

# **Microcystins as Lead Structures for Anticancer Agents**

**Dissertation**

der Mathematisch-Naturwissenschaftlichen Fakultät  
der Eberhard Karls Universität Tübingen  
zur Erlangung des Grades eines  
Doktors der Naturwissenschaften  
(Dr. rer. nat.)

vorgelegt von

**Julia Moschny**

aus Sulzbach-Rosenberg

Tübingen

2020



Gedruckt mit Genehmigung der Mathematisch-Naturwissenschaftlichen Fakultät der  
Eberhard Karls Universität Tübingen.

Tag der mündlichen Qualifikation:

05.11.2020

Stellvertretender Dekan:

Prof. Dr. József Fortágh

1. Berichterstatter:

Prof. Dr. Timo H. J. Niedermeyer

2. Berichterstatter:

Prof. Dr. Harald Groß



# Danksagung

In den letzten fünf Jahren hat mich eine Vielzahl von Leuten von Beginn der Promotion bis zur Abgabe der Dissertation begleitet und in Form von fachlicher, technischer und persönlicher Unterstützung zum Entstehen dieser Arbeit beigetragen. Dafür möchte ich allen Mitarbeitern des Lehrstuhls für Mikrobiologie/Biotechnologie der Universität Tübingen und den Mitgliedern des Instituts für Pharmazeutische Biologie der Martin-Luther-Universität Halle-Wittenberg danken.

Mein besonderer Dank gilt:

Prof. Dr. Timo Niedermeyer für das spannende Projekt, seine Unterstützung und Betreuung während der letzten fünf Jahre und für die Freiräume in der Gestaltung des Projekts, die mir auch Platz für meine persönliche Entfaltung boten. Außerdem möchte ich mich für die vielen Gelegenheiten bedanken, Konferenzen in Deutschland und weltweit besucht zu haben.

Prof. Dr. Harald Groß für die fachliche Betreuung und die Erstellung des Gutachtens, sowie der Ermutigung an der Weiterbildung zur Fachapothekerin teilzunehmen.

Dan und Heike Enke, Wolfram Lorenzen und Alexandra Hilfer für die fruchtbare Zusammenarbeit bei den Patentierungen und der Publikation und für ihre Unterstützung bei der Kultivierung von Cyanobakterien, der Aufreinigung von Microcystin-Derivaten und bei den HPLC–MS Messungen.

Andreas Kulik für die zahllosen HPLC–MS-Messungen.

Dr. Robert Eckenstaler für die Fluoreszenz-Mikroskopie-Versuche.

Thomas Härtner, Elke Klenk und Anja Wodak für ihr Organisationstalent, mit dem sie einen reibungsfreien Ablauf im Labor gewährleisteten.

meinem Master-Studenten Philipp Schneider für die wertvolle Vorarbeit zur Publikation.

Nico, Steffen, Tomasz und Paul für die gemeinsamen Stunden im Labor, die lustigen Diskussionen über laborrelevante und -irrelevante Dinge und die vielen besonderen Erlebnisse auf AG-Ausflügen, gemeinsamen Konferenz-Besuchen oder beim Feierabendbier.

Ulli für die unterhaltsamen und gelächterreichen Mittagspausen beim Kochen im Institut.

Ronja für fünf Jahre gemeinsames Lachen und Weinen, für ihre Hilfe und lieben Worte in allen Labor- und Lebenslagen und für ihr ausdauerndes, immer offenes Ohr.

meinen Eltern und meiner Schwester für ihren unerschütterlichen Glauben an mich und meine Ziele und für ihre uneingeschränkte Unterstützung aus der Ferne.

Vielen herzlichen Dank Julian für die anregenden fachlichen Diskussionen, deine konstruktive Kritik, sowie für deine endlose Geduld und liebevolle Unterstützung!



# Zusammenfassung

Krebserkrankungen entwickeln sich weltweit zum größten Problem für das Gesundheitswesen. Obwohl immer mehr Behandlungsmöglichkeiten zur Verfügung stehen, die die Sterblichkeit nachweislich reduzieren, gibt es immer noch eine große Anzahl an Karzinomen, die nur schlecht darauf anspricht. Ein Großteil der Krebstherapeutika geht auf einen natürlichen Ursprung zurück. Eine Klasse zytotoxischer Naturstoffe bilden dabei die Microcystine, die zyklische Peptide aus Cyanobakterien sind. Allerdings kommen sie aufgrund ihrer schwerwiegenden Lebertoxizität nicht für einen direkten Einsatz am Patienten in Frage, weshalb neue Wege für eine klinische Anwendung verfolgt werden müssen.

Das Ziel der vorgelegten Arbeit bestand darin, Microcystine mit bioorthogonalen („klickbaren“) chemischen Gruppen zu funktionalisieren, durch die es möglich würde sie als aktive Komponenten in Antikörper-Wirkstoff-Konjugaten zu nutzen.

Zunächst wurde eine vielseitig einsetzbare Methode entwickelt und optimiert um Microcystine in ausreichender Menge aus Cyanobakterien zu isolieren. Dabei kamen verschiedene Extraktions- und Trennungsvorgänge, wie Flüssig-Flüssig-Extraktion, Flash- und Größenausschluss-Chromatographie und semipräparative HPLC zum Einsatz. Die einzelnen Schritte wurden zu einem effizienten Arbeitsablauf kombiniert, der auf drei unterschiedliche Mengen an Ausgangsmaterial ausgelegt ist. Ein integraler Bestandteil war außerdem die strukturunabhängige Quantifizierung von Microcystin-Derivaten mittels HPLC, die an einen evaporativen Lichtstreu-Detektor gekoppelt ist. Um die isolierten Microcystine strukturell und biologisch zu charakterisieren, wurden eine MS<sup>2</sup>-basierte Methode zur Strukturdereplikation und ein Zytotoxizitäts-Assay etabliert, der Rückschluss auf die Transporter-Selektivität der jeweiligen Derivate zulässt.

Die Funktionalisierung der Microcystine mit klickbaren Gruppen gelang mittels Vorläufer-dirigierter Biosynthese. Indem Azido- und Alkyn-modifizierte Aminosäuren zur Kulturbrühe von Microcystin-produzierenden Stämmen gegeben wurden, wurden über 40 neue, klickbare Microcystine, einschließlich mehrerer, doppelt funktionalisierter Varianten, gebildet. Bei der Untersuchung der Einbaugeschwindigkeit eines Substrats stellte sich allerdings heraus, dass nur ein kleiner Prozentsatz der eingesetzten Aminosäure in Form von „klickbaren“ Microcystin wiedergefunden wurde. Um die verbliebene Menge an Substrat zurückzuverfolgen, wurde eine vergleichende DC-Methode mit einem fluorogenen Färbereagenz entwickelt. Dabei zeigte sich, dass auch andere Metabolite die bioorthogonale Funktion trugen. Dies ist ein wichtiger Aspekt, weil die klickbaren Microcystine auch für physiologische Studien in den Cyanobakterien genutzt werden sollten.

Eines der „klickbaren“ Microcystine wurde isoliert und mit einem fluorogenen Farbstoff konjugiert. Sowohl das klickbare als auch das fluoreszenzmarkierte Microcystin wurden hinsichtlich ihrer Zytotoxizität charakterisiert. Die Aufnahme des fluoreszierenden Derivats in die Zellen wurde durch Fluoreszenz-Mikroskopie-Aufnahmen visualisiert. Die Datensätze aus beiden Versuchen zeigten, dass weder die bioorthogonale Gruppe noch der Fluoreszenz-Farbstoff einen Einfluss auf die pharmakologischen Eigenschaften der Microcystine haben. Diese Tatsache ist von entscheidender Bedeutung, wenn klickbare Microcystine zukünftig als Leitstrukturen für die Krebstherapie genutzt werden sollen.



## Summary

Cancer is emerging as one of the main health issues worldwide. Although the development of conventional and, more recently, targeted therapies has contributed significantly to reduce cancer mortality, there is still a large number of malignancies with only poor responsiveness. Most clinically used anticancer drugs originate from natural sources. One such class of cytotoxic natural products are microcystins, cyanobacterial cyclic peptides. Because of their severe hepatotoxicity, however, they are inapt for a direct use as anticancer agents, and new ways were sought for their potential clinical application.

The aim of the research presented here was to study whether bioorthogonal (clickable) functions can be introduced into microcystins, allowing for their use as warheads in antibody-drug-conjugates.

In order to isolate microcystins in sufficient yields from the cyanobacterial biomass, an optimized and versatile protocol was compiled by combining different extraction modes and chromatographic techniques, such as liquid-liquid extraction, flash and size-exclusion chromatography, and semi-preparative HPLC. The workflow was optimized for three different amounts of starting material, covering a few milligrams to several grams. Furthermore, an HPLC method based on evaporative light-scattering detection was developed and validated, enabling a structure-independent quantification of microcystin variants. Lastly, the methodic toolbox was complemented with a MS<sup>2</sup> method for structure dereplication and a cytotoxicity screening assay, which assesses the transport selectivity of the microcystin variants.

Simultaneously, an approach called precursor-directed biosynthesis was applied to generate clickable microcystins. Supplementing different azide or terminal alkyne-containing amino acid analogs into the cultivation medium of microcystin-producing cyanobacteria strains led to more than 40 new structures with bioorthogonal groups, including several dual-functionalized congeners. When studying the kinetics of substrate incorporation in more detail, it was observed that most of the alkyne-containing amino acid was not recovered as clickable microcystin. In order to trace back the lost amounts of substrate, a comparative TLC method was developed involving a bioorthogonal, fluorogenic dye as TLC stain. This revealed that the bioorthogonal groups were also present in other metabolites, highlighting an important aspect if the clickable microcystins should also be used for physiological studies within the cyanobacteria.

One clickable microcystin was isolated and labeled with a fluorogenic dye. Both the clickable microcystin and the resulting conjugate were characterized in terms of cytotoxicity. The transportability of the fluorescent microcystin was further demonstrated

by fluorescence microscopy. The data showed that neither incorporation of the unnatural functional group nor attachment of the fluorescent label significantly affects the pharmacological properties of the microcystin, emphasizing the suitability of clickable microcystins as lead structures for anticancer agents.

## Declaration of Contributions

*Parts of this thesis have already been published in Moschny, J., Lorenzen, W., Hilfer, A., Eckenstaler, R., Jahns S., Enke, H., Enke D., Schneider P., Benndorf R., Niedermeyer T.H.J. 2020. Precursor-Directed Biosynthesis and Fluorescence Labeling of Clickable Microcystins. *J Nat Prod* **2020**, 83, 1960–1970. (date: May 28, 2020). (A.4. Publication) All contents, including text, figures, and tables were adapted and reprinted with the permission of the American Chemical Society, Copyright 2020. Adapted paragraphs and sections are indicated by footnotes or a note in the beginning of the chapter, respectively.*

*The authors' contributions are as follows:*

Author	Scientific ideas [%]	Data generation [%]	Data analysis and interpretation [%]	Paper writing [%]
Julia Moschny	50	30	65	60
Wolfram Lorenzen	5	20	10	10
Alexandra Hilfer	0	20	0	0
Robert Eckenstaler	5	5	10	5
Stefan Jahns	0	10	2.5	0
Heike Enke	7.5	5	0	0
Dan Enke	12.5	0	0	0
Philipp Schneider	0	5	0	0
Ralf A. Benndorf	0	0	2.5	0
Timo H. J. Niedermeyer	20	5	10	25



# Table of Content

<b>1. Introduction</b> .....	<b>19</b>
1.1. Cancer – an Emerging, Global Health Issue .....	19
1.1.1. Estimated Prevalence, Incidence and Mortality Rates.....	20
1.1.2. Conventional Therapy: Tumor Resection and Radiotherapy .....	23
1.1.3. Conventional Chemotherapy.....	24
1.1.4. Targeted Chemotherapy and the Problem of Drug Resistance .....	28
1.1.5. Natural Product-Derived Anticancer Agents.....	31
1.2. Microcystins – Promising Candidates for Cytotoxic Drugs.....	36
1.2.1. Structure, Diversity and Biosynthesis.....	37
1.2.2. Mode of Action and Structure–Activity Relationship .....	41
1.2.3. OATPs—the MCs Cellular Gateway and their Role in Cancer .....	44
1.2.4. Microcystins as Warheads for ADCs and Beyond .....	45
1.3. Aim of the Thesis .....	50
<b>2. Materials and Methods</b> .....	<b>52</b>
2.1. Chemicals and Instruments.....	52
2.2. Cultivation of Cyanobacteria .....	55
2.2.1. Media.....	55
2.2.2. Cyanobacterial Strains.....	57
2.2.3. Determination of the Optical Density at 750 nm .....	58
2.2.4. Preparation of Precultures of Cyanobacteria.....	58
2.2.5. Cultivation of Cyanobacteria in Shaking Flasks.....	58
2.2.6. Cultivation of Cyanobacteria in Centrifuge Tubes .....	58
2.2.7. Cultivation in CellDEG HD10 Cultivators.....	59
2.2.8. Supplementation Experiments .....	59
2.2.9. Uptake of Prtyr into <i>M. aeruginosa</i> CBT 480.....	59
2.2.10. Continuous Supplementation System for PDB.....	60
2.3. Processing of Cyanobacterial Biomass and Supernatants .....	61
2.3.1. Extraction with Methanol + 0.05 % Trifluoroacetic Acid .....	61
2.3.2. Evaluation of Biphasic Systems and Re-extraction with <i>n</i> -Butanol.....	61
2.3.3. Evaluation of a Three-Phase System.....	62
2.3.4. Two-step Liquid–Liquid Extraction of Cyanobacterial Biomass .....	62
2.3.5. Quick Extraction for Qualitative Analysis.....	63
2.4. Analytical HPLC .....	63
2.4.1. Generic Method for Method Development on Luna Columns .....	65
2.4.2. Quantification of MCs by HPLC–ELSD .....	65
2.4.3. Quantification of Prtyr in <i>M. aeruginosa</i> CBT 480 Culture Supernatant...	67
2.4.4. Quantification of MC-PrtyrR from the Biomass of CBT 480.....	68
2.5. HPLC–MS.....	69

2.6. Thin-Layer Chromatography (TLC) .....	71
2.6.1. TLC of Samples Obtained from the CuAAC Reaction .....	71
2.6.2. TLC of Templates .....	71
2.7. Preparative LC Methods .....	72
2.7.1. Solid-Phase Extraction (SPE) .....	72
2.7.2. Flash Chromatography .....	72
2.7.3. Size-Exclusion Chromatography .....	73
2.7.4. Semi-preparative HPLC .....	73
2.7.5. Isolation of MC-PrtyrR ( <b>3</b> ) at Cyano Biotech GmbH .....	75
2.8. NMR Spectroscopy .....	75
2.9. Chemical Synthesis: CuAAC Reactions .....	75
2.9.1. CuAAC Reaction with Templates .....	76
2.9.2. Conjugation of MC-PrtyrR ( <b>3</b> ).....	76
2.10. Measurement of the Excitation and Emission Spectra of MC-(O-((7-hydroxy-2H-chromen-3-yl)-1H-1,2,3-triazol-4-yl)methyl)YR .....	76
2.11. Cell Culture Methods .....	77
2.11.1. Cell Culture Media and Reagents .....	77
2.11.2. Cell Lines.....	79
2.11.3. Cultivation of Cell Lines from Cryo-Preserved Stocks .....	79
2.11.4. Changing the Medium.....	79
2.11.5. Passaging of Cell Lines .....	80
2.11.6. Testing for Mycoplasma Contamination by PCR .....	80
2.11.7. Treatment of Mycoplasma-Contaminated Cell Lines .....	82
2.11.8. Cryo-Preservation of Cell Lines.....	82
2.11.9. Counting of Cells .....	83
2.11.9.1. Counting of Cells with a Neubauer Hemocytometer .....	83
2.11.9.2. Counting of Cells with an Automated Cell Counter .....	84
2.11.10. Determination of Cell Abundance by Staining with Sulforhodamine B .....	84
2.11.11. Determination of the Seeding Density .....	85
2.11.12. Cytotoxicity Assay .....	85
2.11.13. Fluorescence Microscopy.....	86
<b>3. Results and Discussion .....</b>	<b>87</b>
3.1. A Toolbox for Microcystin Isolation, Analysis and Screening .....	87
3.1.1. Optimization of Microcystin Extraction.....	88
3.1.2. Pre-Purification by Flash and Size Exclusion Chromatography .....	94
3.1.3. Isolation of Microcystins by Semi-Preparative HPLC.....	99
3.1.4. Quantification of Microcystins by HPLC-ELSD .....	103
3.1.5. Workflow for Microcystin Isolation and Structure Dereplication by MS <sup>2</sup> .....	109
3.1.6. Assay Establishment for Cytotoxicity Screening.....	113
3.2. Precursor-Directed Biosynthesis and Fluorescence Labeling of Clickable Microcystins.....	116
3.2.1. Clickable Microcystins from Various <i>Microcystis</i> strains.....	119
3.2.2. The Uptake of Prtyr in <i>M. aeruginosa</i> CBT 480.....	127

3.2.3. The Use of Prtyr in <i>M. aeruginosa</i> CBT 480.....	130
3.2.4. Fluorescence Labeling of MC-PrtyrR (3) and Biological Characterization of the Conjugate.....	137
<b>4. Conclusion .....</b>	<b>142</b>
4.1. The Toolbox for MC Isolation and Quantification.....	142
4.2. Implications for <i>In Vivo</i> Imaging and Other Applications of PDB.....	143
4.3. Clickable MCs in ADC.....	144
<b>5. References.....</b>	<b>145</b>

## Appendix

A.1. List of Abbreviations.....	179
A.2. Supplementary Information to Chapter 1.1.....	180
A.3. Supplementary Information to Chapter 3.1.....	182
A.4. Publication .....	191
A.5. Supplementary information to Chapter 3.3.....	202
A.6. Copyright Licenses .....	251





Nothing in life is to be feared, it is only to be understood. Now is the time to understand more, so that we may fear less.

**Marie Skłodowska Curie**  
**(First female Nobel laureate)**



# 1. INTRODUCTION

## 1.1. Cancer – an Emerging, Global Health Issue

Cancer is the most feared disease in industrialized countries, mainly because of its high mortality rates.<sup>1,2</sup> Only surpassed by coronary diseases, cancer emerged as the second leading cause of deaths in the United States in 2017 with a proportion of 21.3%.<sup>3,4</sup> With regard to the numbers of premature deaths at the ages 30–69 years, it even ranks first for many countries with a high Human Development Index<sup>[1]</sup> (HDI, Figure 1).<sup>6,7</sup> Since the global increase in HDI has promoted a decline in the mortality rates of infectious diseases, cancer is expected to advance as the leading cause of death worldwide in the 21<sup>st</sup> century accounting for an estimated number of 9.6 million deaths in 2018.<sup>8</sup>

In addition to its lethality, another noteworthy aspect in the fear of cancer is the “aggressive nature of treatments”.<sup>2</sup> Adverse effects, such as pain, suffering, and the loss of hair, often inspire a greater dread in patients than the cancer itself.<sup>9–11</sup> Especially chemotherapy is still associated with many negative side effects imposing a long ordeal on the patients during recurrent cycles of therapy.<sup>12</sup>

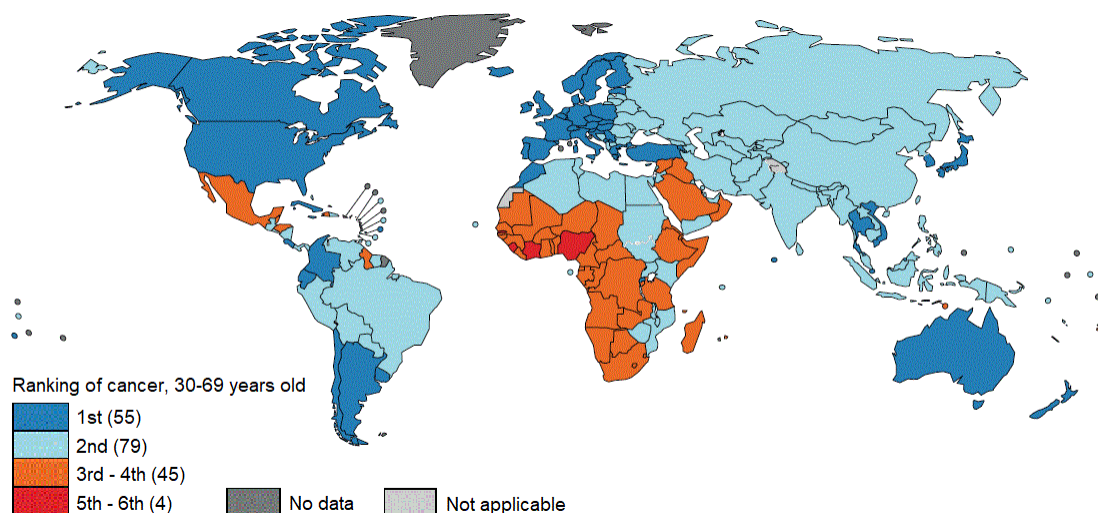


**Figure 1.** Global map of cancer as leading cause of premature death (i.e. at ages 30–69 years) predicted for 2018. The ranking within the respective country is indicated by different colors with the number of countries in parentheses. Dark blue, first leading cause; bright blue, second leading cause; orange, third and fourth leading cause; red, fifth and sixth leading cause; dark grey, no data available; light grey, ranking not applicable. Reprinted from Wild *et al.*<sup>7</sup>

<sup>[1]</sup> Human development index (HDI): the HDI reflects the developmental state of the respective country taking into account life expectancy, education, and standard of living.<sup>5</sup>

## 1. Introduction

---

In the past decades, many novel and better tolerable strategies have been developed for the treatment of cancer.<sup>13,14</sup> These approaches not only helped to increase the incidence-free survival rates, they also contributed to improving the quality of life in cancer patients. Still, such therapies are not available for all types of cancer yet, and there are even some malignancies that only respond poorly to targeted and/or conventional therapies.<sup>15–17</sup>

Another problem in cancer treatment consists in the emergence of drug resistance in many cancers. Under the selection pressure of conventional or targeted therapy, some cancer cells manage to evade the cytotoxic effects of the drugs.<sup>18</sup> These resistant clones then form a new malignancy, which is not susceptible to the treatment any more, and in some cases, the resistance mechanisms even confer resistance to other chemotherapeutics. Due to these two challenges and with cancer emerging as a global health problem, the exploration of new therapeutic options has to go on.

### 1.1.1. Estimated Prevalence, Incidence and Mortality Rates

Regarding the estimated, 5-year prevalence, more than 43 million people have been diagnosed with cancer in 2018.<sup>19</sup> The most common cancer sites are the breasts (15.7 %), colorectum (10.9 %), prostate (8.5 %), and lung (4.9 %). With two of the four most frequent cancers arising from primary and secondary sexual characteristics, there are significant differences in cancer prevalence between men and women (Figure 2A and B). Men mainly suffer from prostate (17.7 %) cancer whereas almost one-third (30.1 %) of the cases in females is attributed to breast cancer. In summary, the 5-year prevalence in 2018 covering all types of cancer is estimated to be higher in women with 22.8 million cases compared to 21.0 million cases in men.

These types of cancer mainly occur in adults at ages above 50 years and they dominate the 5-year prevalence statistics of all ages due to their high incidence rates.<sup>8,19</sup> In children and adolescents, however, the most common malignancies originate from other types of tissues (Figure 2C).<sup>19–21</sup> Leukemia (26.7 %) ranks first as the most common cancer in childhood before brain cancer and other cancers of the central nervous system (grouped as BNS, 9 %), and non-Hodgkin lymphoma (NHL, 7.2 %). Together with thyroid cancer, they account for around half of the 1.2 million cancer cases in patients of ages 0–24 years.

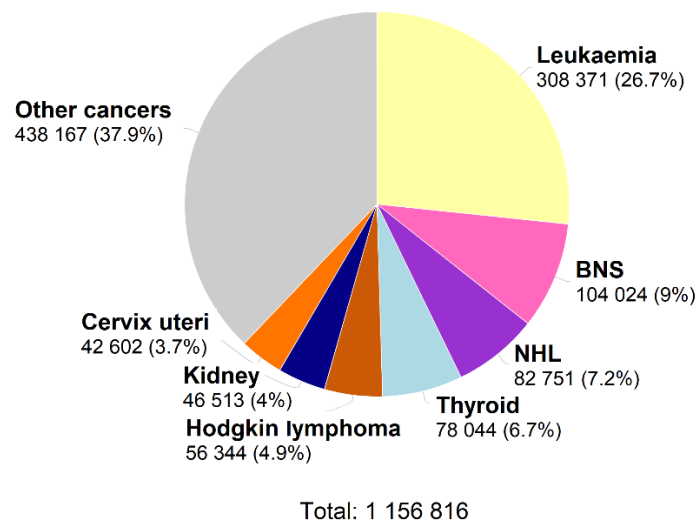
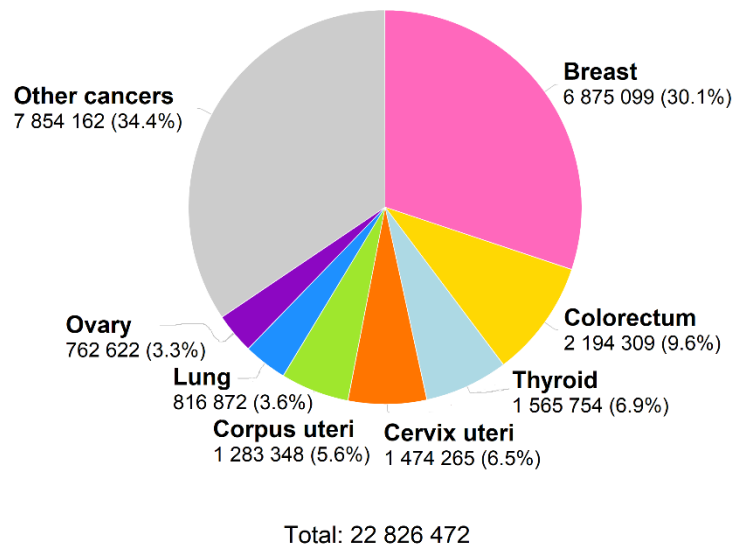
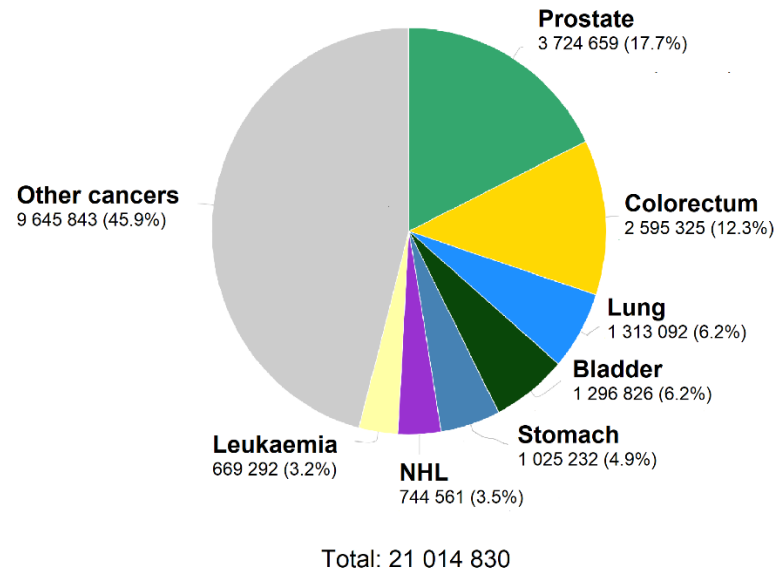


**Figure 2.** Estimated number of prevalent cases (5-year) in 2018, worldwide, all cancers, (A) males, all ages; (B) females, all ages; (C) both sexes, ages 0–24 years. NHL, non-Hodgkin lymphoma; BNS, brain and central nervous system. Data source: GLOBOCAN 2018.<sup>19</sup>

## 1. Introduction

---

Many, formerly developing countries are gradually acquiring the standards of industrialized and wealthy countries, which is associated with population ageing and alterations in lifestyle. These socio-demographic and behavioral changes led to a continuous rise in cancer incidence rates worldwide.<sup>22–24</sup> Within six years only, the number of new cases per year has increased by approximately 30 %, from 14 million new cases in 2012 to estimated 18 million in 2018.<sup>8,25</sup> Since this developmental progress is expected to continue over the upcoming 20 years, predictions foresee an additional 50 % increase in cancer incidence to more than 27 million new cancer cases in 2040, making cancer an even more important, global health issue.<sup>24,26</sup>

As a result of this persisting global evolution, the estimated site-specific cancer incidence rate in 2018 is congruent with the estimated 5-year prevalence. The highest incidence rate by far is predicted for breast cancer with an age-standardized rate<sup>[2]</sup> of almost 50 per 100,000 person-years (Figure 3) followed by prostate cancer.<sup>8,19</sup> However, the mortality rates of breast and prostate cancer are comparatively low despite their high numbers of incidence and prevalence indicating good chances of a long-term survival after diagnosis.

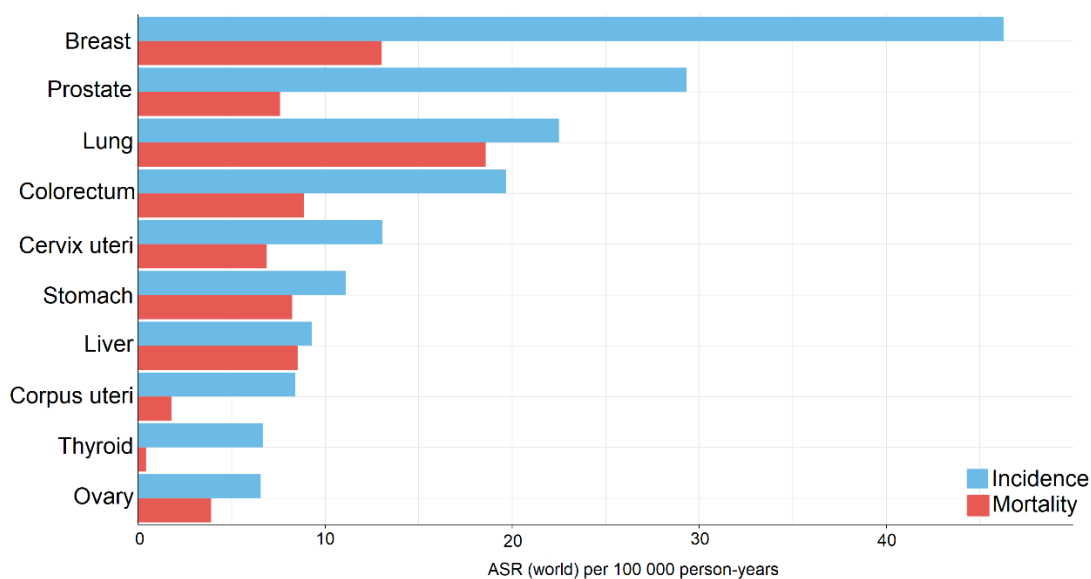


**Figure 3.** Estimated age-standardized incidence (blue) and mortality (red) rates (ASR) of the ten most frequent types of cancer in 2018, worldwide, both sexes, all ages, expressed as age-standardized rate (ASR) per 100 000 person-years. Data source: GLOBOCAN 2018.<sup>19</sup>

---

<sup>[2]</sup> Age-standardized rate (ASR): an ASR is a summary measure of the rate that would have been observed if the population had a standard age structure.<sup>19</sup>

Lung cancer exhibits the highest mortality rate of all types to cancer. Since the incidence rate of lung cancer is not as high as for breast cancer, the gap between incidence and mortality rates shrinks as their values converge. This peculiarity implies poor prognosis for the respective type of cancer.

Stomach cancer shows a comparable relation of incidence and mortality rates as lung cancer, but in case of liver cancer, the gap is narrowest with almost identical incidence and mortality rates. Both these cancers are fatal malignancies with poor survival rates. They represent the third (stomach cancer) and fourth (liver cancer) leading causes of cancer death in respect of the estimated, absolute numbers worldwide for 2018.<sup>19,27,28</sup>

In summary, the mortality rates of most types of cancer have been increasing worldwide over the past decades. However, this trend reverses if only the numbers of western and industrialized countries are taken into evaluation. The mortality rates of all types of cancers taken together have declined significantly in high-income countries of Europe and Northern America while the survival rates have improved.<sup>29,30</sup> This favorable development is predominantly due to substantial advances in cancer management and treatment.

### 1.1.2. Conventional Therapy: Tumor Resection and Radiotherapy

The well-established treatment options of cancer comprise surgery, radiotherapy and chemotherapy. With an evolving understanding of human and cancer biology, new therapeutic strategies have emerged like cancer vaccination, hematopoietic stem cell transplantation, or gene therapy. A detailed characterization of their rationales and mode of actions (MoAs) would go beyond the scope of this thesis, and their applications and recent developments can be retrieved from elsewhere.<sup>14,31–33</sup> However, it is noteworthy that these new approaches are limited to a few types of cancer and/or require specific genotypes and phenotypes. In consequence, the conventional treatment options are still indispensable in modern cancer therapy.

Tumor resection by surgery holds the best potential for cure when solid and locally confined diseases are concerned, because the tumor burden is significantly diminished within a short period. Whereas surgeons endeavored to remove all the malignant tissue and readily accepted the prospect of severe mutilations and amputations in earlier times, nowadays, a more conservative way is followed, which includes the preservation of function and reconstructive or plastic surgery.<sup>34,35</sup> Recent progress in surgical techniques further supported these efforts allowing for microscopic resections and, thus, increasing the chances to achieve tumor-free margins while removing only a minimal amount of tissue.

## 1. Introduction

---

Another treatment option for solid tumors is radiotherapy. It employs electromagnetic waves (e.g. X-rays or gamma rays) or particulate radiation as ionizing radiation, which causes DNA damage and leads to the induction of cell death.<sup>36,37</sup> It is either generated externally in a linear accelerator and directed as a beam towards the tumor (teletherapy), or materials with radioactive nuclei are implanted inside or adjacent to the tumor (brachytherapy).<sup>38</sup> The therapeutically used nuclei comprise alpha emitters like <sup>226</sup>Ra, <sup>137</sup>Cs, or <sup>125</sup>I, and beta emitters like <sup>32</sup>P, <sup>90</sup>Y, and <sup>131</sup>I.<sup>39</sup> With the development of cancer-specific carriers, systemic targeted radionuclide therapy became an alternative way of administering radioactive isotopes.<sup>38</sup> Due to their conjugation with the carriers, they are directly transported and delivered to the cancer after administration, exposing only malignant cells to the ionizing radiation.

Both, tumor resection and radiotherapy rarely work as a stand-alone therapy. They are usually combined with each other or chemotherapy. In the adjuvant therapy concept, chemotherapy follows surgery or radiation therapy in order to treat residual cancer tissue or micrometastases and prevent the tumor's recurrence.<sup>40</sup> In contrast, the neoadjuvant concept involves chemotherapy prior to tumor resection, so the tumor is shrunk to a resectable size. If the cancer has metastasized and spread to multiple sites or cannot be removed surgically out of other reasons, chemotherapy often remains the only effective therapeutic option.

### 1.1.3. Conventional Chemotherapy

Malignant cells exhibit a fast cell division rate by completing the cell cycle more often than healthy cells.<sup>41</sup> The cell cycle consists of two major phases, the mitotic (M) phase and the interphase, which is further subdivided into the G1, S, and G2 phase.<sup>42,43</sup> Before the dividing cell transition to a subsequent phase, it needs to pass several checkpoints.<sup>44</sup> If it fails, e.g. due to DNA damage upon treatment with cytotoxic agents, the cell cycle is arrested, leading to the induction of cell death. After the M phase is completed, the parent and daughter cell enter the G0 phase under normal circumstances and are quiesced. In degenerated cells, however, it is possible that both cells directly proceed to G1 reentering the cell cycle anew.<sup>40</sup>

Conventional chemotherapy exploits this higher cell cycle activity, and the different classes of cytotoxic agents interfere with its progress at different points (Figure 4).<sup>40</sup> The conventional chemotherapeutics form five major classes based on their MoA: antimetabolites, topoisomerase inhibitors, microtubule-targeting agents, alkylating agents, and cytotoxic antibiotics.<sup>45</sup> The antimetabolites exert their cytotoxicity during the



S phase, when new nucleoside bases are synthesized, and the DNA is replicated.<sup>40</sup> Due to their resemblance to natural substrates, they act as competitive inhibitors in essential, biosynthetic routes. The folate antagonists methotrexate and pemetrexed inhibit the *de novo* synthesis of pyrimidine nucleotides through inhibition of the dihydrofolate reductase (for the detailed MoA, refer to Figure A1 in the appendix).<sup>46</sup> Pyrimidine (e.g. fluorouracil and cytarabine) and purine (e.g. mercaptopurine and pentostatin) analogs are incorporated as false nucleotides into the DNA, causing the newly synthesized strand to break and, thus, blocking DNA synthesis.<sup>45,46</sup>

The enzymes topoisomerase I and II control the three-dimensional organization of DNA by catalyzing the relaxation of supercoiled DNA prior to replication and transcription.<sup>47,48</sup> Consequently, topoisomerase inhibitors like topotecan and etoposide hamper DNA synthesis in the S phase and protein biosynthesis in the G2 phase. Furthermore, the anthracyclines, which are often categorized as “antitumor antibiotics” together with bleomycin, were characterized as topoisomerase II inhibitors.<sup>40,49</sup>

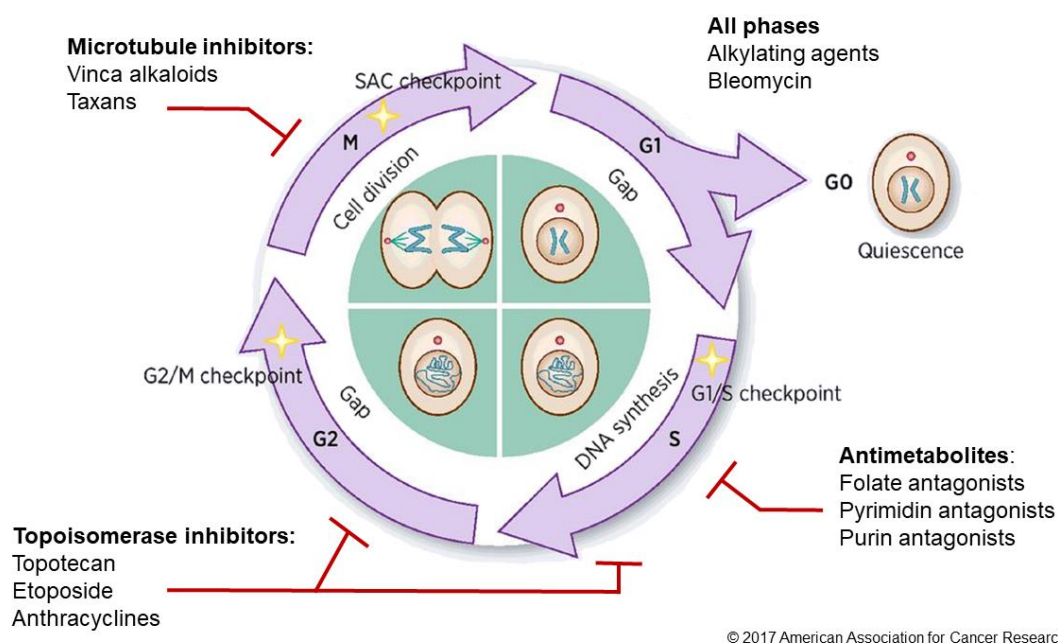


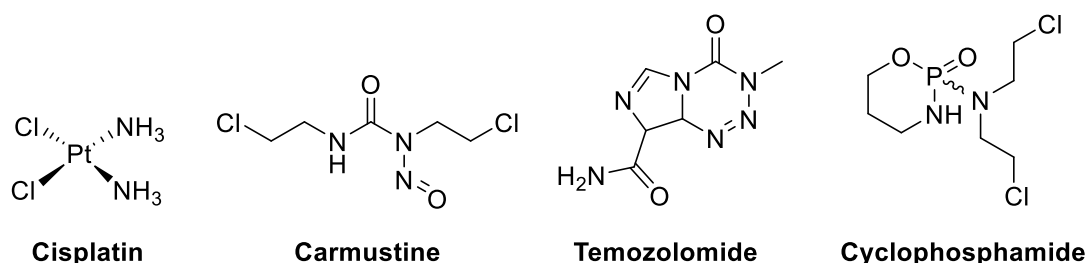
**Figure 4.** Cell cycle inhibitors in conventional chemotherapy. A schematic representation of mammalian cell division and inhibitors that interfere with the various phases. Mitogenic signals trigger the cell cycle initiation (G1), in which the cell prepares for DNA synthesis. Cells transition through S phase, where DNA synthesis occurs, the G2-gap phase and mitotic (M) phase, where cell division occurs. Yellow stars depict three cell-cycle checkpoints: G1–S (the DNA replication checkpoint), G2–M (the DNA damage checkpoint), and SAC (the spindle assembly checkpoint). Blunt red arrows indicate indirect inhibition of the respective phases by the cytotoxic agents. Adapted and modified from Mills *et al.*<sup>50</sup> Reproduced with the permission of the American Association for Cancer Research (Document A1).

## 1. Introduction

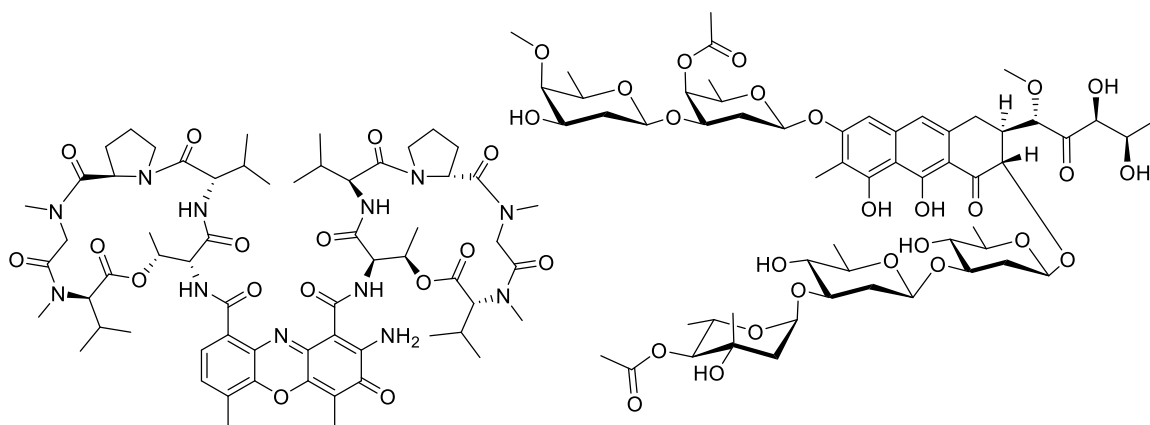
---

Although cells are most sensitive to cytotoxic drugs in the M phase, the microtubule inhibitors are the only class impeding the cell cycle in this phase. By polymerization of the protein monomers  $\alpha$ - and  $\beta$ -tubulin, the microtubules form the mitotic spindle, which is responsible for transporting the chromosomes to its poles during mitosis. All inhibitors bind to  $\beta$ -tubulin, but they differ in their effects caused upon binding. The vinca alkaloids have destabilizing effects on the tubulin polymer preventing the assembly of the mitotic spindle.<sup>51</sup> In contrast, the taxans stabilize the tubulin polymers and mitotic spindle, so it cannot be disassembled and mitosis is not terminated properly.

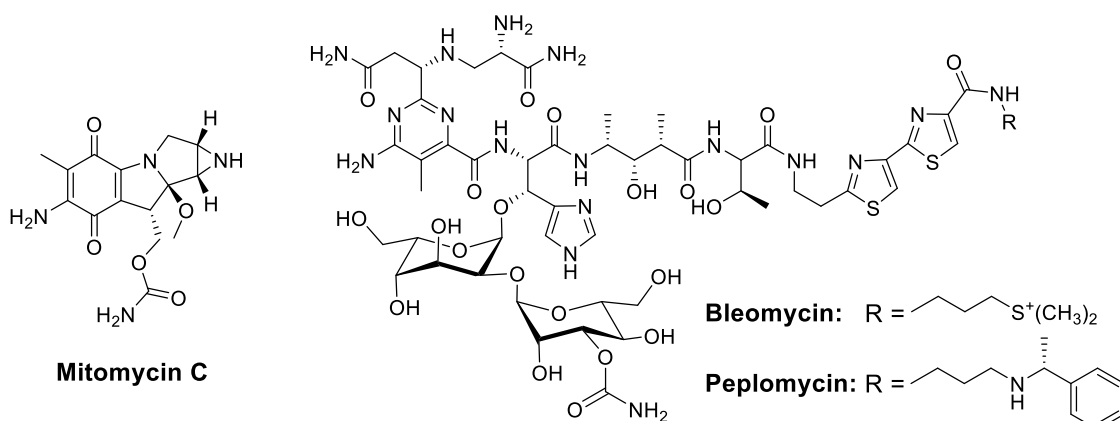
The alkylating chemotherapeutics represent the largest and structurally most diverse class among the cytotoxic agents. They are further subdivided by their functionalities into platinum complexes (e.g. cisplatin), nitrosoureas (e.g. carmustine), triazenes (e.g. temozolomide), and nitrogen mustards (e.g. cyclophosphamide), which are derived from mustard gas, a chemical warfare agent used in World War I.<sup>45,52</sup> Despite the differences in their respective MoAs, all alkylating agents share the generation of a highly reactive intermediate as the essential, common step. These intermediates covalently bind to nucleotides and form DNA adducts compromising DNA functionality and integrity. DNA modified in such a manner cannot be transcribed properly, and protein biosynthesis comes to a halt. Thus, the pharmacologic activity of alkylating agents is independent of the cell cycle.



Likewise structurally diverse, the cytotoxic antibiotics are classified separately from the alkylating agents. Although they also inflict DNA damage through covalent binding, their MoAs go beyond alkylating reactions. The chromopeptide actinomycin D, the anthraquinone glycoside chromomycin A<sub>3</sub>, the quinone mitomycin C, and the glycopeptides bleomycin and peplomycin bind to various motifs of the DNA while azinomycin B additionally cross-links the double strands.<sup>53–59</sup> Bleomycin further cleaves the DNA double strand due to the formation of free radicals.<sup>60</sup> A similar MoA underlies the cytotoxicity of the enediyne neocarzinostatin, which was approved for cancer treatment in form of the polymer conjugate zinothalamer.<sup>61–63</sup>



Actinomycin D

Chromomycin A<sub>3</sub>

Neocarzinostatin

Targeting the cell cycle in order to hamper the growth of cancerous cells has been employed successfully for more than sixty years, and conventional chemotherapy still plays an important role in cancer treatment. However, it comes with a high price. Since cytotoxic drugs also hit other, fast proliferating cells like epithelial cells, conventional chemotherapy is associated with severe side effects like the loss of hair, nausea, and diarrhea, which further leads to malabsorption and malnutrition. This inspired the search for so-called targeted therapies, which aim at more distinctive features of cancer cells than the higher cell cycle activity.

### 1.1.4. Targeted Chemotherapy and the Problem of Drug Resistance

The extensive study of cancer cell biology revealed several new targets for chemotherapy, the majority of which are tyrosine kinases.<sup>64</sup> Tyrosine kinases transfer phosphate from adenosine triphosphate (ATP) to tyrosine residues of effector proteins, what mostly leads to their activation. In consequence, tyrosine kinases are important members of cell signaling pathways controlling cell differentiation, function, growth, survival and migration.

Membrane-bound tyrosine kinases are also called receptor tyrosine kinases and feature an extracellular receptor domain and a catalytic intracellular kinase domain.<sup>65</sup> Solute, non-receptor tyrosine kinases only possess the catalytic kinase domain and are located in the cytosol, the nucleus, and the inner surface of the membrane. Under physiologic conditions, the activity of both types is tightly regulated, maintaining a low degree of protein phosphorylation in non-proliferating cells.<sup>64</sup>

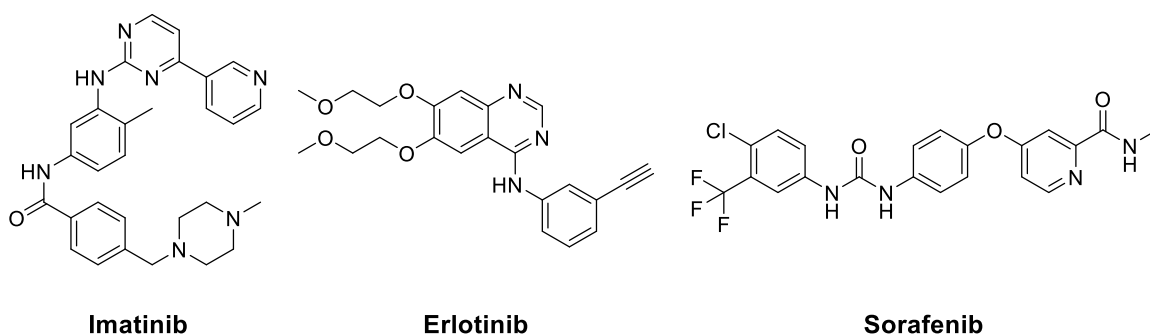
The binding of a ligand activates the receptor tyrosine kinases and stimulates their autophosphorylation, which creates a binding site for effector proteins, and activates subsequent signaling pathways.<sup>65</sup> In case of the non-receptor tyrosine kinases, inhibitory proteins control their activity and only dissociate from the complex when intracellular signals cause either autophosphorylation or the *trans*-phosphorylation by other kinases.<sup>66</sup> The tyrosine kinases remain active until a termination signal, e.g. dephosphorylation by a phosphatase, arises and sets them back into an inactive state.

In degenerated cells, these rigid control mechanisms can be disrupted in manifold ways.<sup>64</sup> Due to mutations in the gene, the autoregulation of tyrosine kinases can be perturbed, and the receptor or solute tyrosine kinases are constitutively activated without external trigger.<sup>67-69</sup> Similar effects are observed if a fusion protein of both types arises, e.g. from chromosomal translocation.<sup>70-72</sup> Further reasons for the dysregulation and over-activation of tyrosine kinases are gene overexpression or upregulation of the respective tyrosine kinase, or an abnormal expression of regulatory factors, such as inhibitory proteins.<sup>73,74</sup> As a result of the tyrosine kinase hyperactivity, cancer cells can proliferate faster, evade pro-apoptotic signals more easily, or become more resistant to cytotoxic drugs. It can further promote angiogenesis, invasiveness and the metastatic potential of solid tumors.<sup>64</sup>

Examples of non-receptor tyrosine kinases exploited for targeted cancer therapy are BCR-ABL in chronic myelogenous leukemia (CML), the anaplastic lymphoma kinase (ALK) in non-small cell lung cancer, the Janus kinase (JAK) in myelofibrosis, and mTOR in breast, pancreatic and lung cancer, and renal cell carcinoma.<sup>13</sup> All of them can be

inhibited by small molecules, which bind to the catalytic center in competition to ATP, e.g. like imatinib to BCR-ABL.<sup>75</sup> In addition to non-receptor tyrosine kinases, other solute protein kinases have been identified as targets for anticancer therapy, i.e. serine-threonine kinases, phosphoinositide 3-kinases, and cyclin-dependent kinases.<sup>76–78</sup> They are equally involved in cell signaling as tyrosine kinases, but their aberrant regulation in cancer cells is less frequent.

The main, druggable receptor tyrosine kinases in cancer cells are the endothelial growth factor receptor (EGFR) and the vascular endothelial growth factor receptors (VEGFR1–3). In contrast to solute tyrosine kinases, three strategies are available to influence the activity of receptor tyrosine kinases pharmacologically.<sup>79</sup> Small molecules, e.g. erlotinib and sorafenib, have a similar MoA to the inhibitors of solute tyrosine kinases and act as competitive inhibitors of the intracellular catalytic subunit.<sup>45</sup> Furthermore, macromolecular proteins called biologicals, i.e. monoclonal antibodies (mAbs), are applied to block the activity of receptor tyrosine kinases from the extracellular side. mAbs feature the particularity to recognize one specific antigen and bind it with extraordinary high affinity. Thus, mAbs targeting receptor tyrosine kinases serve either as neutralizing agents (e.g. bevacizumab) by capturing the ligand and preventing its binding to the receptor, or as direct receptor antagonists (e.g. cetuximab) by blocking the binding site without receptor activation.<sup>79</sup>



This specific binding of mAbs to surface antigens promoted the development of other targeted therapies as cancer cells can express various unique antigens (cluster of differentiation, CD), which are absent in healthy cells.<sup>80–82</sup> The concept of immunotherapy further makes use of the mAbs' capability to trigger a host immune response after binding to the antigen. That way, therapeutic mAbs directed against a cancer-specific CD (e.g. rituximab, directed against CD20 in non-Hodgkin lymphoma) "label" the malignant cells and stimulate the antibody-dependent cell-mediated cytotoxicity (ADCC), which leads to cancer cell death through cytotoxic cells of the immune system.<sup>83</sup>

## 1. Introduction

Another approach in targeted therapy combines the cancer specificity of mAbs with the cytotoxic potential of small molecules. The cytotoxic agents are conjugated with the mAbs via a cleavable linker (Figure 5A), forming a so-called antibody-drug-conjugate (ADC).<sup>84–87</sup> Instead of eliciting an immune response, binding of the ADC to the cancer-specific CD prompts the opsonization of the conjugate, which is subsequently taken up into the cancer cell by endocytosis (Figure 5B). Endosomal and lysosomal processing leads to cleavage of the linker and the cytotoxic agents is eventually released into the cytoplasm, where it can take effect and cause induction of apoptosis and cell death.<sup>87</sup>

By May 2020, four ADCs have been approved by the U.S. Food and Drug Administration (FDA) and the European Medical Agency (EMA).<sup>87</sup> Gemtuzumab ozogamicin and inotuzumab ozogamicin carry an *N*-acetyl- $\gamma$ -calicheamicin-dimethyl hydrazide payload, which belongs to the DNA damaging agents.<sup>88</sup> The mAb gemtuzumab targets CD33 and the ADC is used in the treatment of refractory acute myeloid leukemia while inotuzumab ozogamicin is approved for the treatment of CD22<sup>+</sup> B-cell acute lymphoblastic leukemia.<sup>89,90</sup> Brentuximab vedotin is used for the treatment of CD30<sup>+</sup> Hodgkin lymphoma and peripheral T-cell lymphoma.<sup>91</sup> Its cytotoxic agent monomethyl auristatin E (MMAE) is a microtubule inhibitor just like the payload mertansine of the fourth ADC trastuzumab emtansine.<sup>92</sup> Trastuzumab is directed at the receptor tyrosine kinase HER2, which is often expressed in breast cancer cells.

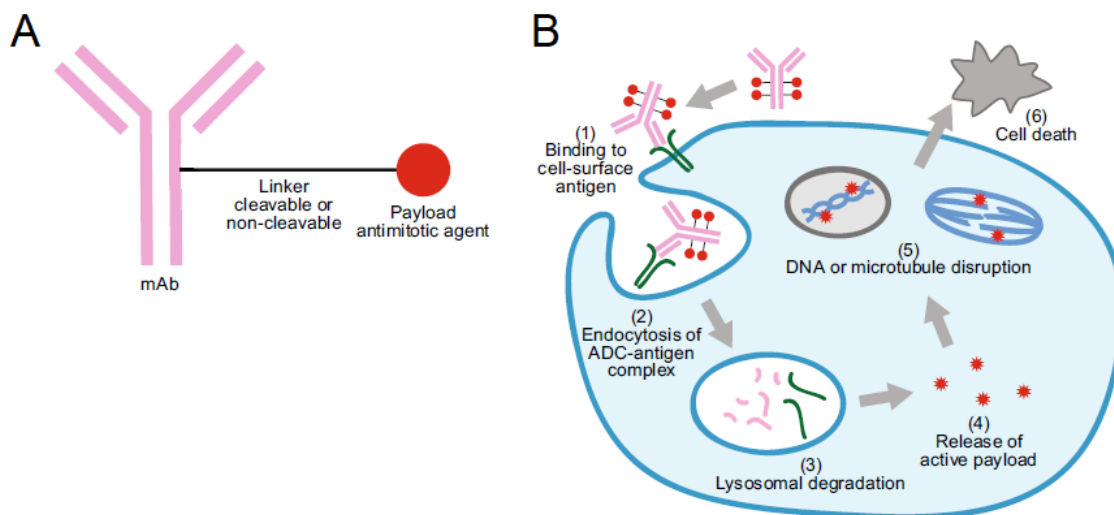


**Figure 5.** Schematic representation of an antibody-drug-conjugate (ADC, A) and its mode of action against a cancer cell (B). (A) The ADC consists of a monoclonal antibody (mAb, rose), which is conjugated to an antimetabolic agent (payload, red circle) by a cleavable or non-cleavable linker (black line). (B) The ADC circulating in the blood stream binds to a surface antigen (1), and the ADC-antigen complex is taken up into the cancer cell by endocytosis (2). The ADC is cleaved and degraded in the lysosome (3), releasing the cytotoxic agent (red circles) into the cytoplasm (4). There, it binds to its target (5) and causes either DNA or microtubule disruption, leading to the induction of cell death (6). Adapted and modified from Tsuchikama and An.<sup>93</sup> (open access)

A major advantage of ADCs in comparison to conventional chemotherapy consists in the targeted and efficient delivery of the anticancer drug to degenerated cells. On the one hand, this significantly attenuates adverse side effects, as healthy cells and tissues are not harmed. On the other hand, the use of ADCs enables an accumulation of the cytotoxic agent in the target cell, reducing the dosage needed to see a clinical effect and, thus, increasing the tolerability of the therapy and improving the therapeutic index. Due to these two advantages, ADCs also open a way to extend the arsenal of chemotherapeutics with new cytotoxic agents, which have great potential, but are too toxic for clinical use when applied as untargeted molecules.

The search for novel, directed therapies revealed new targets for anticancer treatment and granted access to new chemotherapeutic compounds for their clinical use. However, it did not help to overcome the problem of cancer drug resistance. It is common knowledge that many types of cancer rapidly develop drug resistance mechanisms during conventional chemotherapy, but more recently, also resistances against targeted therapies have been reported.<sup>94–97</sup> Out of this reason, the efforts to find new therapeutic options may not dwindle and the search must continue in every possible direction considering new ideas and old resources likewise. The oldest source of all are natural products, which served as lead structure for many clinically used drugs.<sup>98</sup>

### 1.1.5. Natural Product-Derived Anticancer Agents

Biologic materials, such as plants, fungi, and bacteria have always been important sources for the discovery of new therapeutic agents.<sup>99–101</sup> From 1981 to 2019, 23.5 % of all drugs approved by the FDA were natural products (NPs) or synthetically modified derivatives thereof.<sup>98</sup> Additional 25 % were of synthetic origin, but bore either a NP pharmacophore (3.2 %) or structural features similar to NPs (22.5 %) acting as NP mimics.

In respect to anticancer drugs, the proportion of NP-derived agents is even higher. Omitting the numbers of high-molecular weight biologicals and vaccines (62 together), 185 small molecules have been approved for cancer therapy from 1981 to 2019, 84 % of which either originate from a NP lead structure (40 %) or are synthetic NP mimicking substances (44 %; Figure 6).<sup>98</sup> Since various protein kinases have been identified as new targets for cancer therapy, a notable share of the NP mimicry is due to the upsurge in approvals of protein kinase inhibitors over the past two decades.<sup>64,76,98,102–106</sup> Most of them are synthetic and classified as NP mimicry because of their similarity to the natural substrate ATP.<sup>107,108</sup>

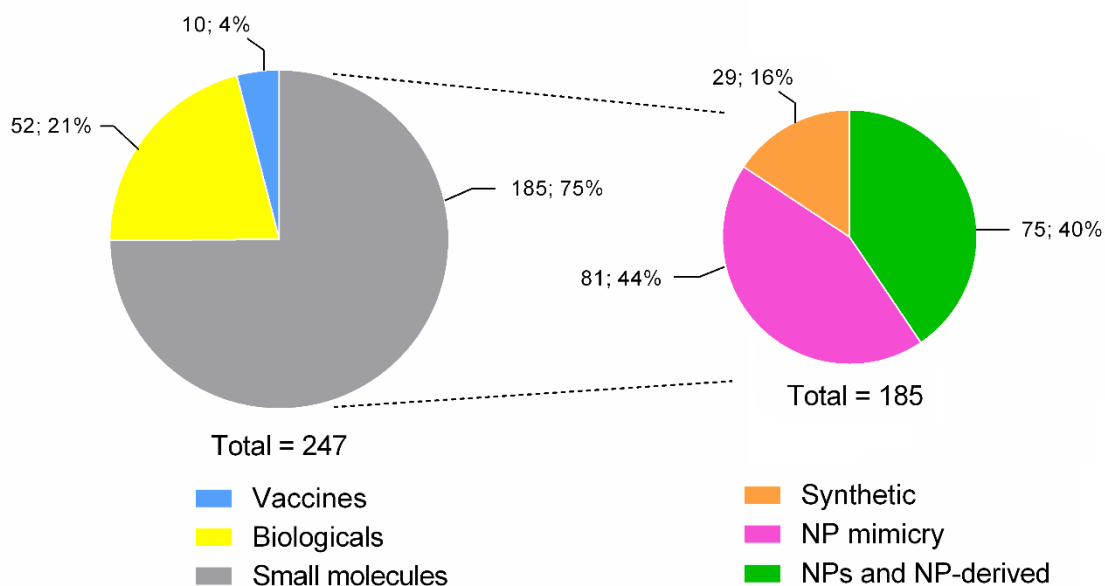
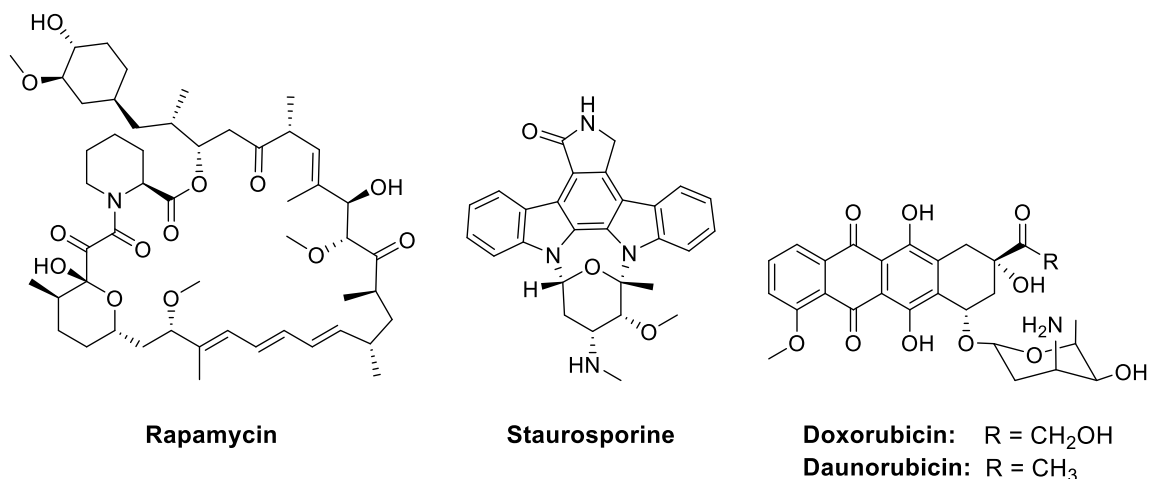


**Figure 6.** Total number of approved anticancer drugs, sorted by the categories vaccines (blue), biologicals (yellow), and small molecules (grey, left pie) and portion of synthetic drugs (orange), NP mimicry (magenta), and NP-/NP-derived agents (green) within the small molecules category (right pie). Data used to generate this figure from Newman and Cragg.<sup>98</sup>

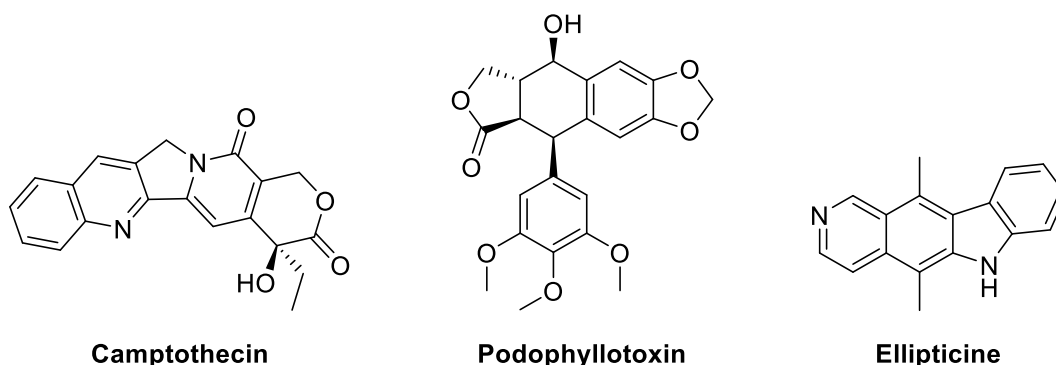
When regarding the origins of most of the approved anticancer agents, it is obvious that bacterial strains of the genus *Streptomyces* have ever been a rich source for cytotoxic agents. Three of the approved tyrosine kinase inhibitors are derived from NP lead structures: the mTOR inhibiting rapamycins everolimus and temsirolimus, and midostaurin, a semi-synthetic derivative of staurosporine.<sup>109–111</sup> Both, rapamycin and staurosporine, were originally isolated from *Streptomyces* sp. Four additional staurosporine analogs are currently under clinical investigation.<sup>112–114</sup> Although many other NPs inhibit protein kinases and, thus, exhibit anticancer activity, only few of them have made the way from bench to bedside (yet).<sup>115–117</sup>



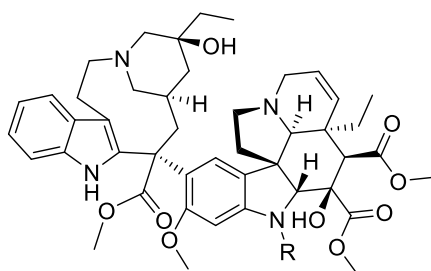


The other NP or NP-derived anticancer agents isolated from *Streptomyces* fall within the scope of conventional chemotherapy. All cytotoxic antibiotics (see chapter 1.1.3.), as well as the anthracyclines are derived from *Streptomyces* sp.<sup>53–63,118</sup> Doxorubicin and daunorubicin were isolated from *Streptomyces peuceticus* in the early 1960s and, later on, the first of their substance class to be approved for cancer therapy.<sup>118</sup>

Another important source for cytotoxic agents are plants, from which most of the remaining inhibitors of topoisomerase I/II were isolated. The topoisomerase I inhibitors belotecan, irinotecan, or topotecan are derived from the *Camptotheca* alkaloid camptothecin.<sup>119</sup> Etoposide and teniposide, which target topoisomerase II, are partialsynthetic products obtained by modification of podophyllotoxin, the main toxic lignan in the plant genus *Podophyllum*.<sup>120</sup> The alkaloid ellipticine, another inhibitor of topoisomerase II, was isolated from *Ochrosia elliptica* of the plant family apocynaceae.<sup>121–123</sup> Due to its poor water solubility, the more hydrophilic form elliptinium acetate was approved for clinical use.<sup>124</sup>

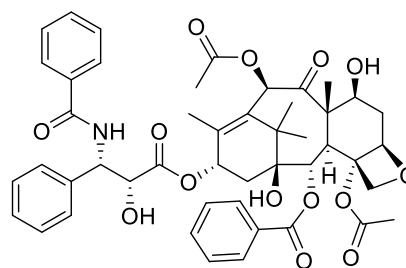


In addition to the topoisomerase inhibitors, most of the microtubule disrupting agents originate from plants. The vinca alkaloids vinblastine and vincristine were isolated from the Madagascar periwinkle *Caranthus roseus* (L.) G. Don around 1960, and they have been in clinical use for almost 60 years now.<sup>51</sup> Subsequently, three additional semi-synthetic derivatives were approved, i.e. vindesine, vinorelbine, and vinflunine. The vinca alkaloids disrupt the mitotic spindle by destabilizing the microtubules while the other tubulin-interfering drugs enact stabilizing effects.<sup>125</sup> These are the taxols paclitaxel and its semi-synthetic derivatives docetaxel and cabazitaxel.<sup>126</sup> Paclitaxel is also a plant-derived cytotoxic agent and was discovered in the stem bark of *Taxus brevifolia*.<sup>127</sup>



**Vinblastine:** R = CH<sub>3</sub>

**Vincristine:** R = COH



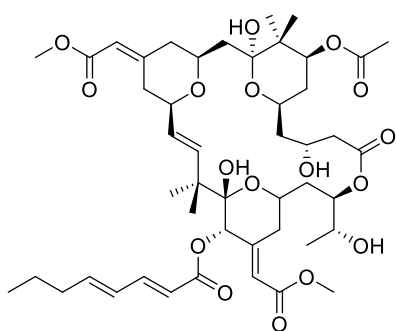
**Paclitaxel**

However, with the exploration and exploitation of new, sometimes extreme habitats and the advances in microbial cultivation techniques, more and more new microorganisms are grown in the laboratory environment. Thus, it is not surprising that many of the new NP-derived chemotherapeutics or potential drug candidates originate from other, e.g. marine sources.<sup>110,117,128</sup> One of the first marine drugs approved for cancer therapy was the protein kinase inhibitor bryostatin-1, which is produced by the brown bryozoan *Bugula neritina*.<sup>129,130</sup> The FDA and EMA granted bryostatin-1 orphan drug status for the treatment of oesophageal cancer.<sup>131,132</sup>

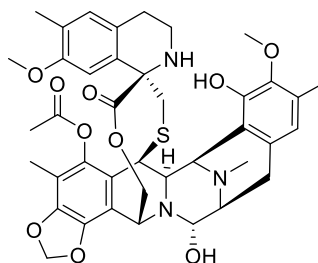
Indeed, the investigation of new biological resources did not only reveal new structural motifs for pharmacophores, but also promoted the discovery of new binding sites in known targets or even completely new MoA. In 2007, the tetrahydroisoquinoline trabectedin isolated from the marine ascidian *Ecteinascidia turbinata* was approved as a DNA-binding agent with a novel way of DNA modification.<sup>133,134</sup> Instead of targeting the *N*-7 or *O*-6 position of the heterocycle in guanine, as most other alkylating chemotherapeutics do, trabectedin binds to the exocyclic amino group attached to the *N*-2 position. Other new MoA comprise the inhibition of protein synthesis by the ascidian NP plitidepsin (dehydrodimenin B) and the inhibition of the histone deacetylase by romidepsin, which was found in the soil bacterium *Chromobacterium violaceum*.<sup>128,135–137</sup>

A particularly interesting example of drugs from marine sources is MMAE. Firstly, it is the microtubule-inhibiting warhead of two ADCs, brentuximab vedotin and polatuzumab vedotin, and, thus, represents one of the first cytotoxic agents employed in this strategy. Secondly, it belongs to a group of peptides called dolastatins and targets a binding site in tubulin specific for antimetabolic peptides, preventing tubulin polymerization.<sup>138</sup> The first variant dolastatin 10 was originally isolated from the sea hare *Dolabella auricularia*, but it was rediscovered in several genera of cyanobacteria in

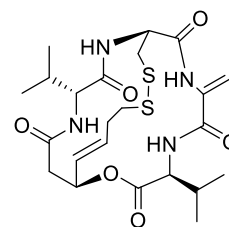
addition to further derivatives, suggesting that dolastatins are of cyanobacterial rather than animal origin.<sup>139–144</sup>



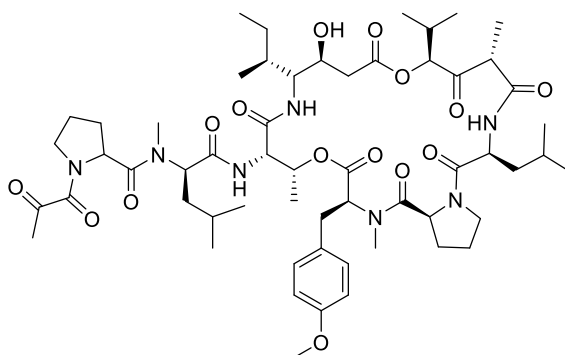
**Broystatin-1**



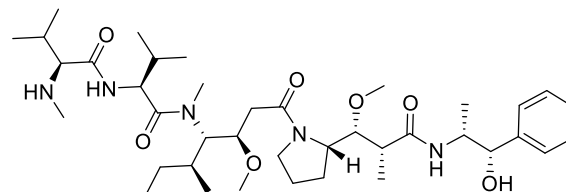
**Trabectedin**



**Romidepsin**



**Plitidepsin**



**Monomethyl auristatin E**

Since at least this finding, cyanobacteria were recognized as prolific source for new specialized metabolites, especially cytotoxic agents.<sup>145–154</sup> The cryptophycins, another class of cyanobacterial toxins, revealed intriguing anticancer activity in preclinical studies,<sup>155</sup> and one particularly potent substance class is still waiting for a breakthrough in their clinical development: the microcystins.

## 1.2. Microcystins – Promising Candidates for Cytotoxic Drugs

The microcystins (MCs) are cyclic heptapeptides produced by cyanobacteria, an ancient phylum of bacteria formerly termed blue-green algae. Their name comes from the Greek word κύανος (*kyanos*, “dark blue”) referring to their deep blue-green coloration, which is due to high contents of blue phycocyanin and green chlorophyll *a* within the thylakoid membranes. The light-harvesting pigment enables the cyanobacteria to use photosynthesis and, thus, prevail under autotrophic conditions.

Based on morphological markers, the cyanobacterial phylum is categorized into nine orders, each of which is further subdivided into families, genera and species by means of morphology, 16s rRNA sequences and other genetic markers.<sup>156</sup> MC-producing strains originate from several different orders, and most often belong to the genera *Dolichospermum* (formerly *Anabaena*), *Microcystis*, *Nostoc*, *Oscillatoria* (Figure 7), or *Planktothrix*.<sup>157–163</sup> This wide-spread occurrence of MC biosynthetic genes in only distantly related strains indicates a high degree of conservation, and attributes a meaningful role to the MCs during the evolution of cyanobacteria - which one, however, is still not clear.

MCs are the main toxic compounds in freshwater reservoirs infested with cyanobacterial blooms. Upon exposure, they induce severe hepatotoxicity in livestock and humans alike.<sup>164,165</sup> Thus, they drew a lot of public and scientific attention and many efforts were invested to understand their impact on ecosystems and public health.<sup>166–175</sup>

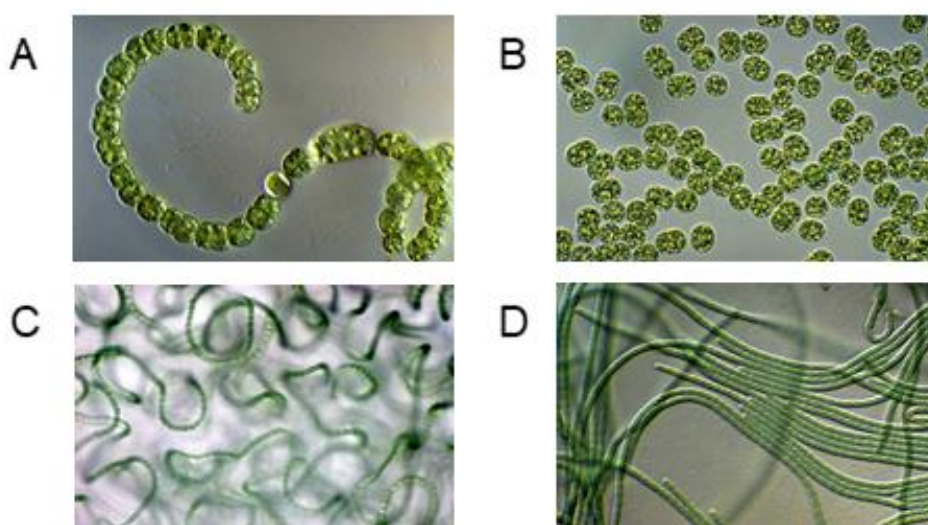


**Figure 7.** Microscopic images of cyanobacterial genera capable of microcystin production: (A) *Dolichospermum* (formerly *Anabaena*), (B) *Microcystis*, (C) *Nostoc*, and (D) *Oscillatoria*. Source: Phycokey.<sup>176</sup>

## 1.2.1. Structure, Diversity and Biosynthesis

Whereas early reports of a toxin derived from algal blooms of the genus *Microcystis* date back to 1944, Bishop and coworkers were the first to acknowledge the peptic structure of the “fast-death factor” in 1959.<sup>177,178</sup> Since then, many efforts were invested to identify the toxic substance, but it was not until 1984 when the structure of MC-LA (formerly cyanoginosin-LA) was finally elucidated.<sup>179–183</sup>

MCs consist of seven amino acids forming a cyclic, peptidic backbone, as depicted in Figure 8. Their most noticeable characteristic is the unusual  $\beta$ -amino acid in position 5 (2S,3S,8S,9S)-3-amino-9-methoxy-2,6,8-trimethyl-10-phenyldeca-4E,6E-dienoic acid, referred to by the acronym “Adda”. It originates from a polyketide synthase (PKS) system and represents a structural feature that most MCs have in common.<sup>184,185</sup> Further non-proteinogenic amino acids occur in positions 1, 3, 6, and 7, all of which are incorporated in D-configuration. Interestingly, these residues are highly conserved with varying patterns of alkylation or hydroxylation only (Figure 8).

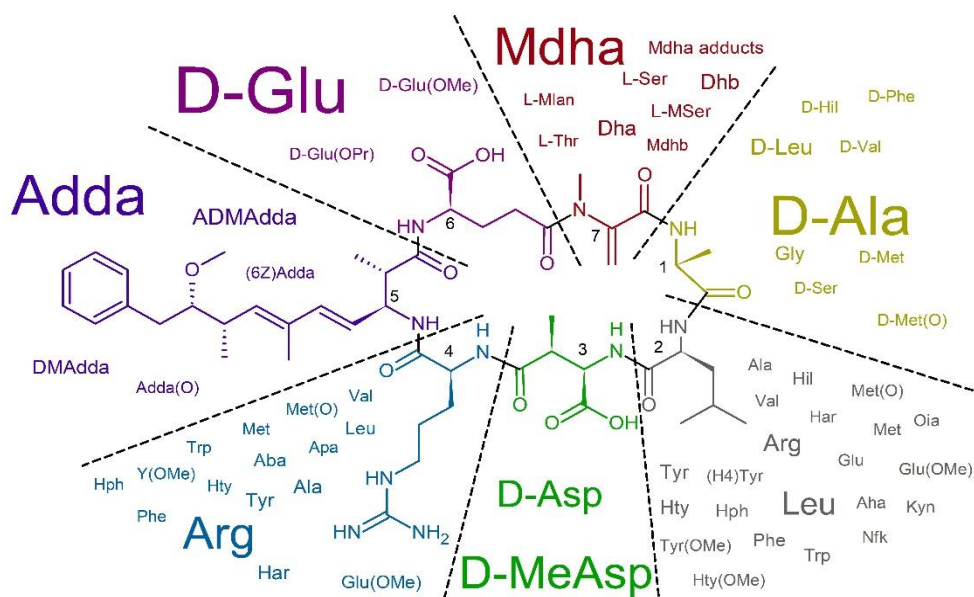


**Figure 8.** General structure of microcystins (MCs). Prevalence of residues found within microcystins is proportional to the font size of the respective residue. Non-proteinogenic amino acids are abbreviated as follows: Aha, aminoheptanoic acid; Aba, 1-2-aminobutanoic acid; Adda, 3-amino-9-methoxy-2,6,8-trimethyl-10-phenyldeca-4,6-dienoic acid; ADMAdda, *O*-acetyl-*O*-demethylAdda; Apa, aminopropionic acid; Dha, dehydroalanine; Dhb, dehydrobutyrine; DMAdda, *O*-demethylAdda; (H4)Tyr, 1,2,3,4-tetrahydrotyrosine; Har, homoarginine; Hil, homoisoleucine; Hph, homophenylalanine; Hty, homotyrosine; Kyn, kynurenine; Lan, lanthionine; MeAsp,  $\beta$ -methyl aspartic acid; Mdha, *N*-methyldehydroalanine; Mdhb, *N*-methyldehydrobutyrate; Mlan, *N*-methylanthionine; Met(O), methionine-*S*-oxide; Mser, *N*-methylserine; Nfk, *N*-formylkynurenine; Oia, oxindolyalanine; (OMe) *O*-methyl-. Amino acids in position 2 and 4 have L-configuration. Reprinted with permission from Moschny J. *et al.*<sup>194</sup> Copyright 2020 American Chemical Society.

The most frequent amino acid observed in position 1 is D-Ala while variants with other residues are only rarely described. Positions 3 and 6 bear derivatives of D-aspartic and D-glutamic acid, respectively, and they are integrated into the peptide ring via the carboxyl group on the  $\gamma$ - $\delta$ -carbon. *N*-methyldehydro D-alanine (Mdha) is the main residue found in position 7. Since the double bond forms a highly-reactive,  $\alpha,\beta$ -unsaturated carbonyl, or Michael system, this amino acid can undergo nucleophilic additions, e.g. with thiol groups of free cysteine residues in proteins.

In contrast, the amino acids in positions 2 and 4 are always L-configured and structurally highly diverse. They include proteinogenic as well as non-proteinogenic amino acids, which can be aromatic, aliphatic, or basic, resulting in an extremely high structural diversity of MCs with more than 270 variants described in the literature.<sup>186</sup> Due to this high variability in positions 2 and 4, these residues are specified in the MC nomenclature by using the single-letter code for proteinogenic and the three-letter code for non-proteinogenic amino acids.<sup>187</sup>

MCs belong to a group of NP called non-ribosomal peptides (NRP). This means that they are not of ribosomal origin, but products of a NRP synthetase (NRPS).<sup>188</sup> NRPSs consist of several, collinearly arranged modules, each of which is responsible for the incorporation of a single amino acid. The modules are further organized in three major domains: an adenylation (A) domain, a thiolation domain, and a condensation (C) domain. While the C domain catalyzes the peptide bond formation and, thus, the elongation of the peptide chain, the A and thiolation domains confer substrate recognition and activation, respectively.<sup>189–193</sup> In consequence, the peptide sequence is determined by the substrate specificity of the respective A domains, and a relaxed substrate specificity promotes structural diversity.

The NRPS enzyme complex of MCs is additionally associated with PKS units forming an integrated PKS–NRPS system.<sup>185,195</sup> In *Microcystis* sp., the biosynthetic gene cluster *mcy* is organized into two bidirectional operons, *mcyABC* and *mcyDEFGHIJ* (Figure A2).<sup>185</sup> The predicted products of the ten genes *mcyA–J* are summarized in Table 1.

Since cyanobacteria are difficult to genetically manipulate and the heterologous expression of MCs has been established just recently,<sup>196</sup> the biosynthetic route is mainly proposed based on homology to known biosynthetic pathways and only partially confirmed by experimental data.<sup>197</sup> It starts with the formation of Adda by loading the mixed NRPS-PKS McyG with an activated phenylpropanoid precursor, which is truncated to give phenylacetate (Figure 9).<sup>198</sup> The aliphatic chain is elongated by repetitive addition of malonyl-CoA with intermitting steps of methylation and

dehydrogenation.<sup>185,199</sup> Thereby, the S-adenosyl-L-methionine (SAM)-dependent methyltransferase McyJ is responsible for the O-methylation on C-9 of Adda.<sup>200,201</sup> In the last step, an aminotransferase attaches an amino group to the C-3 carbon to generate a  $\beta$ -amino acid before the C domain of the mixed NRPS–PKS unit McyE transfers Adda to D-Glu.<sup>185</sup>

**Table 1.** Overview of the single genes in the *mcy* biosynthetic gene cluster in *Microcystis* sp. and their predicted products. NRPS, non-ribosomal peptide synthetase; PKS, polyketide synthase. Data to generate this table was taken from Tillett *et al.*<sup>185</sup>

Encoding gene	Putative gene product	Encoding gene	Putative gene product
<i>mcyA</i>	NRPS	<i>mcyF</i>	Aspartate racemase
<i>mcyB</i>	NRPS	<i>mcyG</i>	Mixed PKS–NRPS
<i>mcyC</i>	NRPS	<i>mcyH</i>	ABC transporter
<i>mcyD</i>	PKS	<i>mcyI</i>	Tailoring enzyme
<i>mcyE</i>	Mixed PKS–NRPS	<i>mcyJ</i>	Tailoring enzyme

The other five amino acids are incorporated by the NRPSs encoded in the *mcyABC* region.<sup>185</sup> The modules of McyA direct the incorporation of the residues in positions 7 and 1, and often include an N-methyltransferase, which transfers a methyl group to the amino group in position 7 yielding Mdha. McyB also consists of two NRPS modules, but their A domains highly differ in their strictness of substrate specificity. One of them only recognizes aspartate and few of its derivatives, which are incorporated in position 3. The other activates the precursors found in position 2. The structural diversity of the residues is highest in this position and several MC variants with very different amino acids in position 2 can co-occur in one single cyanobacterial strain.<sup>202</sup> This implies a certain substrate promiscuity of the respective A domain, which was also confirmed by *in vitro* experiments. Meyer *et al.* demonstrated that the isolated A domain of McyB can activate very different amino acids like Val, Tyr, Gly, or Leu.<sup>203</sup>

Likewise, the isolated A domain of the NRPS McyC can recognize and activate structurally diverse precursors *in vitro*.<sup>203</sup> These findings are not surprising, as McyC is responsible for incorporation of the amino acids in position 4, the position with the second highest structural variability in its residues. After the last amino acid in position 4 is linked to the peptide chain, the peptide is released from the multi-enzyme complex and cyclized by the elimination of water.<sup>185</sup> The underlying mechanisms and putative enzymes involved in this step have not been identified yet.

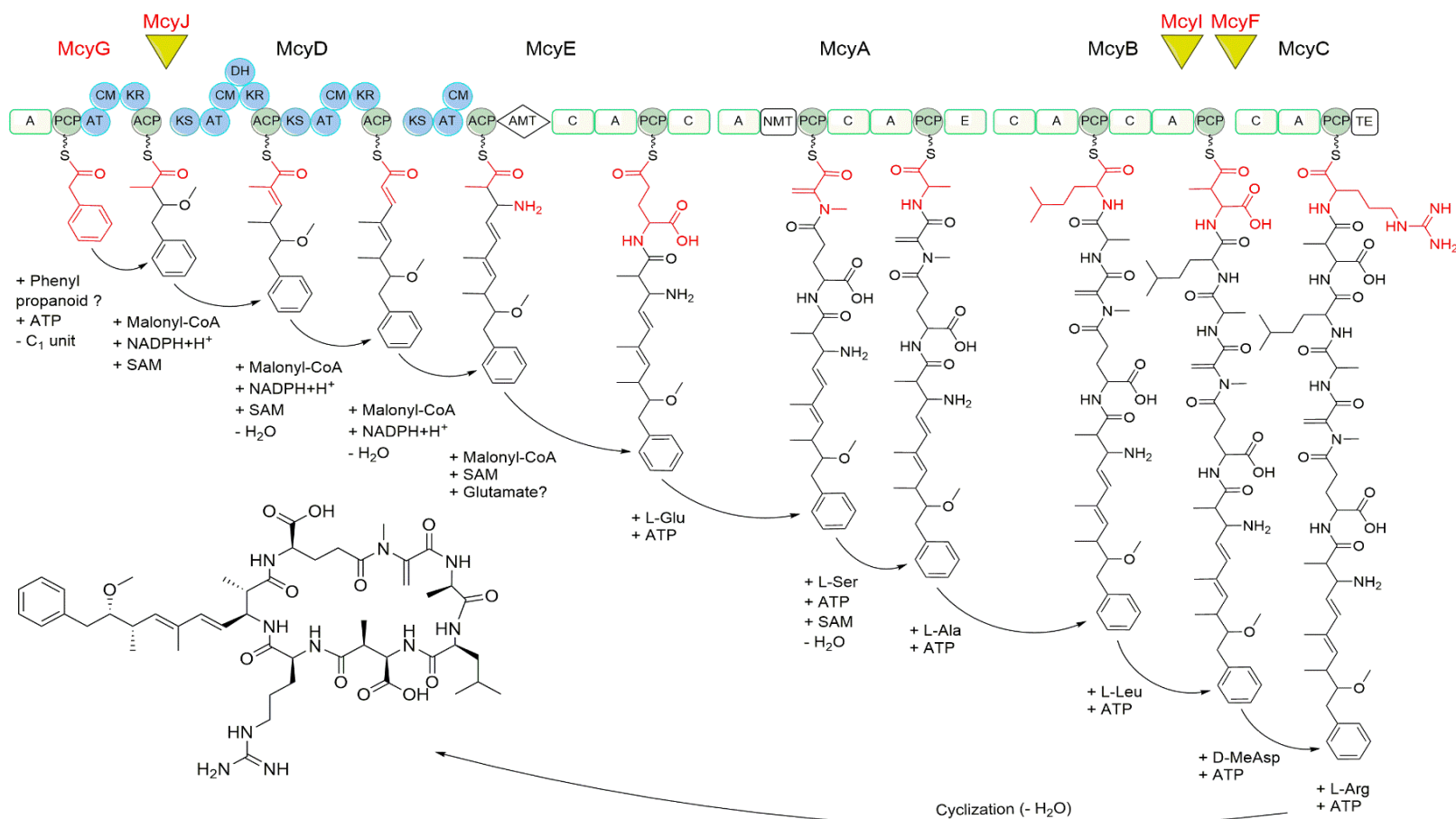


**Figure 9.** Schematic biosynthesis of MC-LR. Biochemically characterized enzymes are highlighted in red while the function of the remaining is based on bioinformatic predictions. Precursors that are incorporated or modified by the respective module are highlighted in red. PKS domains (blue): KS, ketoacyl synthase, AT, acyltransferase, DH, dehydratase, KR, ketoreductase, ACP, acyl carrier protein, CM, C-methyltransferase; AMT, glutamate-semialdehyde aminotransferase; NRPS domains (green rectangles): A, adenylation domain; C, condensation domain, E, epimerization domain; NMT, N-methyltransferase; PCP, peptidyl carrier protein, TE, thioesterase domain. ATP, adenosine triphosphate; SAM, S-adenosyl-L-methionine; NADP(H), nicotinamide adenine dinucleotide phosphate; D-MeAsp,  $\beta$ -methyl aspartic acid. Data used to generate this figure from Dittmann *et al.*<sup>197</sup>



The relaxed substrate specificity of NRPSs like McyB and McyC represents a biosynthetic particularity often observed in cyanobacterial NRP biosynthesis. It is the main reason for the numerous MC variants described in the literature.<sup>146,204</sup> The diversity in amino acid composition inevitably leads to differences in the physico-chemical properties of different MC variants, e.g. solubility, hydrophilicity, or an altered interaction with targets. Still, the toxicity of MC variants with differing amino acids in positions 2 and 4 ranges in the same magnitude indicating that the pharmacophore is located in the conserved part.

### 1.2.2. Mode of Action and Structure–Activity Relationship

The MCs have first been discovered as hepatotoxins, but recent studies suggest that they also affect kidneys, the heart and the reproductive system.<sup>205–207</sup> In 1990, MacKintosh *et al.* discovered the eukaryotic serine–threonine protein phosphatase (PP) subfamilies 1 and 2A as the main intracellular targets of the MCs.<sup>208</sup> PP1 and PP2A are expressed in all eukaryotic cells, and act as counterpart to protein kinases by catalyzing the dephosphorylation of serine and threonine residues. Consequently, they play a crucial role in the regulation of cell signaling pathways, which control cell division and cell cycle progression, metabolism, protein synthesis, and the expression of receptors and ion channels.<sup>209–212</sup>

The inhibition of PP1 and PP2A by MCs leads to a hyperphosphorylation of signaling proteins causing a disturbance of these pathways.<sup>213–216</sup> Although MCs have a similar affinity towards PP1 and PP2A, most of the dysregulations arise from malfunctions of PP2A substrates.<sup>214,217</sup> For instance, PP2A tightly regulates the function of p53, a nuclear factor involved in the control of apoptosis.<sup>218</sup> Its hyperphosphorylation alters the expression of other pro-apoptotic proteins like Bax and Bcl-2, which induce apoptosis by disruption of the mitochondrial membrane permeability.<sup>219–222</sup> Another effector protein of PP2A inhibition is the calcium–calmodulin-dependent protein kinase II.<sup>222–224</sup> If it is not under proper control, it stimulates the generation of reactive oxygen species, resulting in DNA damage and the induction of apoptosis in response to MC exposure.<sup>225</sup>

MC exposure and PP inhibition further activates members of the mitogen-activated protein kinase (MAPK) pathway.<sup>226,227</sup> As a consequence, the cytoskeleton is modified and disrupted, which is another key factor in the MC-mediated induction of apoptosis.<sup>228–231</sup> However, active MAPK pathways are also associated with the expression of proto-oncogenes like c-Jun, c-Fos, or c-Myc.<sup>232,233</sup> Indeed, an upregulation of their expression was linked to MC exposure.<sup>234</sup> Several *in vitro* and *in vivo* studies further demonstrated

that exposure to low levels of MCs promoted cell degeneration and tumor growth while cytotoxicity was only observed under high concentrations of MCs.<sup>235</sup> Thus, MCs elicit a dualistic effect in eukaryotic cells: depending on the concentration the cells were exposed to, MCs can act either as cytotoxic or tumor promoting agents.

MCs bind with an extraordinary high affinity to PP1 and PP2A (picomolar IC<sub>50</sub> values).<sup>208</sup> As evident from the crystal structure of PP1 complexed with MC-LR, the stringent binding is due to the perfect fit of the Adda<sup>5</sup> side chain into the hydrophobic pocket formed by Cys127, Ile130, Ile133, Tyr134, and Trp206 of the catalytic subunit.<sup>236-240</sup> In PP2A, the amino acids Gln122, Ile123, His191, and Trp200 confer the hydrophobic interaction between Adda<sup>5</sup> and the catalytic subunit,<sup>241</sup> as depicted in Figure 9. Secondly, the free carboxyl group of D-Glu<sup>6</sup> and the carbonyl group of Adda<sup>5</sup> bind to water molecules coordinated by two metal ions on the active site of the catalytic subunit.

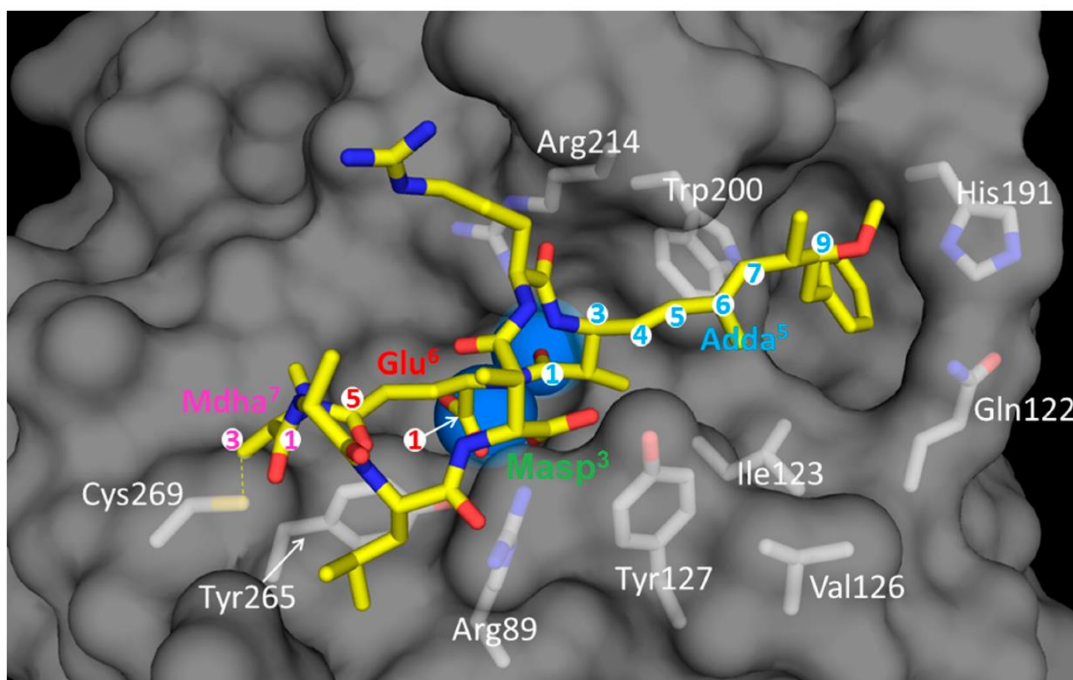
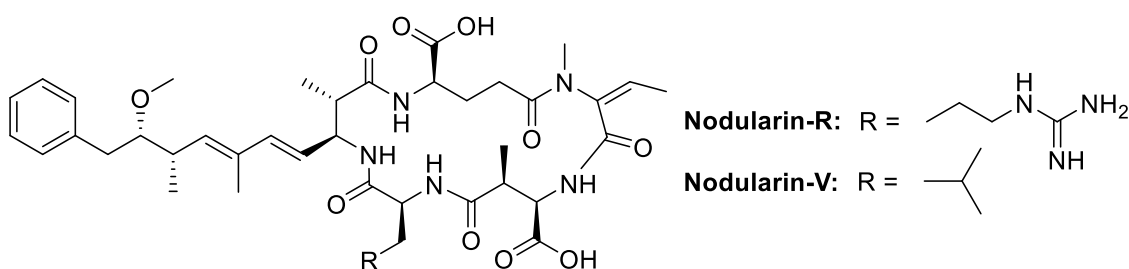


**Figure 9.** X-ray crystallographic structure showing the interaction of MC-LR with the PP2A catalytic subunit and its adjacent amino acid side chains. Important interactions are described in the text. Mdma<sup>7</sup>, Glu<sup>6</sup>, Adda<sup>5</sup>, and Masp<sup>3</sup> moieties, and selected carbons in these amino acids are labeled in magenta, red, pale blue and green, respectively. The large blue spheres represent the catalytic metal ions, and the dashed yellow line shows the location, where the covalent bonds is formed over time between Cys269 and Mdma<sup>7</sup> of MC-LR. Adapted and modified from Bouaïcha *et al.*<sup>186</sup> (open access); based on data provided by Xu *et al.*<sup>242</sup>

*In vitro* studies employing truncated versions of MCs showed that dipeptides, which consisted of Adda<sup>5</sup> and one other amino acid, maintained activity,<sup>243,244</sup> confirming the essential motifs for binding as deduced from X-ray crystallography. Furthermore, changes in the configuration of Adda<sup>5</sup> and esterification of the free carboxylic group in D-Glu<sup>6</sup> abrogate PP inhibition and MC-mediated cytotoxicity.<sup>245,246</sup>

A third interaction takes place between the  $\alpha,\beta$ -unsaturated carbonyl of Mdha<sup>7</sup> and a cysteine residue of the PP, which undergo a nucleophilic addition to form a covalent bond. However, this conjugation is not essential for PP inhibition, but stabilizes the complex and prolongs the interaction.<sup>247,248</sup> More recently, computational modeling revealed an additional region for MC–PP interaction.<sup>240,249</sup> The free carboxylic acid of D-MeAsp<sup>3</sup> forms a hydrogen bond with Arg96 and Tyr134 in PP1, and Arg89 and Tyr127 in PP2A, respectively, so it is interesting to note that all target-binding sites of the MCs lie within the highly conserved amino acid residues. Thus, the high natural diversity of the amino acids in positions 2 and 4 hardly influences the MC inhibitory activity, and also their substitution with unnatural derivatives show little divergence to their natural derivatives.<sup>250,251</sup>

Considering their new MoA and their exceptional high potency, MCs and other NP-based PP inhibitors have been discussed as lead structures for the development of novel anticancer agents.<sup>252,253</sup> Nodularin-R and nodularin-V (motuporin) are cyanobacterial, cyclic pentapeptides closely related to the MCs as they share a similar biosynthetic route.<sup>184,254,255</sup> The nodularins also feature the Adda<sup>5</sup>–D-Glu<sup>6</sup> motif but instead of Mdha<sup>7</sup>, they carry (*N*-methyl)-2-amino-dehydrobutyric acid (Mdhb). Although the additional methyl group sterically impedes a nucleophilic addition and the formation of a covalent bond, they inhibit PP1/2A with equal potency as the MCs.<sup>253</sup>



Other equipotent inhibitors of PP1/2A are the marine NPs okadaic acid and calyculin A–H, and tautomycin, which was isolated from *Streptomyces spiroverticillatus*.<sup>256–260</sup> All of them exhibit high cytotoxicity against various cancer cell lines due to their PP inhibitory activity.<sup>253,261,262</sup> Despite the sophisticated rationale and promising *in vitro* data, none of

these PP inhibitors has successfully completed clinical testing. Since they are highly cytotoxic, a systemic application would lead to fatal side-effects, making the original, underivatized compounds unsuitable for the use in patients. However, such drawbacks can be overcome by employing so-called targeted therapies, which direct the cytotoxic agent to cancer cells only. MCs are especially suited for these approaches because of their pharmacokinetics.

### 1.2.3. OATPs—the MCs Cellular Gateway and their Role in Cancer

The free carboxylic acids and resulting hydrophilicity prevent the MCs from crossing cellular membranes passively and unaided, and they rely on an active uptake. Fisher *et al.* demonstrated that this uptake is mediated by three transmembrane proteins, which are members of the organic anion transporting polypeptide (OATP) family: OATP1A2, OATP1B1, and OATP1B3.<sup>263</sup>

The OATP superfamily is found in humans, rodents, chicken, and fish.<sup>264,265</sup> Based on computational models, they are predicted to consist of six extracellular and five intracellular loops and twelve transmembrane domains, which form a pore through the membrane for substrate transport.<sup>266</sup> The transport mechanisms are not fully understood yet, but evidence suggests that OATPs have several binding sites and transfer their substrates by anion exchange with bicarbonate or glutathione in an ATP-independent manner.<sup>267–273</sup>

Thus, the majority of OATP substrates are anions.<sup>269</sup> Some OATPs, however, are also capable of transporting neutral or even cationic molecules, so their substrate spectrum covers a high variety of substances including endogenous metabolites such as thyroid hormones, conjugated steroids, or bile acids, and xenobiotics like drugs, toxins, and other exogenous NPs.<sup>268,269,274</sup> When regarding the structural diversity of pharmaceutical agents and the wide spectrum of indications they cover, it is not surprising that OATPs play an important role in drug–drug interactions.<sup>275</sup>

Although OATPs are found in manifold epithelia of the human body, the distribution of the single subtypes varies between the types of tissue.<sup>269</sup> The expression of OATP1A2 spreads throughout the whole body, with the highest levels detected in the brain, lung, kidneys, liver and testes.<sup>276,277</sup> In contrast, OATP1B1 and OATP1B3 are exclusively located in the liver, where they are responsible for the clearance of drugs and toxins from the system.<sup>278–282</sup> This is the reason for the severe hepatotoxicity of MCs. Interestingly, the abundances of OATP1B1 and OATP1B3 in hepatocytes differ. OATP1B1 is expressed to a much higher extent than OATP1B3.<sup>283,284</sup>

This distribution pattern of OATPs drastically changes when malignant tissue is concerned. OATP1B3 has been shown to be expressed or upregulated in breast, colon, lung, ovarian, pancreas, and prostate cancers, and it even might promote tumor survival and growth.<sup>285–288</sup> Since OATP1B3 is also essential for the uptake of many chemotherapeutics into cancer cells, it has been discussed as target for directed anticancer therapy.<sup>287,289–291</sup> Thus, OATP1B3 might also serve as cancer-specific gateway for anticancer agents derived from MCs.<sup>252</sup> By identifying MC variants, which are selectively transported by OATP1B3 and not OATP1B1, the hepatic uptake and, in consequence, the hepatotoxicity should significantly be diminished. This should further reduce adverse side effects and improve the tolerability of MC-based drugs opening a way for their clinical development.

Following this rationale, 22 MC congeners were already screened for their OATP1B1/OATP1B3 transport selectivity, and, indeed, some structural features favoring the transport by OATP1B3 over OATP1B1 were determined.<sup>292</sup> However, no MC with true OATP1B3 specificity was found, and the established structure–activity relationships (SAR) still lack important information. Further screenings are required to complete the SAR and identify a potential MC drug candidate.

### 1.2.4. Microcystins as Warheads for ADCs and Beyond

The clinical development of MC-based treatments could further be promoted by employing the MCs as warheads in the design of new ADCs. Following this strategy already enabled the clinical application of MMAE, a semi-synthetic derivative of the cyanobacterial peptide dolastatin 10, in form of the ADC brentuximab vedotin. Due to its clinical success, brentuximab vedotin was included in first line treatment of CD30<sup>+</sup> peripheral T-cell lymphomas and is further discussed for first line treatment of CD30<sup>+</sup> Hodgkin lymphoma.<sup>293,294</sup>

The design of ADCs requires four considerations to be taken into account: (1) the selection of a suitable target and mAb, (2) the application of a compatible linker, (3) picking a potent warhead, and (4) the mechanism to link the single segments with each other.<sup>85,87,295</sup> Of course, developing a new ADC is not a straightforward procedure, and it is self-evident that the order of steps is interchangeable and that going back and forth several times is inevitable.

The identification of suitable targets and the generation of mAbs that bind to it specifically and with high affinity is the most time and cost-consuming part in the process.<sup>295</sup> Several cancer-specific mAbs are already available, as are the platforms for

## 1. Introduction

---

discovering new surface antigens and the biotechnological processes for mAb production.<sup>81,82</sup> However, finding an attachment site for the payloads remains challenging, as it may not interfere with the mAb's integrity and binding, or provoke immunogenicity.

In the past decade, much progress has been made in the conception and chemistry of ADC linkers. They need to fulfill several requirements, e.g. chemical stability while circulating in the blood stream and a reliable release of the cytotoxic agent in the lysosome.<sup>296</sup> For this purpose, cleavable linkers are prone to degradation in the lysosomal milieu, i.e. by proteases like cathepsin B when featuring a valine–citrulline dipeptide motif, by reductive conjugation with glutathione, or due to sensitivity to low pH.<sup>93,296,297</sup> Non-cleavable linkers resist the lysosomal degradation and rather depend on a complete decomposition of the mAb moiety for drug release. This chemical stability also prevents the ADC to release the drug too early, e.g. into the blood stream.<sup>93</sup>

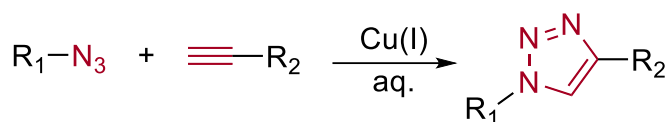
Initially, the linker chemistry exploited nucleophilic groups like -NH<sub>2</sub> of lysine or -SH of cysteine residues in order to affix the linkers to the mAbs. Since a mAb possesses dozens of free lysine or cysteine residues, and the reaction is never quantitative, the conjugation resulted in a heterogeneous mixture of ADCs with varying drug-to-antibody ratios.<sup>298</sup> Thus, newer methods aim at a site-specific conjugation, e.g. by genetic engineering or enzymatic modification of the mAb in order to introduce modified or unnatural amino acids, which provide a “reactive handle” for conjugation.<sup>93,296</sup>

Similar aspects need to be contemplated when the connection of the linker to the cytotoxic agent is concerned. First, the attachment may not interfere with the drug's binding site to the target to avoid loss of or decrease in activity. Secondly, the reaction should occur under mild conditions, so that neither the mAb nor the anticancer agent is compromised. Chemical reactions that meet these terms conjoin under the concept of bioorthogonal chemistry, which allows for *in vivo* conjugations under physiologic conditions.<sup>299–305</sup>

Bioorthogonal chemistry is closely associated with the concept of click chemistry, most prominently the copper(I)-catalyzed azide–alkyne cycloaddition (CuAAC), in which an azide reacts with a terminal alkyne to form a triazole (Scheme 1).<sup>306–309</sup> Other examples are the strain-promoted azide–alkyne cycloaddition, the photo-activated Staudinger ligation of azides and aryl phosphines, and the conjugation of cyclized double bounds with tetrazines (inverse electron-demand Diels-Alder).<sup>[3]</sup>

---

<sup>[3]</sup> Paragraph adapted and modified from Moschny, J.; Lorenzen, W.; Hilfer, A.; Eckenstaler, R.; Jahns, S.; Enke, H.; Enke, D.; Schneider, P.; Benndorf, R. A.; Niedermeyer, T. H. J. Precursor-directed biosynthesis and fluorescence labeling of clickable microcystins. *J Nat Prod* **2020**, 83, 1960–1970. Copyright 2020 American Chemical Society.



**Scheme 1.** The copper(I)-catalyzed azide–alkyne cycloaddition (CuAAC).

The reasons why MCs are highly suited as lead structures for anticancer drugs have been elaborated thoroughly in chapter 1.2.2. For initiating the preclinical development of a MC-based ADC, the question of how to attach the linker to the cyclic peptide needs to be addressed first. Unfortunately, MCs do not bear reactive or easily modifiable residues like lysine or cysteine except for Mdha<sup>7</sup>. Although the  $\alpha,\beta$ -unsaturated carbonyl can easily be linked to a nucleophile, as it has been done beforehand,<sup>310–313</sup> it is located too closely to the pharmacophore Adda<sup>5</sup>–D-Glu<sup>6</sup>. Using Mdha<sup>7</sup> as attachment site for the linker can put the MCs activity and potency at risk.

Consequently, the “reactive handle”, i.e. a bioorthogonal or “clickable” group, has to be introduced into the MCs exogenously. Total synthesis of MCs has already been established in 1996, and Zemskov *et al.* found a way to install O-propargyl tyrosine, which has a terminal alkyne group and is accessible for click chemistry, in position 4 of a MC derivative.<sup>251,314</sup> This approach, however, required about thirty steps and, accordingly, had a low overall yield.

Microbial NPs offer another way to introduce unnatural, functional groups into a molecule of interest: precursor-directed biosynthesis (PDB).<sup>315</sup> In this strategy, the growth medium of a microorganism is supplemented with an artificial precursor that can be incorporated into the NP instead of the natural substrate.<sup>316</sup> It has frequently been applied to the modifications of NPs from various organisms, including cyanobacterial specialized metabolites, and proved especially efficient for the insertion of clickable groups into polyketides and peptides.<sup>317–328</sup> [4]

Cyanobacteria are ideally suited for PDB of unnatural peptides, as they are phototrophic organisms that can be cultivated in medium containing inorganic nutrients only. This facilitates the cellular uptake of supplemented organic substrates if the required uptake transporters are present, as they do not compete with other organic nutrients present in the medium. In addition, the extraordinarily high innate flexibility of cyanobacterial NRPS domains, which is apparent for MCs from *in vitro* data as well as

[4] Paragraph adapted and modified from Moschny, J.; Lorenzen, W.; Hilfer, A.; Eckenstaler, R.; Jahns, S.; Enke, H.; Enke, D.; Schneider, P.; Benndorf, R. A.; Niedermeyer, T. H. J. Precursor-directed biosynthesis and fluorescence labeling of clickable microcystins. *J Nat Prod* **2020**, 83, 1960–1970. Copyright 2020 American Chemical Society.

their high natural diversity, potentially allows the acceptance of modified substrates without the need to manipulate the biosynthesis genes to extend the substrate specificity.<sup>146,203</sup> [5]

Furthermore, employing PDB for the generation of clickable MCs is associated with another advantage. After supplementation of the substrate, the clickable MCs are present in the living cyanobacteria and can be exploited for *in vivo* labeling and other physiological studies shedding a new light on the up-to-date unsolved role of MCs in cyanobacteria.<sup>299,303,329</sup>

Plenty of efforts have been invested to understand the physiological function of MCs in cyanobacteria. Most studies suggest that MCs are involved in the adaption to high light conditions and that they grant an advantage to MC-producing strains over non-producing strains under high irradiances.<sup>330–337</sup> Moreover, the biosynthesis of MCs is affected by the availability of various nutrients like iron, nitrogen and phosphorus, but the findings were not conclusive.<sup>338–341</sup> Other theories hypothesize that MCs are mediators in microbial communication because co-cultivation of MC-producing cyanobacteria with other microorganisms stimulated MC production as well.<sup>342,343</sup>

Labeling studies aiming to localize the MCs within the cyanobacteria by means of immunogold labeling, turned out likewise ambiguous. Whereas most of the studies reported an accumulation of MCs within the thylakoid membranes, one study demonstrated the highest labeling density within the nucleoplasmic area.<sup>344–347</sup> At least, all studies agreed on a cumulative occurrence of MCs in the periphery of polyphosphate bodies indicating a connection of MCs to phosphorous storage.

However, immunogold labeling is associated with one major drawback. Antibodies risen against MCs recognize the Adda-containing motif as hapten, but the sequence Adda<sup>5</sup>-D-Glu<sup>6</sup>-Mdha<sup>7</sup> is also hypothesized as interaction site with target proteins.<sup>330,347,348</sup> Consequently, immunogold labeling is likely to identify free, solute MCs only, while MCs bound to their targets are not visualized and the true site of MC action remains hidden.

This could be overcome by exploiting clickable MCs, which are present within the cyanobacteria after supplementation experiments. The substrate specificity of the A-domains is most relaxed in position 2 and 4, so clickable MCs with a bioorthogonal function in position 2 and/or 4 are expected to be formed. Consequently, the attachment site of the label would be located on the opposite site of the molecule and would not

---

[5] Paragraph adapted and modified from Moschny, J.; Lorenzen, W.; Hilfer, A.; Eckenstaler, R.; Jahns, S.; Enke, H.; Enke, D.; Schneider, P.; Benndorf, R. A.; Niedermeyer, T. H. J. Precursor-directed biosynthesis and fluorescence labeling of clickable microcystins. *J Nat Prod* **2020**, 83, 1960–1970. Copyright 2020 American Chemical Society.



## 1.2. Microcystins – Promising Drug Candidates for Cytotoxic Drugs

interfere with the putative binding site of the MC effector proteins. Since both, CuAAC-modified fluorescent probes and gold nanoparticles have been described, the clickable MCs could prove useful for MC localization by *in vivo* fluorescence microscopy or electron microscopy.<sup>349–354</sup>

### 1.3. Aim of the Thesis

Since cancer is evolving as a serious, global health problem and the demand for new, potent therapeutics will never recede, the aim of this thesis was the identification of MCs that can serve as lead structures for the development of anticancer agents. For this purpose, new chemical functions that can be modified by biorthogonal (click) chemistry should be introduced into the MCs allowing for their conjugation with a cancer-specific antibody or other carrier.

MCs mainly occur inside the cyanobacteria cells. In consequence, a versatile extraction and isolation protocol was devised and optimized, enabling an efficient and high-yielding MC recovery. For extraction from the cyanobacterial biomass, various solvents and combinations thereof, including biphasic systems, were evaluated in terms of their selectivity and MC extraction efficiency. Subsequently, different chromatographic methods, i.e. flash chromatography, size-exclusion chromatography and semi-preparative HPLC were tested for the isolation of pure MCs, and, in the end, arranged into a sophisticated workflow. The last step comprised a structure-independent quantitation method. Since a gravimetric determination is not accurate enough for small amounts, the applicability of HPLC coupled to an evaporative light scattering detector (ELSD) was investigated, and a method was developed, optimized and validated for the designated purpose.

In order to test the bioactivity and transportability of the modified MCs, a cytotoxicity assay was established involving cell lines with stable expression of OATP1B1 and OATP1B3, respectively. The results of the cytotoxicity assay were validated and verified regarding their consistency with previously reported OATP selectivity for MC transport. This cytotoxicity assay in combination with the workflow for MC isolation represents the starting point for the isolation and characterization of the modified MCs.

The second part of this thesis strived for the generation of new, clickable MCs by means of PDB. A number of cyanobacterial strains and amino acids were selected, and a supplementation protocol was devised. The incorporation of substrates was monitored by HPLC–MS. A strain–substrate combination with a high incorporation rate was selected to determine the kinetics of substrate uptake and production of the clickable MC and to deduce parameters that can be used for optimization of the supplementation protocol. The same substrate–strain combination was further evaluated concerning its suitability for *in vivo* labeling of the clickable MC by examining a potential substrate incorporation into other specialized metabolites. For this purpose, a comparative TLC

method was adapted involving a TLC stain based on a CuAAC reaction with a fluorogenic dye.

Simultaneously, one clickable MC was isolated, and the postulated structure was dereplicated by HRMS<sup>2</sup> and confirmed by NMR spectroscopy. The compound was linked to a fluorogenic dye, and the conjugate was biologically characterized in two ways. The cytotoxicity of the conjugated in relation to the natural and clickable MC was evaluated. The fluorescent MC was further employed in fluorescence microscopy studies to investigate its uptake by OATPs in order to confirm the suitability of clickable and conjugated MCs as lead structures for anticancer therapy.

## 2. MATERIALS AND METHODS

### 2.1. Chemicals and Instruments

All chemicals used for extraction, chromatography, chemical synthesis or any other sort of analysis are listed in Table 2. 3-Azido-6-bromo-7-hydroxycoumarin was kindly provided by Chambers Hughes, University of Tübingen. All other reagents used for the cultivation of cyanobacteria and cell culture are detailed in chapters 1.1 and 1.1.

**Table 2.** Chemicals, solvents and other materials used for chromatography, extraction and chemical synthesis.

Chemicals	Vendor
Acetonitrile (ACN)	J. T. Baker® Avantor Performance Materials, Deventer, NL and Honeywell Specialty Chemicals GmbH, Seelze, DE
Aminoguanidine hydrochloride	Carl Roth GmbH & Co. KG, Karlsruhe, DE
3-Azido-7-hydroxycoumarin	Carl Roth GmbH & Co. KG, Karlsruhe, DE
<i>n</i> -Butanol (BuOH)	Merck KGaA, Darmstadt, DE
Butyl acetate (BuAcO)	Merck KGaA, Darmstadt, DE
Certified reference material (CRM) MC-LR	National Research Council of Canada's Metrology Research Center, Ottawa, CA
Certified reference material (CRM) MC-RR	National Research Council of Canada's Metrology Research Center, Ottawa, CA
Copper(II) sulfate × 5 H <sub>2</sub> O	Carl Roth GmbH & Co. KG, Karlsruhe, DE
Dimethyl sulfoxide (DMSO)	Merck KGaA, Darmstadt, DE
Dimethyl sulfoxide- <i>d</i> <sub>6</sub> (DMSO- <i>d</i> <sub>6</sub> )	Sigma-Aldrich, St. Louis, USA
Ethyl acetate (EtAcO)	Sigma-Aldrich, St. Louis, USA
Formic acid (FA)	Merck KGaA, Darmstadt, DE
<i>n</i> -Hexane	Merck KGaA, Darmstadt, DE
HP-TLC plates, Silica 60, 10 × 10 cm	Merck KGaA, Darmstadt, DE
Methanol (MeOH)	Sigma-Aldrich, St. Louis, USA
2-Propanol	Merck KGaA, Darmstadt, DE
Pyridine	Merck KGaA, Darmstadt, DE
Sephadex LH-20	Merck KGaA, Darmstadt, DE
Sodium ascorbate	Carl Roth GmbH & Co. KG, Karlsruhe, DE
Trifluoroacetic acid (TFA)	Sigma-Aldrich, St. Louis, USA Carl Roth GmbH & Co. KG, Karlsruhe, DE
Water (MS purity grade)	AppliChem GmbH, Darmstadt, DE

**Table 3.** HPLC and HPLC–MS systems.

System	Specification	Component
Agilent 1100 Series	G1322A	Degasser
	G1311A	Quaternary Pump (low-pressure gradient)
	G1313A	Autosampler
	G1316A	Column compartment
	G1315B	Diode array detector
	G1364C	Fraction collector
Agilent 1260 Infinity	G4225A	Degasser
	G1312C	Binary pump (high-pressure gradient)
	G1329B	Autosampler
	G1330B	Thermostat
	G1316A	Column compartment
	G1315D	Diode array detector
Agilent 1200	G1379B	Degasser
	G1312A	Binary pump (high-pressure gradient)
	G1330A	Sample thermostat
	G1367B	Autosampler
	G1316A	Column thermostat
	G1315B	Diode array detector
Agilent 6330 Ion Trap		Electron spray ionization (ESI)–ion trap
Hitachi LaChrom	L-7612	Degasser
	L-7100	Quaternary pump (low-pressure gradient)
	L-7200	Autosampler
	L-7544	Diode array detector
	L-7485	Fluorescence detector
Knauer Azura	P 2.1L	Preparative HPLC pump (4 modules; high-pressure gradient)
	E0012	Dynamic mixing chamber
	DAD 2.1L	Diode array detector
	Foxy R2	Fraction collector
Thermo Fisher Scientific UltiMate 3000	LPG-3400SD	Quaternary pump (low-pressure gradient)
	WPS-3000TSL	Autosampler
	TCC-3000SD	Column oven
	DAD-3000	Diode array detector
	AFC-3000	Fraction collector

## 2. Materials and Methods

---

**Table 3.** HPLC and HPLC–MS systems (continued).

System	Specification	Component
Thermo Fisher Scientific UltiMate 3000	LPG-3400A	Quaternary pump (low-pressure gradient)
	WPS-3400SL	Autosampler
	W.O. electronics Jetstream 2	Column oven
	PDA-3000	Diode array detector
	Dionex RF2000	Fluorescence detector
Thermo Fisher Scientific UltiMate 3000	DGP-3600A	Quaternary pump (low-pressure gradient)
	WPS-3000TSL	Autosampler
	TCC-3100 1x2P-10P	Column oven
	PDA-3000	Diode array detector
Thermo Fisher Scientific Q Exactive Plus		ESI–quadrupole–orbitrap
Sedere LT-ELSD	Sedex 85 LT	Evaporative light scattering detector (ELSD)

## 2.2. Cultivation of Cyanobacteria

### 2.2.1. Media

The cyanobacterial cultivation medium BG11 was described by Rippka *et al.*<sup>355</sup> and its components are listed in Table 4. All stock solution were prepared separately by dissolving the components in demineralized water at the respective concentrations. Stock solutions 1–7 were autoclaved at 121 °C for sterilization. Solutions 8–10 were sterile-filtered through a membrane filter with 0.22 µm pore size. The stock solutions were added to 949 mL demineralized water, which was autoclaved at 121 °C prior to use, under aseptic conditions using the volumes specified in Table 4.

The ready-to-use BG11 medium and stock solutions 1–7, 9 and 10 were stored at room temperature. Stock solution 7 was protected from light to prevent precipitation. Solution 8 was kept at 4 °C and also protected from light.

**Table 4.** Composition of BG11 medium.

Stock solution	Components	Concentration in stock [g/L]	Volume per L medium [mL]	Final concentration [g/L]
1	NaNO <sub>3</sub>	300	5	1.5
2	K <sub>2</sub> HPO <sub>4</sub>	6.25	5	0.032
3	MgSO <sub>4</sub> × 7 H <sub>2</sub> O	15	5	0.750
4	CaCl <sub>2</sub> × 2 H <sub>2</sub> O	7.2	5	0.036
5	Ethylenediaminetetraacetic acid (EDTA)	0.2	5	1.00 · 10 <sup>-3</sup>
6	Na <sub>2</sub> CO <sub>3</sub>	8.0	5	0.040
7	Citric acid	1.2	5	6.00 · 10 <sup>-3</sup>
	Ammonium ferric citrate	1.2		6.00 · 10 <sup>-3</sup>
8	H <sub>3</sub> BO <sub>3</sub>	2.86	1	2.86 · 10 <sup>-3</sup>
	MnCl <sub>2</sub> × 4 H <sub>2</sub> O	1.81		1.81 · 10 <sup>-3</sup>
	ZnSO <sub>4</sub> × 7 H <sub>2</sub> O	0.22		0.22 · 10 <sup>-3</sup>
	Na <sub>2</sub> MoO <sub>4</sub> × 2 H <sub>2</sub> O	0.39		0.39 · 10 <sup>-3</sup>
	CuSO <sub>4</sub> × 5 H <sub>2</sub> O	0.08		0.08 · 10 <sup>-3</sup>
	Co(NO <sub>3</sub> ) <sub>2</sub> × 6 H <sub>2</sub> O	0.05		0.05 · 10 <sup>-3</sup>
9	NaHCO <sub>3</sub>	84.1	5	0.421
10	TES free acid	229.3	10	2.29

## 2. Materials and Methods

MLA medium was prepared as described by Bolch and Blackburn.<sup>356</sup> Firstly, a 40-times higher concentrated (40x) MLA nutrient mix was prepared from stock solutions, which are detailed in Table 5. Stock solutions 1–5 were made separately by dissolving the substances in demineralized water. For stock solution 6 and 7, primary stock solutions of biotin, vitamin B<sub>12</sub>, CuSO<sub>4</sub> × 5 H<sub>2</sub>O, ZnSO<sub>4</sub> × 7 H<sub>2</sub>O, CoCl<sub>2</sub> × 6 H<sub>2</sub>O, and Na<sub>2</sub>MoO<sub>4</sub> × 2 H<sub>2</sub>O were prepared first with concentrations also specified in Table 5. The corresponding amounts of vitamin and trace metal were dissolved in demineralized water.

**Table 5.** Compositions and volumes of stock solutions required to prepare 250 mL of 40x MLA nutrient mix.

Stock solution	Components	Concentration in stock [g/L]	Volume [mL] per 250 mL
1	MgSO <sub>4</sub> × 7 H <sub>2</sub> O	49	10
2	NaNO <sub>3</sub>	85	20
3	K <sub>2</sub> HPO <sub>4</sub>	6.96	50
4	H <sub>3</sub> BO <sub>3</sub>	15	10
5	Na <sub>2</sub> SeO <sub>3</sub> × 5 H <sub>2</sub> O	2.63 · 10 <sup>-3</sup>	10
6	Thiamine HCl	0.100	10
	Biotin (0.5 mL of primary stock)	5 · 10 <sup>-5</sup>	
	Vitamin B <sub>12</sub> (0.5 mL of primary stock)	5 · 10 <sup>-5</sup>	
	Primary stocks: Biotin	0.1	
	Vitamin B <sub>12</sub>	0.1	
7	Na <sub>2</sub> EDTA	4.36	10
	FeCl <sub>3</sub> × 6 H <sub>2</sub> O	1.58	
	NaHCO <sub>3</sub>	0.60	
	MnCl <sub>2</sub> × 4 H <sub>2</sub> O	0.36	
	CuSO <sub>4</sub> × 5 H <sub>2</sub> O (10 mL of primary stock)	0.010	
	ZnSO <sub>4</sub> × 7 H <sub>2</sub> O (10 mL of primary stock)	0.022	
	CoCl <sub>2</sub> × 6 H <sub>2</sub> O (10 mL of primary stock)	0.010	
	Na <sub>2</sub> MoO <sub>4</sub> × 2 H <sub>2</sub> O (10 mL of primary stock)	6.00 · 10 <sup>-3</sup>	
Primary stocks: CuSO <sub>4</sub> × 5 H <sub>2</sub> O	1.00		
	ZnSO <sub>4</sub> × 7 H <sub>2</sub> O	2.20	
	CoCl <sub>2</sub> × 6 H <sub>2</sub> O	1.00	
	Na <sub>2</sub> MoO <sub>4</sub> × 2 H <sub>2</sub> O	0.60	

0.5 mL primary stock solutions of biotin and vitamin B<sub>12</sub> were added per liter of stock solution 6, in which the other component, thiamine HCl, had been dissolved. In case of stock solution 7, Na<sub>2</sub>EDTA, FeCl<sub>3</sub> × 6 H<sub>2</sub>O, NaHCO<sub>3</sub>, and MnCl<sub>2</sub> × 4 H<sub>2</sub>O were dissolved



in demineralized water corresponding to 80 % of the final volume. Subsequently, 10 mL of primary stocks of  $\text{CuSO}_4 \times 5 \text{ H}_2\text{O}$ ,  $\text{ZnSO}_4 \times 7 \text{ H}_2\text{O}$ ,  $\text{CoCl}_2 \times 6 \text{ H}_2\text{O}$ , and  $\text{Na}_2\text{MoO}_4 \times 2 \text{ H}_2\text{O}$  per liter of solution 7 were added before it was made up to the final volume with demineralized water. The respective volumes of stock solutions 1–7 indicated in Table 5 were added to 130 mL demineralized water to give 250 mL of 40x MLA nutrient mix, which was sterilized by filtration through a filter with 0.22  $\mu\text{m}$  pore size.

The remaining two stock solutions 8 and 9 (Table 6) were prepared by dissolving the substances in demineralized water and autoclaving them at 121 °C. The volumes of the 40x MLA nutrient mix and stock solutions 8 and 9 were added aseptically to 964 mL sterile, demineralized water giving 1 L ready-to-use MLA medium. The medium and all stock solutions were kept at 4 °C and protected from light.

**Table 6.** Composition of stock solutions and volumes of 40x MLA nutrient mix and stock solutions used to prepare 1 L MLA medium.

Stock solution	Components	Concentration in stock [g/L]	Volume [mL] per L
-	40x-concentrated MLA nutrient mix	-	25
8	$\text{NaHCO}_3$	85	10
9	$\text{CaCl}_2$	6.96	1

### 2.2.2. Cyanobacterial Strains

*The Microcystis strains CBT 1 and CBT 275, the Nodularia strains CBT 750 and CBT 786, and the Planktothrix rubescens strain CBT 329 belong to the strain collection of our corporation partner Cyano Biotech GmbH (Berlin, Germany) and were grown by Heike Enke and Alexandra Hilfer. The Microcystis strain CAWBG11 was obtained from the strain collection of the Cawthron Institute (Nelson, New Zealand) and was also grown at the Cyano Biotech GmbH by Heike Enke and Alexandra Hilfer.*

The *Microcystis aeruginosa* strain CBT 480 and the *Microcystis* strains CBT 633 and 959 were provided by our corporation partner Cyano Biotech GmbH (Berlin, Germany). The strains were grown continuously in tubes filled with 5 mL BG11 (“stock cultures”). While *M. aeruginosa* CBT 480 grew best at 28 °C and a photon flux of 20–30  $\mu\text{mol}\cdot\text{s}^{-1}\cdot\text{m}^{-2}$  under continuous illumination (Lumilux de Lux, Daylight, Osram), the *Microcystis* strains CBT 633 and 959 preferred low light conditions (photon flux 10–15  $\mu\text{mol}\cdot\text{s}^{-1}\cdot\text{m}^{-2}$ ) at 28 °C.

## 2. Materials and Methods

---

### 2.2.3. Determination of the Optical Density at 750 nm

For the cultivation of *Microcystis* strains, which grow in a homogenous suspension, the cell density was determined by measuring the optical density at 750 nm ( $OD_{750}$ ) using a Biomate 3S spectrophotometer (Thermo Fisher Scientific). Firstly, the background  $OD_{750}$  of BG11 medium ("blank") was measured and set to zero. Subsequently, the  $OD_{750}$  of the culture was determined. If a growth curve was to be established, high-density samples with  $OD_{750} \geq 0.9$  were diluted with BG11 medium to  $0.2 \leq OD_{750} \leq 0.8$ . The original  $OD_{750}$  was calculated by multiplication of the measured value with the dilution factor.

### 2.2.4. Preparation of Precultures of Cyanobacteria

All subsequent experiments involving the cultivation of the cyanobacterial strains were started with the inoculation of precultures. Depending on the cell density, 1–3 mL of stock culture was added to 30 mL medium in sterile, closed 100 mL-Erlenmeyer flasks. The precultures were put on an orbital shaker set at 120 rpm, and grown at 28 °C and a photon flux of 20–30  $\mu\text{mol}\cdot\text{s}^{-1}\cdot\text{m}^{-2}$  (*M. aeruginosa* CBT 480) or 10–15  $\mu\text{mol}\cdot\text{s}^{-1}\cdot\text{m}^{-2}$  (*Microcystis* strains CBT 633 and 959) under continuous illumination. All strains took about 14 to 21 d to reach a suitable density.

### 2.2.5. Cultivation of Cyanobacteria in Shaking Flasks

The  $OD_{750}$  of precultures was adjusted to 0.4 to 0.5 with BG11 medium, and 30 mL culture was transferred to sterile Erlenmeyer flasks closed with cotton. The cultures were grown under the same conditions as for pre-cultivation for 7 to 14 d.

### 2.2.6. Cultivation of Cyanobacteria in Centrifuge Tubes

Two holes with diameters of about 4 mm were drilled into the lids of 50 mL-centrifuge tubes. Silicon tubing with a tight fit were pulled through each hole to reach the bottom of the centrifuge tube and the lid was screwed back onto the tube. One of the hoses was equipped with an Acro 37 TF venting filter (diameter: 37 mm; flow rate: 3.58 L/min; Pall Laboratory, Port Washington, USA) to allow for aeration of the culture with sterile gas. The other hose was closed with cotton and aluminum foil. The assembled system was autoclaved at 121 °C for sterilization.

The OD<sub>750</sub> of precultures was adjusted to 0.4–0.5 with BG11 medium, and 30 mL culture was transferred into the autoclaved centrifuge tubes. The hose equipped with the inline gas filter was connected to external gas supply and the cultures were aerated with 5 % CO<sub>2</sub> in synthetic air at a gas flow of 2 L/min. The cultures were grown at 28 °C and a photon flux of 20–30 μmol·s<sup>-1</sup>·m<sup>-2</sup> under continuous illumination. Due to the rapid evaporation of medium, every 7 days, the medium was refilled up to 30 mL.

### 2.2.7. Cultivation in CellDEG HD10 Cultivators

HD10 cultivators (CellDEG, Berlin, DE) are polystyrene tubes with bottom-mounted gas supply membranes. They were used in combination with the HDC 45.10 platform (CellDEG) mounted on an orbital shaker and connected to a growth control unit (CellDEG), which controls the gas mixing and intensity of the light source. HD10 cultivators were inoculated with 10 mL cyanobacterial culture adjusted to an OD<sub>750</sub> of 0.5–0.6 and grown under high light conditions (100 μmol·s<sup>-1</sup>·m<sup>-2</sup>) with bubble-free supply of 5 % CO<sub>2</sub> on a shaker at 260 rpm.

### 2.2.8. Supplementation Experiments

*Most of the supplementation experiments were kindly performed by Heike Enke and Alexandra Hilfer at the Cyano Biotech GmbH. Exceptions were the supplementation of *M. aeruginosa* CBT 480 with Prtyr and Azphe, the supplementation of *Microcystis* CBT 633 with Azabu and Prlys, and the supplementation of *Microcystis* CBT 959 with Azabu.*

The vendors of the modified amino acids and the protocol of the supplementation experiments are specified in Moschny *et al.*<sup>194</sup> (A.4. Publication)

### 2.2.9. Uptake of Prtyr into *M. aeruginosa* CBT 480

The uptake studies of Prtyr into *M. aeruginosa* CBT 480 were carried out as described by Moschny *et al.*<sup>194</sup> (A.4. Publication)

### 2.2.10. Continuous Supplementation System for PDB

Two 500-mL-Schott bottles were provided with two, stacked screw threads on the walls and equipped with connectors for tubing. One bottle was designated as substrate reservoir and the other as cultivation chamber. The upper tubing of the substrate reservoir was equipped with a venting filter to allow for pressure equalization whereas the lower was connected to tubing, which was further attached to the inlet connector of a Pharmacia LKB P-1 peristaltic pump (Cytiva (formerly GE Healthcare Science), Marlborough, MA, USA). Another tube was affixed to the outlet connector of the pump and pulled through a hole drilled into the bottle lid, so it protruded about 5 cm into the cultivation chamber.

A second hole was drilled into the lid and a tube equipped with a venting filter for CO<sub>2</sub> supply was pulled through until it almost reached the bottom of the cultivation chamber. A magnetic stir bar was placed into the cultivation chamber and the lid equipped with the two tubes was reattached to the bottle. The upper tubing connector of the cultivation chamber was connected to tubing filled with cotton for pressure equalization. In order to allow for harvesting of the culture without disassembling the system, a tube was attached to the lower connector of the cultivation chamber and closed with two clamps set about 30 cm apart. For sterilization, the inner tube of the circular pump casing was taken out of the pump and the assembled system was autoclaved at 121 °C. A Prtyr stock solution in BG11 medium was prepared in the concentration as calculated and sterile-filtered into the substrate reservoir using a bottle-top filter with 0.22 µm pore size.

The cultivation chamber was inoculated with 95 mL of *M. aeruginosa* CBT 480 preculture adjusted to OD<sub>750</sub> 0.6 and supplemented with 5 mL of 1 mM Prtyr stock (final concentration: 50 µM). The cultivation chamber was put on a magnetic stirrer set at 100 rpm and the tube for harvesting was submerged in 70 % (v/v) ethanol to prevent contamination of the culture after harvest. The culture was grown for 24 h under low light conditions (photon flux 10–15 µmol·s<sup>-1</sup>·m<sup>-2</sup>) at 28 °C to allow for adaption to the new system. The next day, the pump was set to the lowest possible flow rate (7.5 µL/min) and the culture was grown at 28 °C and 5 % CO<sub>2</sub> supply (2 L/min) under medium light conditions (photon flux: 50 µmol·s<sup>-1</sup>·m<sup>-2</sup>).

### 2.3. Processing of Cyanobacterial Biomass and Supernatants

In the course of harvesting, the cyanobacterial samples were transferred into centrifuge tubes or bottles, and the biomass was separated from the supernatant by centrifugation at 5000 rpm for 30 min. Small-scale samples of 1 mL were centrifuged at 10,000 g for 5 min. The supernatant (if needed) and cyanobacterial biomass was frozen at -80 °C for 24 h and, subsequently, lyophilized for at least 48 h using a Lyovac GT2 (Heraeus Holding, Hanau, DE).

Additional lyophilized biomass of *M. aeruginosa* CBT 480 was provided by our corporation partner Cyano Biotech GmbH for the purpose of method development.

#### 2.3.1. Extraction with Methanol + 0.05 % Trifluoroacetic Acid

Lyophilized cyanobacterial biomass was suspended in methanol (MeOH) supplemented with 0.05 % (v/v) trifluoroacetic acid (TFA; 20 mL/g dried biomass) and extracted in three cycles. Each cycle consisted of sonication for 5 min with a sonotrode (output control: 5, 30 % duty cycle) on ice, shaking at room temperature for 20 min, sonication for 5 min (same parameters) on ice, shaking at room temperature for 20 min and centrifugation at 9,000 rpm and 4 °C for 20 min. In between the cycles, the supernatants were collected, and fresh MeOH + 0.05 % (v/v) TFA (50 mg/mL dried biomass) was added to the biomass pellet.

The pooled supernatants were transferred into a dry, empty-weighed vessel and dried *in vacuo* with either a rotary evaporator or an EZ-2 Elite vacuum centrifuge (GeneVac, Suffolk, UK). Subsequently, the dried, crude extracts were weighed to determine the yield.

#### 2.3.2. Evaluation of Biphasic Systems and Re-extraction with *n*-Butanol

A total volume of 2 mL of various biphasic systems were prepared and equilibrated by shaking at room temperature for 1 h. 10 mg of dried extract (MeOH + 0.05 % TFA) were weighed into centrifuge tubes and the biphasic systems were added. The extract was solubilized within the two-phase systems by sonication using an ultrasonic bath. Subsequently, the centrifuge tubes were shaken at room temperature for 2 h. After centrifugation at 14,000 g at room temperature for 30 min, the two phases were separated and transferred into empty-weighed centrifuge tubes, while the insoluble pellet was discarded.

## 2. Materials and Methods

---

Both phases were dried *in vacuo* in an EZ-2 Elite vacuum centrifuge and redissolved in 1 mL MeOH for HPLC analysis.

The dried aqueous phases were dissolved in an *n*-butanol–water system (1:1; 6 mg/mL total volume) and the mixture was shaken at room temperature for 30 min. The organic layer was decanted, collected in a centrifuge tube and replaced by 1 mL water-saturated *n*-butanol. This process was repeated twice. The organic layers were collected separately and dried *in vacuo* before redissolving in 1 mL MeOH for HPLC analysis.

### 2.3.3. Evaluation of a Three-Phase System

2 g of lyophilized biomass of *M. aeruginosa* CBT 480 were extracted in three cycles with a ternary system consisting of 13 mL *n*-hexane, 13 mL methyl acetate, 10 mL acetonitrile and 13 mL water (total volume: 50 mL). The same cycle sequence as described in chapter 2.3.1. was applied. In between each cycle, the three phases were separated and collected, and the pellet was mixed with the same volume of fresh, three-phase solvent system. The respective phases were pooled and dried *in vacuo*. The dried extract was dissolved in 10 mL methanol and subjected to HPLC analysis.

### 2.3.4. Two-step Liquid–Liquid Extraction of Cyanobacterial Biomass

Lyophilized, cyanobacterial biomass was resuspended in a biphasic system consisting of equal parts *n*-hexane, butyl acetate, methanol and water (20 mL/g dried biomass) in three cycles. The mixture was sonicated twice with a sonotrode (output control: 5; 30 % duty cycle) for 5 min on ice and thoroughly shaken in between. Subsequently, the samples were shaken for 20 min to 1 h at room temperature. After centrifugation at 9000 rpm for 20 min at 4 °C, the phases were separated and the organic and aqueous phases were collected separately. If a semi-solid, intermediate phase had formed, it was removed prior to phase separation and pooled with the pellet afterwards. The pellet (and intermediate phase) were resuspended in a fresh aliquot of the biphasic system (50 mL/g dried biomass) and the extraction cycle started anew with sonication.

The pooled, organic phases were dried on a rotary evaporator (waterbath: 40 °C). The pooled aqueous phases were concentrated on a rotary evaporator to remove the major part of methanol, and the volume was made up to the initial volume of the aqueous phase with water. Subsequently, the extract was transferred into a separation funnel and an equal volume of water-saturated *n*-butanol was added.

The mixture was shaken thoroughly for 15 min, and the phases were let to separate for several hours. When complete, the *n*-butanol layer was collected and replaced with the same volume of fresh *n*-butanol, and the process was repeated twice. The organic phases were pooled, dried *in vacuo*, and redissolved in methanol for preparative LC.

### 2.3.5. Quick Extraction for Qualitative Analysis

The quick extraction for qualitative analysis was carried out as described by Moschny *et al.*<sup>194</sup>

## **2.4. Analytical HPLC**

The components of the two instruments used for HPLC–DAD, an Agilent 1260 Infinity (Agilent, Waldbronn, DE) and an UltiMate 3000 (Thermo Fisher Scientific, Waltham, USA), are summarized in Table 3. For all analytical measurements, the diode array detector (DAD) was equipped with a standard 10-mm flow cell. For HPLC–DAD analysis coupled to fluorescence detection an UltiMate 3000 (Thermo Fisher Scientific) was used as specified in Table 3. All other method parameters are listed in Table 7 to Table 13. Prior to analysis, all samples were centrifuged at 14,000 g for 5 min and the supernatants were transferred into HPLC vials.

The following HPLC columns were used as indicated in the methods: Nucleosil 100 C<sub>18</sub> (5 μm; 100 Å; 4.6 mm ID × 125 mm; Dr. Maisch GmbH, Ammerbuch-Entringen, DE), VDSpher PUR 100 C<sub>18</sub>-E (5 μm, 100 Å; 4.6 mm ID × 250 mm; VDS optilab, Berlin, DE), Kinetex C<sub>18</sub> (2.6 μm, 100 Å; 3.0 mm ID × 100 mm, Phenomenex, Torrance, US), Luna C<sub>18</sub> (5 μm, 100 Å; 4.6 mm ID × 250 mm, Phenomenex), Luna PH (5 μm, 100 Å; 4.6 mm ID × 250 mm, Phenomenex), and Luna PFP (5 μm, 100 Å; 4.6 mm ID × 250 mm, Phenomenex).

## 2. Materials and Methods

**Table 7.** Analytical HPLC screening method using a Nucleosil 100 C<sub>18</sub> column.

Parameter	Value
Instrument	Agilent 1260 Infinity
Column	Nucleosil-100 C <sub>18</sub> (5 μm; 100 Å; 4.6 mm ID × 125 mm)
Solvents	A: H <sub>2</sub> O + 0.1 % FA B: ACN + 0.1 % FA
Elution	Gradient: 4.5–100 % B over 15 min; plateau 100 % B for 5 min
Flow rate	0.85 mL/min
Temperature	20 °C
DAD settings	Channel 1: 210 nm Channel 2: 230 nm Channel 3: 260 nm Channel 5: 280 nm Full scan: 210–500 nm Channel 6: 310 nm Channel 7: 360 nm Channel 8: 434 nm
ELSD settings	Temperature: 40 °C N <sub>2</sub> pressure: 4 bar Gain: 8

**Table 8.** HPLC–DAD–fluorescence method using a VDSpher PUR 100 C<sub>18</sub>-E column.

Parameter	Value
Instrument	UltiMate 3000
Column	VDSpher PUR 100 C <sub>18</sub> -E (5 μm, 100 Å; 4.6 mm ID × 250 mm)
Solvents	A: H <sub>2</sub> O + 0.1 % FA B: ACN + 0.1 % FA
Elution	Gradient: 5.0–100 % B over 25 min; plateau 100 % B for 5 min
Flow rate	1.0 mL/min
Temperature	37 °C
DAD settings	Channel 1: 210 nm Channel 2: 230 nm Channel 3: 238 nm Full scan: 210–500 nm Channel 4: 360 nm Channel 5: 410 nm
Fluorescence detector settings	Excitation wavelength (λ <sub>ex</sub> ): 365 nm Emission wavelength (λ <sub>em</sub> ): 475 nm

Data obtained from Agilent systems were analyzed with ChemStation (version B.04.03, Agilent) whereas HPLC–DAD data from UltiMate 3000 systems were analyzed with Chromeleon 7 (version 7.2.6., Thermo Fisher Scientific). For HPLC–DAD–fluorescence measurements, Chromeleon 6 (version 6.8., Thermo Fisher Scientific) was used for data analysis. If a (semi-)quantitative estimation was required, the peaks were integrated manually.



### 2.4.1. Generic Method for Method Development on Luna Columns

For the method development on Luna columns, the following generic method was applied using the column and gradient as indicated in the Results and Discussion section.

**Table 9.** Generic parameters for the method development on analytical Luna columns.

Parameter	Value
Instrument	Agilent 1260 Infinity
Column	as indicated
Solvents	A: H <sub>2</sub> O + 0.1 % FA B: ACN + 0.1 % FA
Elution	Initial gradient as indicated; plateau 100 % B for 5 min
Flow rate	1.0 mL/min
Temperature	25 °C
DAD settings	Channel 1: 210 nm Channel 2: 230 nm Channel 3: 260 nm Channel 5: 280 nm Full scan: 210–500 nm
	Channel 6: 310 nm Channel 7: 360 nm Channel 8: 434 nm

### 2.4.2. Quantification of MCs by HPLC–ELSD

The methods employed for the quantification of MCs are specified in Table 10 and Table 11. Before each measurement, calibration was carried out by injecting five volumes between 9.2 and 24.3  $\mu$ L of certified reference material (CRM) MC-RR in triplicate corresponding to 100, 200, 250, 300, and 350 ng on-column. The ELSD response areas were averaged, and the log(ELSD response area) was plotted against the log(amount in ng) to generate a linear calibration curve using Prism 6 (version 6.01; GraphPad Software Inc., San Diego, USA).

Samples for quantification were dissolved in DMSO and the concentration adjusted in a manner that an injection volume between 1 to 15  $\mu$ L resulted in an ELSD response area in the medium range of the calibration curve. Each sample was injected in triplicate and the concentration was calculated by means of the equation obtained from linear regression.

## 2. Materials and Methods

**Table 10.** HPLC–ELSD method for the quantification of MC variants on an Agilent 1260 Infinity.

Parameter	Value
Instrument	Agilent 1260 Infinity
Column	Kinetex C <sub>18</sub> (2.6 μm, 100 Å; 3.0 mm ID × 100 mm; Phenomenex)
Solvents	A: H <sub>2</sub> O + 0.1 % FA B: ACN + 0.1 % FA
Elution	Gradient: 10–100 % B over 10 min; plateau 100 % B for 3 min
Flow rate	0.65 mL/min
Temperature	50 °C
DAD settings	Channel 1: 210 nm Channel 2: 230 nm Channel 3: 254 nm Channel 5: 280 nm Full scan: 210–500 nm Channel 6: 310 nm Channel 7: 360 nm Channel 8: 434 nm
ELSD settings	Temperature: 40 °C N <sub>2</sub> pressure: 4 bar Gain: 11

**Table 11.** HPLC–ELSD method for the quantification of MC variants on an UltiMate3000.

Parameter	Value
Instrument	UltiMate 3000
Column	Kinetex C <sub>18</sub> (2.6 μm, 100 Å; 3.0 mm ID × 100 mm)
Solvents	A: H <sub>2</sub> O + 0.1 % FA B: ACN + 0.1 % FA
Elution	Gradient: 10–100 % B over 10 min; plateau 100 % B for 3 min
Flow rate	0.65 mL/min
Temperature	25 °C
DAD settings	Channel 1: 210 nm Channel 2: 254 nm Full scan: 210–500 nm Channel 3: 280 nm Channel 4: 360 nm
ELSD settings	Temperature: 40 °C N <sub>2</sub> pressure: 4 bar Gain: 11

### 2.4.3. Quantification of Prtyr in *M. aeruginosa* CBT 480 Culture Supernatant

The HPLC–DAD parameters for the quantification of Prtyr from the culture supernatant are specified in Table 12. For calibration, the 1 mM Prtyr stock solution was diluted by 1:10 with water to obtain a 100  $\mu$ M solution. Volumes of 1.0, 3.0, 5.0, 7.5, and 10  $\mu$ L, corresponding to 0.10, 0.30, 0.50, 0.75, and 1.0 nmol Prtyr on column, were injected in triplicate. The peak areas in the UV chromatograms monitored at 254 nm were averaged and plotted against the amount of Prtyr to establish a linear calibration curve ( $R^2 = 0.999$ ) using Prism 6.

The culture supernatants were processed as described above. After lyophilization, they were redissolved in 100  $\mu$ L water and 10  $\mu$ L were injected in triplicate under the same conditions and analysis was done as described above. The peak areas were averaged and the amount of Prtyr was calculated from the equation obtained from linear regression. Taking in to account the original volume, the concentration of Prtyr in the sample was further calculated.

To determine the uptake kinetics of Prtyr into *M. aeruginosa*, the calculated concentration was further plotted against the sampling time  $t$  in h using Prism 6. A curve was fitted corresponding to a first-order decay (equation:  $y = (y_0 - \text{plateau}) \cdot e^{-(k \cdot x)} + \text{plateau}$ ) with a goodness of fit of  $R^2 = 0.990$ . The plateau was constrained to 0 because Prtyr was taken up completely. The half-life  $t_{1/2}$  and uptake rate  $k$  were deduced from the fitted curve.

**Table 12.** HPLC–DAD method for the quantification of Prtyr from the culture supernatant.

Parameter	Value
Instrument	UltiMate 3000
Column	Kinetex C <sub>18</sub> (2.6 $\mu$ m, 100 Å; 3.0 mm ID $\times$ 100 mm)
Solvents	A: H <sub>2</sub> O + 0.1 % FA B: ACN + 0.1 % FA
Elution	Plateau 100 % A over 5 min Linear gradient: 0–100 % B over 7 min Plateau 100 % B for 3 min
Flow rate	0.85 mL/min
Temperature	25 °C
DAD settings	Channel 1: 210 nm                      Channel 3: 280 nm Channel 2: 254 nm                      Channel 4: 360 nm Full scan: 210–500 nm

## 2. Materials and Methods

---

### 2.4.4. Quantification of MC-PrtyrR from the Biomass of CBT 480

The HPLC–DAD parameters for the quantification of MC-PrtyrR from the biomass are specified in Table 13. A stock solution of MC-PrtyrR was prepared at a concentration of 1 mM in methanol by using the pure compound isolated from *M. aeruginosa* CBT 480. The stock solution was further diluted by 1:10 with methanol to obtain a 100 µM solution and 1, 5, and 10 µL of this solution corresponding to 0.1, 0.5, and 1.0 nmol MC-PrtyrR on column were injected in triplicate. The peak areas in the UV chromatograms monitored at 238 nm were averaged and plotted against the amount of MC-PrtyrR to establish a linear calibration curve ( $R^2 = 0.999$ ) using Prism 6.

The biomass samples were processed as described above. After lyophilization, the samples were dissolved in 20 µL methanol. 15 µL of this solution was injected and analyzed under the same conditions as calibration was carried out. The content of MC-PrtyrR in each sample was calculated by means of the equation obtained from linear regression, and extrapolated to the original sample volume (the amount in 20 µL HPLC sample equals the amount in 1 mL culture sample before processing). Subsequently, the total amount of MC-PrtyrR in the culture was calculated with the total culture volume being 20 mL - n (number of samples drawn before).

The resulting amount of MC-PrtyrR per culture was further transformed into percentage of the maximum theoretically possible amount of MC-PrtyrR. Assuming a complete incorporation of Prtyr into MC-PrtyrR, the maximum theoretically possible amount of MC-PrtyrR was 1 µmol (50 µM Prtyr in 20 mL culture volume) per culture. The values were plotted against the incubation time with Prism 6.

**Table 13.** HPLC–DAD method for the quantification of MC-PrtyrR from the biomass of *M. aeruginosa* CBT 480.

Parameter	Value
Instrument	UltiMate 3000
Column	Kinetex C <sub>18</sub> (2.6 µm, 100 Å; 3.0 mm ID × 100 mm)
Solvents	A: H <sub>2</sub> O + 0.1 % FA B: ACN + 0.1 % FA
Elution	Gradient: 5–100 % B over 15 min; plateau 100 % B for 3 min
Flow rate	0.85 mL/min
Temperature	25 °C
DAD settings	Channel 1: 210 nm Channel 2: 238 nm Full scan: 210–500 nm Channel 3: 254 nm Channel 4: 360 nm

## 2.5. HPLC–MS

*Dr. Wolfram Lorenzen and Alexandra Hilfer performed a part of the HPLC–MS measurements on an LCMS-8040 Tandem Quadrupole Mass Spectrometer coupled to a Nexera HPLC (Shimadzu) at the Technical University of Applied Sciences Wildau. The raw data was made available to me for further analysis.*

Table 3 specifies the components of the HPLC–MS systems used in this thesis: an Agilent 1200 coupled to an Agilent 6330 Ion Trap and an UltiMate 3000 coupled to a Q Exactive Plus (Thermo Fisher Scientific). The DAD of each system was equipped with a standard 10-mm flow cell. All other method parameters are listed in Table 14 and Table 15. Prior to analysis, all samples were centrifuged at 14,000 g for 5 min and the supernatants were transferred into HPLC vials. The parameters of the measurements performed on the Nexera HPLC system coupled to a LCMS-8040 Tandem Quadrupole Mass Spectrometer are specified in the journal article by Moschny *et al.*<sup>194</sup> (A.4. Publication)

Data obtained from the Agilent system was analyzed with DataAnalysis for 6300 Series Ion Trap (version 3.4.; Bruker Corporation, Billerica, MA, USA), while FreeStyle 1.5 (Thermo Fisher Scientific) was used for data from the Q Exactive plus. All other HPLC–MS data were analyzed with ACD/MS Workbook Suite 2017 (Advanced Chemistry Development, Toronto, CA). MS<sup>2</sup> spectra were exported to the mzML format with MSConvert (version 3.0.19363)<sup>357</sup> and annotated with the *in silico* fragmentation tool mMass (version 5.5.0) following the instructions in the user's guide.<sup>358</sup>

## 2. Materials and Methods

**Table 14.** HPLC–MS method for an Agilent 1200 system coupled to an Agilent 6630 Ion Trap.

Parameter	Value
Instruments	Agilent 1200 and Agilent 6330 Ion Trap
Column	Nucleosil 100 C <sub>18</sub> (3 μm; 100 Å; 2 mm ID × 100 mm)
Solvents	A: H <sub>2</sub> O + 0.1 % FA B: ACN + 0.06 % FA
Elution	Gradient: 10–100 % B over 15 min; plateau 100 % B for 2 min
Flow rate	0.40 mL/min
Temperature	40 °C
DAD settings	Channel 1: 220 nm Channel 2: 260 nm Channel 3: 280 nm Full scan: 230–600 nm Channel 4: 360 nm Channel 5: 435 nm
Injection volume	2.5 μL
Tune settings	Capillary voltage - 3.5 kV Gas temperature: 350 °C
Ion trap settings	Target <i>m/z</i> 1000
MS <sup>n</sup> parameters	Target <i>m/z</i> 1045.5 (positive mode); fragmentation voltage: 0.40 V Target <i>m/z</i> 995.5 (positive mode); fragmentation voltage: 0.40 V Target <i>m/z</i> 1083.5 (positive mode); fragmentation voltage: 0.35 V Multiple reaction monitoring: MS <sup>2</sup> target <i>m/z</i> 1070.5 (positive mode); fragmentation voltage: 0.35 V MS <sup>3</sup> target <i>m/z</i> 1042.6; fragmentation voltage: 0.35 V

**Table 15.** HPLC–MS method for an UltiMate 3000 coupled to a Q Exactive Plus.

Parameter	Value
Instruments	UltiMate 3000 and Q Exactive Plus
Column	Kinetex C <sub>18</sub> (2.6 μm; 100 Å; 2.1 mm ID × 50 mm)
Solvents	A: H <sub>2</sub> O + 0.1 % FA B: ACN + 0.1 % FA
Elution	Gradient: 5 - 100 % B over 7.5 min; plateau 100 % B for 5 min
Flow rate	0.60 mL/min
Temperature	50 °C
Injection volume	2 μL
HESI source settings	Spray voltage: 3.5 kV Sheath gas flow rate: 55 L/min Aux gas flow rate: 15 L/min Sweep gas flow rate: 3 L/min Capillary temperature: 380 °C S-lens RF level: 50 V Aux gas heater temperature: 450 °C
MS settings	Full MS resolution: 70000 Stepped NCE 30, 40, 50

## 2.6. Thin-Layer Chromatography (TLC)

### 2.6.1. TLC of Samples Obtained from the CuAAC Reaction

10  $\mu\text{L}$  of samples were spotted on a Silica 60 HP-TLC plate (10  $\times$  10 cm) and air-dried. The plate was put in a TLC chamber saturated with mobile phase and developed in a mixture of *n*-butanol:water:pyridine (3:1:1) as mobile phase for 1 h (travel distance: 8 cm). The plate was air-dried and analyzed by UV-detection at 365 nm without further staining. The retardation factor ( $R_f$ ) was determined by dividing the travel distance of a substance by the travel distance of the mobile phase.

### 2.6.2. TLC of Templates

In a modification of the method, the templates used for the CuAAC reaction were spotted on the HP-TLC plate. 2.5  $\mu\text{L}$  of water, 1 M Prtyr stock, 200  $\mu\text{M}$  MC-YR stock, and 1 mM MC-PrtyrR stock were applied, while 5  $\mu\text{L}$  of both methanol extracts, *M. aeruginosa* CBT 480 + Prtyr and *M. aeruginosa* CBT 480 control were used. The plate was developed and analyzed as described above.

$\text{CuSO}_4 \times 5 \text{H}_2\text{O}$  was dissolved in demineralized water at a concentration of 100 mM (stock solution). A 200 mM stock solution of tris(3-hydroxypropyltriazolyl-methyl)amine (THPTA) was prepared in demineralized water. 3-Azido-6-bromo-7-hydroxycoumarin was dissolved in DMSO at a final concentration of 10 mM. All stock solutions were stored at  $-20 \text{ }^\circ\text{C}$  and protected from light. A sodium ascorbate solution of 100 mM in demineralized water was always prepared directly before use.

A TLC stain (2 mL per plate) containing 100  $\mu\text{M}$   $\text{CuSO}_4$ , 500  $\mu\text{M}$  THPTA, 10  $\mu\text{M}$  3-azido-6-bromo-7-hydroxycoumarin, and 250  $\mu\text{M}$  sodium ascorbate in water was prepared from the stock solutions described above. The HP-TLC plate was stained by homogenously spraying the stain on the plate and heating at  $70 \text{ }^\circ\text{C}$  for 20 s. Subsequently, the slightly wet plate was analyzed by UV detection at 365 nm and the  $R_f$  was determined as described above.

### **2.7. Preparative LC Methods**

Prior to each preparative LC step, the dried sample was dissolved in a suitable solvent as described below. Solubilization was aided by putting the sample–solvent mixture into an ultrasonic bath for up to 30 min. Insoluble residues were removed by centrifugation at room temperature either at 14,000 g for 5 min (volumes  $\leq$  2 mL) or at 5,000 g for 30 min (volumes  $>$  2 mL). The supernatant was decanted and the pellet was discarded.

#### 2.7.1. Solid–Phase Extraction (SPE)

A Strata C<sub>18</sub>-E SPE cartridge (55  $\mu$ m, 70 Å, 200 mg sorbent; Phenomenex) was mounted on an SPE manifold and preconditioned with two column volumes of water by applying vacuum. The sample was slowly loaded on the cartridge and washed once with one column volume water. The products were eluted with two column volumes methanol, dried *in vacuo* in a vacuum centrifuge and redissolved in DMSO.

#### 2.7.2. Flash Chromatography

Flash chromatography was performed on an Azura preparative HPLC system (Knauer Wissenschaftliche Geräte GmbH, Berlin (DE)) in the configuration as listed in Table 3. The dimension of the Sepacore C<sub>18</sub> flash cartridge (Büchi Labortechnik AG, Flawil, CH) was chosen depending on the amount of extract as recommended by the manufacturer. The dried extract was redissolved in 50 % (v/v) methanol in water at the highest possible concentration. Initially, the cartridge was purged with three to five column volumes of 100 % methanol before equilibrating for with five column volumes at starting conditions. 5 mL of extract were injected and fractionated by employing a linear gradient of 30–80 % methanol over 40 min at a flow rate of 25 mL/min. Fractions were collected every minute. Lastly, the cartridge was purged with 100 % methanol for 20 min. The fractions with the same constituents were pooled and dried *in vacuo*. If the fraction composition was unknown, 1 mL of sample were drawn prior to drying and analyzed by HPLC–DAD or HPLC–MS.



### 2.7.3. Size-Exclusion Chromatography

Sephadex LH-20 dry material was resuspended in mobile phase and let sit to swell and form a homogenous slurry for 4 h. Careful not to produce any air bubbles or inclusions in the column bed, the slurry was poured into an empty gravity-flow glass column (25 mm ID × 900 mm), and the stationary phase was let to settle for 4 h by purging with mobile phase. 130 mg of methanol extract was dissolved in 4 mL mobile phase and loaded on the column. The flow rate was adjusted to about 30 mL/h. Fractions were collected every 20 min over 21 h. The fractions were dried *in vacuo* and reconstituted in 500 µL methanol before subjecting them to HPLC–DAD analysis.

### 2.7.4. Semi-preparative HPLC

An Agilent 1100 instrument consisting of the modules summarized in Table 3 was used for semi-preparative HPLC. The DAD was equipped with a 3-mm semi-preparative flow cell. If fluorescence detection was required, a Hitachi LaChrom chromatographer (Merck KGaA) with the components listed in Table 3 was used. The method details are summarized in Table 16 to Table 20. Fractions, which were identical in composition and/or contained the compound(s) of interest, were pooled and dried *in vacuo*. For analytical HPLC or HPLC–MS analysis, the fractions were dissolved in methanol.

**Table 16.** Semi-preparative HPLC method on a Luna PFP column using a gradient of 30–60 % acetonitrile in water.

Parameter	Value
Instrument	Agilent 1100
Column	Luna PFP (5 µm, 100 Å; 10 mm ID × 250 mm; Phenomenex)
Solvents	A: H <sub>2</sub> O + 0.1 % FA B: ACN + 0.1 % FA
Elution	Gradient: 30–60 % B over 20 min; plateau 100 % B for 5 min
Flow rate	4.5 mL/min
Temperature	20 °C
DAD settings	Channel 1: 230 nm                      Channel 2: 238 nm Full scan: 210–500 nm
Fraction collection	Peak-based: threshold 150 mAU, slope 15 mAU/s

## 2. Materials and Methods

**Table 17.** Semi-preparative HPLC method on a Luna C<sub>18</sub> column using a gradient of 30–50 % acetonitrile in water.

Parameter	Value
Instrument	Agilent 1100
Column	Luna C <sub>18</sub> (5 µm, 100 Å; 10 mm ID × 250 mm; Phenomenex)
Solvents	A: H <sub>2</sub> O + 0.1 % FA B: ACN + 0.1 % FA
Elution	Gradient: 30–50 % B over 20 min; plateau 100 % B for 5 min
Flow rate	4.5 mL/min
Temperature	20 °C
DAD settings	Channel 1: 230 nm                      Channel 2: 238 nm Full scan: 210–500 nm
Fraction collection	Peak-based: threshold 150 mAU, slope 15 mAU/s

**Table 18.** Semi-preparative HPLC method on a Luna C<sub>18</sub> column using a gradient of 30–40 % acetonitrile in water.

Parameter	Value
Instrument	Agilent 1100
Column	Luna C <sub>18</sub> (5 µm, 100 Å; 10 mm ID × 250 mm)
Solvents	A: H <sub>2</sub> O + 0.1 % FA B: ACN + 0.1 % FA
Elution	Gradient: 30–40 % B over 18 min; plateau 100 % B for 5 min
Flow rate	4.5 mL/min
Temperature	20 °C
DAD settings	Channel 1: 230 nm                      Channel 2: 238 nm Full scan: 210–500 nm
Fraction collection	Peak-based: threshold 150 mAU, slope 15 mAU/s

**Table 19.** Semi-preparative HPLC method on an analytical Luna C<sub>18</sub> column using a gradient of 30–50 % acetonitrile in water and a fluorescence detector for peak identification.

Parameter	Value
Instrument	Hitachi LaChrom
Column	Luna C <sub>18</sub> (5 µm, 100 Å; 4.6 mm ID × 250 mm)
Solvents	A: H <sub>2</sub> O + 0.1 % FA B: ACN + 0.1 % FA
Elution	Gradient: 30–50 % B over 15 min; plateau 100 % B for 5 min;
Flow rate	1.5 mL/min
Temperature	Ambient
DAD settings	Channel 1: 210 nm                      Channel 2: 238 nm Channel 3: 360 nm                      Channel 4: 410 nm Full scan: 210–500 nm
Fluorescence detector settings	Excitation wavelength ( $\lambda_{ex}$ ): 404 nm Emission wavelength ( $\lambda_{em}$ ): 480 nm

**Table 20.** Semi-preparative HPLC method on an analytical Luna C<sub>18</sub> column using a gradient of 5–70 % acetonitrile in water and a fluorescence detector for peak identification.

Parameter	Value
Instrument	Hitachi LaChrom
Column	Luna C <sub>18</sub> (5 μm, 100 Å; 4.6 mm ID × 250 mm)
Solvents	A: H <sub>2</sub> O + 0.1 % FA B: ACN + 0.1 % FA
Elution	Gradient: 5–70 % B over 15 min; plateau 100 % B for 5 min;
Flow rate	1.5 mL/min
Temperature	Ambient
DAD settings	Channel 1: 210 nm                      Channel 2: 238 nm Channel 3: 360 nm                    Channel 4: 410 nm Full scan: 210–500 nm
Fluorescence detector settings	Excitation wavelength (λ <sub>ex</sub> ): 404 nm Emission wavelength (λ <sub>em</sub> ): 480 nm

### 2.7.5. Isolation of MC-PrtyrR (3) at Cyano Biotech GmbH

*MC-PrtyrR* was mainly isolated by Dr. Wolfram Lorenzen, Cyano Biotech GmbH according to the following protocol. The isolated compound was transferred to our labs.

MC-PrtyrR (3) was isolated according to the procedure described by Moschny *et al.*<sup>194</sup> (A.4. Publication)

## 2.8. NMR Spectroscopy

NMR spectroscopy of 3 was performed as described by Moschny *et al.*<sup>194</sup> (A.4. Publication)

## 2.9. Chemical Synthesis: CuAAC Reactions

Aminoguanidine was dissolved in methanol at a concentration of 100 mM and stored at 4 °C. 3-Azido-7-hydroxycoumarin was dissolved in DMSO at a final concentration of 10 mM, and the solution was stored at -20 °C and protected from light. A sodium ascorbate solution of 100 mM in demineralized water was always prepared directly before use. All other stock solutions were prepared and stored as described above.

### 2.9.1. CuAAC Reaction with Templates

1  $\mu\text{L}$   $\text{CuSO}_4$  stock solution and 2.5  $\mu\text{L}$  THPTA stock solution were pre-incubated in a small amount of water for several minutes. After addition of 50  $\mu\text{L}$  aminoguanidine stock solution and 10  $\mu\text{L}$  3-azido-6-bromo-7-hydroxycoumarin stock solution, the templates were added to the reaction mix (volumes see Table 21). The volume was made up to 975  $\mu\text{L}$  with demineralized water, and the reaction was started by addition of 25  $\mu\text{L}$  of sodium ascorbate solution. The reaction mix was incubated for 90 min at room temperature.

**Table 21.** Volumes of templates used for the CuAAC reaction.

Template	Volume	Template	Volume
Water (Blank)	1 $\mu\text{L}$	MC-PrtyrR (1 mM stock solution)	20 $\mu\text{L}$
MC-YR (200 $\mu\text{M}$ stock solution)	100 $\mu\text{L}$	CBT 480 + Prtyr extract (20 mg/mL)	100 $\mu\text{L}$
Prtyr (1 mM stock solution)	20 $\mu\text{L}$	CBT 480 control extract	35 $\mu\text{L}$

### 2.9.2. Conjugation of MC-PrtyrR (3)

The conjugation of **3** to 3-azido-7-hydroxycoumarin was performed as described by Moschny *et al.*<sup>194</sup> (A.4. Publication)

## 2.10. Measurement of the Excitation and Emission Spectra of MC-(O-((7-hydroxy-2H-chromen-3-yl)-1H-1,2,3-triazol-4-yl)methyl)YR

MC-(O-((7-hydroxy-2H-chromen-3-yl)-1H-1,2,3-triazol-4-yl)methyl)YR (**5**) was dissolved in DMSO to a final concentration of 90 mM and diluted by 1:10 with standard minimal essential medium with supplements as used for cell culture. The excitation spectra for both solutions were recorded from 230–500 nm at a fixed emission wavelength of 480 nm with a TECAN Infinite M200 Pro plate reader (TECAN, Männedorf (CH)). Accordingly, the emission spectra were measured from 400–700 nm with fixed excitation at 404 nm. The measurement was repeated with DMSO and standard minimal essential medium to determine the background fluorescence. The background-corrected curves were plotted using Prism 6. The excitation maximum was found to be 404 nm, the emission maximum was determined as 474 nm for the solution in cell culture medium.

## 2.11. Cell Culture Methods

### 2.11.1. Cell Culture Media and Reagents

All media, chemicals and other reagents used in cell culture and cytotoxicity testing are listed in Table 22. 10× phosphate-buffered saline (PBS) was prepared by dissolving the components in Table 23 in Milli-Q water and autoclaving at 121 °C. The solution was stored at 4 °C. 1× PBS was prepared from this stock by 1:10 dilution with demineralized water, autoclaved and stored at 4 °C until further use.

Fetal bovine serum (FBS) was heat-inactivated (HI) prior to use by heating at 60 °C in a temperature-controlled water bath for 30 min and stored at -20 °C until further use. G418 stock solution (50 mg/mL in sterile PBS) and dimethyl sulfoxide (DMSO) were sterilized by filtration through a membrane filter with 0.22 µm pore size and stored at 4 °C. 1 M sodium butyrate stock solution was prepared by dissolving 2.2 g substance in 20 mL sterile PBS. The stock solution was sterile-filtered using a membrane filter with 0.22 µm pore size and stored at 4 °C. 10× trypsin-EDTA was diluted 1:10 with sterile PBS to 1× trypsin-EDTA under aseptic conditions and stored at -20 °C until further use. Working stocks of 1× trypsin-EDTA were kept at 4 °C to avoid repetitive cycles of thawing and freezing.

Growth medium (minimal essential medium, MEM) was supplemented with 10 % (v/v) HI-FBS, 2 mM glutamine and 1× NEAA prior to use and kept at 4 °C up to 12 months at maximum. During that period, working stocks were regularly checked for turbidity and floating particles, which indicate a microbial contamination. The selection markers G418 and hygromycin B were added at the respective concentration during cell maintenance, i.e. changing media or sub-culturing. Freezing media (MEM) was supplemented with G418 or hygromycin B at the respective concentrations, 40 % HI-FBS and 20 % DMSO and stored at 4 °C.

50× Tris-acetate-EDTA (TAE) buffer containing 242 g/L tris base, 57.1 mL/L acetic acid, and 18.6 g/L Na<sub>2</sub>EDTA was prepared in demineralized water and diluted by 1:100 to obtain a 0.5× working stock. All stocks were stored at 4 °C.

## 2. Materials and Methods

---

**Table 22.** Media, chemicals and reagents used for cell culture.

Reagent	Vendor
<b>Media and supplements</b>	
100× Antibiotic antimycotic solution	Sigma-Aldrich, St. Louis, USA
Fetal bovine serum (FBS)	Sigma-Aldrich, St. Louis, USA
G418 disodium salt	Sigma-Aldrich, St. Louis, USA
Hygromycin B solution (50 mg/mL)	InvivoGen, San Diego, USA
Minimal essential medium (MEM)	Sigma-Aldrich, St. Louis, USA
100× Non-essential amino acid mix (NEAA)	Sigma-Aldrich, St. Louis, USA
Roti-CELL® glutamine solution (200 mM)	Carl Roth GmbH & Co. KG, Karlsruhe, DE
Sodium butyrate	Sigma-Aldrich, St. Louis, US
<b>Other reagents</b>	
Acetic acid	Merck KGaA, Darmstadt, DE
5-Fluorouracil	Sigma-Aldrich, St. Louis, USA
Poly-D-lysine	Sigma-Aldrich, St. Louis, USA
Plasmocin	InvivoGen, San Diego, USA
Sulforhodamine B	Sigma-Aldrich, St. Louis, USA
Trichloroacetic acid	Merck KGaA, Darmstadt, DE
Tris base	Carl Roth GmbH & Co. KG, Karlsruhe, DE
Trypan blue	Sigma-Aldrich, St. Louis, USA
10× Trypsin–EDTA	Sigma-Aldrich, St. Louis, USA
<b>Mycoplasma PCR</b>	
Desoxy nucleotide triphosphates (dNTPs)	Qiagen, Venlo, NL
GPO-3 primer (5'-GGGAGCAAACAGGATTAGATACCCT-3')	Integrated DNA Technologies, Inc., Iowa, USA
MGSO primer (5'-TGCACCATCTGTCACTCTGTTAACCTC-3')	Integrated DNA Technologies, Inc., Iowa, USA
PCR buffer (including gel loading buffer)	Qiagen, Venlo, NL
Q-solution	Qiagen, Venlo, NL
Taq DNA polymerase	Genaxxon, Ulm, DE
<b>Gel electrophoresis</b>	
Agarose	Carl Roth GmbH & Co. KG, Karlsruhe, DE
DNA marker	Bio-Rad Laboratories, Inc., Hercules, USA
Ethidium bromide	Carl Roth GmbH & Co. KG, Karlsruhe, DE
Tris-acetate-EDTA (TAE)	Carl Roth GmbH & Co. KG, Karlsruhe, DE

**Table 23.** Composition of phosphate-buffered saline (PBS).

<u>Component</u>	<u>Concentration</u>
NaCl	80 g/L
KCl	2.0 g/L
Na <sub>2</sub> HPO <sub>4</sub> × 2 H <sub>2</sub> O	14.4 g/L
KH <sub>2</sub> PO <sub>4</sub>	2.4 g/L

### 2.11.2. Cell Lines

The cell lines and their respective culturing conditions are specified in Moschny *et al.*<sup>194</sup> (A.4. Publication)

### 2.11.3. Cultivation of Cell Lines from Cryo-Preserved Stocks

9 mL of growth medium, pre-warmed in a temperature-controlled water bath at 37 °C, were put into a T-25 cell culture flask and supplemented with the selection markers in their respective concentrations. The cryo-preserved cell lines were rapidly thawed at 37 °C, and after careful resuspension, the cells were transferred into the cell culture flask and incubated 37 °C.

After two days, the medium was carefully aspirated and replaced by fresh growth medium containing the selection markers in their required concentrations. If the cells did not fully adhere, the cell suspension was transferred into a sterile centrifuge tube and spun down at 150× g for 7 min at room temperature. The cell pellet was resuspended in growth medium with selection markers and transferred into a new T-25 cell culture flask. This procedure was repeated until the cells were completely adherent and reached a confluency of 80–90 %.

After two to four days, 1 mL of culture medium of each cell line was drawn to test for mycoplasma contamination. The samples were stored at -20 °C.

### 2.11.4. Changing the Medium

For each cell line, the medium was exchanged every two to three days. The spent culture medium was aspirated, and fresh growth medium was let to trickle down the flask wall carefully, so the cells were not accidentally detached due to shear forces. Finally, the selection markers were supplemented in their respective concentrations.

## 2. Materials and Methods

---

### 2.11.5. Passaging of Cell Lines

When the cells had reached a confluency of 80–90 % (every three to four days depending on the cell line), they were sub-cultured (“passaged”) according to the following protocol. Growth medium, 1× PBS, and 1× trypsin–EDTA were pre-warmed in a temperature-controlled water bath at 37 °C. The culture medium was carefully aspirated and the cells were washed with 5 mL PBS. After the PBS had been aspirated, the cells were treated with 2 mL trypsin–EDTA and incubated at 37 °C for several minutes to allow for a sufficient cell detachment.

Protein digest was stopped by addition of 3 mL growth medium, and the cells were carefully flushed from the flask surface. The cell suspension was transferred into a sterile centrifuge tube and spun down at 150× g for 7 min at room temperature. In the meantime, 9 mL of growth medium were put into a new T-25 cell culture flask and supplemented with the respective amounts of selection marker. After centrifugation, the supernatant was aspirated, and the cell pellet was resuspended in growth medium. The cells were split at ratios between 1:3 and 1:5 using between 3 and 5 mL of growth media for resuspending the cell pellet and 1 mL of suspension for inoculation of the new flask.

All cell lines were continuously sub-cultured until a passage number of around 40 was reached. Since at this point, the metabolism and behavior of the cells can change drastically, the old cultures were discarded and new ones were prepared from cryo-preserved stocks.

### 2.11.6. Testing for Mycoplasma Contamination by PCR

Before cell lines can be cryo-preserved and stored in liquid nitrogen, they need to be free of mycoplasma because the contamination can spread to other cryo-stocks in the liquid nitrogen. Due to its sensitivity and reliability, mycoplasma contamination was monitored regularly by PCR as described by van Kuppeveld *et al.*<sup>359</sup> Samples for testing were drawn on the second day after taking cryo-preserved stocks into culture, or immediately if cultured cell lines were obtained from another research group.

1 mL of culture medium was drawn and centrifuged at 14,000× g for 5 min at room temperature. The supernatant was aspirated and discarded, and the pellet was dissolved in 100 µL sterile Milli-Q water. The samples were heated to 95 °C and kept at this temperature for 3 min. Condensed water on the lid was spun down by brief centrifugation. If necessary, the samples (“templates”) were stored at -20 °C until further processing.



The components and volumes of the PCR mix are listed in Table 24. A master-mix containing components 1–7 was prepared of the respective volumes corresponding to  $n + 1$  templates. 21.5  $\mu\text{L}$  of master mix were put into sterile PCR tubes, and the templates were added. Sterile, demineralized water was used as negative control. A sample tested positively for contamination served as positive control. The PCR cycling program is detailed in Table 25. After the PCR program was finished, the samples were stored at 4  $^{\circ}\text{C}$  until further analysis.

**Table 24.** Composition of the PCR mix used for testing cell lines for mycoplasma contamination.

No	Component	Volume [ $\mu\text{L}$ ]
1	Sterile, demineralized water	12.5
2	Q-solution	5.0
3	PCR buffer (including gel loading buffer)	2.5
4	dNTPs	0.5
5	GPO-3 primer	0.5
6	MGSO primer	0.5
7	Taq DNA polymerase	0.5
8	Template	3.0

An agarose gel was prepared from a 1.5 % (w/v) agarose solution supplemented with 0.25  $\mu\text{g}/\text{mL}$  ethidium bromide. The gel was transferred into a horizontal gel electrophoresis chamber filled with 0.5 $\times$  TAE buffer. 10  $\mu\text{L}$  of each PCR sample and 3  $\mu\text{L}$  of DNA marker were loaded on the gel and the electrophoresis was run at 135 V for about 30 min. The gel was analyzed by UV detection at 254 nm and documented by taking photographs. The positive control and contaminated samples showed a DNA fragment with 280 base pairs.

**Table 25.** PCR cycling program for testing cell lines for mycoplasma contamination.

Step	Temperature [ $^{\circ}\text{C}$ ]	Time [min]	Cycles (n = 30)
Initial denaturation	94	3	
DNA denaturation	94	0.5	Start
Primer annealing	54	1	
DNA elongation	72	1	End
Final elongation	72	10	

## 2. Materials and Methods

---

### 2.11.7. Treatment of Mycoplasma-Contaminated Cell Lines

If a cell line tested positive for contamination with mycoplasma, it was treated with Plasmocin for mycoplasma eradication. Plasmocin was supplemented with the growth medium of the contaminated cell line at concentrations of 12.5 µg/mL, 25 µg/mL, and 37.5 µg/mL and treatment was maintained for at least two weeks, during which the contaminated cells were passaged as usual. Mycoplasma elimination was confirmed by PCR two and four weeks after the end of treatment before the cell lines were designated as “mycoplasma-free”.

### 2.11.8. Cryo-Preservation of Cell Lines

As soon as cell lines had been proven free of mycoplasma, stocks for cryo-preservation were prepared. During routine passaging, the cell lines were additionally seeded on a 14.5-cm cell culture dish or T-75 cell culture flask at a split ratio of 1:2 to 3:5. Cells were grown until they reached a confluency of 80–90 % and the medium was changed every second day including the day directly before cryo-preservation.

The cells were harvested by trypsination as described for cell passaging using 10 mL of 1× PBS for washing, 5 mL of 1× trypsin–EDTA for detaching and 8 mL growth medium to stop protein digest. After centrifugation and removal of the supernatant, the pellet was resuspended in 5 (if a 14.5-cm cell culture dish was used) or 4 (if a T-75 cell culture flask was used) mL of growth medium supplemented with selection marker.

900 µL of cell suspension were added to 900 µL cold freezing medium in sterile, cryogenic tubes and thoroughly mixed. The tubes were closed tightly and put into a Mr. Frosty freezing container (Thermo Fisher Scientific), which was filled with 2-propanol. The container was put at -80 °C, where the cells were slowly frozen with a cooling rate of -1 °C/min. After one day, the tubes were transferred to a liquid nitrogen storage container and stored in both the liquid and the vapor nitrogen phase.

### 2.11.9. Counting of Cells

#### 2.11.9.1. Counting of Cells with a Neubauer Hemocytometer

A 0.4 % (w/v) trypan blue stock solution was prepared in demineralized water. Cells were harvested and trypsinized as described in chapter 2.11.5. After centrifugation, the cell pellet was resuspended in 8 mL growth medium supplemented with selection marker. A 1 mL aliquot was taken out, and cells were stained with 10  $\mu$ L of trypan blue stock solution. The cell suspension was mixed gently for several minutes. After homogenization of the cell suspension, 5  $\mu$ L was transferred on a Neubauer hemocytometer (VWR, Radnor, USA), and the cells were fixed by placing a cover slip on top. The cell number was determined by counting the cells within each of the five quadrants highlighted in Figure 10 under an inverted light microscope (VWR) at 10x magnification.

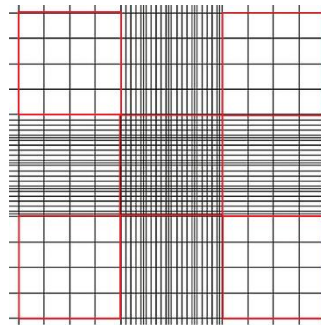


**Figure 10.** Schematic overview of a Neubauer cell counting chamber. The quadrants, of which the cell number was determined, are highlighted in red.

If the number per quadrant did not range between 30–80 cells, the concentration of the cell suspension was adjusted by either dilution or centrifugation of the stock cell suspension and reconstitution in less volume. Dead cells appeared as dark blue spheres and were omitted from counting. The numbers of cells per quadrant were averaged, and multiplication by a factor of 10,000 gave the number of cells per mL. If the original cell suspension had to be diluted for counting, the dilution factor was further included to obtain the number of cells per mL. The counting was repeated twice with two new aliquots of the stained cell suspension and thorough cleaning of the counting chamber in between. The values of the three independent counts were averaged. If an outlier was identified, the counting was repeated a fourth time.

## 2. Materials and Methods

---

### 2.11.9.2. Counting of Cells with an Automated Cell Counter

Cells were harvested and trypsinized as described in chapter 2.11.5. After centrifugation, the cell pellet was resuspended in 8 mL growth medium supplemented with selection marker. A 1 mL aliquot was taken out and cells were stained with 10  $\mu$ L of trypan blue stock solution. The cell suspension was applied on an EVE cell counting slide (NanoEnTek Inc., Seoul, KR) and counted with an EVE automated cell counter.

### 2.11.10. Determination of Cell Abundance by Staining with Sulforhodamine B

The cell abundance, which correlates with cell viability for adherent growing cell lines, was determined by staining with sulforhodamine B (SRB).<sup>360</sup> A 10 % (w/v) solution of trichloroacetic acid (TCA) in demineralized water was prepared. SRB was dissolved in 1 % (v/v) acetic acid at a concentration of 0.57 % (w/v) giving a 10 $\times$  stock solution, which was diluted by 1:10 with 1 % (v/v) acetic acid to 0.057 % (w/v) as working stock. Lastly, 10 mM tris base was prepared in demineralized water, and the pH was adjusted to 10.5. All solutions were stored at 4  $^{\circ}$ C.

For cell fixation, 100  $\mu$ L cold TCA was directly added to the cells grown in 96-well plates and incubated for 1 h at 4  $^{\circ}$ C. Subsequently, the medium/TCA mixture was removed and the fixated cell layer was washed three times with 200  $\mu$ L demineralized water. The plates were dried completely with pressurized air or at room temperature over night. The dry cell layer was stained with 100  $\mu$ L SRB working stock and incubated at 4  $^{\circ}$ C for 30 min. Having removed the staining solution, the cells were washed three times with 200  $\mu$ L of 1 % (v/v) acetic acid. The plate was dried with pressurized air or by sitting at room temperature over night.

200  $\mu$ L of 10 mM tris base (pH 10.5) was added to solubilize the stain, and the plate was shaken on an orbital shaker until the dye was homogenously dissolved. The absorbance at 510 nm was measured with a TECAN Infinite M200 Pro plate reader. Prism 6 was used for normalization and plotting of the data.

#### 2.11.11. Determination of the Seeding Density

In order to establish an assay for cytotoxicity screening, the ideal seeding density in 96-well flat bottom plates was determined. Exponentially growing cells (confluency 70–90 %) were harvested by trypsination and counted as described above. The cell concentration was adjusted in a manner that 100  $\mu$ L contained the desired number of cells per well.

The HEK293 OATP1B1 control and HEK293 OATP1B3 control cell lines were seeded at seven different densities between 5,000 and 100,000 cells per well in 100  $\mu$ L growth medium and incubated over night. The 1 M sodium butyrate stock solution was diluted to 20 mM with growth medium and 100  $\mu$ L were added to the cells (final concentration: 10 mM). The cells were incubated for another 24 h. Subsequently, the culture medium containing the inducer was carefully removed and substituted with fresh growth medium without selection marker. After 48 h, the cells were fixed and stained. The data was analyzed with Prism 6.

#### 2.11.12. Cytotoxicity Assay

Exponentially growing cells (confluency 70–90 %) were harvested by trypsination and counted as described above. The cell concentration was adjusted in a manner that 100  $\mu$ L contained the desired number of cells per well. The four cell lines (HEK293 OATP1B1 control, tHEK293 OATP1B1, HEK293 OATP1B3 control, and HEK293 OATP1B3) were seeded at a density of 50,000 cells per well in growth medium with selection marker.

After 24 h, sodium butyrate was added to a final concentration of 10 mM as described earlier and the cells were incubated for another 24 h. Dilutions of MCs were prepared in growth medium without selection marker at final concentrations ranging from 100 pM to 2  $\mu$ M. Likewise, 1 % (v/v) DMSO and 38 mM 5-fluorouracil solutions were prepared. Subsequently, the culture medium containing the inducer was removed and replaced by the MC-containing dilutions in triplicate. After 48 h, the cells were fixed, stained and analyzed as described above. After normalization, Prism 6 was used to plot the data. A sigmoidal, four-parameter logarithmic curve, from which the EC<sub>50</sub> values were deduced, was fitted using the log<sub>10</sub>(x) values of the concentration. The model can also be described by  $Y = \text{Bottom} + (\text{Top} - \text{Bottom}) / (1 + 10^{((\text{LogEC}_{50} - X) \cdot \text{HillSlope})})$ . The measurements were repeated twice for all cell lines.

### 2.11.13. Fluorescence Microscopy

*The following experiment was performed in corporation with Dr. Robert Eckenstaler, University of Halle-Wittenberg, DE.*

MC-(O-((7-hydroxy-2H-chromen-3-yl)-1H-1,2,3-triazol-4-yl)methyl)YR (5) was dissolved in DMSO at a final concentration of 90 mM. The HEK293 OATP1B1 control, the HEK293 OATP1B1, the HEK293 OATP1B3 control, and the HEK293 OATP1B3 cell lines were seeded into a 96-well at a cell density of 50,000 cells per well and treated as described above for cytotoxicity testing. All subsequent steps of the measurement are described by Moschny *et. al.*<sup>194</sup> (A.4. Publication)

## 3. RESULTS AND DISCUSSION

### 3.1. A Toolbox for Microcystin Isolation, Analysis and Screening

A major intention in natural product research is to isolate a compound of interest from a complex matrix; a good yield and high degree of purity of the product are of similar importance. The process follows a basic scheme that consists of (1) the extraction of the target molecule from the producing organism, (2) its separation from other extract components, (3) its quantitation and structural characterization.

In the first step, the substance is mostly withdrawn from the solid biomass with a solvent, supported by physical disruption of the cellular structures, i.e. cell walls and membranes. The method, also referred to as liquid extraction, is never selective for one compound only, so the resulting crude extract also contains undesired metabolites and contaminants, from which the compound of interest must be separated.

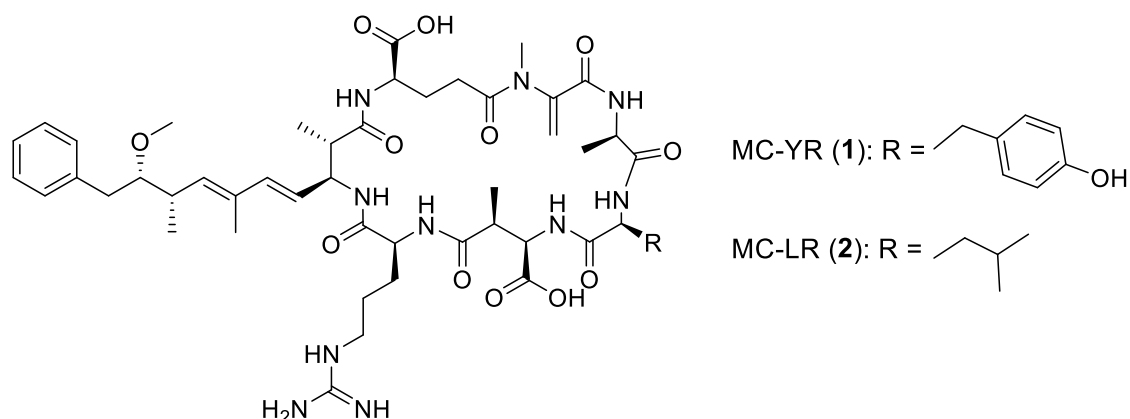
This is achieved by various methods of liquid chromatography (LC) including gravity column, flash, and high performance liquid chromatography (HPLC), which dissects the sample components based on their interactions with a stationary and mobile phase. The coupling to online detectors, such as single wavelength and photo diode array detectors (DAD) enables a direct monitoring of the analysis and selective collection of the fraction(s) with the compound of interest.

In the majority of cases, one such step is not sufficient to obtain a pure compound and the combination of several chromatographic principles proves beneficial. The analyte separation usually relies on adsorption and partition processes, size exclusion, or ion exchange, but also some specialized materials, e.g. modified with antibodies for immunochromatography, are available. However, the common methods mainly employ normal phase separations on highly hydrophilic silica gel, and reversed phase (RP) columns, in which the silica is conjugated with organic side chains in order to implement a separation based on hydrophobic interactions.

Once the pure compound is at hand, its chemical structure needs to be identified or confirmed by spectroscopic and spectrometric means. Nuclear magnetic resonance (NMR) spectroscopy, mass spectrometry (MS), and tandem-MS ( $MS^2$ ) represent feasible tools for both purposes. NMR in combination with MS rather provides comprehensive data for the *de novo* structure elucidation, whereas  $MS^2$  is more convenient for a rapid dereplication of known compounds.

### 3. Results and Discussion

Although most protocols hardly deviate from this workflow, the detailed method of each step needs to be specifically tailored to the analyte of interest and its chemical properties, as well as the composition of the matrix. Thus, an optimized process for the isolation of MCs should be established covering all steps from extraction, to their purification, to their quantification and structure elucidation/dereplication. Lyophilized biomass from the *M. aeruginosa* strain CBT 480, which produces MC-YR (**1**) and MC-LR (**2**) as the main variants, served as template for method development.



Since this study further strived to discover and nominate new MCs as drug candidates for anticancer therapy, also a screening assay was required to assess their cytotoxic potential. A cell culture assay had to be established and validated in terms of consistency with previously reported results. Such data was already available for **1**, so the isolated compound from *M. aeruginosa* CBT 480 was used as test MC for the cytotoxicity assay's establishment and validation.

#### 3.1.1. Optimization of Microcystin Extraction

The efficient and quantitative recovery of MCs from the cyanobacterial biomass demanded an extraction protocol adopted to their chemical properties, i.e. solubility and polarity. Furthermore, the right choice of solvent(s) should minimize the co-extraction of proteins, carbohydrates, lipids and other, undesired substances facilitating the subsequent MC isolation procedure significantly.

Most protocols employed mixtures of methanol and water combined with sonication or extensive stirring in order to lyse the cells, but also the use of other primary alcohols and acetonitrile are reported.<sup>361-371</sup> However, the best MC extraction rate was observed for methanol acidified with 0.05 % trifluoroacetic acid (TFA),<sup>372</sup> so 10 g lyophilized biomass of *M. aeruginosa* CBT 480 was extracted with this solvent mixture.



In total, 1.63 g crude extract was obtained from this process, and it was characterized by HPLC–DAD–MS (Table 14). The base peak chromatogram (BPC) (Figure 11A) revealed two peaks at retention times ( $t_R$ ) between 9 and 10 min, which were attributed to **1** and **2** by means of their characteristic UV spectrum (Figure 11B). The typical absorption maximum at 238 nm arises from the Adda side-chain. Since Adda is a mandatory feature of the MCs, all variants show similar UV spectra.<sup>310</sup> Furthermore, the detected molecular ions with  $m/z$  1045.6 and 995.6 were consistent with  $[1+H]^+$  and  $[2+H]^+$ , respectively.

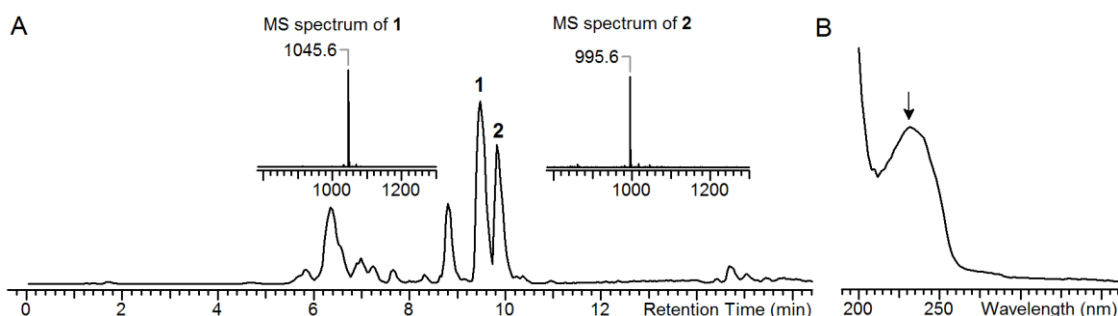


**Figure 11.** (A) Base peak chromatogram (BPC, positive mode) of a *M. aeruginosa* CBT 480 methanol extract containing MC-YR (**1**) and MC-LR (**2**). (B) UV spectrum of MC-YR (**1**) with the black arrow indicating the typical absorption maximum of MCs at 238 nm.

Since the solvent lacked an aqueous component, many lipophilic compounds, e.g. chlorophylls and fatty acids, were co-extracted, lending the extract a dark green color and oily consistence. If this crude is directly applied to semi-preparative HPLC, the lipophilic impurities can damage RP columns by irreversible binding to the stationary phase.<sup>373</sup> Thus, a further pre-purification step, i.e. flash or column chromatography, was necessary to remove these impurities prior to MC isolation via semi-preparative HPLC.

Another possibility to diminish co-extraction of lipids right from the start consists in liquid–liquid extraction (LLE) of MCs with a biphasic solvent system. These systems are composed of two or more, immiscible solvents, which form two separate phases: usually an upper, rather hydrophobic, organic layer and a lower, aqueous one. In systems with chloroform, dichloromethane, or other poly-halogenated hydrocarbons, the lipophilic phase is located below the aqueous phase due to the higher densities of halogenated hydrocarbons.

If the biomass is extracted with a two-phase system, the components partition between the phases in dependence of their polarity. This behavior is indexed by the compound's partition coefficient  $P$ , which reflects the ratio of the concentration contained in the organic phase to the concentration within the aqueous phase for an octanol–water

### 3. Results and Discussion

---

system. More frequently, the literature quotes the logP with positive values for lipophilic and negative ones for hydrophilic substances.

Although a logP of 4 classifies the MCs as rather lipophilic,<sup>374</sup> they were still expected to accumulate in water/methanol phases due to their good solubility in primary alcohols and water–methanol mixtures.<sup>375</sup> In contrast, the hydrophobic chlorophylls and fats should migrate into the organic phases and, thus, be separated from the MCs what has already been shown.<sup>367</sup>

Nine LLE systems (Table 26) were tested whether they sufficiently solubilize the MCs by simultaneously removing the lipophilic contaminants. They consisted of either *n*-hexane, butyl acetate (BuAcO), methanol (MeOH) and water, or *n*-hexane, ethyl acetate (EtAcO), MeOH and water, or chloroform, MeOH and water at three different ratios. 10 mg of CBT 480 extract was partitioned within 2 mL of each system and after drying and reconstitution in methanol, both phases were analyzed by HPLC–DAD (Table 7).

The main idea of this approach was that the MCs should quantitatively accumulate within the aqueous phase while the organic solvents would trap the lipophilic constituents hampering their co-extraction alongside the MCs. Consequently, the criteria MC extraction efficiency (MCEE), MC accumulation (MCA), and degree of co-extractions (CoE) were characterized by semi-quantitative estimations in order to assess the extraction performance. The MC peak areas were taken from the HPLC–DAD chromatograms monitored at 230 nm while the amount of impurities was determined from the UV-chromatograms recorded at 210 nm. The UV-chromatogram (210 nm) overlays of the aqueous and organic phases of each system are compiled in Figure A3–Figure A10.

The MCEE was calculated by the sum of peak areas attributed to MCs in both phases taken together, and the MCA was defined as MC peak area in each phase divided by the MCEE. Lastly, the total peak areas within the  $t_R$  window from 12–18 min corresponding to an elution with 80–100 % acetonitrile were designated as a measure for the CoE. The results are summarized in Table 26.

Surprisingly, the LLE of the CBT 480 sample caused an irreversible phase break in system 9 most likely due to the presence of amphiphilic, detergent-like compounds in the extract. This led to the formation of an extremely stable emulsion that even persisted after high-speed centrifugation, so no data were obtained for this system.

In terms of MCEE, systems 2, 3, 6, and 8 stood out as they achieved values of 1000 mAU·s and above whereas the MCEE of the other systems only ranged between 600 to 850 mAU·s indicating an incomplete recovery of MCs from the extract. Systems 1–6 were further able to quantitatively accumulate the extracted MCs at rates of 98–100 % within the aqueous phases, at which the minor loss of 1.2 % to the organic

phase of system 3 is neglectable. Solely in the chloroform-containing systems, the MCs partitioned between both phases. This was less prominent in system 8 than in 7. Still, a loss of MCs of almost 20 % is not tolerable if also low abundant congeners shall be recovered sufficiently for their isolation and bioactivity testing, so these LLE systems proved unfeasible for MC extraction.

When assessing the CoE, it was evident that nearly all systems concentrated the lipid impurities within the organic phases since the total peak areas at  $t_R$  between 12 and 17 min were distinctly lower for the aqueous phases. The only exception was system 5, in which the aqueous phase contained more hydrophobic contaminants than the organic phase out of unknown reasons. The higher CoE of the aqueous phases in system 4 and 6 also suggested that the systems with ethyl acetate performed inferior compared to systems 1–3 containing butyl acetate instead.

**Table 26.** Composition of the nine, biphasic systems and calculated parameters for assessing the extraction performance. MCEE, MC extraction efficiency; MCA, MC accumulation; CoE, degree of co-extractions; BuAcO, butyl acetate; MeOH, methanol; OP, organic phase; AP, aqueous phase; EtAcO, ethyl acetate; N/A: data not available.

N <sup>o</sup>	Solvent system	MCEE [mAU·s]	phase	MCA [%]	CoE [mAU·s]
1	<i>n</i> -Hexane : BuAcO : MeOH : H <sub>2</sub> O 8 : 2 : 8 : 2	634.6	OP	0	340.6
			AP	100	158.9
2	<i>n</i> -Hexane : BuAcO : MeOH : H <sub>2</sub> O 6.6 : 3.4 : 6.6 : 3.4	1116.9	OP	0	693.3
			AP	100	282.0
3	<i>n</i> -Hexane : BuAcO : MeOH : H <sub>2</sub> O 5 : 5 : 5 : 5	1259.4	OP	1.2	862.3
			AP	98.8	132.7
4	<i>n</i> -Hexane : EtAcO : MeOH : H <sub>2</sub> O 8 : 2 : 8 : 2	704.2	OP	0	463.8
			AP	100	327.7
5	<i>n</i> -Hexane : EtAcO : MeOH : H <sub>2</sub> O 6.6 : 3.4 : 6.6 : 3.4	658.7	OP	0	270.3
			AP	100	327.9
6	<i>n</i> -Hexane : EtAcO : MeOH : H <sub>2</sub> O 5 : 5 : 5 : 5	1372.3	OP	0	548.4
			AP	100	226.7
7	CHCl <sub>3</sub> : MeOH : H <sub>2</sub> O 12 : 6 : 2	846.1	OP	46.4	549.7
			AP	53.6	185.2
8	CHCl <sub>3</sub> : MeOH : H <sub>2</sub> O 1 : 1 : 1	1050.0	OP	18.7	542.3
			AP	81.3	6.2
9	CHCl <sub>3</sub> : MeOH : H <sub>2</sub> O 5 : 12 : 3	N/A	OP	N/A	N/A
			AP	N/A	N/A

### 3. Results and Discussion

---

Since ethyl acetate is less hydrophobic, it is better miscible with methanol and water, decreasing the polarity of the aqueous phase so lipophilic compounds were better solubilized. The least CoE was found for system 8, in which almost none late eluting components were detectable.

Taking all three parameters, MCEE, MCA, and CoE into account, the best LLE performance was observed for systems 3 and 6. They attained a decent recovery of MCs from the extract and accumulated them in the methanol/water phase by simultaneously withdrawing lipophilic constituents into the organic phase. Although system 6 was superior regarding the extraction efficiency, the LLE with system 3 was taken up as standard method into the optimized workflow because the extent of impurity co-extraction was more favorable. Especially when the extract input is scaled-up for preparative LC, a smaller load of chlorophylls and lipids wears down the HPLC columns less rapidly.

Interestingly, LLE systems consisting of equal parts of *n*-hexane and *n*-butanol or ethyl methyl ketone were described for the MC purification before.<sup>367</sup> They also proved highly capable of removing lipid substances from the MCs but did not perform as well as the systems 3 and 6. Due to their formation of an additional intermediate phase, the MCs spread over two layers and did not accumulate within the polar one. In the present study, this effect was only discernible for the chloroform-containing systems with an almost 1:1 distribution of the MCs in system 7.

Despite all its benefits, the LLE with system 3 also bore a major, not-anticipated drawback. The high water content of the aqueous phase facilitated a notable extraction of hydrophilic impurities, especially polysaccharides, which have similar, detrimental effects on HPLC columns as strongly hydrophobic compounds. Consequently, the extract obtained from LLE with system 3 is not suitable for the direct use in semi-preparative HPLC either.

In order to circumvent this problem, two studies applied *n*-butanol as a water-immiscible solvent to extract the MCs from an aqueous sample.<sup>370,371</sup> Due to their higher affinity towards primary alcohols, the MCs migrate into the *n*-butanol layer while sugars, amino acids and other water-soluble analytes remain in the aqueous phase. Thus, the dried, MC-containing aqueous phase of system 3 was dissolved in a two-phase system made from *n*-butanol and water, and extracted with *n*-butanol in three cycles.

After drying and reconstitution in methanol, the samples of the three *n*-butanol phases and the aqueous phase were analyzed by HPLC–DAD (Table 7). The UV chromatogram overlay in Figure 12 illustrates that the MCs at  $t_R$  8.83 (**1**) and 9.15 min (**2**) were enriched within the *n*-butanol layer of the first extraction step (black) and they remained detectable in the second (blue) and third (grey) extraction step as well. Only minor, hydrophilic

impurities ( $t_R$  window from 1.5–4 min) were present in all three organic layers, but they accumulated in the aqueous phase (red trace). The aqueous phase did not show any signals of MCs, indicating a quantitative MC accumulation within the *n*-butanol layers.

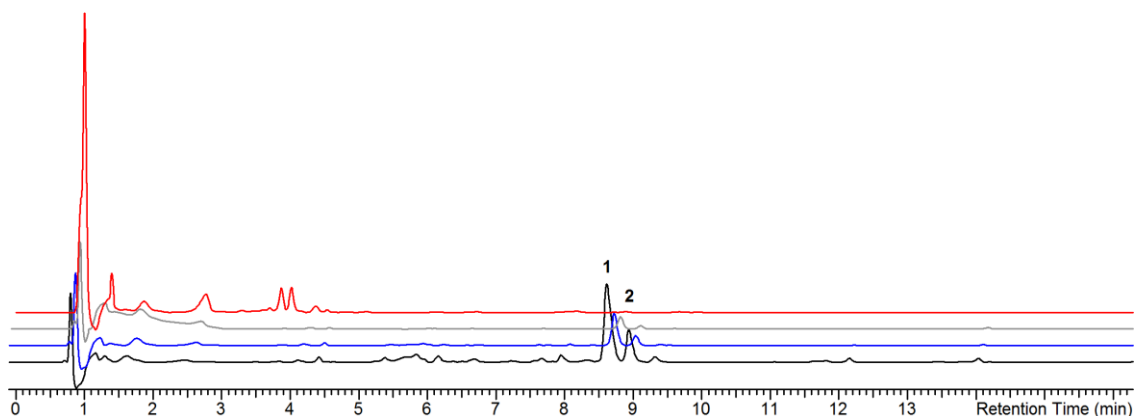


**Figure 12.** UV chromatogram (230 nm) overlay of the *n*-butanol layers obtained from three subsequent extraction steps (black, first step; blue, second step; grey, third step) and the aqueous phase (red, upper trace) obtained from a *M. aeruginosa* CBT 480 sample containing MC-YR (1) and MC-LR (2).

Conclusively, the process proved feasible for removing the hydrophilic contaminants while minimizing the loss of the target molecules. Since the two-stage LLE with complementary, biphasic systems eliminated most of the hydrophilic and hydrophobic compounds, the resulting fraction is sufficiently pre-purified for direct subjection to semi-preparative HPLC.

In an attempt to merge the two steps into one and reduce the time for extraction by half, a three-phase system was tested, which formed a lower aqueous, an intermediate methyl acetate/acetonitrile layer, and an upper organic phase with *n*-hexane.<sup>376,377</sup> 2 g of lyophilized biomass of *M. aeruginosa* CBT 480 was extracted in three cycles with a ternary system consisting of 13 mL *n*-hexane, 13 mL methyl acetate, 10 mL acetonitrile and 13 mL water. After drying and redissolving in methanol, composition of the three phases was analyzed by HPLC–DAD (Table 7).

Notwithstanding the assumption that the MCs would concentrate in the intermediate phase, the main MC peaks appeared within the aqueous layer (red trace), as it is visible in the chromatogram overlay in Figure 13. Since the intermediate phase was mainly composed of methyl acetate/acetonitrile, it was probably not polar enough to extract the MCs, and they migrated into the aqueous layer. Additionally, notable amounts of hydrophilic impurities were observed as well, and the aqueous phase of the ternary system was composed similarly to the corresponding phase of system 3. Thus, the ternary solvent system did not offer any advantage over the two-stage protocol.

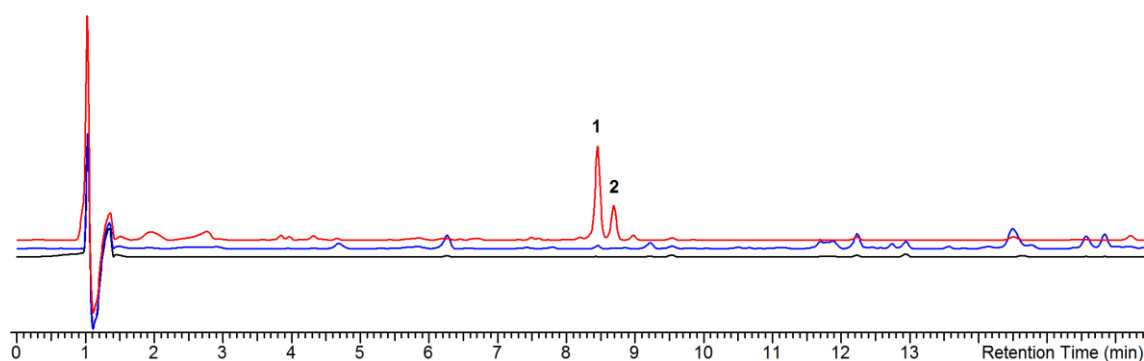


**Figure 13.** UV chromatogram (230 nm) overlay of the upper (black, lower trace), intermediate (blue, middle trace) and aqueous (red, upper trace) phases of the ternary solvent system used for extraction of *M. aeruginosa* CBT 480 containing MC-YR (1) and MC-LR (2).

In summary, two extraction protocols for MCs were established, which can be applied in dependence of the analytical question and purpose. The extraction with methanol/0.05 % TFA poses a fast and easy way for the qualitative characterization of cyanobacterial biomass samples regarding their MC content. If the MCs shall be isolated quantitatively from biomass samples between 1 and 100 g, the two-step LLE provided a fast and feasible method because the resulting extract is suitable for MC isolation by semi-preparative HPLC right away.

Nevertheless, this procedure was difficult to apply to large batches (> 100 g lyophilized biomass) as the handling of big volumes is limited to the laboratory equipment, e.g. size and weight of the (filled) separation funnel. With increasing volumes of the phases, also thorough and prolonged mixing is crucial for a proper partition of the components so manual shaking would not only be tiring but also insufficient.

Thus, a specialized extraction apparatus would have been necessary, which included fixtures for mechanical cell lysis and an outlet valve on the bottom for phase separation. Since this type of instrument was not available in all laboratories, and splitting of the sample into several extraction cycles would have been too tedious, large bulks needed to be extracted with methanol/0.05 % TFA. For the work-up of this crude extract, further pre-purification protocols were required, e.g. by flash or column chromatography.

#### 3.1.2. Pre-Purification by Flash and Size Exclusion Chromatography

During the 1980s and 1990s, various chromatographic techniques were developed for the isolation of MCs and comprehensively reviewed.<sup>365,378-381</sup> Frequently applied methods covered gravity column chromatography on NP or RP silica beds, size exclusion chromatography (SEC) on Sephadex materials, and ion exchange chromatography, as well as combinations thereof.

As a modification of classic glass columns, silica-based stationary phases were packed into pressure-resistant plastic cartridges, so a (binary) pump could be connected for transferring the mobile phase at a higher flow rate and enabling the elution with a continuous gradient. This technique became known as flash or medium pressure liquid chromatography if a pressure above 10 bar is achieved. Both are precious tools for the pre-purification of extracts obtained from biological samples.<sup>382,383</sup>

Because of the high flow rates, the overall run times usually lie between 30 and 60 min, reducing the time for analysis by more than 20-fold compared to gravity column chromatography. Furthermore, the cartridge capacities range up to 75 g of analyte mixture. These two advantages make flash chromatography highly suitable for the processing of crude extracts from large-scale samples.

Flash chromatography, mainly on RP-C<sub>18</sub> modified silica, was already employed for the fractionation of MC-containing samples using water acetonitrile or water/methanol as mobile phases.<sup>384-387</sup> Yet, it mostly represented the last step in the course of MC isolation and the samples were already characterized by a high degree of purity, so no information was provided whether high-abundant impurities were removed with similar efficiency. As these drawbacks hampered the direct method transfer, a new protocol needed to be developed for the application of flash chromatography to the extracts.

The methanol extract of CBT 480 was loaded on a Sepacore C<sub>18</sub> flash cartridge, and several chromatographic conditions were tested. The optimum gradient was found to be 30–80 % methanol in water over 40 min with fraction collection in 1-minute intervals. Online monitoring by DAD facilitated the direct identification of the MCs. Five fractions containing **1**, two fractions containing both **1** and **2**, and four fractions containing **2** were obtained. Identically composed fractions were pooled and dried, and after reconstitution in methanol, they were analyzed by HPLC–DAD (Table 7) in order to determine their degree of purity.

The chromatograms of the **1**- and **2**-containing fractions (Figure 14) disclosed only minor impurities in the medium polar range. The lipophilic contaminants were adequately removed. Consequently, flash chromatography afforded a sample ready for semi-preparative HPLC by simultaneous separation of the MCs. The overlapping fractions with both variants can be recycled in later isolation processes. Interestingly, the **1**-containing fraction (Figure 14A) was exceptionally clean considering that it was obtained from the extract after one chromatographic separation. However, neither the resolution of **1** and **2**, nor the degree of purity could be reproduced in the following experiments, and the  $t_R$  of the MCs shifted dramatically from run to run. This may be due to the reuse of the flash cartridge, which is actually designed for single-use only.

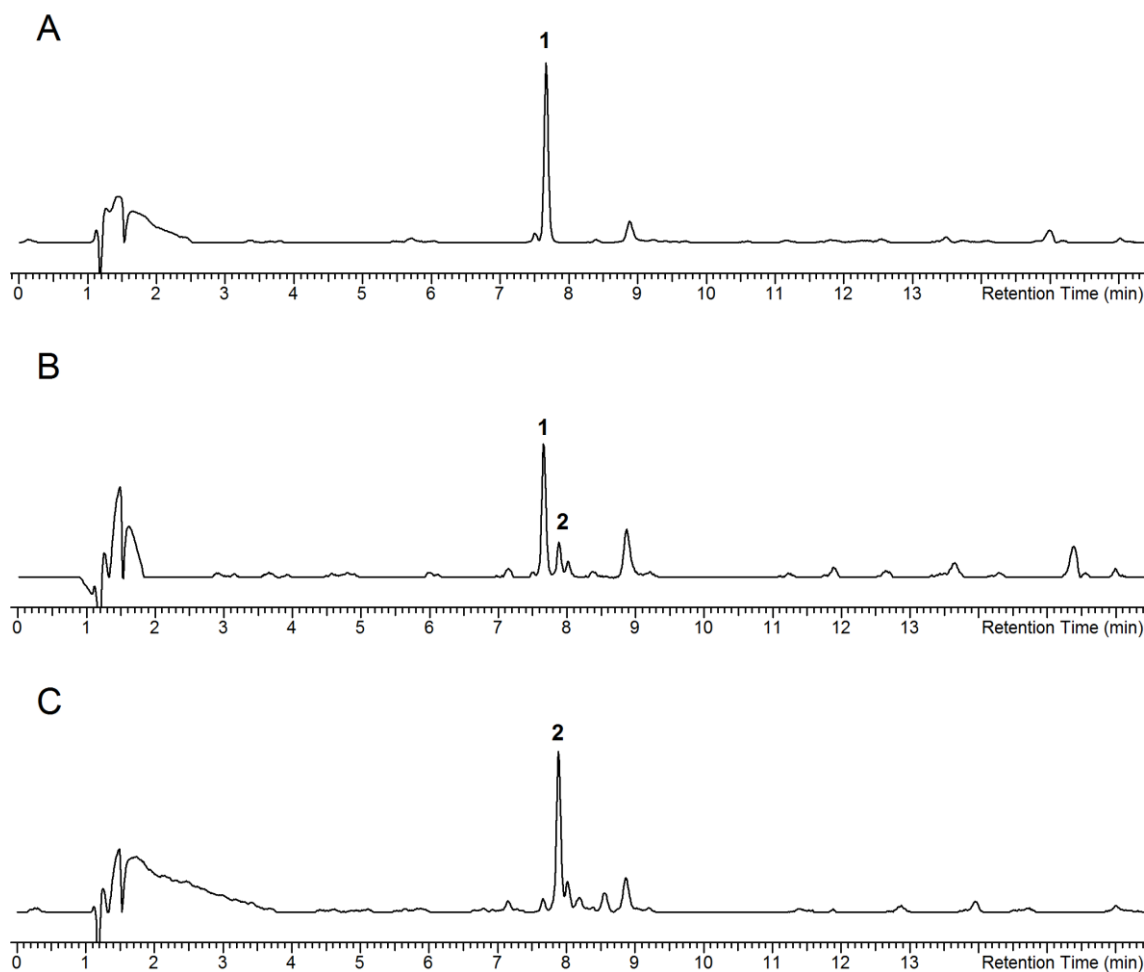


**Figure 14.** UV chromatograms (230 nm) of MC-containing fractions obtained from the fractionation of the methanol extract of *M. aeruginosa* CBT 480 by flash chromatography. The fractions either contained (A) MC-YR (**1**), (B) both, MC-YR (**1**) and MC-LR (**2**), or (C) MC-LR (**2**) only.

Analogously to RP-HPLC columns, the quality of the stationary phase declines by multiple usage due to the irreversible binding of lipophilic compounds. This reduces the performance and reproducibility over time, impeding the predictability how well the single MCs will be resolved. Since the use of a new RP-C<sub>18</sub> cartridge for each run would have been too costly, it needed to be carefully pondered whether this drawback was bearable or if methods relying on other chromatographic principles might have been superior.

For instance, gel filtration on Sephadex columns represents a technique that is orthogonal to LC on stationary phases with silica. Whereas herein, the analytes are separated by their interactions and adsorption on the stationary phase, mainly size exclusion effects are responsible for analyte retention on Sephadex column beds. The materials consist of a three-dimensional network of cross-linked polydextran chains. Most often, Sephadex LH-20 is used, where the sugar units are modified with hydroxypropyl groups prior to polymerization to increase the lipophilicity of the matrix.<sup>388</sup>



When the dry Sephadex LH-20 powder is suspended in liquids, it swells and forms a gel with regularly sized pores. The degree of swelling and the pore size depends on the polarity of the solvent: the higher the hydrophilicity, the smaller the pores and, thus, the better the retention of small molecules. In addition to these size exclusion mechanisms, also adsorption processes at the polymer affect the separation, but only to a minor degree.

For the purification of MCs, column chromatography with Sephadex LH-20 in methanol proved useful for the removal of pigments and large proteins.<sup>389-394</sup> The MCs with their molecular weight (MW) of around 1000 Da were well retained within the medium-sized pores while the high molecular proteins passed right through the column. Replicating this approach, a glass column was packed with Sephadex LH-20 in methanol and loaded with the methanol extract of *M. aeruginosa* CBT 480. The sample was eluted over 21 h with a flow rate of 30 mL/h resulting in 63 fractions by collecting every 20 minutes.

Since no optical detector was available, every single fraction had to be checked for the presence of MCs by analytical HPLC–DAD (Table 7). Judging from the  $t_R$ , fraction 14 contained **2** only, and within the subsequent two, 15 and 16, both variants were detected followed by number 17 with **1** only (Figure A11). Additionally, three to five other substances were present in all four samples.

Despite the higher MW of **1** with 1045.5 Da, it eluted more slowly from the size-exclusion column than **2** with a MW of 995.5 Da, demonstrating the impact of adsorption processes in SEC with Sephadex LH-20. The additional hydroxyl group seemed to intensify the hydrophilic interactions between **1** and the dextran chains of Sephadex LH-20 to such an extent that it was better retained on the column than the smaller MC-LR. Considering that these effects are even more prominent when the polarity of the solvent increases and the matrix swells more extensively, SEC on Sephadex LH-20 might also be capable of providing a baseline separation of **1** and **2** by addition of water to the mobile phase.

Thus, employing 50 % (v/v) methanol in water as solvent was hypothesized to resolve the two congeners better, and another gravity column was prepared accordingly. After loading the methanol extract of *M. aeruginosa* CBT 480, the analysis ran for 24 h at a flow rate of 27 mL/min with the interval of the fraction collector set to 20 minutes. The fractions were characterized by analytical HPLC–DAD (Table 7). The higher degree of matrix swelling also caused the pores to shrink so the MCs dwelled longer on the column and **2** was not detected until fraction 40 to 43. After two intermediate fractions without any MCs, **1** followed in fraction 46 to 48 (Figure A12). The UV chromatograms also

### 3. Results and Discussion

revealed only few other compounds, so the MCs can be directly isolated from the pooled fractions.

Figure 15 outlines the distribution of the two MC congeners for the SEC experiments with (A) methanol and (B) 50 % (v/v) methanol in water by plotting the relative abundance of **1** and **2** in each fraction obtained from integration of the peak areas in the UV chromatograms. In both set-ups, **2** eluted first (black line in Figure 15) and spreads over four fractions. The red line indicates that **2** can mainly be found in three fractions, which are 16–18 in Figure 16A and 46 to 48 in Figure 16B.

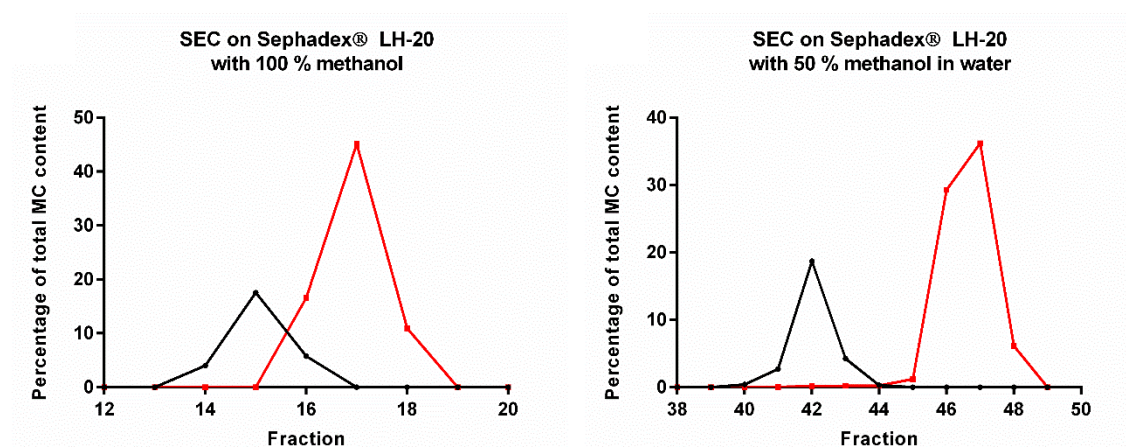


**Figure 15.** Distribution of MC-LR (black) and MC-YR (red) over fractions obtained from SEC on Sephadex LH-20 with (A) 100 % methanol and (B) 50 % (v/v) methanol in water.

Interestingly, the resolution of **2** and **1** improved by increasing the polarity of the solvent. Whereas the two lines overlapped in Figure 15A and both variants co-eluted in fraction 16 with methanol, the use of 50 % (v/v) methanol led to a true baseline separation yielding the MC-free inter-fraction 44. As expected, the extent of adsorption processes and hydrophilic interactions augmented due to the more extensive swelling of the Sephadex LH-20 material so **1** was relatively better retained than **2**, increasing the  $t_R$  gap between the two variants.

Two further trials confirmed the reproducibility of these findings by maintaining the baseline separation of the MCs, but the degree of resolution decreased slightly. This may be caused by recycling of the stationary phase, which compromised the retention capacity over time. A good deal of the column bed further got lost in repetitive cycles of column filling, emptying and re-preparation. However, this can easily be come by with thorough washing of the material with different organic solvents and replacing the lost material.

In conclusion, the performance of SEC was significantly higher with aqueous methanol than methanol only. Both chromatographic steps were equally able to remove hydrophobic impurities, e.g. chlorophylls, but with 50 % methanol in water as eluent, the MCs were already pre-separated, facilitating the final isolation process. However, employing an aqueous portion in the mobile phase led to a 2- to 3-fold increase in analysis run time. When compared to flash chromatography, gel filtration on Sephadex LH-20 turned out to be superior in terms of MC resolution and reproducibility, while both methods produced equally pure fractions for semi-preparative HPLC.

However, the low loading capacities on Sephadex LH-20 are a major disadvantage: even for the largest glass columns available, the loading capacity is restricted to a few hundreds of milligrams. Additionally, the long run times of 24 h, and the need to re-prepare the column in between individual runs render repetitive SEC of a single sample inefficient and time-consuming. Hence, flash chromatography on a RP-C<sub>18</sub> cartridge is the method of choice for large batches of cyanobacterial biomass when a crude extract with several grams is obtained. For smaller samples that still require an extraction with methanol and yield 500 mg of extract or less, gel filtration on Sephadex LH-20 is more suitable as pre-purification step before the MCs are isolated by semi-preparative HPLC.

#### 3.1.3. Isolation of Microcystins by Semi-Preparative HPLC

Pure MCs were mostly prepared by (semi-)preparative HPLC on RP-C<sub>18</sub> columns with either isocratic or gradient elution.<sup>364,365,395-410</sup> The mobile phases included mixtures of acetonitrile and water, or methanol and water with TFA or formic acid (FA) as modifiers. Although some studies also reported the use of ion exchange chromatography or hydrophilic interaction liquid chromatography, these methods did not prevail, and HPLC on C<sub>18</sub> columns emerged as the standard method for MC analysis.<sup>411-415</sup>

With the technical progress, manifold new modifications of silica evolved for RP-HPLC. Nowadays, dozens of such stationary phases are commercially available.<sup>416-418</sup> Especially aromatic ligands, such as phenylhexyl (PH) or pentafluorophenyl (PFP), are of immense interest for the separation of MCs as they do not only interact with the analytes by standard, hydrophobic adsorption and partitioning processes, but also by  $\pi$ - $\pi$  stacking of aromatic residues.<sup>419-423</sup>

All MCs share the aromatic Adda side chain as common, structural element and, thus, should feature an overall good affinity to aromatic, stationary phases. Furthermore, some variants possess an additional aromatic amino acid in either one or both variable

### 3. Results and Discussion

---

positions. Due to the stronger  $\pi$ - $\pi$  electron interactions, they should elute notably later than derivatives with aliphatic residues in positions 2 and 4.

In order to test this hypothesis, the separation was evaluated on three different analytical columns: a Luna C<sub>18</sub>, a Luna PH, and a Luna PFP column, all of them identical in length, diameter, particle and pore size. As test mixture, pre-purified fractions from flash and size exclusion chromatography containing **1** and **2** were pooled, dried, and dissolved in methanol. The mobile phase composition and all other parameters are specified in Table 9.

Firstly, a gradient from 20–50 % acetonitrile in water over 20 min was applied and, for assessing the MC separation quality, the peak resolution R on each column was calculated according to the formula

$$R = \frac{t_{R2} - t_{R1}}{\frac{1}{2} (W_1 + W_2)}$$

with W referring to the total peak width in min.<sup>424</sup> The results are summarized in Table 27. Since the Luna PH column even revealed a lower resolution of the MCs than the Luna C<sub>18</sub> column, it was omitted from further gradient optimization. For the other two stationary phases, the gradient was adjusted to 30–60 % acetonitrile in water over 20 min in order to shift the MC peaks to an earlier  $t_R$ . The resulting chromatograms of the optimized gradients recorded at 230 nm are shown in Figure 16.

**Table 27.** Peak resolution R of MC-YR (**1**) and MC-LR (**2**) on a Phenomenex Luna PH, C<sub>18</sub>, and PFP column eluted with two different gradients. PH, phenylhexyl; PFP, pentafluorophenyl.

Column	Gradient	R
Luna PH	20–50 % acetonitrile in H <sub>2</sub> O	2.48
Luna C <sub>18</sub>	20–50 % acetonitrile in H <sub>2</sub> O	2.60
	30–60 % acetonitrile in H <sub>2</sub> O	2.64
Luna PFP	20–50 % acetonitrile in H <sub>2</sub> O	6.16
	30–60 % acetonitrile in H <sub>2</sub> O	6.13

The calculated R of around 2.6 as well as the black chromatogram in Figure 16 illustrate that the Luna C<sub>18</sub> achieved a proper baseline separation of **1** and **2** irrespective of which of the two gradients was employed. Theoretically, this would be satisfactory for the isolation of both variants, but the scale-up to a semi-preparative dimension may still be problematic due to the often-observed decline in chromatographic performance on

bigger columns. Furthermore, care must be taken not to overload the column since the resulting peak broadening and tailing impair the separation efficiency, and cause the substances to co-elute, contradicting the often-used practice of column over-loading in preparative chromatography.

By contrast, **1** and **2** were separated on the PFP phase with a 2.3-times higher  $R$  with either of the two gradients. As apparent from the red chromatogram in Figure 16, the aromatic modification increased the difference in  $t_R$  to 1.12 min compared to only 0.18 min on the  $C_{18}$  phase, and furthermore, delayed the elution of the MCs by 6–7 min. This confirms the assumption that the  $\pi$ – $\pi$  stacking effects between Adda and the PFP residues strengthen the interaction of the MCs and the stationary phase, leading to a better analyte retention. HPLC–MS analysis (Table 14) identified the first eluting peak as compound **2**, while the second peak was attributed to **1**. This confirms the hypothesis that the additional aromatic residue in **1** amplifies the impact of the  $\pi$ – $\pi$  stacking effects leading to later elution and, thus, reversing the elution order of **1** and **2** compared to standard  $C_{18}$  columns.

The extra-ordinary high resolution of the two MC variants enabled an easy scale-up to a semi-preparative Luna PFP column (Table 16), without needing to mind the loading capacities. The dried *n*-butanol phase obtained from two-step LLE was reconstituted in methanol and fractionated in 14 runs, at which compounds **1** and **2** were collected.

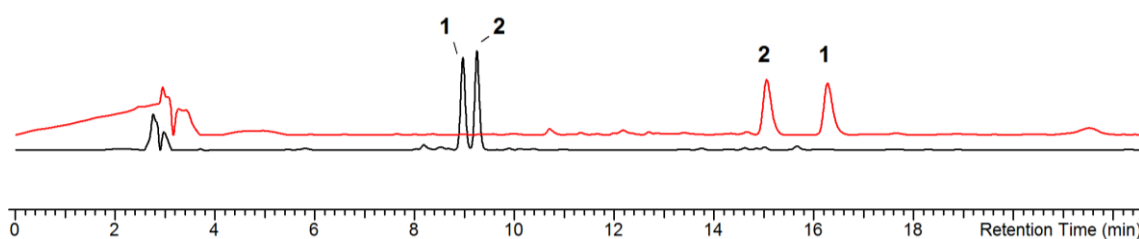


**Figure 16.** UV chromatogram (230 nm) of a sample containing MC-YR (**1**) and MC-LR (**2**), analyzed on a Luna  $C_{18}$  (black trace) and Luna PFP (red trace) column applying a gradient from 30–60 % acetonitrile in water.

Although **1** was separated from **2** properly and no co-eluting substances were notable during fractionation, HPLC–DAD (Table 7) still uncovered about 10 % impurities at a wavelength of 210 nm in both samples. Since the MCs were meant for the use in bioactivity assays, they needed to be as pure as possible. All contaminants had to be removed prior to testing, necessitating another isolation step via semi-preparative HPLC.

### 3. Results and Discussion

---

An optimized gradient from 30–50 % acetonitrile in water on a Luna C<sub>18</sub> column proved feasible for the purification of **1**. After scaling up to semi-preparative dimensions (Table 17) **1** was isolated with high purity according to the UV (210 nm), the evaporative light scattering detector (ELSD), and total ion chromatogram (TIC; Figure A13).

In case of **2**, the procedure was not as straightforward. The method development involved a number of isocratic, gradient, and step gradient elution modes on an analytical Luna C<sub>18</sub> column. In the end, a shallow gradient from 30–40 % acetonitrile in water over 18 min led to a baseline separation of the sample constituents. The method was scaled up to suit a 10 mm column (Table 18) and **2** was purified with comparable purity as **1** (Figure A14).

With this final step, the isolation procedure was completed, and the isolated MCs matched the mandatory purity standard for the cytotoxicity screening. Though a single, all-in-one isolation method for semi-preparative HPLC would have been preferable, this two-step approach is still expedient, and the additional time expenses are tolerable.

One aspect that also needed to be considered in this context is the high heterogeneity of cyanobacterial samples. The template biomass from *M. aeruginosa* CBT 480 was rather simple in terms of metabolite composition and MC content with two variants only. Indeed, much more derivatives can occur within one strain, so the methods always have to be adapted to the respective analytical question.<sup>161,202,409,425</sup> There will never be a Swiss Army knife for the isolation of MCs via semi-preparative HPLC.

With increasing complexity of the sample, also the amounts of the single MCs vary significantly. Their general production rate is already very low, and the amount of **1** and **2** isolated from 1 g extract during the course of method development was less than 1 mg, which hampered an accurate gravimetric determination with standard laboratory balances. This problem became even more eminent when minor, low abundant MC congeners were isolated. However, knowing the exact amount of test substance was crucial for bioactivity testing since otherwise, the calculation of the 50 % inhibition or efficacy concentration (IC<sub>50</sub> or EC<sub>50</sub>, respectively) would have been incorrect. This fact highlights the necessity of a precise quantification method, which could be applied to every MC variant irrespective of the chemical structure.

#### 3.1.4. Quantification of Microcystins by HPLC–ELSD

At the early stages of MC analysis, HPLC–UV with single wavelength monitoring or DAD was the only reliable technique available for quantification.<sup>415</sup> Due to the easy and straightforward method development and low priced instrumentation, this approach is still frequently applied and was even included in the current ISO guidelines for MC analysis.<sup>369,426–435</sup>

Yet, the optical properties strongly depend on the chemical structures, and since the molar absorptivities differ between the single MCs, an appropriate calibration standard for each congener is mandatory.<sup>436,437</sup> Chemical reference materials (CRM) are only available for a few MCs, so the quantitation of new or uncommon variants would come with a high uncertainty. Out of this reason, HPLC–UV was inept for the purpose of this study, in which a universal method for all MCs was required.

With the advances in protein production and purification, complementary, biochemical techniques arose, which were mostly based on the immunological recognition of MCs.<sup>438–440</sup> Especially enzyme-linked immunosorbent assays (ELISA) enjoyed enormous popularity, so many kits for the in-field use were launched on the market during the past years.<sup>245,441–452</sup> Simultaneously, enzymatic assays utilizing the bioactivity of PP inhibition were developed for the quantitative estimation of MCs with comparable detection limits and performances.<sup>431,432,435,455–456</sup>

Both assays were designed for the quantitation of the overall MC content in a structure-independent manner, fulfilling the most important requirement for the aforementioned application. The lack of a chromatographic step, however, hampers the discrimination of the single MCs regarding their identity and individual abundances. This drawback was negligible as the MCs will already be purified and characterized prior to quantification.

Still, direct coupling to a HPLC system was highly desirable, so the purity assessment and quantitation can be carried out within one run instead of two separate experiments. Three studies reported a post-column, offline detection of MCs by ELISA and/or PP inhibition assay for HPLC.<sup>457,458</sup> After fractionation into a microtiter plate, the fractions served directly as samples for the assays without solvent evaporation or other intermediate steps. However, the pipetting and read-out of the assays still had to be done manually, and the microtiter plates needed to be prepared, e.g. coated with antibody in case of ELISA. Taking all of this together, this procedure is more time-consuming than quantification with an online detector directly coupled to the HPLC, and not feasible for medium through-put analysis.

### 3. Results and Discussion

---

Much progress was made in the development of quantitative MS and tandem-MS techniques, mostly coupled to LC via electron spray ionization (ESI), but also matrix-assisted laser desorption ionization for the analysis of dry, crude samples has been described.<sup>459–469</sup> Since the ionization efficiency diverges from one run to the other, the use of an internal standard (IS) is recommended in addition to the external calibration.<sup>470–472</sup> Stunningly, only half of the cited approaches mention an IS at all: most often, other peptides such as enkephalin or nodularin were used, and only in four publications the gold standard was employed, an isotopically labeled MC.<sup>459,462,468,473</sup> For the present study, nodularin or enkephalin did not suit as IS as the method needed to be transferable to different mass spectrometers without requiring a re-validation, so the use of isotopically labelled MCs would have been inevitable. Since neither these nor CRM standards for external calibration are easily accessible, MS was no option for the quantification of MCs either.

Another mass-sensitive detector for HPLC is the evaporative light scattering detector (ELSD).<sup>474</sup> Evaporative light scattering belongs to the aerosol-based detection techniques and was used for the quantification of a broad spectrum of substances.<sup>475–485</sup> Remarkably, the chemical structures of the analytes only have little impact on the signal response, enabling the application of ELSD as a universal quantification method for many, structurally diverse natural products.<sup>486</sup> Still, aerosol-based detection of MCs is only found once within the literature for the purpose of MC purity assessment, because in contrast to DAD, ELSD also uncovers contaminants without chromophore.<sup>396</sup> Consequently, a suitable HPLC–DAD–ELSD method would provide reliable information about both, MC content and the degree of purity, within one run.

Firstly, the chromatographic parameters were optimized in terms of peak shape and detector response. The general method set-up comprised a RP-C<sub>18</sub> analytical column and acetonitrile and water (both with 0.1 % FA) as mobile phase. Furthermore, CRM MC-RR and MC-LR were used for method development. Due to the different boiling points of acetonitrile and water, the response of the ELSD varies in dependence of the mobile phase composition.<sup>487,488</sup> Out of this reason, an isocratic elution is preferred over a gradient in order to ensure a uniform evaporation of the mobile phase throughout the analysis.

However, gradient elution gave sharper peaks and facilitated the detection of impurities. This effect was even more pronounced by switching from a porous silica Nucleosil 100 C<sub>18</sub> column (Table 7; modified ELSD setting: gain 11) to a core-shell Kinetex C<sub>18</sub> column with 2.6 µm particle size (Table 10). The peak height increased more than threefold whereas the peak width was reduced by more than a half (Figure 17). In



addition to the detector response, the background noise was slightly higher, but it did not interfere with peak integration.

The design of the core-shell column accounts for shorter diffusion paths of the analytes, resulting in sharper peaks and a better separation.<sup>489–491</sup> The latter is further enhanced by the smaller particle size, increasing the ratio of stationary phase to carrier material and, thus, the number of theoretical plates. Since these columns produce a comparable peak resolution in shorter run times than those with porous silica, the method was reduced to a gradient ramp of 10–100 % acetonitrile in water (both with 0.1 % FA) over 10 min.

As a result, the resolution of MC-RR and MC-LR decreased. The new  $t_R$  of 5.1 and 5.9 min corresponded to mobile phase compositions of 55.9 % and 63.1 % acetonitrile in water, respectively. This minor difference is neglectable in terms of ELSD response, and the gradient elution represents an acceptable compromise for the detection of impurities and an exact quantitation of MCs.

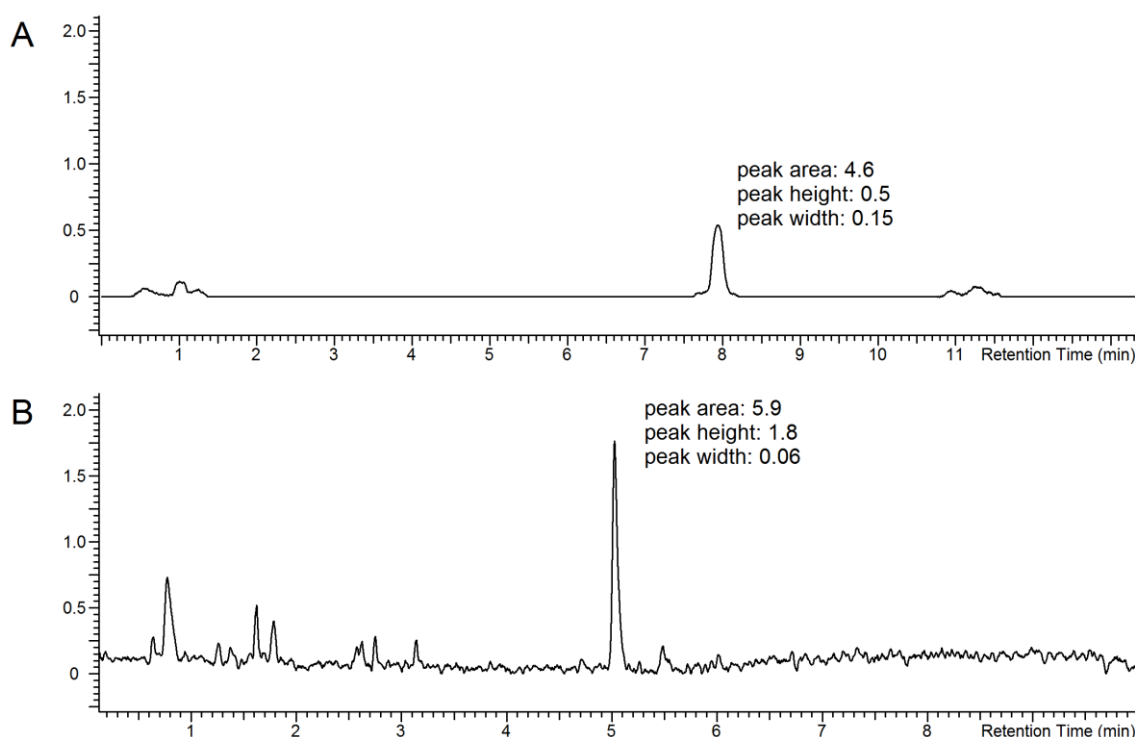


**Figure 17.** (A) HPLC–ELSD chromatogram of CRM MC-RR (51.4 ng on-column) using a porous-silica Nucleosil 100 C<sub>18</sub> column. Peak area, height, and width of the peak of MC-RR are depicted in the chromatogram. (B) HPLC-ELSD chromatogram of CRM MC-RR (51.4 ng on-column) using a core-shell Kinetex C<sub>18</sub> column. Peak area, height, and width of the peak of MC-RR are depicted in the chromatogram.

### 3. Results and Discussion

---

When the chromatographic conditions were fully set, the ELSD parameters were optimized in a second step. One crucial setting is the appropriate evaporation temperature. Whereas the mobile phase is insufficiently vaporized at values below 40 °C, elevated temperatures of 60 °C and more are prone to decompose or sublime the substances.<sup>484,492–494</sup> For MC-RR, the signal intensity was best at 40 °C and did not improve by raising the evaporation temperature to 50 or 60 °C, respectively.

Lastly, the signal-to-noise ratio (SNR) was regulated by adjustment of the digital signal amplification, also referred to as gain. Starting at 8, the gain was sequentially increased by increments of 1. When set to 11, the best detector response was observed while the background noise remained low. Higher values just raised the background noise disproportionately.

The final HPLC and ELSD settings are summarized in Table 10. Next, the method was validated by determining the following specifications: linearity, accuracy, intra- and inter-day precision, which both are an indicator for reproducibility, the limit of detection (LOD), and limit of quantification (LOQ).<sup>495</sup> The specificity as well as the selectivity were excluded from the validation because the method was meant for the analysis of pure compounds only, and interfering effects of the matrix could be ruled out.

CRM MC-RR was used as external calibrant. Five different amounts between 100 and 300 ng were injected in order to establish a calibration curve. Since the ELSD signal correlates with the analyte quantity in an exponential manner, a linear correlation is obtained by plotting the logarithmic values according to the following equation:

$$\log A = a \cdot \log m + b$$

in which A refers to the ELSD response area and m to the amount of analyte, while a and b describe the slope and y-intercept, respectively.<sup>494</sup> Figure 18 depicts the calibration curve with its equation and the goodness of fit, which was deduced from linear regression as  $R^2 = 0.991$ , indicating a suitable linearity. The logarithmic transformation, however, limits the applicability to the selected range.

Subsequently, the ability of a structure-independent quantification was verified by injection of 150 and 200 ng CRM MC-LR. The theoretical amount calculated from the calibration curve of MC-RR was compared to the true value, and the degree of consistency was defined as measure for accuracy, as shown in Table 28. Each sample was analyzed in triplicate, and the whole sequence including the calibration was repeated on two further days, from which the intra- and inter-day precisions were estimated, respectively.

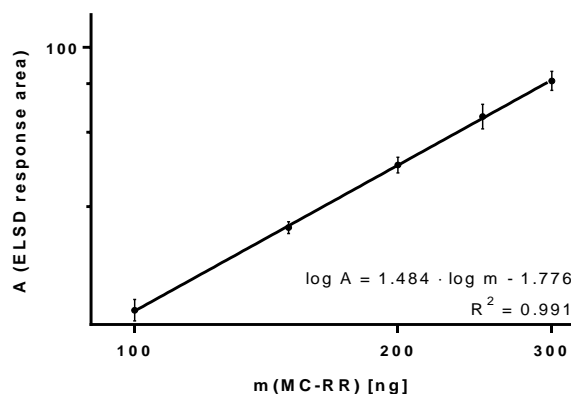


**Figure 18.** ELSD calibration curve obtained from five different amounts of CRM MC-RR (100, 150, 200, 250, and 300 ng) on column by plotting the log(ELSD response area) against the log(amount of MC-RR). The equation and goodness of fit ( $R^2$ ) are depicted in the graph.

Regarding the values of the single sequences, 200 ng MC-LR was determined with a higher accuracy than 150 ng, and the intra-day precision also proved superior as characterized by the mostly lower standard deviations. The superior accuracy is reflected in the average, which comes close to 100 % for 200 ng MC-LR. No notable differences were observed for the inter-day precision, whose values converge around 1 ng and 0.7 % for both amounts, respectively. In summary, all values for accuracy, intra- and inter-day precision lie in an adequate range, qualifying this HPLC–ELSD method for a valid, structure-independent quantification method of MCs.

**Table 28.** True and calculated values of CRM MC-LR, and the respective accuracy determined in three independent sequences including the respective standard deviations. The average of the three independent measurements and their corresponding standard deviation (inter-day precision) were further calculated from these values.

True [ng]	Calculated values [ng]/ accuracy [%]			Average	Inter-day precision
	1 <sup>st</sup> sequence	2 <sup>nd</sup> sequence	3 <sup>rd</sup> sequence		
150	152.5 ± 2.12	152.4 ± 5.75	154.2 ± 2.89	153.0 ng	± 0.99 ng
	101.7 ± 1.41	101.6 ± 3.83	102.8 ± 1.93	102.0 %	± 0.66 %
200	201.2 ± 2.03	202.6 ± 1.32	199.5 ± 5.72	201.0 ng	± 1.42 ng
	100.6 ± 1.01	101.2 ± 0.65	99.8 ± 2.86	100.5 %	± 0.71 %

External circumstances prompted the transfer of the method to a new laboratory and a different experimental set-up. Instead of an Agilent 1260 Infinity, the HPLC instrumentation comprised a Thermo Scientific UltiMate 3000, but still coupled to the

### 3. Results and Discussion

---

same model of ELSD, so these parameters were not changed. The column and CRM also remained the same. The new method specifications are compiled in Table 11.

In harmonization to the previous validation procedure, a five-point, external calibration with CRM MC-RR was performed, which was used for the quantitative estimation of 150 and 200 ng of MC-LR in order to determine the accuracy and intra-day precision as described above. The goodness of fit with  $R^2 = 0.996$  again proved a high linearity of detector response after logarithmic transformation and the accuracy of MC-LR quantification reached values of  $99.3 \pm 1.3 \%$  and  $101 \pm 2.4 \%$  corresponding to  $149 \pm 1.9$  ng and  $202 \pm 4.8$  ng as calculated values for CRM MC-LR, respectively.

Contrary to the values of the previous validation, the accuracy as well as the intra-day precision for 150 ng MC-LR were slightly better than for 200 ng MC-LR. When comparing the values and deviations of the single sequences (Table 28), it is apparent that they were consistent for both amounts confirming a successful method transfer from the University of Tübingen to the University of Halle-Wittenberg.

The final parameters LOD and LOQ were determined by continuously lowering the injected amount of MC-RR to a minimum of 1 ng on-column, for which no ELSD signal was observed anymore. Whereas quantitative measurements are derived from the integrated peak area, the SNR was calculated from the peak height according to the following equation:<sup>424</sup>

$$\text{SNR} = \frac{\text{Peak height (signal)}}{\text{Average height (background noise)}}$$

The LOD is defined as three times the SNR,<sup>495</sup> which was reached at an on-column amount of 8 ng MC-RR. 19 ng yielded an SNR of 14.5. This value was slightly higher than the minimal SNR of 10, as which the LOQ is defined. Still, this amount of MC-RR was accepted as LOQ since the missing data for 16, 17, and 18 ng of MC-RR were not complemented and a linear extrapolation of the peak height to an SNR of 10 is not valid.

These two parameters were the last stage of the validation process. The values of linearity, accuracy, intra- and inter-day precision showed that the HPLC–ELSD method provided reliable and reproducible results for the structure-independent quantification of MCs. Since the linear range was determined for 100 to 300 ng and the accuracy was verified for 150 and 200 ng, the MC on-column amount must be fitted to these values by adjusting either the sample concentration or injection volume. If lower or higher quantities shall be analyzed, a different calibration curve and new validation is required, especially to check whether the detector response remains linear after logarithmic transformation.

Judging from the inter-laboratory precision, the method is also characterized by a certain robustness. The change of the HPLC instrumentation did not affect the accuracy and reproducibility, so it could be easily transferred to a new laboratory. However, a more elaborated validation design is required to enable a definite statement on the method robustness, e.g. by testing other ELSD models or mobile phase constitutions.

In terms of LOD and LOQ, the HPLC–ELSD method is comparable to MC quantification by HPLC–DAD, but it is much less sensitive than ELISA, the PP inhibition assay, and HPLC–MS, which all achieve detection limits in the picogram range.<sup>411,429,432–434</sup> Furthermore, its applicability is strictly limited to pure compounds as HPLC–ELSD only allows for an analyte discrimination based on the  $t_R$  and cannot attribute errors arising from co-eluting substances.

In conclusion, the efforts led to the establishment of a validated HPLC–ELSD method, which is capable of quantifying low amounts of MCs in a structure-independent manner. Another benefit consists in the simple and straightforward method transfer, so it can be easily adopted by other analysts. The establishment of the HPLC–ELSD method was the last step required for MC analysis, and all the methods described so far were compiled into a workflow.

#### 3.1.5. Workflow for Microcystin Isolation and Structure Dereplication by MS<sup>2</sup>

The quantification by HPLC–ELSD was the last part the protocol specifically developed for a rapid MC isolation and analysis. All the steps were assembled into a workflow, which is depicted in Scheme 2. Depending on the amount of biomass, one of the two extraction procedures was selected. Whereas the sample obtained from the two subsequent LLE steps was directly applicable to semi-preparative HPLC, the methanol extract has to be further purified beforehand.

Here again, the choice of the appropriate LC method depended on the amount of extract generated by liquid extraction with methanol. SEC on Sephadex LH-20 was better suited for smaller samples due to its higher separation efficiency, but limited in throughput capacity. Thus, large samples were best cleaned up by flash chromatography, since manifold cartridge sizes are available and enable an easy scalability.

In the next step, either the extract of the two-step LLE or the MC-containing fractions obtained from LC purification were submitted to semi-preparative HPLC on a Luna PFP column employing a gradient from 30–50 % acetonitrile in water with 0.1 % FA as modifier. This separation fractionated the MC variants based on the number of aromatic

### 3. Results and Discussion

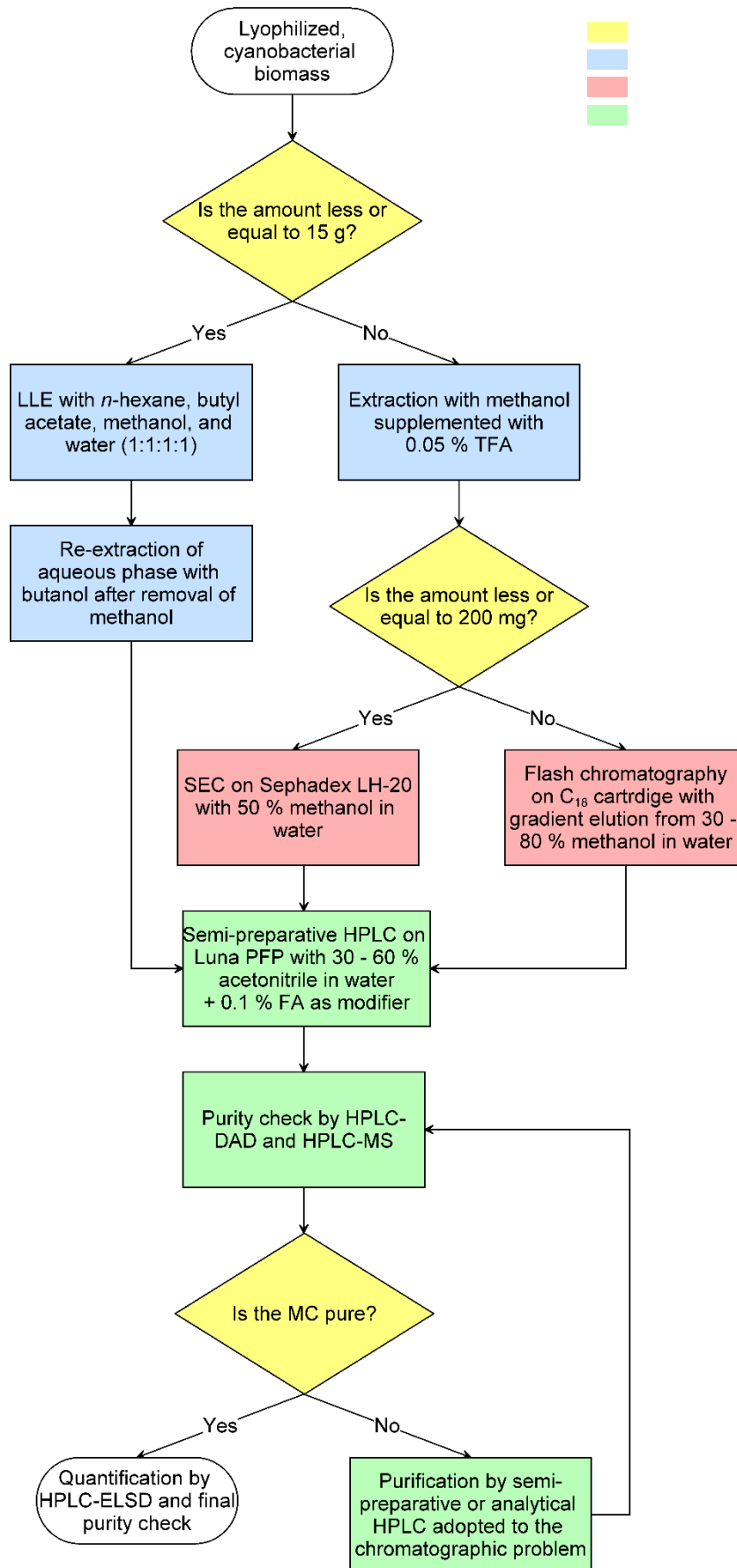
---

residues and eventually yielded pure compounds, which are evaluated by analytical HPLC–DAD and HPLC–MS.

If more than one substance was present, the sample was fractionated in another HPLC run in either semi-preparative or analytical scale using a method that was adopted to the respective separation problem. The resulting fractions were checked by HPLC–DAD and HPLC–MS once again, and the cycle of isolation via HPLC and purity assessment iterated until the sample reached a satisfying grade of purity. Finally, the quantity of each MC was determined by HPLC–ELSD.

As a proof of concept, **1** and **2** were isolated from 13 g lyophilized CBT 480 biomass following the left branch of the workflow in Scheme 2. After the first purity check by HPLC–MS, the MCs were isolated by semi-preparative HPLC on a Luna C<sub>18</sub> column employing the method in Table 17 for **1** and the method in Table 18 for **2**. Quantification by HPLC–ELSD revealed a total yield of 688 µg of **1** and 765 µg of **2**. Since the amounts were sufficient, both samples were adjusted to a concentration of 200 µM with DMSO and designated as stock solutions for the establishment and validation of the cytotoxicity assay.

The straightforward workflow was designed for the targeted isolation of MCs, whose structures were either known or could be predicted after modification via PDB, in which an amino acid was substituted by a distinct, artificial substrate. Knowing the postulated types and sequence of the amino acid residues made it possible to dereplicate the structures by MS<sup>2</sup>. In this approach, target molecular ions are fragmented through collision with atomic or sub-atomic particles, and the fragment spectra are recorded.<sup>496–499</sup> The fragmentation usually follows basic chemical principles, and similar patterns are observed for related compounds irrespective of the instrumentation.

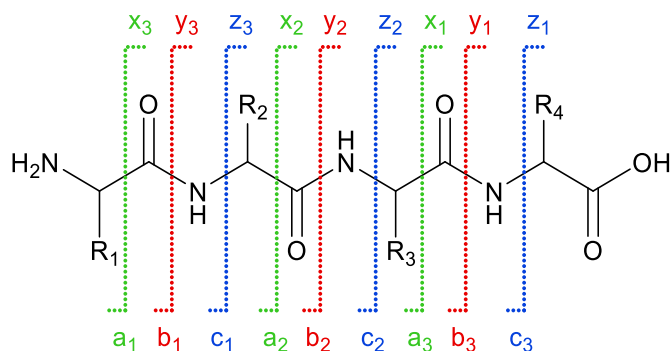


**Scheme 2.** Workflow for MC isolation and analysis. Abbreviations as defined in the text.

### 3. Results and Discussion

Peptides and proteins are fragmented into their oligomers and monomers when the amide bonds are cleaved during fragmentation. In this process, the charge can be retained on either the C- or N-terminal fragment. Depending on where the bond is cleaved, charged C-terminal fragments form *x*, *y*, or *z* ions, and ions originating from charged N-terminal fragments are classed as *a*, *b*, and *c*.<sup>500,501</sup> The number of amino acid monomers in the fragment sequence is indexed (Scheme 3).

If the peptide bond is broken between the carbonyl-carbon and the nitrogen, *y* and *b* ions are obtained. Cleavage between the  $\alpha$ -carbon and the carbonyl-carbon leads to the formation of *a* ions (- CO (28 Da) in relation to the *b* ion) and *x* ions (+ CO (28 Da) in relation to the *y* ion). The *c* ions (+ NH<sub>2</sub> (19 Da) in relation to the *b* ion) and *z* ions (- NH<sub>2</sub> (19 Da) in relation to the *y* ion) ions are formed in consequence of cleavage in between the nitrogen and  $\alpha$ -carbon. The same nomenclature is applied to the fragmentation of cyclic peptides after linearization to obtain a C- and N- terminus.



**Scheme 3.** Peptide fragmentation scheme and nomenclature of the resulting ions.

Peptide fragmentation strictly follows these few, easy principles, and MS<sup>2</sup> became a popular tool for the structural assignment of linear and cyclic peptides, even of non-ribosomal origin.<sup>502–506</sup> The efforts to establish a way for *de novo* sequencing of unknown peptides from MS<sup>2</sup> spectra promoted the development of new algorithms and computer-aided tools leading to a broad array of software for peptide identification and peak annotation.<sup>507–515</sup>

Since most of these programs demand a high computing power and time, the less complex *in silico* fragmentation engine mMass was used in this study.<sup>358</sup> mMass had already proven valuable for the fast dereplication of MCs.<sup>161,292,516</sup> It generates a list of all possible daughter ions of a given peptide sequence and also includes neutral losses, which are defined for each monomer in a library. In the second step, the calculated fragments are matched to the peaks of the MS<sup>2</sup> spectrum and the outcome is scored dependent on the overall matched intensities.



The structure dereplication could be performed at any stage of the MC isolation process, but the purity check by HPLC–MS proved as the most suitable. Both MCs were fragmented by selected ion monitoring at  $m/z$  1045.5 and  $m/z$  995.5 (Table 14), and the MS<sup>2</sup> spectra of **1** and **2** (Figure A15 and Figure A16) were annotated with mMass (Table A1 and Table A2). The matched intensities covered 81 % of the total intensities for **1** and 75 % for **2**.

Both spectra feature characteristic fragments of MCs with  $m/z$  599, corresponding to the  $b^3$  and  $y^3$  ions with the sequences Masp<sup>3</sup>–Arg<sup>4</sup>–Adda<sup>5</sup> or Arg<sup>4</sup>–Adda<sup>5</sup>–Glu<sup>6</sup>, and  $m/z$  375, which is consistent with the  $z^3$  ion with the sequence Adda'–Glu<sup>6</sup>–Mdha<sup>7</sup> (Adda': truncated form of Adda).<sup>461,517–519</sup> In the MS<sup>2</sup> spectrum of **1**, three other fragments characteristic for MC-YR with  $m/z$  916, 603, and 520 were detectable.<sup>519–521</sup> The analogous fragments for **2** with  $m/z$  866, 553, and 470 were further observed in the MS<sup>2</sup> of **2**. Consequently, mMass proved to be a fast and easy-to-use software tool for the structure dereplication of **1** and **2** isolated from *M. aeruginosa* CBT 480. This was the last tool necessary for the chemical characterization of MCs before they were to be submitted to a cytotoxicity assay.

#### 3.1.6. Assay Establishment for Cytotoxicity Screening

Since one of the primary goals of this thesis was the identification of new MCs as lead structures for anticancer therapy, the establishment of a reliable, *in vitro* screening assay was indispensable in order to characterize the cytotoxic potential of the new variants. As mentioned in the beginning, MCs cannot cross the membrane by diffusion but depend on an active uptake, which is mainly mediated by OATP1B1 and OATP1B3.<sup>263</sup> Thus, suitable model cell lines must express these transporters at a high and stable level.

Furthermore, the assay read-out should clearly state the affinities towards the single subtypes OATP1B1 and OATP1B3. Many studies report the use of primary hepatocytes of either rodent or human origin for the cytotoxicity characterization of MCs and related compounds.<sup>520–528</sup> However, these types of cells mostly co-express both transporters, so they were inept as reporter cell lines for this project. A system was required, in which OATP expression was introduced exogenously.

Such models were not only designed for the toxicological profiling of MCs, but also for studying the uptake of pharmaceuticals because OATPs play an important role in hepatic drug uptake and drug–drug interactions. For this purpose, well characterized standard cell lines, e.g. Chinese hamster ovarian or human embryonal kidney (HEK and HEK293) cells, were stably transfected with a vector for the expression of

### 3. Results and Discussion

either OATP1B1 or OATP1B3.<sup>524,529–533</sup> Dr. Jörg König from the University of Erlangen-Nürnberg kindly provided such an OATP screening system involving HEK293 cell lines transfected with an inducible expression vector for OATP1B1 and OATP1B3.<sup>529</sup>

After routine testing for mycoplasma contamination, the ideal seeding density of the two control cell lines was determined because they were growing the fastest (OATP1B3 control) and the slowest (OATP1B1 control). Most studies incubated the cells with MCs for 48 h, so the experiment was designed accordingly. The ideal seeding density was defined as the highest cell number per well that reached a confluency of about 80–90 % after 48 h. A seeding density of 50,000 cells per well met these parameters (Figure A17). Intensive monitoring of the cell confluency during the cytotoxicity testing confirmed that this seeding density also worked well for the HEK293 OATP1B1 and HEK293 OATP1B3 cell lines.

Since full data sets on the OATP selectivity were already available,<sup>292</sup> the assay should be established and validated with compound **1** isolated from *M. aeruginosa* CBT 480. All four cell lines of the OATP expression system were incubated at various concentrations for 48 h and viable cells were strained with SRB followed by photometrical quantification. After normalization and mathematical transformation, a sigmoidal curve was fitted, from which the EC<sub>50</sub> was calculated.

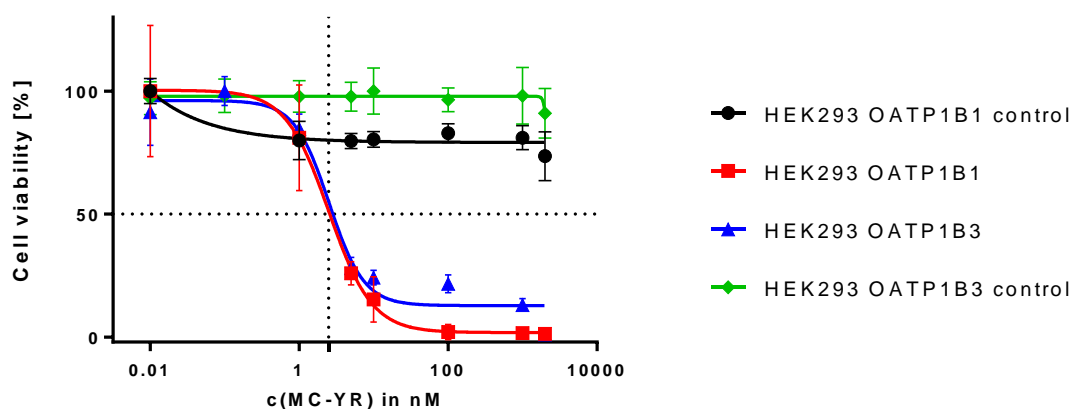


**Figure 19.** Bioactivity of MC-YR (**1**) against HEK293 OATP1B1 control (black circles), HEK293 OATP1B1 (red squares), HEK293 OATP1B3 (blue triangles), and HEK293 OATP1B3 control (green diamonds). The EC<sub>50</sub> is marked with a dashed line.

The HEK293 OATP expression system gave results as expected. The black and green lines in Figure 19 indicate that **1** did not affect the HEK293 OATP1B1 control and HEK293 OATP1B3 control cells, respectively. In contrast, the HEK293 OATP1B1 cell line strongly reacted to exposure of **1** exhibiting an EC<sub>50</sub> value of 2.5 nM. A similar EC<sub>50</sub> value was also determined for the cell line expressing OATP1B1.

Two further biological replicates supported the bioactivity of **1** in this cell line system. A sigmoidal inhibition curve was fitted for all three data sets. For HEK293 OATP1B1, the  $R^2$  equaled 0.93, and the mean  $EC_{50}$  was calculated as 4.5 nM with a 95 % confidence interval (CI) ranging from 2.9–7.2 nM. Accordingly, the fitted curve for HEK293 OATP1B3 gave an  $R^2$  of 0.96 and a mean  $EC_{50}$  of 3.0 nM covered by a 95% CI from 2.1–4.3 nM.

These results not only suggested a proper functionality of both OATPs, but also implied a validity of the assay design and data analysis. The goodness of fit confirmed that the increments in MC concentration were chosen adequately and that the sigmoidal plotting was a suitable mathematical model. Judging from the narrow 95% CI of both  $EC_{50}$  values, the assay further featured a good reproducibility, in which the HEK293 OATP1B1 cells performed less robust than HEK293 OATP1B3 as seen by the slightly wider 95 % CI window.

Since this OATP expression system was established from a completely different cell line, the  $EC_{50}$  of **1** cannot directly be compared to the values reported for HeLa cells.<sup>292</sup> However, the authors defined the ratio  $EC_{50}$  (OATP1B1)/ $EC_{50}$  (OATP1B3) as a measure for the MC transporter selectivity, which only depends on the interaction between the MCs and OATPs and not on the cell line. This renders the ratio an appropriate index to check the consistency of the current results with the preceding findings. Indeed, the presented assay yielded a ratio of  $EC_{50}$  (OATP1B1)/ $EC_{50}$  (OATP1B3) of 1.5 for **1** while previously, it was determined as 2.0. In this context, the minor difference of 0.5 is well tolerable. Thus, the results are highly reproducible and coherent with the findings of the prior study.

The validation revealed a very good assay performance. It enabled the screening of new MCs in terms of their general toxicity and OATP selectivity, so they can be put into context with the previous findings on the structural features that favor an OATP1B3 preference. This cytotoxicity assay represented the last step in the method development. With its successful establishment, the toolbox for MC isolation, analysis, and biological characterization was completed and ready to use on new MC derivatives.

## 3.2. Precursor-Directed Biosynthesis and Fluorescence Labeling of Clickable Microcystins

The main goal of this thesis was to design MC-based lead structures, which can serve as payload for ADCs. In order to conjugate the MCs with the linker moiety of an ADC, new chemical functions that can be modified via click chemistry should be introduced by means of PDB. Simultaneously, this method can serve as starting point for physiological studies, e.g. by using the bioorthogonal handles in the clickable MCs for *in vivo* fluorescence labeling in the cyanobacteria.

However, Okumura and coworkers did not succeed in PDB of MCs in a *Planktothrix rubescens* strain.<sup>321</sup> When comparing the structural diversity of MCs from different genera, it becomes clear that only few [Asp<sup>3</sup>Dhb<sup>7</sup>]-MC variants have ever been isolated from *Planktothrix*.<sup>535</sup> Indeed, the majority of MCs were found in strains of the genus *Microcystis*, indicating a relatively low substrate specificity of the A domains of McyB and McyC. Thus, six *Microcystis* strains were chosen for PDB studies: CBT 480, CBT 1, and CBT 959 (all three producers of MC-LR and MC-YR), CBT 275, a producer of MC-LR, MC-LF, and MC-LW, the MC-RR producing strain CBT633, and CAWBG11, which has been shown to produce more than 20 different MC variants.<sup>202</sup>

As the structural variability of MCs is most pronounced in positions 2 and 4, the substrate specificity of the respective biosynthesis enzymes (McyB and McyC) is lower than the specificity of the other biosynthesis enzymes involved in MC biosynthesis. Thus, nine amino acid derivatives with either an azido or terminal alkyne group resembling the natural amino acids found in these positions were selected for PDB studies. In the selected MC-producing strains, the amino acids in positions 2 and 4 were mostly found to be either aliphatic (e.g. Leu), basic (Arg), or aromatic (e.g. Tyr). In consequence, two aromatic (*p*-azido-L-phenylalanine and *O*-2-propyn-1-yl-L-tyrosine), as well as six aliphatic functionalized amino acids with side chain lengths of up to four carbons (6-azido-L-norleucine, 5-azido-L-norvaline, 2-amino-4-azido-L-butyric acid, 3-azido-L-alanine, *N*6-[(2-propyn-1-yloxy)carbonyl]-L-lysine, and propyn-1-yl-L-glycine, were

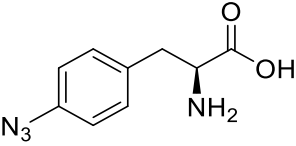
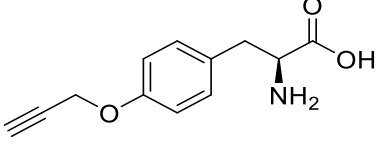
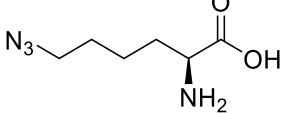
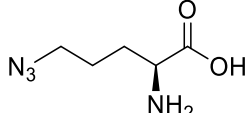
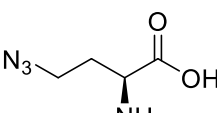
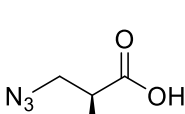
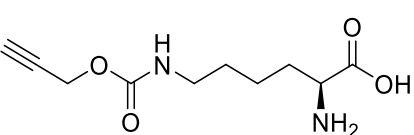
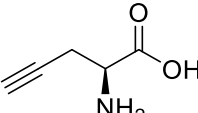
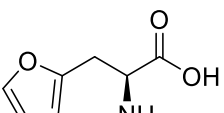
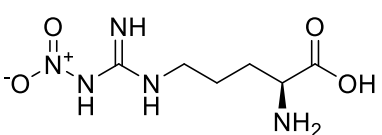
selected as artificial precursors (for structures and acronyms of these substrates, see Table 29. In addition to these substrates modifiable via CuAAC, two amino acids with bioorthogonal functionalities with other reactivities were chosen: 3-(2-furyl)-L-alanine (Furala) as an analog of aromatic amino acids, and *N*<sub>ω</sub>-nitro-L-arginine (Narg) as a potential substitute for Arg.<sup>[6]</sup>

---

<sup>[6]</sup> Paragraph adapted and modified from Moschny, J.; Lorenzen, W.; Hilfer, A.; Eckenstaler, R.; Jahns, S.; Enke, H.; Enke, D.; Schneider, P.; Benndorf, R. A.; Niedermeyer, T. H. J. Precursor-directed biosynthesis and fluorescence labeling of clickable microcystins. *J Nat Prod* **2020**, 83, 1960–1970. Copyright 2020 American Chemical Society.

### 3. Results and Discussion

**Table 29.** List of substrates used for precursor-directed biosynthesis (PDB). Reprinted with permission from Moschny *et al.*<sup>194</sup> Copyright 2020 American Chemical Society.

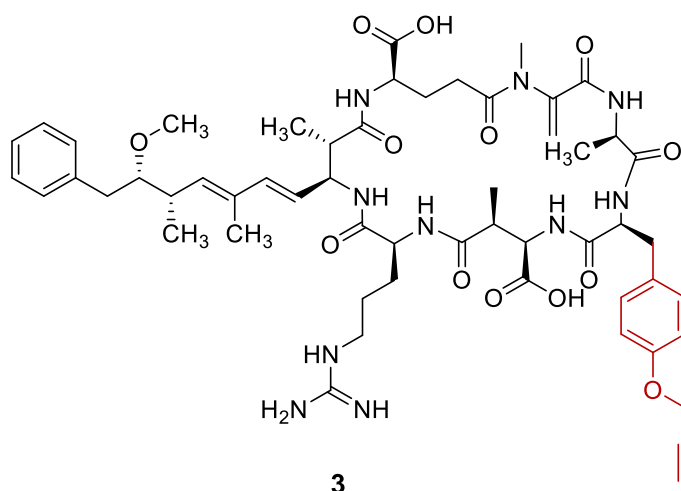
Name	Acronym	Structure
<i>p</i> -Azido-L-phenylalanine	Azphe	
O-2-Propyn-1-yl-L-tyrosine	Prtyr	
6-Azido-L-norleucine	Aznle	
5-Azido-L-norvaline	Aznva	
2-Amino-4-azido-L-butyric acid	Azabu	
3-Azido-L-alanine	Azala	
<i>N</i> 6-[(2-Propyn-1-yloxy)carbonyl]-L-lysine	Prlys	
Propyn-1-yl-L-glycine	Prgly	
3-(2-Furyl)-L-alanine	Furala	
<i>N</i> <sub>ω</sub> -Nitro-L-arginine	Narg	

3.2.1. Clickable Microcystins from Various *Microcystis* strains

This chapter is adapted and modified from Moschny, J.; Lorenzen, W.; Hilfer, A.; Eckenstaler, R.; Jahns, S.; Enke, H.; Enke, D.; Schneider, P.; Benndorf, R. A.; Niedermeyer, T. H. J. Precursor-directed biosynthesis and fluorescence labeling of clickable microcystins. *J Nat Prod* **2020**, 83, 1960–1970. Copyright 2020 American Chemical Society.

Supplementation of the precursors to the medium revealed that some of these substrates negatively affected the growth of the cyanobacterial strains. For example, Azphe impaired the growth of the *Microcystis aeruginosa* strain CBT 480 at concentrations of 30  $\mu\text{M}$  and above, whereas Prtyr was well tolerated at concentrations of up to 100  $\mu\text{M}$ . Consequently, to reduce peak substrate concentrations, an iterative supplementation scheme was devised, and the substrates were added to the cultivation media every 24 h to a final concentration of 30  $\mu\text{M}$ . This precursor incubation protocol proved feasible for all strains and amino acid analogs. After cultivation, the cyanobacterial biomass of the supplemented and control cultures was harvested and extracted. The extracts were analyzed by LC–MS.

*M. aeruginosa* CBT 480 naturally produces **1** and **2**. Analyses of the biomass extracts of cultures supplemented with 30  $\mu\text{M}$  Azphe showed that, indeed, a new compound with  $m/z$  1070.6 ( $[\text{M}+\text{H}]^+$ ) could be observed (Figure 20A and B). This corresponds to the calculated  $m/z$  of the protonated molecule  $[\text{MC-AzpheR}+\text{H}]^+$ , suggesting a replacement of Tyr in position 2 by Azphe. Supplementation with Prtyr following the same protocol resulted the biosynthesis of MC-PrtyrR (**3**;  $m/z$  1083.5, consistent with  $[\text{3} + \text{H}]^+$  (Figure 20C and D).



### 3. Results and Discussion

$MS^2$  and  $MS^3$  data of the two compounds were consistent with the hypothesized structures: The spectra feature a characteristic fragment of MCs with  $m/z$  599, corresponding to the  $b^3$  and  $y^3$  ions with the sequences Masp–Arg–Adda or Arg–Adda–Glu, indicating that the new peak is a MC with Arg in position 4.<sup>358</sup> Furthermore, fragment ions analogous to the characteristic fragment ions with  $m/z$  916, 911, 620, and 603 for  $[1+H]^+$  were observed with a distinct shift of -3 for  $[MC\text{-AzpheR} - N_2+H]^+$  and +38 for  $[3+H]^+$  (Figure A18 and Figure A19, Table A3 and Table A4).

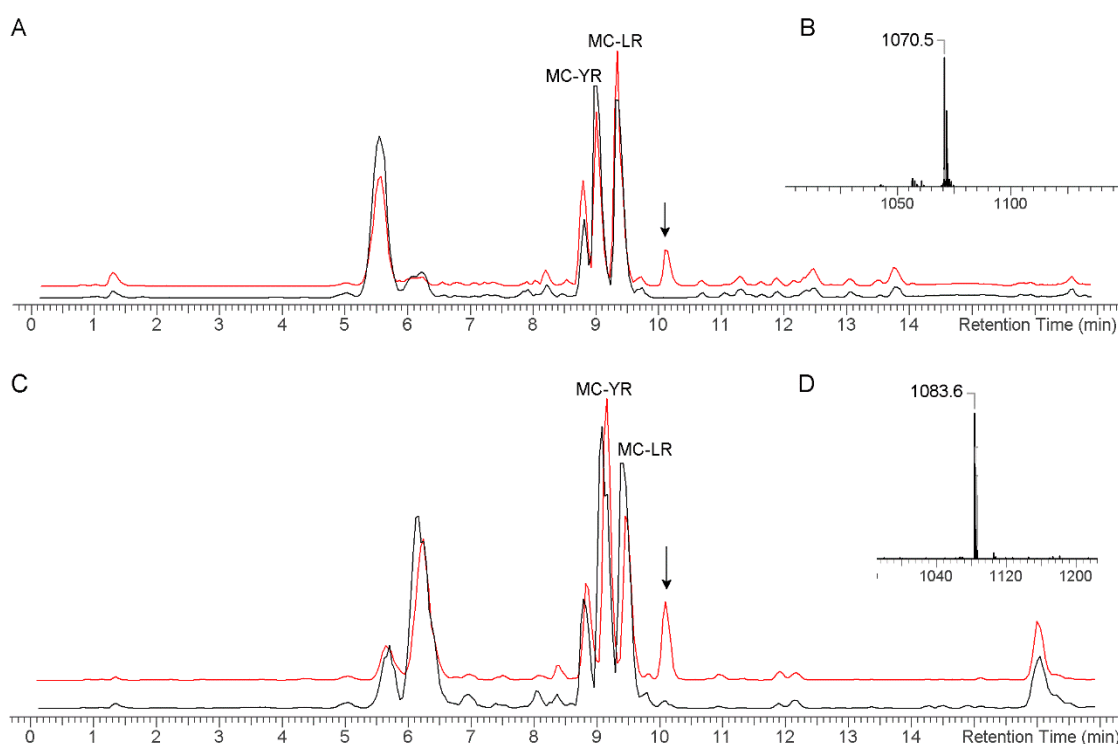


**Figure 20.** Precursor-directed biosynthesis with *M. aeruginosa* CBT480 and the substrates Azphe and Prtyr. (A) Base peak chromatogram (BPC, pos. mode) overlay of an *M. aeruginosa* CBT 480 control culture (black, lower trace) and a culture supplemented with 30  $\mu$ M Azphe (red, upper trace); the black arrow indicates an additional peak in the supplemented culture. (B) Mass spectrum of  $[MC\text{-AzpheR}+H]^+$  ( $t_R$  10.1 min) produced by CBT 480 supplemented with 30  $\mu$ M Azphe. (C) BPC (pos. mode) overlay of an *M. aeruginosa* CBT 480 control culture (black, lower trace) and a culture supplemented with 30  $\mu$ M Prtyr (red, upper trace); the black arrow indicates an additional peak in the supplemented culture. (D) Mass spectrum of  $[MC\text{-PrtyrR}(3)+H]^+$  ( $t_R$  10.2 min) produced by CBT 480 supplemented with 30  $\mu$ M Prtyr. Adapted with permission from Moschny *et al.*<sup>194</sup> Copyright 2020 American Chemical Society.



Encouraged by these findings, all 10 substrates were supplemented to *M. aeruginosa* CBT 480 and the five other *Microcystis* strains. The results of the PDB studies are summarized in Table 30. In addition to the aromatic amino acid analogs Azphe and Prtyr, *M. aeruginosa* CBT 480 was also capable of incorporating the aliphatic, medium-chain length amino acids Prlys, Aznva and Aznle in position 2 instead of Leu (Figure A20–Figure A22). However, the short-chain length amino acid analogs (Azala and Azabu) were not accepted, indicating a binding preference for sterically demanding precursors. Furthermore, the Arg residue in position 4 of **1** could be replaced by Prgly (Figure A23), resulting in MC-LPrgly, which features the clickable functional group in position 4. The analogous product MC-YPrgly was not detectable.

Another MC-LR and MC-YR-producing *Microcystis* strain, CBT 1, was found to possess an identical substrate recognition pattern. It was also capable of incorporating the aromatic amino acid analogs Azphe and Prtyr (Figure A24 and Figure A25), as well as the long chain derivatives Prlys, Aznva, and Aznle (Figure A26–Figure A28) in position 2. Furthermore, Prgly replaced the Arg residue in position in **2**, but not in **1** (Figure A29). In summary, PDB with CBT 1 resulted in the exact same products as PDB with *M. aeruginosa* CBT 480 (Table 30).

In contrast to *M. aeruginosa* CBT 480 and *Microcystis* CBT 1, the *Microcystis* strain CBT 275 showed a very strict substrate specificity in position 2. It did not incorporate any of the selected amino acid derivatives instead of Leu. It rather exhibited broad flexibility in position 4, which was already evident from its naturally produced variants (**2**, -LF, and -LW). CBT 275 incorporated both aromatic analogs Azphe and Prtyr, as well as the four sterically more demanding aliphatic clickable amino acids Aznle, Aznva, Azabu, and Prlys (Figure A30–Figure A35). Thus, it was capable of producing six clickable MCs with both azido and terminal alkyne groups in position 4.

Of all *Microcystis* strains selected for PDB, CBT 633 showed the lowest natural structural diversity of natural MCs, producing MC-RR as the predominant congener. Because the A-domains of McyB and McyC did not seem to possess any affinity towards aromatic amino acids, PDB with the substrates Azphe and Prtyr was not tested. CBT 633 accepted all four aliphatic amino acid derivatives with two or more carbons in their side-chains (Aznle, Aznva, Azabu, and Prlys, Figure A36–Figure A39) as substrates replacing either one of the two Arg residues in position 2 and 4. Whereas both possible isomers were found for the incorporation of Azabu and Prlys (MC-AzabuR and -RAzabu, and MC-PrlysR and -RPrlys), only one product was detected for the supplementation with Aznle (MC-AznleR) and Aznva (MC-AznvaR), indicating a less stringent substrate acceptance of McyB compared to McyC.

**Table 30.** Overview of PDB studies (substrate–strain combinations). The strains used and their main natural MC-congeners are given in the first row. Clickable MCs detected in the supplemented cultures are given in the respective table cells. n/a, data not available; -, no PDB product detectable. Substrate abbreviations see Table 29. Reprinted with permission from Moschny *et al.*<sup>194</sup> Copyright 2020 American Chemical Society.

Substrate	Strain (main naturally produced congeners)					
	CBT 480 (MC-(L/Y)R)	CBT 1 (MC-(L/Y)R)	CBT 275 (MC-L(R/F/W))	CBT 633 (MC-RR)	CBT 959 (MC-(L/Y)R)	CAWBG11 (MC-(L/F/Y/W/R)(A/Abu/L/R))
Azphe	MC-AzpheR	MC-AzpheR	MC-LAzphe	n/a	MC-AzpheR	MC-Azphe(R/A)
Prtyr	MC-PrtyrR	MC-PrtyrR	MC-LPrtyr	n/a	MC-PrtyrR	MC-Prtyr(R/A/Abu/L)
Aznle	MC-AznleR	MC-AznleR	MC-LAznle	MC-AznleR	MC-AznleR	MC-Aznle(R/A/Abu/L) MC-AznleAznle
Aznva	MC-AznvaR	MC-AznvaR	MC-LAznva	MC-AznvaR	MC-AznvaR MC-(L/Y)Aznva MC-AznvaAznva	MC-(R/F/Y/W/L)Aznva MC-Aznva(A/Abu/R) MC-AznvaAznva
Azabu	-	-	MC-LAzabu	MC-AzabuR MC-RAzabu	MC-(L/Y)Azabu	MC-(R/F/Y/W/L)Azabu MC-AzabuR
Azala	-	-	-	-	MC-(L/Y)Azala	MC-(F/W/L)Azala
Prlys	MC-PrlysR	MC-PrlysR	MC-LPrlys	MC-PrlysR MC-RPrlys	MC-PrlysR	MC-Prlys(R/A)
Prgly	MC-LPrgly	MC-LPrgly	-	-	MC-(L/Y)Prgly	MC(R/F/Y/W/L)Prgly MC-PrglyR
Furala	-	-	MC-LFurala	-	-	n/a
Narg	MC-(L/Y)Narg	MC-(L/Y)Narg	MC-LNarg	MC-NargR MC-RNarg MC-NargNarg	MC-(L/Y)Narg	n/a

Except for *Microcystis* CBT 633, all strains reported so far showed a substrate flexibility in either position 2 or position 4. The *Microcystis* strains CBT 959 and CAWBG11 distinguished themselves by being capable of incorporating the clickable amino acids in both positions likewise. *Microcystis* CBT 959, which mainly produces MC-LR and MC-YR, accepted the aromatic and long-chain aliphatic substrates in position 2, whereas the short-chain amino acids were incorporated instead of arginine in position 4 (Figure A40–Figure A53). Due to the overlap in substrate acceptance for Aznva, all theoretically possible products with Aznva in position 2 or 4 (MC-AznvaR, MC-LAznva, and MC-YAznva) as well as the dual functionalized variant MC-AznvaAznva could be detected.

A similar pattern of substrate recognition was observed for *Microcystis* CAWBG11. The naturally produced MCs of *Microcystis* CAWBG11 contain the aromatic amino acids Phe, Tyr, and Trp in position 2 only whereas the smaller amino acids Ala and Abu are exclusively found in position 4. Leu and Arg occur in both positions. This biosynthetic behavior was also reflected in the substrate acceptance during the PDB studies.

Both aromatic analogs Azphe and Prtyr as well as the two bulkier analogs Aznle and Prlys were incorporated in position 2 (Figure A54–Figure A65). For Prtyr and Aznle, all theoretically possible products were observed (Figure A56–Figure A63). The isomers MC-AznleL, MC-AznleR, and MC-PrlysR were confirmed also by HRMS2 (Figure A66–Figure A68 and Table A5–Table A7). Interestingly, also the variant MC-AznleAznle arising from the dual incorporation of Aznle was detectable (Figure A69), but not the analogous products with Phe, Tyr, Trp, Leu, or Arg in position 2 and Aznle in position 4. This suggests that these sterically more demanding precursors prevented the binding of Aznle to the A-domain of McyC. Thus, the substrate acceptance seems not only to be determined by the architecture of the respective A- and C-domains, but might also be influenced by steric or electrostatic effects mediated by the constituents of the peptide chain bound to the NRPS.<sup>203</sup> However, further *in-* and *ex-vivo* studies are required to confirm this hypothesis. In the case of Azphe and Prlys, similar causes may have led to the formation of the PDB products and MC-AzpheR and MC-AzpheA (Figure A54 and Figure A55), and MC-PrlysR and MC-PrlysA (Figure A64 and Figure A65), respectively, lacking the combinations of Azphe and Prlys with Abu or Leu.

Due to its intermediate size and side-chain length, Aznva served as substrate for both A-domains of McyB and McyC in CAWBG11. In addition to its incorporation in position 2, yielding MC-AznvaA, MC-AznvaAbu, and MC-AznvaR (Figure A70–Figure A72), Aznva was also found in position 4 in combination with Arg, Phe, Tyr, Trp, and Leu (Figure A72–Figure A76). The structure of MC-LAznva was confirmed by HRMS2

### 3. Results and Discussion

---

(Figure A77 and Table A8). The dual functionalized MC-AznvaAznva was observed, as well (Figure A78).

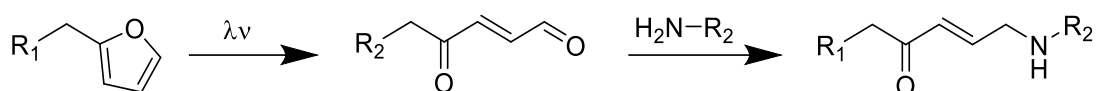
The short-chain aliphatic amino acids Azala, Azabu, and Prgly were mainly accepted as precursors in position 4, but the number of new products differed between the individual derivatives. PDB with Azala resulted in three new MCs bearing either Phe, Trp, or Leu in position 2 (Figure A79–Figure A81), while all possible combinations of Azabu and Prgly with the naturally occurring residues in position 2 were observed (Figure A82–Figure A91). The structures of MC-LAzabu and MC-LPrgly were both dereplicated by HRMS<sup>2</sup> (Figure A92 and Figure A93, Table A9 and Table A10). Additionally, both substrates were further accepted in position 2, but only in combination with Arg in position 4 yielding MC-AzabuR and MC-PrglyR (Figure A86–Figure A91). These differences in product formation observed for the supplementation with Azala, Azabu, and Prgly may also be due to the steric effects of the peptide chain bound to the NRPS, as discussed above.

In addition to the common [D-Masp<sup>3</sup>]MCs, many of the *Microcystis* strains also produce the respective [D-Asp<sup>3</sup>]MC congeners, but in much lower amounts. The corresponding PDB products for these [D-Asp<sup>3</sup>]MC congeners were observed in those cases, where the acceptance of the clickable amino acid analog was high (data not shown).

Due to the surprising substrate flexibility of various MC producing *Microcystis* strains as well as the simplicity of this precursor supplementation strategy, this method should also be transferred to the modification of nodularins via PDB. The chemical relation of nodularins to MCs and the overlaps in their biosynthetic pathways suggest that nodularin should be equally accessible as the MCs.<sup>184,254,255</sup> However, the supplementation of two *Nodularia* strains, CBT 750 and CBT 786, with various clickable precursors did not result in any new nodularin derivative. Taking into account that only 10 natural nodularin congeners are known, it seems that the substrate specificity of NdaB is much stricter than the specificity of McyB and McyC.<sup>255,535</sup>

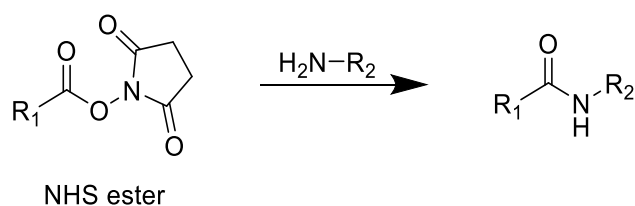
Interestingly, also the filamentous, [D-Asp<sup>3</sup>,E-Dhb<sup>7</sup>]MC-RR-producing *Planktothrix rubescens* strain CBT 329 did not accept any of the azide and alkyne functionalized amino acids as substrates for MC production. This agrees with the findings of Okumura *et al.*, who reported that the *Planktothrix* strain they used for PDB studies did not incorporate the supplemented precursors into MCs.<sup>321</sup> Further considering the lower MC diversity in the genus *Planktothrix* compared to the genus *Microcystis*, these findings support the initial hypothesis that the potential for PDB of MCs is much higher in the genus *Microcystis*.<sup>535</sup> Due to the selection of this genus for the PDB studies, previous drawbacks were overcome making MCs amenable for the modification via PDB.

In addition to the CuAAC, the bioorthogonal toolbox encompasses several other functional groups for the convenient conjugation of biomolecules.<sup>300,536</sup> One of these is the photo-inducible furyl group, which undergoes ring-opening under UV irradiation, forming a highly reactive unsaturated dicarbonyl moiety (Scheme 4).<sup>537</sup> By subsequent addition of nucleophiles, this mechanism has been used for the labeling of nucleotides and peptides.<sup>538–541</sup> Consequently, Furala was chosen as an additional bioorthogonal substrate. Despite its aromaticity, none of the MC-YR-producing strains accepted it as a substrate in position 2. Only *Microcystis* strain CBT 275 incorporated Furala as an analog to Phe in position 4, resulting in the formation of MC-LFurala (Figure A94).



**Scheme 4.** Ring opening of a furyl group under UV irradiation and subsequent conjugation with a nucleophile.

Furthermore, the efficient and specific coupling of primary amines to *N*-hydroxysuccinimide esters has been widely used for quantitative proteomics, protein crosslinking and labeling (Scheme 5), which could also be applied to MCs bearing a primary amine group.<sup>542–550</sup> Because direct supplementation of L-Lys and its homologs to any of the strains did not yield such a MC variant, an alternative route via Narg was chosen. This derivative decomposes to L-ornithine upon ammonolysis, resulting in a primary amine.<sup>551</sup> All the *Microcystis* strains readily accepted it as an Arg substitute, and incorporated it at position 4 (CBT 480, CBT 1, CBT 275, and CBT 959, Figure A95–Figure A101), or position 2 or/and 4 (CBT 633, Figure A102 and Figure A103). Due to the obviously close similarity of Narg to Arg, even *Planktothrix rubescens* strain CBT 329 was capable of incorporating Narg into [D-Asp<sup>3</sup>,E-Dhb<sup>7</sup>]MC-RR (Figure A104).



**Scheme 5.** Conjugation of a N-hydroxysuccinimide (NHS) ester with a primary amine.

### 3. Results and Discussion

---

In order to generate dual-functionalized clickable MCs, the simultaneous supplementation with two substrates was tested as a proof-of-principle in two cases. Simultaneous supplementation of the MC-YR-producing strains CBT 480 and CBT 1 with Narg and the Tyr analogs Azphe or Prtyr led to the production of the expected bifunctionalized derivatives bearing the *N*<sub>ω</sub>-nitroguanidine group in position 4 and either an azide or terminal alkyne function at position 2 (Figure A105–Figure A108), in addition to the mono-functionalized MC variants.

In summary, the precursor supplementation studies resulted in a total of 41 new MCs accessible to derivatization by CuAAC “click” chemistry, of which 28 feature an azido and 13 a terminal alkyne group in addition to two variants bearing azido groups in both positions 2 and 4. One additional congener with a furyl moiety, four with a *N*<sub>ω</sub>-nitroguanidine residue, and two dual-functionalized MCs with orthogonal bioorthogonal functional groups were generated.

Clickable MCs have been described before by Zemskov *et al.*, who introduced terminal alkyne groups into two MC derivatives by total synthesis, with one being identical to the MC-LPrtyr described here.<sup>251,313</sup> However, as described above, a complex synthesis with a low total yield was required in order to obtain the final product. This is not feasible for larger-scale production. In contrast, about 10 mg of **3** were isolated from a 20-L batch of *M. aeruginosa* CBT 480 (about 16 g of dry biomass) after a cultivation for one week under unoptimized conditions. Although total synthesis allows for a completely free choice of amino acid building blocks and their sequence, precursor-directed biosynthesis outperforms this approach in terms of time and cost-effectiveness, if the functionalization is to be located in positions 2 or 4.

Alternative procedures of chemically modifying natural MCs mainly involve the derivatization of Mdha<sup>7</sup> by nucleophilic additions, e.g. of thiols and subsequent cleavage.<sup>311,312,552</sup> Zemskov *et al.* even employed this approach for introducing clickable groups into a natural MC congener by addition of propargyl amine.<sup>313</sup> If the clickable MC, however, shall be used for *in vivo* labelling or as starting point for the development of MC-based anticancer agents, the location of the attachment site for a probe or carrier is crucial. Thus, Mdha<sup>7</sup> is only of limited use for this purpose due to its proximity to the pharmacophore, which is also discussed as interaction site with targets in the cyanobacterium. Affixing, e.g. a fluorescent tag, might put the affinity to the targets at a risk.<sup>330,553</sup> Only recently, the derivatization of MCs on D-Glu<sup>6</sup> with diazomethane was applied to analytical purposes.<sup>554</sup> Since D-Glu<sup>6</sup> belongs to the pharmacophore Adda<sup>5</sup>–Glu<sup>6</sup>–Mdha<sup>7</sup> and is essential for PP binding and inhibition, this residue is off-limits for derivatization as well if activity is to be maintained.<sup>236,244</sup>

Out of this reason, especially position 2 is better suited for designing MCs for subsequent conjugation. The introduction of a terminal alkyne into another position than 7 has only been achieved by means of total synthesis, and so far, no azido-modified MC has been reported. Other authors describe the semi-synthetic modification of natural microcystins by fluorescence labelling of arginine residues in position 4.<sup>555,556</sup> Indeed, it is most likely possible to transfer this method to introduce terminal alkynes and azides as well. Still, this has only been done on purified MCs and, due to the abundance of arginine, this approach is not feasible for *in vivo* labelling. Furthermore, semi-synthetic derivatization to obtain a pure, chemically modified variant always requires the isolation of a natural MC from cyanobacteria beforehand, unless it is purchased from a vendor. Thus, the time and efforts for chemical derivatization even add up to the time necessary to purify the MC.

Semi-synthetic derivatization, however, might be applied to introduce clickable functions into nodularin-R. Since PDB of nodularin-R was only successful with Narg, which also requires a chemical modification to give a primary amine for conjugation, direct derivatization of Arg in position 3 might be more feasible. Natural variants are produced in higher amounts than products derived from PDB giving higher yields after isolation compared to the Narg-containing variant and, in consequence, more starting material for semi-synthesis. If the method developed by Shreder *et al.* for Arg<sup>4</sup>-containing MCs can be transferred to nodularin-R,<sup>555</sup> this might also be a way to establish terminal alkyne or azide groups amenable for CuAAC reactions in nodularins.

#### 3.2.2. The Uptake of Prtyr in *M. aeruginosa* CBT 480

Of all *Microcystis* strains used for PDB studies, *M. aeruginosa* CBT 480 showed the best potential for PDB with the substrate Prtyr. It tolerated Prtyr at concentrations of up to 50  $\mu$ M without impairments in its growth rate (Figure A109). Other advantages are its general fast growth compared to the other *Microcystis* strains and the efficient incorporation of Prtyr into **3**, which gives a distinct signal in HPLC–DAD as well as HPLC–MS (Figure 20C).

In order to further improve the PDB efficiency with *M. aeruginosa* CBT 480 and the substrate Prtyr, the kinetics of Prtyr uptake and formation of **3** were investigated. Prtyr was added to the cultivation medium to a final concentration of 50  $\mu$ M, and samples were taken immediately and at time intervals of 4 to 24 h. All three replicates exhibited a good and comparable growth rate (Figure A109). The amount of Prtyr in the medium as well as the extractable amount of **3** in the biomass were quantified by HPLC–DAD (Table 12

### 3. Results and Discussion

and Table 13) in biological triplicate using a Prtyr and MC-Prtyr standard curve for calibration (Figure A110).<sup>[7]</sup>

As it can be seen in Figure 21, the uptake of Prtyr follows first-order kinetics ( $R^2 = 0.990$ ) with a half-life  $t_{1/2}$  of 14.4 h (95 % CI: [12.3 – 17.3 h]). The substrate was completely consumed after 96 h, thus sampling was stopped at this time point. In contrast, the amount of extractable **3** in the biomass most likely increases in an exponential manner during the first 36 h reaching a maximum at 48 h. Fitting of the corresponding curve, however, gave a poor goodness of fit.<sup>[6]</sup>

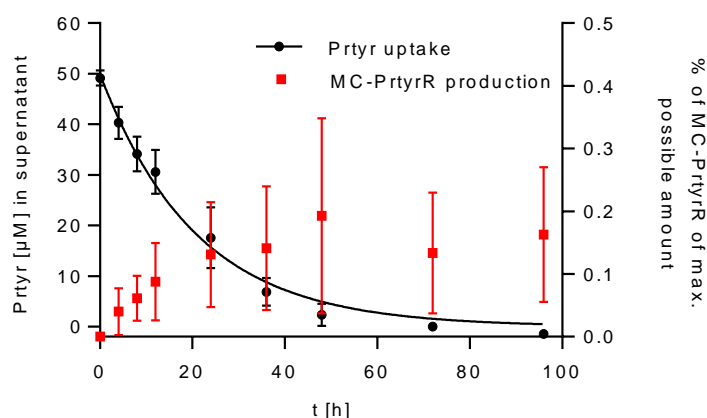


**Figure 21.** Prtyr concentration in the supernatant (black circles) and the amount of MC-PrtyrR (**3**) expressed as percentage of the maximum possible amount (red squares) in *M. aeruginosa* CBT 480 over 96 h (three biological replicates). Reprinted with permission from Moschny *et al.*<sup>194</sup> Copyright 2020 American Chemical Society.

One possibility to improve PDB efficiency consisted in maintaining a constantly high concentration of substrate in the culture supernatant. Thus, a cultivation system for the continuous supply of *M. aeruginosa* CBT 480 with Prtyr was designed (Figure 22). Two Schott bottles were provided with two stacked screw threads on the walls and equipped with connectors for tubing. One of the bottles was further equipped with inlet tubing for CO<sub>2</sub> supply and an outlet hose to allow for harvesting of the culture without disassembling of the system. A peristaltic pump, which continuously supplied a Prtyr stock solution to the culture at a flow rate of 7.5 µL/min, was installed in between the two bottles.

The main goal of this system was to achieve a steady state in terms of Prtyr supplementation, i.e. the rate of supplementation of Prtyr equals the uptake rate, so that

<sup>[7]</sup> Paragraph adapted and modified from Moschny, J.; Lorenzen, W.; Hilfer, A.; Eckenstaler, R.; Jahns, S.; Enke, H.; Enke, D.; Schneider, P.; Benndorf, R. A.; Niedermeyer, T. H. J. Precursor-directed biosynthesis and fluorescence labeling of clickable microcystins. *J Nat Prod* **2020**, 83, 1960–1970. Copyright 2020 American Chemical Society.



the concentration of Prtyr in the culture supernatant remained constant. The concentration in the steady state ( $c_{ss}$ ) is defined as

$$c_{ss} = \frac{R_0}{k_e \cdot V}$$

with  $R_0$  referring to the supplementation rate,  $k_e$  to the Prtyr uptake constant and  $V$  to the culture volume.<sup>557</sup> The  $c_{ss}$  was defined as 50  $\mu\text{M}$  because this concentration of Prtyr was well tolerated and used for determination of the uptake kinetics. The uptake constants differed in between the replicates of the uptake studies and ranged between 0.05 and 0.06 per h as deduced from the equations of the Prtyr uptake kinetics. For the subsequent calculations, the value for  $k_e$  was set to 0.06 per h. The system was inoculated with 100 mL culture corresponding to  $V$ .

Based on these parameters, the supplementation rate  $R_0$  of Prtyr was calculated as 5 nmol/h. Taking into account the flow rate of the pump, the concentration of the Prtyr stock solution was calculated as 0.66 mM. The culture was grown under these conditions for several weeks and small amounts of biomass were continuously harvested. During this period, no contamination of the system was observed and the culture maintained a healthy state.

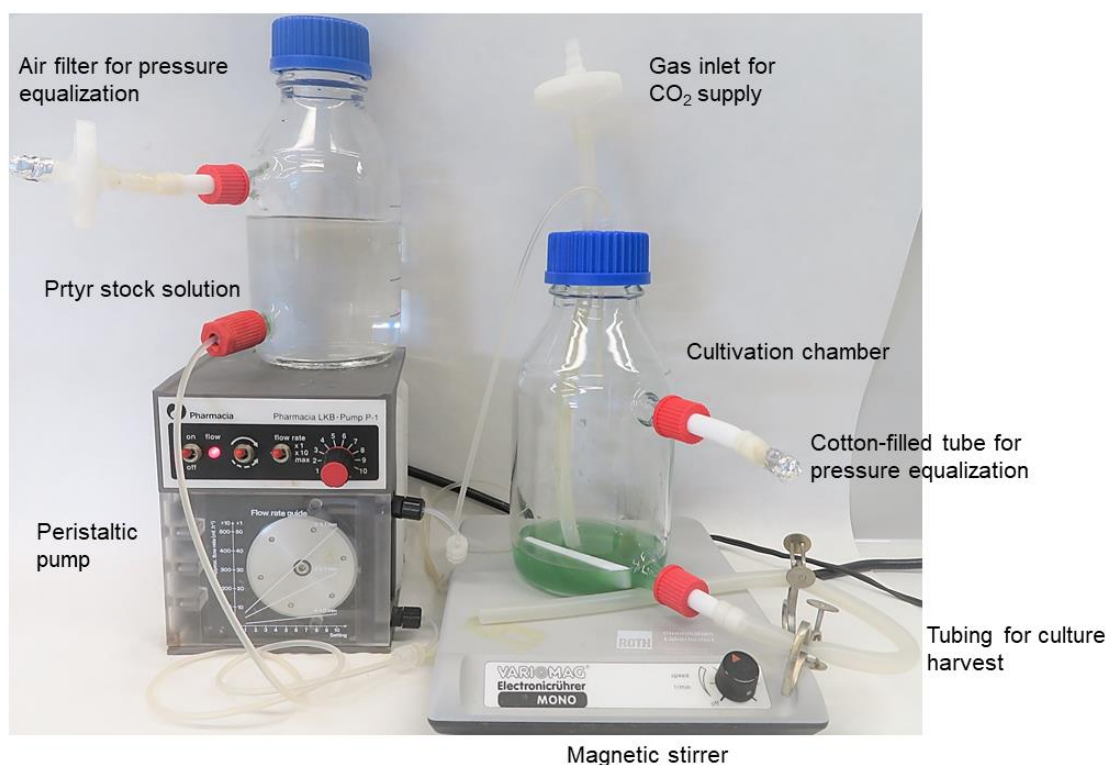


**Figure 22.** A continuous feeding system designed for the supplementation of cyanobacterial cultures with PDB substrates. Components are labeled in the figure.

### 3. Results and Discussion

---

These observations demonstrated that it was possible to grow *M. aeruginosa* CBT 480 under continuous supplementation with the substrate Prtyr without impeding the culture's fitness. However, the set-up requires further validation before conclusions can be made about its superiority over the standard supplementation protocol. On the one hand, the concentration of Prtyr needs to be monitored over time to check whether it maintains the  $c_{ss}$  of 50  $\mu\text{M}$ . Since the culture volume changes during cultivation, it is most likely that adaptations are necessary to keep the concentration at this level, e.g. by increasing the flow rate of the pump or changing the concentration of the Prtyr stock solution. On the other hand, data on the production of **3** are relevant to compare the yield of clickable MC of the continuous to a one-time supplementation. As evident from Figure 21, the production rate of **3** seems to correlate with the uptake of Prtyr. When taking a closer look at the amounts of **3**, however, it becomes clear that a big share of the substrate was lost in a one-time supplementation. This indicates an accumulation of Prtyr within the cyanobacteria or an ulterior use of the substrate in the biosynthesis of other specialized metabolites

#### 3.2.3. The Use of Prtyr in *M. aeruginosa* CBT 480

Interestingly, less than 0.2 % of the supplemented Prtyr was recovered as extractable **3**. Meissner *et al.* showed that, depending on the light conditions, about 30–60 % of the total MC content is bound to proteins and, thus, not extracted with methanol but detectable in the insoluble fraction.<sup>558</sup> However, this fact still leaves more than 99 % of the total Prtyr input unaccounted for. It is possible that the substrate accumulated within the cells due to a much faster Prtyr uptake compared to the production of **3**, which might slow down once a physiologically relevant total MC concentration is reached within the cyanobacterial cells. Also, part of the supplemented Prtyr may have been lost in the primary metabolism of both the *Microcystis* strain and the associated microorganisms. Because the culture of *M. aeruginosa* CBT 480 used for the PDB experiments was not axenic, co-cultivated heterotrophic bacteria might also have taken up Prtyr to use it as carbon and nitrogen source.<sup>[8]</sup>

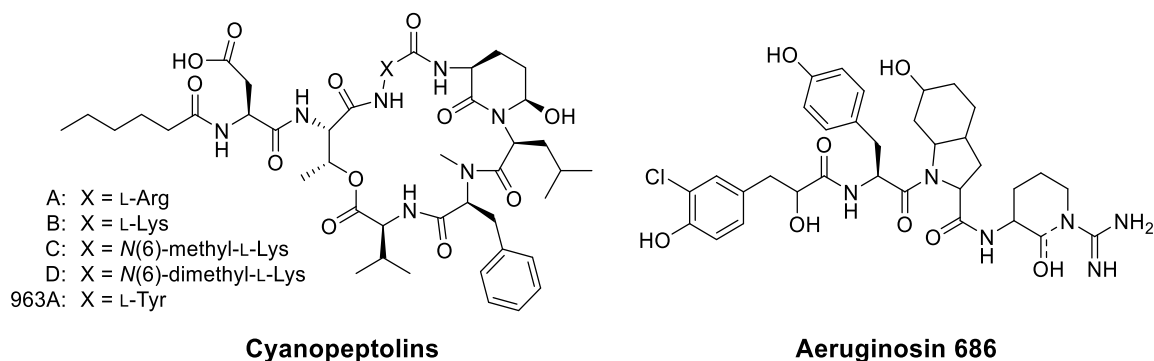
Another possibility might be the incorporation of Prtyr into other specialized metabolites of *M. aeruginosa* CBT 480. Genetic analysis revealed that cyanobacterial genomes contain about five biosynthetic gene clusters in average, but the individual

---

<sup>[8]</sup> Paragraph adapted and modified from Moschny, J.; Lorenzen, W.; Hilfer, A.; Eckenstaler, R.; Jahns, S.; Enke, H.; Enke, D.; Schneider, P.; Benndorf, R. A.; Niedermeyer, T. H. J. Precursor-directed biosynthesis and fluorescence labeling of clickable microcystins. *J Nat Prod* **2020**, 83, 1960–1970. Copyright 2020 American Chemical Society.

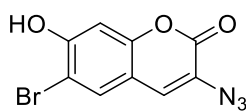
### 3.2. PDB and Fluorescence Labeling of Clickable Microcystins

numbers can reach up to 23, many of which encode up-to-date unknown metabolites.<sup>154,559,560</sup> *M. aeruginosa* PCC 7806, the probably best-characterized *M. aeruginosa* strain of all, has been shown to possess two other NRPS and NRPS–PKS encoding biosynthetic gene clusters in addition to *mcy*.<sup>561</sup> Their main products were identified as cyanopeptolins A–D and 963A, and the tautomers aeurginosin 686A and B, respectively.<sup>562–564</sup>



As evident from the structures, both NRPs feature a Tyr and in case of cyanopeptolin 963A, this Tyr residue is even located in a hypervariable position and can also be substituted by Arg (cyanopeptolin A), Lys (cyanopeptolin B) or derivatives of the latter (cyanopeptolins C and D). Thus, it is not surprising that PDB with *M. aeruginosa* PCC 7806 and clickable Tyr analogs, which was conducted by our cooperation partner Cyano Biotech GmbH, not only yielded clickable MCs, but also gave new, azido and propargyl modified cyanopeptolins (personal correspondence).

These findings and the high amounts of unaccounted Prtyr in the PDB studies prompted the search for other specialized metabolites in *M. aeruginosa* CBT 480, which are amenable for modification by PDB with Prtyr. For this purpose, methanol extracts of an *M. aeruginosa* CBT 480 culture supplemented with Prtyr and a non-treated control culture were labeled with 3-azido-6-bromo-7-hydroxycoumarin (**4**) applying the optimized CuAAC protocol of Hong *et al.*<sup>565</sup> Compound **4** is a brominated, fluorogenic probe and was developed to affix a fluorescent and MS-sensitive tag to propargyl residues in proteins.<sup>566</sup> Recently, it was applied to identify endogenous terminal alkyne containing natural products in the cyanobacterium *Moorea producens*.<sup>567</sup>



**4**

### 3. Results and Discussion

The reaction mixtures were spotted on a NP HP-TLC plate together with a blank reaction mix and standards of **1**, Prtyr, and **3**, all labeled in the same manner with **4** as negative (Blank and **1**) and positive controls (Prtyr and **3**), respectively. After development, the HP-TLC plate was analyzed by UV detection at 365 nm without further staining and by determination of the retardation factor  $R_f$  (Figure 23).

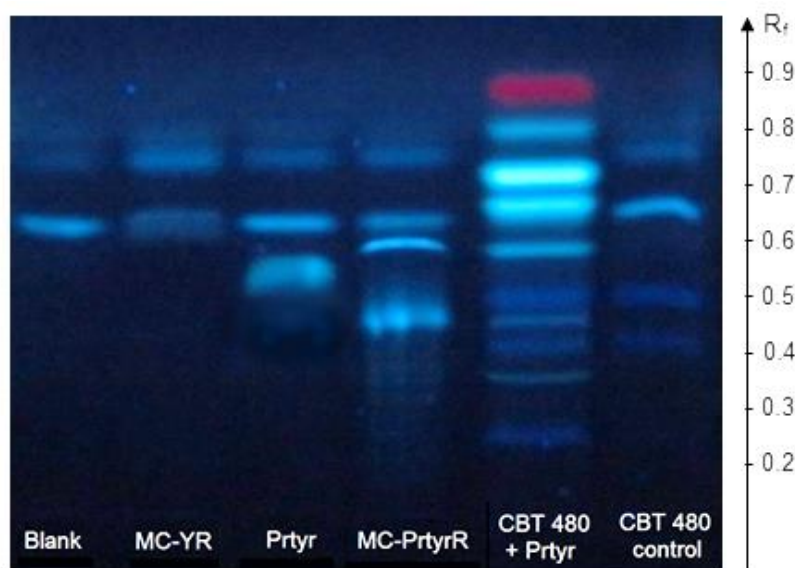


**Figure 23.** HP-TLC plate (UV detection at 365 nm) of a blank, of standards of MC-YR (**1**), Prtyr, and MC-PrtyrR (**3**) and of methanol extracts of an *M. aeruginosa* CBT 480 culture supplemented with Prtyr and a control culture, after conjugation with 3-azido-6-bromo-7-hydroxycoumarin (**4**).

The blank reaction mix showed two bands, an intense one with  $R_f$  0.63 and a weaker one with  $R_f$  0.74 probably due to ring opening of the lactone in aqueous solution. This further indicates that **4** is not fluorogenic at an excitation wavelength of 365 nm, but exhibits a residual, blue background fluorescence. The other negative control, **1**, displayed a similar pattern of bands with inversed intensities. The fluorescently labeled product of Prtyr gave a blue fluorescent band with  $R_f$  0.55 while for MC-PrtyrR two blue fluorescent products were observed. This, however, was to be expected as the stock solution of MC-PrtyrR (fluorescently labeled product with  $R_f$  0.46) contained small amounts of the artifact MC-PrtyrR(GluOMe), which corresponds to the band with  $R_f$  0.59.

Interestingly, the sample of *M. aeruginosa* CBT 480 supplemented with Prtyr exhibited several blue fluorescent bands with  $R_f$  values between 0.25 and 0.8. One of the bands was linked to the fluorescently labeled product of MC-PrtyrR, and the band with  $R_f$  0.58 might arise from accumulated Prtyr. The difference in  $R_f$  (0.03) is most likely due to inaccuracies in the determination of  $R_f$ . All other blue fluorescent bands, including the two most intense ones with  $R_f$  values of 0.71 and 0.66, could not be linked to any known

or expected product, suggesting that P<sub>tyr</sub> might indeed have been incorporated into other metabolites or that MC degradation products were present in the extract.

When taking a close look at the *M. aeruginosa* CBT 480 control, it becomes clear that the sample not only exhibited two bands from background fluorescence of unconjugated **4**, but also showed two additional, blue fluorescent bands with R<sub>f</sub> values of 0.42 and 0.5. Corresponding bands are also present in the sample of *M. aeruginosa* CBT 480 supplemented with P<sub>tyr</sub>, indicating that they can emerge out of two different reasons. Firstly, cyanobacteria have been shown to exhibit a strong, blue autofluorescence, which emanates from the pigments phycocyanin (maximum emission wavelength,  $\lambda_{em\ max.}$  650 nm) and allophycocyanin ( $\lambda_{em\ max.}$  665 nm).<sup>568,569</sup> Secondly, around 30 different compounds or classes of metabolites, all of which carry a terminal alkyne, were discovered in cyanobacteria.<sup>567,570</sup> Although such compounds exclusively occurred in strains of marine habitats while *M. aeruginosa* are freshwater cyanobacteria, the presence of endogenous, terminal alkynes-containing NPs in *M. aeruginosa* CBT 480 cannot fully be excluded.

Furthermore, the input amounts of extract template are remarkably different between the sample of *M. aeruginosa* CBT 480 supplemented with P<sub>tyr</sub> and the corresponding control sample. The extract of *M. aeruginosa* CBT 480 with P<sub>tyr</sub> was much higher concentrated as it is evident from the strong red fluorescent band with R<sub>f</sub> 0.87 of chlorophyll *a*, which is absent in the control. Thus, the putative additional, blue fluorescent bands of *M. aeruginosa* CBT 480 with P<sub>tyr</sub> could also be present in the control, but may not be discernible if their intensities fall below the limit of detection. In other words, their presence in *M. aeruginosa* CBT 480 supplemented with P<sub>tyr</sub> cannot be unambiguously linked to the incorporation of P<sub>tyr</sub> in specialized metabolites other than MCs based on this set of data.

Out of this reason, the HP-TLC method was adapted in order to overcome this drawback. Instead of performing the CuAAC reaction prior to HP-TLC analysis, the crude templates, i.e. a water blank, the stock solutions of **1**, P<sub>tyr</sub>, and **3**, as well as the methanol extracts of a *M. aeruginosa* CBT 480 culture supplemented with P<sub>tyr</sub> and a control culture, were spotted on the plate. The bands were evaluated by UV detection at 365 nm. The volumes of the two *M. aeruginosa* CBT 480 extracts were optimized to give red fluorescent bands of chlorophyll *a* (R<sub>f</sub> 0.87) with comparable intensities.

Afterwards, the CuAAC reaction was performed on the HP-TLC plate by using the reaction mixture as TLC staining reagent. The mixture, which contained the same components as for conjugation except for the templates was sprayed on the plate and let to air-dry at room temperature. Optimization of the staining procedure revealed that

### 3. Results and Discussion

lowering the concentration of **4** from 100  $\mu\text{M}$  to 10  $\mu\text{M}$  with simultaneous heating at 70  $^{\circ}\text{C}$  for 10 s gave the best SNR. The TLC stain could be stored at 4  $^{\circ}\text{C}$  for up to four weeks without losing its staining ability. Storage durations beyond that period were not investigated.

Before the staining, no signals for both the negative (blank and **1**) and positive (Prtyr and **3**), controls were observed (Figure 24A). The two methanol extracts of the *M. aeruginosa* CBT 480 cultures exhibited an identical pattern of red and blue fluorescent bands confirming the assumption that part of the signals in the cyanobacterial extracts are due to autofluorescence. Even though the intensities of a few, individual bands differed between the two templates, the overall amount spotted on the HP-TLC plate seemed to be in the same range.

After staining with the CuAAC reaction mix (Figure 25B), a blue-green fluorescent band for Prtyr appeared with  $R_f$  0.59 while four signals became discernible for **3**. The two major bands with  $R_f$  0.64 and  $R_f$  0.49 belonged to MC-PrtyrR(GluOMe) and compound **3**, respectively. The two fainter ones had  $R_f$  values of 0.61 and 0.44 and might arise from ring opening of the respective MC variant. Like the blank and negative control **1**, the methanol extract of the *M. aeruginosa* CBT 480 control culture did not show any new bands after staining. This indicates that *M. aeruginosa* CBT 480 does not produce any endogenous metabolites with a terminal alkyne moiety.

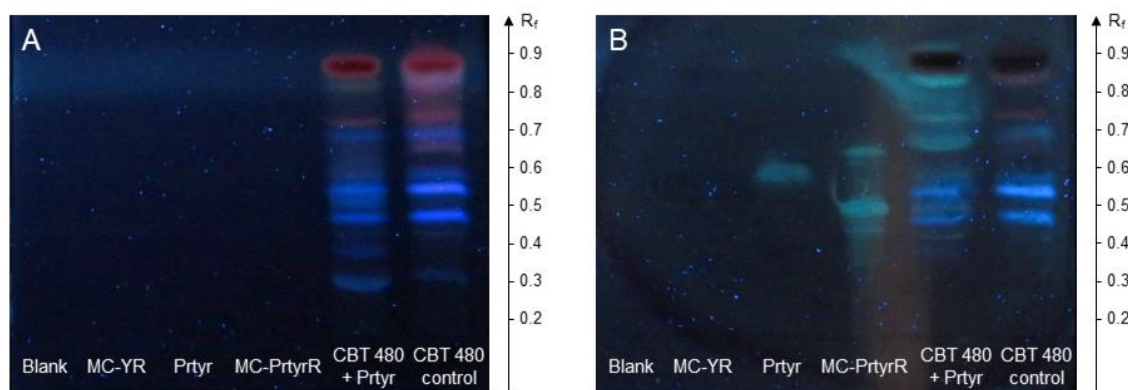


**Figure 24.** HP-TLC plate (UV detection at 365 nm) of a water blank, the stock solutions of MC-YR (**1**), Prtyr, and MC-PrtyrR (**3**), and methanol extracts of an *M. aeruginosa* CBT 480 culture supplemented with Prtyr and a control culture, before (A) and after (B) staining with a CuAAC reaction mix.

In contrast, the sample of *M. aeruginosa* CBT 480 supplemented with Prtyr exhibited seven additional, blue-green fluorescent bands after staining with the CuAAC reaction mix. Two signals corresponded to Prtyr and **3**. The other five bands had  $R_f$  values of 0.41, 0.66, 0.73, 0.83 and 0.92, indicating that at least five other products of *M.*

*aeruginosa* CBT 480 bear a terminal alkyne that can be labeled with **4**. Judging from their  $R_f$  values, four of them are intermediate ( $R_f$  0.66 and 0.73) to strongly ( $R_f$  0.83 and 0.92) hydrophobic while only one is hydrophilic with an even lower  $R_f$  than **3**. However, no information could be obtained about the chemical nature of these additional compounds, and it is unclear whether they are chemically related to MCs or not. Further studies would be needed to elucidate the structures of these clickable compounds.

This is the first report of applying a fluorogenic CuAAC reaction as TLC stain for the *in situ* labeling of terminal alkynes. Schröder *et al.* developed a TLC stain based on the CuAAC click reaction for the identification of azides and primary amines with propargylic alcohol.<sup>571</sup> The read-out, however, involved the discoloration of the TLC plate after successful conjugation, i.e. the detection of white spots on a white TLC plate what is likely prone to false positives and definitively less sensitive than the detection of fluorescent bands.

Another method combined radio-TLC with an alkyne-functionalized  $^{18}\text{F}$ -positron emitter in order to identify organic azides.<sup>572</sup> Although radiation can be detected with higher sensitivity than fluorescence, this technique requires special technical equipment for detection and the handling of radioactive substances. Thus, it cannot be adapted as easily as the method described here.

Comparative TLC of the methanol extract obtained from PDB studies before and after conjugation with a fluorogenic dye proved a fast and easy tool to pinpoint clickable groups in the extract. The findings were also confirmed by HPLC coupled to a fluorescence detector (Table 8). The HPLC–fluorescence chromatogram overlay (Figure A111) shows that after conjugation with **4**, the extract of *M. aeruginosa* CBT 480 supplemented with Prtyr exhibited five additional peaks, which were absent in the control extract.

The information gained from this technique could be extended by an additional dimension when coupling it to MS via a TLC–MS interface.<sup>573</sup> Since **4** also carries bromine as MS-tag, the  $m/z$  values of the conjugated products should be dissectible from other signals revealing potential masses of other PDB-modified metabolites. No such TLC–MS interface was available, and a method using the MS-imaging MALDI source was not established yet, so the extract of *M. aeruginosa* supplemented with Prtyr was labeled with **4** and the reaction mix was analyzed by HPLC–HRMS (Table 15). The TIC was searched for halogenated compounds using the software tool HaloSeeker 1.0, which was especially designed for this purpose.<sup>574</sup>

Unfortunately, the tool only revealed false positive hits and varying different parameters of analysis did not make a difference. The main problem seemed to consist

### 3. Results and Discussion

---

in the peak-picking because the overall intensity of peaks was very low. Consequently, it was not possible to identify the masses of the other potential PDB products from the available set of data, but this might be overcome by optimizing the HPLC–HRMS conditions. Due to the complexity of the sample, a manual search for brominated analytes was not practical.

A major disadvantage of this HPLC–HRMS analysis is the loss of information concerning the missing fluorescence detection. Either installing an online HPLC–fluorescence detector before the MS or developing a TLC–MS method as mentioned above would help to correlate the fluorescence of peaks/bands to MS signals of brominated compounds and, thus, facilitate the identification of the  $m/z$  values belonging to the alkyne-containing compounds.

Still, the application of comparative TLC of the *M. aeruginosa* CBT 480 extract obtained from PDB studies provided important indications for the use of Prtyr in metabolites other than MCs. Although the nature of these metabolites could not be established and a certain risk remained that the fluorescent bands arose from artifacts, this is crucial knowledge in case the PDB-modified MCs were to be used for physiological studies in cyanobacteria.

Kurmayer *et al.* used alkyne-labeled MCs and anabaenopeptins for *in vivo* fluorescence microscopy in a *Planktothrix argadhii* and *M. aeruginosa* strain.<sup>575</sup> Even though they contemplated the possibility of an untargeted incorporation of the clickable amino acids, they dismissed it based on manual comparison of HPLC–MS (ion trap) data. However, this approach is questionable since low-abundant compounds or such with bad ionization properties can easily be overlooked. Additionally, the manual comparison of HPLC–MS data set is time-consuming and automated methods require high computing capacities and are still under development. In contrast, the comparative TLC analysis is easy to adapt, fast and provides more comprehensive data.

If it is further coupled to MS, this not only allows for the identification of the alkyne-labeled metabolites, but even enables the application of PDB for an untargeted discovery of new NPs. By transferring the PDB experiments into a format suitable for screening, various cyanobacteria strains could be supplemented with clickable amino acids or other CuAAC-modified precursors. After extraction, comparative TLC should reveal the incorporation of the precursors while the metabolites can be dereplicated by means of HRMS data and NP database research. Conceding that discovered masses are not catalogued, the clickable precursors are most likely incorporated into unknown specialized metabolites. In such cases, the bioorthogonal handle presents another advantage. It could further facilitate the purification of the putative, new NP by introducing



an affinity tag (e.g. biotin) via a CuAAC reaction and enriching it on suitable solid support materials (e.g. agarose beads) prior to analysis.<sup>576,577</sup>

As obvious from this short reasoning, the possibilities to make use of MCs and other specialized metabolites, which are derivatized with clickable functions, are not exhausted yet. In addition to studying their physiological role, they can also serve for pharmacological studies in target cells, producing relevant information on their suitability as lead structures for drug development.

#### 3.2.4. Fluorescence Labeling of MC-PrtyrR (3) and Biological Characterization of the Conjugate

*This chapter is adapted and modified from Moschny, J.; Lorenzen, W.; Hilfer, A.; Eckenstaler, R.; Jahns, S.; Enke, H.; Enke, D.; Schneider, P.; Benndorf, R. A.; Niedermeyer, T. H. J. Precursor-directed biosynthesis and fluorescence labeling of clickable microcystins. *J Nat Prod* **2020**, 83, 1960–1970. Copyright 2020 American Chemical Society.*

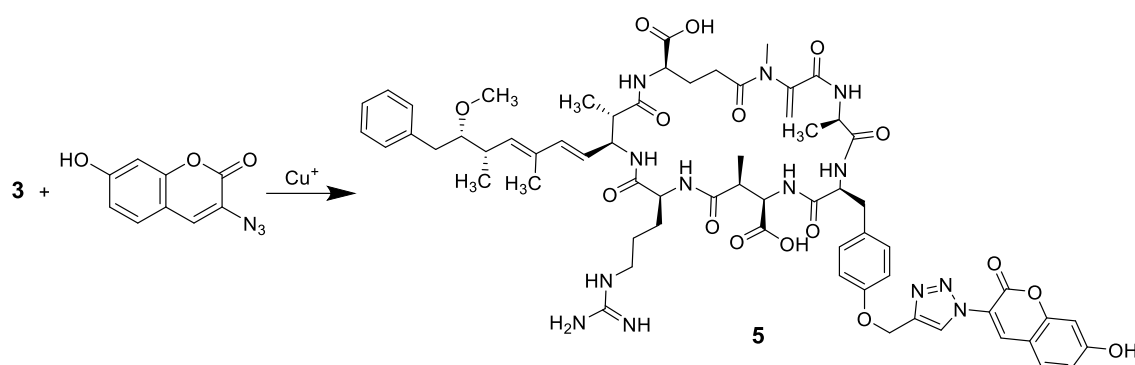
Compound **3** was isolated from *M. aeruginosa* CBT 480 (Figure A112) by Dr. Wolfram Lorenzen (see chapter 2.7.5) and its postulated structure was confirmed by NMR spectroscopy and HRMS (Figure A 113 and Figure A122; Table A11). The total yield was 40 mg isolated from 63.5 g dry biomass. Judging from HPLC–DAD, HRMS, and NMR data, the substance contained about 10 % impurities, most likely the *O*-methyl ester of D-Glu<sup>6</sup>, MC-PrtyrR(GluOMe), as major impurity. This variant was not detectable in the crude extract, so it was presumably formed as artifact during purification, e.g. by using methanol supplemented with TFA as mobile phase in preparative HPLC. Such esterification under acidic conditions has been observed previously.<sup>578,579</sup> Since the peak of the impurity is chromatographically resolved from the product peak, the impact of the impurity on future experiments was estimated to be neglectable. Thus, compound **3** was not further purified.

Since the development of the fluorogenic 3-azido-7-hydroxycoumarin by Sivakumar *et al.* in 2004, fluorescence labeling of terminal alkynes belongs to the most prominent applications of CuAAC with more than 500 publications referring to this work.<sup>349,580</sup> One advantage of this probe is its low molecular weight, making it highly suitable for studies in which major structural changes in the molecule of interest are undesired (e.g. in target binding or interaction studies). Thus, this coumarin derivative was chosen as a fluorogenic tag to design a fluorescent MC congener as a probe for uptake and cytotoxicity studies. Using an optimized reaction protocol of Hong *et al.*,<sup>565</sup> 3-azido-7-

### 3. Results and Discussion

hydroxycoumarin was conjugated with **3**, yielding the fluorescent MC derivative MC-(O-((7-hydroxy-2H-chromen-3-yl)-1H-1,2,3-triazol-4-yl)methyl)YR (**5**).

Compound **5** was purified from the reaction mix by solid-phase extraction (SPE) and semi-preparative HPLC (Table 19 and Table 20; Figure A123). HRMS<sup>2</sup> data of **5** were consistent with the postulated structure (Figure A124 and Table A12). Due to an error in the SPE protocol, a significant amount of product was lost in the work-up. Consequently, no yield could be calculated for the conjugation reaction. The remaining low amount was quantified by HPLC–ELSD (Table 11).



**Scheme 6.** Conjugation of MC-PrtyrR (**3**) with 3-azido-7-hydroxycoumarin yielding the blue fluorescent MC-PrtyrR-coumarin conjugate MC-(O-((7-hydroxy-2H-chromen-3-yl)-1H-1,2,3-triazol-4-yl)methyl)YR (**5**).

The cytotoxicity of the fluorescent MC **5**, its clickable precursor **3**, and the native MC **1** was determined. Structural modifications can influence cytotoxicity in two ways. On one hand, binding of the MC to its targets PP1 and PP2A could be influenced. As it is known that the pharmacophore of MCs is the Adda<sup>5</sup>–D-Glu<sup>6</sup> substructure, the modification site (position 2) is as far away as possible from the pharmacophore, and the effect of the derivatization on PP binding was suspected to be low.<sup>236,243,244</sup>

On the other hand, the structural modifications could also have an effect on the uptake of MCs into cells by OATP1B1 and OATP1B3. Although both transporters possess a broad substrate tolerance,<sup>269</sup> it is unpredictable whether they are still capable of transporting **5** into cells. The chemical features in naturally occurring MC that might affect MC uptake by both transporters have been studied before.<sup>292,524</sup>

Furthermore, semi-synthetically modified MC variants carrying different fluorescent tags were tested against the liver carcinoma cell line HuH-7 and a HEK293 cell line expressing drOATP1D1, an OATP-subtype from zebrafish.<sup>556,581</sup> Although no data on the cytotoxicity of the fluorescent MC on the drOATP1D1 expressing HEK293 cells were provided, cellular uptake was demonstrated by fluorescence microscopy. However, transport by human OATP has not been studied. Comparable fluorescence microscopy

data were also obtained for HuH-7 cells, but as for most cell lines established from primary cells, HuH-7 cells were shown to significantly downregulate OATP expression when cultured.<sup>582</sup> Thus, not surprisingly, the  $EC_{50}$  of both the fluorescent MC and MC-LR were found to be about 20  $\mu$ M, which is about 1000-fold higher than the values usually found for MCs.<sup>292,525,583</sup> This makes it difficult to estimate the OATP transportability of the fluorescent MC compared to the native MC.

Thus, the cytotoxicity of **1**, **3**, and **5** against OATP1B1- and OATP1B3-expressing HEK293 cells and the corresponding control cell lines was determined (Figure 25). As expected, all three MC derivatives were inactive against both empty vector control cell lines (no OATP expression). In contrast, they exhibited pronounced activity against the OATP1B1- and OATP1B3-expressing cells, with  $EC_{50}$  values in the low nanomolar range. The differences between the three derivatives are statistically insignificant, indicating that the coumarin label affects neither the transport nor the PP1/PP2A inhibition.

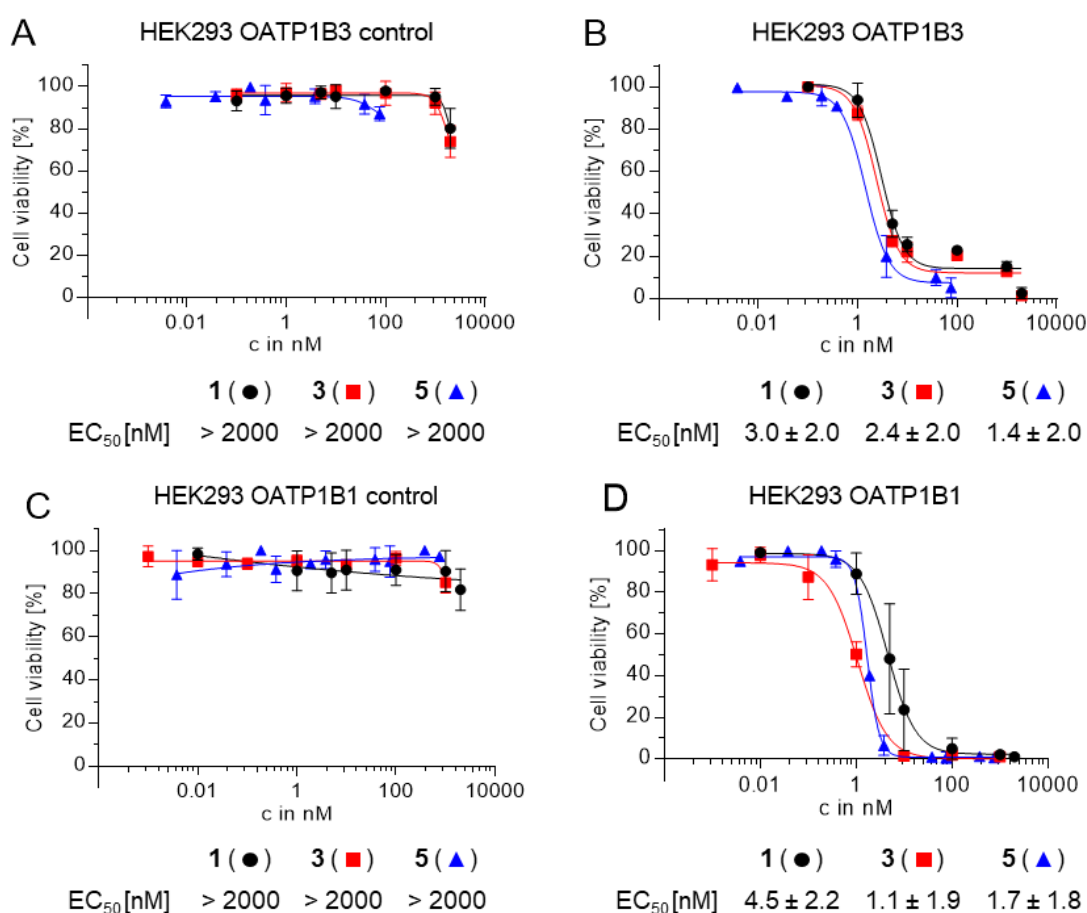


**Figure 25.** Cytotoxicity of MC-YR (**1**, black circles), MC-PrtyrR (**3**, red squares), and MC-(O-((7-hydroxy-2H-chromen-3-yl)-1H-1,2,3-triazol-4-yl)methyl)YR (**5**, blue triangles) against HEK293 OATP1B3 control cells (A), HEK293 OATP1B3 cells (B), HEK293 OATP1B1 control cells (C), and HEK293 OATP1B1 cells (D). Adapted with permission from Moschny *et al.*<sup>194</sup> Copyright 2020 American Chemical Society.

### 3. Results and Discussion

The fluorescent MC **5** was used for uptake studies into OATP1B3-expressing HEK293 cells as well as the corresponding control cells. Prior to the measurements, the excitation and emission spectra of **5** in growth medium and DMSO (Figure A125) was recorded in order to identify suitable wavelengths for fluorescence microscopy. Time-lapse measurements revealed that the probe accumulated rapidly in OATP1B3<sup>+</sup> cells. Within 14 min of exposure to 100 nM of **5**, maximum fluorescence intensity in the cells was reached, with a simultaneous decrease in background fluorescence (Figure 26). For the control cells, no staining was observed, but background fluorescence was slightly reduced over time due to photo-bleaching of the dye. Similar results were obtained for OATP1B1<sup>+</sup> HEK293 cells and their control cells (Figure A126).

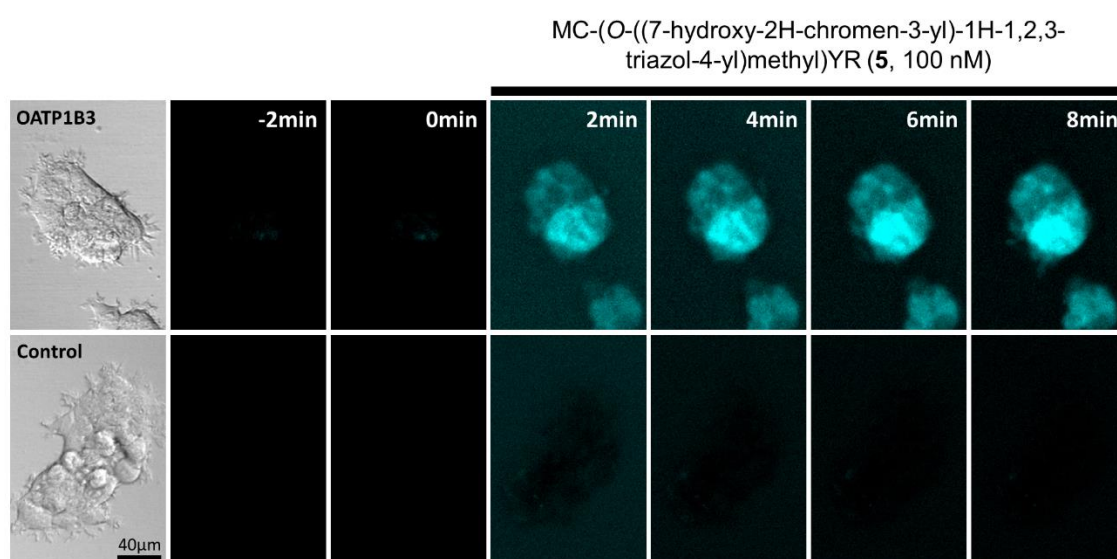


**Figure 26.** Fluorescence time-lapse microscopy of OATP1B3<sup>+</sup> HEK293 cells (upper row) and the corresponding control cells (lower row) before and after exposure to 100 nM MC-(O-((7-hydroxy-2H-chromen-3-yl)-1H-1,2,3-triazol-4-yl)methyl)YR (**5**). The first picture of each row depicts the brightfield image of the selected cell colony. After 8 min, the increase in fluorescence intensity was not visually discernible anymore. Adapted with permission from Moschny *et al.*<sup>194</sup> Copyright 2020 American Chemical Society.

In comparison to previous MC uptake studies, in which fluorescence imaging was performed after 30 min and 4 h, respectively, this time-lapse recording showed that the main part of the probe is taken up within the first 15 min.<sup>556,581</sup> Afterward, photo-bleaching effects of the dye outweighed the gain in fluorescence intensity per cell, leading to an overall signal decrease. These findings are in accordance with the previously described OATP1B1 and OATP1B3 uptake kinetics for MC-LR by Fischer *et al.*, who chose an incubation time of 15 min to determine the Michaelis constant  $K_M$  and the maximal velocity  $V_{max}$ .<sup>524</sup>

### 3.2. PDB and Fluorescence Labeling of Clickable Microcystins

The roughly homogenous distribution of signal intensity throughout the whole cell indicates a cytosolic localization of **5**, but further measurements at higher resolutions and in combination with a cytosolic marker are required to confirm this hypothesis. In addition, more statistical replicates are needed in order to determine the kinetic parameters for the uptake of the MC-coumarin conjugate by OATP1B1 and OATP1B3.

# 4. CONCLUSION

The presented work aimed at the identification of MC variants, which can be used as lead structures for the development of MC-based anticancer agents. For this purpose, an optimized method for MC isolation and quantification was developed. These efforts led to a sophisticated and versatile workflow, which offers three different routes covering amounts of starting material from only few milligrams to several grams.

The main approach to set the starting point for a clinical development of MCs consisted in the introduction of bioorthogonal groups into the peptides. This was achieved by means of PDB, which proved feasible for the generation of an array of clickable MCs. When investigating the underlying kinetics, the apparent, but unforeseen incorporation of the substrate into other metabolites raised new implications for using PDB as basis for *in vivo* labeling. One of the clickable MCs was linked to a fluorogenic dye, and the resulting conjugate was biologically characterized providing important information on the suitability of conjugated, clickable MCs as anticancer lead structures.

This chapter will give an overview of the key findings of the thesis, including the main conclusions drawn from the results.

## 4.1. The Toolbox for MC Isolation and Quantification

In the presented work, a straightforward protocol for the fast isolation of MCs was established. Since the MCs are produced in rather low amounts, it is important that they are quantitatively isolated from the biomass. In addition to isolation efficiency, time plays a crucial role in natural product research. A technique that proves fast and feasible for low amounts of starting material may turn out to be time-consuming and inefficient when transferred to larger amounts due to its limitations in through-put. Taking this into account, the workflow was compiled in a manner that three different routes became available, which were optimized in terms of input amount.

Even despite this sophisticated method, the possibility remained that the yields of isolated MCs fell below weighable quantities. In consequence, a HPLC–ELSD method was developed for MC quantification. Its thorough validation qualified it for a structure-independent quantification of MCs in the nanogram range. To the best of my knowledge, this is the first method matching both these criteria — structure-independence and high sensitivity. Due to its simplicity, the method can easily be adapted or transferred to other laboratory environments.

## 4.2. Implications for *In Vivo* Imaging and Other Applications of PDB

Using PDB to insert bioorthogonal functions and exploiting them for *in vivo* labeling and other physiologic studies has been done for many natural products, including MCs. With the detection of other, supposedly clickable functions in cyanobacteria after PDB, doubts arise about the reliability of all of these data if the incorporation of the substrate or a substructure of it into other specialized metabolites had not been ruled out explicitly. There is a certain amount of risk that a significant share of detected signals or other findings result from artifacts or false positive labeling.

If PDB in *Microcystis* sp. shall still be used for studying the function of MCs in cyanobacteria, the strain has to be selected with great care. When choosing a strain, of which the whole genome sequence is available, genome mining might reveal putative biosynthetic gene clusters of interfering, specialized metabolites. However, the products of many biosynthetic gene clusters are still obscure. Thus, it is inevitable to check for the presence of the bioorthogonal functions elsewhere than the MCs unless the findings can be unambiguously attributed to MCs, e.g. by combination of the read-out with immuno-based techniques or HRMS<sup>2</sup> showing MC-specific fragments.

The herein developed, comparative analysis of an extract before and after conjugation with a MS-tagged fluorescence dye represents an easily adaptable and versatile method, which has not been reported up to date. Likewise, the use of a CuAAC-based TLC stain employing a fluorogenic probe has not been described previously. It can also be applied to the rapid identification of endogenous terminal alkynes.

By fine-tuning of the HRMS parameters, the MS tag should further disclose the exact mass and, in consequence, the sum formula of the labeled specialized metabolites, facilitating their dereplication. Following this reasoning, PDB might even prove a useful tool for the discovery of new natural products in cases the exact mass and, consequently, the metabolite is unknown

### 4.3. Clickable MCs in ADC

PDB led to the generation of more than 40 clickable MCs comprising several different bioorthogonal functionalities. The majority of them possess a new, yet undescribed chemical structure except for one variant obtained by total synthesis. One clickable MC has been isolated in decent yield (10 mg per 20 L culture). The obtainable yield offers room for improvement because the conditions of substrate supplementation have not been optimized yet. This is a noteworthy fact as the supply of material is essential for the clinical development of a new therapeutic, and economic consideration are as important as pharmacological ones for its success.

Furthermore, the biological characterization of the clickable MC and the fluorescent conjugate provided promising *in vitro* data. The bioorthogonal group did not affect the activity of both variants, indicating a potential suitability of the clickable MCs as anticancer drugs. Out of this reason, the modified MCs and their generation by means of PDB were protected by two patents.<sup>584,585</sup> This is the first step towards the development of a new targeted therapy based on MC lead structures, which might help to fight the mortality of cancer and abate the people's fear.



## 5. REFERENCES

- (1) Vrinten, C.; Waller, J.; Wagner, C. von; Wardle, J. Cancer fear: facilitator and deterrent to participation in colorectal cancer screening. *Cancer Epidemiol Biomarkers Prev* **2015**, *24*, 400–405.
- (2) Morrell, L.; Li, S. S.; Wordsworth, S.; Wilson, R.; Rees, S.; Barker, R. Cancer as the “perfect storm”? A qualitative study of public attitudes to health conditions. *Health Sci Rep* **2018**, *1*, e16.
- (3) Kochanek, K. D.; Murphy, S. L.; Xu, J.; Arias, E. Deaths: final data for 2017. *Natl Vital Stat Rep* **2019**, *68*.
- (4) Siegel, R. L.; Miller, K. D.; Jemal, A. Cancer statistics, 2020. *CA Cancer J Clin* **2020**, *70*, 7–30.
- (5) United Nations Development Programme. *Human development report 1990*; UNDP: New York, NY, 1990.
- (6) World Health Organization. *Global health estimates 2016: deaths by cause, age, sex, by country and by region 2000–2016*; WHO: Geneva, 2018.
- (7) Cao, B.; Soerjomataram, I.; Bray, F. The burden and prevention of premature deaths from non-communicable diseases, including cancer: a global perspective. In *World cancer report: cancer research for cancer prevention*; Wild, C. P., Weiderpass, E., Stewart, B. W., Eds.; IARC: Lyon, France, 2020; pp 16–22.
- (8) Bray, F.; Ferlay, J.; Soerjomataram, I.; Siegel, R. L.; Torre, L. A.; Jemal, A. Global cancer statistics 2018: GLOBOCAN estimates of incidence and mortality worldwide for 36 cancers in 185 countries. *CA Cancer J Clin* **2018**, *68*, 394–424.
- (9) Moser, R. P.; Arndt, J.; Han, P. K.; Waters, E. A.; Amsellem, M.; Hesse, B. W. Perceptions of cancer as a death sentence: prevalence and consequences. *J Health Psychol* **2014**, *19*, 1518–1524.
- (10) Quaife, S. L.; Winstanley, K.; Robb, K. A.; Simon, A. E.; Ramirez, A. J.; Forbes, L. J. L.; Brain, K. E.; Gavin, A.; Wardle, J. Socioeconomic inequalities in attitudes towards cancer: an international cancer benchmarking partnership study. *Eur J Cancer Prev* **2015**, *24*, 253–260.
- (11) Murphy, P. J.; Marlow, L. A. V.; Waller, J.; Vrinten, C. What is it about a cancer diagnosis that would worry people? A population-based survey of adults in England. *BMC Cancer* **2018**, *18*, 1–10.
- (12) Vrinten, C.; McGregor, L. M.; Heinrich, M.; Wagner, C. von; Waller, J.; Wardle, J.; Black, G. B. What do people fear about cancer? A systematic review and meta-synthesis of cancer fears in the general population. *Psycho-Oncol* **2017**, *26*, 1070–1079.
- (13) Do, K. T.; Kummar, S. Therapeutic targeting of cancer cells: era of molecularly targeted agents. In *Abeloff's clinical oncology*, 6th edition; Niederhuber, J. E., Armitage, J. O., Doroshow, J. H., Kastan, M. B., Tepper, J. E., Eds.; Elsevier Inc: Philadelphia, PA, 2020; 420–430.
- (14) Dobrenkov, K.; Cheung, N.-K. V. Therapeutic antibodies and immunologic conjugates. In *Abeloff's clinical oncology*, 6th edition; Niederhuber, J. E., Armitage, J. O., Doroshow, J. H., Kastan, M. B., Tepper, J. E., Eds.; Elsevier Inc: Philadelphia, PA, 2020; 486–499.
- (15) Su, W.; Zhang, X.; Cai, X.; Peng, M.; Wang, F.; Wang, Y. BIM deletion polymorphism predicts poor response to EGFR-TKIs in nonsmall cell lung cancer: an updated meta-analysis. *Medicine* **2019**, *98*, e14568.
- (16) Marin, J. J. G.; Briz, O.; Herraiez, E.; Lozano, E.; Asensio, M.; Di Giacomo, S.; Romero, M. R.; Osorio-Padilla, L. M.; Santos-Llamas, A. I.; Serrano, M. A.; *et al.* Molecular bases of the poor response of liver cancer to chemotherapy. *Clin Res Hepatol Gastroenterol* **2018**, *42*, 182–192.

## 5. References

---

- (17) Jukkola, A.; Bloigu, R.; Soini, Y.; Savolainen, E.-R.; Holli, K.; Blanco, G. c-erbB-2 Positivity is a factor for poor prognosis in breast cancer and poor response to hormonal or chemotherapy treatment in advanced disease. *Eur J Cancer* **2001**, *37*, 347–354.
- (18) Rueff, J.; Rodrigues, A. S. *Cancer drug resistance*; Springer: New York, NY, 2016.
- (19) Ferlay, J.; Ervik M.; Lam F.; Colombet M.; Mery L.; Piñeros M.; Znaor A.; Soerjomataram, I.; Bray, F. Global cancer observatory: cancer today. <https://gco.iarc.fr/today> (accessed March 20, 2020).
- (20) Gupta, S.; Harper, A.; Ruan, Y.; Barr, R.; Frazier, A. L.; Ferlay, J.; Steliarova-Foucher, E.; Fidler-Benaoudia, M. M. International trends in the incidence of cancer among adolescents and young adults. *J Natl Cancer Inst* **2020**, djaa007.
- (21) Johnston, W. T.; Erdmann, F.; Newton, R.; Steliarova-Foucher, E.; Schüz, J.; Roman, E. Childhood cancer: estimating regional and global incidence. *Cancer Epidemiol* **2020**, 101662.
- (22) Omran, A. R. The epidemiologic transition: a theory of the epidemiology of population change. *Milbank Mem Fund Q* **1971**, *49*, 509–538.
- (23) Bray, F. Transitions in human development and the global cancer burden. In *World cancer report 2014*; Stewart, B. W., Wild, C. P., Eds.; IARC: Lyon, France, 2014; pp 54–68.
- (24) Fidler-Benaoudia, Miranda M; Bray, F. Transitions in human development and the global cancer burden. In *World cancer report: cancer research for cancer prevention*; Wild, C. P., Weiderpass, E., Stewart, B. W., Eds.; IARC: Lyon, France, 2020; pp 34–44.
- (25) Forman, D.; Ferlay, J. The global and regional burden of cancer. In *World cancer report 2014*; Stewart, B. W., Wild, C. P., Eds.; IARC: Lyon, France, 2014; pp 16–53.
- (26) Bray, F.; Møller, B. Predicting the future burden of cancer. *Nat Rev Cancer* **2006**, *6*, 63–74.
- (27) Brenner, H.; Rothenbacher, D.; Arndt, V. Epidemiology of stomach cancer. In *Cancer epidemiology*; Verma, M., Ed.; Humana Press: Totowa, NY, 2009; pp 467–477.
- (28) Forner, A.; Llovet, J. M.; Bruix, J. Hepatocellular carcinoma. *Lancet* **2012**, *379*, 1245–1255.
- (29) Ferlay, J. The IARC cancer mortality database. <http://www-dep.iarc.fr/WHODb/WHODb.htm> (accessed March 22, 2020).
- (30) Arnold, M.; Rutherford, M. J.; Bardot, A.; Ferlay, J.; Andersson, T. M.-L.; Myklebust, T. Å.; Tervonen, H.; Thursfield, V.; Ransom, D.; Shack, L.; *et al.* Progress in cancer survival, mortality, and incidence in seven high-income countries 1995–2014 (ICBP SURVMARK-2): a population-based study. *Lancet Oncol* **2019**, *20*, 1493–1505.
- (31) Davar, D.; Tarhini, A. A.; Kirkwood, J. M. Immunotherapy of cancer. In *Principles of Oncology*; The American Cancer Society, Ed.; John Wiley & Sons, Inc: Hoboken, NJ, 2018; pp 244–266.
- (32) Zeidner, J. F.; Kanakry, C. G.; Luznik, L. Hematopoietic stem cell transplantation for cancer. In *Principles of Oncology*; The American Cancer Society, Ed.; John Wiley & Sons, Inc: Hoboken, NJ, 2018; pp 284–292.
- (33) Talmadge, J. E.; Cowan, K. H. Gene therapy in oncology. In *Abeloff's clinical oncology*, 6th edition; Niederhuber, J. E., Armitage, J. O., Doroshow, J. H., Kastan, M. B., Tepper, J. E., Eds.; Elsevier Inc: Philadelphia, PA, 2020; 470–485.
- (34) Pollock, R. E.; Choti, M. A.; Morton, D. L. Principles of surgical oncology. In *Holland-Frei cancer medicine*, 8th edition; Hong, W. K., Bast, Robert C., Jr, Hait, W. N., Kufe, D. W., Pollock, R. E., Weichselbaum, R. R., Holland, J. F., Frei, E., Eds.; PMPH USA, Ltd: Shelton, CT, 2010; pp 499–509.
- (35) Sicard, M. A.; Li, B. D. Surgical oncology overview. In *Principles of Oncology*; The American Cancer Society, Ed.; John Wiley & Sons, Inc: Hoboken, NJ, 2018; pp 193–203.
- (36) Puck, T. T.; Marcus, P. I. Action of X-rays on mammalian cells. *J Exp Med* **1956**, *103*, 653–666.
- (37) Terasima, T.; Tolmach, L. J. Changes in X-ray sensitivity of HeLa cells during the division cycle. *Nature* **1961**, *190*, 1210–1211.

- (38) Deville, Curtiland, Jr.; Shukla, G.; Rengan, R.; Thomas, C. R., JR. Radiotherapy. In *Principles of Oncology*; The American Cancer Society, Ed.; John Wiley & Sons, Inc: Hoboken, NJ, 2018; pp 204–219.
- (39) Zeman, E. M.; Schreiber, E. C.; Tepper, J. E. Basics of radiation therapy. In *Abeloff's clinical oncology*, 6th edition; Niederhuber, J. E., Armitage, J. O., Doroshow, J. H., Kastan, M. B., Tepper, J. E., Eds.; Elsevier Inc: Philadelphia, PA, 2020; pp 431–460.
- (40) Harvey, R. D.; Khuri, F. R. Cytotoxic chemotherapy. In *Principles of Oncology*; The American Cancer Society, Ed.; John Wiley & Sons, Inc: Hoboken, NJ, 2018; pp 220–235.
- (41) Hartwell, L. H.; Kastan, M. B. Cell cycle control and cancer. *Science* **1994**, *266*, 1821–1828.
- (42) Howard, A.; Pelc, S. R. Synthesis of nucleoprotein in bean root cells. *Nature* **1951**, *167*, 599–600.
- (43) Steel, G. G. Autoradiographic analysis of the cell cycle: Howard and Pelc to the present day. *Int J Radiat Biol Relat Stud Phys Chem Med* **1986**, *49*, 227–235.
- (44) Kastan, M. B.; Bartek, J. Cell-cycle checkpoints and cancer. *Nature* **2004**, *432*, 316–323.
- (45) Mutschler, E.; Geisslinger, G.; Kroemer, H. K.; Ruth, P.; Schäfer-Korting, M., Eds. *Arzneimittelwirkungen: Lehrbuch der Pharmakologie und Toxikologie*, 9. Auflage; Wissenschaftliche Verlagsgesellschaft: Stuttgart, 2008.
- (46) Kaye, S. B. New antimetabolites in cancer chemotherapy and their clinical impact. *Br J Cancer* **1998**, *78* (Suppl 3), 1–7.
- (47) Champoux, J. J. DNA topoisomerases: structure, function, and mechanism. *Annu Rev Biochem* **2001**, *70*, 369–413.
- (48) Thomas, A.; Pommier, Y. Targeting topoisomerase I in the era of precision medicine. *Clin Cancer Res* **2019**, *25*, 6581–6589.
- (49) Wassermann, K.; Markovits, J.; Jaxel, C.; Capranico, G.; Kohn, K. W.; Pommier, Y. Effects of morpholinyl doxorubicins, doxorubicin, and actinomycin D on mammalian DNA topoisomerases I and II. *Mol Pharmacol* **1990**, *38*, 38–45.
- (50) Mills, C. C.; Kolb, E. A.; Sampson, V. B. Recent advances of cell-cycle inhibitor therapies for pediatric cancer. *Cancer Res* **2017**, *77*, 6489–6498.
- (51) Kingston, D. G. I. Tubulin-interactive natural products as anticancer agents. *J Nat Prod* **2009**, *72*, 507–515.
- (52) More, G. S.; Thomas, A. B.; Chitlange, S. S.; Nanda, R. K.; Gajbhiye, R. L. Nitrogen mustards as alkylating agents: a review on chemistry, mechanism of action and current US FDA status of drugs. *Anticancer Agents Med Chem* **2019**, *19*, 1080–1102.
- (53) Yoo, H.; Rill, R. L. Actinomycin D binding to unstructured, single-stranded DNA. *J Mol Recognit* **2001**, *14*, 145–150.
- (54) Wells, R. D.; Larson, J. E. Studies on the binding of actinomycin D to DNA and DNA model polymers. *J Mol Biol* **1970**, *49*, 319–342.
- (55) Waksman, S. A.; Geiger, W. B.; Reynolds, D. M. Strain specificity and production of antibiotic substances: VII. Production of actinomycin by different actinomycetes. *PNAS* **1946**, *32*, 117–120.
- (56) Kamiyama, M. Mechanism of action of chromomycin A3. III. On the binding of chromomycin A3 with DNA and physiochemical properties of the complex. *J Biochem* **1968**, *63*, 566–572.
- (57) Crooke, S. T.; Bradner, W. T. Mitomycin C: a review. *Cancer Treat Rev* **1976**, *3*, 121–139.
- (58) Takeshita, M.; Grollman, A. P.; Ohtsubo, E.; Ohtsubo, H. Interaction of bleomycin with DNA. *PNAS* **1978**, *75*, 5983–5987.
- (59) Armstrong, R. W.; Salvati, M. E.; Nguyen, M. Novel interstrand cross-links induced by the antitumor antibiotic carzinophilin/azinomycin B. *J Am Chem Soc* **1992**, *114*, 3144–3145.
- (60) Takeuchi, T. Antitumor antibiotics discovered and studied at the Institute of Microbial Chemistry. *J Cancer Res Clin Oncol* **1995**, *121*, 505–510.

## 5. References

---

- (61) Beerman, T. A.; Goldberg, I. H. DNA strand scission by the antitumor protein neocarzinostatin. *Biochem Biophys Res Commun* **1974**, *59*, 1254–1261.
- (62) Dedon, P. C.; Goldberg, I. H. Free-radical mechanisms involved in the formation of sequence-dependent bistranded DNA lesions by the antitumor antibiotics bleomycin, neocarzinostatin, and calicheamicin. *Chem Res Toxicol* **1992**, *5*, 311–332.
- (63) Povirk, L. F. DNA damage and mutagenesis by radiomimetic DNA-cleaving agents: bleomycin, neocarzinostatin and other enediynes. *Mutat Res* **1996**, *355*, 71–89.
- (64) Krause, D. S.; van Etten, R. A. Tyrosine kinases as targets for cancer therapy. *N Engl J Med* **2005**, *353*, 172–187.
- (65) Lemmon, M. A.; Schlessinger, J. Cell signaling by receptor tyrosine kinases. *Cell* **2010**, *141*, 1117–1134.
- (66) Gocek, E.; Moulas, A. N.; Studzinski, G. P. Non-receptor protein tyrosine kinases signaling pathways in normal and cancer cells. *Crit Rev Clin Lab Sci* **2014**, *51*, 125–137.
- (67) Lynch, T. J.; Bell, D. W.; Sordella, R.; Gurubhagavatula, S.; Okimoto, R. A.; Brannigan, B. W.; Harris, P. L.; Haserlat, S. M.; Supko, J. G.; Haluska, F. G.; *et al.* Activating mutations in the epidermal growth factor receptor underlying responsiveness of non-small cell lung cancer to gefitinib. *N Engl J Med* **2004**, *350*, 2129–2139.
- (68) Pao, W.; Miller, V.; Zakowski, M.; Doherty, J.; Politi, K.; Sarkaria, I.; Singh, B.; Heelan, R.; Rusch, V.; Fulton, L.; *et al.* EGF receptor gene mutations are common in lung cancers from "never smokers" and are associated with sensitivity of tumors to gefitinib and erlotinib. *PNAS* **2004**, *101*, 13306–13311.
- (69) Sordella, R.; Bell, D. W.; Haber, D. A.; Settleman, J. Gefitinib-sensitizing EGFR mutations in lung cancer activate anti-apoptotic pathways. *Science* **2004**, *305*, 1163–1167.
- (70) Graux, C.; Cools, J.; Melotte, C.; Quentmeier, H.; Ferrando, A.; Levine, R.; Vermeesch, J. R.; Stul, M.; Dutta, B.; Boeckx, N.; *et al.* Fusion of *NUP214* to *ABL1* on amplified episomes in T-cell acute lymphoblastic leukemia. *Nat Genet* **2004**, *36*, 1084–1089.
- (71) Cazzaniga, G.; Tosi, S.; Aloisi, A.; Giudici, G.; Daniotti, M.; Pioltelli, P.; Kearney, L.; Biondi, A. The tyrosine kinase *Abl*-related gene *arg* is fused to *ETV6* in an AML-M4Eo patient with a t(1;12)(q25;p13): molecular cloning of both reciprocal transcripts. *Blood* **1999**, *94*, 4370–4373.
- (72) Cools, J.; DeAngelo, D. J.; Gotlib, J.; Stover, E. H.; Legare, R. D.; Cortes, J.; Kutok, J.; Clark, J.; Galinsky, I.; Griffin, J. D. A tyrosine kinase created by fusion of the *PDGFRA* and *FIP1L1* genes as a therapeutic target of imatinib in idiopathic hypereosinophilic syndrome. *N Engl J Med* **2003**, *348*, 1201–1214.
- (73) Chesi, M.; Nardini, E.; Brents, L. A.; Schröck, E.; Ried, T.; Kuehl, W. M.; Bergsagel, P. L. Frequent translocation t(4;14)(p16.3;q32.3) in multiple myeloma is associated with increased expression and activating mutations of fibroblast growth factor receptor 3. *Nat Genet* **1997**, *16*, 260–264.
- (74) Watanabe, D.; Ezo, S.; Fujimoto, M.; Kimura, A.; Saito, Y.; Nagai, H.; Tachibana, I.; Matsumura, I.; Tanaka, T.; Kanegane, H.; *et al.* Suppressor of cytokine signalling-1 gene silencing in acute myeloid leukaemia and human haematopoietic cell lines. *Br J Haematol* **2004**, *126*, 726–735.
- (75) Druker, B. J.; Talpaz, M.; Resta, D. J.; Peng, B.; Buchdunger, E.; Ford, J. M.; Lydon, N. B.; Kantarjian, H.; Capdeville, R.; Ohno-Jones, S.; *et al.* Efficacy and safety of a specific inhibitor of the BCR-ABL tyrosine kinase in chronic myeloid leukemia. *N Engl J Med* **2001**, *344*, 1031–1037.
- (76) Shapiro, G. I. Cyclin-dependent kinase pathways as targets for cancer treatment. *J Clin Oncol* **2006**, *24*, 1770–1783.
- (77) Okkenhaug, K.; Graupera, M.; Vanhaesebroeck, B. Targeting PI3K in cancer: impact on tumor cells, their protective stroma, angiogenesis, and immunotherapy. *Cancer Discov* **2016**, *6*, 1090–1105.

- (78) Capra, M.; Nuciforo, P. G.; Confalonieri, S.; Quarto, M.; Bianchi, M.; Nebuloni, M.; Boldorini, R.; Pallotti, F.; Viale, G.; Gishizky, M. L.; *et al.* Frequent alterations in the expression of serine/threonine kinases in human cancers. *Cancer Res* **2006**, *66*, 8147–8154.
- (79) Kessler, E.; Brittain, P.; Davis, S. L.; Leong, S.; Eckhardt, S. G.; Lieu, C. H. Targeted therapies. In *Principles of Oncology*; The American Cancer Society, Ed.; John Wiley & Sons, Inc: Hoboken, NJ, 2018; pp 267–283.
- (80) Weiner, L. M.; Dhodapkar, M. V.; Ferrone, S. Monoclonal antibodies for cancer immunotherapy. *Lancet* **2009**, *373*, 1033–1040.
- (81) Weiner, L. M.; Surana, R.; Wang, S. Monoclonal antibodies: versatile platforms for cancer immunotherapy. *Nat Rev Immunol* **2010**, *10*, 317–327.
- (82) Sliwkowski, M. X.; Mellman, I. Antibody therapeutics in cancer. *Science* **2013**, *341*, 1192–1198.
- (83) Nimmerjahn, F.; Ravetch, J. V. Fcγ receptors: old friends and new family members. *Immunity* **2006**, *24*, 19–28.
- (84) Thomas, A.; Teicher, B. A.; Hassan, R. Antibody–drug conjugates for cancer therapy. *Lancet Oncol* **2016**, *17*, e254–e262.
- (85) Polakis, P. Antibody Drug Conjugates for Cancer Therapy. *Pharmacol Rev* **2016**, *68*, 3–19.
- (86) Beck, A.; Goetsch, L.; Dumontet, C.; Corvaia, N. Strategies and challenges for the next generation of antibody–drug conjugates. *Nat Rev Drug Discov* **2017**, *16*, 315–337.
- (87) Khongorzul, P.; Ling, C. J.; Khan, F. U.; Ihsan, A. U.; Zhang, J. Antibody–drug conjugates: a comprehensive review. *Mol Cancer Res* **2020**, *18*, 3–19.
- (88) Ricart, A. D. Antibody–drug conjugates of calicheamicin derivative: gemtuzumab ozogamicin and inotuzumab ozogamicin. *Clin Cancer Res* **2011**, *17*, 6417–6427.
- (89) Bross, P. F.; Beitz, J.; Chen, G.; Chen, X. H.; Duffy, E.; Kieffer, L.; Roy, S.; Sridhara, R.; Rahman, A.; Williams, G. Approval summary: gemtuzumab ozogamicin in relapsed acute myeloid leukemia. *Clin Cancer Res* **2001**, *7*, 1490–1496.
- (90) Lamb, Y. N. Inotuzumab ozogamicin: first global approval. *Drugs* **2017**, *77*, 1603–1610.
- (91) Younes, A.; Bartlett, N. L.; Leonard, J. P.; Kennedy, D. A.; Lynch, C. M.; Sievers, E. L.; Forero-Torres, A. Brentuximab vedotin (SGN-35) for relapsed CD30-positive lymphomas. *N Engl J Med* **2010**, *363*, 1812–1821.
- (92) Verma, S.; Miles, D.; Gianni, L.; Krop, I. E.; Welslau, M.; Baselga, J.; Pegram, M.; Oh, D.-Y.; Diéras, V.; Guardino, E.; *et al.* Trastuzumab emtansine for HER2-positive advanced breast cancer. *N Engl J Med* **2012**, *367*, 1783–1791.
- (93) Tsuchikama, K.; An, Z. Antibody–drug conjugates: recent advances in conjugation and linker chemistries. *Protein Cell* **2018**, *9*, 33–46.
- (94) Liu, W.-J.; Du, Y.; Wen, R.; Yang, M.; Xu, J. Drug resistance to targeted therapeutic strategies in non-small cell lung cancer. *Pharmacol Ther* **2020**, *206*, 107438.
- (95) Feng, W. W.; Wilkins, O.; Bang, S.; Ung, M.; Li, J.; An, J.; Del Genio, C.; Canfield, K.; DiRenzo, J.; Wells, W.; *et al.* CD36-mediated metabolic rewiring of breast cancer cells promotes resistance to HER2-targeted therapies. *Cell Rep* **2019**, *29*, 3405–3420.
- (96) Kozar, I.; Margue, C.; Rothengatter, S.; Haan, C.; Kreis, S. Many ways to resistance: how melanoma cells evade targeted therapies. *Biochim Biophys Acta Rev Cancer* **2019**, *1871*, 313–322.
- (97) Horikawa, N.; Abiko, K.; Matsumura, N.; Baba, T.; Hamanishi, J.; Yamaguchi, K.; Murakami, R.; Taki, M.; Ukita, M.; Hosoe, Y.; *et al.* Anti-VEGF therapy resistance in ovarian cancer is caused by GM-CSF-induced myeloid-derived suppressor cell recruitment. *Br J Cancer* **2020**, *122*, 778–788.
- (98) Newman, D. J.; Cragg, G. M. Natural products as sources of new drugs over the nearly four decades from 01/1981 to 09/2019. *J Nat Prod* **2020**, *83*, 770–803.

## 5. References

---

- (99) Filho, V. C., Ed. *Natural products as source of molecules with therapeutic potential*; Springer Nature Switzerland AG: Cham, 2018.
- (100) Zhang, L.; Demain, A. L. *Natural products: Drug discovery and therapeutic medicine*; Humana Press Inc: Totowa, NJ, 2005.
- (101) Cragg, G. M.; Grothaus, P. G.; Newman, D. J. New horizons for old drugs and drug leads. *J Nat Prod* **2014**, *77*, 703–723.
- (102) Sebolt-Leopold, J. S.; Herrera, R. Targeting the mitogen-activated protein kinase cascade to treat cancer. *Nat Rev Cancer* **2004**, *4*, 937–947.
- (103) Gschwind, A.; Fischer, O. M.; Ullrich, A. The discovery of receptor tyrosine kinases: targets for cancer therapy. *Nat Rev Cancer* **2004**, *4*, 361–370.
- (104) Baselga, J. Targeting tyrosine kinases in cancer: the second wave. *Science* **2006**, *312*, 1175–1178.
- (105) Roberts, P. J.; Der, C. J. Targeting the Raf-MEK-ERK mitogen-activated protein kinase cascade for the treatment of cancer. *Oncogene* **2007**, *26*, 3291–3310.
- (106) Griner, E. M.; Kazanietz, M. G. Protein kinase C and other diacylglycerol effectors in cancer. *Nat Rev Cancer* **2007**, *7*, 281–294.
- (107) Noble, M. E. M.; Endicott, J. A.; Johnson, L. N. Protein kinase inhibitors: insights into drug design from structure. *Science* **2004**, *303*, 1800–1805.
- (108) Wu, P.; Nielsen, T. E.; Clausen, M. H. Small-molecule kinase inhibitors: an analysis of FDA-approved drugs. *Drug Discov Today* **2016**, *21*, 5–10.
- (109) Caravatti, G.; Meyer, T.; Fredenhagen, A.; Trinks, U.; Mett, H.; Fabbro, D. Inhibitory activity and selectivity of staurosporine derivatives towards protein kinase C. *Bioorg Med Chem Lett* **1994**, *4*, 399–404.
- (110) Cragg, G. M.; Pezzuto, J. M. Natural products as a vital source for the discovery of cancer chemotherapeutic and chemopreventive agents. *Med Princ Pract* **2016**, *25 Suppl 2*, 41–59.
- (111) Hartford, C. M.; Ratain, M. J. Rapamycin: something old, something new, sometimes borrowed and now renewed. *Clin Pharmacol Ther* **2007**, *82*, 381–388.
- (112) Vézina, C.; Kudelski, A.; Sehgal, S. N. Rapamycin (AY-22,989), a new antifungal antibiotic. I. Taxonomy of the producing streptomycete and isolation of the active principle. *J Antibiot* **1975**, *28*, 721–726.
- (113) Oka, S.; Kodama, M.; Takeda, H.; Tomizuka, N.; Suzuki, H. Staurosporine, a potent platelet aggregation inhibitor from a *Streptomyces* species. *Agric. Bio. Chem.* **1986**, *50*, 2723–2727.
- (114) Carles, F.; Bourg, S.; Meyer, C.; Bonnet, P. PKIDB: a curated, annotated and updated database of protein kinase inhibitors in clinical trials. *Molecules* **2018**, *23*, 908.
- (115) Guerra, B.; Issinger, O.-G. Natural compounds and derivatives as Ser/Thr protein kinase modulators and inhibitors. *Pharmaceuticals (Basel)* **2019**, *12*, 4.
- (116) Liu, J.; Hu, Y.; Waller, D. L.; Wang, J.; Liu, Q. Natural products as kinase inhibitors. *Nat Prod Rep* **2012**, *29*, 392–403.
- (117) Haefner, B. Drugs from the deep: marine natural products as drug candidates. *Drug Discov Today* **2003**, *8*, 536–544.
- (118) Minotti, G.; Menna, P.; Salvatorelli, E.; Cairo, G.; Gianni, L. Anthracyclines: molecular advances and pharmacologic developments in antitumor activity and cardiotoxicity. *Pharmacol Rev* **2004**, *56*, 185–229.
- (119) Thomas, C. J.; Rahier, N. J.; Hecht, S. M. Camptothecin: current perspectives. *Bioorg Med Chem* **2004**, *12*, 1585–1604.
- (120) Clark, P. I.; Slevin, M. L. The clinical pharmacology of etoposide and teniposide. *Clin Pharmacokinet* **1987**, *12*, 223–252.
- (121) Goodwin, S.; Smith, A. F.; Horning, E. C. Alkaloids of *Ochrosia elliptica* Labill. *J Am Chem Soc* **1959**, *81*, 1903–1908.

- (122) Auclair, C. Multimodal action of antitumor agents on DNA: the ellipticine series. *Arch Biochem Biophys* **1987**, *259*, 1–14.
- (123) Froelich-Ammon, S. J.; Patchan, M. W.; Osheroff, N.; Thompson, R. B. Topoisomerase II binds to ellipticine in the absence or presence of DNA. Characterization of enzyme-drug interactions by fluorescence spectroscopy. *J Biol Chem* **1995**, *270*, 14998–15004.
- (124) Darwiche, N.; El-Banna, S.; Gali-Muhtasib, H. Cell cycle modulatory and apoptotic effects of plant-derived anticancer drugs in clinical use or development. *Expert Opin Drug Discov* **2007**, *2*, 361–379.
- (125) Jordan, A.; Hadfield, J. A.; Lawrence, N. J.; McGown, A. T. Tubulin as a target for anticancer drugs: agents which interact with the mitotic spindle. *Med Res Rev* **1998**, *18*, 259–296.
- (126) Khrapunovich-Baine, M.; Menon, V.; Yang, C.-P. H.; Northcote, P. T.; Miller, J. H.; Angeletti, R. H.; Fiser, A.; Horwitz, S. B.; Xiao, H. Hallmarks of molecular action of microtubule stabilizing agents: effects of epothilone B, ixabepilone, peloruside A, and laulimalide on microtubule conformation. *J Biol Chem* **2011**, *286*, 11765–11778.
- (127) Wani, M. C.; Taylor, H. L.; Wall, M. E.; Coggon, P.; McPhail, A. T. Plant antitumor agents. VI. The isolation and structure of taxol, a novel antileukemic and antitumor agent from *Taxus brevifolia*. *J Am Chem Soc* **1971**, *93*, 2325–2327.
- (128) Jimenez, P. C.; Wilke, D. V.; Branco, P. C.; Bauermeister, A.; Rezende-Teixeira, P.; Gaudêncio, S. P.; Costa-Lotufo, L. V. Enriching cancer pharmacology with drugs of marine origin. *Br J Pharmacol* **2020**, *177*, 3–27.
- (129) Kollár, P.; Rajchard, J.; Balounová, Z.; Pazourek, J. Marine natural products: bryostatins in preclinical and clinical studies. *Pharm Biol* **2014**, *52*, 237–242.
- (130) Pettit, G. R.; Herald, C. L.; Doubek, D. L.; Herald, D. L.; Arnold, E.; Clardy, J. Isolation and structure of bryostatin-1. *J Am Chem Soc* **1982**, *104*, 6846–6848.
- (131) Search orphan drug designations and approvals. <http://www.accessdata.fda.gov/scripts/opdlisting/oopd/index.cfm> (accessed April 1st, 2020).
- (132) European Medicines Agency. *Public summary of positive opinion for orphan designation of bryostatin-1 for the treatment of oesophageal cancer: EU/3/02/099*, 2007.
- (133) A review of trabectedin (ET-743): a unique mechanism of action. *Mol Cancer Ther* **2010**, *9*, 2157–2163.
- (134) Wright, A. E.; Forleo, D. A.; Gunawardana, G. P.; Gunasekera, S. P.; Koehn, F. E.; McConnell, O. J. Antitumor tetrahydroisoquinoline alkaloids from the colonial ascidian *Ecteinascidia turbinata*. *J Org Chem* **1990**, *55*, 4508–4512.
- (135) Sakai, R.; Rinehart, K. L.; Kishore, V.; Kundu, B.; Faircloth, G.; Gloer, J. B.; Carney, J. R.; Namikoshi, M.; Sun, F.; Hughes, R. G.; *et al.* Structure–activity relationships of the didemnins. *J Med Chem* **1996**, *39*, 2819–2834.
- (136) Ueda, H.; Nakajima, H.; Hori, Y.; Fujita, T.; Nishimura, M.; Goto, T.; Okuhara, M. FR901228, a novel antitumor bicyclic depsipeptide produced by *Chromobacterium violaceum* No. 968. I. Taxonomy, fermentation, isolation, physico-chemical and biological properties, and antitumor activity. *J Antibiot* **1994**, *47*, 301–310.
- (137) Nakajima, H.; Kim, Y. B.; Terano, H.; Yoshida, M.; Horinouchi, S. FR901228, a potent antitumor antibiotic, is a novel histone deacetylase inhibitor. *Exp Cell Res* **1998**, *241*, 126–133.
- (138) Bai, R. L.; Pettit, G. R.; Hamel, E. Binding of dolastatin 10 to tubulin at a distinct site for peptide antimetabolic agents near the exchangeable nucleotide and vinca alkaloid sites. *J Biol Chem* **1990**, *265*, 17141–17149.
- (139) Bai, R.; Pettit, G. R.; Hamel, E. Dolastatin 10, a powerful cytostatic peptide derived from a marine animal. *Biochem Pharmacol* **1990**, *39*, 1941–1949.
- (140) Harrigan, G. G.; Yoshida, W. Y.; Moore, R. E.; Nagle, D. G.; Park, P. U.; Biggs, J.; Paul, V. J.; Mooberry, S. L.; Corbett, T. H.; Valeriote, F. A. Isolation, structure determination, and biological activity of dolastatin 12 and lyngbyastatin 1 from *Lyngbya majuscula*/*Schizothrix calcicola* cyanobacterial assemblages. *J Nat Prod* **1998**, *61*, 1221–1225.

## 5. References

---

- (141) Harrigan, G. G.; Luesch, H.; Yoshida, W. Y.; Moore, R. E.; Nagle, D. G.; Paul, V. J.; Mooberry, S. L.; Corbett, T. H.; Valeriote, F. A. Symplostatin 1: a dolastatin 10 analogue from the marine cyanobacterium *Symploca hydroides*. *J Nat Prod* **1998**, *61*, 1075–1077.
- (142) Mitchell, S. S.; Faulkner, D. J.; Rubins, K.; Bushman, F. D. Dolastatin 3 and two novel cyclic peptides from a palauan collection of *Lyngbya majuscula*. *J Nat Prod* **2000**, *63*, 279–282.
- (143) Nogle, L. M.; Gerwick, W. H. Isolation of four new cyclic depsipeptides, antanapeptins A–D, and dolastatin 16 from a Madagascan collection of *Lyngbya majuscula*. *J Nat Prod* **2002**, *65*, 21–24.
- (144) Luesch, H.; Yoshida, W. Y.; Moore, R. E.; Paul, V. J.; Mooberry, S. L.; Corbett, T. H. Symplostatin 3, a new dolastatin 10 analogue from the marine cyanobacterium *Symploca* sp. VP452. *J Nat Prod* **2002**, *65*, 16–20.
- (145) Moore, R. E. Cyclic peptides and depsipeptides from cyanobacteria: a review. *J Ind Microbiol* **1996**, *16*, 134–143.
- (146) Welker, M.; von Döhren, H. Cyanobacterial peptides—nature's own combinatorial biosynthesis. *FEMS Microbiol Rev* **2006**, *30*, 530–563.
- (147) Gademann, K.; Portmann, C. Secondary metabolites from cyanobacteria: complex structures and powerful bioactivities. *Curr Org Chem* **2008**, *12*, 326–341.
- (148) Jones, A. C.; Gu, L.; Sorrels, C. M.; Sherman, D. H.; Gerwick, W. H. New tricks from ancient algae: natural products biosynthesis in marine cyanobacteria. *Curr Opin Chem Biol* **2009**, *13*, 216–223.
- (149) Tan, L. T. Filamentous tropical marine cyanobacteria: a rich source of natural products for anticancer drug discovery. *J Appl Phycol* **2010**, *22*, 659–676.
- (150) Jones, A. C.; Monroe, E. A.; Eisman, E. B.; Gerwick, L.; Sherman, D. H.; Gerwick, W. H. The unique mechanistic transformations involved in the biosynthesis of modular natural products from marine cyanobacteria. *Nat Prod Rep* **2010**, *27*, 1048–1065.
- (151) Singh, R. K.; Tiwari, S. P.; Rai, A. K.; Mohapatra, T. M. Cyanobacteria: an emerging source for drug discovery. *J Antibiot* **2011**, *64*, 401–412.
- (152) Kehr, J.-C.; Picchi, D. G.; Dittmann, E. Natural product biosyntheses in cyanobacteria: a treasure trove of unique enzymes. *Beilstein J Org Chem* **2011**, *7*, 1622–1635.
- (153) Niedermeyer, T. H. J. Anti-infective natural products from cyanobacteria. *Planta Med* **2015**, *81*, 1309–1325.
- (154) Dittmann, E.; Gugger, M.; Sivonen, K.; Fewer, D. P. Natural product biosynthetic diversity and comparative genomics of the cyanobacteria. *Trends Microbiol* **2015**, *23*, 642–652.
- (155) Liang, J.; Moore, R. E.; Moher, E. D.; Munroe, J. E.; Al-awar, R. S.; Hay, D. A.; Varie, D. L.; Zhang, T. Y.; Aikins, J. A.; Martinelli, M. J.; *et al.* Cryptophycins-309, 249 and other cryptophycin analogs: preclinical efficacy studies with mouse and human tumors. *Invest New Drugs* **2005**, *23*, 213–224.
- (156) Komárek, J. Review of the cyanobacterial genera implying planktic species after recent taxonomic revisions according to polyphasic methods: state as of 2014. *Hydrobiologia* **2016**, *764*, 259–270.
- (157) Krishnamurthy, T.; Carmichael, W. W.; Sarver, E. W. Toxic peptides from freshwater cyanobacteria (blue-green algae). I. Isolation, purification and characterization of peptides from *Microcystis aeruginosa* and *Anabaena flos-aquae*. *Toxicon* **1986**, *24*, 865–873.
- (158) Watanabe, M. F.; Oishi, S.; Harada, K.-I.; Matsuura, K.; Kawai, H.; Suzuki, M. Toxins contained in *Microcystis* species of cyanobacteria (blue-green algae). *Toxicon* **1988**, *26*, 1017–1025.
- (159) Sivonen, K.; Namikoshi, M.; Evans, W. R.; Fardig, M.; Carmichael, W. W.; Rinehart, K. L. Three new microcystins, cyclic heptapeptide hepatotoxins, from *Nostoc* sp. strain 152. *Chem Res Toxicol* **1992**, *5*, 464–469.



- (160) Sivonen, K.; Namikoshi, M.; Evans, W. R.; Carmichael, W. W.; Sun, F.; Rouhiainen, L.; Luukkainen, R.; Rinehart, K. L. Isolation and characterization of a variety of microcystins from seven strains of the cyanobacterial genus *Anabaena*. *Appl Environ Microbiol* **1992**, *58*, 2495–2500.
- (161) Niedermeyer, T. H. J.; Schmieder, P.; Kurmayer, R. Isolation of microcystins from the cyanobacterium *Planktothrix rubescens* strain No. 80. *Nat Prod Bioprospect* **2014**, *4*, 37–45.
- (162) Brittain, S.; Mohamed, Z. A.; Wang, J.; Lehmann, V. K. B.; Carmichael, W. W.; Rinehart, K. L. Isolation and characterization of microcystins from a River Nile strain of *Oscillatoria tenuis* Agardh ex Gomont. *Toxicon* **2000**, *38*, 1759–1771.
- (163) Luukkainen, R.; Sivonen, K.; Namikoshi, M.; Fardig, M.; Rinehart, K. L.; Niemela, S. I. Isolation and identification of eight microcystins from thirteen *Oscillatoria agardhii* strains and structure of a new microcystin. *Appl Environ Microbiol* **1993**, *59*, 2204–2209.
- (164) Watanabe, M. F.; Harada, K.-I.; Carmichael, W. W.; Fujiki, H.; Editors. *Toxic Microcystis*; CRC Press, 1996.
- (165) Dawson, R. M. The toxicology of microcystins. *Toxicon* **1998**, *36*, 953–962.
- (166) Duy, T. N.; Lam, P. K. S.; Shaw, G. R.; Connell, D. W. Toxicology and risk assessment of freshwater cyanobacterial (blue-green algal) toxins in water. *Rev Environ Contam Toxicol* **2000**, *163*, 113–185.
- (167) Briand, J.-F.; Jacquet, S.; Bernard, C.; Humbert, J.-F. Health hazards for terrestrial vertebrates from toxic cyanobacteria in surface water ecosystems. *Vet Res* **2003**, *34*, 361–377.
- (168) Zurawell, R. W.; Chen, H.; Burke, J. M.; Prepas, E. E. Hepatotoxic cyanobacteria: a review of the biological importance of microcystins in freshwater environments. *J Toxicol Environ Health B Crit Rev* **2005**, *8*, 1–37.
- (169) Wiegand, C.; Pflugmacher, S. Ecotoxicological effects of selected cyanobacterial secondary metabolites a short review. *Toxicol Appl Pharmacol* **2005**, *203*, 201–218.
- (170) Zanchett, G.; Oliveira-Filho, E. C. Cyanobacteria and cyanotoxins: from impacts on aquatic ecosystems and human health to anticarcinogenic effects. *Toxins* **2013**, *5*, 1896–1917.
- (171) Pavagadhi, S.; Balasubramanian, R. Toxicological evaluation of microcystins in aquatic fish species: current knowledge and future directions. *Aquat Toxicol* **2013**, *142-143*, 1–16.
- (172) De Figueiredo, D. R.; Azeiteiro, U. M.; Esteves, S. M.; Gonçalves, F. J. M.; Pereira, M. J. Microcystin-producing blooms—a serious global public health issue. *Ecotoxicol Environ Saf* **2004**, *59*, 151–163.
- (173) Codd, G. A.; Morrison, L. F.; Metcalf, J. S. Cyanobacterial toxins: risk management for health protection. *Toxicol Appl Pharmacol* **2005**, *203*, 264–272.
- (174) Dittmann, E.; Wiegand, C. Cyanobacterial toxins—occurrence, biosynthesis and impact on human affairs. *Mol Nutr Food Res* **2006**, *50*, 7–17.
- (175) Svirčev, Z.; Drobac, D.; Tokodi, N.; Mijović, B.; Codd, G. A.; Meriluoto, J. Toxicology of microcystins with reference to cases of human intoxications and epidemiological investigations of exposures to cyanobacteria and cyanotoxins. *Arch Toxicol* **2017**, *91*, 621–650.
- (176) Baker A. L.; *et al.* Phycokey—an image based key to algae (PS Protista), cyanobacteria, and other aquatic objects. <http://cfb.unh.edu/phycokey/phycokey.htm> (accessed May 24, 2020).
- (177) Steyn, D. G. Poisoning of animals and human beings by algae. *S Afr J Sci* **1944**, *41*, 243–244.
- (178) Bishop, C. T.; Anet, E. F. L. J.; Gorham, P. R. Isolation and identification of the fast-death factor in *Microcystis aeruginosa* NRC-1. *Can J Biochem Physiol* **1959**, *37*, 453–471.
- (179) Botes, D. P.; Tuinman, A. A.; Wessels, P. L.; Viljoen, C. C.; Kruger, H.; Williams, D. H.; Santikarn, S.; Smith, R. J.; Hammond, S. J. The structure of cyanoginosin-LA, a cyclic heptapeptide toxin from the cyanobacterium *Microcystis aeruginosa*. *J Chem Soc, Perkin Trans I* **1984**, 2311–2318.

## 5. References

---

- (180) Botes, D. P.; Kruger, H.; Viljoen, C. C. Isolation and characterization of four toxins from the blue-green alga, *Microcystis aeruginosa*. *Toxicon* **1982**, *20*, 945–954.
- (181) Gorham, P. R.; Carmichael, W. W. Phycotoxins from blue-green algae. *Pure Appl Chem* **1980**, *52*, 165–174.
- (182) Elleman, T. C.; Falconer, I. R.; Jackson, A. R.; Runnegar, M. T. Isolation, characterization and pathology of the toxin from a *Microcystis aeruginosa* (= *Anacystis cyanea*) bloom. *Aust J Biol Sci* **1978**, *31*, 209–218.
- (183) Murthy, J. R.; Capindale, J. B. A new isolation and structure for the endotoxin from *Microcystis aeruginosa* NRC-1. *Can J Biochem* **1970**, *48*, 508–510.
- (184) Rinehart, K. L.; Harada, K.; Namikoshi, M.; Chen, C.; Harvis, C. A.; Munro, M. H. G.; Blunt, J. W.; Mulligan, P. E.; Beasley, V. R.; et al. Nodularin, microcystin, and the configuration of Adda. *J Am Chem Soc* **1988**, *110*, 8557–8558.
- (185) Tillett, D.; Dittmann, E.; Erhard, M.; von Döhren, H.; Börner, T.; Neilan, B. A. Structural organization of microcystin biosynthesis in *Microcystis aeruginosa* PCC7806: an integrated peptide–polyketide synthetase system. *Chem Biol* **2000**, *7*, 753–764.
- (186) Bouaïcha, N.; Miles, C. O.; Beach, D. G.; Labidi, Z.; Djabri, A.; Benayache, N. Y.; Nguyen-Quang, T. Structural diversity, characterization and toxicology of microcystins. *Toxins* **2019**, *11*, 714.
- (187) Carmichael, W. W.; Beasley, V.; Bunner, D. L.; Eloff, J. N.; Falconer, I.; Gorham, P.; Harada, K.-I.; Krishnamurthy, T.; Min-Juan, Y.; Moore, R. E.; et al. Naming of cyclic heptapeptide toxins of cyanobacteria (blue-green algae). *Toxicon* **1988**, *26*, 971–973.
- (188) Dittmann, E.; Neilan, B. A.; Erhard, M.; von Döhren, H.; Börner, T. Insertional mutagenesis of a peptide synthetase gene that is responsible for hepatotoxin production in the cyanobacterium *Microcystis aeruginosa* PCC 7806. *Mol Microbiol* **1997**, *26*, 779–787.
- (189) Weber, T.; Baumgartner, R.; Renner, C.; Marahiel, M. A.; Holak, T. A. Solution structure of PCP, a prototype for the peptidyl carrier domains of modular peptide synthetases. *Structure* **2000**, *8*, 407–418.
- (190) Stachelhaus, T.; Mootz, H. D.; Bergendahl, V.; Marahiel, M. A. Peptide bond formation in nonribosomal peptide biosynthesis. Catalytic role of the condensation domain. *J Biol Chem* **1998**, *273*, 22773–22781.
- (191) Stachelhaus, T.; Hüser, A.; Marahiel, M. A. Biochemical characterization of peptidyl carrier protein (PCP), the thiolation domain of multifunctional peptide synthetases. *Chem Biol* **1996**, *3*, 913–921.
- (192) Stachelhaus, T.; Marahiel, M. A. Modular structure of genes encoding multifunctional peptide synthetases required for non-ribosomal peptide synthesis. *FEMS Microbiol Lett* **1995**, *125*, 3–14.
- (193) Stachelhaus, T.; Marahiel, M. A. Modular structure of peptide synthetases revealed by dissection of the multifunctional enzyme GrsA. *J Biol Chem* **1995**, *270*, 6163–6169.
- (194) Moschny, J.; Lorenzen, W.; Hilfer, A.; Eckenstaler, R.; Jahns, S.; Enke, H.; Enke, D.; Schneider, P.; Benndorf, R. A.; Niedermeyer, T. H. J. Precursor-directed biosynthesis and fluorescence labeling of clickable microcystins. *J Nat Prod* **2020**, *83*, 1960–1970.
- (195) Nishizawa, T.; Ueda, A.; Asayama, M.; Fujii, K.; Harada, K.; Ochi, K.; Shirai, M. Polyketide synthase gene coupled to the peptide synthetase module involved in the biosynthesis of the cyclic heptapeptide microcystin. *J Biochem* **2000**, *127*, 779–789.
- (196) Cullen, A.; Pearson, L. A.; Mazmouz, R.; Liu, T.; Soeriyadi, A. H.; Ongley, S. E.; Neilan, B. A. Heterologous expression and biochemical characterisation of cyanotoxin biosynthesis pathways. *Nat Prod Rep* **2019**, *36*, 1117–1136.
- (197) Dittmann, E.; Fewer, D. P.; Neilan, B. A. Cyanobacterial toxins: biosynthetic routes and evolutionary roots. *FEMS Microbiol Rev* **2013**, *37*, 23–43.

- (198) Hicks, L. M.; Moffitt, M. C.; Beer, L. L.; Moore, B. S.; Kelleher, N. L. Structural characterization of *in vitro* and *in vivo* intermediates on the loading module of microcystin synthetase. *ACS Chem Biol* **2006**, *1*, 93–102.
- (199) Moore, R. E.; Chen, J. L.; Moore, B. S.; Patterson, G. M. L.; Carmichael, W. W. Biosynthesis of microcystin-LR. Origin of the carbons in the Adda and Masp units. *J Am Chem Soc* **1991**, *113*, 5083–5084.
- (200) Liu, T.; Mazmouz, R.; Pearson, L. A.; Neilan, B. A. Mutagenesis of the microcystin tailoring and transport proteins in a heterologous cyanotoxin expression system. *ACS Synth Biol* **2019**, *8*, 1187–1194.
- (201) Christiansen, G.; Fastner, J.; Erhard, M.; Börner, T.; Dittmann, E. Microcystin biosynthesis in *Planktothrix*: genes, evolution, and manipulation. *J Bacteriol* **2003**, *185*, 564–572.
- (202) Puddick, J.; Prinsep, M. R.; Wood, S. A.; Kaufononga, S. A. F.; Cary, S. C.; Hamilton, D. P. High levels of structural diversity observed in microcystins from *Microcystis* CAWBG11 and characterization of six new microcystin congeners. *Mar Drugs* **2014**, *12*, 5372–5395.
- (203) Meyer, S.; Kehr, J.-C.; Mainz, A.; Dehm, D.; Petras, D.; Süssmuth, R. D.; Dittmann, E. Biochemical dissection of the natural diversification of microcystin provides lessons for synthetic biology of NRPS. *Cell Chem Biol* **2016**, *23*, 462–471.
- (204) Börner, T.; Dittmann, E. Molecular biology of cyanobacterial toxins. In *Harmful cyanobacteria*; Huisman, J., Matthijs, H. C. P., Visser, P. M., Eds.; Aquatic Ecology Series 3; Springer: Dordrecht, 2005; pp 25–40.
- (205) Chen, L.; Chen, J.; Zhang, X.; Xie, P. A review of reproductive toxicity of microcystins. *J Hazard Mater* **2016**, *301*, 381–399.
- (206) Wang, Q.; Xie, P.; Chen, J.; Liang, G. Distribution of microcystins in various organs (heart, liver, intestine, gonad, brain, kidney and lung) of Wistar rat via intravenous injection. *Toxicol* **2008**, *52*, 721–727.
- (207) Milutinović, A.; Zorc-Pleskovič, R.; Petrovič, D.; Zorc, M.; Šuput, D. Microcystin-LR induces alterations in heart muscle. *Folia Biol (Praha)* **2006**, *52*, 116–118.
- (208) MacKintosh, C.; Beattie, K. A.; Klumpp, S.; Cohen, P.; Codd, G. A. Cyanobacterial microcystin-LR is a potent and specific inhibitor of protein phosphatases 1 and 2A from both mammals and higher plants. *FEBS Lett* **1990**, *264*, 187–192.
- (209) Ceulemans, H.; Bollen, M. Functional diversity of protein phosphatase-1, a cellular economizer and reset button. *Physiol Rev* **2004**, *84*, 1–39.
- (210) Cohen, P. T. W. Protein phosphatase 1—targeted in many directions. *J Cell Sci* **2002**, *115*, 241–256.
- (211) Janssens, V.; Goris, J. Protein phosphatase 2A: a highly regulated family of serine/threonine phosphatases implicated in cell growth and signalling. *Biochem J* **2001**, *353*, 417–439.
- (212) Millward, T. A.; Zolnierowicz, S.; Hemmings, B. A. Regulation of protein kinase cascades by protein phosphatase 2A. *Trends Biochem Sci* **1999**, *24*, 186–191.
- (213) Buratti, F. M.; Manganeli, M.; Vichi, S.; Stefanelli, M.; Scardala, S.; Testai, E.; Funari, E. Cyanotoxins: producing organisms, occurrence, toxicity, mechanism of action and human health toxicological risk evaluation. *Arch Toxicol* **2017**, *91*, 1049–1130.
- (214) McLellan, N. L.; Manderville, R. A. Toxic mechanisms of microcystins in mammals. *Toxicol Res* **2017**, *6*, 391–405.
- (215) Valério, E.; Vasconcelos, V.; Campos, A. New insights on the mode of action of microcystins in animal cells—a review. *Mini Rev Med Chem* **2016**, *16*, 1032–1041.
- (216) Campos, A.; Vasconcelos, V. Molecular mechanisms of microcystin toxicity in animal cells. *Int J Mol Sci* **2010**, *11*, 268–287.
- (217) Liu, J.; Sun, Y. The role of PP2A-associated proteins and signal pathways in microcystin-LR toxicity. *Toxicol Lett* **2015**, *236*, 1–7.

## 5. References

---

- (218) Li, H.-H.; Cai, X.; Shouse, G. P.; Piluso, L. G.; Liu, X. A specific PP2A regulatory subunit, B56 $\gamma$ , mediates DNA damage-induced dephosphorylation of p53 at Thr55. *EMBO J* **2007**, *26*, 402–411.
- (219) Fu, W.-Y.; Chen, J.-P.; Wang, X.-M.; Xu, L.-H. Altered expression of p53, Bcl-2 and Bax induced by microcystin-LR *in vivo* and *in vitro*. *Toxicol* **2005**, *46*, 171–177.
- (220) Zegura, B.; Zajc, I.; Lah, T. T.; Filipic, M. Patterns of microcystin-LR induced alteration of the expression of genes involved in response to DNA damage and apoptosis. *Toxicol* **2008**, *51*, 615–623.
- (221) Xing, M.-L.; Wang, X.-F.; Xu, L.-H. Alteration of proteins expression in apoptotic FL cells induced by MC-LR. *Environ Toxicol* **2008**, *23*, 451–458.
- (222) Morselli, E.; Galluzzi, L.; Kroemer, G. Mechanisms of p53-mediated mitochondrial membrane permeabilization. *Cell Res* **2008**, *18*, 708–710.
- (223) Huang, B.; Yang, C.-S.; Wojton, J.; Huang, N.-J.; Chen, C.; Soderblom, E. J.; Zhang, L.; Kornbluth, S. Metabolic control of Ca<sup>2+</sup>/calmodulin-dependent protein kinase II (CaMKII)-mediated caspase-2 suppression by the B55 $\beta$ /protein phosphatase 2A (PP2A). *J Biol Chem* **2014**, *289*, 35882–35890.
- (224) Kajihara, R.; Fukushige, S.; Shioda, N.; Tanabe, K.; Fukunaga, K.; Inui, S. CaMKII phosphorylates serine-10 of p27 and confers apoptosis resistance to HeLa cells. *Biochem Biophys Res Commun* **2010**, *401*, 350–355.
- (225) Krakstad, C.; Herfindal, L.; Gjertsen, B. T.; Boe, R.; Vintermyr, O. K.; Fladmark, K. E.; Doskeland, S. O. CaM-kinase II-dependent commitment to microcystin-induced apoptosis is coupled to cell budding, but not to shrinkage or chromatin hypercondensation. *Cell Death Differ.* **2006**, *13*, 1191–1202.
- (226) Komatsu, M.; Furukawa, T.; Ikeda, R.; Takumi, S.; Nong, Q.; Aoyama, K.; Akiyama, S.-I.; Keppler, D.; Takeuchi, T. Involvement of mitogen-activated protein kinase signaling pathways in microcystin-LR-induced apoptosis after its selective uptake mediated by OATP1B1 and OATP1B3. *Toxicol Sci* **2007**, *97*, 407–416.
- (227) Daily, A.; Monks, N. R.; Leggas, M.; Moscow, J. A. Abrogation of microcystin cytotoxicity by MAP kinase inhibitors and *N*-acetyl cysteine is confounded by OATP1B1 uptake activity inhibition. *Toxicol* **2010**, *55*, 827–837.
- (228) Yang, F.; Wen, C.; Zheng, S.; Yang, S.; Chen, J.; Feng, X. Involvement of MAPK/ERK1/2 pathway in microcystin-induced microfilament reorganization in HL7702 hepatocytes. *J Toxicol Environ Health A* **2018**, *81*, 1135–1141.
- (229) Zhou, M.; Tu, W.-W.; Xu, J. Mechanisms of microcystin-LR-induced cytoskeletal disruption in animal cells. *Toxicol* **2015**, *101*, 92–100.
- (230) Zeng, J.; Tu, W.-W.; Lazar, L.; Chen, D.-N.; Zhao, J.-S.; Xu, J. Hyperphosphorylation of microfilament-associated proteins is involved in microcystin-LR-induced toxicity in HL7702 cells. *Environ Toxicol* **2015**, *30*, 981–988.
- (231) Chen, D.-N.; Zeng, J.; Wang, F.; Zheng, W.; Tu, W.-W.; Zhao, J.-S.; Xu, J. Hyperphosphorylation of intermediate filament proteins is involved in microcystin-LR-induced toxicity in HL7702 cells. *Toxicol Lett* **2012**, *214*, 192–199.
- (232) Dunn, K. L.; Espino, P. S.; Drobnic, B.; He, S.; Davie, J. R. The Ras-MAPK signal transduction pathway, cancer and chromatin remodeling. *Biochem Cell Biol* **2005**, *83*, 1–14.
- (233) Zhang, W.; Liu, H. T. MAPK signal pathways in the regulation of cell proliferation in mammalian cells. *Cell Res* **2002**, *12*, 9–18.
- (234) Li, H.; Xie, P.; Li, G.; Hao, L.; Xiong, Q. *In vivo* study on the effects of microcystin extracts on the expression profiles of proto-oncogenes (c-fos, c-jun and c-myc) in liver, kidney and testis of male Wistar rats injected i.v. with toxins. *Toxicol* **2009**, *53*, 169–175.
- (235) Gehringer, M. M. Microcystin-LR and okadaic acid-induced cellular effects: a dualistic response. *FEBS Lett* **2004**, *557*, 1–8.

- (236) Goldberg, J.; Huang, H.-B.; Kwon, Y.-G.; Greengard, P.; Nairn, A. C.; Kuriyan, J. Three-dimensional structure of the catalytic subunit of protein serine/threonine phosphatase-1. *Nature* **1995**, *376*, 745–753.
- (237) Craig, M.; Luu, H. A.; McCready, T. L.; Williams, D.; Andersen, R. J.; Holmes, C. F. Molecular mechanisms underlying the interaction of motuporin and microcystins with type-1 and type-2A protein phosphatases. *Biochem Cell Biol* **1996**, *74*, 569–578.
- (238) Gauss, C.-M.; Sheppeck, J. E.; Nairn, A. C.; Chamberlin, R. A molecular modeling analysis of the binding interactions between the okadaic acid class of natural product inhibitors and the Ser–Thr phosphatases, PP1 and PP2A. *Bioorg Med Chem* **1997**, *5*, 1751–1773.
- (239) Webster, K. L.; Maude, A. B.; O'Donnell, M. E.; Mehrotra, A. P.; Gani, D. Design and preparation of serine–threonine protein phosphatase inhibitors based upon the nodularin and microcystin toxin structures. Part 3. *J Chem Soc, Perkin Trans I* **2001**, 1673–1695.
- (240) Fontanillo, M.; Köhn, M. Microcystins: synthesis and structure–activity relationship studies toward PP1 and PP2A. *Bioorg Med Chem* **2018**, *26*, 1118–1126.
- (241) Xing, Y.; Xu, Y.; Chen, Y.; Jeffrey, P. D.; Chao, Y.; Lin, Z.; Li, Z.; Strack, S.; Stock, J. B.; Shi, Y. Structure of protein phosphatase 2A core enzyme bound to tumor-inducing toxins. *Cell* **2006**, *127*, 341–353.
- (242) Xu, Y.; Xing, Y.; Chen, Y.; Chao, Y.; Lin, Z.; Fan, E.; Yu, J. W.; Strack, S.; Jeffrey, P. D.; Shi, Y. Structure of the protein phosphatase 2A holoenzyme. *Cell* **2006**, *127*, 1239–1251.
- (243) Gullledge, B. M.; Aggen, J. B.; Eng, H.; Sweimeh, K.; Chamberlin, A. R. Microcystin analogues comprised only of Adda and a single additional amino acid retain moderate activity as PP1/PP2A inhibitors. *Bioorg Med Chem Lett* **2003**, *13*, 2907–2911.
- (244) Gullledge, B. M.; Aggen, J. B.; Chamberlin, A. R. Linearized and truncated microcystin analogues as inhibitors of protein phosphatases 1 and 2A. *Bioorg Med Chem Lett* **2003**, *13*, 2903–2906.
- (245) Rinehart, K. L.; Namikoshi, M.; Choi, B. W. Structure and biosynthesis of toxins from blue-green algae (cyanobacteria). *J Appl Phycol* **1994**, *6*, 159–176.
- (246) An, J.; Carmichael, W. W. Use of a colorimetric protein phosphatase inhibition assay and enzyme linked immunosorbent assay for the study of microcystins and nodularins. *Toxicon* **1994**, *32*, 1495–1507.
- (247) MacKintosh, R. W.; Dalby, K. N.; Campbell David G.; Cohen, P. T. W.; Cohen, P.; MacKintosh, C. The cyanobacterial toxin microcystin binds covalently to cysteine-273 on protein phosphatase 1. *FEBS Lett* **1995**, *371*, 236–240.
- (248) Zhang, Z.; Zhao, S.; Deans-Zirattu, S.; Bai, G.; Lee, E. Y. Mutagenesis of the catalytic subunit of rabbit muscle protein phosphatase-1. *Mol Cell Biochem* **1993**, *127-128*, 113–119.
- (249) Pereira, S. R.; Vasconcelos, V. M.; Antunes, A. Computational study of the covalent bonding of microcystins to cysteine residues—a reaction involved in the inhibition of the PPP family of protein phosphatases. *FEBS J* **2013**, *280*, 674–680.
- (250) Chen, Y. M.; Lee, T. H.; Lee, S. J.; Huang, H. B.; Huang, R.; Chou, H. N. Comparison of protein phosphatase inhibition activities and mouse toxicities of microcystins. *Toxicon* **2006**, *47*, 742–746.
- (251) Zemskov, I.; Altaner, S.; Dietrich, D. R.; Wittmann, V. Total synthesis of microcystin-LF and derivatives thereof. *J Org Chem* **2017**, *82*, 3680–3691.
- (252) Sainis, I.; Fokas, D.; Vareli, K.; Tzakos, A. G.; Kounnis, V.; Briasoulis, E. Cyanobacterial cyclopeptides as lead compounds to novel targeted cancer drugs. *Mar Drugs* **2010**, *8*, 629–657.
- (253) McCluskey, A.; Sim, A. T. R.; Sakoff, J. A. Serine–threonine protein phosphatase inhibitors. Development of potential therapeutic strategies. *J Med Chem* **2002**, *45*, 1151–1175.
- (254) de Silva, E. D.; Williams, D. E.; Andersen, R. J.; Klux, H.; Holmes, C. F. B.; Allen, T. M. Motuporin, a potent protein phosphatase inhibitor isolated from the Papua New Guinea sponge *Theonella swinhoei* Gray. *Tetrahedron Lett* **1992**, *33*, 1561–1564.

## 5. References

---

- (255) Moffitt, M. C.; Neilan, B. A. Characterization of the nodularin synthetase gene cluster and proposed theory of the evolution of cyanobacterial hepatotoxins. *Appl Environ Microbiol* **2004**, *70*, 6353–6362.
- (256) Tachibana, K.; Scheuer, P. J.; Tsukitani, Y.; Kikuchi, H.; van Engen, D.; Clardy, J.; Gopichand, Y.; Schmitz, F. J. Okadaic acid, a cytotoxic polyether from two marine sponges of the genus *Halichondria*. *J Am Chem Soc* **1981**, *103*, 2469–2471.
- (257) Kato, Y.; Fusetani, N.; Matsunaga, S.; Hashimoto, K.; Fujita, S.; Furuya, T. Calyculin A. A novel antitumor metabolite from the marine sponge *Discodermia calyx*. *J Am Chem Soc* **1986**, *108*, 2780–2781.
- (258) Kato, Y.; Fusetani, N.; Matsunaga, S.; Hashimoto, K.; Koseki, K. Isolation and structure elucidation of calyculins B, C, and D, novel antitumor metabolites, from the marine sponge *Discodermia calyx*. *J Org Chem* **1988**, *53*, 3930–3932.
- (259) Ishihara, H.; Martin, B. L.; Brautigam, D. L.; Karaki, H.; Ozaki, H.; Kato, Y.; Fusetani, N.; Watabe, S.; Hashimoto, K.; Uemura, D.; *et al.* Calyculin A and okadaic acid: inhibitors of protein phosphatase activity. *Biochem Biophys Res Commun* **1989**, *159*, 871–877.
- (260) MacKintosh, C.; Klumpp, S. Tautomycin from the bacterium *Streptomyces verticillatus*. Another potent and specific inhibitor of protein phosphatases 1 and 2A. *FEBS Lett* **1990**, *277*, 137–140.
- (261) Adler, J. T.; Cook, M.; Luo, Y.; Pitt, S. C.; Ju, J.; Li, W.; Shen, B.; Kunnimalaiyaan, M.; Chen, H. Tautomycetin and tautomycin suppress the growth of medullary thyroid cancer cells via inhibition of glycogen synthase kinase-3 $\beta$ . *Mol Cancer Ther* **2009**, *8*, 914–920.
- (262) Pinchot, S. N.; Adler, J. T.; Luo, Y.; Ju, J.; Li, W.; Shen, B.; Kunnimalaiyaan, M.; Chen, H. Tautomycin suppresses growth and neuroendocrine hormone markers in carcinoid cells through activation of the Raf-1 pathway. *Am J Surg* **2009**, *197*, 313–319.
- (263) Fischer, W. J.; Altheimer, S.; Cattori, V.; Meier, P. J.; Dietrich, D. R.; Hagenbuch, B. Organic anion transporting polypeptides expressed in liver and brain mediate uptake of microcystin. *Toxicol Appl Pharmacol* **2005**, *203*, 257–263.
- (264) Hagenbuch, B.; Gui, C. Xenobiotic transporters of the human organic anion transporting polypeptides (OATP) family. *Xenobiotica* **2008**, *38*, 778–801.
- (265) Popovic, M.; Zaja, R.; Smital, T. Organic anion transporting polypeptides (OATP) in zebrafish (*Danio rerio*): phylogenetic analysis and tissue distribution. *Comp Biochem Physiol A Mol Integr Physiol* **2010**, *155*, 327–335.
- (266) Hagenbuch, B.; Meier, P. J. The superfamily of organic anion transporting polypeptides. *Biochim Biophys Acta Biomembr* **2003**, *1609*, 1–18.
- (267) Hong, W.; Wu, Z.; Fang, Z.; Huang, J.; Huang, H.; Hong, M. Amino acid residues in the putative transmembrane domain 11 of human organic anion transporting polypeptide 1B1 dictate transporter substrate binding, stability, and trafficking. *Mol Pharm* **2015**, *12*, 4270–4276.
- (268) Stieger, B.; Hagenbuch, B. Organic anion transporting polypeptides. *Curr Top Membr* **2014**, *73*, 205–232.
- (269) Roth, M.; Obaidat, A.; Hagenbuch, B. OATPs, OATs and OCTs: the organic anion and cation transporters of the *SLCO* and *SLC22A* gene superfamilies. *Br J Pharmacol* **2012**, *165*, 1260–1287.
- (270) DeGorter, M. K.; Ho, R. H.; Leake, B. F.; Tirona, R. G.; Kim, R. B. Interaction of three regiospecific amino acid residues is required for OATP1B1 gain of OATP1B3 substrate specificity. *Mol Pharm* **2012**, *9*, 986–995.
- (271) Mandery, K.; Sticht, H.; Bujok, K.; Schmidt, I.; Fahrmayr, C.; Balk, B.; Fromm, M. F.; Glaeser, H. Functional and structural relevance of conserved positively charged lysine residues in organic anion transporting polypeptide 1B3. *Mol Pharmacol* **2011**, *80*, 400–406.

- (272) Miyagawa, M.; Maeda, K.; Aoyama, A.; Sugiyama, Y. The eighth and ninth transmembrane domains in organic anion transporting polypeptide 1B1 affect the transport kinetics of estrone-3-sulfate and estradiol-17 $\beta$ -D-glucuronide. *J Pharmacol Exp Ther* **2009**, *329*, 551–557.
- (273) Gui, C.; Hagenbuch, B. Amino acid residues in transmembrane domain 10 of organic anion transporting polypeptide 1B3 are critical for cholecystokinin octapeptide transport. *Biochemistry* **2008**, *47*, 9090–9097.
- (274) Bossuyt, X.; Müller, M.; Meier, P. J. Multispecific amphipathic substrate transport by an organic anion transporter of human liver. *J Hepatol* **1996**, *25*, 733–738.
- (275) Fahrmayr, C.; Fromm, M. F.; König, J. Hepatic OATP and OCT uptake transporters: their role for drug–drug interactions and pharmacogenetic aspects. *Drug Metab Rev* **2010**, *42*, 380–401.
- (276) Kullak-Ublick, G. A.; Hagenbuch, B.; Stieger, B.; Scheingart, C. D.; Hofmann, A. F.; Wolkoff, A. W.; Meier, P. J. Molecular and functional characterization of an organic anion transporting polypeptide cloned from human liver. *Gastroenterology* **1995**, *109*, 1274–1282.
- (277) Steckelbroeck, S.; Nassen, A.; Ugele, B.; Ludwig, M.; Watzka, M.; Reissinger, A.; Clusmann, H.; Lütjohann, D.; Siekmann, L.; Klingmüller, D.; *et al.* Steroid sulfatase (STS) expression in the human temporal lobe: enzyme activity, mRNA expression and immunohistochemistry study. *J Neurochem* **2004**, *89*, 403–417.
- (278) Abe, T.; Kakyo, M.; Tokui, T.; Nakagomi, R.; Nishio, T.; Nakai, D.; Nomura, H.; Unno, M.; Suzuki, M.; Naitoh, T.; *et al.* Identification of a novel gene family encoding human liver-specific organic anion transporter LST-1. *J Biol Chem* **1999**, *274*, 17159–17163.
- (279) Hsiang, B.; Zhu, Y.; Wang, Z.; Wu, Y.; Sasseville, V.; Yang, W. P.; Kirchgessner, T. G. A novel human hepatic organic anion transporting polypeptide (OATP2). Identification of a liver-specific human organic anion transporting polypeptide and identification of rat and human hydroxymethylglutaryl-CoA reductase inhibitor transporters. *J Biol Chem* **1999**, *274*, 37161–37168.
- (280) König, J.; Cui, Y.; Nies, A. T.; Keppler, D. Localization and genomic organization of a new hepatocellular organic anion transporting polypeptide. *J Biol Chem* **2000**, *275*, 23161–23168.
- (281) König, J.; Cui, Y.; Nies, A. T.; Keppler, D. A novel human organic anion transporting polypeptide localized to the basolateral hepatocyte membrane. *Am J Physiol Gastrointest Liver Physiol* **2000**, *278*, G156–G164.
- (282) Abe, T.; Unno, M.; Onogawa, T.; Tokui, T.; Kondo, T. N.; Nakagomi, R.; Adachi, H.; Fujiwara, K.; Okabe, M.; Suzuki, T.; *et al.* LST-2, a human liver-specific organic anion transporter, determines methotrexate sensitivity in gastrointestinal cancers. *Gastroenterology* **2001**, *120*, 1689–1699.
- (283) Briz, O.; Romero, M. R.; Martinez-Becerra, P.; Macias, R. I. R.; Perez, M. J.; Jimenez, F.; San Martin, F. G.; Marin, J. J. G. OATP8/1B3-mediated cotransport of bile acids and glutathione: an export pathway for organic anions from hepatocytes? *J Biol Chem* **2006**, *281*, 30326–30335.
- (284) Michalski, C.; Cui, Y.; Nies, A. T.; Nuessler, A. K.; Neuhaus, P.; Zanger, U. M.; Klein, K.; Eichelbaum, M.; Keppler, D.; König, J. A naturally occurring mutation in the *SLC21A6* gene causing impaired membrane localization of the hepatocyte uptake transporter. *J Biol Chem* **2002**, *277*, 43058–43063.
- (285) Nakanishi, T.; Tamai, I. Solute carrier transporters as targets for drug delivery and pharmacological intervention for chemotherapy. *J Pharm Sci* **2011**, *100*, 3731–3750.
- (286) Buxhofer-Ausch, V.; Secky, L.; Wlcek, K.; Svoboda, M.; Kounnis, V.; Briasoulis, E.; Tzakos, A. G.; Jaeger, W.; Thalhammer, T. Tumor-specific expression of organic anion transporting polypeptides: transporters as novel targets for cancer therapy. *J Drug Deliv* **2013**, 863539.
- (287) Thakkar, N.; Lockhart, A. C.; Lee, W. Role of organic anion transporting polypeptides (OATPs) in cancer therapy. *AAPS J* **2015**, *17*, 535–545.
- (288) Lee, W.; Belkhir, A.; Lockhart, A. C.; Merchant, N.; Glaeser, H.; Harris, E. I.; Washington, M. K.; Brunt, E. M.; Zaika, A.; Kim, R. B.; *et al.* Overexpression of OATP1B3 confers apoptotic resistance in colon cancer. *Cancer Res* **2008**, *68*, 10315–10323.

## 5. References

---

- (289) Schulte, R. R.; Ho, R. H. Organic anion transporting polypeptides: emerging roles in cancer pharmacology. *Mol Pharmacol* **2019**, *95*, 490–506.
- (290) Liu, T.; Li, Q. Organic anion transporting polypeptides: a novel approach for cancer therapy. *J Drug Target* **2014**, *22*, 14–22.
- (291) Hays, A.; Apte, U.; Hagenbuch, B. Organic anion transporting polypeptides expressed in pancreatic cancer may serve as potential diagnostic markers and therapeutic targets for early stage adenocarcinomas. *Pharm Res* **2013**, *30*, 2260–2269.
- (292) Niedermeyer, T. H. J.; Daily, A.; Swiatecka-Hagenbruch, M.; Moscow, J. A. Selectivity and potency of microcystin congeners against OATP1B1 and OATP1B3 expressing cancer cells. *PLoS ONE* **2014**, *9*, e91476.
- (293) Richardson, N. C.; Kasamon, Y. L.; Chen, H.; de Claro, R. A.; Ye, J.; Blumenthal, G. M.; Farrell, A. T.; Pazdur, R. FDA approval summary: brentuximab vedotin in first-line treatment of peripheral T-cell lymphoma. *Oncologist* **2019**, *24*, e180–e187.
- (294) Eichenauer, D. A.; Plütschow, A.; Kreissl, S.; Sökler, M.; Hellmuth, J. C.; Meissner, J.; Mathas, S.; Topp, M. S.; Behringer, K.; Klapper, W.; *et al.* Incorporation of brentuximab vedotin into first-line treatment of advanced classical Hodgkin's lymphoma: final analysis of a phase 2 randomised trial by the German Hodgkin Study Group. *Lancet Oncol* **2017**, *18*, 1680–1687.
- (295) Jackson, D.; Stover, D. Using the lessons learned from the clinic to improve the preclinical development of antibody drug conjugates. *Pharm Res* **2015**, *32*, 3458–3469.
- (296) Jain, N.; Smith, S. W.; Ghone, S.; Tomczuk, B. Current ADC linker chemistry. *Pharm Res* **2015**, *32*, 3526–3540.
- (297) Dubowchik, G. M.; Firestone, R. A.; Padilla, L.; Willner, D.; Hofstead, S. J.; Mosure, K.; Knipe, J. O.; Lasch, S. J.; Trail, P. A. Cathepsin B-labile dipeptide linkers for lysosomal release of doxorubicin from internalizing immunoconjugates: model studies of enzymatic drug release and antigen-specific *in vitro* anticancer activity. *Bioconjug Chem* **2002**, *13*, 855–869.
- (298) Panowski, S.; Bhakta, S.; Raab, H.; Polakis, P.; Junutula, J. R. Site-specific antibody drug conjugates for cancer therapy. *mAbs* **2014**, *6*, 34–45.
- (299) Prescher, J. A.; Bertozzi, C. R. Chemistry in living systems. *Nat Chem Biol* **2005**, *1*, 13–21.
- (300) Patterson, D. M.; Nazarova, L. A.; Prescher, J. A. Finding the right (bioorthogonal) chemistry. *ACS Chem Biol* **2014**, *9*, 592–605.
- (301) Row, R. D.; Prescher, J. A. Constructing new bioorthogonal reagents and reactions. *Acc. Chem. Res.* **2018**, *51*, 1073–1081.
- (302) Ramil, C. P.; Lin, Q. Bioorthogonal chemistry: strategies and recent developments. *Chem Commun* **2013**, *49*, 11007–11022.
- (303) Gordon, C. G.; Bertozzi, C. R. *In vivo* applications of bioorthogonal chemistries. In *Chemoselective and bioorthogonal ligation reactions*; Algar, W. R., Dawson, P. E., Medintz, I. L., Eds.; Wiley-VCH Verlag GmbH & Co. KGaA: Weinheim, 2017; pp 417–457.
- (304) Qin, L.-H.; Hu, W.; Long, Y.-Q. Bioorthogonal chemistry: optimization and application updates during 2013–2017. *Tetrahedron Lett* **2018**, *59*, 2214–2228.
- (305) Devaraj, N. K. The future of bioorthogonal chemistry. *ACS Cent Sci* **2018**, *4*, 952–959.
- (306) Kolb, H. C.; Finn, M. G.; Sharpless, K. B. Click chemistry: diverse chemical function from a few good reactions. *Angew Chem Int Ed Engl* **2001**, *40*, 2004–2021.
- (307) Tornøe, C. W.; Christensen, C.; Meldal, M. Peptidotriazoles on solid phase: [1,2,3]-triazoles by regioselective copper(I)-catalyzed 1,3-dipolar cycloadditions of terminal alkynes to azides. *J Org Chem* **2002**, *67*, 3057–3064.
- (308) Rostovtsev, V. V.; Green, L. G.; Fokin, V. V.; Sharpless, K. B. A stepwise Huisgen cycloaddition process: copper(I)-catalyzed regioselective "ligation" of azides and terminal alkynes. *Angew Chem Int Ed Engl* **2002**, *41*, 2596–2599.
- (309) McKay, C. S.; Finn, M. G. Click chemistry in complex mixtures: bioorthogonal bioconjugation. *Chem Biol* **2014**, *21*, 1075–1101.



- (310) Kondo, F.; Ikai, Y.; Oka, H.; Okumura, M.; Ishikawa, N.; Harada, K.; Matsuura, K.; Murata, H.; Suzuki, M. Formation, characterization, and toxicity of the glutathione and cysteine conjugates of toxic heptapeptide microcystins. *Chem Res Toxicol* **1992**, *5*, 591–596.
- (311) Miles, C. O.; Sandvik, M.; Nonga, H. E.; Rundberget, T.; Wilkins, A. L.; Rise, F.; Ballot, A. Thiol derivatization for LC–MS identification of microcystins in complex matrices. *Environ Sci Technol* **2012**, *46*, 8937–8944.
- (312) Miles, C. O.; Sandvik, M.; Nonga, H. E.; Rundberget, T.; Wilkins, A. L.; Rise, F.; Ballot, A. Identification of microcystins in a Lake Victoria cyanobacterial bloom using LC–MS with thiol derivatization. *Toxicol* **2013**, *70*, 21–31.
- (313) Zemskov, I.; Kropp, H. M.; Wittmann, V. Regioselective cleavage of thioether linkages in microcystin conjugates. *Chem Eur J* **2016**, *22*, 10990–10997.
- (314) Humphrey, J. M.; Aggen, J. B.; Chamberlin, A. R. Total synthesis of the serine–threonine phosphatase inhibitor microcystin-LA. *J Am Chem Soc* **1996**, *118*, 11759–11770.
- (315) Birch, A. J. The biosynthesis of antibiotics. *Pure Appl Chem* **1963**, *7*, 527–538.
- (316) Thiericke, R.; Rohr, J. Biological variation of microbial metabolites by precursor-directed biosynthesis. *Nat Prod Rep* **1993**, *3*, 265–289.
- (317) Lowden, P. A. S.; Böhm, G. A.; Metcalfe, S.; Staunton, J.; Leadlay, P. F. New rapamycin derivatives by precursor-directed biosynthesis. *Chembiochem* **2004**, *5*, 535–538.
- (318) Magarvey, N. A.; Beck, Z. Q.; Golakoti, T.; Ding, Y.; Huber, U.; Hemscheidt, T. K.; Abelson, D.; Moore, R. E.; Sherman, D. H. Biosynthetic characterization and chemoenzymatic assembly of the cryptophycins. Potent anticancer agents from *Nostoc* cyanobionts. *ACS Chem Biol* **2006**, *1*, 766–779.
- (319) Kirschning, A.; Taft, F.; Knobloch, T. Total synthesis approaches to natural product derivatives based on the combination of chemical synthesis and metabolic engineering. *Org Biomol Chem* **2007**, *5*, 3245–3259.
- (320) Portmann, C.; Prestinari, C.; Myers, T.; Scharfe, J.; Gademann, K. Directed biosynthesis of phytotoxic alkaloids in the cyanobacterium *Nostoc* 78-12A. *Chembiochem* **2009**, *10*, 889–895.
- (321) Okumura, H. S.; Philmus, B.; Portmann, C.; Hemscheidt, T. K. Homotyrosine-containing cyanopeptolins 880 and 960 and anabaenopeptins 908 and 915 from *Planktothrix agardhii* CYA 126/8. *J Nat Prod* **2009**, *72*, 172–176.
- (322) Grünschow, S.; Rackham, E. J.; Elkins, B.; Newill, P. L. A.; Hill, L. M.; Goss, R. J. M. New pacidamycin antibiotics through precursor-directed biosynthesis. *Chembiochem* **2009**, *10*, 355–360.
- (323) Harvey, C. J. B.; Puglisi, J. D.; Pande, V. S.; Cane, D. E.; Khosla, C. Precursor directed biosynthesis of an orthogonally functional erythromycin analogue: selectivity in the ribosome macrolide binding pocket. *J Am Chem Soc* **2012**, *134*, 12259–12265.
- (324) Zhu, X.; Zhang, W. Tagging polyketides/non-ribosomal peptides with a clickable functionality and applications. *Front Chem* **2015**, *3*, 11.
- (325) Boecker, S.; Zobel, S.; Meyer, V.; Süßmuth, R. D. Rational biosynthetic approaches for the production of new-to-nature compounds in fungi. *Fungal Genet Biol* **2016**, *89*, 89–101.
- (326) Wang, C.; Monger, A.; Wang, L.; Fu, P.; Piyachaturawat, P.; Chairoungdua, A.; Zhu, W. Precursor-directed generation of indolocarbazoles with topoisomerase II $\alpha$  inhibitory activity. *Mar Drugs* **2018**, *16*, 168.
- (327) Guo, H.; Schmidt, A.; Stephan, P.; Raguž, L.; Braga, D.; Kaiser, M.; Dahse, H.-M.; Weigel, C.; Lackner, G.; Beemelmans, C. Precursor-directed diversification of cyclic tetrapeptidic pseudoxylallemycins. *Chembiochem* **2018**, *19*, 2307–2311.
- (328) Telfer, T. J.; Richardson-Sanchez, T.; Gotsbacher, M. P.; Nolan, K. P.; Tieu, W.; Codd, R. Analogues of desferrioxamine B (DFOB) with new properties and new functions generated using precursor-directed biosynthesis. *BioMetals* **2019**, *32*, 395–408.

## 5. References

---

- (329) Baskin, J. M.; Prescher, J. A.; Laughlin, S. T.; Agard, N. J.; Chang, P. V.; Miller, I. A.; Lo, A.; Codelli, J. A.; Bertozzi, C. R. Copper-free click chemistry for dynamic *in vivo* imaging. *PNAS* **2007**, *104*, 16793–16797.
- (330) Zilliges, Y.; Kehr, J.-C.; Meissner, S.; Ishida, K.; Mikkat, S.; Hagemann, M.; Kaplan, A.; Börner, T.; Dittmann, E. The cyanobacterial hepatotoxin microcystin binds to proteins and increases the fitness of *Microcystis* under oxidative stress conditions. *PLoS ONE* **2011**, *6*, e17615.
- (331) Straub, C.; Quillardet, P.; Vergalli, J.; Tandeau de Marsac, N.; Humbert, J.-F. A day in the life of *Microcystis aeruginosa* strain PCC 7806 as revealed by a transcriptomic analysis. *PLoS ONE* **2011**, *6*, e16208.
- (332) LeBlanc Renaud, S.; Pick, F. R.; Fortin, N. Effect of light intensity on the relative dominance of toxigenic and nontoxigenic strains of *Microcystis aeruginosa*. *Appl Environ Microbiol* **2011**, *77*, 7016–7022.
- (333) Meissner, S.; Steinhauser, D.; Dittmann, E. Metabolomic analysis indicates a pivotal role of the hepatotoxin microcystin in high light adaptation of *Microcystis*. *Environ Microbiol* **2015**, *17*, 1497–1509.
- (334) Briand, E.; Yéprémian, C.; Humbert, J.-F.; Quiblier, C. Competition between microcystin- and non-microcystin-producing *Planktothrix agardhii* (cyanobacteria) strains under different environmental conditions. *Environ Microbiol* **2008**, *10*, 3337–3348.
- (335) Ding, Y.; Song, L.; Sedmak, B. UVB radiation as a potential selective factor favoring microcystin-producing bloom-forming cyanobacteria. *PLoS ONE* **2013**, *8*, e73919.
- (336) Yang, Z.; Kong, F.; Shi, X.; Yu, Y.; Zhang, M. Effects of UV-B radiation on microcystin production of a toxic strain of *Microcystis aeruginosa* and its competitiveness against a non-toxic strain. *J Hazard Mater* **2015**, *283*, 447–453.
- (337) Tonietto, A.; Petriz, B. A.; Araújo, W. C.; Mehta, A.; Magalhães, B. S.; Franco, O. L. Comparative proteomics between natural *Microcystis* isolates with a focus on microcystin synthesis. *Proteome Sci* **2012**, *10*, 38.
- (338) Pineda-Mendoza, R. M.; Zúñiga, G.; Martínez-Jerónimo, F. Microcystin production in *Microcystis aeruginosa*: effect of type of strain, environmental factors, nutrient concentrations, and N:P ratio on *mcyA* gene expression. *Aquat Ecol* **2016**, *50*, 103–119.
- (339) Yeung, A. C. Y.; D'Agostino, P. M.; Poljak, A.; McDonald, J.; Bligh, M. W.; Waite, T. D.; Neilan, B. A. Physiological and proteomic responses of continuous cultures of *Microcystis aeruginosa* PCC 7806 to changes in iron bioavailability and growth rate. *Appl Environ Microbiol* **2016**, *82*, 5918–5929.
- (340) Mowe, M. A. D.; Abbas, F.; Porojan, C.; Mitrovic, S. M.; Lim, R. P.; Furey, A.; Yeo, D. C. J. Roles of nitrogen and phosphorus in growth responses and toxin production (using LC–MS/MS) of tropical *Microcystis ichthyoblabe* and *M. flos-aquae*. *J Appl Phycol* **2016**, *28*, 1543–1552.
- (341) Gobler, C. J.; Burkholder, J. M.; Davis, T. W.; Harke, M. J.; Johengen, T.; Stow, C. A.; van de Waal, D. B. The dual role of nitrogen supply in controlling the growth and toxicity of cyanobacterial blooms. *Harmful Algae* **2016**, *54*, 87–97.
- (342) Kaplan, A.; Harel, M.; Kaplan-Levy, R. N.; Hadas, O.; Sukenik, A.; Dittmann, E. The languages spoken in the water body (or the biological role of cyanobacterial toxins). *Front Microbiol* **2012**, *3*, 138.
- (343) Bittencourt-Oliveira, M. d. C.; Chia, M. A.; Bezerra de Oliveira, H. S.; Cordeiro Araújo, M. K.; Molica, R. J. R.; Tadeu Santos Dias, C. Allelopathic interactions between microcystin-producing and non-microcystin-producing cyanobacteria and green microalgae: implications for microcystins production. *J Appl Phycol* **2015**, *27*, 275–284.
- (344) Shi, L.; Carmichael, W. W.; Miller, I. Immunogold localization of hepatotoxins in cyanobacterial cells. *Arch Microbiol* **1995**, *163*, 7–15.

- (345) Young, F. M.; Thomson, C.; Metcalf, J. S.; Lucocq, J. M.; Codd, G. A. Immunogold localisation of microcystins in cryosectioned cells of *Microcystis*. *J Struct Biol* **2005**, *151*, 208–214.
- (346) Gerbersdorf, S. U. An advanced technique for immuno-labelling of microcystins in cryosectioned cells of *Microcystis aeruginosa* PCC 7806 (cyanobacteria): implementations of an experiment with varying light scenarios and culture densities. *Toxicon* **2006**, *47*, 218–228.
- (347) Young, F. M.; Morrison, L. F.; James, J.; Codd, G. A. Quantification and localization of microcystins in colonies of a laboratory strain of *Microcystis* (cyanobacteria) using immunological methods. *Eur J Phycol* **2008**, *43*, 217–225.
- (348) Mhadhbi, H.; Ben-Rejeb, S.; Cl eroux, C.; Martel, A.; Delahaut, P. Generation and characterization of polyclonal antibodies against microcystins—application to immunoassays and immunoaffinity sample preparation prior to analysis by liquid chromatography and UV detection. *Talanta* **2006**, *70*, 225–235.
- (349) Sivakumar, K.; Xie, F.; Cash, B. M.; Long, S.; Barnhill, H. N.; Wang, Q. A fluorogenic 1,3-dipolar cycloaddition reaction of 3-azidocoumarins and acetylenes. *Org Lett* **2004**, *6*, 4603–4606.
- (350) Shieh, P.; Dien, V. T.; Beahm, B. J.; Castellano, J. M.; Wyss-Coray, T.; Bertozzi, C. R. CalFluors: a universal motif for fluorogenic azide probes across the visible spectrum. *J Am Chem Soc* **2015**, *137*, 7145–7151.
- (351) Le Droumaguet, C.; Wang, C.; Wang, Q. Fluorogenic click reaction. *Chem Soc Rev* **2010**, *39*, 1233–1239.
- (352) Zhou, Y.; Wang, S.; Zhang, K.; Jiang, X. Visual detection of copper(II) by azide- and alkyne-functionalized gold nanoparticles using click chemistry. *Angew Chem Int Ed Engl* **2008**, *47*, 7454–7456.
- (353) Luo, W.; Gobbo, P.; McNitt, C. D.; Sutton, D. A.; Popik, V. V.; Workentin, M. S. "Shine & click" photo-induced interfacial unmasking of strained alkynes on small water-soluble gold nanoparticles. *Chemistry* **2017**, *23*, 1052–1059.
- (354) Elliott, E. W.; Ginzburg, A. L.; Kennedy, Z. C.; Feng, Z.; Hutchison, J. E. Single-step synthesis of small, azide-functionalized gold nanoparticles: versatile, water-dispersible reagents for click chemistry. *Langmuir* **2017**, *33*, 5796–5802.
- (355) Rippka, R.; Deruelles, J.; Waterbury, J. B.; Herdman, M.; Stanier, R. Y. Generic assignments, strain histories and properties of pure cultures of cyanobacteria. *J Gen Microbiol* **1979**, *111*, 1–61.
- (356) Bolch, C. J. S.; Blackburn, S. I. Isolation and purification of Australian isolates of the toxic cyanobacterium *Microcystis aeruginosa* K utz. *J Appl Phycol* **1996**, *8*, 5–13.
- (357) Chambers, M. C.; Maclean, B.; Burke, R.; Amodei, D.; Ruderman, D. L.; Neumann, S.; Gatto, L.; Fischer, B.; Pratt, B.; Egertson, J.; *et al.* A cross-platform toolkit for mass spectrometry and proteomics. *Nat Biotechnol* **2012**, *30*, 918–920.
- (358) Niedermeyer, T. H. J.; Strohal, M. mMass as a software tool for the annotation of cyclic peptide tandem mass spectra. *PLoS ONE* **2012**, *7*, e44913.
- (359) van Kuppeveld, F. J.; Johansson, K. E.; Galama, J. M.; Kissing, J.; B olske, G.; van der Logt, J. T.; Melchers, W. J. Detection of mycoplasma contamination in cell cultures by a mycoplasma group-specific PCR. *Appl Environ Microbiol* **1994**, *60*, 149–152.
- (360) Vichai, V.; Kirtikara, K. Sulforhodamine B colorimetric assay for cytotoxicity screening. *Nat Protoc* **2006**, *1*, 1112–1116.
- (361) Cerasino, L.; Meriluoto, J.; Bl aha, L.; Carmeli, S.; Kaloudis, T.; Mazur-Marzec, H. Extraction of Cyanotoxins from Cyanobacterial Biomass. In *Handbook of cyanobacterial monitoring and cyanotoxin analysis*; Meriluoto, J., Spoof, L., Codd, G. A., Eds.; Wiley: Chichester, West Sussex, 2017; pp 350–353.
- (362) Rogers, S.; Puddick, J.; Wood, S. A.; Dietrich, D. R.; Hamilton, D. P.; Prinsep, M. R. The effect of cyanobacterial biomass enrichment by centrifugation and GF/C filtration on subsequent microcystin measurement. *Toxins* **2015**, *7*, 821–834.

## 5. References

---

- (363) Lagoutte, B.; Tunkelrott, M.-L.; Feraudet-Tarisse, C.; Dano, J.; Volland, H. Fast and direct extraction of cell-associated hepatotoxins from toxic cyanobacteria. *Water Environ Res* **2014**, *86*, 470–477.
- (364) Sano, T.; Takagi, H.; Nishikawa, M.; Kaya, K. NIES certified reference material for microcystins, hepatotoxic cyclic peptide toxins from cyanobacterial blooms in eutrophic water bodies. *Anal Bioanal Chem* **2008**, *391*, 2005–2010.
- (365) Msagati, T. A. M.; Siame, B. A.; Shushu, D. D. Evaluation of methods for the isolation, detection and quantification of cyanobacterial hepatotoxins. *Aquat Toxicol* **2006**, *78*, 382–397.
- (366) Spoof, L.; Vesterkvist, P.; Lindholm, T.; Meriluoto, J. Screening for cyanobacterial hepatotoxins, microcystins and nodularin in environmental water samples by reversed-phase liquid chromatography–electrospray ionisation mass spectrometry. *J Chromatogr A* **2003**, *1020*, 105–119.
- (367) Ramanan, S.; Tang, J.; Velayudhan, A. Isolation and preparative purification of microcystin variants. *J Chromatogr A* **2000**, *883*, 103–112.
- (368) Fastner, J.; Flieger, I.; Neumann, U. Optimised extraction of microcystins from field samples—a comparison of different solvents and procedures. *Water Res* **1998**, *32*, 3177–3181.
- (369) Lawton, L. A.; Edwards, C.; Codd, G. A. Extraction and high-performance liquid chromatographic method for the determination of microcystins in raw and treated waters. *Analyst* **1994**, *119*, 1525.
- (370) Kungsuwan, A.; Noguchi, T.; Matsunaga, S.; Watanabe, M. F.; Watabe, S.; Hashimoto, K. Properties of two toxins isolated from the blue-green alga *Microcystis aeruginosa*. *Toxicon* **1988**, *26*, 119–125.
- (371) Kungsuwan, A. Isolation of two toxins from the blue-green alga *Microcystis aeruginosa*. *Nippon Suisan Gakkai Shi* **1987**, *53*, 2051–2054.
- (372) Barco, M.; Lawton, L. A.; Rivera, J.; Caixach, J. Optimization of intracellular microcystin extraction for their subsequent analysis by high-performance liquid chromatography. *J Chromatogr A* **2005**, *1074*, 23–30.
- (373) Rabel, F. M. Care of reverse phase high performance liquid chromatographic columns when injecting extracts of fat- or oil-based preparations. *J Assoc Off Anal Chem* **1981**, *64*, 1258.
- (374) Rivasseau, C.; Martins, S.; Hennion, M.-C. Determination of some physicochemical parameters of microcystins (cyanobacterial toxins) and trace level analysis in environmental samples using liquid chromatography. *J Chromatogr A* **1998**, *799*, 155–169.
- (375) Harada, K.-I. Chemistry and detection of microcystins. *Toxic Microcystis* **1996**, 103–148.
- (376) Skrzecz, A.; Shaw, D.; Maczynski, A.; Skrzecz, A. IUPAC-NIST solubility data series 69. Ternary alcohol–hydrocarbon–water systems. *J Phys Chem Ref Data* **1999**, *28*, 983–1235.
- (377) Sugi, H.; Katayama, T. Liquid–liquid equilibrium data for three ternary systems of aqueous alcohol solutions and applicability of the analytical solutions of groups. *J Chem Eng Jpn* **1977**, *10*, 400–402.
- (378) Trojanowicz, M. Chromatographic and capillary electrophoretic determination of microcystins. *J Sep Sci* **2010**, *33*, 359–371.
- (379) Lawton, L. A.; Edwards, C. Purification of microcystins. *J Chromatogr A* **2001**, *912*, 191–209.
- (380) Meriluoto, J. Chromatography of microcystins. *Anal Chim Acta* **1997**, *352*, 277–298.
- (381) Pérez, S.; Aga, D. S. Recent advances in the sample preparation, liquid-chromatography tandem-mass spectrometric analysis and environmental fate of microcystins in water. *Trends Anal Chem* **2005**, *24*, 658–670.
- (382) Weber, P.; Hamburger, M.; Schafroth, N.; Potterat, O. Flash chromatography on cartridges for the separation of plant extracts: rules for the selection of chromatographic conditions and comparison with medium pressure liquid chromatography. *Fitoterapia* **2011**, *82*, 155–161.

- (383) Blunt, J. W.; Calder, V. L.; Fenwick, G. D.; Lake, R. J.; McCombs, J. D.; Munro, M. H. G.; Perry, N. B. Reverse phase flash chromatography: a method for the rapid partitioning of natural product extracts. *J Nat Prod* **1987**, *50*, 290–292.
- (384) Lawton, L. A.; McElhiney, J.; Edwards, C. Purification of closely eluting hydrophobic microcystins (peptide cyanotoxins) by normal-phase and reversed-phase flash chromatography. *J Chromatogr A* **1999**, *848*, 515–522.
- (385) Edwards, C.; Lawton, L. A.; Coyle, S. M.; Ross, P. Laboratory-scale purification of microcystins using flash chromatography and reversed-phase high-performance liquid chromatography. *J Chromatogr A* **1996**, *734*, 163–173.
- (386) Cremer, J.; Meyer, H.; Henning, K. Separation of methylated and non-methylated cyanoginosin-LR homologues of the cyanobacterium *Microcystis aeruginosa* strain PCC 7806 by reversed-phase medium-pressure liquid chromatography. *J Chromatogr A* **1991**, *558*, 430–434.
- (387) Cremer, J.; Henning, K. Application of reversed-phase medium-pressure liquid chromatography to the isolation, separation and amino acid analysis of two closely related peptide toxins of the cyanobacterium *Microcystis aeruginosa* strain PCC 7806. *J Chromatogr A* **1991**, *587*, 71–80.
- (388) Henke, H. *Präparative Gelchromatographie an Sephadex LH-20*; Obernburg, 1994.
- (389) Baier, W.; Loleit, M.; Fischer, B.; Jung, G.; Neumann, U.; Weiß, M.; Weckesser, J.; Hoffmann, P.; Bessler, W.G.; Mittenbühler, K. Generation of antibodies directed against the low-immunogenic peptide-toxins microcystin-LR/RR and nodularin. *Int J Immunopharmacol* **2000**, *22*, 339–353.
- (390) Lee, T.-H.; Chen, Y.-M.; Chou, H.-N. First report of microcystins in Taiwan. *Toxicon* **1998**, *36*, 247–255.
- (391) Jakobi, C.; Rinehart, K. L.; Codd, G. A.; Carmienke, I.; Weckesser, J. Occurrence of toxic water blooms containing microcystins in a German lake over a three year period. *Syst Appl Microbiol* **1996**, *19*, 249–254.
- (392) Boland, M. P.; Smillie, M. A.; Chen, D. Z. X.; Holmes, C. F. B. A unified bioscreen for the detection of diarrhetic shellfish toxins and microcystins in marine and freshwater environments. *Toxicon* **1993**, *31*, 1393–1405.
- (393) Craig, M.; McCready, T. L.; Luu, H. A.; Smillie, M. A.; Dubord, P.; Holmes, C. F. B. Identification and characterization of hydrophobic microcystins in Canadian freshwater cyanobacteria. *Toxicon* **1993**, *31*, 1541–1549.
- (394) Namikoshi, M.; Rinehart, K. L.; Sakai, R.; Stotts, R. R.; Dahlem, A. M.; Beasley, V. R.; Carmichael, W. W.; Evans, W. R. Identification of 12 hepatotoxins from a Homer Lake bloom of the cyanobacteria *Microcystis aeruginosa*, *Microcystis viridis*, and *Microcystis wesenbergii*: nine new microcystins. *J Org Chem* **1992**, *57*, 866–872.
- (395) Hiskia, A.; Spooft, L.; Kaloudis, T.; Meriluoto, J. Determination of cyanotoxins by high-performance liquid chromatography with photodiode array. In *Handbook of cyanobacterial monitoring and cyanotoxin analysis*; Meriluoto, J., Spooft, L., Codd, G. A., Eds.; Wiley: Chichester, West Sussex, 2017; pp 203–211.
- (396) Edwards, C.; Lawton, L. A. Assessment of microcystin purity using charged aerosol detection. *J Chromatogr A* **2010**, *1217*, 5233–5238.
- (397) Krüger, T.; Christian, B.; Luckas, B. Development of an analytical method for the unambiguous structure elucidation of cyclic peptides with special appliance for hepatotoxic desmethylated microcystins. *Toxicon* **2009**, *54*, 302–312.
- (398) Purdie, E. L.; Young, F. M.; Menzel, D.; Codd, G. A. A method for acetonitrile-free microcystin analysis and purification by high-performance liquid chromatography, using methanol as mobile phase. *Toxicon* **2009**, *54*, 887–890.

## 5. References

---

- (399) Lombardo, M.; Pinto, F. C. R.; Vieira, J. M. S.; Honda, R. Y.; Pimenta, A. M. C.; Bemquerer, M. P.; Carvalho, L. R.; Kiyota, S. Isolation and structural characterization of microcystin-LR and three minor oligopeptides simultaneously produced by *Radiocystis feernandoi* (Chroococcales, Cyanobacteria): a Brazilian toxic cyanobacterium. *Toxicon* **2006**, *47*, 560–566.
- (400) Oudra, B.; Loudiki, M.; Sbiyyaa, B.; Martins, R.; Vasconcelos, V.; Namikoshi, N. Isolation, characterization and quantification of microcystins (heptapeptides hepatotoxins) in *Microcystis aeruginosa* dominated bloom of Lalla Takerkoust lake–reservoir (Morocco). *Toxicon* **2001**, *39*, 1375–1381.
- (401) Habermehl, G. G.; Krebs, H. C.; Nemes, P.; Nagy, G.; Scheiber, P. Occurrence of toxin producing cyanobacteria in Hungary. Isolation, separation and identification of microcystins. *Z Naturforsch B Chem Sci* **1997**, *52*, 107–109.
- (402) Edwards, C.; Lawton, L. A.; Coyle, S. M.; Ross, P. Automated purification of microcystins. *J Chromatogr A* **1996**, *734*, 175–182.
- (403) Lawton, L. A.; Edwards, C.; Beattie, K. A.; Pleasance, S.; Dear, G. J.; Codd, G. A. Isolation and characterization of microcystins from laboratory cultures and environmental samples of *Microcystis aeruginosa* and from an associated animal toxicosis. *Nat Toxins* **1995**, *3*, 50–57.
- (404) Azevedo, S. M. F. O.; Evans, W. R.; Carmichael, W. W.; Namikoshi, M. First report of microcystins from a Brazilian isolate of the cyanobacterium *Microcystis aeruginosa*. *J Appl Phycol* **1994**, *6*, 261–265.
- (405) Kos, P.; Gorzo, G.; Suranyi, G.; Borbely, G. Simple and efficient method for isolation and measurement of cyanobacterial hepatotoxins by plant tests (*Sinapis alba*). *Anal Biochem* **1995**, *225*, 49–53.
- (406) Luukkainen, R.; Namikoshi, M.; Sivonen, K.; Rinehart, K. L.; Niemelä, S. I. Isolation and identification of 12 microcystins from four strains and two bloom samples of *Microcystis* spp.: structure of a new hepatotoxin. *Toxicon* **1994**, *32*, 133–139.
- (407) Namikoshi, M.; Choi, B. W.; Sun, F.; Rinehart, K. L.; Evans, W. R.; Carmichael, W. W. Chemical characterization and toxicity of dihydro derivatives of nodularin and microcystin-LR, potent cyanobacterial cyclic peptide hepatotoxins. *Chem Res Toxicol* **1993**, *6*, 151–158.
- (408) Sivonen, K.; Skulberg, O. M.; Namikoshi, M.; Evans, W. R.; Carmichael, W. W.; Rinehart, K. L. Two methyl ester derivatives of microcystins, cyclic heptapeptide hepatotoxins, isolated from *Anabaena flos-aquae* strain CYA 83/1. *Toxicon* **1992**, *30*, 1465–1471.
- (409) Sivonen, K.; Carmichael, W. W.; Namikoshi, M.; Rinehart, K. L.; Dahlem, A. M.; Niemela, S. I. Isolation and characterization of hepatotoxic microcystin homologs from the filamentous freshwater cyanobacterium *Nostoc* sp. strain 152. *Appl Environ Microbiol* **1990**, *56*, 2650–2657.
- (410) Martin, C.; Sivonen, K.; Matern, U.; Dierstein, R.; Weckesser, J. Rapid purification of the peptide toxins microcystin-LR and nodularin. *FEMS Microbiol Lett* **1990**, *56*, 1–5.
- (411) Cerasino, L. Analysis of microcystins and nodularin by ultra high-performance liquid chromatography tandem mass spectrometry. In *Handbook of cyanobacterial monitoring and cyanotoxin analysis*; Meriluoto, J., Spoof, L., Codd, G. A., Eds.; Wiley: Chichester, West Sussex, 2017; pp 379–384.
- (412) Triantis, T. M.; Kaloudis, T.; Zervou, S.-K.; Hiskia, A. Determination of microcystins and nodularin in filtered and drinking water by LC-MS/MS. In *Handbook of cyanobacterial monitoring and cyanotoxin analysis*; Meriluoto, J., Spoof, L., Codd, G. A., Eds.; Wiley: Chichester, West Sussex, 2017; pp 372–378.
- (413) Dell'Aversano, C.; Eaglesham, G. K.; Quilliam, M. A. Analysis of cyanobacterial toxins by hydrophilic interaction liquid chromatography–mass spectrometry. *J Chromatogr A* **2004**, *1028*, 155–164.
- (414) Spoof, L.; Meriluoto, J. Rapid separation of microcystins and nodularin using a monolithic silica C18 column. *J Chromatogr A* **2002**, *947*, 237–245.

- (415) Gathercole, P. S.; Thiel, P. G. Liquid chromatographic determination of the cyanoginosins, toxins produced by the cyanobacterium *Microcystis aeruginosa*. *J Chromatogr A* **1987**, *408*, 435–440.
- (416) Galea, C.; Mangelings, D.; Vander Heyden, Y. Characterization and classification of stationary phases in HPLC and SFC—a review. *Anal Chim Acta* **2015**, *886*, 1–15.
- (417) Qiu, H.; Liang, X.; Sun, M.; Jiang, S. Development of silica-based stationary phases for high-performance liquid chromatography. *Anal Bioanal Chem* **2011**, *399*, 3307–3322.
- (418) Przybyciel, M. Novel phases for HPLC separations. *LC GC N Am* **2006**, *24*, 49–52.
- (419) Sadek, P. C.; Carr, P. W. Study of solute retention in reversed-phase high-performance liquid chromatography on hydrocarbonaceous and three fluorinated bonded phases. *J Chromatogr A* **1984**, *288*, 25–41.
- (420) Tanaka, N.; Tokuda, Y.; Iwaguchi, K.; Araki, M. Effect of stationary phase structure on retention and selectivity in reversed-phase liquid chromatography. *J Chromatogr A* **1982**, *239*, 761–772.
- (421) Blevins, D. D. The synthesis and characterization of bonded phase chromatographic adsorbents. Ph.D. dissertation, Univ. Arizona, Tucson, Arizona, 1982.
- (422) Haas, A.; Köhler, J.; Hemetsberger, H. Fluorinated ligands in HPLC. *Chromatographia* **1981**, *14*, 341–344.
- (423) Lochmüller, C. H.; Amoss, C. W. 3-(2,4,5,7-tetranitrofluorenimino)-propyldiethoxysiloxane—a highly selective, bonded  $\pi$ -complexing phase for high-pressure liquid chromatography. *J Chromatogr A* **1975**, *108*, 85–93.
- (424) Rücker, G.; Neugebauer, M.; Willems, G. G. *Instrumentelle pharmazeutische Analytik*, 5., überarb. Aufl.; Wissenschaftliche Verlagsgesellschaft: Stuttgart, 2013.
- (425) Namikoshi, M.; Yuan, M.; Sivonen, K.; Carmichael, W. W.; Rinehart, K. L.; Rouhiainen, L.; Sun, F.; Brittain, S.; Otsuki, A. Seven new microcystins possessing two L-glutamic acid units, isolated from *Anabaena* sp. strain 186. *Chem Res Toxicol* **1998**, *11*, 143–149.
- (426) Preeti, T.; Hariharan, G.; Rajarajeswari, G. R. Histopathological and biochemical effects of cyanobacterial cells containing microcystin-LR on Tilapia fish. *Water Environ J* **2016**, *30*, 135–142.
- (427) Wu, X.; Xiao, B.; Li, R.; Wang, Z.; Chen, X.; Chen, X. Rapid quantification of total microcystins in cyanobacterial samples by periodate-permanganate oxidation and reversed-phase liquid chromatography. *Anal Chim Acta* **2009**, *651*, 241–247.
- (428) Oliveira, A. C. P.; Magalhães, V. F.; Soares, R. M.; Azevedo, S. M. F. O. Influence of drinking water composition on quantitation and biological activity of dissolved microcystin (cyanotoxin). *Environ Toxicol* **2005**, *20*, 126–130.
- (429) Rapala, J.; Erkomaa, K.; Kukkonen, J.; Sivonen, K.; Lahti, K. Detection of microcystins with protein phosphatase inhibition assay, high-performance liquid chromatography–UV detection and enzyme-linked immunosorbent assay: comparison of methods. *Anal Chim Acta* **2002**, *466*, 213–231.
- (430) Fastner, J.; Codd, G. A.; Metcalf, J. S.; Woiitke, P.; Wiedner, C.; Utkilen, H. An international intercomparison exercise for the determination of purified microcystin-LR and microcystins in cyanobacterial field material. *Anal Bioanal Chem* **2002**, *374*, 437–444.
- (431) Robillot, C.; Vinh, J.; Puiseux-Dao, S.; Hennion, M.-C. Hepatotoxin production kinetics of the cyanobacterium *Microcystis aeruginosa* PCC 7820, as determined by HPLC–mass spectrometry and protein phosphatase bioassay. *Environ Sci Technol* **2000**, *34*, 3372–3378.
- (432) Wirsing, B.; Flury, T.; Wiedner, C.; Neumann, U.; Weckesser, J. Estimation of the microcystin content in cyanobacterial field samples from German lakes using the colorimetric protein–phosphatase inhibition assay and RP-HPLC. *Environ Toxicol* **1999**, *14*, 23–29.
- (433) Ward, C. J.; Beattie, K. A.; Lee, E. Y. C.; Codd, G. A. Colorimetric protein phosphatase inhibition assay of laboratory strains and natural blooms of cyanobacteria: comparisons with high-performance liquid chromatographic analysis for microcystins. *FEMS Microbiol Lett* **1997**, *153*, 465–473.

## 5. References

---

- (434) Lee, H. S.; Jeong, C. K.; Lee, H. M.; Choi, S. J.; Do, K. S.; Kim, K.; Kim, Y. H. On-line trace enrichment for the simultaneous determination of microcystins in aqueous samples using high-performance liquid chromatography with diode-array detection. *J Chromatogr A* **1999**, *848*, 179–184.
- (435) ISO 20179:2005. Water quality — Determination of microcystins — Method using solid phase extraction (SPE) and high performance liquid chromatography (HPLC) with ultraviolet (UV) detection
- (436) Harada, K.-I.; Ogawa, K.; Matsuura, K.; Nagai, H.; Murata, H.; Suzuki, M.; Itezono, Y.; Nakayama, N.; Shirai, M.; Nakano, M. Isolation of two toxic heptapeptide microcystins from an axenic strain of *Microcystis aeruginosa*, K-139. *Toxicon* **1991**, *29*, 479–489.
- (437) Harada, K.-I.; Matsuura, K.; Suzuki, M.; Watanabe, M. F.; Oishi, S.; Dahlem, A. M.; Beasley, V. R.; Carmichael, W. W. Isolation and characterization of the minor components associated with microcystins-LR and -RR in the cyanobacterium (blue-green algae). *Toxicon* **1990**, *28*, 55–64.
- (438) Hu, C.; Lee, J. A novel proof-of-concept sandwich immunoassay for screening microcystin in cyanobacteria based on michael addition reaction. *Anal Sci* **2019**, *35*, 107–111.
- (439) Weller, M. G.; Zeck, A.; Eikenberg, A.; Nagata, S.; Ueno, Y.; Niessner, R. Development of a direct competitive microcystin immunoassay of broad specificity. *Anal Sci* **2001**, *17*, 1445–1448.
- (440) Mehto, P.; Ankelo, M.; Hinkkanen, A.; Mikhailov, A.; Eriksson, J. E.; Spoo, L.; Meriluoto, J. A time-resolved fluoroimmunoassay for the detection of microcystins, cyanobacterial peptide hepatotoxins. *Toxicon* **2001**, *39*, 831–836.
- (441) Lebogang, L.; Jantra, J.; Hedström, M.; Mattiasson, B. Electrochemical flow-ELISA for rapid and sensitive determination of microcystin-LR using automated sequential injection system. *Sensors (Basel)* **2017**, *17*.
- (442) Zeck, A.; Weller, M. G.; Bursill, D.; Niessner, R. Generic microcystin immunoassay based on monoclonal antibodies against Adda. *Analyst* **2001**, *126*, 2002–2007.
- (443) Zeck, A.; Eikenberg, A.; Weller, M. G.; Niessner, R. Highly sensitive immunoassay based on a monoclonal antibody specific for [4-arginine]microcystins. *Anal Chim Acta* **2001**, *441*, 1–13.
- (444) Mikhailov, A.; Härmälä-Braskén, A.-S.; Meriluoto, J.; Sorokina, Y.; Dietrich, D.; Eriksson, J. E. Production and specificity of mono and polyclonal antibodies against microcystins conjugated through *N*-methyldehydroalanine. *Toxicon* **2001**, *39*, 477–483.
- (445) Metcalf, J. S.; Bell, S. G.; Codd, G. A. Production of novel polyclonal antibodies against the cyanobacterial toxin microcystin-LR and their application for the detection and quantification of microcystins and nodularin. *Water Res* **2000**, *34*, 2761–2769.
- (446) McElhiney, J.; Lawton, L. A.; Porter, A. J. R. Detection and quantification of microcystins (cyanobacterial hepatotoxins) with recombinant antibody fragments isolated from a naive human phage display library. *FEMS Microbiol Lett* **2000**, *193*, 83–88.
- (447) Nagata, S.; Tsutsumi, T.; Yoshida, F.; Ueno, Y. A new type sandwich immunoassay for microcystin: production of monoclonal antibodies specific to the immune complex formed by microcystin and an anti-microcystin monoclonal antibody. *Nat Toxins* **1999**, *7*, 49–55.
- (448) Tsutsumi, T.; Nagata, S.; Yoshida, F.; Ueno, Y. Anti-idiotypic monoclonal antibodies against anti-microcystin antibody and their use in enzyme immunoassay. *Toxicon* **1998**, *36*, 235–245.
- (449) Nagata, S.; Tsutsumi, T.; Hasegawa, A.; Yoshida, F.; Ueno, Y.; Watanabe, M. F. Enzyme immunoassay for direct determination of microcystins in environmental water. *J AOAC Int* **1997**, *80*, 408–417.
- (450) McDermott, C.M.; Feola, R.; Plude, J. Detection of cyanobacterial toxins (microcystins) in waters of northeastern Wisconsin by a new immunoassay technique. *Toxicon* **1995**, *33*, 1433–1442.



- (451) Chu, F. S.; Huang, X.; Wei, R. D. Enzyme-linked immunosorbent assay for microcystins in blue-green algal blooms. *J Assoc Off Anal Chem* **1990**, *73*, 451–456.
- (452) Brooks, W. P.; Codd, G. A. Immunoassay of hepatotoxic cultures and water blooms of cyanobacteria using *Microcystis aeruginosa* peptide toxin polyclonal antibodies. *Environ Technol* **1988**, *9*, 1343–1348.
- (453) Heresztyn, T.; Nicholson, B. C. Determination of cyanobacterial hepatotoxins directly in water using a protein phosphatase inhibition assay. *Water Res* **2001**, *35*, 3049–3056.
- (454) Wong, B. S. F.; Lam, P. K. S.; Xu, L.; Zhang, Y.; Richardson, B. J. A colorimetric assay for screening microcystin class compounds in aquatic systems. *Chemosphere* **1999**, *38*, 1113–1122.
- (455) Fontal, O. I.; Vieytes M. R.; Baptista de Sousa J. M. V.; Louzao M. C.; Botana L. M. A fluorescent microplate assay for microcystin-LR. *Anal Biochem* **1999**, *269*, 289–296.
- (456) Lambert, T. W.; Boland, M. P.; Holmes, C. F. B.; Hrudey, S. E. Quantitation of the microcystin hepatotoxins in water at environmentally relevant concentrations with the protein phosphatase bioassay. *Environ Sci Technol* **1994**, *28*, 753–755.
- (457) Zeck, A.; Weller, M. G.; Niessner, R. Multidimensional biochemical detection of microcystins in liquid chromatography. *Anal Chem* **2001**, *73*, 5509–5517.
- (458) Holmes, C. F. B. Liquid chromatography-linked protein phosphatase bioassay; a highly sensitive marine bioscreen for okadaic acid and related diarrhetic shellfish toxins. *Toxicon* **1991**, *29*, 469–477.
- (459) Attard, T. J.; Carter, M. D.; Fang, M.; Johnson, R. C.; Reid, G. E. Structural characterization and absolute quantification of microcystin peptides using collision-induced and ultraviolet photo-dissociation tandem mass spectrometry. *J Am Soc Mass Spectrom* **2018**, *29*, 1812–1825.
- (460) Karlsson, K. M.; Spooft, L. E. M.; Meriluoto, J. A. O. Quantitative LC–ESI–MS analyses of microcystins and nodularin-R in animal tissue—matrix effects and method validation. *Environ Toxicol* **2005**, *20*, 381–389.
- (461) Bateman, K. P.; Thibault, P.; Douglas, D. J.; White, R. L. Mass spectral analyses of microcystins from toxic cyanobacteria using on-line chromatographic and electrophoretic separations. *J Chromatogr A* **1995**, *712*, 253–268.
- (462) Kohoutek, J.; Procházková, T.; Adamovský, O.; Palíková, M.; Hilscherová, K. Stable-isotope dilution LC-MS/MS method for quantitative determination of microcystin conjugates with cysteine and glutathione in biotic matrices. *Anal Bioanal Chem* **2019**, *411*, 5267–5275.
- (463) Fayad, P. B.; Roy-Lachapelle, A.; Duy, S. V.; Prévost, M.; Sauvé, S. On-line solid-phase extraction coupled to liquid chromatography tandem mass spectrometry for the analysis of cyanotoxins in algal blooms. *Toxicon* **2015**, *108*, 167–175.
- (464) Roegner, A. F.; Schirmer, M. P.; Puschner, B.; Brena, B.; Gonzalez-Sapienza, G. Rapid quantitative analysis of microcystins in raw surface waters with MALDI MS utilizing easily synthesized internal standards. *Toxicon* **2014**, *78*, 94–102.
- (465) Puddick, J.; Prinsep, M. R.; Wood, S. A.; Cary, S. C.; Hamilton, D. P. Enhanced sample preparation for quantitation of microcystins by matrix-assisted laser desorption/ionisation-time of flight mass spectrometry. *Phytochem Anal* **2012**, *23*, 285–291.
- (466) Oehrle, S. A.; Southwell, B.; Westrick, J. Detection of various freshwater cyanobacterial toxins using ultra-performance liquid-chromatography tandem-mass spectrometry. *Toxicon* **2010**, *55*, 965–972.
- (467) Xu, W.; Chen, Q.; Zhang, T.; Cai, Z.; Jia, X.; Xie, Q.; Ren, Y. Development and application of ultra performance liquid chromatography-electrospray ionization tandem triple quadrupole mass spectrometry for determination of seven microcystins in water samples. *Anal Chim Acta* **2008**, *626*, 28–36.
- (468) Howard, K. L.; Boyer, G. L. Quantitative analysis of cyanobacterial toxins by matrix-assisted laser desorption ionization mass spectrometry. *Anal Chem* **2007**, *79*, 5980–5986.

## 5. References

---

- (469) Barco, M.; Flores, C.; Rivera, J.; Caixach, J. Determination of microcystin variants and related peptides present in a water bloom of *Planktothrix (Oscillatoria) rubescens* in a Spanish drinking water reservoir by LC/ESI–MS. *Toxicol* **2004**, *44*, 881–886.
- (470) Bungert, D.; Heinzle, E.; Tholey, A. Quantitative matrix-assisted laser desorption/ionization mass spectrometry for the determination of enzyme activities. *Anal Biochem* **2004**, *326*, 167–175.
- (471) Bucknall, M.; Fung, K. Y. C.; Duncan, M. W. Practical quantitative biomedical applications of MALDI–TOF mass spectrometry. *J Am Soc Mass Spectrom* **2002**, *13*, 1015–1027.
- (472) Horak, J.; Werther, W.; Schmid, E. R. Optimisation of the quantitative determination of chlormequat by matrix-assisted laser desorption/ionisation mass spectrometry. *Rapid Commun Mass Spectrom* **2001**, *15*, 241–248.
- (473) Wharton, R. E.; Ojeda-Torres, G.; Cunningham, B.; Feyereisen, M. C.; Hill, K. L.; Abbott, N. L.; Seymour, C.; Hill, D.; Lang, J.; Hamelin, E. I.; *et al.* Quantification of microcystin-LR in human urine by immunocapture liquid chromatography tandem mass spectrometry. *Chem Res Toxicol* **2018**, *31*, 898–903.
- (474) Mourey, T. H.; Oppenheimer, L. E. Principles of operation of an evaporative light-scattering detector for liquid chromatography. *Anal Chem* **1984**, *56*, 2427–2434.
- (475) Leulmi, N.; Sighel, D.; Defant, A.; Khenaka, K.; Boulahrouf, A.; Mancini, I. Enhanced production and quantitative evaluation of nigericin from the Algerian soil-living *Streptomyces yousseoufiensis* SF10 strain. *Fermentation* **2019**, *5*, 13.
- (476) Zhang, H.-Q.; Liu, P.; Duan, J.-A.; Dong, L.; Shang, E.-X.; Qian, D.-W.; Zhu, Z.-H.; Li, H.-W.; Li, W.-W. Comparative analysis of carbohydrates, nucleosides and amino acids in different parts of *Trichosanthes kirilowii* Maxim by (ultra) high-performance liquid chromatography coupled with tandem-mass spectrometry and evaporative light scattering detector Methods. *Molecules* **2019**, *24*.
- (477) Sut, S.; Franceschi, C.; Peron, G.; Poloniato, G.; Dall'Acqua, S. Development and validation of an HPLC–ELSD method for the quantification of 1-triacontanol in solid and liquid samples. *Molecules* **2018**, *23*.
- (478) Lin, C.-Z.; Zhang, R.-J.; Yao, Y.-F.; Huang, X.-D.; Zheng, R.-B.; Wu, B.-J.; Zhu, C.-C. Qualitative and quantitative analysis of the major constituents in WLJ herbal tea using multiple chromatographic techniques. *Molecules* **2018**, *23*.
- (479) Shao, J.; Cao, W.; Qu, H.; Pan, J.; Gong, X. A novel quality by design approach for developing an HPLC method to analyze herbal extracts: a case study of sugar content analysis. *PLoS ONE* **2018**, *13*, e0198515.
- (480) Huang, D.; Zhao, X.; Liu, X.; Chao, R. Determination of five aminoalcohol-diterpenoid alkaloids in the lateral root of *Aconitum carmichaeli* by HPLC–ELSD with SPE. *J Chromatogr Sci* **2017**, *55*, 940–945.
- (481) Remeur, C.; Le Borgne, E.; Gauthier, L.; Grougnet, R.; Deguin, B.; Poullain, C.; Litaudon, M. HPLC–ELSD quantification and centrifugal partition chromatography isolation of 8-O-acetylharpagide from *Oxera coronata* (Lamiaceae). *Phytochem Anal* **2017**, *28*, 242–246.
- (482) Sastre, F.; Ferreira, F.; Pedreschi, F. MALDI–TOF mass spectrometry and reversed-phase HPLC–ELSD chromatography for structural and quantitative studies of major steroid saponins in commercial extracts of *Yucca schidigera* Roetzl. *J Pharm Biomed Anal* **2016**, *120*, 270–282.
- (483) Lee, G. J.; Shin, B.-K.; Yu, Y.-H.; Ahn, J.; Kwon, S. W.; Park, J. H. Systematic development of a group quantification method using evaporative light scattering detector for relative quantification of ginsenosides in ginseng products. *J Pharm Biomed Anal* **2016**, *128*, 158–165.
- (484) Magnusson, L. E.; Risle, D. S.; Koropchak, J. A. Aerosol-based detectors for liquid chromatography. *J Chromatogr A* **2015**, *1421*, 68–81.
- (485) Heron, S.; Maloumbi, M. G.; Dreux, M.; Verette, E.; Tchaplal, A. Method development for a quantitative analysis performed without any standard using an evaporative light-scattering detector. *J Chromatogr A* **2007**, *1161*, 152–156.

- (486) Adnani, N.; Michel, C. R.; Bugni, T. S. Universal quantification of structurally diverse natural products using an evaporative light-scattering detector. *J Nat Prod* **2012**, *75*, 802–806.
- (487) de Villiers, A.; Górecki, T.; Lynen, F.; Szucs, R.; Sandra, P. Improving the universal response of evaporative light-scattering detection by mobile phase compensation. *J Chromatogr A* **2007**, *1161*, 183–191.
- (488) Mathews, B. T.; Higginson, P. D.; Lyons, R.; Mitchell, J. C.; Sach, N. W.; Snowden, M. J.; Taylor, M. R.; Wright, A. G. Improving quantitative measurements for the evaporative light-scattering detector. *Chromatographia* **2004**, *60*, 625–633.
- (489) Gritti, F.; Guiochon, G. Comparative study of the performance of columns packed with several new fine silica particles. Would the external roughness of the particles affect column properties? *J Chromatogr A* **2007**, *1166*, 30–46.
- (490) Fekete, S.; Fekete, J.; Ganzler, K. Shell and small particles; evaluation of new column technology. *J Pharm Biomed Anal* **2009**, *49*, 64–71.
- (491) Horvath, C.; Lipsky, S. R. Column design in high pressure liquid chromatography. *J Chromatogr Sci* **1969**, *7*, 109–116.
- (492) Aruda, W. O.; Walfish, S.; Krull, I. S. Review and optimization of linearity and precision in quantitative HPLC-ELSD with chemometrics. *LC GC N Am* **2008**, *26*, 1032,1034-1040,1042.
- (493) Young, C. S.; Dolan, J. W. Success with evaporative light-scattering detection. Part 2. Tips and techniques. *LC GC N Am* **2004**, *22*, 244,246-250.
- (494) Young, C. S.; Dolan, J. W. Success with evaporative light-scattering detection. *LC GC N Am* **2003**, *21*, 120, 122, 126, 128.
- (495) Bliesner, D. M. *Validating chromatographic methods: a practical guide*; John Wiley & Sons, Inc: Hoboken, NJ, 2006.
- (496) Himmelsbach, M. 10 years of MS instrumental developments—Impact on LC–MS/MS in clinical chemistry. *J Chromatogr B* **2012**, *883-884*, 3–17.
- (497) Jennings, K. R. MS/MS instrumentation. *Proc Phytochem Soc Eur* **1996**, *40*, 25–43.
- (498) Boyd, R. K. Linked-scan techniques for MS/MS using tandem-in-space instruments. *Mass Spec Rev* **1994**, *13*, 359–410.
- (499) Burlingame, A. L.; Baillie, T. A.; Russell, D. H. Mass spectrometry. *Anal Chem* **1992**, *64*, 467R-502R.
- (500) Roepstorff, P.; Fohlman, J. Proposal for a common nomenclature for sequence ions in mass spectra of peptides. *Biomed Mass Spectrom* **1984**, *11*, 601.
- (501) Johnson, R. S.; Martin, S. A.; Biemann, K.; Stults, J. T.; Watson, J. T. Novel fragmentation process of peptides by collision-induced decomposition in a tandem mass spectrometer: differentiation of leucine and isoleucine. *Anal Chem* **1987**, *59*, 2621–2625.
- (502) Medzihradszky, K. F.; Chalkley, R. J. Lessons in *de novo* peptide sequencing by tandem mass spectrometry. *Mass Spec Rev* **2015**, *34*, 43–63.
- (503) Mohimani, H.; Yang, Y.-L.; Liu, W.-T.; Hsieh, P.-W.; Dorrestein, P. C.; Pevzner, P. A. Sequencing cyclic peptides by multistage mass spectrometry. *Proteomics* **2011**, *11*, 3642–3650.
- (504) Seidler, J.; Zinn, N.; Boehm, M. E.; Lehmann, W. D. *De novo* sequencing of peptides by MS/MS. *Proteomics* **2010**, *10*, 634–649.
- (505) Semmler, A.; Weber, R.; Przybylski, M.; Wittmann, V. *De novo* sequencing of peptides on single resin beads by MALDI-FTICR tandem mass spectrometry. *J Am Soc Mass Spectrom* **2010**, *21*, 215–219.
- (506) Eckart, K. Mass spectrometry of cyclic peptides. *Mass Spec Rev* **1994**, *13*, 23–55.
- (507) Vyatkina, K.; Dekker, L. J. M.; Wu, S.; VanDuijn, M. M.; Liu, X.; Tolić, N.; Luider, T. M.; Paša-Tolić, L. *De novo* sequencing of peptides from high-resolution bottom-up tandem-mass spectra using top-down intended Mmethods. *Proteomics* **2017**, *17*.

## 5. References

---

- (508) Yang, H.; Chi, H.; Zhou, W.-J.; Zeng, W.-F.; He, K.; Liu, C.; Sun, R.-X.; He, S.-M. OpenpNovo: *De novo* peptide sequencing with thousands of protein modifications. *J Proteome Res* **2017**, *16*, 645–654.
- (509) Novák, J.; Lemr, K.; Schug, K. A.; Havlíček, V. CycloBranch: *de novo* sequencing of nonribosomal peptides from accurate product ion mass spectra. *J Am Soc Mass Spectrom* **2015**, *26*, 1780–1786.
- (510) Yan, Y.; Kusalik, A.; Wu, F.-X. Recent developments in computational methods for *de novo* peptide sequencing from tandem-mass spectrometry (MS/MS). *Protein Pept Lett* **2015**, *22*, 983–991.
- (511) Hubbard, S. J. Computational approaches to peptide identification via tandem MS. *Methods Mol Biol* **2010**, *604*, 23–42.
- (512) Bertsch, A.; Leinenbach, A.; Pervukhin, A.; Lubeck, M.; Hartmer, R.; Baessmann, C.; Elnakady, Y. A.; Müller, R.; Böcker, S.; Huber, C. G.; *et al.* *De novo* peptide sequencing by tandem-MS using complementary CID and electron transfer dissociation. *Electrophoresis* **2009**, *30*, 3736–3747.
- (513) Liu, W.-T.; Ng, J.; Meluzzi, D.; Bandeira, N.; Gutierrez, M.; Simmons, T. L.; Schultz, A. W.; Lington, R. G.; Moore, B. S.; Gerwick, W. H.; *et al.* Interpretation of tandem-mass spectra obtained from cyclic nonribosomal peptides. *Anal Chem* **2009**, *81*, 4200–4209.
- (514) Ng, J.; Bandeira, N.; Liu, W.-T.; Ghassemian, M.; Simmons, T. L.; Gerwick, W. H.; Lington, R.; Dorrestein, P. C.; Pevzner, P. A. Dereplication and *de novo* sequencing of nonribosomal peptides. *Nat Methods* **2009**, *6*, 596 EP -.
- (515) Fischer, B.; Roth, V.; Roos, F.; Grossmann, J.; Baginsky, S.; Widmayer, P.; Gruissem, W.; Buhmann, J. M. NovoHMM: a hidden Markov model for *de novo* peptide sequencing. *Anal Chem* **2005**, *77*, 7265–7273.
- (516) Bogialli, S.; Bortolini, C.; Di Gangi, I. M.; Di Gregorio, F. N.; Lucentini, L.; Favaro, G.; Pastore, P. Liquid chromatography-high resolution mass spectrometric methods for the surveillance monitoring of cyanotoxins in freshwaters. *Talanta* **2017**, *170*, 322–330.
- (517) Yuan, M.; Namikoshi, M.; Otsuki, A.; Rinehart, K. L.; Sivonen, K.; Watanabe, M. F. Low-energy collisionally activated decomposition and structural characterization of cyclic heptapeptide microcystins by electrospray ionization mass spectrometry. *J Mass Spectrom* **1999**, *34*, 33–43.
- (518) Kubwabo, C.; Vais, N.; Benoit, F. M. Characterization of microcystins using in-source collision-induced dissociation. *Rapid Commun Mass Spectrom* **2005**, *19*, 597–604.
- (519) Mayumi, T.; Kato, H.; Imanishi, S.; Kawasaki, Y.; Hasegawa, M.; Harada, K.-I. Structural characterization of microcystins by LC/MS/MS under ion trap conditions. *J Antibiot* **2006**, *59*, 710–719.
- (520) Woolbright, B. L.; Williams, C. D.; Ni, H.; Kumer, S. C.; Schmitt, T.; Kane, B.; Jaeschke, H. Microcystin-LR induced liver injury in mice and in primary human hepatocytes is caused by oncotic necrosis. *Toxicol* **2017**, *125*, 99–109.
- (521) Shimizu, K.; Sano, T.; Kubota, R.; Kobayashi, N.; Tahara, M.; Obama, T.; Sugimoto, N.; Nishimura, T.; Ikarashi, Y. Effects of the amino acid constituents of microcystin variants on cytotoxicity to primary cultured rat hepatocytes. *Toxins* **2013**, *6*, 168–179.
- (522) Ufelmann, H.; Krüger, T.; Luckas, B.; Schrenk, D. Human and rat hepatocyte toxicity and protein phosphatase 1 and 2A inhibitory activity of naturally occurring desmethyl-microcystins and nodularins. *Toxicology* **2012**, *293*, 59–67.
- (523) Herfindal, L.; Myhren, L.; Kleppe, R.; Krakstad, C.; Selheim, F.; Jokela, J.; Sivonen, K.; Døskeland, S. O. Nostocyclopeptide-M1: a potent, nontoxic inhibitor of the hepatocyte drug transporters OATP1B3 and OATP1B1. *Mol Pharm* **2011**, *8*, 360–367.
- (524) Fischer, A.; Hoeger, S. J.; Stemmer, K.; Feurstein, D. J.; Knobloch, D.; Nussler, A.; Dietrich, D. R. The role of organic anion transporting polypeptides (OATPs/SLCOs) in the toxicity of different microcystin congeners *in vitro*: a comparison of primary human hepatocytes and OATP-transfected HEK293 cells. *Toxicol Appl Pharmacol* **2010**, *245*, 9–20.

- (525) Boaru, D. A.; Dragoş, N.; Schirmer, K. Microcystin-LR induced cellular effects in mammalian and fish primary hepatocyte cultures and cell lines: a comparative study. *Toxicology* **2006**, *218*, 134–148.
- (526) Batista, T.; de Sousa, G.; Suput, J. S.; Rahmani, R.; Šuput, D. Microcystin-LR causes the collapse of actin filaments in primary human hepatocytes. *Aquat Toxicol* **2003**, *65*, 85–91.
- (527) McDermott, C. M.; Nho, C. W.; Howard, W.; Holton, B. The cyanobacterial toxin, microcystin-LR, can induce apoptosis in a variety of cell types. *Toxicon* **1998**, *36*, 1981–1996.
- (528) Battle, T.; Touchard, C.; Moulds, H. J.; Dowsett, B.; Stacey, G. N. New cell substrates for *in vitro* evaluation of microcystin hepato-cytotoxicity. *Toxicol In Vitro* **1997**, *11*, 557–567.
- (529) Seithel, A.; Eberl, S.; Singer, K.; Auge, D.; Heinkele, G.; Wolf, N. B.; Dörje, F.; Fromm, M. F.; König, J. The influence of macrolide antibiotics on the uptake of organic anions and drugs mediated by OATP1B1 and OATP1B3. *Drug Metab Dispos* **2007**, *35*, 779–786.
- (530) Ikehara, T.; Nakashima, J.; Nakashima, S.; Yasumoto, T. Different responses of primary normal human hepatocytes and human hepatoma cells toward cyanobacterial hepatotoxin microcystin-LR. *Toxicon* **2015**, *105*, 4–9.
- (531) Lancaster, C. S.; Sprowl, J. A.; Walker, A. L.; Hu, S.; Gibson, A. A.; Sparreboom, A. Modulation of OATP1B-type transporter function alters cellular uptake and disposition of platinum chemotherapeutics. *Mol Cancer Ther* **2013**, *12*, 1537–1544.
- (532) Picard, N.; Levoir, L.; Lamoureux, F.; Yee, S. W.; Giacomini, K. M.; Marquet, P. Interaction of sirolimus and everolimus with hepatic and intestinal organic anion-transporting polypeptide transporters. *Xenobiotica* **2011**, *41*, 752–757.
- (533) Hirano, M.; Maeda, K.; Shitara, Y.; Sugiyama, Y. Contribution of OATP2 (OATP1B1) and OATP8 (OATP1B3) to the hepatic uptake of pitavastatin in humans. *J Pharmacol Exp Ther* **2004**, *311*, 139–146.
- (534) Niedermeyer, T. H. J. Microcystin congeners described in the literature. <http://dx.doi.org/10.6084/m9.figshare.880756> (accessed on March 28, 2020).
- (535) Spoo, L.; Catherine, A. Appendix 3: tables of microcystins and nodularins. In *Handbook of cyanobacterial monitoring and cyanotoxin analysis*; Meriluoto, J., Spoo, L., Codd, G. A., Eds.; Wiley: Chichester, West Sussex, 2017; pp 526–537.
- (536) Sletten, E. M.; Bertozzi, C. R. Bioorthogonal chemistry: fishing for selectivity in a sea of functionality. *Angew Chem Int Ed Engl* **2009**, *48*, 6974–6998.
- (537) Halila, S.; Velasco, T.; Clercq, P. D.; Madder, A. Fine-tuning furan toxicity: fast and quantitative DNA interchain cross-link formation upon selective oxidation of a furan containing oligonucleotide. *Chem Commun* **2005**, 936–938.
- (538) Stevens, K.; Madder, A. Furan-modified oligonucleotides for fast, high-yielding and site-selective DNA inter-strand cross-linking with non-modified complements. *Nucleic Acids Res* **2009**, *37*, 1555–1565.
- (539) Deceuninck, A.; Madder, A. From DNA cross-linking to peptide labeling: on the versatility of the furan-oxidation-conjugation strategy. *Chem Commun* **2009**, 340–342.
- (540) Hoogewijs, K.; Buyst, D.; Winne, J. M.; Martins, J. C.; Madder, A. Exploiting furan's versatile reactivity in reversible and irreversible orthogonal peptide labeling. *Chem Commun* **2013**, *49*, 2927–2929.
- (541) Carrette, L. L. G.; Gyssels, E.; de Laet, N.; Madder, A. Furan oxidation based cross-linking: a new approach for the study and targeting of nucleic acid and protein interactions. *Chem Commun* **2016**, *52*, 1539–1554.
- (542) Anderson, G. W.; Zimmerman, J. E.; Callahan, F. M. *N*-Hydroxysuccinimide esters in peptide synthesis. *J Am Chem Soc* **1963**, *85*, 3039.
- (543) Anderson, G. W.; Zimmerman, J. E.; Callahan, F. M. The use of esters of *N*-hydroxysuccinimide in peptide synthesis. *J Am Chem Soc* **1964**, *86*, 1839–1842.

## 5. References

---

- (544) Lomant, A. J.; Fairbanks, G. Chemical probes of extended biological structures: synthesis and properties of the cleavable protein cross-linking reagent [<sup>35</sup>S]dithiobis(succinimidyl propionate). *J Mol Biol* **1976**, *104*, 243–261.
- (545) Trester-Zedlitz, M.; Kamada, K.; Burley, S. K.; Fenyö, D.; Chait, B. T.; Muir, T. W. A modular cross-linking approach for exploring protein interactions. *J Am Chem Soc* **2003**, *125*, 2416–2425.
- (546) Ross, P. L.; Huang, Y. N.; Marchese, J. N.; Williamson, B.; Parker, K.; Hattan, S.; Khainovski, N.; Pillai, S.; Dey, S.; Daniels, S.; *et al.* Multiplexed protein quantitation in *Saccharomyces cerevisiae* using amine-reactive isobaric tagging reagents. *Mol Cell Proteomics* **2004**, *3*, 1154–1169.
- (547) Aggarwal, K.; Choe, L. H.; Lee, K. H. Shotgun proteomics using the iTRAQ isobaric tags. *Briefings Funct Genomics Proteomics* **2006**, *5*, 112–120.
- (548) Wiese, S.; Reidegeld, K. A.; Meyer, H. E.; Warscheid, B. Protein labeling by iTRAQ: a new tool for quantitative mass spectrometry in proteome research. *Proteomics* **2007**, *7*, 340–350.
- (549) Evans, C.; Noirel, J.; Ow, S. Y.; Salim, M.; Pereira-Medrano, A. G.; Couto, N.; Pandhal, J.; Smith, D.; Pham, T. K.; Karunakaran, E.; *et al.* An insight into iTRAQ: where do we stand now? *Anal Bioanal Chem* **2012**, *404*, 1011–1027.
- (550) Ward, C. C.; Kleinman, J. I.; Nomura, D. K. NHS-esters as versatile reactivity-based probes for mapping proteome-wide ligandable hotspots. *ACS Chem Biol* **2017**, *12*, 1478–1483.
- (551) Kuenzi, H.; Manneberg, M.; Studer, R. O. Ammonolysis of nitroarginine and nitroarginine-containing peptides. Side reactions. *Helv Chim Acta* **1974**, *57*, 566–572.
- (552) Miles, C. O.; Sandvik, M.; Haande, S.; Nonga, H.; Ballot, A. LC–MS analysis with thiol derivatization to differentiate Dhb(7)- from Mdha(7)-microcystins: analysis of cyanobacterial blooms, *Planktothrix* cultures and European crayfish from Lake Steinsfjorden, Norway. *Environ Sci Technol* **2013**, *47*, 4080–4087.
- (553) Wei, N.; Hu, L.; Song, L.; Gan, N. Microcystin-bound protein patterns in different cultures of *Microcystis aeruginosa* and field samples. *Toxins* **2016**, *8*.
- (554) Mallia, V.; Uhlig, S.; Rafuse, C.; Meija, J.; Miles, C. O. Novel microcystins from *Planktothrix prolifica* NIVA-CYA 544 identified by LC–MS/MS, functional group derivatization and <sup>15</sup>N-labeling. *Mar Drugs* **2019**, *17*, 643.
- (555) Shreder, K. R.; Liu, Y.; Nomanhboy, T.; Fuller, S. R.; Wong, M. S.; Gai, W. Z.; Wu, J.; Leventhal, P. S.; Lill, J. R.; Corral, S. Design and synthesis of AX7574: a microcystin-derived, fluorescent probe for serine/threonine phosphatases. *Bioconjug Chem* **2004**, *15*, 790–798.
- (556) Grundler, V.; Faltermann, S.; Fent, K.; Gademann, K. Preparation of fluorescent microcystin derivatives by direct arginine labelling and their biological evaluation. *Chembiochem* **2015**, *16*, 1657–1662.
- (557) Schiffter, H. A. *Pharmakokinetik: Modelle und Berechnungen ; mit 25 Tabellen und 323 mathematischen Formeln*, 2. unveränderte Auflage; Wiss. Verl.-Ges: Stuttgart, 2015.
- (558) Meissner, S.; Fastner, J.; Dittmann, E. Microcystin production revisited: conjugate formation makes a major contribution. *Environ Microbiol* **2013**, *15*, 1810–1820.
- (559) Shih, P. M.; Wu, D.; Latifi, A.; Axen, S. D.; Fewer, D. P.; Talla, E.; Calteau, A.; Cai, F.; Tandeau de Marsac, N.; Rippka, R.; *et al.* Improving the coverage of the cyanobacterial phylum using diversity-driven genome sequencing. *PNAS* **2013**, *110*, 1053–1058.
- (560) Calteau, A.; Fewer, D. P.; Latifi, A.; Coursin, T.; Laurent, T.; Jokela, J.; Kerfeld, C. A.; Sivonen, K.; Piel, J.; Gugger, M. Phylum-wide comparative genomics unravel the diversity of secondary metabolism in cyanobacteria. *BMC Genomics* **2014**, *15*, 977.
- (561) Frangeul, L.; Quillardet, P.; Castets, A.-M.; Humbert, J.-F.; Matthijs, H. C. P.; Cortez, D.; Tolonen, A.; Zhang, C.-C.; Gribaldo, S.; Kehr, J.-C.; *et al.* Highly plastic genome of *Microcystis aeruginosa* PCC 7806, a ubiquitous toxic freshwater cyanobacterium. *BMC Genomics* **2008**, *9*, 274.

- (562) Martin, C.; Oberer, L.; Ino, T.; König, W. A.; Busch, M.; Weckesser, J. Cyanopeptolins, new depsipeptides from the cyanobacterium *Microcystis* sp. PCC 7806. *J Antibiot* **1993**, *46*, 1550–1556.
- (566) Bister, B.; Keller, S.; Baumann, H. I.; Nicholson, G.; Weist, S.; Jung, G.; Süssmuth, R. D.; Jüttner, F. Cyanopeptolin 963A, a chymotrypsin inhibitor of *Microcystis* PCC 7806. *J Nat Prod* **2004**, *67*, 1755–1757.
- (564) Ishida, K.; Welker, M.; Christiansen, G.; Cadel-Six, S.; Bouchier, C.; Dittmann, E.; Hertweck, C.; Tandeau de Marsac, N. Plasticity and evolution of aeruginosin biosynthesis in cyanobacteria. *Appl Environ Microbiol* **2009**, *75*, 2017–2026.
- (565) Hong, V.; Presolski, S. I.; Ma, C.; Finn, M. G. Analysis and optimization of copper-catalyzed azide-alkyne cycloaddition for bioconjugation. *Angew Chem Int Ed Engl* **2009**, *48*, 9879–9883.
- (566) Yang, L.; Chumsae, C.; Kaplan, J. B.; Moulton, K. R.; Wang, D.; Lee, D. H.; Zhou, Z. S. Detection of alkynes via click chemistry with a brominated coumarin azide by simultaneous fluorescence and isotopic signatures in mass spectrometry. *Bioconjug Chem* **2017**, *28*, 2302–2309.
- (567) Moss, N. A.; Seiler, G.; Leão, T. F.; Castro-Falcón, G.; Gerwick, L.; Hughes, C. C.; Gerwick, W. H. Nature's combinatorial biosynthesis produces vatiamides A-F. *Angew Chem Int Ed Engl* **2019**, *58*, 9027–9031.
- (568) Bittersmann, E.; Vermaas, W. Fluorescence lifetime studies of cyanobacterial photosystem II mutants. *Biochim Biophys Acta Bioenerg* **1991**, *1098*, 105–116.
- (569) Vermaas, W. F. J.; Timlin, J. A.; Jones, H. D. T.; Sinclair, M. B.; Nieman, L. T.; Hamad, S. W.; Melgaard, D. K.; Haaland, D. M. *In vivo* hyperspectral confocal fluorescence imaging to determine pigment localization and distribution in cyanobacterial cells. *PNAS* **2008**, *105*, 4050–4055.
- (570) Chai, Q.-Y.; Yang, Z.; Lin, H.-W.; Han, B.-N. Alkynyl-containing peptides of marine origin: a review. *Mar Drugs* **2016**, *14*.
- (571) Schröder, T.; Gartner, M.; Grab, T.; Bräse, S. A new azide staining reagent based on "click chemistry". *Org Biomol Chem* **2007**, *5*, 2767–2769.
- (572) Bouvet, V.; Wuest, M.; Wuest, F. Copper-free click chemistry with the short-lived positron emitter fluorine-18. *Org Biomol Chem* **2011**, *9*, 7393–7399.
- (573) García-Rojas, N. S.; Moreno-Pedraza, A.; Rosas-Román, I.; Ramírez-Chávez, E.; Molina-Torres, J.; Winkler, R. Mass spectrometry imaging of thin-layer chromatography plates using laser desorption/low-temperature plasma ionisation. *Analyst* **2020**, *145*, 3885–3891.
- (574) León, A.; Cariou, R.; Hutinet, S.; Hurel, J.; Guitton, Y.; Tixier, C.; Munsch, C.; Antignac, J.-P.; Dervilly-Pinel, G.; Le Bizec, B. HaloSeeker 1.0: a user-friendly software to highlight halogenated chemicals in nontargeted high-resolution mass spectrometry data sets. *Anal Chem* **2019**, *91*, 3500–3507.
- (575) Kurmayer, R.; Entfellner, E.; Weisse, T.; Offterdinger, M.; Rentmeister, A.; Deng, L. Chemically labeled toxins or bioactive peptides show a heterogeneous intracellular distribution and low spatial overlap with autofluorescence in bloom-forming cyanobacteria. *Sci Rep* **2020**, *10*, 2781.
- (576) Vila, A.; Tallman, K. A.; Jacobs, A. T.; Liebler, D. C.; Porter, N. A.; Marnett, L. J. Identification of protein targets of 4-hydroxynonenal using click chemistry for *ex vivo* biotinylation of azido and alkynyl derivatives. *Chem Res Toxicol* **2008**, *21*, 432–444.
- (577) Parker, C. G.; Pratt, M. R. Click chemistry in proteomic investigations. *Cell* **2020**, *180*, 605–632.
- (578) Foss, A. J.; Miles, C. O.; Samdal, I. A.; Løvberg, K. E.; Wilkins, A. L.; Rise, F.; Jaabæk, J. A. H.; McGowan, P. C.; Aabel, M. T. Analysis of free and metabolized microcystins in samples following a bird mortality event. *Harmful Algae* **2018**, *80*, 117–129.
- (579) Harada, K.-I.; Tsuji, K.; Watanabe, M. F.; Kondo, F. Stability of microcystins from cyanobacteria—III. Effect of pH and temperature. *Phycologia* **1996**, *35*, 83–88.
- (580) Scifinder search for citing references, accessed on May 27, 2020.

## 5. References

---

- (581) Faltermann, S.; Prétôt, R.; Pernthaler, J.; Fent, K. Comparative effects of nodularin and microcystin-LR in zebrafish: 1. Uptake by organic anion transporting polypeptide Oatp1d1 (*Slco1d1*). *Aquat Toxicol* **2016**, *171*, 69–76.
- (582) Jouan, E.; Le Vée, M.; Denizot, C.; Parmentier, Y.; Fardel, O. Drug transporter expression and activity in human hepatoma HuH-7 cells. *Pharmaceutics* **2017**, *9*, 3.
- (583) Monks, N. R.; Liu, S.; Xu, Y.; Yu, H.; Bendelow, A. S.; Moscow, J. A. Potent cytotoxicity of the phosphatase inhibitor microcystin LR and microcystin analogues in OATP1B1- and OATP1B3-expressing HeLa cells. *Mol Cancer Ther* **2007**, *6*, 587–598.
- (584) Niedermeyer, T.H.J., Enke, H., Kramer, D., Moschny, J., Lorenzen, W., Jahns, S. Modified microcystins and nodularins. **2017**. EP17170183.0
- (585) Niedermeyer, T.H.J., Enke, H., Kramer, D., Moschny, J., Lorenzen, W., Jahns, S. Method for modifying microcystins and nodularins. **2017**. EP17170184.8



# APPENDIX



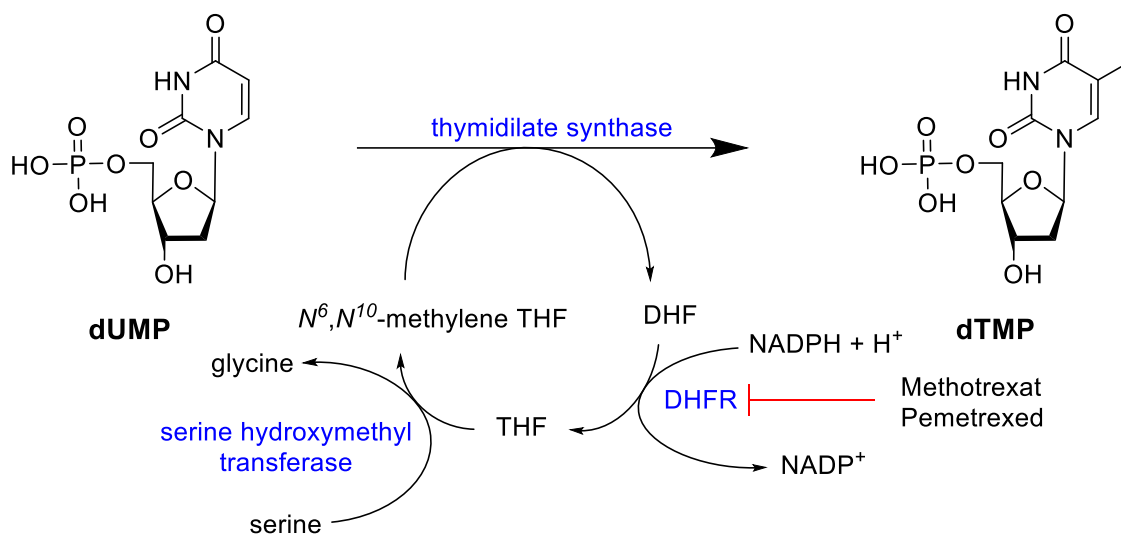
## A.1. List of Abbreviations

Abbreviation (Abb.)	Meaning	Abb.	Meaning
A (domain)	Adenylation domain	HDI	Human development index
Aabu	2-amino-4-azido-L-butyric	HEK	Human embryonal kidney
ACN	Acetonitrile	HI	Heat-inactivated
ADC	Antibody-drug conjugate	HPLC	High-performance liquid chromatography
Adda	(2S,3S,8S,9S)-3-amino-9-methoxy-2,6,8-trimethyl-10-phenyldeca-4,6-dienoic acid	HP-TLC	High-performance thin layer chromatography
ATP	Adenosine triphosphate	IS	Internal standard
Azala	3-Azido-L-alanine	LC	Liquid chromatography
Aznle	6-Azido-L-norleucine	LLE	Liquid-liquid extraction
Aznva	5-Azido-L-norvaline	LOD	Limit of detection
Azphe	p-azido-L-phenylalanine	LOQ	Limit of quantification
BPC	Base-peak chromatogram	mAb	Monoclonal antibody
BuAcO	Butyl acetate	MAPK	Mitogen-activated protein kinase
BuOH	<i>n</i> -Butanol	MC	Microcystin
C (domain)	Condensation domain	MCA	Microcystin accumulation
CD	Cluster of differentiation	MCEE	Microcystin extraction efficiency
CI	Confidence interval	<i>mcy</i>	Microcystin biosynthetic gene cluster
CoE	Degree of co-extractions	Mdha	<i>N</i> -methyldehydro D-alanine
CRM	Certified reference material	Mdhb	( <i>N</i> -methyl)-2-amino-dehydrobutyric acid
CuAAC	Copper(I)-catalyzed azide-alkyne cycloaddition	MEM	Minimal essential medium
DAD	Diode array detector	MeOH	Methanol
DMSO	Dimethyl sulfoxide	MMAE	Monomethyl auristatin E
EC <sub>50</sub>	50% efficacy concentration	MoA	Mode of action
EDTA	Ethylendiaminetetraacetic acid	MS	Mass spectrometry
ELSD	Evaporative light-scattering detector	MS <sup>2</sup>	Tandem-mass spectrometry
EMA	European Medical Agency	MW	Molecular weight
ESI	Electron spray ionization	Narg	<i>N</i> <sub>ω</sub> -Nitro-L-arginine
EtAcO	Ethyl acetate	NHL	Non-Hodgkin lymphoma
FA	Formic acid	NP	Natural product
FBS	Fetal bovine serum	NRP	Non-ribosomal peptide
FDA	Food and Drug Administration	NRPS	Non-ribosomal peptide synthase
Furala	3-(2-furyl)-L-alanine	OATP	Organic anion transporting polypeptide

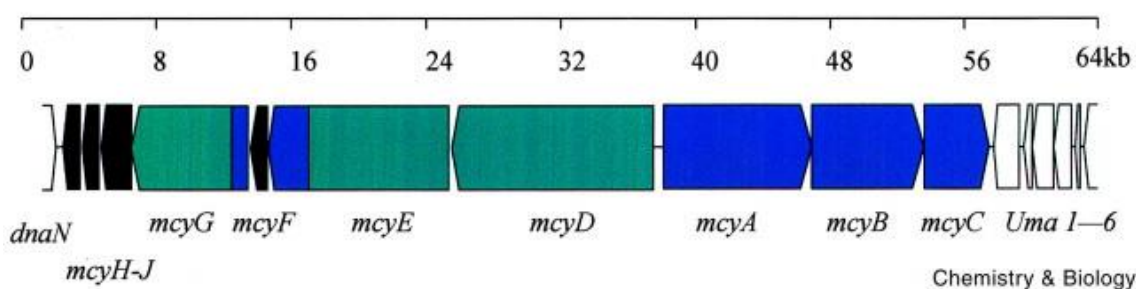
**List of Abbreviations (continued).**

Abb.	Meaning	Abb.	Meaning
OD <sub>750</sub>	Optical density at 750 nm	RP	Reversed phase
PBS	Phosphate-buffered saline	SAM	S-Adenosyl-L-methionine
PDB	Precursor-directed biosynthesis	SAR	Structure–activity relationship
PFP	Pentafluorophenyl	SEC	Size-exclusion chromatography
PH	Phenylhexyl	SNR	Signal–to–noise ratio
PKS	Polketide synthase	SPE	Solid-phase extraction
PP	Protein phosphatase	SRB	Sulforhodamine B
Prgly	Propyn-1-yl-L-glycine	TAE	Tris-acetate-EDTA
Prlys	<i>N</i> 6-[(2-propyn-1-yloxy)carbonyl]-L-lysine	TCA	Trichloroacetic acid
Prtyr	<i>O</i> -(2-propyn-1-yl)-L-tyrosine	TFA	Trifluoroacetic acid
R <sub>f</sub>	Retardation factor	THPTA	Tris(3-hydroxypropyltriazolyl-methyl)amine
PFP	Pentafluorophenyl	TIC	Total ion chromatogram
PH	Phenylhexyl	<i>t<sub>R</sub></i>	Retention time
R	Peak resolution		

## A.2. Supplementary Information to Chapter 1.1.: Cancer – an Emerging, Global Health Issue



**Figure A1.** Mode of action (MoA) of methotrexate and pemetrexed. The folate analogues methotrexate and pemetrexed inhibit the dihydrofolate reductase (DHFR), which reduces dihydrofolic acid (DHF) to tetrahydrofolic acid (THF). THF is further converted to  $N^6,N^{10}$ -methylene THF by a serine hydroxymethyl transferase.  $N^6,N^{10}$ -methylene THF acts as cofactor in the conversion of desoxy uridine monophosphate (dUMP) to desoxy thymidine monophosphate (dTMP) by the thymidylate synthase. Due to the shortage of THF, and in consequence  $N^6,N^{10}$ -methylene THF supply upon DHFR inhibition, methotrexate and pemetrexed indirectly inhibit the thymidylate synthase and, thus, thymidine synthesis. Enzymes are marked in blue caption and the red, blunt ended arrow indicates inhibition. Figure adapted and modified from Proteopedia (<https://proteopedia.org/wiki/index.php/Methotrexate>; accessed on May 24, 2020).



**Figure A2.** Organization of the gene cluster for microcystin biosynthesis. The direction of transcription and relative sizes of the open reading frames (ORFs) deduced from the analysis of the nucleotide sequence are indicated. ORFs containing regions homologous to non-ribosomal peptide synthetases or polyketide synthetases are indicated in blue and green, respectively. Additional ORFs of putative microcystin tailoring function are indicated in black. Non-microcystin synthetase ORFs are shown in white. Reproduced from Tillet *et al.*<sup>185</sup> with the permission of Elsevier (Document A2).

### A.3. Supplementary Information to Chapter 3.1.: A Toolbox for Microcystin Isolation, Analysis and Screening

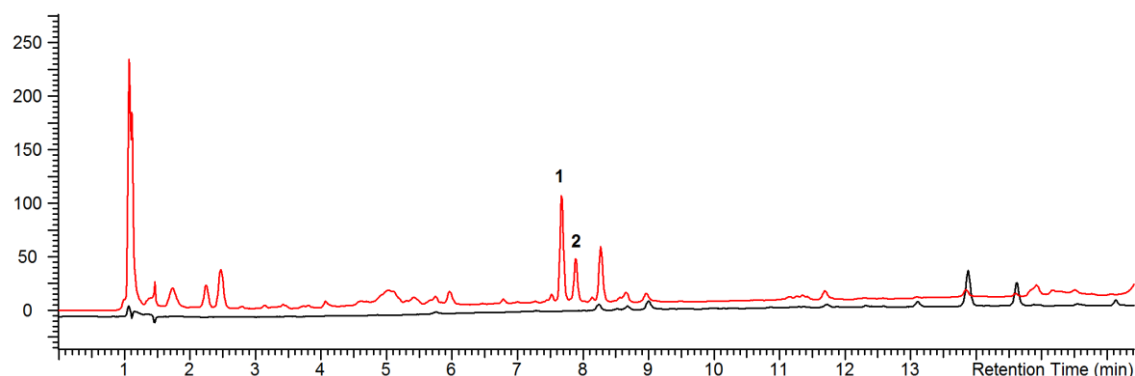


**Figure A3.** HPLC-UV chromatogram (210 nm) overlay of the aqueous (red, upper trace) and organic (black, lower trace) of solvent system 1 (n-hexane:buty lacetate:methanol:water = 8:2:8:2) after partition of an *M. aeruginosa* CBT 480 sample containing MC-YR (1) and MC-LR (2).

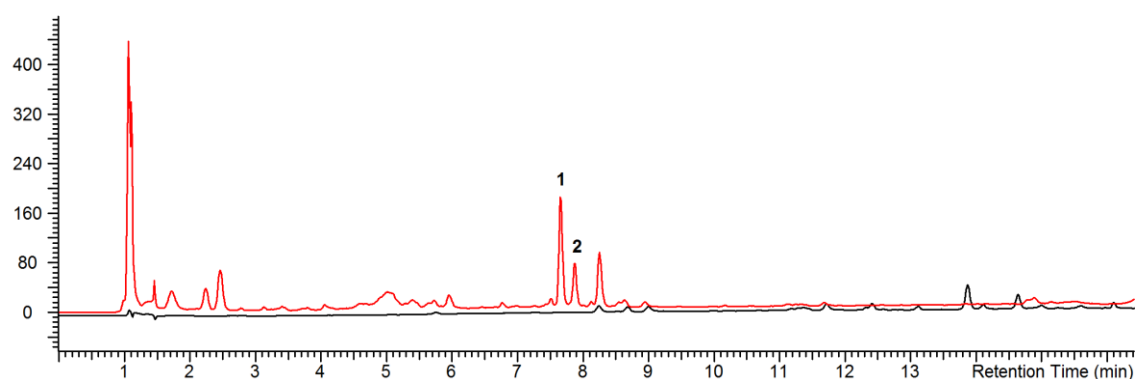


**Figure A4.** HPLC-UV chromatogram (210 nm) overlay of the aqueous (red, upper trace) and organic (black, lower trace) of the biphasic solvent system 2 (n-hexane:butyl acetate:methanol:water = 6.6:3.4: 6.6:3.4) after partition of an *M. aeruginosa* CBT 480 sample containing MC-YR (1) and MC-LR (2).

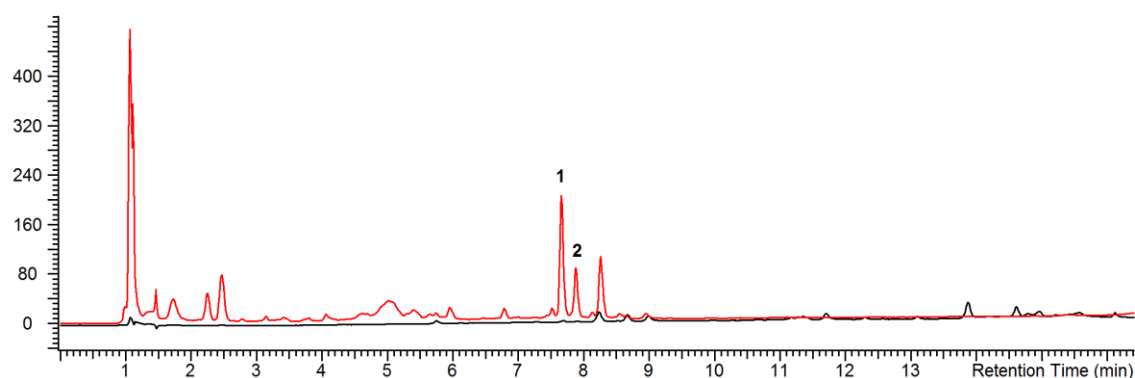


**Figure A5.** HPLC-UV chromatogram (210 nm) overlay of the aqueous (red, upper trace) and organic (black, lower trace) of the biphasic solvent system 3 (n-hexane:butyl acetate:methanol:water = 1:1:1:1) after partition of an *M. aeruginosa* CBT 480 sample containing MC-YR (1) and MC-LR (2).

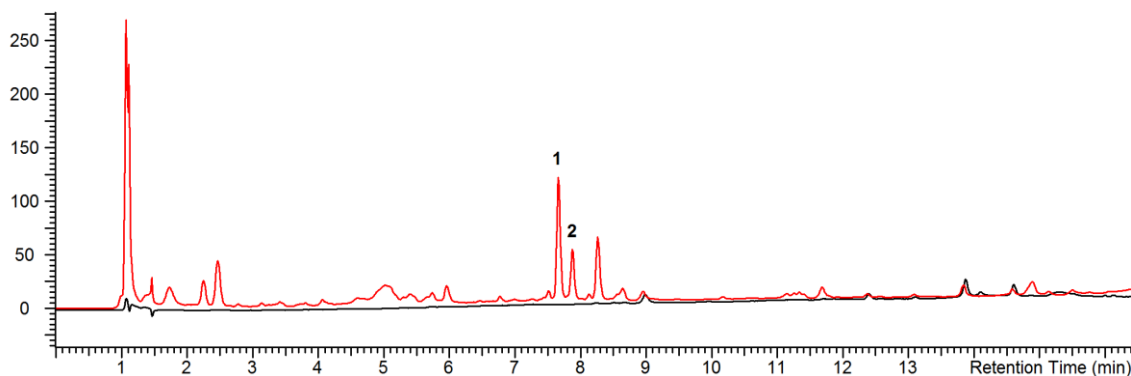


**Figure A6.** HPLC-UV chromatogram (210 nm) overlay of the aqueous (red, upper trace) and organic (black, lower trace) of the biphasic solvent system 4 (n-hexane:ethyl acetate:methanol: water = 8:2:8:2) after partition of an *M. aeruginosa* CBT 480 sample containing MC-YR (1) and MC-LR (2).

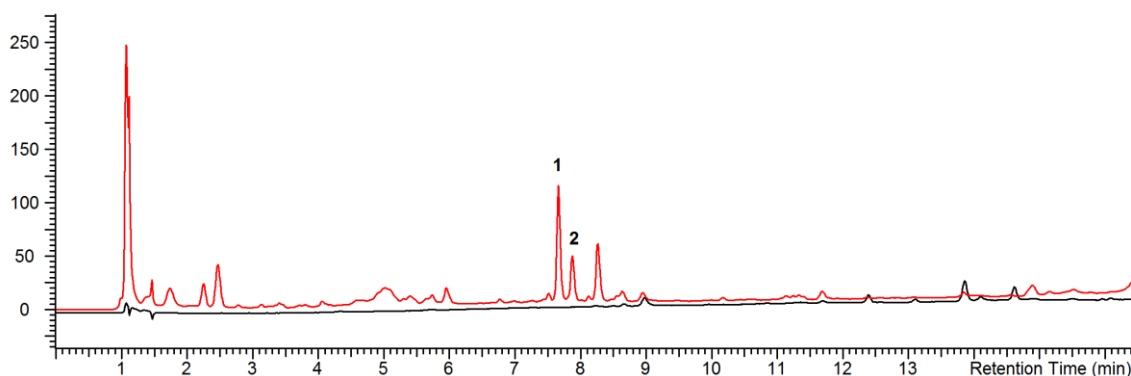


**Figure A7.** HPLC-UV chromatogram (210 nm) overlay of the aqueous (red, upper trace) and organic (black, lower trace) of the biphasic solvent system 5 (n-hexane:ethyl acetate:methanol: water = 6.6:3.4:6.6:3.4) after partition of an *M. aeruginosa* CBT 480 sample containing MC-YR (1) and MC-LR (2).

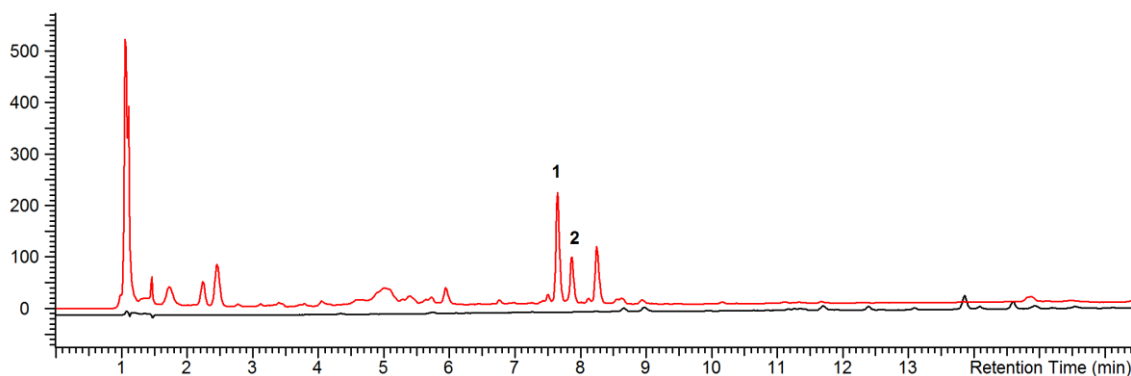


**Figure A8.** HPLC-UV chromatogram (210 nm) overlay of the aqueous (red, upper trace) and organic (black, lower trace) of the biphasic solvent system 6 (n-hexane:ethyl acetate:methanol: water = 1:1:1:1) after partition of an *M. aeruginosa* CBT 480 sample containing MC-YR (1) and MC-LR (2).

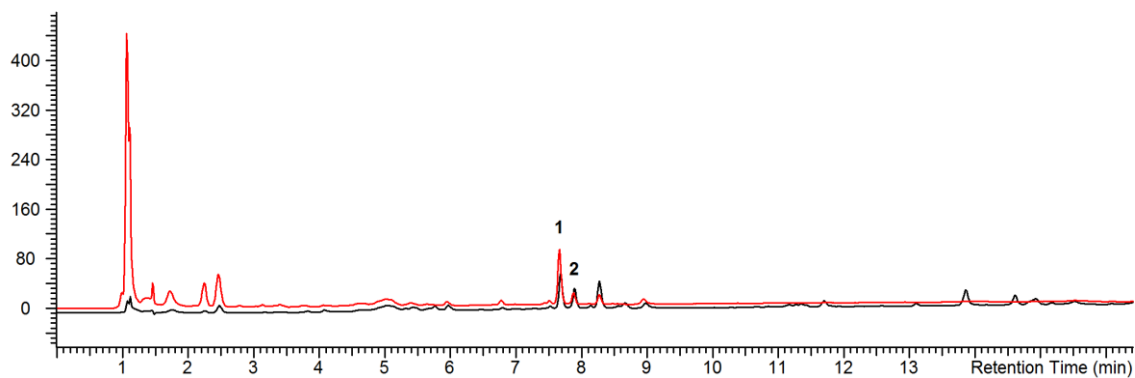


**Figure A9.** HPLC-UV chromatogram (210 nm) overlay of the aqueous (red, upper trace) and organic (black, lower trace) of the biphasic solvent system 7 (chloroform:methanol: water = 6:3:1) after partition of an *M. aeruginosa* CBT 480 sample containing MC-YR (1) and MC-LR (2).

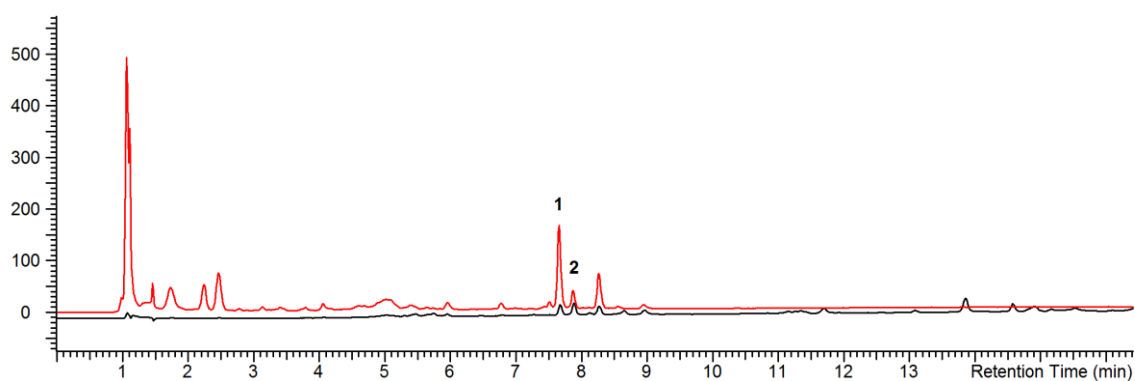


**Figure A10.** HPLC-UV chromatogram (210 nm) overlay of the aqueous (red, upper trace) and organic (black, lower trace) of the biphasic solvent system 7 (chloroform:methanol: water = 1:1:1) after partition of an *M. aeruginosa* CBT 480 sample containing MC-YR (1) and MC-LR (2).



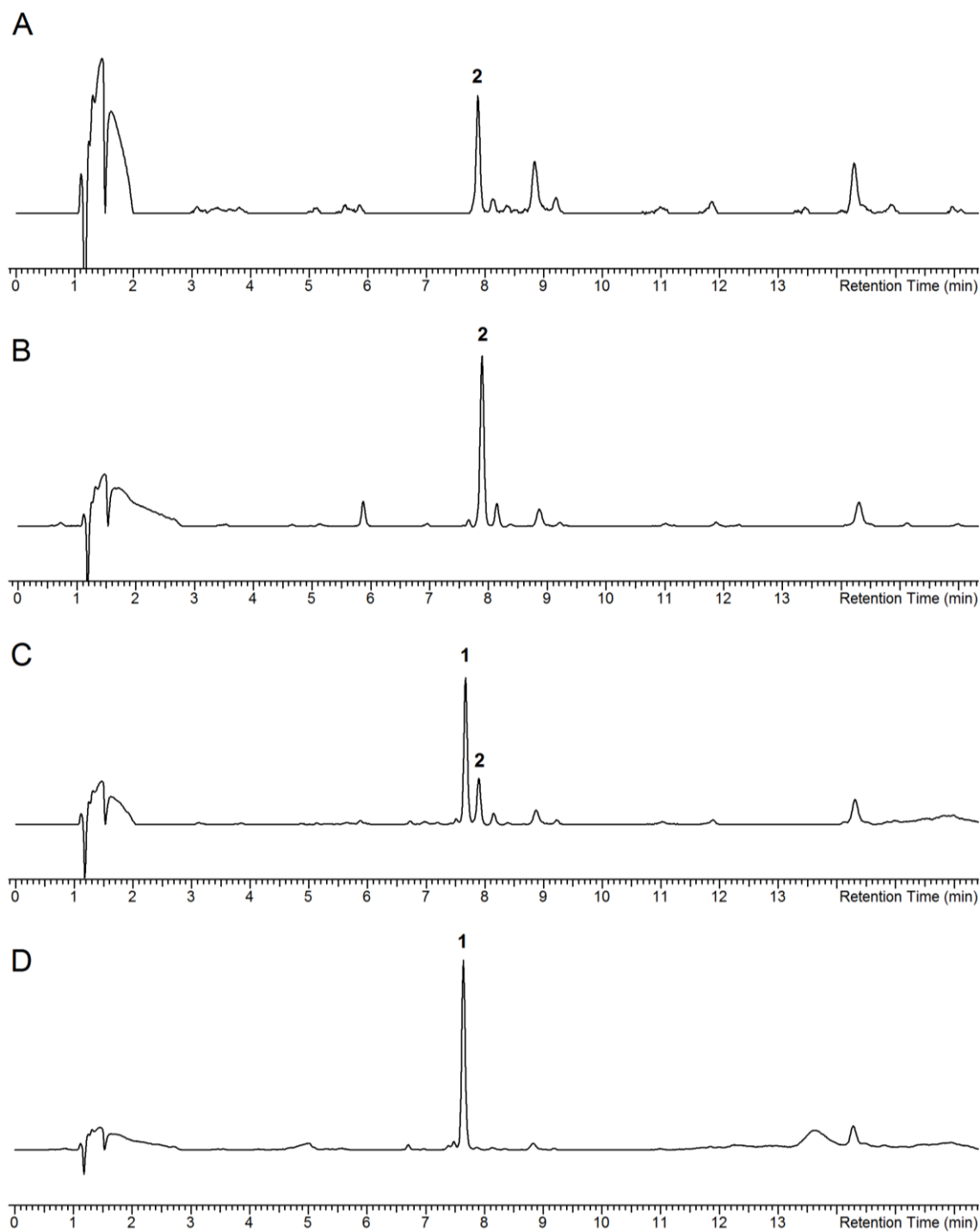


**Figure A11.** UV chromatograms (230 nm) of fraction 14, 15, 16, and 17 obtained from size-exclusion chromatography (SEC) of a *M. aeruginosa* CBT 480 methanol extract on Sephadex LH-20 with methanol. (A) UV chromatogram (230 nm) of fraction 14 with MC-LR (2). (B) UV chromatogram (230 nm) of fraction 15 with MC-LR (2). (C) UV chromatogram (230 nm) of fraction 16 with MC-YR (1) and MC-LR (2). (D) UV chromatogram (230 nm) of fraction 17 with MC-YR (1).

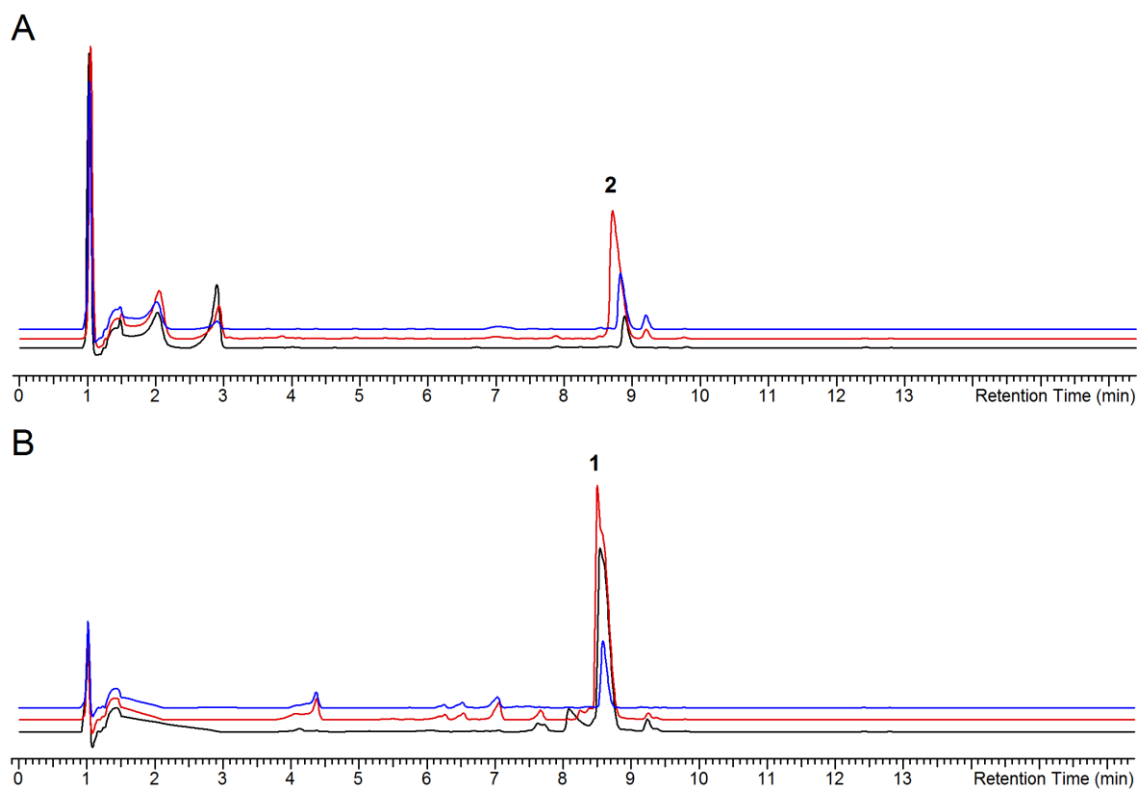


**Figure A12.** UV chromatogram (230 nm) overlays of MC-containing fractions obtained from size-exclusion chromatography (SEC) of a *M. aeruginosa* CBT 480 methanol extract on Sephadex LH-20 with 50 % (v/v) methanol in water. (A) UV chromatogram (230 nm) overlay of fractions 41, 42, and 43 containing MC-LR (**2**). (B) UV chromatogram (230 nm) overlay of fractions 46, 47, and 48 containing MC-YR (**1**).

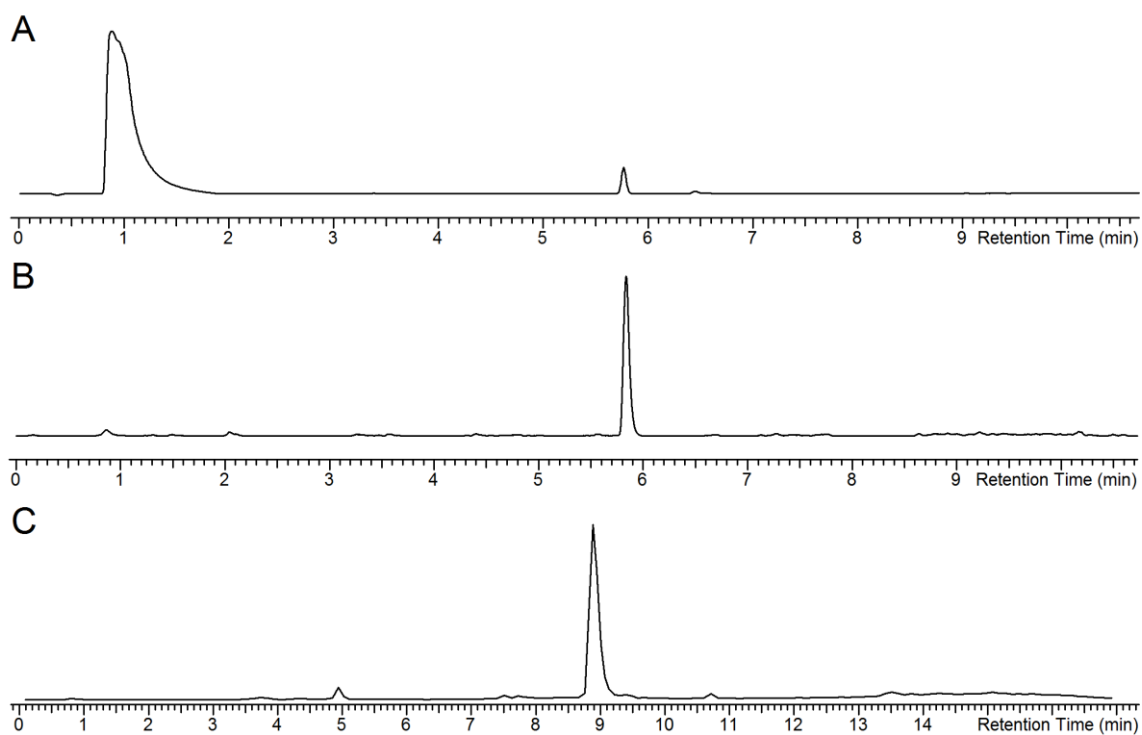


**Figure A13.** UV chromatogram (210 nm; A), HPLC-ELSD chromatogram (B) and total ion chromatogram (TIC, C) of MC-YR (**1**) in DMSO, isolated from *M. aeruginosa* CBT 480.

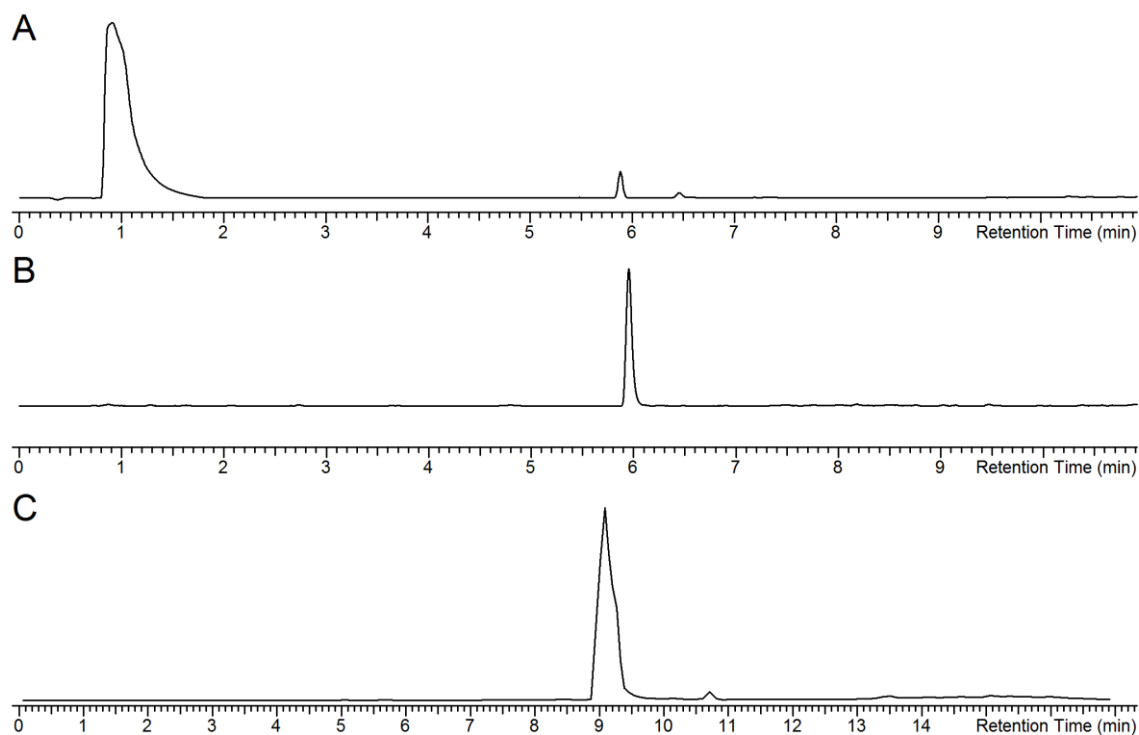


**Figure A14.** UV chromatogram (210 nm; A), HPLC-ELSD chromatogram (B) and TIC (C) of MC-LR (2) in DMSO, isolated from *M. aeruginosa* CBT 480. Peak shoulder at  $t_R$  9.3 min contains the same  $m/z$  of 995.5 and as peak apex and no additional  $m/z$  values. The shoulder most likely arose from peak tailing due to overloading.

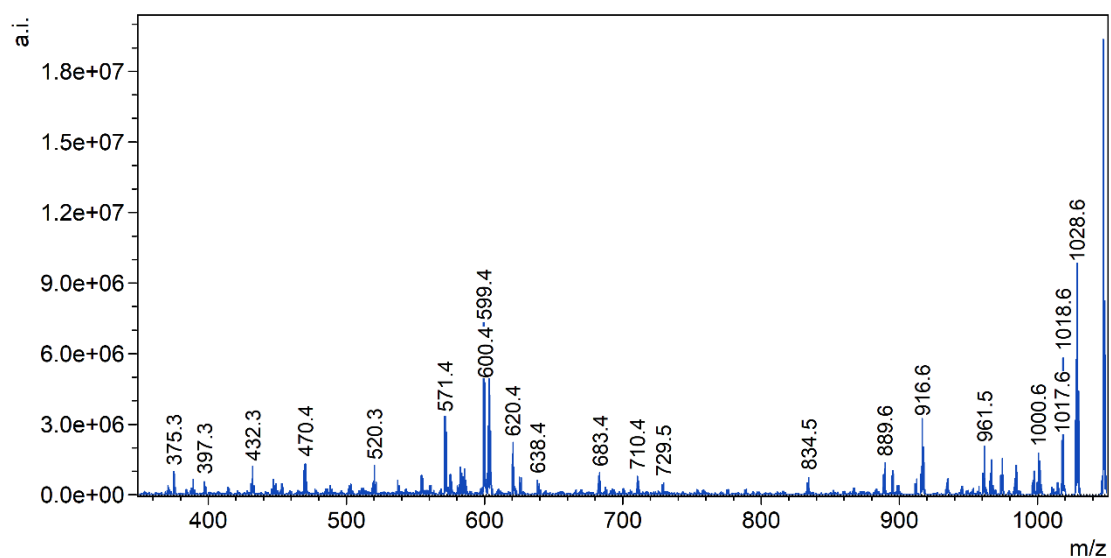


**Figure A15.** MS<sup>2</sup> spectrum of MC-YR (1) with  $m/z$  1045.5.

**Table A1.** Annotation of the MS<sup>2</sup> spectrum of MC-YR (1). Mdha, *N*-methyl dehydroalanine; Masp,  $\beta$ -methyl aspartic acid; Adda, 3*S*-amino-9*S*-methoxy-2*S*,6,8*S*-trimethyl-10-phenyldeca-4*E*,6*E*-dienoic acid.

<i>m/z</i>	Annotation	Ion	Difference [Da]
1028.6	M - NH <sub>3</sub> + H <sup>+</sup>	-	+ 0.1
1017.6	M - CO + H <sup>+</sup>	-	+ 0.1
1006.6	M - CO - NH <sub>3</sub> + H <sup>+</sup>	-	+ 0.1
961.5	Ala-Tyr-Masp-Arg-Adda-Glu - H <sub>2</sub> O + H <sup>+</sup>	c <sup>6</sup>	+ 0.1
916.6	Mdha-Ala-Tyr-Masp-Arg-Adda + H <sup>+</sup> or Arg-Adda-Glu-Mdha-Ala-Tyr + H <sup>+</sup>	b <sup>6</sup> /y <sup>6</sup>	+ 0.1
889.6	Ala-Tyr-Masp-Arg-Adda-Glu - CO - NH <sub>3</sub> + H <sup>+</sup>	a <sup>6</sup>	+ 0.1
834.5	Masp-Arg-Adda-Glu-Mdha-Ala - CH <sub>3</sub> O	z <sup>6</sup>	+ 0.1
729.5	Adda-Glu-Mdha-Ala-Tyr - CH <sub>3</sub> O	b <sup>5</sup> /y <sup>5</sup>	+ 0.1
710.4	Masp-Arg-Adda-Glu - H <sub>2</sub> O + H <sup>+</sup>	b <sup>4</sup> /y <sup>4</sup>	0.0
683.4	Masp-Arg-Adda-Glu - CO - NH <sub>3</sub> + H <sup>+</sup>	b <sup>4</sup> /y <sup>4</sup>	+ 0.1
620.4	Mdha-Ala-Tyr-Masp-Arg + H <sup>+</sup>	c <sup>5</sup>	+ 0.1
603.4	Mdha-Ala-Tyr-Masp-Arg + H	b <sup>5</sup> /y <sup>5</sup>	+ 0.1
600.4	Tyr-Masp-Arg-Adda - C <sub>9</sub> H <sub>10</sub> O + H <sup>+</sup>	a <sup>3</sup>	+ 0.1
599.4	Masp-Arg-Adda + H <sup>+</sup> or Arg-Adda-Glu + H <sup>+</sup>	b <sup>3</sup> /y <sup>3</sup>	+ 0.1
571.4	Masp-Arg-Adda + H <sup>+</sup> or Arg-Adda-Glu + H <sup>+</sup>	a <sup>3</sup>	+ 0.1
520.3	Ala-Tyr-Masp-Arg + H <sup>+</sup>	b <sup>4</sup> /y <sup>4</sup>	+ 0.1
470.4	Arg-Adda + H <sup>+</sup>	b <sup>2</sup> /y <sup>2</sup>	+ 0.1
432.3	Tyr-Masp-Arg + H <sup>+</sup>	z <sup>3</sup>	+ 0.1
397.3	Adda-Glu - H <sub>2</sub> O + H <sup>+</sup>	a <sup>2</sup>	+ 0.1
375.3	C <sub>11</sub> H <sub>14</sub> O-Glu-Mdha + H <sup>+</sup>	z <sup>3</sup>	+ 0.1

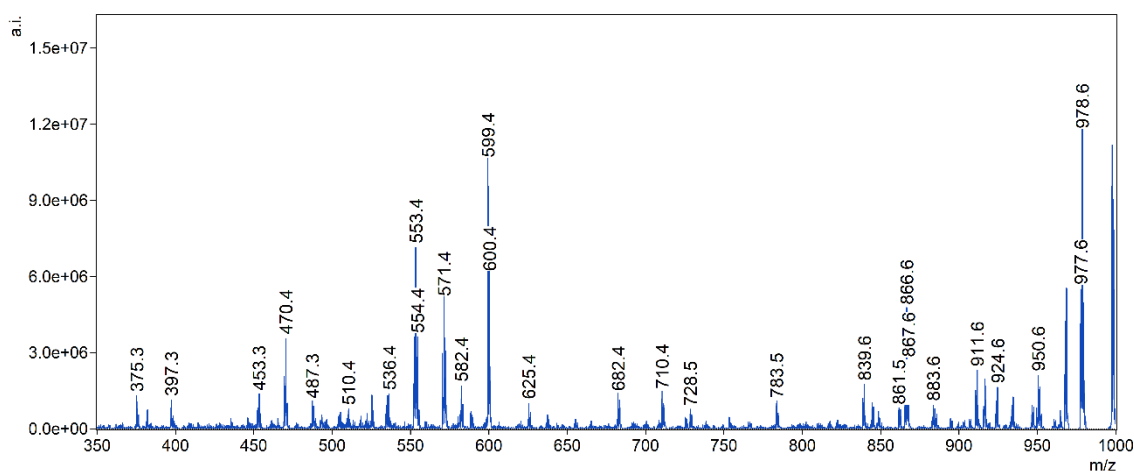


**Figure A16.** MS<sup>2</sup> spectrum of MC-LR (2) with *m/z* 995.5.

**Table A2.** Annotation of the MS<sup>2</sup> spectrum of MC-LR (2). Mdha, *N*-methyl dehydroalanine; Masp,  $\beta$ -methyl aspartic acid; Adda, 3*S*-amino-9*S*-methoxy-2*S*,6,8*S*-trimethyl-10-phenyldeca-4*E*,6*E*-dienoic acid.

<i>m/z</i>	Annotation	Ion	Difference [Da]
978.6	M - NH <sub>3</sub> + H <sup>+</sup>	-	+ 0.1
977.6	M - H <sub>2</sub> O + H <sup>+</sup>	-	+ 0.1
967.6	M - CO + H <sup>+</sup>	-	+ 0.1
950.6	M - CO - NH <sub>3</sub> + H <sup>+</sup>	-	+ 0.1
924.6	Leu-Masp-Arg-Adda-Glu-Mdha + H <sup>+</sup>	b <sup>6</sup> /y <sup>6</sup>	+ 0.1
911.6	Ala-Leu-Masp-Arg-Adda-Glu - H <sub>2</sub> O + H <sup>+</sup>	c <sup>6</sup>	+ 0.1
883.6	Mdha-Ala-Leu-Masp-Arg-Adda + H <sup>+</sup> or Arg-Adda-Glu-Mdha-Ala-Leu + H <sup>+</sup>	c <sup>6</sup>	+ 0.1
867.6	Ala-Leu-Masp-Arg-Adda-Glu - NH <sub>3</sub> + H <sup>+</sup>	a <sup>6</sup>	+ 0.1
866.6	Mdha-Ala-Leu-Masp-Arg-Adda + H <sup>+</sup> or Arg-Adda-Glu-Mdha-Ala-Leu + H <sup>+</sup>	b <sup>6</sup> /y <sup>6</sup>	+ 0.1
861.5	M - C <sub>9</sub> H <sub>10</sub> O + H <sup>+</sup>	-	0.0
839.6	Mdha-Ala-Leu-Masp-Arg-Adda - CO <sub>2</sub> + H <sup>+</sup> or Arg-Adda-Glu-Mdha-Ala-Leu - CO <sub>2</sub> + H <sup>+</sup>	c <sup>6</sup>	0.0
783.5	Ala-Leu-Masp-Arg-Adda + H <sup>+</sup>	b <sup>5</sup> /y <sup>5</sup>	+ 0.1
728.5	Masp-Arg-Adda-Glu + H <sup>+</sup>	b <sup>4</sup> /y <sup>4</sup>	+ 0.1
710.4	Adda-Glu-Mdha-Ala-Leu + H <sup>+</sup>	b <sup>5</sup> /y <sup>5</sup>	0.0
682.4	Glu-Mdha-Ala-Leu-Masp-Arg + H <sup>+</sup> or Arg-Adda-Glu-Mdha + H <sup>+</sup>	b <sup>6</sup> /y <sup>6</sup> b <sup>4</sup> /y <sup>4</sup>	+ 0.1 0.0
625.4	Arg-Adda-Glu + H <sup>+</sup> or Masp-Arg-Adda + H <sup>+</sup>	x <sup>3</sup>	+ 0.1
599.4	Masp-Arg-Adda + H <sup>+</sup> or Arg-Adda-Glu + H <sup>+</sup>	b <sup>3</sup> /y <sup>3</sup>	+ 0.1
582.4	Masp-Arg-Adda - NH <sub>3</sub> + H <sup>+</sup> or Arg-Adda-Glu - NH <sub>3</sub> + H <sup>+</sup>	b <sup>3</sup> /y <sup>3</sup>	+ 0.1
571.4	Masp-Arg-Adda + H <sup>+</sup> or Arg-Adda-Glu + H <sup>+</sup>	a <sup>3</sup>	+ 0.1
554.4	Masp-Arg-Adda - NH <sub>3</sub> + H <sup>+</sup> or Arg-Adda-Glu - NH <sub>3</sub> + H <sup>+</sup>	a <sup>3</sup>	+ 0.1
553.4	Mdha-Ala-Leu-Masp-Arg + H <sup>+</sup>	b <sup>5</sup> /y <sup>5</sup>	+ 0.1
536.4	Leu-Masp-Arg-Adda - C <sub>9</sub> H <sub>10</sub> O - CN <sub>2</sub> H <sub>2</sub> + H <sup>+</sup>	b <sup>4</sup> /y <sup>4</sup>	+ 0.1
487.3	Arg-Adda + H <sup>+</sup> or Ala-Leu-Masp-Arg + H <sup>+</sup>	c <sup>2</sup> c <sup>4</sup>	0.0 0.0
470.4	Arg-Adda + H <sup>+</sup>	b <sup>2</sup> /y <sup>2</sup>	+ 0.1
453.3	Arg-Adda + H <sup>+</sup> or Ala-Leu-Masp-Arg + H <sup>+</sup>	z <sup>2</sup> z <sup>4</sup>	0.0 + 0.1
397.3	Adda-Glu - H <sub>2</sub> O + H <sup>+</sup>	a <sup>2</sup>	+ 0.1
375.3	C <sub>11</sub> H <sub>14</sub> O-Glu-Mdha + H <sup>+</sup>	z <sup>3</sup>	+ 0.1

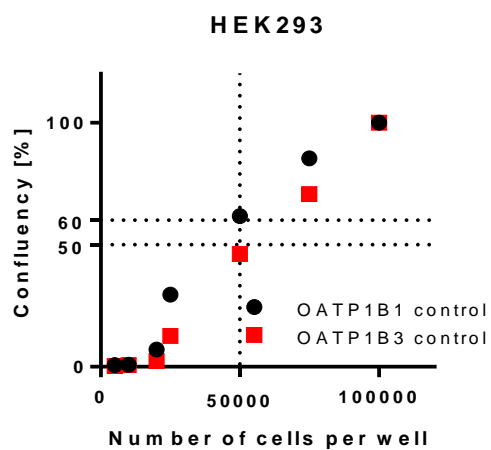


**Figure A17.** Determination of the ideal seeding density for the HEK293 OATP1B1 control cell line (black circles) and HEK293 OATP1B3 control cell line (red squares).

## A.4. Publication

JOURNAL OF  
NATURAL  
PRODUCTS

pubs.acs.org/jnp

Article

## Precursor-Directed Biosynthesis and Fluorescence Labeling of Clickable Microcystins

Julia Moschny, Wolfram Lorenzen, Alexandra Hilfer, Robert Eckenstaler, Stefan Jahns, Heike Enke, Dan Enke, Philipp Schneider, Ralf A. Benndorf, and Timo H. J. Niedermeyer\*

Cite This: *J. Nat. Prod.* 2020, 83, 1960–1970

Read Online

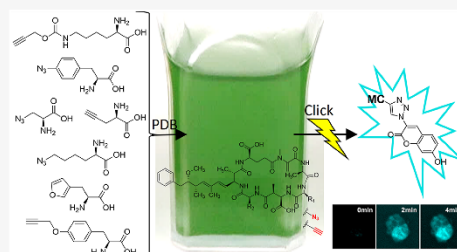
ACCESS |

Metrics & More

Article Recommendations

Supporting Information

**ABSTRACT:** Microcystins, cyclic nonribosomal heptapeptides, are the most well-known cyanobacterial toxins. They are exceptionally well studied, but open questions remain concerning their physiological role for the producing microorganism or their suitability as lead compounds for anticancer drug development. One means to study specialized metabolites in more detail is the introduction of functional groups that make a compound amenable for bioorthogonal, so-called click reactions. Although it was reported that microcystins cannot be derivatized by precursor-directed biosynthesis, we successfully used this approach to prepare clickable microcystins. Supplementing different azide- or terminal alkyne containing amino acid analogues into the cultivation medium of microcystin-producing cyanobacteria strains, we found that these strains differ strongly in their substrate acceptance. Exploiting this flexibility, we generated more than 40 different clickable microcystins. We conjugated one of these derivatives with a fluorogenic dye and showed that neither incorporation of the unnatural amino acid analogue nor attachment of the fluorescent label significantly affects the cytotoxicity against cell lines expressing the human organic anion transporting polypeptides 1B1 or 1B3. Using time-lapse microscopy, we observed that the fluorescent microcystin is rapidly taken up into eukaryotic cells expressing these transporters.



More than 50 years have passed since the discovery of microcystins (MCs) as the main toxins in freshwater reservoirs infested with cyanobacterial blooms.<sup>1–3</sup> Since then, MCs have drawn a lot of public and scientific attention. They became the most cited cyanobacterial toxins, with more than 10 000 publications containing the keyword “microcystin” being published.<sup>4</sup> Many efforts have been undertaken to study their impact on ecosystems<sup>5–10</sup> and public health.<sup>5,11–14</sup> The toxicology of MCs has been intensely studied.<sup>15–19</sup> They inhibit the eukaryotic protein phosphatases 1 and 2A (PP1 and PP2A) with picomolar IC<sub>50</sub> values, resulting in the induction of cell death.<sup>20</sup> Because none of the clinically used anticancer therapeutics has this mode of action, MCs have been discussed as lead structures for anticancer drug development.<sup>21,22</sup> However, no MC has entered a clinical trial so far because they are highly hepatotoxic after systemic application.<sup>15,16</sup> Also, many questions concerning their physiological role for MC-producing cyanobacteria are still unanswered.<sup>23–27</sup>

These two research questions encouraged us to try to introduce bioorthogonal functional groups into MCs,<sup>28–30</sup> which would result in new possibilities for studying these potent toxins.<sup>31–34</sup> Bioorthogonal chemistry is closely associated with the concept of click chemistry,<sup>35,36</sup> most prominently the copper(I)-catalyzed azide–alkyne cyclo-

addition (CuAAC), in which an azide reacts with a terminal alkyne to form a triazole.<sup>37,38</sup>

Although a total synthetic route to clickable MCs has been described before,<sup>39</sup> this synthesis required about 30 steps and, accordingly, had a low overall yield. Thus, we sought an alternative approach to introduce azido or terminal alkyne groups into MCs. MCs are products of an integrated polyketide synthase/nonribosomal peptide synthetase system (PKS-NRPS).<sup>40</sup> About 250 natural MC derivatives have been described in the literature.<sup>41</sup> This high natural variability is mainly due to the low substrate specificity of the A-domains responsible for substrate recognition for positions 2 and 4 of the MC core structure and the adjacent C-domains of subsequent modules (Figure 1).<sup>42</sup>

Consequently, we hypothesized that MCs should be modifiable via precursor-directed biosynthesis (PDB).<sup>43</sup> In this strategy, the growth medium of a microorganism is

Received: March 6, 2020

Published: May 28, 2020



ACS Publications

© 2020 American Chemical Society and American Society of Pharmacognosy

1960

<https://dx.doi.org/10.1021/acs.jnatprod.0c00251>  
*J. Nat. Prod.* 2020, 83, 1960–1970

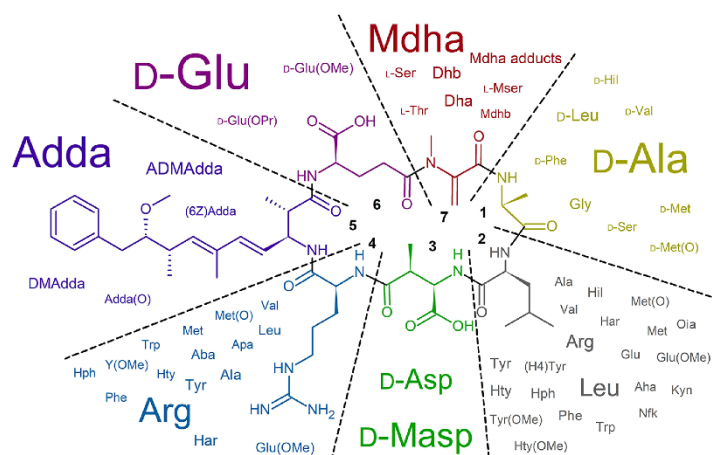


**Figure 1.** General structure of microcystins. Prevalence of residues found within microcystins is proportional to the font size of the respective residue. Nonproteinogenic amino acids are abbreviated as follows: Aha, aminoheptanoic acid; Aba, 2-aminobutanoic acid; Adda, (2*S*,3*S*,4*E*,6*E*,8*S*,9*S*)-3-amino-9-methoxy-2,6,8-trimethyl-10-phenyldeca-4,6-dienoic acid; ADMAdda, 9-*O*-acetylDMAdda; Apa, aminopropionic acid; Dha, dehydroalanine; Dhb, dehydrobutyrine; DMAdda, 9-*O*-desmethylAdda; (H4)Tyr, 1,2,3,4-tetrahydrotyrosine; Har, homoarginine; Hil, homoisoleucine; Hph, homophenylalanine; Hty, homotyrosine; Kyn, kynurenine; Lan, lanthionine; Mdan, *N*-methyldehydroalanine; Mdhb, *N*-methyldehydrobutyrate; Masp, erythro- $\beta$ -methyl-isospartic acid; Mlan, *N*-methylanthionine; Met(O), methionine-*S*-oxide; Mser, *N*-methylserine; Nfk, *N*-formylkynurenine; Oia, oxindolalanine; (OMe) *O*-methyl. Amino acids in pos. 2 and 4 have *L*-configuration. Data used to generate this figure from Bouaïcha et al.<sup>41</sup>

supplemented with an artificial precursor that can be incorporated into the molecule of interest instead of the natural substrate.<sup>44</sup> PDB has frequently been applied to the modifications of natural products from various organisms,<sup>44–51</sup> including cyanobacterial specialized metabolites,<sup>52–54</sup> and proved especially efficient for the insertion of clickable groups into polyketides and peptides.<sup>55–57</sup> Cyanobacteria are ideally suited for PDB of unnatural peptides, as they are phototrophic organisms that can be cultivated in media containing inorganic nutrients only. This facilitates the cellular uptake of supplemented unnatural amino acids if the required uptake transporters are present, as the supplemented amino acids do not compete for uptake with the natural amino acids present in rich media. In addition, the extraordinarily high innate flexibility of cyanobacterial NRPS domains<sup>58</sup> potentially allows the acceptance of modified substrates without the need to manipulate the biosynthesis genes to extend the substrate specificity.

Although Okumura et al. reported that they were not able to structurally modify MCs by PDB,<sup>53</sup> we here demonstrate the successful generation of clickable MCs by supplementation of various clickable amino acids to the medium of cyanobacteria cultures. We identified more than 40 new MC congeners with azido and terminal alkyne groups in positions 2 and 4. In addition, MCs with other bioorthogonal functions and also MCs with a dual functionalization are described. As a proof of concept, one clickable MC was isolated and conjugated with a fluorescent probe. Time-lapse fluorescence microscopy and cytotoxicity assessment revealed that the modifications affected neither the cellular uptake nor the subsequent cytotoxicity of the modified MC.

## RESULTS AND DISCUSSION

**PDB of New Clickable MCs.** As the structural variability of MCs is most pronounced in positions 2 and 4, we hypothesized that the substrate specificity of the respective biosynthesis enzymes (McyB and McyC) should be lower than the specificity of the other biosynthesis enzymes involved in MC biosynthesis. Thus, nine amino acid derivatives with either an azido or terminal alkyne group resembling the natural amino acids found in these positions were selected for PDB studies. As in the studied MC-producing strains the amino acids in positions 2 and 4 were mostly found to be either aliphatic (e.g., Leu), basic (Arg), or aromatic (e.g., Tyr), we selected two aromatic (*p*-azido-*L*-phenylalanine, *O*-2-propyn-1-yl-*L*-tyrosine), as well as six aliphatic functionalized amino acids with side chain lengths of up to four carbons (6-azido-*L*-norleucine, 5-azido-*L*-norvaline, 2-amino-4-azido-*L*-butyric acid, 3-azido-*L*-alanine, *N*6-[(2-propyn-1-yloxy)carbonyl]-*L*-lysine, propyn-1-yl-*L*-glycine) as artificial precursors (structures and acronyms of these substrates, see Table 1). In addition to these substrates modifiable via CuAAC, we chose two amino acids with bioorthogonal functionalities with other reactivities: 3-(2-furyl)-*L*-alanine as an analogue of aromatic amino acids and *N*<sub>ω</sub>-nitro-*L*-arginine as a potential substitute for Arg.

We observed that some of these substrates negatively affected the growth of the cyanobacterial strains. For example, Azphe impaired the growth of the *Microcystis aeruginosa* strain CBT 480 at concentrations of 30  $\mu$ M and above, whereas PrTyr was well tolerated at concentrations of up to 100  $\mu$ M. Consequently, to reduce peak substrate concentrations, an iterative supplementation scheme was devised, and the substrates were added to the cultivation media every 24 h to a final concentration of 30  $\mu$ M. This precursor-incubation protocol proved feasible for all strains and amino acid analogues.



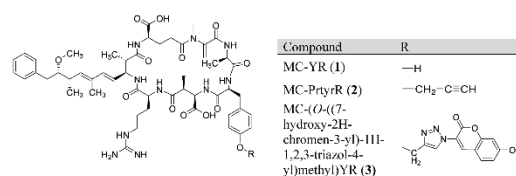
**Table 1. List of Substrates Used for Precursor-Directed Biosynthesis (PDB)**

Name	Acronym	Structure
<i>p</i> -Azido-L-phenylalanine	Azphe	
<i>O</i> -2-Propyn-1-yl-L-tyrosine	Prtyr	
6-Azido-L-norleucine	Aznle	
5-Azido-L-norvaline	Aznva	
2-Amino-4-azido-L-butyric acid	Azabu	
3-Azido-L-alanine	Azala	
N6-[(2-Propyn-1-yloxy)carbonyl]-L-lysine	Prlys	
Propyn-1-yl-L-glycine	Prgly	
3-(2-Furyl)-L-alanine	Furala	
N $\omega$ -Nitro-L-arginine	Narg	

After cultivation, the cyanobacterial biomass of the supplemented and control cultures was harvested and extracted. The extracts were analyzed by LC-MS. As an example, the results of one PDB study with *M. aeruginosa* strain CBT 480 are shown in Figure 2.

**PDB with *M. aeruginosa* CBT 480 and *Microcystis* CBT 1.** *M. aeruginosa* CBT 480 naturally produces MC-LR and MC-YR (1). Analyses of the biomass extracts of cultures supplemented with 30  $\mu$ M Azphe showed that, indeed, a new compound with  $m/z$  1070.6 ( $[M + H]^+$ ) could be

observed. This corresponds to the calculated  $m/z$  of the protonated molecule  $[MC\text{-AzpheR} + H]^+$ , suggesting a replacement of Tyr in position 2 by Azphe. Supplementation with Prtyr following the same protocol resulted in the biosynthesis of MC-PrtyrR (2;  $m/z$  1083.5, consistent with  $[2+H]^+$ ; Supporting Information, Figure S1). MS<sup>2</sup> and MS<sup>3</sup> data of the two compounds were consistent with the hypothesized structures: The spectra feature a characteristic fragment of MCs with  $m/z$  599, corresponding to the b<sup>3</sup> and y<sup>3</sup> ions with the sequences Masp-Arg-Adda or Arg-Adda-Glu,<sup>105</sup> indicating that the new peak is a MC with Arg in position 4. Furthermore, fragment ions analogous to the characteristic fragment ions  $m/z$  916, 911, 620, and 603 of  $[1 + H]^+$  were observed with a distinct shift of  $-3$  for  $[MC\text{-AzpheR} - N_2]^+$  and  $+38$  for  $[2 + H]^+$  (S1, Figures S2 and S3, Tables S1 and S2). Encouraged by these findings, all 10 substrates were supplemented to six different *Microcystis* strains (Table 2).



In addition to the aromatic amino acid analogues Azphe and Prtyr, *M. aeruginosa* CBT 480 was also capable of incorporating the aliphatic, medium-chain length amino acids Prlys, Aznva, and Aznle in position 2 instead of Leu (Figures S4–S6). However, the short-chain length amino acid analogues (Azala and Azabu) were not accepted, indicating a binding preference for sterically demanding precursors. Furthermore, the Arg residue in position 4 of MC-LR could be replaced by Prgly (Figure S7), resulting in MC-LPrgly, which features the clickable functional group in position 4. The analogous product MC-YPrgly was not detectable. Another MC-LR- and MC-YR-producing *Microcystis* strain, CBT 1, was found to possess an identical substrate recognition pattern, resulting in exactly the same products (Table 2 and Figures S8–S13).

**PDB with *Microcystis* CBT 275.** In contrast to *Microcystis aeruginosa* CBT480 and *Microcystis* strain CBT1, *Microcystis* strain CBT 275 showed a very strict substrate specificity in position 2. It did not incorporate any of the selected amino acid derivatives instead of Leu. It rather exhibited broad flexibility in position 4, which was already evident from its

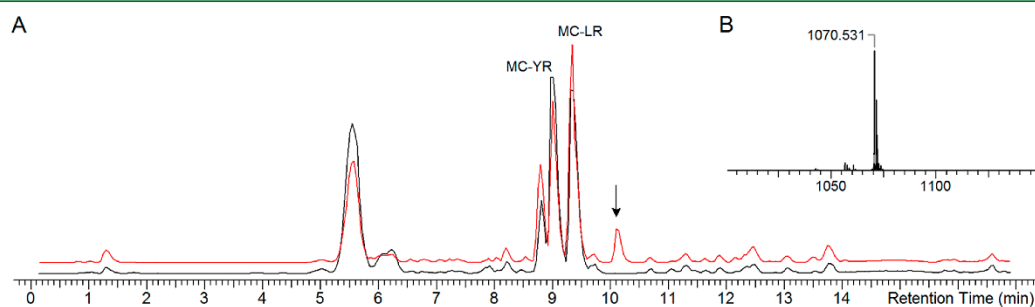


**Figure 2.** (A) Base peak chromatogram (pos. mode) overlay of an *M. aeruginosa* CBT 480 control culture (black, lower trace) and a culture supplemented with 30  $\mu$ M Azphe (red, upper trace); indicates an additional peak in the supplemented culture. (B) Mass spectrum of  $[MC\text{-AzpheR} + H]^+$  ( $t_R$  10.1 min) produced by CBT 480 supplemented with 30  $\mu$ M Azphe.

Table 2. Overview of PDB Studies (Substrate-Strain Combinations)<sup>a</sup>

substrate <sup>b</sup>	strain (main naturally produced congeners)					
	CBT 480 (MC-(L/Y)R)	CBT 1 (MC-(L/Y)R)	CBT 275 (MC-L(R/F/W))	CBT 633 (MC-RR)	CBT 959 (MC-(L/Y)R)	CAWBG11 (MC-(L/F/Y/W/R)(A/Abu/L/R))
Azphe	MC-AzpheR	MC-AzpheR	MC-LAzphe	n/a	MC-AzpheR	MC-Azphe(R/A)
Prtyr	MC-PrtyrR	MC-PrtyrR	MC-LPrtyr	n/a	MC-PrtyrR	MC-Prtyr(R/A/Abu/L)
Aznle	MC-AznleR	MC-AznleR	MC-LAznle	MC-AznleR	MC-AznleR	MC-Aznle(R/A/Abu/L) MC-AznleAznle
Aznva	MC-AznvaR	MC-AznvaR	MC-LAznva	MC-AznvaR	MC-AznvaR MC-(L/Y)Aznva MC-AznvaAznva	MC-(R/F/Y/W/L)Aznva MC-Aznva(A/Abu/R) MC-AznvaAznva
Azabu	-	-	MC-LAzabu	MC-AzabuR MC-RAzabu	MC-(L/Y)Azabu	MC-(R/F/Y/W/L)Azabu MC-AzabuR
Azala	-	-	-	-	MC-(L/Y)Azala	MC-(F/W/L)Azala
Prlys	MC-PrlysR	MC-PrlysR	MC-LPrlys	MC-PrlysR MC-RPrlys	MC-PrlysR	MC-Prlys(R/A)
Prgly	MC-LPrgly	MC-LPrgly	-	-	MC-(L/Y)Prgly	MC(R/F/Y/W/L)Prgly MC-PrglyR
Furala	-	-	MC-LFurala	-	-	n/a
Narg	MC-(L/Y)Narg	MC-(L/Y)Narg	MC-LNarg	MC-NargR MC-RNarg MC-NargNarg	MC-(L/Y)Narg	n/a

<sup>a</sup>The strains used and their main natural MC-congeners are given in the first row. Clickable MCs detected in the supplemented cultures are given in the respective table cells. n/a, data is not available; -, no PDB product detectable. <sup>b</sup>Substrate abbreviations see Table 1.

naturally produced variants (MC-LR, -LF, and -LW). CBT 275 incorporated both aromatic analogues Azphe and Prtyr, as well as the four sterically more demanding aliphatic clickable amino acids Aznle, Aznva, Azabu, and Prlys (Figures S14–S19). Thus, it was capable of producing six clickable MCs with both azido and terminal alkyne groups in position 4.

**PDB with *Microcystis* CBT 633.** Of all *Microcystis* strains selected for PDB, CBT 633 showed the lowest structural diversity of natural MCs, producing MC-RR as the predominant congener. Because the A-domains of McyB and McyC did not seem to possess any affinity toward aromatic amino acids, PDB with the substrates Azphe and Prtyr was not tested. CBT 633 accepted all four aliphatic amino acid derivatives with two or more carbons in their side-chains (Aznle, Aznva, Azabu, and Prlys, Figures S20–S23) as substrates replacing either one of the two arginine residues in position 2 and 4. Whereas both possible isomers were found for the incorporation of Azabu and Prlys (MC-AzabuR and -RAzabu, and MC-PrlysR and -RPrlys), only one product was detected for the supplementation with Aznle (MC-AznleR) and Aznva (MC-AznvaR), indicating a less stringent substrate acceptance of McyB compared to McyC.

**PDB with *Microcystis* CBT 959.** CBT 959, which mainly produces MC-LR and MC-YR, accepted the aromatic and long-chain aliphatic substrates in position 2, whereas the short-chain amino acids were incorporated instead of arginine in position 4 (Figures S24–S37). Because of the overlap in substrate acceptance for Aznva, all theoretically possible products with Aznva in position 2 or 4 (MC-AznvaR, MC-LAznva, and MC-YAznva) as well as the dual functionalized variant MC-AznvaAznva could be detected.

**PDB with *Microcystis* CAWBG11.** A similar pattern of substrate recognition was observed for CAWBG11, a *Microcystis* strain naturally producing a broad spectrum of MCs.<sup>59</sup> While the aromatic amino acids Phe, Tyr, or Trp are used as substrates in position 2 only, the smaller amino acids Ala and Abu are exclusively found in position 4. Leu and Arg occur in

both positions. This biosynthetic behavior was also reflected in the substrate acceptance during the PDB studies.

Both aromatic analogues Azphe and Prtyr as well as the two bulkier analogues Aznle and Prlys were incorporated in position 2 (Figures S38–S49). For Prtyr and Aznle, all theoretically possible products were observed (Figures S40–S47). The isomers MC-AznleL, MC-AznleR, and MC-PrlysR were confirmed also by HRMS<sup>2</sup> (Figures S50–S52 and Tables S3–S5). Interestingly, also the variant MC-AznleAznle arising from the dual incorporation of Aznle (Figure S53) was detectable but not the analogous products with Phe, Tyr, Trp, Leu, or Arg in position 2 and Aznle in position 4. This suggests that these sterically more demanding precursors prevented the binding of Aznle to the A-domain of McyC. Thus, the substrate acceptance seems not only to be determined by the architecture of the respective A- and C-domains<sup>42</sup> but might also be influenced by steric or electrostatic effects mediated by the constituents of the peptide chain bound to the NRPS. However, further *in vivo* and *ex vivo* studies are required to confirm this hypothesis. In the case of Azphe and Prlys, similar causes may have led to the formation of the PDB products and MC-AzpheR and MC-AzpheA (Figures S38 and S39), and MC-PrlysR and MC-PrlysA (Figures S48 and S49), respectively, lacking the combinations of Azphe and Prlys with Abu or Leu.

Because of its intermediate size and side-chain length, Aznva served as substrate for both A-domains of McyB and McyC in CAWBG11. In addition to its incorporation in position 2, yielding MC-AznvaA, MC-AznvaAbu, and MC-AznvaR (Figures S54–S56), Aznva was also found in position 4 in combination with Arg, Phe, Tyr, Trp, and Leu, (Figures S56–S60). The structure of MC-LAznva was confirmed by HRMS<sup>2</sup> (Figure S61 and Table S6). The dual functionalized MC-AznvaAznva was observed, as well (Figure S62).

The short-chain aliphatic amino acids Azala, Azabu, and Prgly were mainly accepted as precursors in position 4, but the number of new products differed between the individual

derivatives. PDB with Azala resulted in three new MCs bearing either Phe, Trp, or Leu in position 2 (SI, Figures S63–S65), while all possible combinations of Azabu and Prgly with the naturally occurring residues in position 2 were observed (Figures S66–S75). The structures of MC-LAzabu and MC-LPrgly were both confirmed by HRMS<sup>2</sup> (Figures S76 and S77, Tables S7 and S8). Additionally, both substrates were further accepted in position 2, but only in combination with Arg in position 4, yielding MC-AzabuR and MC-PrglyR (Figures S70 and S75). These differences in product formation observed for the supplementation with Azala, Azabu, and Prgly may also be due to the steric effects of the peptide chain bound to the NRPS, as discussed above.

In addition to the common [D-Masp<sup>3</sup>]MCs, many of the *Microcystis* strains also produce the respective [D-Asp<sup>3</sup>]MC congeners, but in much lower amounts. We observed the corresponding PDB products for these [D-Asp<sup>3</sup>]MC congeners in those cases, where the acceptance of the clickable amino acid analogue was high (data not shown).

**PDB with *Nodularia* spp. and *Planktothrix rubescens*.** The surprising substrate flexibility of various MC producing *Microcystis* strains as well as the simplicity of our precursor-supplementation strategy prompted us to try the modification of nodularins via PDB. Nodularins are cyclic pentapeptides produced by filamentous *Nodularia* spp. They are chemically related to the MCs, as they also contain the Adda-D-Glu motif.<sup>60–63</sup> However, the supplementation of two *Nodularia* strains, CBT 750 and CBT 786, with various clickable precursors did not result in any new nodularin derivative. Taking into account that only 10 natural nodularin congeners are known,<sup>64</sup> it seems that the substrate specificity of NdaB<sup>65</sup> is much stricter than the specificity of McyB and McyC.

Interestingly, also the filamentous, [D-Asp<sup>3</sup>,E-Dhb<sup>7</sup>]MC-RR-producing *Planktothrix rubescens* strain CBT 329 did not accept any of the azide and alkyne functionalized amino acids as substrates for MC production. This agrees with the findings of Okumura et al.,<sup>53</sup> who reported that the *Planktothrix* strain they used for PDB studies did not incorporate the supplemented precursors into MCs. Considering the lower MC diversity in the genus *Planktothrix* compared to the genus *Microcystis*,<sup>66</sup> we hypothesize that the potential for PDB of MCs is much higher in the genus *Microcystis*. Because of the selection of this genus for our PDB studies, we overcame the previous drawbacks and made MCs amenable for the modification via PDB.

**Dual Functionalization and PDB Using Non-CuAAC Substrates.** In addition to the CuAAC, the bioorthogonal toolbox encompasses several other functional groups for the convenient conjugation of biomolecules.<sup>29,67</sup> One of these is the photoinducible furyl group, which undergoes ring-opening under UV irradiation, forming a highly reactive unsaturated dicarbonyl moiety.<sup>68</sup> By subsequent addition of nucleophiles, this mechanism has been used for the labeling of nucleotides and peptides.<sup>69–72</sup> Consequently, Furala was chosen as an additional bioorthogonal substrate. Despite its aromaticity, none of the MC-YR producing strains accepted it as a substrate in position 2. Only *Microcystis* strain CBT 275 incorporated Furala as an analogue to Phe/Trp in position 4, resulting in the formation of MC-LFurala (Figure S78).

Furthermore, the efficient and specific coupling of primary amines to *N*-hydroxysuccinimide (NHS) esters has been widely used for quantitative proteomics, protein cross-linking, and labeling,<sup>73–81</sup> which could also be applied to MCs bearing

a primary amine group. Because direct supplementation of L-Lys and its homologues to any of the strains did not yield such a MC variant, an alternative route via Narg was chosen. This derivative decomposes to L-ornithine upon ammonolysis, resulting in a primary amine.<sup>82</sup> All the *Microcystis* strains readily accepted it as an Arg substitute, and incorporated it in position 4 (CBT 480, CBT 1, CBT 275, and CBT 959, Figures S79–S85), or position 2 or/and 4 (CBT 633, Figures S86 and S87). Because of the obviously close similarity of Narg to Arg, even *Planktothrix rubescens* strain CBT 329 was capable of incorporating Narg into [D-Asp<sup>3</sup>,E-Dhb<sup>7</sup>]MC-RR (Figure S88).

In order to generate dual-functionalized clickable MCs, the simultaneous supplementation with two substrates was tested as a proof-of-principle in two cases. Simultaneous supplementation of the MC-YR-producing strains CBT 480 and CBT 1 with Narg and the Tyr analogues Azphe or Prtyr led to the production of the expected bifunctionalized derivatives bearing the *N*<sub>ω</sub>-nitroguanidine group in position 4 and either an azide or terminal alkyne function at position 2 (Figures S89–S92), in addition to the monofunctionalized MC variants.

**Summary of PDB Results.** In summary, our precursor-supplementation studies resulted in a total of 41 new MCs accessible to derivatization by CuAAC “click” chemistry, of which 28 feature an azido and 13 feature a terminal alkyne group in addition to two variants bearing azido groups in both positions 2 and 4. One additional congener with a furyl moiety, four with a *N*<sub>ω</sub>-nitro-guanidine residue, and two dual-functionalized MCs with orthogonal bioorthogonal functional groups were generated.

Clickable MCs have been described before by Zemskov et al., who introduced terminal alkyne groups into two MC derivatives by total synthesis, with one being identical to the MC-LPrtyr described here.<sup>39,83</sup> However, as described above, a complex synthesis with a low total yield was required in order to obtain the final product, and this route seems not to be feasible for larger-scale production. In contrast, about 10 mg of **2** were isolated from a 20 L batch of CBT 480 (about 16 g of dry biomass) after a cultivation for 1 week under unoptimized conditions. Although total synthesis allows for a completely free choice of amino acid building blocks and their sequence, precursor-directed biosynthesis outperforms this approach in terms of time and cost-effectiveness, if the functionalization is to be located in positions 2 or 4.

**Kinetics of Prtyr Uptake and Production of **2**.** In order to establish an efficient PDB protocol, we investigated the kinetics of the Prtyr uptake and the formation of **2** in *M. aeruginosa* CBT 480. Prtyr was added to the cultivation medium to a final concentration of 50 μM, and samples were taken immediately and at time intervals of 4 to 24 h. The amount of Prtyr in the medium as well as the extractable amount of **2** in the biomass were determined by HPLC-DAD.

As can be seen in Figure 3, the uptake of Prtyr follows first-order kinetics ( $R^2 = 0.990$ ) with a half-life  $t_{1/2}$  of 14.4 h (95% confidence interval: [12.3–17.3 h]). The substrate was completely consumed after 96 h, thus sampling was stopped at this time point. In contrast, the amount of extractable **2** in the biomass most likely increases in an exponential manner during the first 36 h reaching a maximum at 48 h. Fitting of the corresponding curve, however, gave a poor goodness of fit.

Interestingly, less than 0.2% of the supplemented Prtyr was recovered as extractable **2**. Meissner et al. showed that, depending on the light conditions, about 30–60% of the total

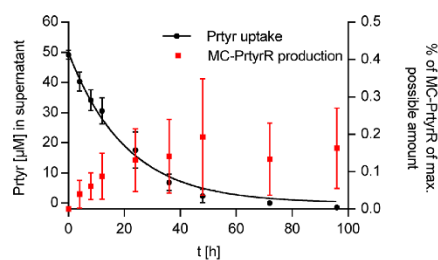


**Figure 3.** Prtyr concentration in the supernatant (black circles) and the amount of MC-PrtyrR (**2**) expressed as percentage of the maximum possible amount (red squares) in *M. aeruginosa* CBT 480 over 96 h (three biological replicates).

MC content is bound to proteins and, thus, not extracted with MeOH but detectable in the insoluble fraction.<sup>84</sup> However, this fact still leaves more than 99% of the total Prtyr input unaccounted for. As the Prtyr concentration within the cyanobacterial biomass was not determined, it is possible that the substrate accumulated within the cells because of a much faster Prtyr uptake compared with the production of **2**, which might slow down once a physiologically relevant total MC concentration is reached within the cyanobacterial cells. Also, part of the supplemented Prtyr may have been lost in the primary metabolism of both the *Microcystis* strain and the associated microorganisms. Because we did not use an axenic culture of *M. aeruginosa* CBT 480 for our experiments, cocultivated heterotrophic bacteria likely also have taken up Prtyr to use it as carbon and nitrogen source.

**Conjugation of **2** with a Fluorescent Probe and Its Biological Characterization.** Compound **2** was isolated from CBT 480 (Figures S93 and S94), and its postulated structure was confirmed by NMR spectroscopy (Table S9 and Figures S95–S103). Since the development of the fluorogenic 3-azido-7-hydroxycoumarin by Sivakumar et al. in 2004,<sup>85</sup> fluorescence labeling of terminal alkynes belongs to the most prominent applications of CuAAC with more than 500 publications referring to this work.<sup>86</sup>

One advantage of this probe is its low molecular weight, making it highly suitable for studies in which major structural changes in the molecule of interest are undesired (e.g., in target binding or interaction studies). Thus, this coumarin derivative was chosen as a fluorogenic tag to design a fluorescent MC congener as a probe for uptake and cytotoxicity studies. Using an optimized reaction protocol of Hong et al.,<sup>87</sup> 3-azido-7-hydroxycoumarin was conjugated with **2**, yielding the fluorescent MC derivative MC-(O-((7-hydroxy-2H-chromen-3-yl)-1H-1,2,3-triazol-4-yl)methyl)YR (**3**). HRMS<sup>2</sup> data of **3** were consistent with the postulated structure (Figure S105 and Table S10).

After purification of **3** by HPLC, the cytotoxicity of the fluorescent MC **3**, its clickable precursor **2**, and the native MC **1** was determined. Structural modification can influence cytotoxicity in two ways. On one hand, binding of the MC to its targets PP1 and PP2A could be influenced. As it is known that the pharmacophore of MCs is the Adda-D-Glu substructure,<sup>88–90</sup> the modification site (position 2) is as far away as possible from the pharmacophore, and we suspected the effect of the derivatization on PP binding to be low.

On the other hand, the structural modification could also have an effect on the uptake of MCs into cells. MCs cannot

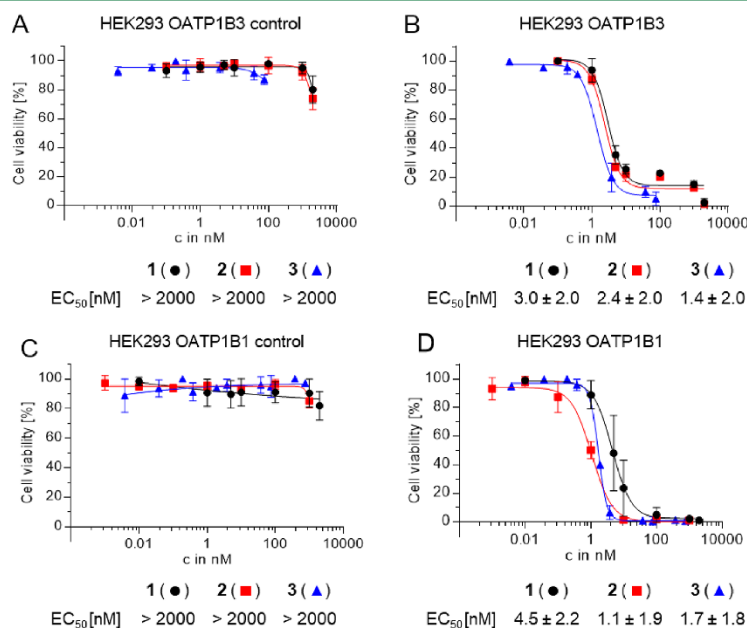


**Figure 4.** Cytotoxicity of **1** (black circles), **2** (red squares), and **3** (blue triangles) against HEK293 OATP1B3 control cells (A), HEK293 OATP1B3 cells (B), HEK293 OATP1B1 control cells (C), and HEK293 OATP1B1 cells (D).

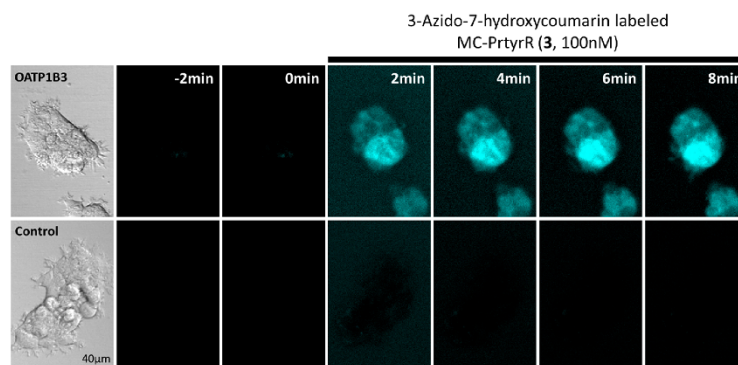


**Figure 5.** Fluorescence time-lapse microscopy of OATP1B3<sup>+</sup> HEK293 cells (upper row) and the corresponding control cells (lower row) before and after exposure to 100 nM **3**. The first picture of each row depicts the brightfield image of the selected cell colony. After 8 min, the increase in fluorescence intensity was not visually discernible anymore (see [Time-Lapse Movie](#)).

penetrate the cell membrane by passive diffusion but depend on active transport, which in humans is mediated by the organic anion transporting polypeptides (OATP) 1B1 and 1B3.<sup>91–94</sup> Although both transporters possess a broad substrate tolerance,<sup>95</sup> it is unpredictable whether they are still capable of transporting **3** into cells.

The chemical features in naturally occurring MC that might affect MC uptake by both transporters have been studied before,<sup>96,97</sup> and even semisynthetically modified MC variants carrying different fluorescent tags were tested against the liver carcinoma cell line HuH-7<sup>98</sup> and a human embryonic kidney (HEK293) cell line expressing drOATP1D1, an OATP-subtype from zebrafish.<sup>99</sup> Although no data on the cytotoxicity of the fluorescent MC on the drOATP1D1 expressing HEK293 cell line was provided, cellular uptake was demonstrated by fluorescence microscopy. However, transport by human OATP has not been studied. Comparable fluorescence microscopy data were also obtained for HuH-7 cells, but as for most cell lines established from primary cells, HuH-7 cells were shown to significantly downregulate OATP expression when cultured.<sup>100</sup> Thus, not surprisingly, the EC<sub>50</sub> of both the fluorescent MC and MC-LR were found to be about 20  $\mu$ M, which is about 1000-fold higher than the values usually found for MCs.<sup>96,97,101</sup> This makes it difficult to estimate the OATP transportability of the fluorescent MC compared with the native MC.

Thus, the cytotoxicity of **1**, **2**, and **3** against OATP1B1- and OATP1B3-expressing HEK293 cells and the corresponding control cell lines was determined ([Figure 4](#)). As expected, all three MC derivatives were inactive against both empty vector control cell lines (no OATP expression). In contrast, they exhibited pronounced activity against the OATP1B1- and OATP1B3-expressing cells, with EC<sub>50</sub> values in the low nanomolar range. The differences between the three derivatives are statistically insignificant, indicating that the coumarin label affects neither the transport nor the PP1/PP2A inhibition.

**Fluorescence Microscopy of MC Uptake into Cells.** The fluorescent MC **3** was used for uptake studies into OATP1B3-expressing HEK293 cells as well as the corresponding control cells. Time-lapse measurements revealed that the probe accumulated rapidly in OATP1B3<sup>+</sup> cells. Within 14 min of exposure to 100 nM **3**, the maximum fluorescence intensity

in the cells was reached, with a simultaneous decrease in background fluorescence ([Figure 5](#), see [Time-Lapse Movie](#)). For the control cells, no staining was observed, but background fluorescence was slightly reduced over time due to photobleaching of the dye. Similar results were obtained for OATP1B1<sup>+</sup> HEK293 cells and their control cells (data not shown).

In comparison to previous MC uptake studies,<sup>98,99</sup> in which fluorescence imaging was performed after 30 min and 4 h, respectively, our time-lapse recording showed that the main part of the probe is taken up within the first 15 min. Afterward, photobleaching effects of the dye outweighed the gain in fluorescence intensity per cell, leading to an overall signal decrease. These findings are in accordance with the previously described OATP1B1 and OATP1B3 uptake kinetics for MC-LR by Fischer et al.,<sup>92</sup> who chose an incubation time of 15 min to determine the Michaelis constant  $K_M$  and the maximal velocity  $V_{max}$ .

The roughly homogeneous distribution of signal intensity throughout the whole cell indicates a cytosolic localization of **3**, but further measurements at higher resolutions and in combination with a cytosolic marker are required to confirm this hypothesis. In addition, more statistical replicates are needed in order to determine the kinetic parameters for the uptake of the MC-coumarin conjugate by OATP1B1 and OATP1B3.

**Potential Uses of Clickable MCs.** The exploitation of a clickable MC to attach a fluorescent tag *ex vivo* is only one of the potential applications arising from the bioorthogonally functionalized MCs. By means of *in vivo* labeling, the MCs could also be localized within the producing cyanobacteria, allowing for new insights into their biological role. Furthermore, the clickable MCs can be conjugated with a suitable carrier or adjuvants potentially enabling the development of MC-based therapeutics.

## ■ EXPERIMENTAL SECTION

**Chemicals and Reagents.** *p*-Azido-*L*-phenylalanine (Azphe), *O*-(2-Propyn-1-yl)-*L*-tyrosine (Prtyr), *N*6-[(2-Propyn-1-yloxy)carbonyl]-*L*-lysine (Prlys), 5-azido-*L*-norvaline (Aznva), and 6-azido-*L*-norleucine (Aznle) hydrochloride were obtained from BAPEKS sia. Propyn-1-yl-*L*-glycine (Prgly), 3-azido-*L*-alanine hydrochloride (Azala), and 2-amino-4-azido-*L*-butyric acid hydrochloride (Aabu), and 3-(2-furyl)-*L*-

alanine (Furala) were purchased from Iris Biotech GmbH. *N*<sub>ω</sub>-Nitro-L-arginine (Narg), 3-azido-7-hydroxycoumarin, sodium ascorbate, tris(3-hydroxypropyltriazolylmethyl)amine (THPTA), and copper(II) sulfate were purchased from Carl Roth GmbH+Co. KG. Aminoguanidine hydrochloride was obtained from Merck KGaA. Acetonitrile in HPLC and MS purity grade as well as formic acid were purchased from Honeywell Specialty Chemicals Seelze GmbH, and water in MS purity grade was obtained from AppliChem GmbH.

**Cyanobacterial Cultivation and Supplementation Experiments.** The *Microcystis* strains CBT 1, CBT 275, CBT 480, CBT 633, CBT 959, *Planktothrix rubescens* CBT 329, and the *Nodularia* strains CBT 750 and CBT 786 were provided by Cyano Biotech GmbH (Berlin, Germany). All strains were cultured in BG11.<sup>102</sup> *Microcystis* CAWBG11 was obtained from the strain collection of the Cawthron Institute, Nelson, New Zealand. It was grown in both BG11 and MLA medium.<sup>59,103,104</sup> Cells were precultivated in Erlenmeyer flasks under low light conditions (30 μmol/s·m<sup>2</sup>) at 28 °C on a shaker at 70 rpm. For CBT 1, CBT 275, CBT 480, CBT 633, and CBT 959, PDB experiments were performed in 10 mL scale using polystyrene tubes with bottom-mounted gas supply membranes (HD10 cultivators, CellDEG GmbH) under high light conditions (100 μmol/s·m<sup>2</sup>) with bubble-free supply with 5% CO<sub>2</sub> on a shaker at 260 rpm. For CAWBG11, PDB experiments were performed in closed Erlenmeyer flasks with 50 mL culture volume under the same conditions as in precultivation. In both schemes, cells were inoculated at an optical density of 0.5 at 750 nm. Stock solutions of the precursors were prepared (1 mM in water) and added to the culture medium right after inoculation to reach a final concentration of 10 μM. Additional precursor was added iteratively every 24 h over 3 days to a final concentration of 30 μM. If strains grew slowly and the substrate was tolerated well, the incubation time was extended to 9 or 15 days, and the concentration of substrate was increased to a final concentration of 90 and 150 μM, respectively. Growth of cultures was monitored daily by measurements of the optical density at 750 nm (OD<sub>750</sub>).

**Biomass Extraction and LC-MS Analysis.** After cultivation, the biomass was separated from the medium by centrifugation and lyophilized. The lyophilized biomass was extracted with MeOH (50 μL/mg dried biomass) in three cycles consisting of sonication for 3 min with a sonotrode (70% power; 60% cycle duty), shaking at room temperature for 10 min, and centrifugation (13 000g; 10 min). After each cycle, the supernatant was collected, and fresh solvent was added to the pellet. The combined supernatants were concentrated to dryness *in vacuo* using a vacuum centrifuge. For LC-MS analysis, the dried extracts were redissolved in MeOH to a final concentration of 2.5 mg extract per mL. After centrifugation, the samples were analyzed with a LC-MS system consisting of an Agilent Ion Trap 6330 coupled to an Agilent 1260 HPLC, a Q Exactive Plus coupled to an UltiMate 3000 HPLC (Thermo Fisher Scientific), or a LCMS-8040 Tandem Quadrupole Mass Spectrometer coupled to a Nexera HPLC (Shimadzu) after separation on a Kinetex 2.6 μm C18 100 Å 100 × 3.0 mm column (Phenomenex). Raw data were analyzed using FreeStyle 1.5 (Thermo Fisher Scientific), ACD/MS Workbook Suite 2017 (Advanced Chemistry Development), or LabSolution Version 5 (Shimadzu). MS<sup>2</sup> spectra were annotated with the *in silico* fragmentation tool mMass.<sup>105</sup>

**Prtyr Uptake and Production of Compound 2.** *Microcystis aeruginosa* strain CBT 480 was precultivated in Erlenmeyer flasks under low light conditions (30 μmol/s·m<sup>2</sup>) at 28 °C on a shaker at 120 rpm. For Prtyr uptake and production studies, the cells were grown in 50 mL centrifuge tubes under the same conditions and supplemented with 5% CO<sub>2</sub> (2 L/h). The experiment was carried out in biological triplicate. Samples of 1 mL were drawn immediately, and after 4, 8, 12, 24, 36, 48, 72, and 96 h. After determination of the OD<sub>750</sub> to monitor the culture growth, the biomass and supernatant were separated by centrifugation at 10 000g for 5 min. Both biomass and supernatant samples were lyophilized. Prtyr was quantified from the supernatant after redissolving the lyophilized sample in MeOH, centrifugation, and analysis by HPLC-DAD on a Thermo UltiMate 3000 instrument. The samples were injected in triplicate on a Kinetex 2.6 μm C18 100 Å 100 × 3.0 mm column and eluted with 100% H<sub>2</sub>O

+ 0.1% (v/v) formic acid over 5 min followed by a linear gradient from 100% H<sub>2</sub>O + 0.1% (v/v) formic acid to 100% MeCN + 0.1% (v/v) formic acid over 7 min at 25 °C. The run was monitored by UV detection at 254 nm, and the peak corresponding to Prtyr was integrated for quantitation. Calibration was carried out under the same conditions giving a linear curve ( $R^2 = 0.999$ ) for concentrations from 0 to 100 μM Prtyr. Data were analyzed using Chromleon 7 (Thermo Fisher Scientific) and processed with PRISM 6 (GraphPad Software Inc.).

In order to determine the production of **2**, the lyophilized biomass was extracted with MeOH as described above. After drying *in vacuo*, the samples were dissolved in MeOH, and **2** was quantified by HPLC-DAD on a Thermo UltiMate 3000 instrument using a Kinetex 2.6 μm C18 100 Å 100 × 3.0 mm column and a linear gradient of 5–100% MeCN + 0.1% (v/v) formic acid in H<sub>2</sub>O + 0.1% (v/v) formic acid over 15 min. Calibration was carried out under the same conditions giving a linear curve ( $R^2 = 0.999$ ) for 0.1 to 1 nmol of **2** on-column, which corresponds to a recovery of 0.2–2% Prtyr as compound **2**. Data were analyzed using Chromleon 7 (Thermo Fisher Scientific) and processed with PRISM 6 (GraphPad Software Inc.).

**Isolation and Structure Elucidation of Compound 2.** First, 63.5 g of dry biomass from a CBT 480 culture supplemented with Prtyr was extracted with 80% MeOH/H<sub>2</sub>O (v/v) (60 mg/mL dried biomass) in two cycles consisting of sonication for 1 min with a sonotrode (100% power; 100% cycle duty) on ice, shaking at room temperature for 20 min, and centrifugation (13 000g; 20 min). After each cycle, the supernatant was collected, and fresh solvent was added to the pellet. The combined supernatants were concentrated to dryness *in vacuo* using a rotary evaporator. The resulting 5.13 g of extract was dissolved in 20% MeOH/H<sub>2</sub>O (v/v) (5 mg/mL), loaded on C18 cartridges on a VersaFlash system (Supelco), and fractionated using a two-step elution with 80% MeOH/H<sub>2</sub>O (v/v) followed by 100% MeOH. The fractions containing **2** (monitored by HPLC) were dried *in vacuo*. The resulting 371 mg of semipure **2** eluted with 80% MeOH/H<sub>2</sub>O (v/v) was redissolved in DMSO/MeOH/MeCN (70:20:10 (v/v/v)) (200 mg/mL) and subjected to semipreparative HPLC on a LC-10 vp series (Shimadzu) using a Gemini 5 μm C6, 10 × 250 mm column (Phenomenex). The analytes were eluted with a linear gradient of aqueous MeOH with 0.025% trifluoroacetic acid, starting with 45%, increasing to 51% in 30.0 min at 55 °C and detection at 238 nm. **2** eluted at 26–27 min. Fractions containing **2** were combined and freeze-dried yielding 40 mg of **2**. Compound **2** was analyzed by LC-HRMS and HPLC-DAD/ELSD (Figures S93 and S94; purity about 90%).

Fifteen milligrams of **2** was dissolved in 1 mL of DMSO-*d*<sub>6</sub>. NMR experiments were performed on a Varian/Agilent VNMRs spectrometer operating at 600 MHz (<sup>1</sup>H). Chemical shifts were referenced to the residual solvent signals ( $\delta_{\text{H}} = 2.50$  ppm,  $\delta_{\text{C}} = 39.5$  ppm). NMR data were analyzed with ACD/Structure Elucidator Suite 2018.2 (Figures S95–S103).

**Conjugation of 2 with 3-Azido-7-hydroxycoumarin.** According to the optimized protocol for click reactions as previously described,<sup>87</sup> 1 μM copper(II) sulfate (50 equiv) and 5 μM THPTA (250 equiv) were preincubated in H<sub>2</sub>O (total volume: 100 mL) for several min. After addition of 125 equiv of aminoguanidine, 5 equiv of 3-azido-7-hydroxycoumarin and 1 equiv of **2**, the reaction was started with 1250 equiv of sodium ascorbate, and stirred for 2 h at room temperature. The reaction mix was loaded on a preconditioned Strata C-18-E SPE cartridge (55 μm, 70 Å, 200 mg sorbent, Phenomenex), eluted with 1 mL of MeOH and dried *in vacuo*. The resulting crude reaction product was redissolved in DMSO, and the fluorescent product **3** was isolated in two steps via HPLC on a Hitachi LaChrom (Merck) coupled to the fluorescence detector module L-7485 with the wavelengths set to 404 nm for excitation and 480 nm for emission. The crude reaction product was prepurified on a Luna C-18 column (5 μm; 4.6 × 250 mm, Phenomenex) with gradient elution from 30–50% MeCN in H<sub>2</sub>O containing 0.1% formic acid as modifier over 15 min. The fractions containing **3** were combined, dried *in vacuo*, and redissolved in MeOH. HPLC-DAD analysis revealed a nonfluorescent byproduct, thus for final purification, the same column was used with

a gradient from 5–70% MeCN in H<sub>2</sub>O containing 0.1% formic acid as modifier over 15 min. The structure of **3** was confirmed by HRMS<sup>2</sup> (Figure S105 and Table S10).

**Quantification of **3** by HPLC-ELSD.** The concentration of the test solution of **3** for the cytotoxicity assays and fluorescence microscopy was quantified by HPLC coupled to an ELSD (Sedex 85, Sedere). Certified reference material (CRM) of MC-RR (9.91 μM, National Research Council, Canada) was used as standard to establish a calibration curve from 100 to 300 ng on-column. Five volumes between 9.2 and 24.3 μL of CRM MC-RR were injected in triplicate on a Kinetex C18 column (100 × 3.1 mm, 5 μm, 100 Å) and eluted with a gradient from 10–100% MeCN in H<sub>2</sub>O (0.1% formic acid each) over 10 min at a flow rate of 0.65 mL/min. Settings of the ELSD were as follows: evaporation temperature 40 °C, gain 11, N<sub>2</sub> pressure 4 bar. ELSD response areas were averaged, and log(ELSD response area) was plotted against log(amount in ng) to generate a linear calibration curve. The accuracy of a structure-independent quantification of MC congeners was checked by injecting 150, 200, and 250 ng of CRM MC-LR (10.2 μM, National Research Council, Canada) in triplicate under identical conditions and found to range between 99.2 and 100.8%. **3** was dissolved in 1 mL of DMSO. Fifteen microliters of this solution was injected in triplicate under the same conditions. The on-column amount was quantified as 146 ng, corresponding to a concentration of 7.58 μM of test solution of **3**. This solution was used as stock solution for all subsequent experiments.

**Cell Culture and Cytotoxicity Assay.** HEK293 cells, stably transfected with the expression vectors pcDNA3.1(+)-OATP1B1 and pcDNA3.1/Hygro(-)-OATP1B3, and the respective empty vectors pcDNA3.1(+) and pcDNA3.1/Hygro(-) as controls were kindly provided by Prof. Dr. Joerg Koenig (Friedrich-Alexander-University Erlangen-Nuernberg, Germany).<sup>106</sup> All four cell lines were maintained in minimal essential medium, supplemented with 10% heat-inactivated fetal bovine serum, nonessential amino acid mix and 2 mM glutamine at 37 °C and 5% CO<sub>2</sub>, and routinely subcultured by trypsinization. HEK293 OATP1B1<sup>+</sup> and the corresponding control cell line were constantly selected with 800 μg/mL G418, while 250 μg/mL of hygromycin B were used for the selection of HEK293 OATP1B3<sup>+</sup> and its empty vector control. Every 3 to 6 months, all cell lines were tested for mycoplasma contamination as described before.<sup>107</sup> Roti-CELL glutamine solution was purchased from Carl Roth GmbH+Co. KG. Hygromycin B solution was obtained from InvivoGen. All other cell culture reagents were purchased from Merck KGaA.

In order to determine the cytotoxicity of **1**, **2**, and **3**, 50 000 cells per well of each cell line were seeded in a 96-well flat-bottom plate in triplicate without the respective selection markers. After 24 h, transporter expression was induced by addition of 10 mM sodium butyrate. After 24 h, the medium containing the inducer was removed, and all cell lines were incubated for 48 h with either **1**, **2**, or **3**, dissolved in standard medium without selection markers, at concentrations from 0.1 nM to 2 μM. Subsequently, the cell lines were fixed, washed, and stained with sulforhodamine B as previously described,<sup>108</sup> and the absorbance at 510 nm was measured with a TECAN Infinite M200 Pro plate reader. After normalization, GraphPad PRISM 6 was used to plot the data. A sigmoidal, four-parameter logarithmic curve, from which the EC<sub>50</sub> were deduced, was fitted using the log<sub>10</sub>(x) values for the concentration. The model can also be described by  $Y = \text{Bottom} + (\text{Top} - \text{Bottom}) / (1 + 10^{-(\text{LogEC}_{50} - X) \cdot \text{HillSlope}})$ . Each measurement was repeated twice independently.

**Measurement of Excitation and Emission Spectra of **3**.** **3** was dissolved in DMSO to a final concentration of 90 mM and diluted 1:10 with standard minimal essential medium with supplements as used for cell culture. The excitation spectra for both solutions were recorded at a fixed emission wavelength of 480 nm with a TECAN Infinite M200 Pro plate reader. Accordingly, the emission spectra were measured with fixed excitation at 404 nm, and the curves were plotted using PRISM 6. The excitation maximum was found to

be 404 nm, the emission maximum was determined as 474 nm for the solution in cell culture medium.

**Fluorescence Microscopy of **3** after Addition to HEK293 Cells.** The four HEK293 cell lines were seeded into a 96-well plate and treated as described above for cytotoxicity profiling. After removal of the inducer, colonies of HEK293 cells were inspected with a confocal laser-scanning microscope (Nikon AIR) equipped with a 10× dry objective (CFI Plan Apo Lambda, Nikon, numerical aperture 0.45) and an O<sub>2</sub>/CO<sub>2</sub> cage incubator (okolab) at 37 °C and 5% CO<sub>2</sub>. Fluorescence of **3** was excited using the 405 nm line of a diode laser (CUBE 405–100C, Coherent), and fluorescence emission was detected in the range of 465–500 nm (GaAsP detector, Nikon). In addition, a brightfield image was acquired using the 514 nm laser line of an argon laser (Melles Griot) and a transmitted light detector (TD, Nikon). Time-lapse video microscopy was applied to monitor the uptake of **3** into the cells. After recording untreated baseline fluorescence levels of the cells for 5 min, **3** was added to the medium at a final concentration of 100 nM and the cells were monitored for an additional 20 min. Images were processed using NIS Elements (Nikon) to enhance brightness and contrast both equally to induced group and control.

## ■ ASSOCIATED CONTENT

### Supporting Information

The Supporting Information is available free of charge at <https://pubs.acs.org/doi/10.1021/acs.jnatprod.0c00251>.

Annotated MS<sup>3</sup> of MC-AzpheR and annotated MS<sup>2</sup> of **2**, LC-MS data for clickable MCs from CBT 480, CBT 1, CBT 633, CBT 275, CBT 959, CAWGB11, and CBT 329. HPLC chromatogram, HRMS spectrum and NMR spectra of **2**; HPLC chromatogram, MS<sup>2</sup> spectrum and annotation of **3** (PDF)

### Web-Enhanced Feature

Time-lapse movie of MC uptake into HEK293 OATP1B3<sup>+</sup>

## ■ AUTHOR INFORMATION

### Corresponding Author

**Timo H. J. Niedermeyer** – Department of Pharmaceutical Biology/Pharmacognosy, Institute of Pharmacy, University of Halle-Wittenberg, 06120 Halle (Saale), Germany; Interfaculty Institute of Microbiology and Infection Medicine, Eberhard Karls University Tübingen, 72076 Tübingen, Germany; [orcid.org/0000-0003-1779-7899](https://orcid.org/0000-0003-1779-7899); Phone: +49 345 55 25765; Email: [timo.niedermeyer@pharmazie.uni-halle.de](mailto:timo.niedermeyer@pharmazie.uni-halle.de); Fax: +49 345 55 27407

### Authors

**Julia Moschny** – Department of Pharmaceutical Biology/Pharmacognosy, Institute of Pharmacy, University of Halle-Wittenberg, 06120 Halle (Saale), Germany; Interfaculty Institute of Microbiology and Infection Medicine, Eberhard Karls University Tübingen, 72076 Tübingen, Germany  
**Wolfram Lorenzen** – Cyano Biotech GmbH, 12489 Berlin, Germany  
**Alexandra Hilfer** – Cyano Biotech GmbH, 12489 Berlin, Germany  
**Robert Eckenstaler** – Department of Clinical Pharmacy and Pharmacotherapy, Institute of Pharmacy, Martin-Luther-University Halle-Wittenberg, 06120 Halle (Saale), Germany  
**Stefan Jahns** – Cyano Biotech GmbH, 12489 Berlin, Germany  
**Heike Enke** – Cyano Biotech GmbH, 12489 Berlin, Germany  
**Dan Enke** – Cyano Biotech GmbH, 12489 Berlin, Germany







## A.5. Supplementary information to Chapter 3.3. - Precursor-Directed Biosynthesis

MS<sup>3</sup> multiple reaction scheme:  $[M+H]^+$   $\xrightarrow{MS^2}$   $[(M-N_2)+H]^+$   $\xrightarrow{MS^3}$  Annotation  
 1070.59  $\longrightarrow$  1042.57  $\longrightarrow$  Annotation

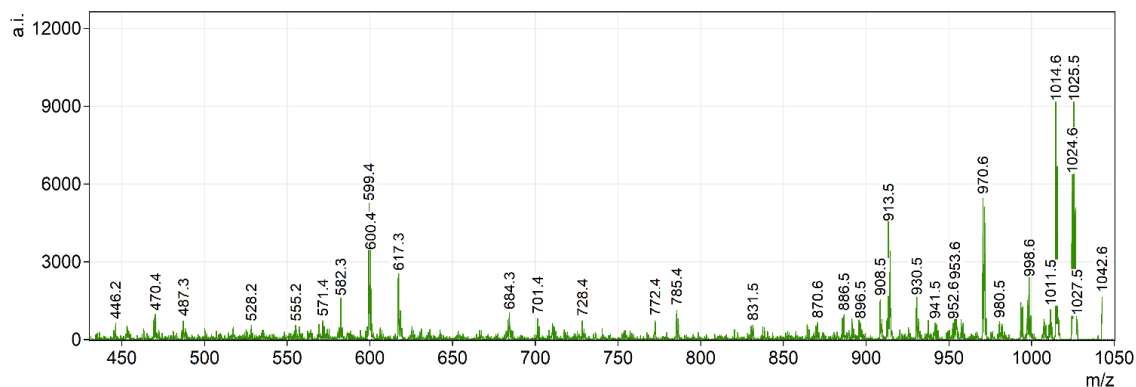
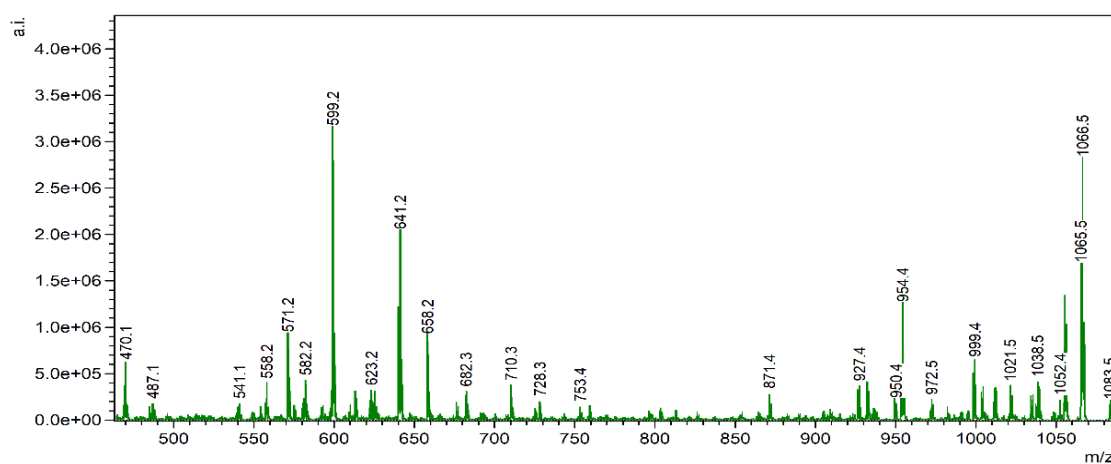


Figure A18. MS<sup>3</sup> spectrum of MC-AzpheR.

Table A3. Annotation of the MS<sup>3</sup> spectrum of MC-AzpheR. Fragments containing Azphe or related species are highlighted in bold. Mdha, *N*-methyl dehydroalanine; Masp,  $\beta$ -methyl aspartic acid; Adda, 3*S*-amino-9*S*-methoxy-2*S*,6,8*S*-trimethyl-10-phenyldeca-4*E*,6*E*-dienoic acid.

<i>m/z</i>	Annotation	Ion	Difference [Da]
1042.6	<b>(M - N<sub>2</sub>) + H<sup>+</sup></b>	-	<b>+ 0.1</b>
1025.5	<b>(M - N<sub>2</sub>) - NH<sub>3</sub> + H<sup>+</sup></b>	-	<b>0.0</b>
1024.6	<b>(M - N<sub>2</sub>) - H<sub>2</sub>O + H<sup>+</sup></b>	-	<b>+ 0.1</b>
1014.6	<b>(M - N<sub>2</sub>) - H<sub>2</sub>CN + H<sup>+</sup></b>	-	<b>+ 0.1</b>
970.6	<b>(M - N<sub>2</sub>) - H<sub>2</sub>CN - CO<sub>2</sub> + H<sup>+</sup></b>	-	<b>0.0</b>
913.5	<b>Mdha-Ala-(Azphe-N<sub>2</sub>)-Masp-Arg-Adda + H<sup>+</sup> or</b> <b>Arg-Adda-Glu-Mdha-Ala-(Azphe - N<sub>2</sub>) + H<sup>+</sup></b>	<b>b<sup>6</sup>/y<sup>6</sup></b> <b>b<sup>6</sup>/y<sup>6</sup></b>	<b>0.0</b>
895.5	<b>Mdha-Ala-(Azphe - N<sub>2</sub>)-Masp-Arg-Adda - H<sub>2</sub>O + H<sup>+</sup> or</b> <b>Arg-Adda-Glu-Mdha-Ala-(Azphe - N<sub>2</sub>) - H<sub>2</sub>O + H<sup>+</sup></b>	<b>b<sup>6</sup>/y<sup>6</sup></b> <b>b<sup>6</sup>/y<sup>6</sup></b>	<b>+ 0.1</b>
886.5	<b>Adda-Glu-Mdha-Ala-(Azphe - N<sub>2</sub>)-Masp + H<sup>+</sup></b>	<b>b<sup>6</sup>/y<sup>6</sup></b>	<b>+ 0.1</b>
785.4	<b>(Azphe - N<sub>2</sub>)-Masp-Arg-Adda + H<sup>+</sup></b>	<b>x<sup>4</sup></b>	<b>0.0</b>
728.4	Masp-Arg-Adda-Glu + H <sup>+</sup>	b <sup>4</sup> /y <sup>4</sup>	0.0
701.4	<b>Glu-Mdha-Ala-(Azphe - N<sub>2</sub> - H<sub>2</sub>CN)-Masp-Arg + H<sup>+</sup></b>	<b>b<sup>6</sup>/y<sup>6</sup></b>	<b>+ 0.1</b>
617.3	<b>Mdha-Ala-(Azphe - N<sub>2</sub>)-Masp-Arg + H<sup>+</sup></b>	<b>c<sup>5</sup></b>	<b>0.0</b>
600.4	<b>Mdha-Ala-(Azphe - N<sub>2</sub>)-Masp-Arg + H<sup>+</sup></b>	<b>b<sup>5</sup>/y<sup>5</sup></b>	<b>+ 0.1</b>
599.4	Masp-Arg-Adda + H <sup>+</sup> or Arg-Adda-Glu + H <sup>+</sup>	b <sup>3</sup> /y <sup>3</sup>	0.0

571.4	Masp-Arg-Adda + H <sup>+</sup> or Arg-Adda-Glu + H <sup>+</sup>	a <sup>3</sup>	+ 0.1
555.2	Mdha-Ala-(Azphe - N <sub>2</sub> - H <sub>2</sub> CN)-Masp-Arg + H <sup>+</sup>	z <sup>5</sup>	0.0
528.2	Glu-Mdha-Ala-(Azphe - N <sub>2</sub> - H <sub>2</sub> CN)-Masp + H <sup>+</sup>	z <sup>5</sup>	+ 0.1
446.2	(Azphe-N <sub>2</sub> )-Masp-Arg + H <sup>+</sup>	b <sup>3</sup> /y <sup>3</sup>	0.0



**Figure A19.** MS<sup>2</sup> spectrum of **3**.

**Table A4.** Annotation of the MS<sup>2</sup> spectrum of **3**. Fragments containing Prtyr are highlighted in bold. Mdha, *N*-methyl dehydroalanine; Masp,  $\beta$ -methyl aspartic acid; Adda, 3*S*-amino-9*S*-methoxy-2*S*,6,8*S*-trimethyl-10-phenyldeca-4*E*,6*E*-dienoic acid.

<i>m/z</i>	Annotation	Ion	Difference [Da]
1083.5	<b>M + H<sup>+</sup></b>	-	0.0
1066.5	<b>M - NH<sub>3</sub> + H<sup>+</sup></b>	-	0.0
1065.5	<b>M - H<sub>2</sub>O + H<sup>+</sup></b>	-	0.0
1012.5	<b>Prtyr-Masp-Arg-Adda-Glu-Mdha + H<sup>+</sup></b>	<b>b<sup>6</sup>/y<sup>6</sup></b>	0.0
954.4	<b>Mdha-Ala-Prtyr-Masp-Arg-Adda + H<sup>+</sup></b> <b>Arg-Adda-Glu- Mdha-Ala-Prtyr + H<sup>+</sup></b>	<b>b<sup>6</sup>/y<sup>6</sup></b> <b>b<sup>6</sup>/y<sup>6</sup></b>	- 0.1
949.5	<b>M - C<sub>9</sub>H<sub>10</sub>O + H<sup>+</sup></b>	-	- 0.1
927.4	<b>Adda-Glu-Mdha-Ala-Prtyr-Masp + H<sup>+</sup></b>	<b>b<sup>6</sup>/y<sup>6</sup></b>	0.0
871.4	<b>Ala-Prtyr-Masp-Arg-Adda + H<sup>+</sup></b>	<b>b<sup>5</sup>/y<sup>5</sup></b>	- 0.1
753.4	Arg-Adda-Glu-Mdha-Ala + H <sup>+</sup>	b <sup>5</sup> /y <sup>5</sup>	- 0.1
728.3	Masp-Arg-Adda-Glu + H <sup>+</sup>	b <sup>4</sup> /y <sup>4</sup>	- 0.1
710.3	Masp-Arg-Adda-Glu - H <sub>2</sub> O + H <sup>+</sup>	b <sup>4</sup> /y <sup>4</sup>	- 0.1
682.3	Arg-Adda-Glu-Mdha + H <sup>+</sup>	b <sup>4</sup> /y <sup>4</sup>	-0.1
658.2	<b>Mdha-Ala-Prtyr-Masp-Adda + H<sup>+</sup></b>	<b>c<sup>5</sup></b>	-0.1
641.2	<b>Mdha-Ala-Prtyr-Masp-Arg + H<sup>+</sup></b>	<b>b<sup>5</sup>/y<sup>5</sup></b>	-0.1
623.2	<b>Mdha-Ala-Prtyr-Masp-Arg + H<sup>+</sup></b>	<b>x<sup>4</sup></b>	- 0.1

599.2	Masp-Arg-Adda + H <sup>+</sup> or Arg-Adda-Glu + H <sup>+</sup>	$y^3/b^3$	- 0.1
571.2	Masp-Arg-Adda + H <sup>+</sup> or Arg-Adda-Glu + H <sup>+</sup>	$a^3$	- 0.1
<b>558.2</b>	<b>Ala-Prtyr-Masp-Arg + H<sup>+</sup></b>	<b><math>b^4/y^4</math></b>	<b>- 0.1</b>

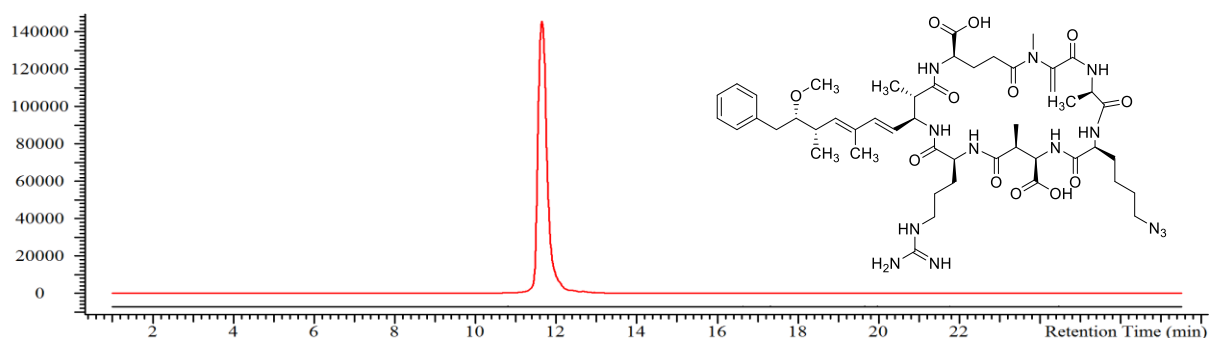


**Figure A20.** Extracted ion chromatogram (EIC,  $m/z$  1036.5, pos. mode) overlay of an *M. aeruginosa* CBT 480 control culture (black, lower trace) and a culture grown with 30  $\mu$ M Aznl (red, upper trace)

	Formula	Ion	Measured $m/z$	Calculated $m/z$	Difference (Da)
MC-AznlR	$C_{49}H_{73}N_{13}O_{12}$	$[M+H]^+$	1036.5	1036.5	0.0

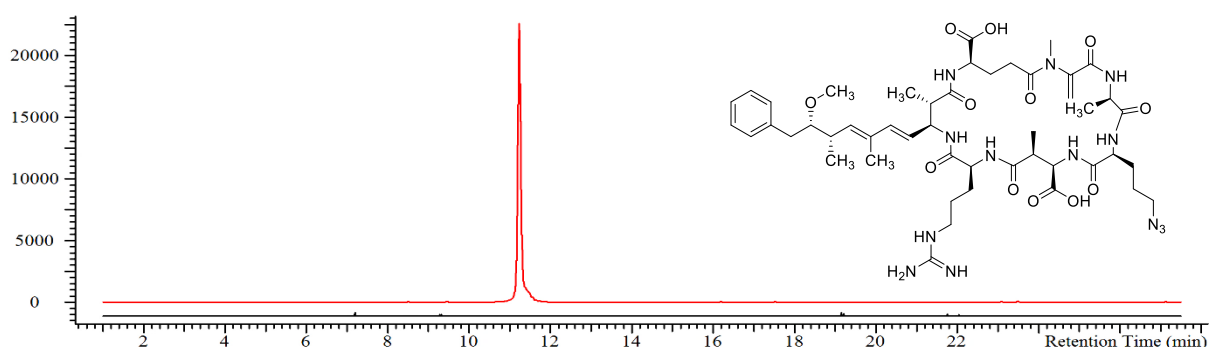


**Figure A21.** EIC ( $m/z$  1022.5, pos. mode) overlay of an *M. aeruginosa* CBT 480 control culture (black, lower trace) and a culture grown with 30  $\mu$ M Azva (red, upper trace).

	Formula	Ion	Measured $m/z$	Calculated $m/z$	Diff. (Da)
MC-AzvaR	$C_{48}H_{71}N_{13}O_{12}$	$[M+H]^+$	1022.5	1022.5	0.0

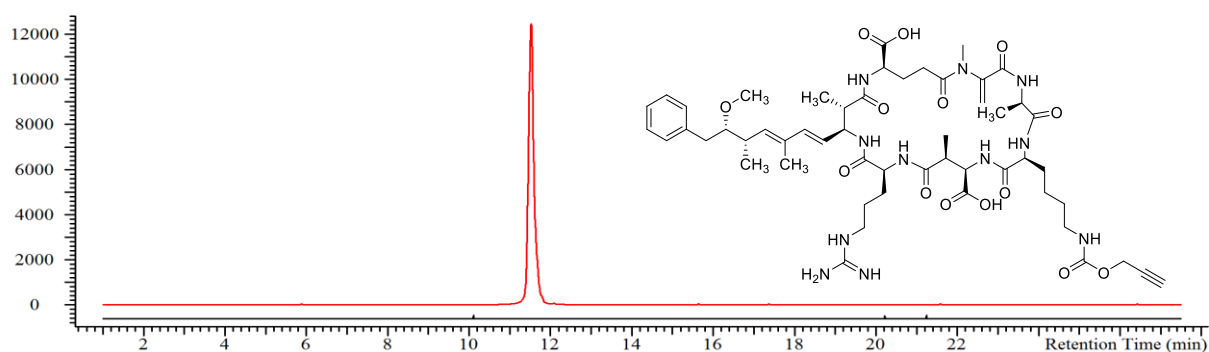


**Figure A22.** EIC ( $m/z$  1092.5, pos. mode) overlay of an *M. aeruginosa* CBT 480 control culture (black, lower trace) and a culture grown with 30  $\mu$ M Prlys (red, upper trace).

	Formula	Ion	Measured $m/z$	Calculated $m/z$	Difference (Da)
MC-PrlysR	$C_{53}H_{77}N_{11}O_{14}$	$[M+H]^+$	1092.5	1092.5	0.0

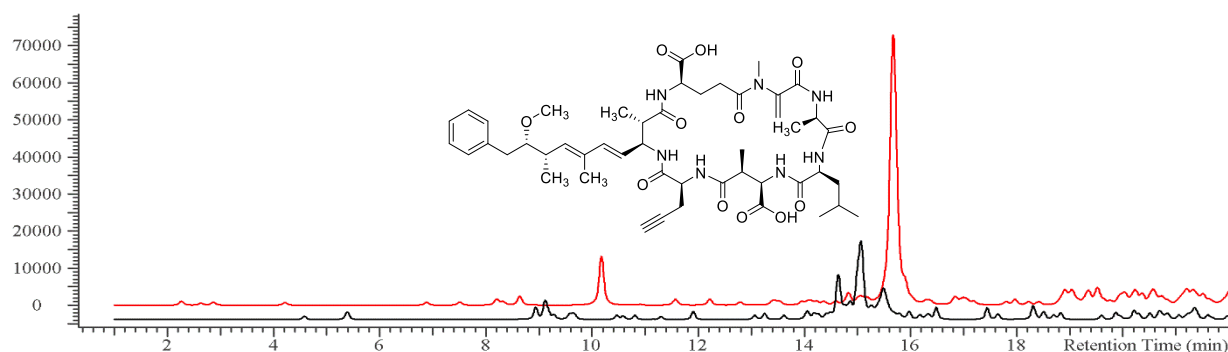


**Figure A23.** EIC ( $m/z$  934.4, pos. mode) overlay of an *M. aeruginosa* CBT 480 control culture (black, lower trace) and a culture grown with 30  $\mu$ M Prgly (red, upper trace).

	Formula	Ion	Measured $m/z$	Calculated $m/z$	Difference (Da)
MC-LPrgly	$C_{48}H_{67}N_7O_{12}$	$[M+H]^+$	934.4	934.4	0.0

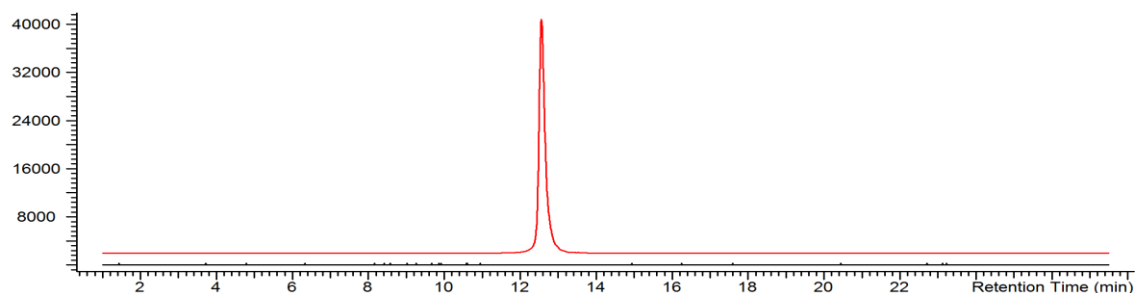


**Figure A24.** EIC ( $m/z$  1070.5, pos. mode) overlay of a *Microcystis* CBT 1 control culture (black, lower trace) and a culture grown with 30  $\mu$ M Azphe (red, upper trace).

	Formula	Ion	Measured $m/z$	Calculated $m/z$	Difference (Da)
MC-AzpheR	$C_{52}H_{71}N_{13}O_{12}$	$[M+H]^+$	1070.5	1070.5	0.0

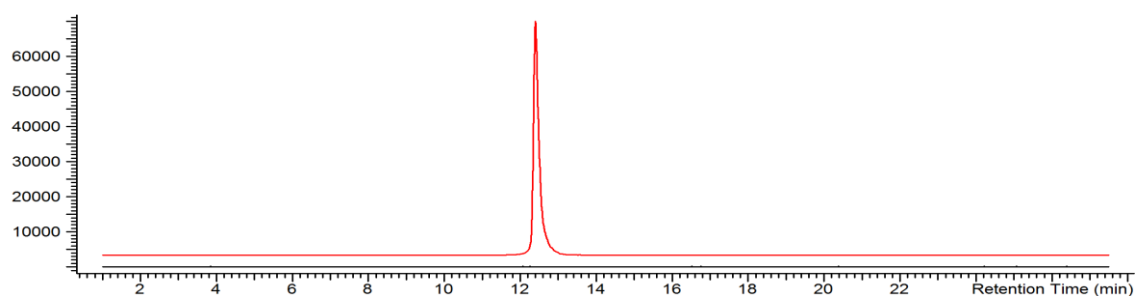


**Figure A25.** EIC ( $m/z$  1083.5, pos. mode) overlay of a *Microcystis* CBT 1 control culture (black, lower trace) and a culture grown with 30  $\mu$ M Prtyr (red, upper trace).

	Formula	Ion	Measured $m/z$	Calculated $m/z$	Difference (Da)
2	$C_{55}H_{74}N_{10}O_{13}$	$[M+H]^+$	1083.5	1083.5	0.0

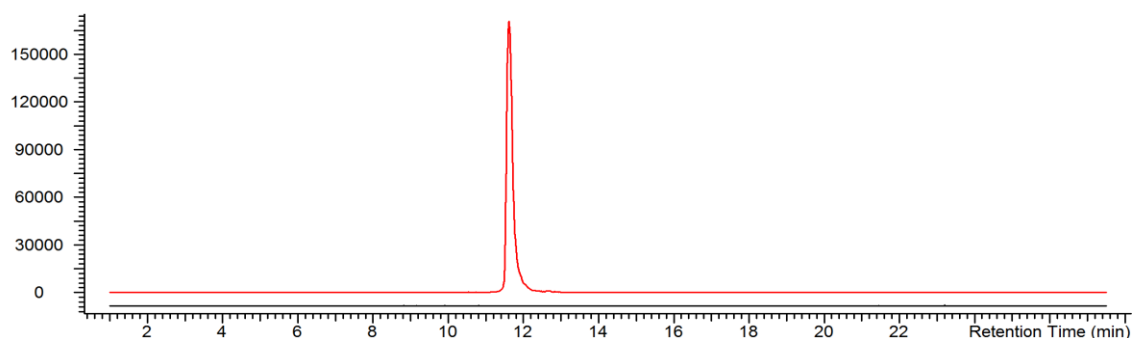


**Figure A26.** EIC ( $m/z$  1036.5, pos. mode) overlay of a *Microcystis* CBT 1 control culture (black, lower trace) and a culture grown with 30  $\mu$ M Aznle (red, upper trace).

	Formula	Ion	Measured $m/z$	Calculated $m/z$	Difference (Da)
MC-AznleR	$C_{49}H_{73}N_{13}O_{12}$	$[M+H]^+$	1036.5	1036.5	0.0

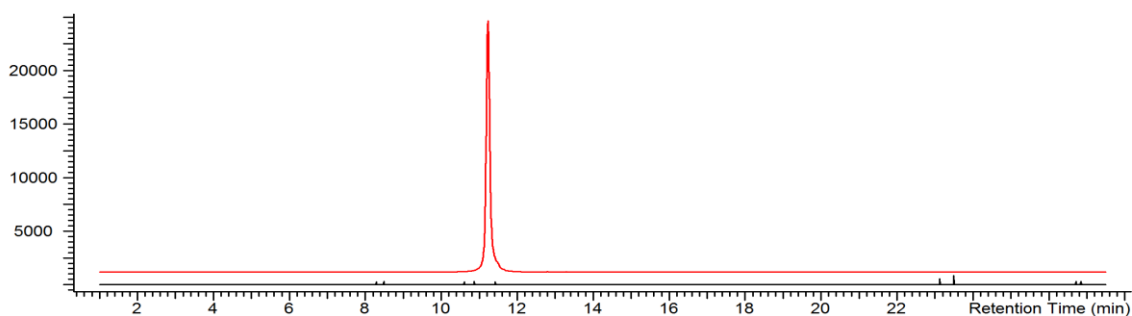


**Figure A27.** EIC ( $m/z$  1022.5, pos. mode) overlay of a *Microcystis* CBT 1 control culture (black, lower trace) and a culture grown with 30  $\mu$ M Aznva (red, upper trace).

	Formula	Ion	Measured $m/z$	Calculated $m/z$	Diff. (Da)
MC-AznvaR	$C_{48}H_{71}N_{13}O_{12}$	$[M+H]^+$	1022.5	1022.5	0.0

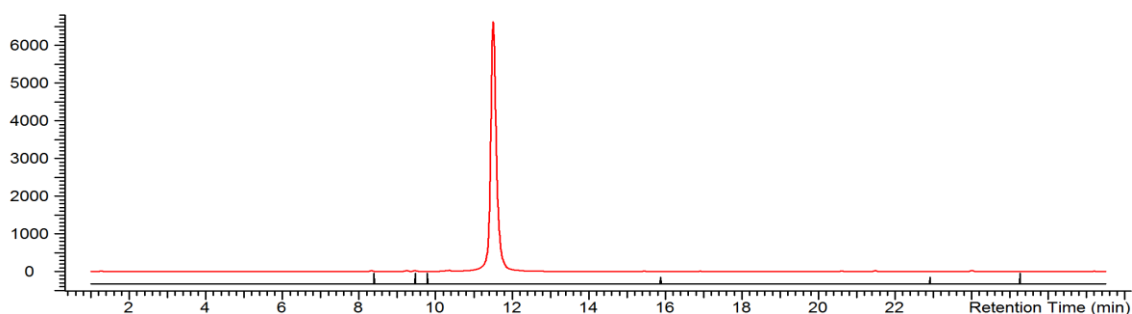


**Figure A28.** EIC ( $m/z$  1092.5, pos. mode) overlay of a *Microcystis* CBT 1 control culture (black, lower trace) and a culture grown with 30  $\mu$ M Prys (red, upper trace).

	Formula	Ion	Measured $m/z$	Calculated $m/z$	Difference (Da)
MC-PrysR	$C_{53}H_{77}N_{11}O_{14}$	$[M+H]^+$	1092.5	1092.5	0.0

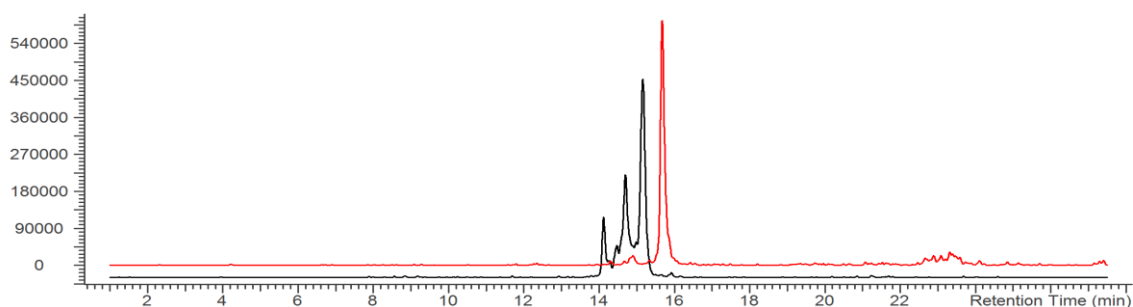


**Figure A29.** EIC ( $m/z$  934.3, pos. mode) overlay of a *Microcystis* CBT 1 control culture (black, lower trace) and a culture grown with 30  $\mu$ M Prgly (red, upper trace).

	Formula	Ion	Measured $m/z$	Calculated $m/z$	Difference (Da)
MC-LPrgly	$C_{48}H_{67}N_7O_{12}$	$[M+H]^+$	934.3	934.4	- 0.1

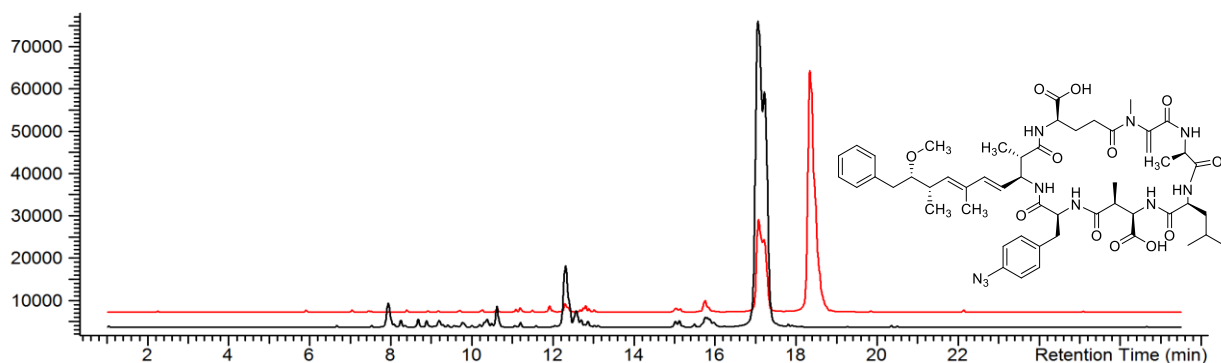


**Figure A30.** EIC ( $m/z$  1025.3, pos. mode) overlay of a *Microcystis* CBT 275 control culture (black, lower trace) and a culture grown with 30  $\mu$ M Azphe (red, upper trace).

	Formula	Ion	Measured $m/z$	Calculated $m/z$	Difference (Da)
MC-LAzphe	$C_{52}H_{70}N_{10}O_{12}$	$[M-H]^+$	1025.3	1025.5	- 0.2

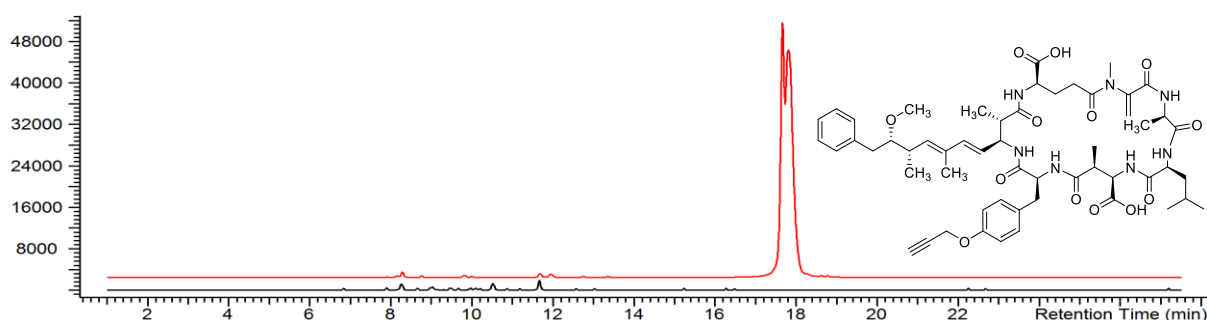


**Figure A31.** EIC ( $m/z$  1038.3, pos. mode) overlay of a *Microcystis* CBT 275 control culture (black, lower trace) and a culture grown with 30  $\mu$ M Prtyr (red, upper trace).

	Formula	Ion	Measured $m/z$	Calculated $m/z$	Difference (Da)
MC-LPrtyr	$C_{55}H_{73}N_7O_{13}$	$[M-H]^-$	1038.3	1038.5	- 0.2



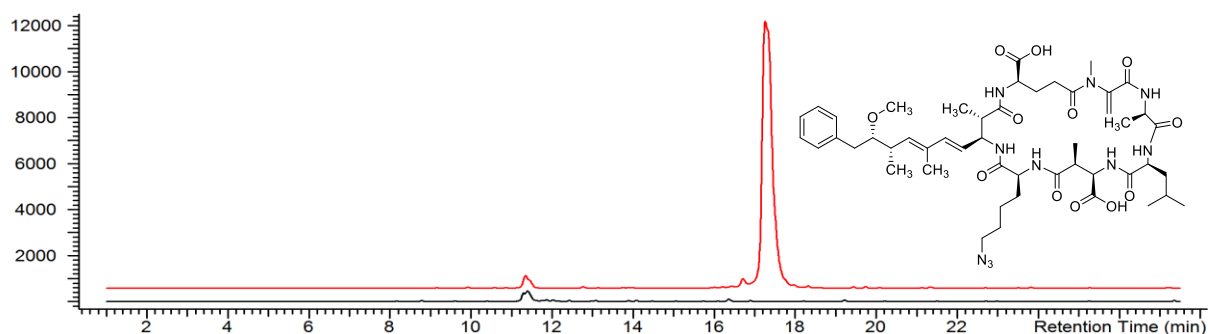


**Figure A32.** EIC ( $m/z$  993.5, pos. mode) overlay of a *Microcystis* CBT 275 control culture (black, lower trace) and a culture grown with 30  $\mu\text{M}$  Aznle (red, upper trace).

	Formula	Ion	Measured $m/z$	Calculated $m/z$	Difference (Da)
MC-LAznle	$\text{C}_{49}\text{H}_{72}\text{N}_{10}\text{O}_{12}$	$[\text{M}+\text{H}]^+$	993.5	993.5	0.0

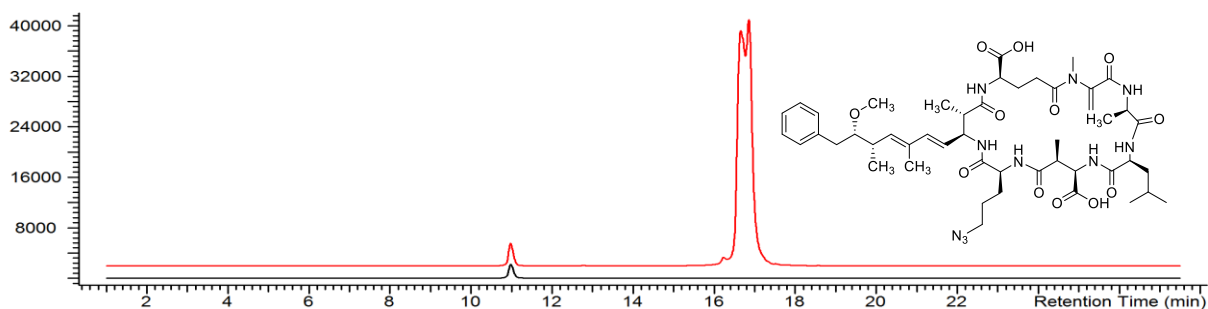


**Figure A33.** EIC ( $m/z$  979.4, pos. mode) overlay of a *Microcystis* CBT 275 control culture (black, lower trace) and a CBT 275 culture grown with 30  $\mu\text{M}$  Aznva (red, upper trace).

	Formula	Ion	Measured $m/z$	Calculated $m/z$	Difference (Da)
MC-LAznva	$\text{C}_{48}\text{H}_{70}\text{N}_{10}\text{O}_{12}$	$[\text{M}+\text{H}]^+$	979.4	979.5	- 0.1

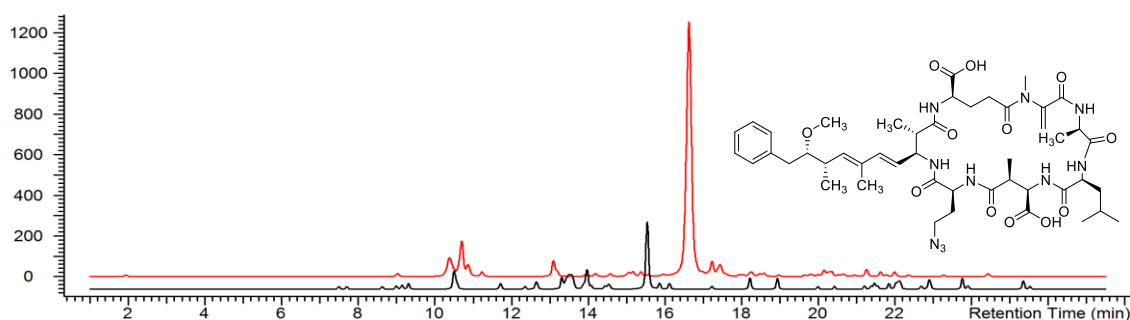


**Figure A34.** EIC ( $m/z$  965.4, pos. mode) overlay of a *Microcystis* CBT 275 control culture (black, lower trace) and a culture grown with 30  $\mu\text{M}$  Azabu (red, upper trace).

	Formula	Ion	Measured $m/z$	Calculated $m/z$	Difference (Da)
MC-LAzabu	$\text{C}_{47}\text{H}_{68}\text{N}_{10}\text{O}_{12}$	$[\text{M}+\text{H}]^+$	965.4	965.5	- 0.1

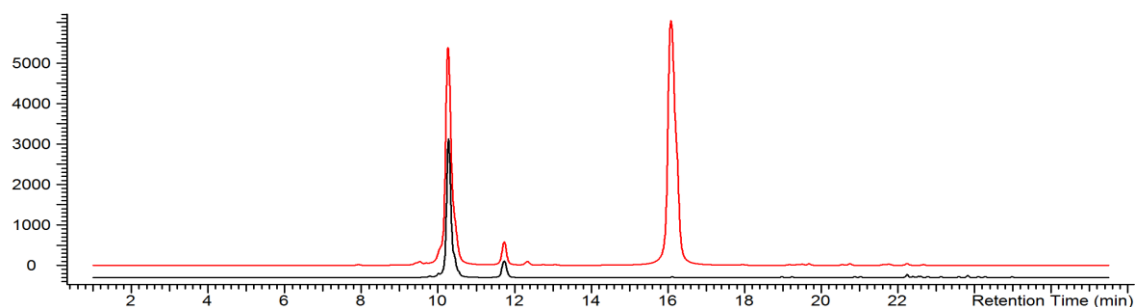


**Figure A35.** EIC ( $m/z$  1049.4, pos. mode) overlay of a *Microcystis* CBT 275 control culture (black, lower trace) and a culture grown with 30  $\mu\text{M}$  Prys (red, upper trace).

	Formula	Ion	Measured $m/z$	Calculated $m/z$	Difference (Da)
MC-LPrys	$\text{C}_{53}\text{H}_{76}\text{N}_8\text{O}_{14}$	$[\text{M}+\text{H}]^+$	1049.4	1049.5	- 0.1

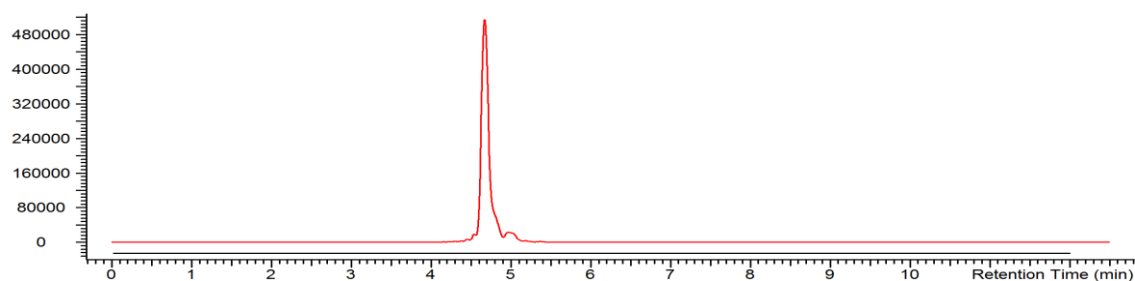


**Figure A36.** EIC ( $m/z$  1036.5574, pos. mode) overlay of a *Microcystis* CBT 633 control culture (black, lower trace) and a culture grown with 30  $\mu\text{M}$  Aznle (red, upper trace). The  $t_R$  is identical with the  $t_R$  of MC-AznleR from CAWBG11 (Figure A60).

	Formula	Ion	Measured $m/z$	Calculated $m/z$	Difference (Da)
MC-AznleR	$\text{C}_{49}\text{H}_{73}\text{N}_{13}\text{O}_{12}$	$[\text{M}+\text{H}]^+$	1036.5573	1036.5574	- 0.0001

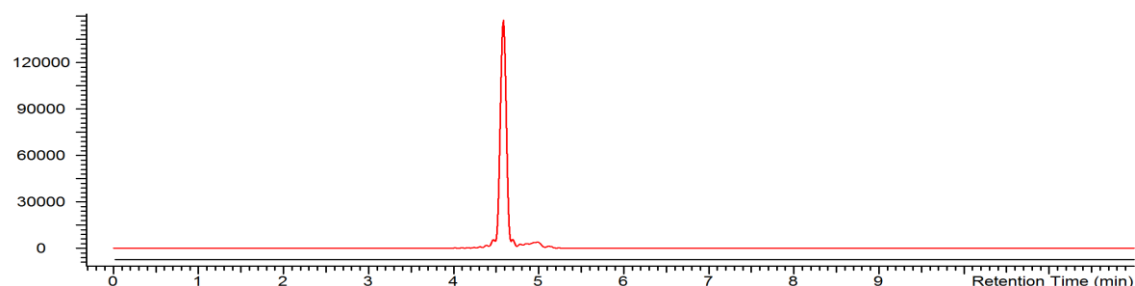


**Figure A37.** EIC ( $m/z$  1022.5418, pos. mode) overlay of a *Microcystis* CBT 633 control culture (black, lower trace) and a culture grown with 30  $\mu\text{M}$  Aznva (red, upper trace). The  $t_R$  (4.60 min; -0.06 min compared to MC-AznleR, see Figure A36) corresponds to the isomer MC-AznvaR.

	Formula	Ion	Measured $m/z$	Calculated $m/z$	Difference (Da)
MC-AznvaR	$\text{C}_{48}\text{H}_{71}\text{N}_{13}\text{O}_{12}$	$[\text{M}+\text{H}]^+$	1022.5418	1022.5418	0.000

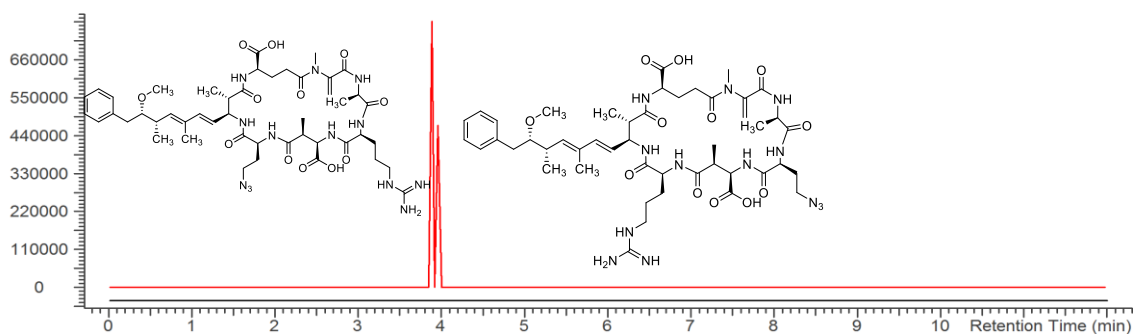


**Figure A38.** EIC ( $m/z$  1008.5242, pos. mode) overlay of a *Microcystis* CBT 633 control culture (black, lower trace) and a culture grown with 30  $\mu$ M Azabu (red, upper trace). The occurrence of two peaks indicates the co-formation of both isomers.

	Formula	Ion	Measured $m/z$	Calculated $m/z$	Difference (Da)
MC-AzabuR	$C_{47}H_{69}N_{13}O_{12}$	$[M+H]^+$	1008.5272	1008.5267	+ 0.0005
MC-RAzabu			1008.5242		-0.0025

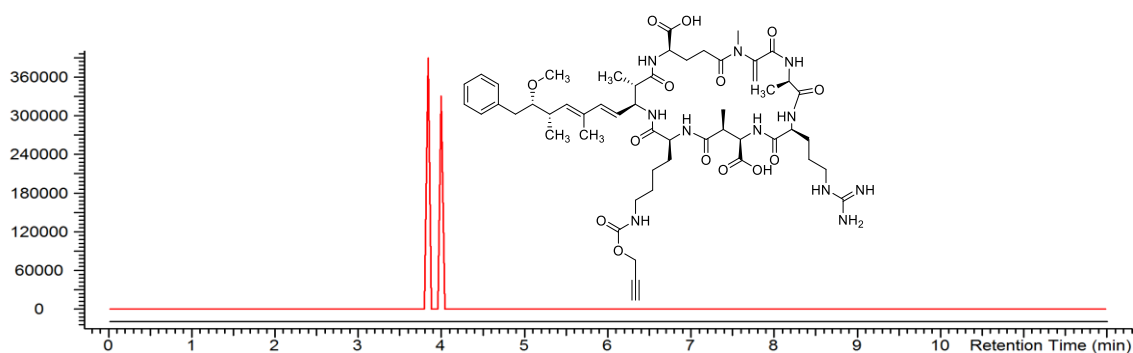


**Figure A39.** EIC ( $m/z$  1092.5724, pos. mode) overlay of a *Microcystis* CBT 633 control culture (black, lower trace) and a culture grown with 30  $\mu$ M Prlys (red, upper trace). The occurrence of two peaks indicates the co-formation of both isomers.

	Formula	Ion	Measured $m/z$	Calculated $m/z$	Difference (Da)
MC-PrlysR	$C_{53}H_{77}N_{11}O_{14}$	$[M+H]^+$	1092.5712	1092.5724	- 0.0012
MC-RPrlys			1092.5717		-0.0007

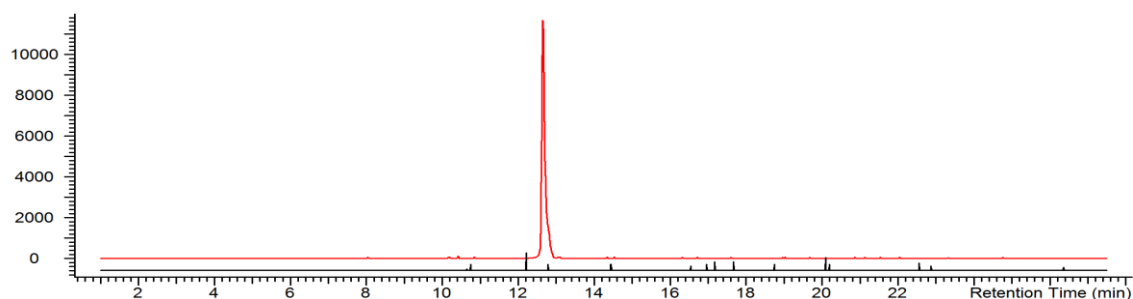


**Figure A40.** EIC ( $m/z$  1070.5, pos. mode) overlay of a *Microcystis* CBT 959 control culture (black, lower trace) and a culture grown with 30  $\mu$ M Azphe (red, upper trace).

	Formula	Ion	Measured $m/z$	Calculated $m/z$	Difference (Da)
MC-AzpheR	$C_{52}H_{71}N_{13}O_{12}$	$[M+H]^+$	1070.5	1070.5	0.0

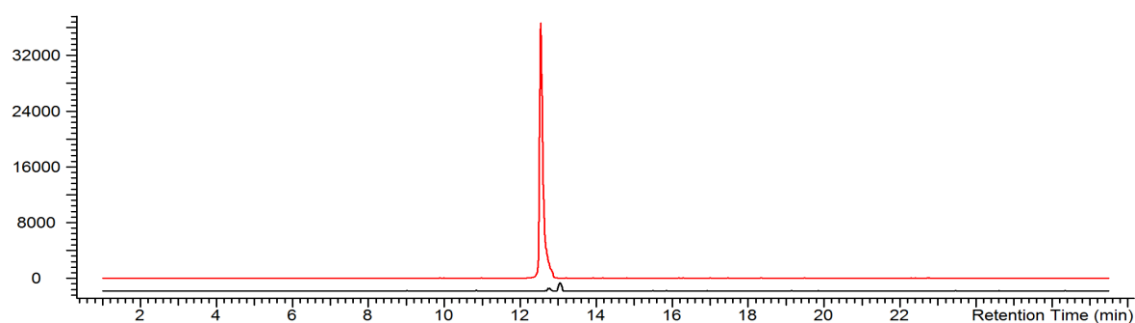


**Figure A41.** EIC ( $m/z$  1083.5, pos. mode) overlay of a *Microcystis* CBT 959 control culture (black, lower trace) and a culture grown with 30  $\mu$ M Prtyr (red, upper trace).

	Formula	Ion	Measured $m/z$	Calculated $m/z$	Difference (Da)
MC-PrtyrR	$C_{55}H_{74}N_{10}O_{13}$	$[M+H]^+$	1083.5	1083.5	0.0

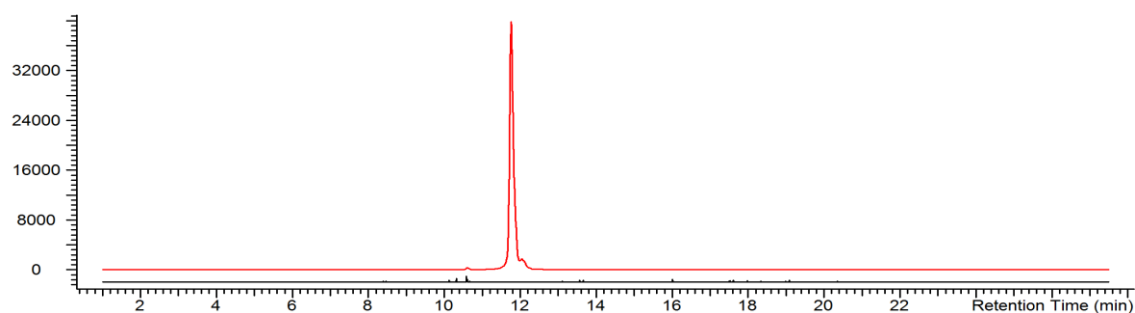


**Figure A42.** EIC ( $m/z$  1036.5, pos. mode) overlay of a *Microcystis* CBT 959 control culture (black, lower trace) and a culture grown with 30  $\mu$ M Aznle (red, upper trace).

	Formula	Ion	Measured $m/z$	Calculated $m/z$	Difference (Da)
MC-AznleR	$C_{49}H_{73}N_{13}O_{12}$	$[M+H]^+$	1036.5	1036.5	0.0

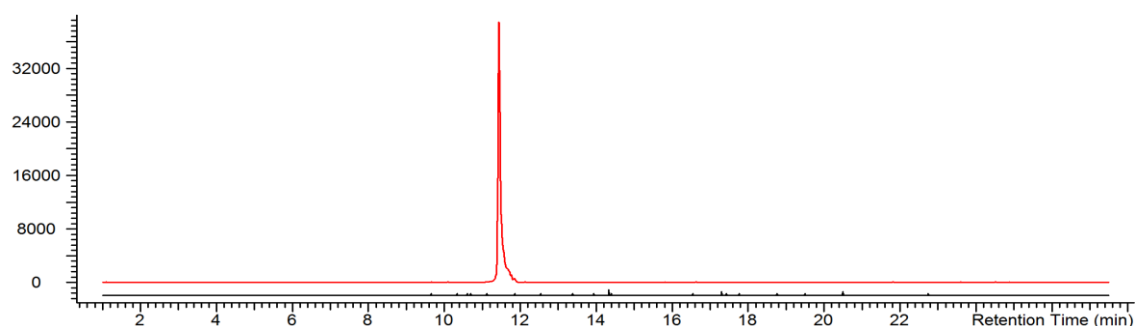


**Figure A43.** EIC ( $m/z$  1022.5, pos. mode) overlay of a *Microcystis* CBT 959 control culture (black, lower trace) and a culture grown with 30  $\mu$ M Aznva (red, upper trace).

	Formula	Ion	Measured $m/z$	Calculated $m/z$	Difference (Da)
MC-AznvaR	$C_{48}H_{71}N_{13}O_{12}$	$[M+H]^+$	1022.5	1022.5	0.0

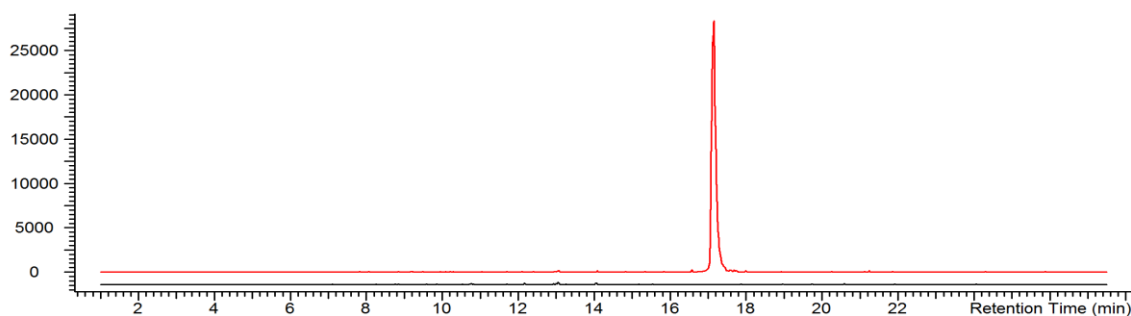


**Figure A44.** EIC ( $m/z$  979.4, pos. mode) overlay of a *Microcystis* CBT 959 control culture (black, lower trace) and a culture grown with 30  $\mu\text{M}$  Aznva (red, upper trace).

	Formula	Ion	Measured $m/z$	Calculated $m/z$	Difference (Da)
MC-LAznva	$\text{C}_{48}\text{H}_{70}\text{N}_{10}\text{O}_{12}$	$[\text{M}+\text{H}]^+$	979.4	979.5	- 0.1

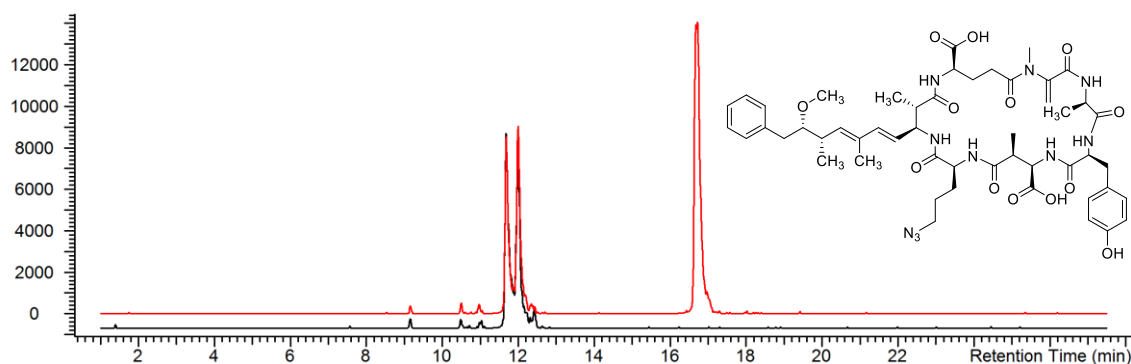


**Figure A45.** EIC ( $m/z$  1029.4, pos. mode) overlay of a *Microcystis* CBT 959 control culture (black, lower trace) and a culture grown with 30  $\mu\text{M}$  Aznva (red, upper trace).

	Formula	Ion	Measured $m/z$	Calculated $m/z$	Difference (Da)
MC-YAznva	$\text{C}_{51}\text{H}_{68}\text{N}_{10}\text{O}_{13}$	$[\text{M}+\text{H}]^+$	1029.4	1029.5	- 0.1

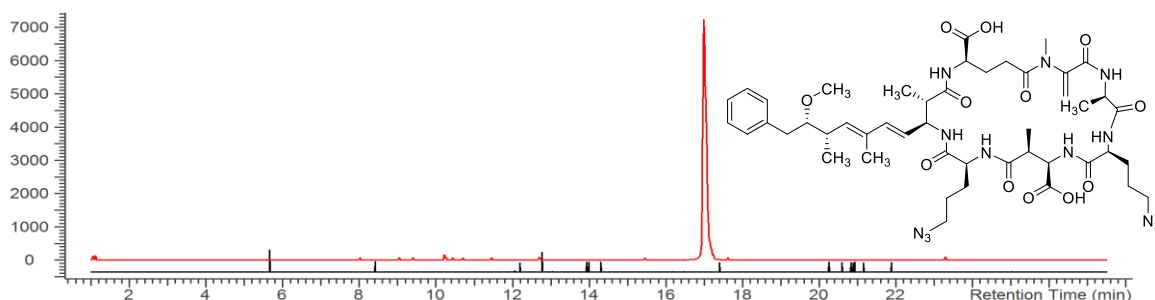


**Figure A46.** EIC ( $m/z$  1006.4, pos. mode) overlay of a *Microcystis* CBT 959 control culture (black, lower trace) and a culture grown with 30  $\mu\text{M}$  Aznva (red, upper trace).

	Formula	Ion	Measured $m/z$	Calculated $m/z$	Difference (Da)
MC-Aznva	$\text{C}_{47}\text{H}_{67}\text{N}_{13}\text{O}_{12}$	$[\text{M}+\text{H}]^+$	1006.4	1006.5	- 0.1

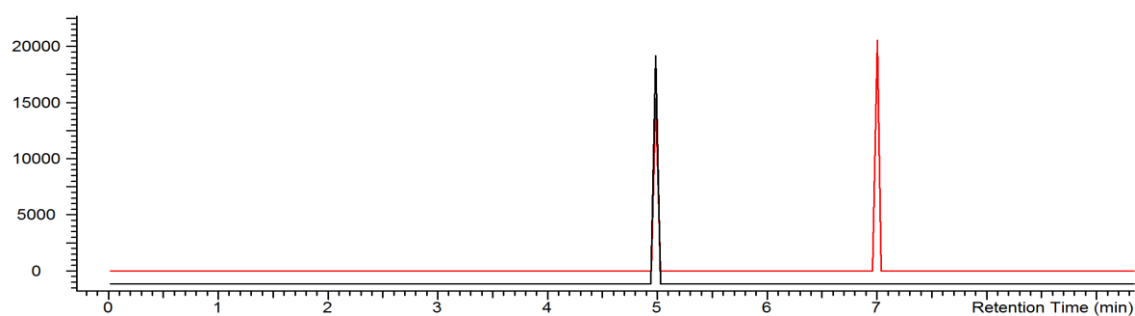


**Figure A47.** EIC ( $m/z$  965.5106, pos. mode) overlay of a *Microcystis* CBT 959 control culture (black, lower trace) and a culture grown with 30  $\mu$ M Azabu (red, upper trace).

	Formula	Ion	Measured $m/z$	Calculated $m/z$	Difference (Da)
MC-LAzabu	$C_{47}H_{68}N_{10}O_{12}$	$[M+H]^+$	965.5106	965.5096	+ 0.001

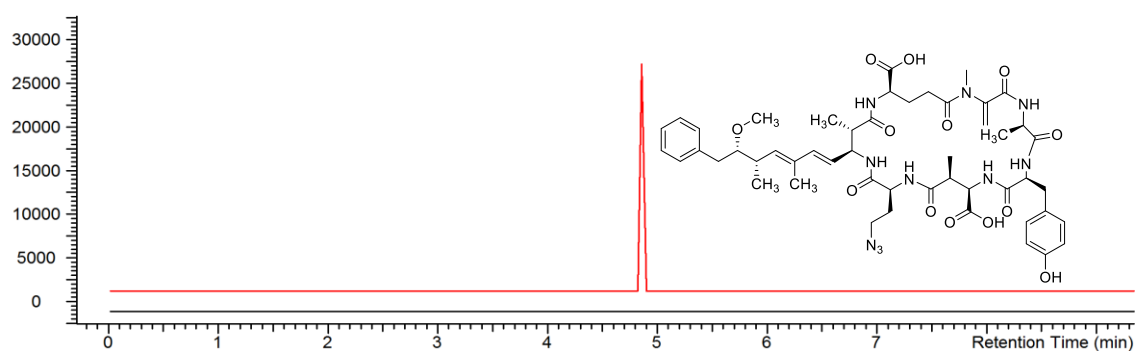


**Figure A48.** EIC ( $m/z$  1015.4879, pos. mode) overlay of a *Microcystis* CBT 959 control culture (black, lower trace) and a culture grown with 30  $\mu$ M Azabu (red, upper trace).

	Formula	Ion	Measured $m/z$	Calculated $m/z$	Difference (Da)
MC-YAzabu	$C_{50}H_{66}N_{10}O_{13}$	$[M+H]^+$	1015.4879	1015.4889	- 0.001

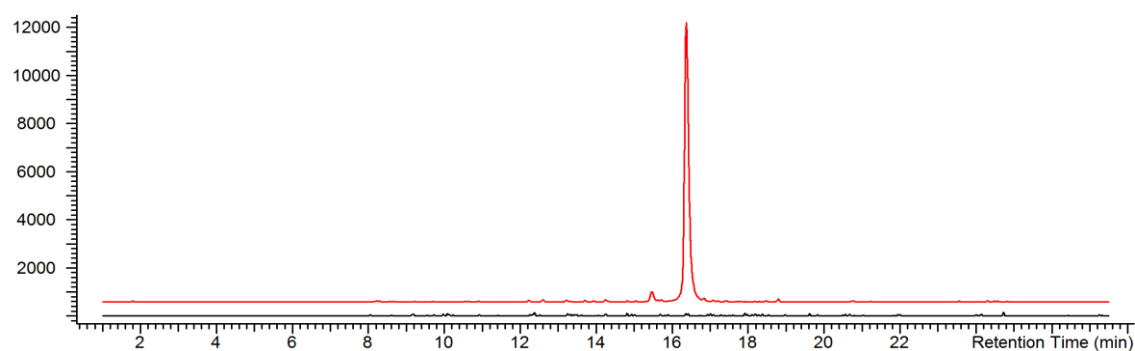


**Figure A49.** EIC ( $m/z$  951.4, pos. mode) overlay of a *Microcystis* CBT 959 control culture (black, lower trace) and a culture grown with 30  $\mu$ M Azala (red, upper trace).

	Formula	Ion	Measured $m/z$	Calculated $m/z$	Difference (Da)
MC-LAzala	$C_{46}H_{66}N_{10}O_{12}$	$[M+H]^+$	951.4	951.4	0.0

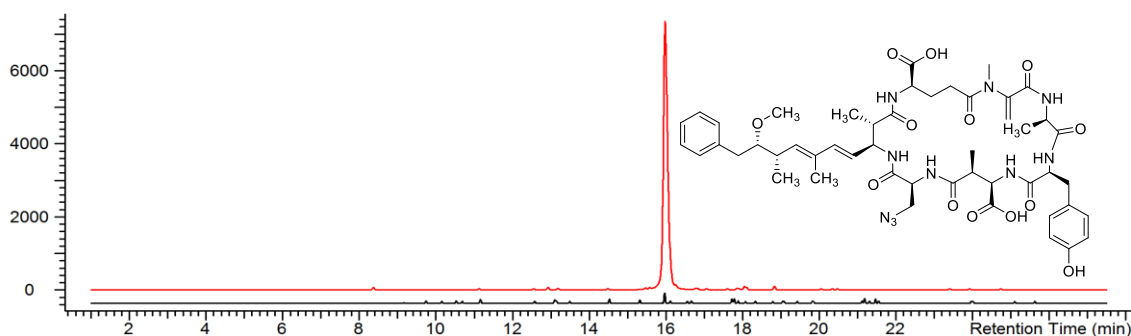


**Figure A50.** EIC ( $m/z$  1001.4, pos. mode) overlay of a *Microcystis* CBT 959 control culture (black, lower trace) and a culture grown with 30  $\mu$ M Azala (red, upper trace).

	Formula	Ion	Measured $m/z$	Calculated $m/z$	Difference (Da)
MC-YAzala	$C_{49}H_{64}N_{10}O_{13}$	$[M+H]^+$	1001.4	1001.4	0.0

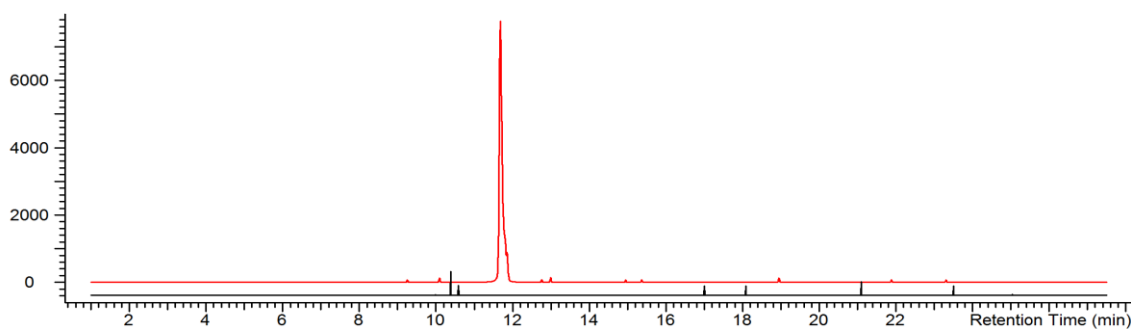


**Figure A51.** EIC ( $m/z$  1092.6, pos. mode) overlay of a *Microcystis* CBT 959 control culture (black, lower trace) and a culture grown with 30  $\mu$ M Prlys (red, upper trace).

	Formula	Ion	Measured $m/z$	Calculated $m/z$	Difference (Da)
MC-PrlysR	$C_{53}H_{77}N_{11}O_{14}$	$[M+H]^+$	1092.6	1092.5	+ 0.1

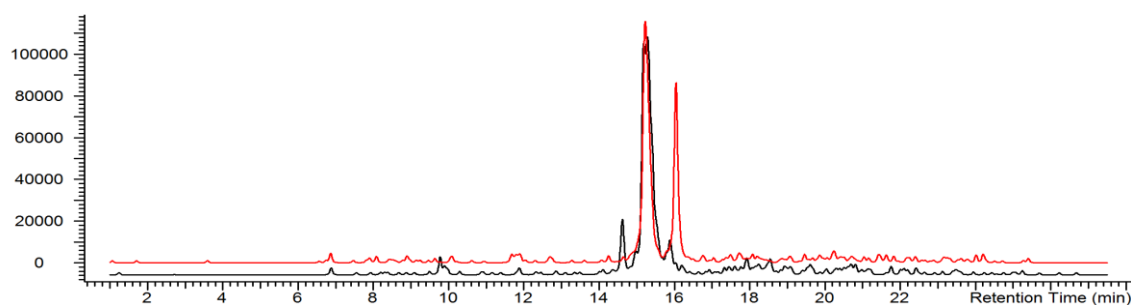


**Figure A52.** EIC ( $m/z$  934.4, pos. mode) overlay of a *Microcystis* CBT 959 control culture (black, lower trace) and a culture grown with 30  $\mu$ M Prgly (red, upper trace).

	Formula	Ion	Measured $m/z$	Calculated $m/z$	Diff. (Da)
MC-LPrgly	$C_{48}H_{67}N_7O_{12}$	$[M+H]^+$	934.4	934.4	0.0

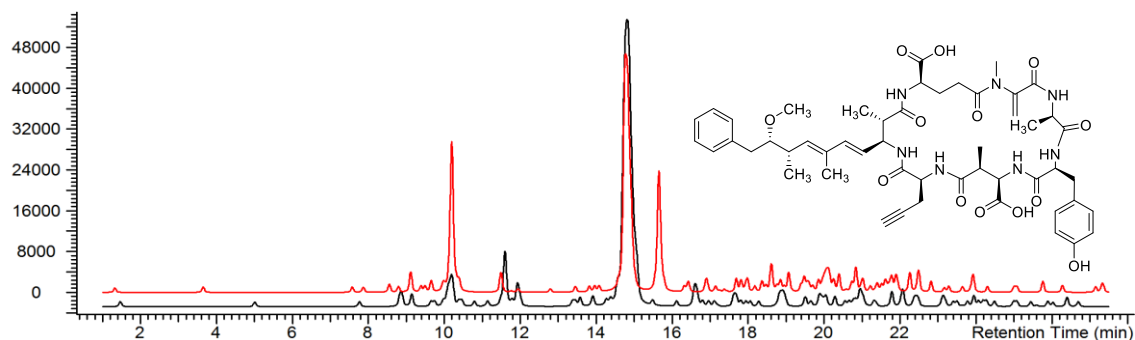


**Figure A53.** EIC ( $m/z$  984.4, pos. mode) overlay of a *Microcystis* sp. CBT 959 control culture (black, lower trace) and a culture grown with 30  $\mu$ M Prgly (red, upper trace).

	Formula	Ion	Measured $m/z$	Calculated $m/z$	Difference (Da)
MC-Yprgly	$C_{51}H_{65}N_7O_{13}$	$[M+H]^+$	984.3	984.4	- 0.1

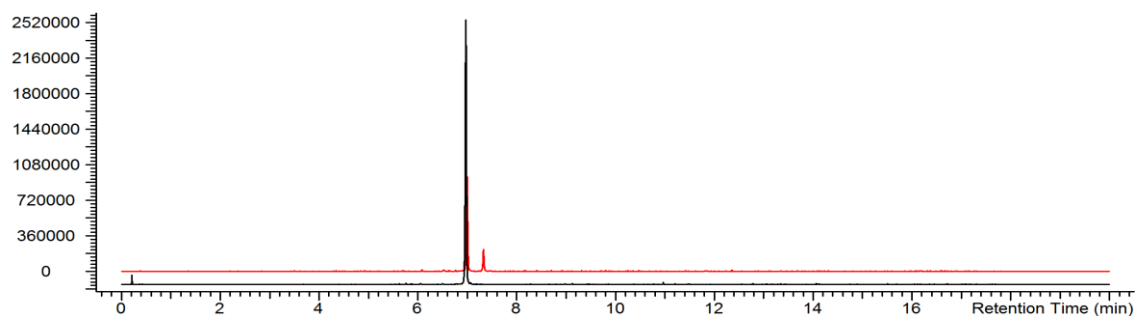


**Figure A54.** EIC ( $m/z$  1070.5, pos. mode) overlay of a *Microcystis* CAWBG11 control culture (black, lower trace) and a culture grown with 30  $\mu$ M Azphe (red, upper trace).

	Formula	Ion	Measured $m/z$	Calculated $m/z$	Difference (Da)
MC-AzpheR	$C_{52}H_{71}N_{13}O_{12}$	$[M+H]^+$	1070.5	1070.5	0.0

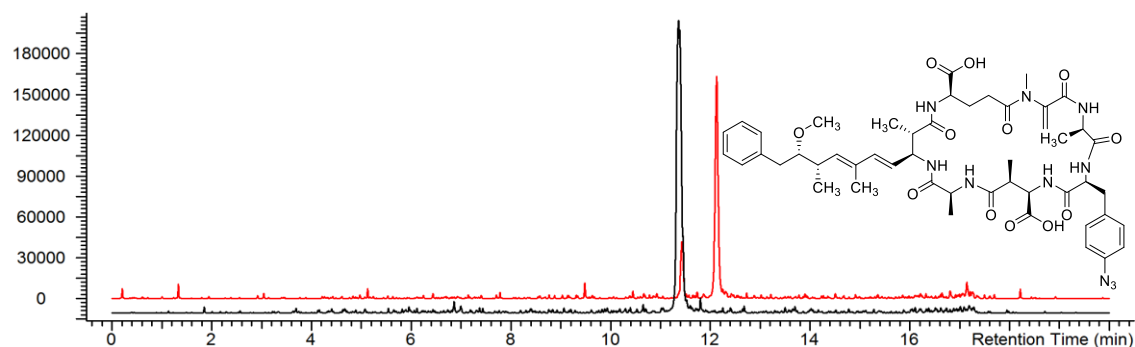


**Figure A55.** EIC ( $m/z$  985.5, pos. mode) overlay of a *Microcystis* CAWBG11 control culture (black, lower trace) and a culture grown with 30  $\mu$ M Azphe (red, upper trace).

	Formula	Ion	Measured $m/z$	Calculated $m/z$	Difference (Da)
MC-AzpheA	$C_{49}H_{64}N_{10}O_{12}$	$[M+H]^+$	985.5	985.4	+ 0.1



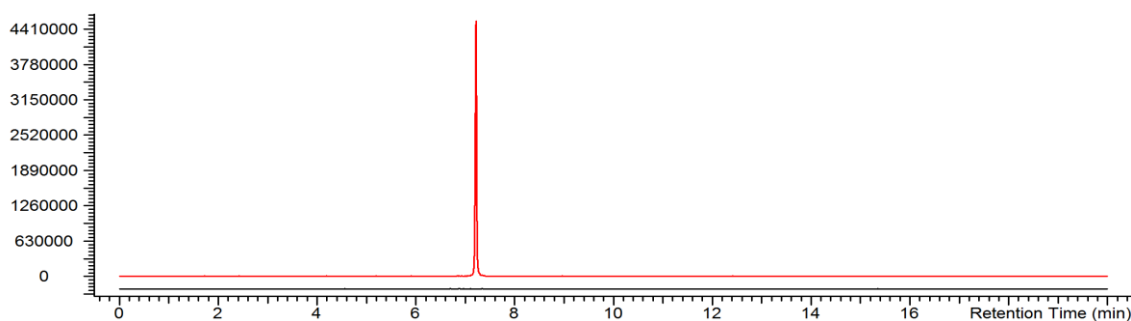


**Figure A56.** EIC ( $m/z$  1083.5, pos. mode) overlay of a *Microcystis* CAWBG11 control culture (black, lower trace) and a culture grown with 30  $\mu$ M Prtyr (red, upper trace).

	Formula	Ion	Measured $m/z$	Calculated $m/z$	Difference (Da)
MC-PrtyrR	$C_{55}H_{74}N_{10}O_{13}$	$[M+H]^+$	1083.5	1083.5	0.0

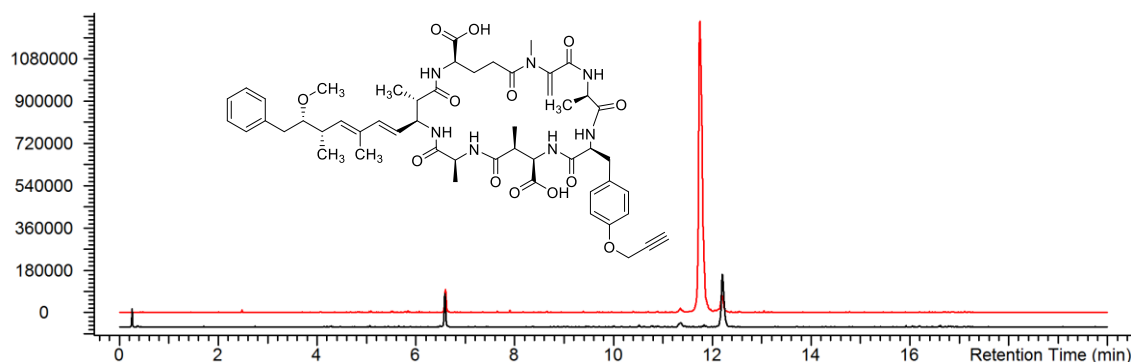


**Figure A57.** EIC ( $m/z$  998.4, pos. mode) overlay of a *Microcystis* CAWBG11 control culture (black, lower trace) and a culture grown with 30  $\mu$ M Prtyr (red, upper trace).

	Formula	Ion	Measured $m/z$	Calculated $m/z$	Difference (Da)
MC-PrtyrA	$C_{52}H_{67}N_7O_{13}$	$[M+H]^+$	998.4	998.4	0.0

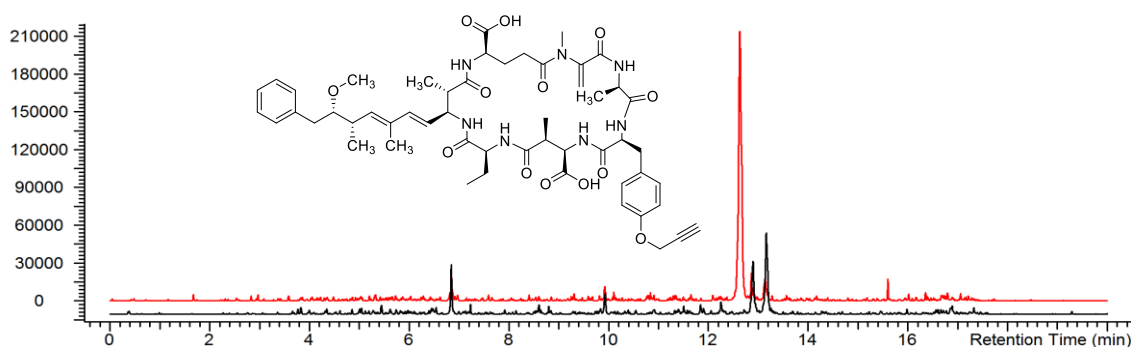


**Figure A58.** EIC ( $m/z$  1012.5, pos. mode) overlay of a *Microcystis* CAWBG11 control culture (black, lower trace) and a culture grown with 30  $\mu$ M Prtyr (red, upper trace).

	Formula	Ion	Measured $m/z$	Calculated $m/z$	Difference (Da)
MC-PrtyrAbu	$C_{53}H_{69}N_7O_{13}$	$[M+H]^+$	1012.5	1012.5	0.0

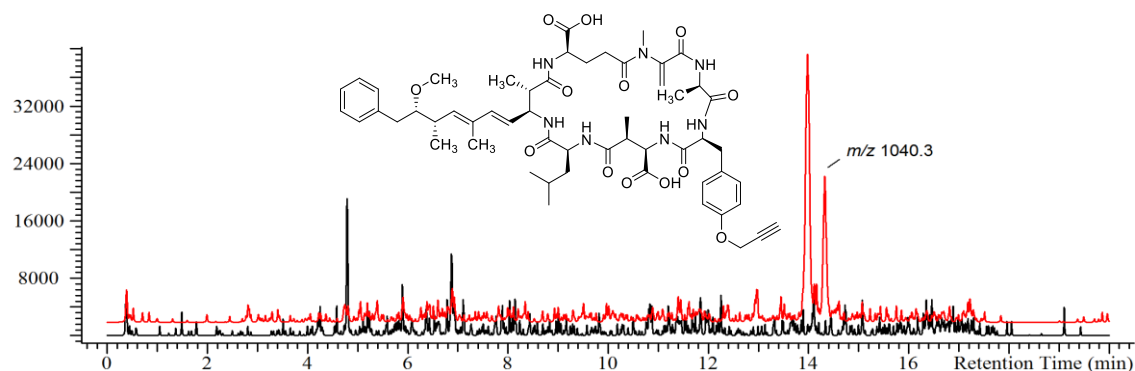


**Figure A59.** EIC ( $m/z$  1040.6, pos. mode) overlay of a *Microcystis* CAWBG11 control culture (black, lower trace) and a culture grown with 30  $\mu$ M Prtyr (red, upper trace).

	Formula	Ion	Measured $m/z$	Calculated $m/z$	Difference (Da)
MC-PrtyrL	$C_{55}H_{73}N_7O_{13}$	$[M+H]^+$	1040.6	1040.5	+ 0.1

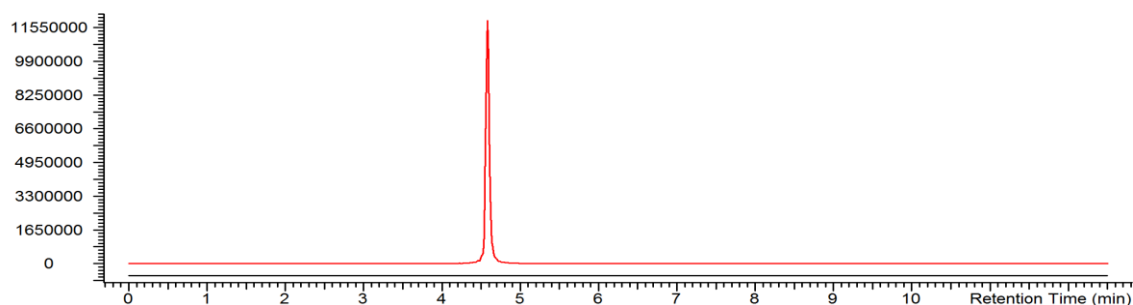


**Figure A60.** EIC ( $m/z$  1036.5574, pos. mode) overlay of a *Microcystis* CAWBG11 control culture (black, lower trace) and a culture grown with 30  $\mu$ M Aznle (red, upper trace). The structure of MC-AznleR was confirmed by MS<sup>2</sup> (Figure A67 and Table A6).

	Formula	Ion	Measured $m/z$	Calculated $m/z$	Difference (Da)
MC-AznleR	$C_{49}H_{73}N_{13}O_{12}$	$[M+H]^+$	1036.5570	1036.5574	- 0.0004

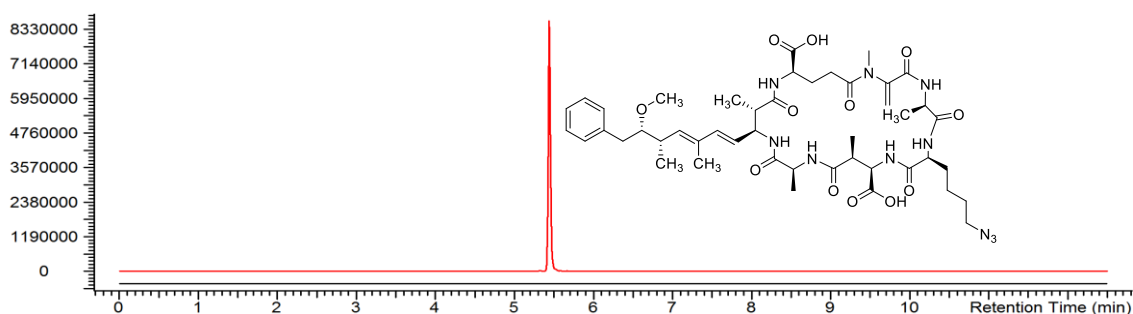


**Figure A61.** EIC ( $m/z$  951.4934, pos. mode) overlay of a *Microcystis* CAWBG11 control culture (black, lower trace) and a culture grown with 30  $\mu$ M Aznle (red, upper trace).

	Formula	Ion	Measured $m/z$	Calculated $m/z$	Difference (Da)
MC-AznleA	$C_{46}H_{66}N_{10}O_{12}$	$[M+H]^+$	951.4924	951.4934	- 0.001

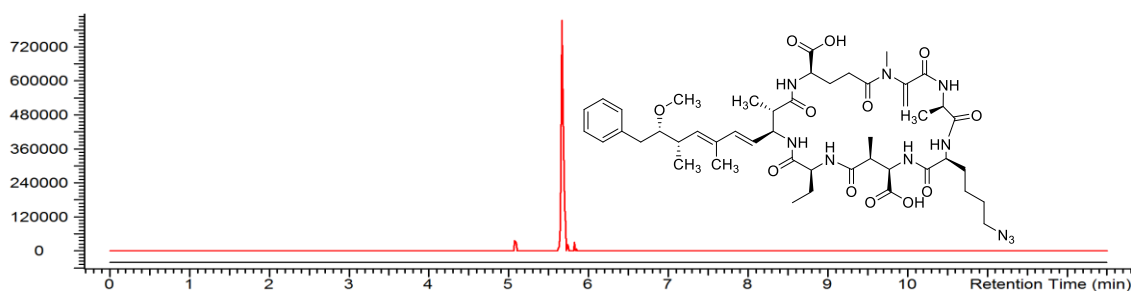


**Figure A62.** EIC ( $m/z$  965.5, pos. mode) overlay of a *Microcystis* CAWBG11 control culture (black, lower trace) and a culture grown with 30  $\mu\text{M}$  Aznle (red, upper trace).

	Formula	Ion	Measured $m/z$	Calculated $m/z$	Difference (Da)
MC-AznleAbu	$\text{C}_{47}\text{H}_{68}\text{N}_{10}\text{O}_{12}$	$[\text{M}+\text{H}]^+$	965.5093	965.5091	+ 0.0002

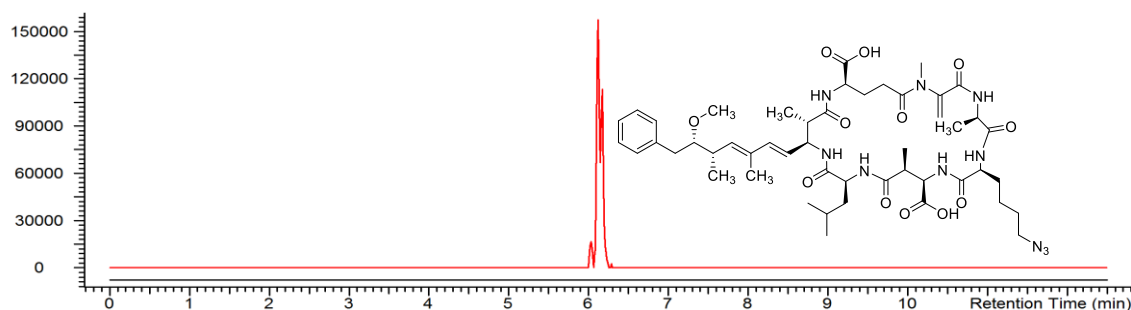


**Figure A63.** EIC ( $m/z$  993.5404, pos. mode) overlay of a *Microcystis* CAWBG11 control culture (black, lower trace) and a culture grown with 30  $\mu\text{M}$  Aznle (red, upper trace). The structure of MC-AznleL was confirmed by MS<sup>2</sup> (Figure A66 and Table A5).

	Formula	Ion	Measured $m/z$	Calculated $m/z$	Difference (Da)
MC-AznleL	$\text{C}_{49}\text{H}_{72}\text{N}_{10}\text{O}_{12}$	$[\text{M}+\text{H}]^+$	993.5410	993.5404	+ 0.0006

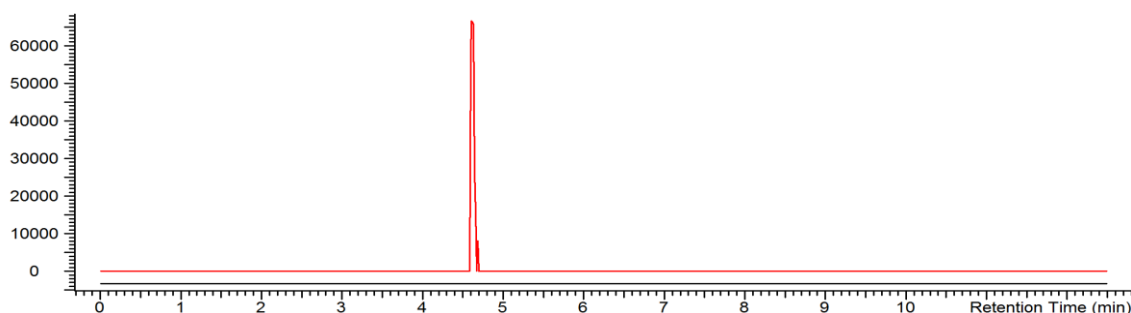


**Figure A64.** EIC ( $m/z$  1092.5724, pos. mode) overlay of a *Microcystis* CAWBG11 control culture (black, lower trace) and a culture grown with 30  $\mu\text{M}$  Prys (red, upper trace). The structure of MC-PrysR was confirmed by MS<sup>2</sup> (Figure A87 and Table A7).

	Formula	Ion	Measured $m/z$	Calculated $m/z$	Difference (Da)
MC-PrysR	$\text{C}_{53}\text{H}_{77}\text{N}_{11}\text{O}_{14}$	$[\text{M}+\text{H}]^+$	1092.5721	1092.5724	- 0.0003

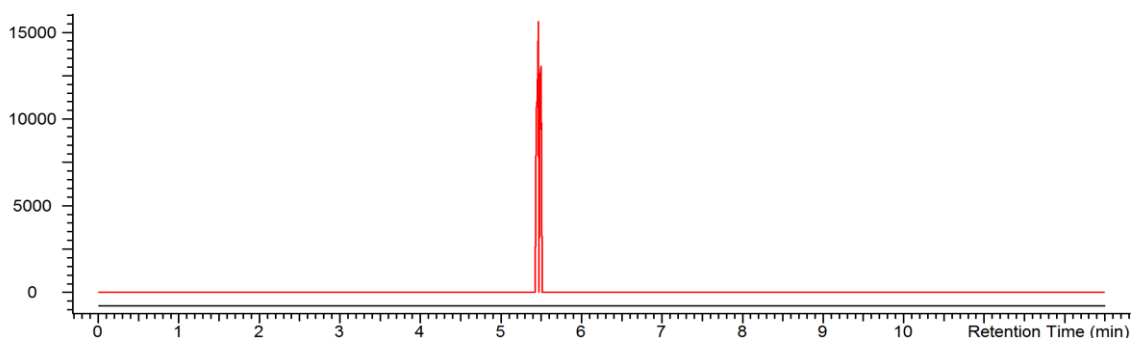


**Figure A65.** EIC ( $m/z$  1007.5084, pos. mode) overlay of a *Microcystis* CAWBG11 control culture (black, lower trace) and a culture grown with 30  $\mu$ M Prys (red, upper trace).

	Formula	Ion	Measured $m/z$	Calculated $m/z$	Difference (Da)
MC-PrysA	$C_{50}H_{70}N_8O_{14}$	$[M+H]^+$	1007.5063	1007.5084	- 0.0021

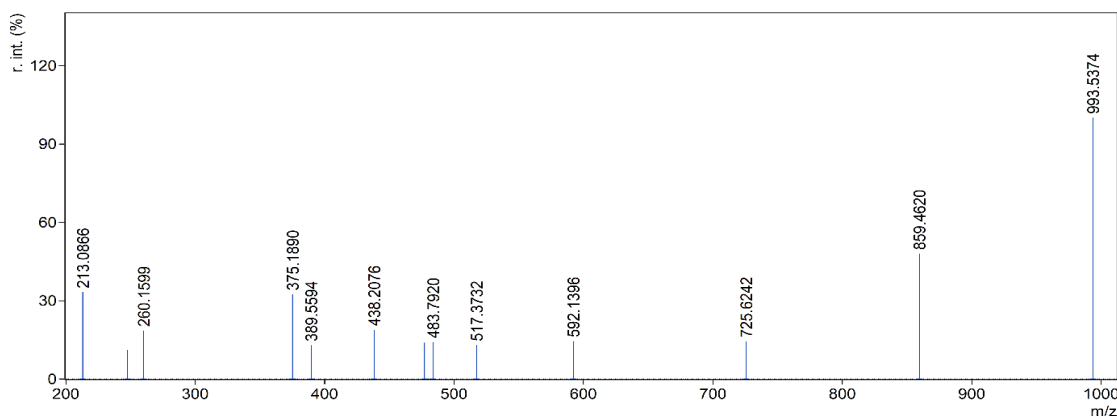


**Figure A66.** MS<sup>2</sup> spectrum of MC-AznleL obtained from PDB with *Microcystis* CAWBG11.

**Table A5.** Annotation of the MS<sup>2</sup> spectrum of MC-AznleL obtained from PDB with *Microcystis* CAWBG11. Fragments characteristic for MC-AznleL are highlighted in bold script. Mdha, *N*-methyl dehydroalanine; Masp,  $\beta$ -methyl aspartic acid; Adda, 3*S*-amino-9*S*-methoxy-2*S*,6,8*S*-trimethyl-10-phenyldeca-4*E*,6*E*-dienoic acid.

$m/z$	Annotation	Ion	Difference [ppm]
993.5374	$M + H^+$	-	- 3.1
	(M - $C_9H_{10}O$ ) + $H^+$	-	- 6.0
859.4620	(aNI - $N_2$ )-Masp-Leu-Adda-Glu-Mdha - $H_2O$ + $H^+$	$z^6$	2.3
<b>438.2076</b>	<b>Mdha-Ala-Aznle-Masp</b> + $H^+$ <b>Glu-Mdha-Ala-Aznle + H<sup>+</sup></b>	$y^4/b^4$	- 4.4
375.1912	(Adda - $C_9H_{10}O$ )-Glu-Mdha + $H^+$	$z^3$	- 6.5
260.1599	Masp-Leu + $H^+$	$c^2$	- 2.4
213.0866	Glu-Mdha + $H^+$	$y^2/b^2$	- 1.1

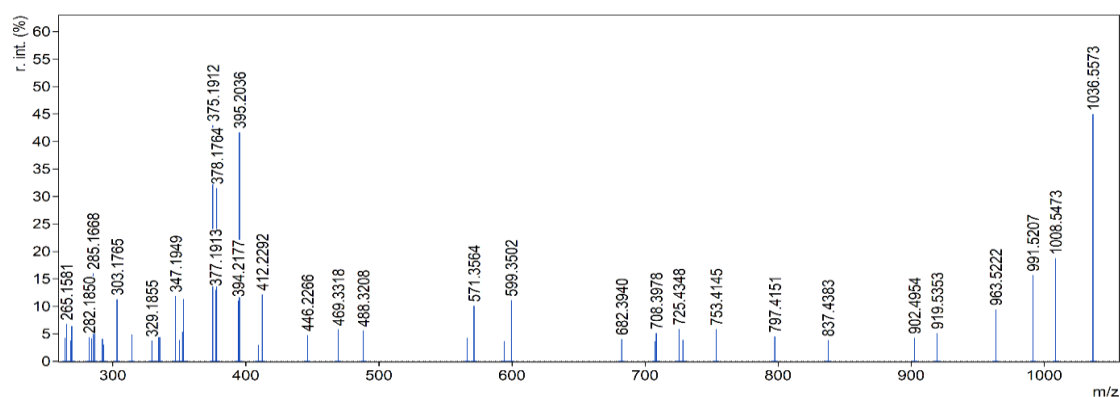


**Figure A67.** MS<sup>2</sup> spectrum of MC-AznleR obtained from PDB with *Microcystis* CAWBG11.

**Table A6.** Annotation of the MS<sup>2</sup> spectrum of MC-AznleR obtained from PDB with *Microcystis* CAWBG11. Fragments characteristic for MC-AznleR are highlighted in bold script. Mdha, *N*-methyl dehydroalanine; Masp,  $\beta$ -methyl aspartic acid; Adda, 3*S*-amino-9*S*-methoxy-2*S*,6*S*,8*S*-trimethyl-10-phenyldeca-4*E*,6*E*-dienoic acid.

<i>m/z</i>	Annotation	Ion	Difference [ppm]	
1036.5573	M + H <sup>+</sup>	-	- 0.2	
1008.5473	(M - N <sub>2</sub> ) + H <sup>+</sup>	-	- 4.0	
991.5207	(M - N <sub>2</sub> - NH <sub>3</sub> ) + H <sup>+</sup>	-	- 4.1	
837.4383	Adda-Glu-Mdha-Ala-(Aznle - HN <sub>3</sub> )-Masp + H <sup>+</sup>	y <sup>6</sup> /b <sup>6</sup>	- 1.2	
753.4145	Ala-(Aznle - HCN <sub>3</sub> )-Masp-(Arg - CH <sub>2</sub> N <sub>2</sub> )-Adda + H <sup>+</sup>	x <sup>5</sup>	- 4.9	
725.4345	(Aznle - N <sub>2</sub> )-Masp-Arg-Adda + H <sup>+</sup>	y <sup>4</sup> /b <sup>4</sup>	+ 0.5	
708.3978	Adda-Glu-Mdha-Ala-(Aznle - HN <sub>3</sub> ) + H <sup>+</sup>	y <sup>5</sup> /b <sup>5</sup>	+ 1.6	
<b>682.3923</b>	<b>Arg-Adda-Glu-Mdha + H<sup>+</sup></b>	<b>y<sup>4</sup>/b<sup>4</sup></b>	<b>+ 2.6</b>	
594.3113	Mdha-Ala-Aznle-Masp-Arg + H <sup>+</sup>	y <sup>5</sup> /b <sup>5</sup>	+ 1.1	
566.3050	Mdha-Ala- (Aznle - N <sub>2</sub> )-Masp-Arg + H <sup>+</sup>	y <sup>5</sup> /b <sup>5</sup>	+ 0.8	
446.2266	(Adda - C <sub>9</sub> H <sub>10</sub> O)-Glu-Mdha-Ala + H <sup>+</sup>	z <sup>4</sup>	- 4.5	
412.2292	(Aznle - N <sub>2</sub> )-Masp-Arg + H <sup>+</sup>	y <sup>3</sup> /b <sup>3</sup>	- 2.5	
395.2036	(Aznle - N <sub>2</sub> )-Masp-Arg - NH <sub>3</sub> + H <sup>+</sup>	y <sup>3</sup> /b <sup>3</sup>	- 0.3	
<b>394.2177</b>	<b>(Glu - CO<sub>2</sub>)-Mdha-Ala-Aznle+ Mdha-Ala-Aznle-(Masp - CO<sub>2</sub>) + H<sup>+</sup></b>	<b>H<sup>+</sup></b>	<b>y<sup>4</sup>/b<sup>4</sup></b>	<b>- 5.0</b>
378.1764	(Aznle - N <sub>2</sub> )-Masp-(Arg - N <sub>2</sub> H <sub>6</sub> ) + H <sup>+</sup>	y <sup>3</sup> /b <sup>3</sup>	- 2.2	
<b>377.1913</b>	<b>Mdha-Ala-Aznle-(Masp - CO<sub>2</sub>) + H<sup>+</sup></b>	<b>z<sup>4</sup></b>	<b>- 5.1</b>	
375.1912	(Adda - C <sub>9</sub> H <sub>10</sub> O)-Glu-Mdha + H <sup>+</sup>	z <sup>3</sup>	- 0.8	
353.1815	(Aznle - N <sub>2</sub> )-Masp-(Arg - CH <sub>5</sub> N <sub>3</sub> ) + H <sup>+</sup>	y <sup>3</sup> /b <sup>3</sup>	- 1.3	
350.1819	(Aznle - N <sub>2</sub> )-Masp-(Arg - N <sub>2</sub> H <sub>6</sub> ) + H <sup>+</sup>	y <sup>3</sup> /b <sup>3</sup>	- 1.1	
335.1707	(Aznle - HN <sub>3</sub> )-Masp-(Arg - N <sub>2</sub> H <sub>6</sub> ) + H <sup>+</sup>	a <sup>3</sup>	<b>- 2.1</b>	
292.1540	(Adda - C <sub>9</sub> H <sub>10</sub> O)-Glu + H <sup>+</sup>	z <sup>2</sup>	- 1.1	
286.1501	Masp-Arg + H <sup>+</sup>	y <sup>2</sup> /b <sup>2</sup>	- 3.2	
284.1240	Glu-Mdha-Ala + H <sup>+</sup>	y <sup>3</sup> /b <sup>3</sup>	- 0.5	

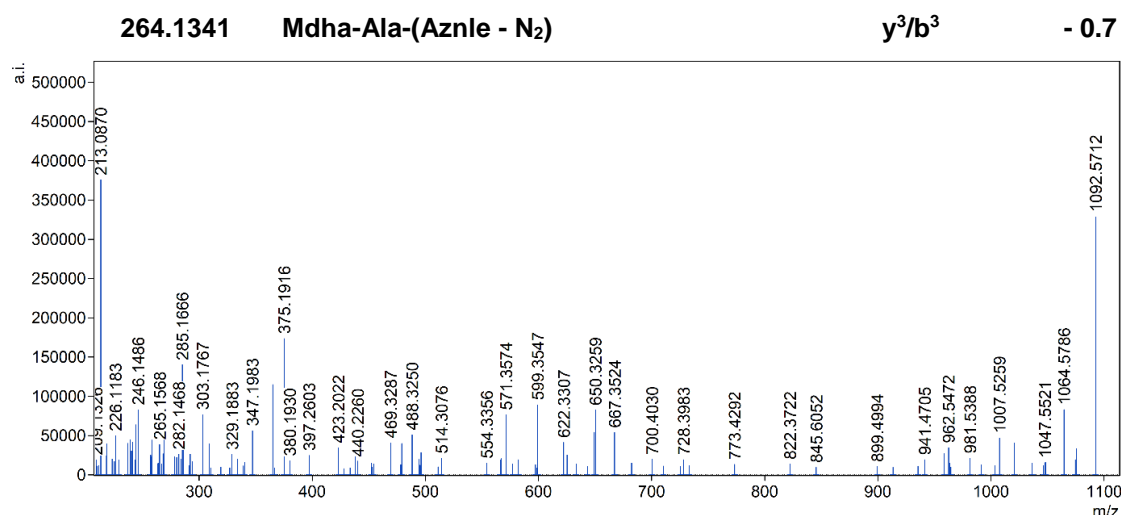


**Figure A68.** MS<sup>2</sup> spectrum of MC-PrllysR obtained from PDB with *Microcystis* CAWBG11.

**Table A7.** Annotation of the MS<sup>2</sup> spectrum of MC-PrllysR obtained from PDB of *Microcystis* CAWBG11. Fragments characteristic for MC-PrllysR are highlighted in bold script. Mdha, *N*-methyl dehydroalanine; Masp,  $\beta$ -methyl aspartic acid; Adda, 3*S*-amino-9*S*-methoxy-2*S*,6,8*S*-trimethyl-10-phenyldeca-4*E*,6*E*-dienoic acid.

<i>m/z</i>	Annotation	Ion	Difference [ppm]
1092.5712	M + H <sup>+</sup>	-	- 1.1
1064.5786	M - CO + H <sup>+</sup>	-	1.0
1007.5259	Ala-Prllys-Masp-Arg-Adda-Glu - CO + H <sup>+</sup>	x <sup>6</sup>	- 6.2
899.4994	Masp-Arg-Adda-Glu-Mdha-Ala + H <sup>+</sup>	c <sup>6</sup>	1.0
<b>728.3983</b>	<b>Masp-Arg-Adda-Glu + H<sup>+</sup></b>	<b>b<sup>4</sup>/y<sup>4</sup></b>	<b>0.8</b>
<b>682.3960</b>	<b>Arg-Adda-Glu-Mdha + H<sup>+</sup></b>	<b>b<sup>4</sup>/y<sup>4</sup></b>	<b>5.5</b>
667.3524	Mdha-Ala-Prllys-Masp-Arg + H <sup>+</sup>	c <sup>5</sup>	0.3
650.3259	Mdha-Ala-Prllys-Masp-Arg + H <sup>+</sup>	b <sup>5</sup> /y <sup>5</sup>	0.3
<b>599.3547</b>	<b>Masp-Arg-Adda + H<sup>+</sup></b>	b <sup>3</sup> /y <sup>3</sup>	- 0.7
<b>571.3574</b>	<b>Masp-Arg-Adda + H<sup>+</sup></b>	a <sup>3</sup>	- 5.0
375.1916	(Adda - C <sub>9</sub> H <sub>10</sub> O)-Glu-Mdha + H <sup>+</sup>	z <sup>3</sup>	0.3
258.1666	Masp-Arg	a <sup>2</sup>	3.9
213.0876	Glu-Mdha + H <sup>+</sup>	y <sup>2</sup> /b <sup>2</sup>	- 1.1

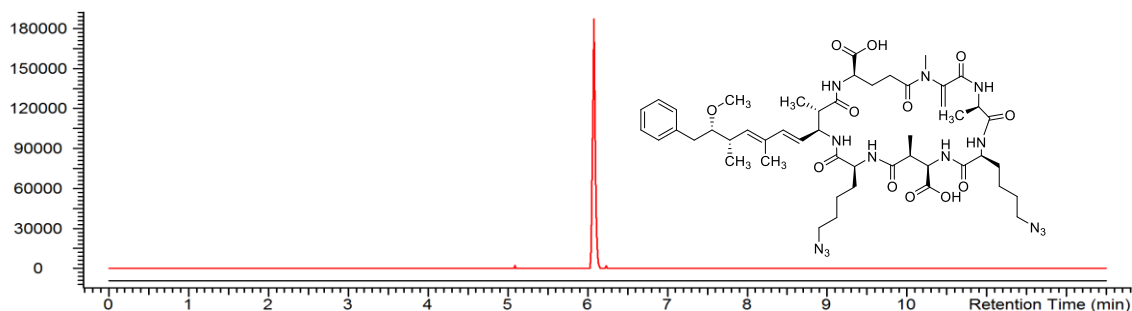


**Figure A69.** EIC ( $m/z$  1034.5418, pos. mode) overlay of a *Microcystis* CAWBG11 control culture (black, lower trace) and a culture grown with 30  $\mu\text{M}$  Aznle (red, upper trace).

	Formula	Ion	Measured $m/z$	Calculated $m/z$	Difference (Da)
MC-AznleAznle	$\text{C}_{49}\text{H}_{71}\text{N}_{13}\text{O}_{12}$	$[\text{M}+\text{H}]^+$	1034.5426	1034.5418	+ 0.0008

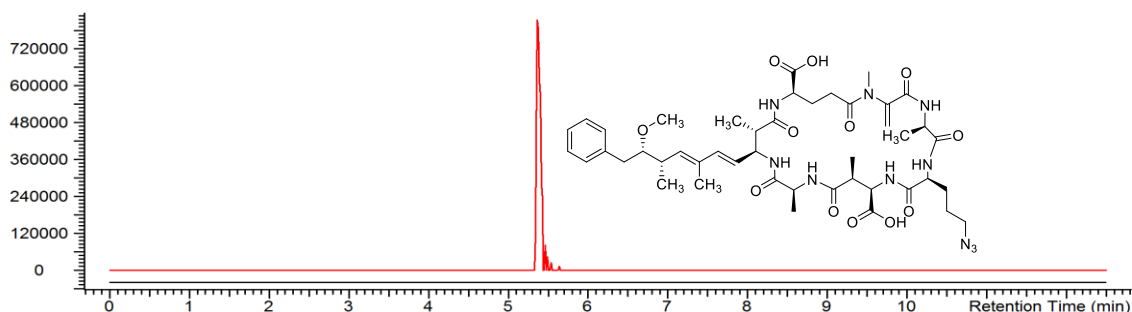


**Figure A70.** EIC ( $m/z$  937.4778, pos. mode) overlay of a *Microcystis* CAWBG11 control culture (black, lower trace) and a culture grown with 30  $\mu\text{M}$  Aznva (red, upper trace).

	Formula	Ion	Measured $m/z$	Calculated $m/z$	Difference (Da)
MC-AznvaA	$\text{C}_{45}\text{H}_{64}\text{N}_{10}\text{O}_{12}$	$[\text{M}+\text{H}]^+$	937.4780	937.4778	+ 0.0002

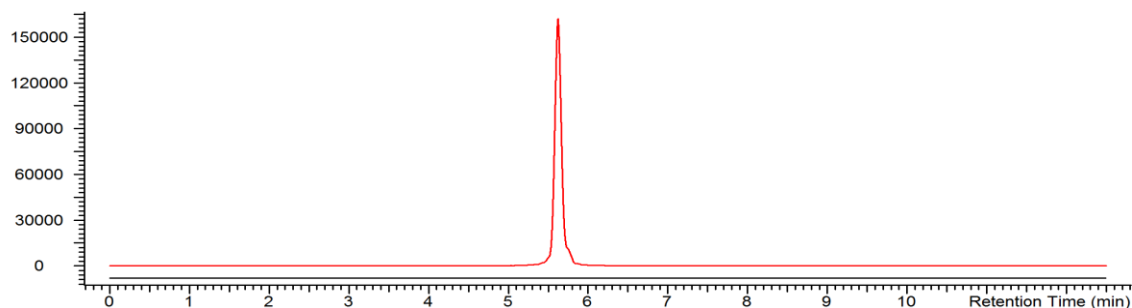


**Figure A71.** EIC ( $m/z$  951.4934, pos. mode) overlay of a *Microcystis* CAWBG11 control culture (black, lower trace) and a culture grown with 30  $\mu\text{M}$  Aznva (red, upper trace).

Formula	Ion	Measured $m/z$	Calculated $m/z$	Difference (Da)
---------	-----	----------------	------------------	-----------------

MC-AznvaAbu C<sub>46</sub>H<sub>66</sub>N<sub>10</sub>O<sub>12</sub> [M+H]<sup>+</sup> 951.4936 951.4934 + 0.0002

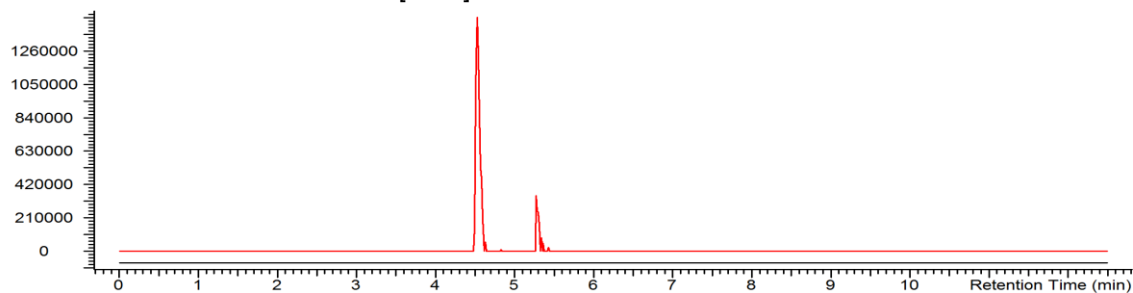


**Figure A72.** EIC ( $m/z$  1022.5418, pos. mode) overlay of a *Microcystis* CAWBG11 control culture (black, lower trace) and a culture grown with 30  $\mu$ M Aznva (red, upper trace). The occurrence of two peaks indicates the co-formation of both isomers.

	Formula	Ion	Measured $m/z$	Calculated $m/z$	Difference (Da)
MC-AznvaR	C <sub>48</sub> H <sub>71</sub> N <sub>13</sub> O <sub>12</sub>	[M+H] <sup>+</sup>	1022.5415	1022.5418	- 0.0003
MC-RAznva			1022.5422		+ 0.0004

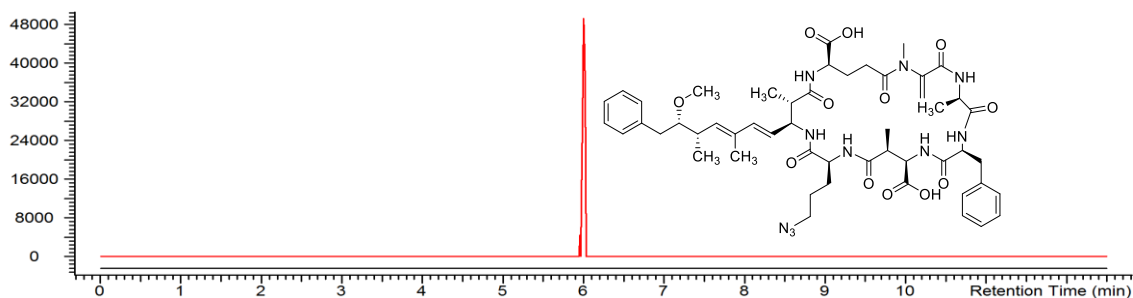


**Figure A73.** EIC ( $m/z$  1013.5091, pos. mode) overlay of a *Microcystis* CAWBG11 control culture (black, lower trace) and a culture grown with 30  $\mu$ M Aznva (red, upper trace).

	Formula	Ion	Measured $m/z$	Calculated $m/z$	Difference (Da)
MC-FAznva	C <sub>51</sub> H <sub>68</sub> N <sub>10</sub> O <sub>12</sub>	[M+H] <sup>+</sup>	1013.5090	1013.5091	- 0.0001

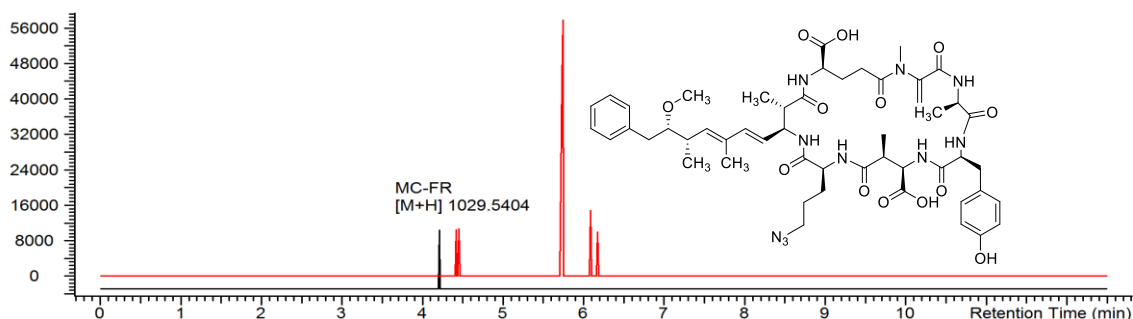


**Figure A74.** EIC ( $m/z$  1029.5040, pos. mode) overlay of a *Microcystis* CAWBG11 control culture (black, lower trace) and a culture grown with 30  $\mu$ M Aznva (red, upper trace).

	Formula	Ion	Measured $m/z$	Calculated $m/z$	Difference (Da)
--	---------	-----	----------------	------------------	-----------------



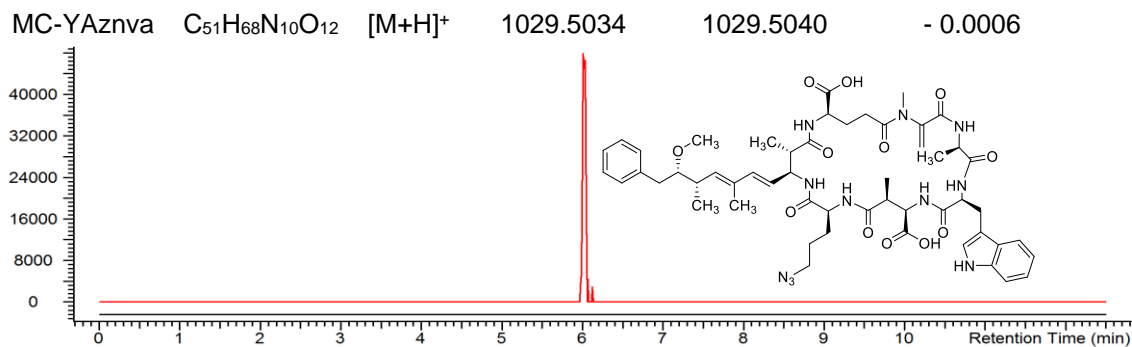


**Figure A75.** EIC ( $m/z$  1052.5200, pos. mode) overlay of a *Microcystis* CAWBG11 control culture (black, lower trace) and a culture grown with 30  $\mu$ M Aznva (red, upper trace).

	Formula	Ion	Measured $m/z$	Calculated $m/z$	Difference (Da)
MC-WAznva	C <sub>53</sub> H <sub>69</sub> N <sub>11</sub> O <sub>12</sub>	[M+H] <sup>+</sup>	1052.5199	1052.5200	- 0.0001

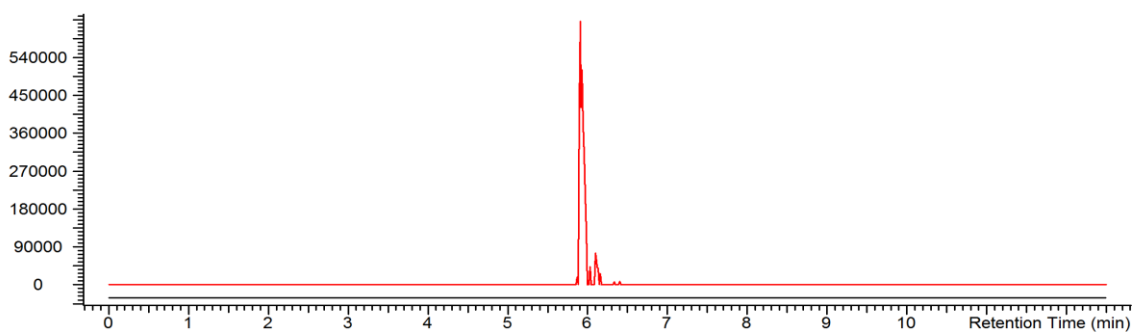


**Figure A76.** EIC ( $m/z$  979.5247, pos. mode) overlay of a *Microcystis* CAWBG11 control culture (black, lower trace) and a culture grown with 30  $\mu$ M Aznva (red, upper trace). The structure of MC-LAznva was confirmed by MS<sup>2</sup> (Figure A77 and Table A8).

	Formula	Ion	Measured $m/z$	Calculated $m/z$	Difference (Da)
MC-LAznva	C <sub>48</sub> H <sub>70</sub> N <sub>10</sub> O <sub>12</sub>	[M+H] <sup>+</sup>	979.5245	979.5247	- 0.0002

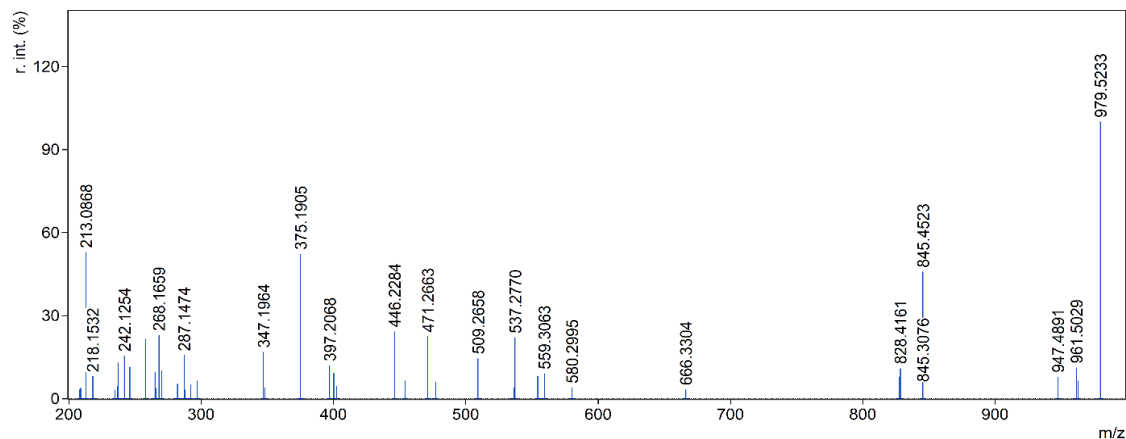


**Figure A77.** MS<sup>2</sup> spectrum of MC-LAznva obtained from PDB with *Microcystis* CAWBG11.

**Table A8.** Annotation of the MS<sup>2</sup> spectrum of MC-LAzvna obtained from PDB with *Microcystis* CAWBG11. Fragments characteristic for MC-LAzvna are highlighted in bold. Mdha, *N*-methyl dehydroalanine; Masp,  $\beta$ -methyl aspartic acid; Adda, 3*S*-amino-9*S*-methoxy-2*S*,6,8*S*-trimethyl-10-phenyldeca-4*E*,6*E*-dienoic acid.

<i>m/z</i>	Annotation	Ion	Difference [ppm]
979.5233	M + H <sup>+</sup>	-	- 1.5
845.3076	(M - C <sub>9</sub> H <sub>10</sub> O) + H <sup>+</sup>	-	+ 0.8
827.4361	(M - C <sub>9</sub> H <sub>10</sub> O - H <sub>2</sub> O) + H <sup>+</sup>	-	- 5.9
580.2995	Adda-Glu-Mdha-Ala + H <sup>+</sup>	z <sup>4</sup>	- 3.8
554.3046	Mdha-Ala-Leu-Masp-Aznva + H <sup>+</sup>	c <sup>5</sup>	+ 0.1
537.2770	Mdha-Ala-Leu-Masp-Aznva + H <sup>+</sup>	y <sup>5</sup> /b <sup>5</sup>	- 1.7
509.2658	Adda-Glu-Mdha + H <sup>+</sup>	z <sup>3</sup>	+ 2.3
477.2358	Mdha-Ala-Leu-Masp-(Aznva - HN <sub>3</sub> ) + H <sup>+</sup>	z <sup>5</sup>	+ 3.0
471.2663	Ala-Leu-Masp-Aznva + H <sup>+</sup>	c <sup>4</sup>	- 2.4
454.3046	Ala-Leu-Masp-Aznva + H <sup>+</sup>	y <sup>4</sup> /b <sup>4</sup>	- 0.4
446.2284	(Adda - C <sub>9</sub> H <sub>10</sub> O)-Glu-Mdha-Ala + H <sup>+</sup>	z <sup>4</sup>	
<b>397.2068</b>	<b>Mdha-Ala-Leu-Masp + H<sup>+</sup></b> <b>Glu-Mdha-Ala-Leu + H<sup>+</sup></b>	<b>y<sup>4</sup>/b<sup>4</sup></b>	<b>- 3.5</b>
375.1905	(Adda - C <sub>9</sub> H <sub>10</sub> O)-Glu-Mdha + H <sup>+</sup>	z <sup>3</sup>	- 2.6
297.4857	Adda + H <sup>+</sup>	z <sup>1</sup>	+ 2.6
292.1529	(Adda - C <sub>9</sub> H <sub>10</sub> O)-Glu + H <sup>+</sup>	z <sup>2</sup>	- 5.0
287.1474	Masp-Aznva + H <sup>+</sup>	c <sup>2</sup>	+ 4.1
270.1192	Masp-Aznva + H <sup>+</sup>	y <sup>2</sup> /b <sup>2</sup>	- 1.7
<b>268.1659</b>	<b>Mdha-Ala-Leu + H<sup>+</sup></b>	<b>y<sup>3</sup>/b<sup>3</sup></b>	<b>+ 1.1</b>
266.1133	Glu-Mdha-Ala - H <sub>2</sub> O + H <sup>+</sup>	y <sup>3</sup> /b <sup>3</sup>	- 0.7
242.1254	Masp-Aznva + H <sup>+</sup>	a <sup>2</sup>	+ 2.4
213.0866	Glu-Mdha + H	y <sup>2</sup> /b <sup>2</sup>	- 1.1

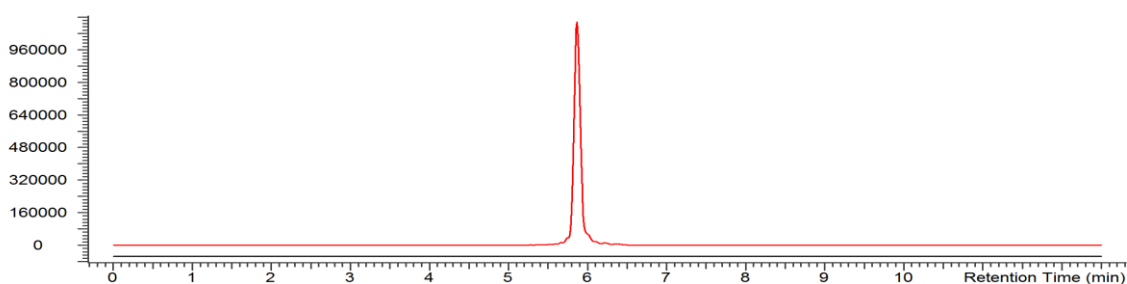


**Figure A78.** EIC (*m/z* 1006.5105, pos. mode) overlay of a *Microcystis* CAWBG11 control culture (black, lower trace) and a culture grown with 30  $\mu$ M Aznva (red, upper trace).

	Formula	Ion	Measured <i>m/z</i>	Calculated <i>m/z</i>	Difference (Da)
MC-AznvaAznva	C <sub>47</sub> H <sub>67</sub> N <sub>13</sub> O <sub>12</sub>	[M+H] <sup>+</sup>	1006.5106	1006.5105	+ 0.0001

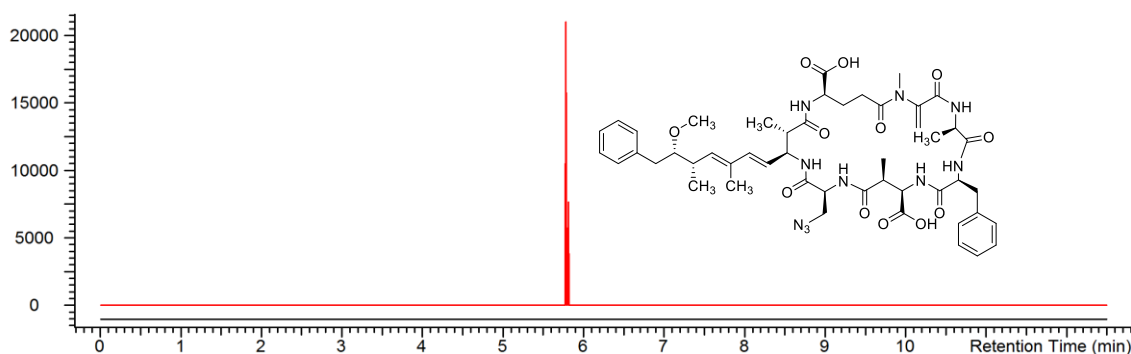


**Figure A79.** EIC ( $m/z$  985.5, pos. mode) overlay of a *Microcystis* CAWBG11 control culture (black, lower trace) and a culture grown with 30  $\mu$ M Azala (red, upper trace).

	Formula	Ion	Measured $m/z$	Calculated $m/z$	Difference (Da)
MC-FAzala	$C_{49}H_{64}N_{10}O_{12}$	$[M+H]^+$	985.4775	985.4778	- 0.0003

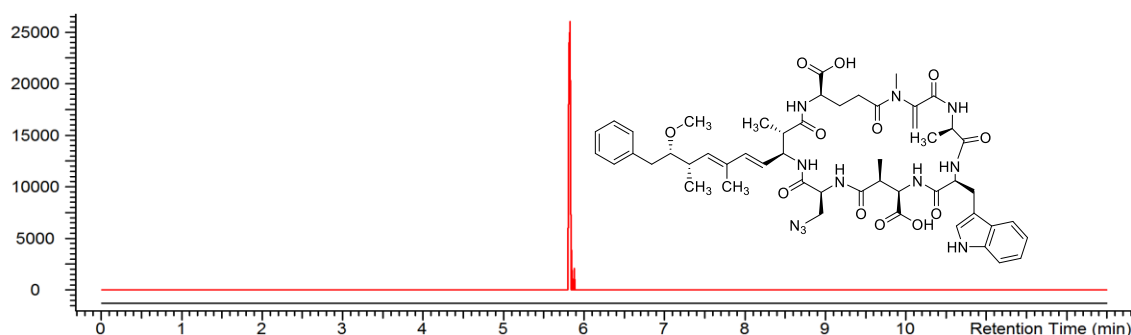


**Figure A80.** EIC ( $m/z$  1024.4887, pos. mode) overlay of a *Microcystis* CAWBG11 control culture (black, lower trace) and a culture grown with 30  $\mu$ M Azala (red, upper trace).

	Formula	Ion	Measured $m/z$	Calculated $m/z$	Difference (Da)
MC-FAzala	$C_{51}H_{65}N_{11}O_{12}$	$[M+H]^+$	1024.4884	1024.4887	- 0.0003

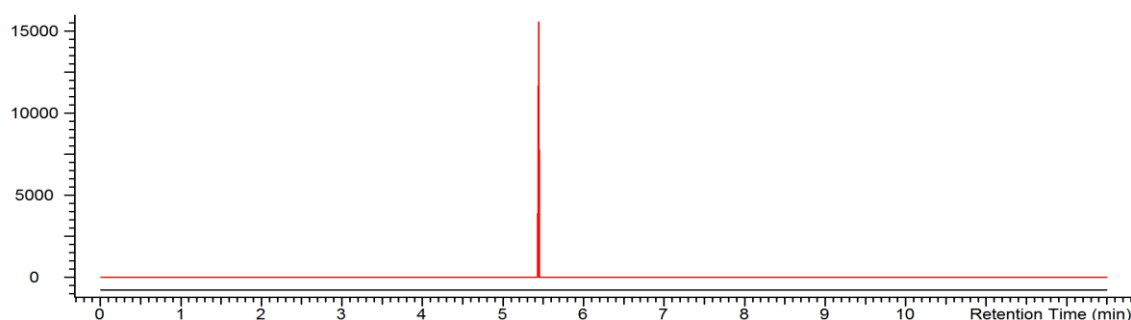


**Figure A81.** EIC ( $m/z$  951.4934, pos. mode) overlay of a *Microcystis* CAWBG11 control culture (black, lower trace) and a culture grown with 30  $\mu$ M Azala (red, upper trace).

	Formula	Ion	Measured $m/z$	Calculated $m/z$	Difference (Da)
MC-LAzala	$C_{46}H_{66}N_{10}O_{12}$	$[M+H]^+$	951.4932	951.4934	- 0.0002

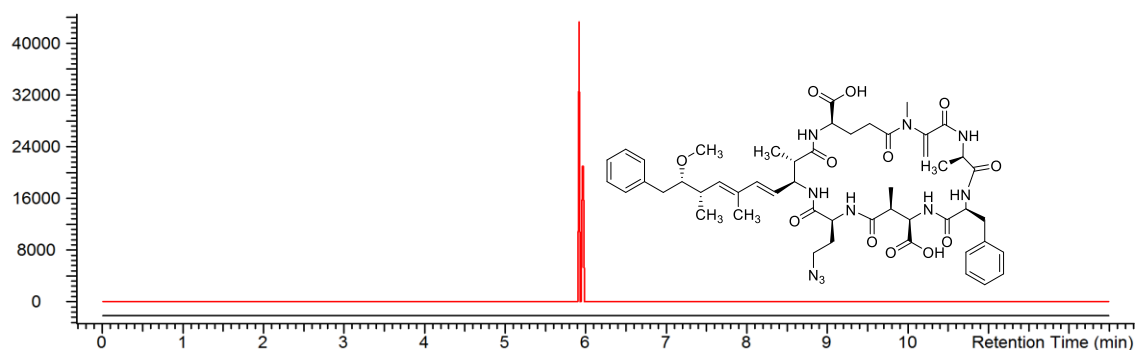


**Figure A82.** EIC ( $m/z$  999.4934, pos. mode) overlay of a *Microcystis* CAWBG11 control culture (black, lower trace) and a culture grown with 30  $\mu$ M Azabu (red, upper trace).

	Formula	Ion	Measured $m/z$	Calculated $m/z$	Difference (Da)
MC-FAzabu	$C_{50}H_{66}N_{10}O_{12}$	$[M+H]^+$	999.4938	999.4934	+ 0.0004

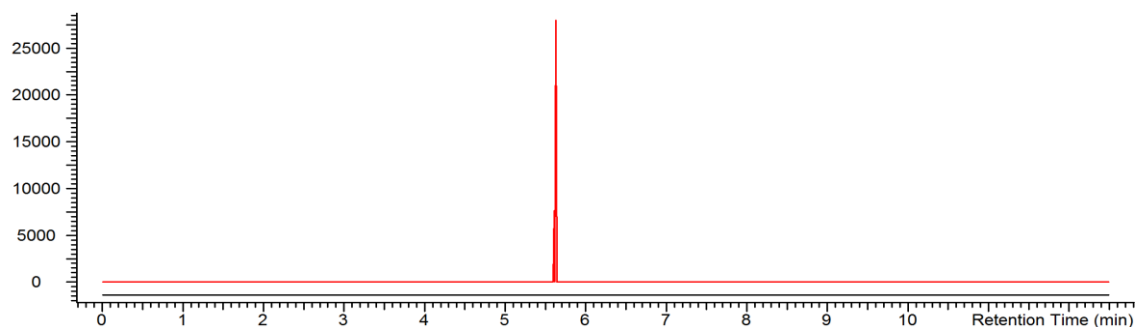


**Figure A83.** EIC ( $m/z$  1015.4884, pos. mode) overlay of a *Microcystis* CAWBG11 control culture (black, lower trace) and a culture grown with 30  $\mu$ M Azabu (red, upper trace).

	Formula	Ion	Measured $m/z$	Calculated $m/z$	Difference (Da)
MC-YAzabu	$C_{50}H_{66}N_{10}O_{13}$	$[M+H]^+$	1015.4833	1015.4884	- 0.0051

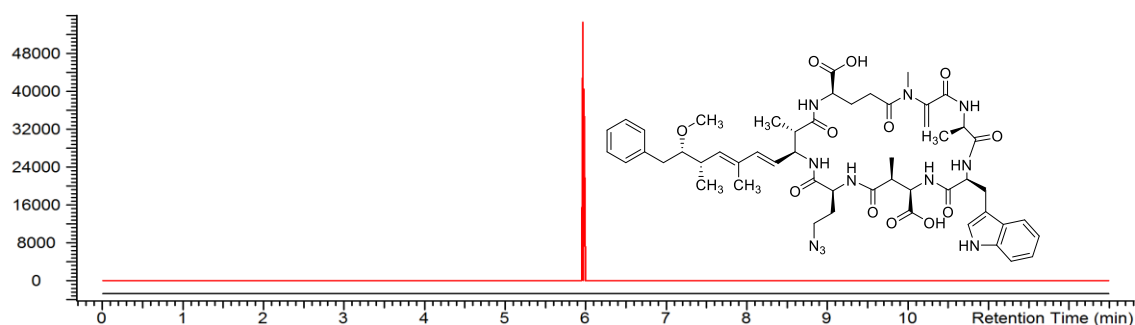


**Figure A84.** EIC ( $m/z$  1038.5043, pos. mode) overlay of a *Microcystis* CAWBG11 control culture (black, lower trace) and a culture grown with 30  $\mu$ M Azabu (red, upper trace).

	Formula	Ion	Measured $m/z$	Calculated $m/z$	Difference (Da)
MC-WAzabu	$C_{52}H_{67}N_{11}O_{12}$	$[M+H]^+$	1038.5039	1038.5043	- 0.0004

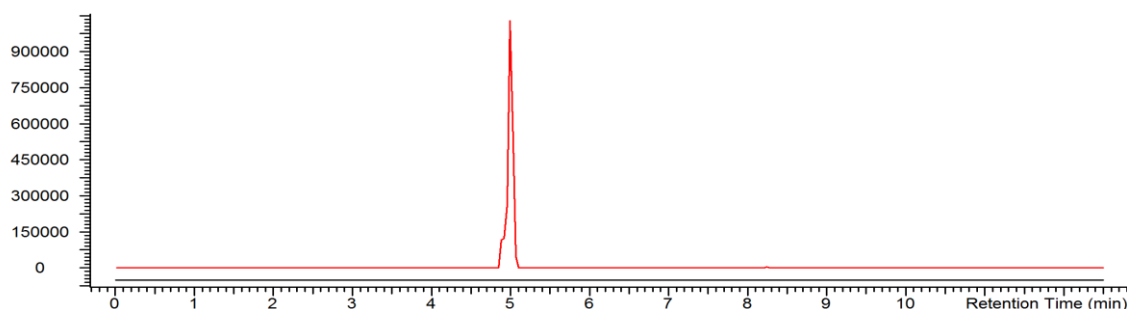


**Figure A85.** EIC ( $m/z$  965.5091, pos. mode) overlay of a *Microcystis* CAWBG11 control culture (black, lower trace) and a culture grown with 30  $\mu\text{M}$  Azabu (red, upper trace). The structure of MC-LAzabu was confirmed by MS<sup>2</sup> (Figure A92 and Table A9).

	Formula	Ion	Measured $m/z$	Calculated $m/z$	Difference (Da)
MC-LAzabu	$\text{C}_{47}\text{H}_{88}\text{N}_{10}\text{O}_{12}$	$[\text{M}+\text{H}]^+$	965.5084	965.5091	- 0.0007

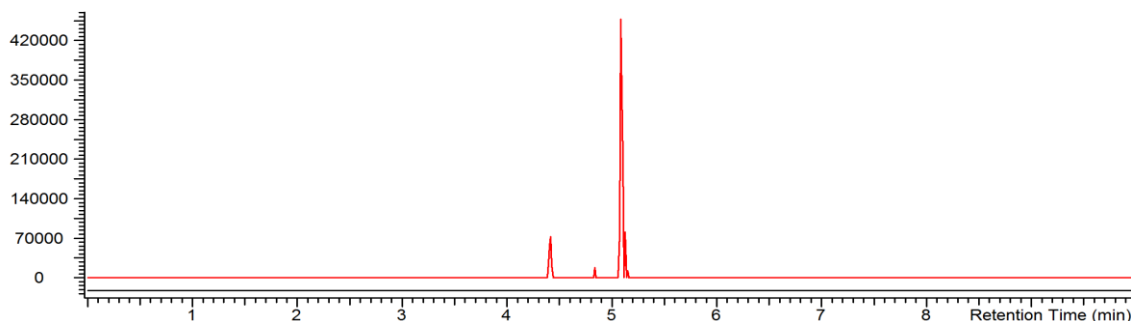


**Figure A86.** EIC ( $m/z$  1008.5261, pos. mode) overlay of a *Microcystis* CAWBG11 control culture (black, lower trace) and a culture grown with 30  $\mu\text{M}$  Azabu (red, upper trace). The occurrence of two peaks indicates the formation of both isomers.

	Formula	Ion	Measured $m/z$	Calculated $m/z$	Difference (Da)
MC-AzabuR	$\text{C}_{47}\text{H}_{69}\text{N}_{13}\text{O}_{12}$	$[\text{M}+\text{H}]^+$	1008.5264	1008.5261	+ 0.0003
MC-RAzabu			1008.5259		- 0.0002

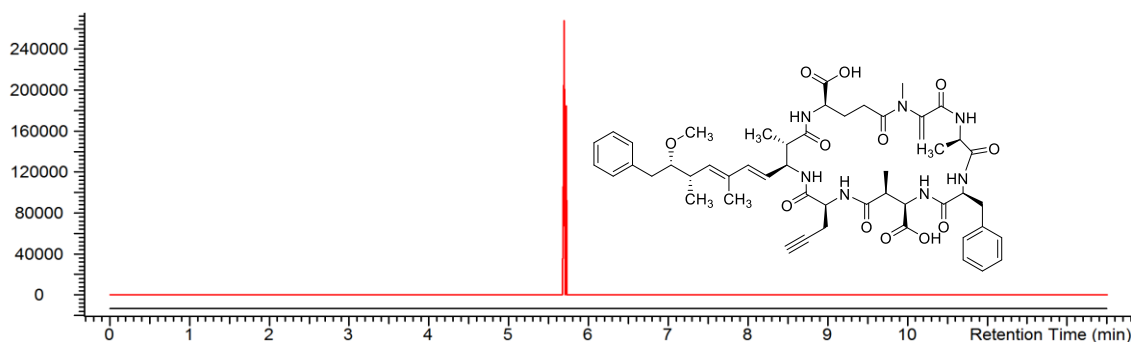


**Figure A87.** EIC ( $m/z$  968.4764, pos. mode) overlay of a *Microcystis* CAWBG11 control culture (black, lower trace) and a culture grown with 30  $\mu\text{M}$  Prgly (red, upper trace).

	Formula	Ion	Measured $m/z$	Calculated $m/z$	Difference (Da)
MC-FPrgly	$\text{C}_{51}\text{H}_{65}\text{N}_7\text{O}_{12}$	$[\text{M}+\text{H}]^+$	968.4764	968.4764	0.0000

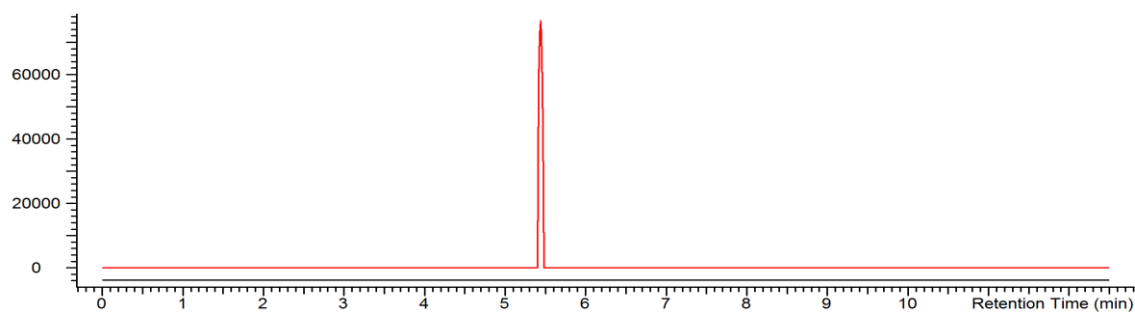


**Figure A88.** EIC ( $m/z$  984.4713, pos. mode) overlay of a *Microcystis* CAWBG11 control culture (black, lower trace) and a culture grown with 30  $\mu$ M Prgly (red, upper trace).

	Formula	Ion	Measured $m/z$	Calculated $m/z$	Difference (Da)
MC-YPrgly	$C_{51}H_{65}N_7O_{13}$	$[M+H]^+$	984.4713	984.4713	0.0000

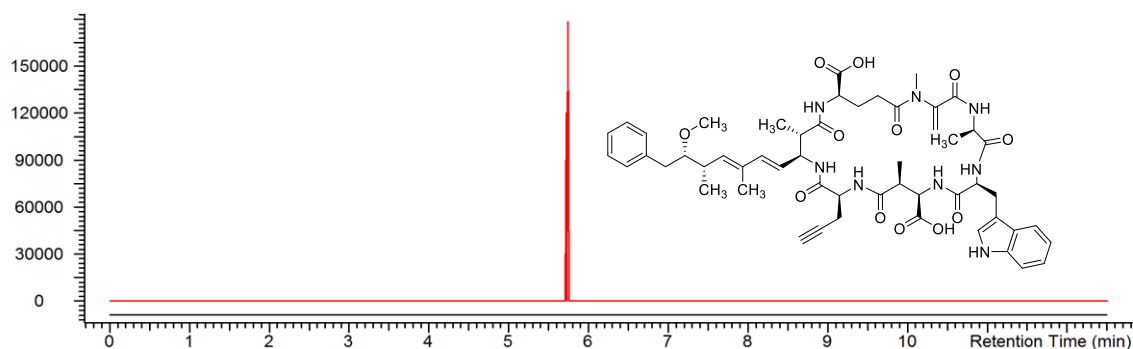


**Figure A89.** EIC ( $m/z$  1007.4873, pos. mode) overlay of a *Microcystis* CAWBG11 control culture (black, lower trace) and a culture grown with 30  $\mu$ M Prgly (red, upper trace).

	Formula	Ion	Measured $m/z$	Calculated $m/z$	Difference (Da)
MC-WPrgly	$C_{53}H_{66}N_8O_{12}$	$[M+H]^+$	1007.4870	1007.4873	- 0.0003

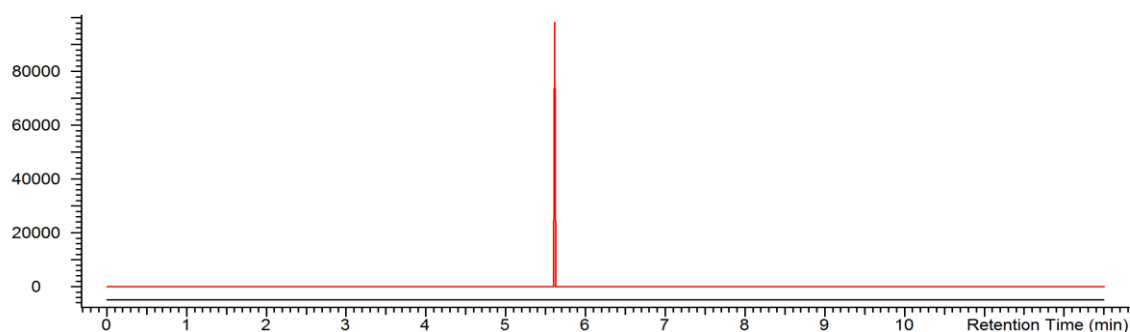


**Figure A90.** EIC ( $m/z$  934.4920, pos. mode) overlay of a *Microcystis* CAWBG11 control culture (black, lower trace) and a culture grown with 30  $\mu$ M Prgly (red, upper trace). The structure of MC-LPrgly was confirmed by MS<sup>2</sup> (Figure A93 and Table A10).

	Formula	Ion	Measured $m/z$	Calculated $m/z$	Difference (Da)
MC-LPrgly	$C_{48}H_{67}N_7O_{12}$	$[M+H]^+$	934.4923	934.4920	+ 0.0003

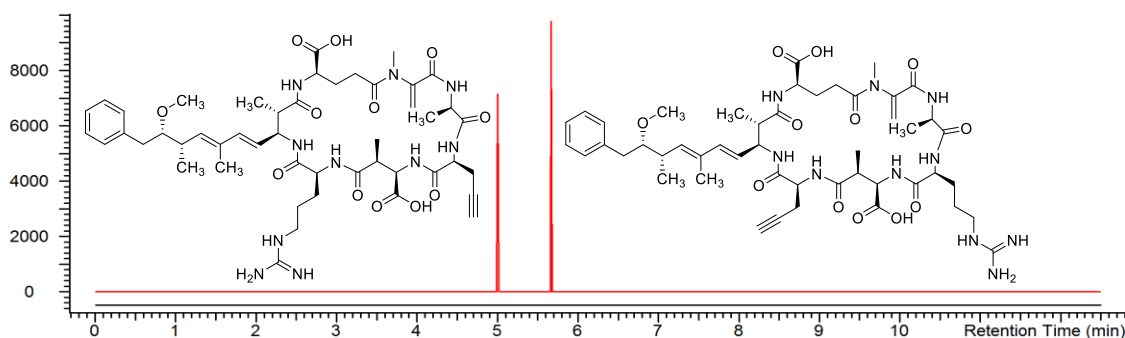


**Figure A91.** EIC ( $m/z$  977.5091, pos. mode) overlay of a *Microcystis* CAWBG11 control culture (black, lower trace) and a culture grown with 30  $\mu$ M Prgly (red, upper trace). The occurrence of two peaks indicates the co-formation of both isomers.

	Formula	Ion	Measured $m/z$	Calculated $m/z$	Difference (Da)
MC-PrglyR	$C_{48}H_{68}N_{10}O_{12}$	$[M+H]^+$	977.5111	977.5091	+ 0.0019
MC-RPrgly			977.5054		- 0.0037

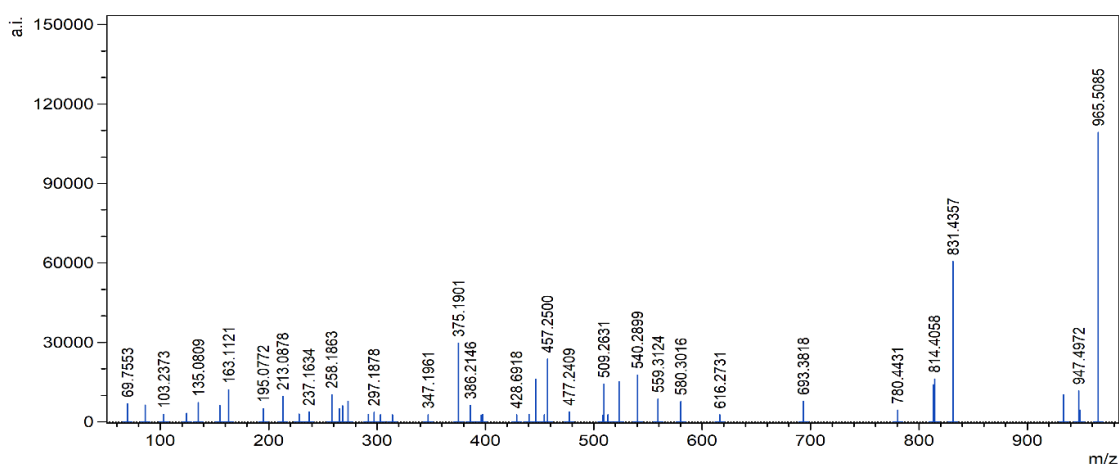


**Figure A92.**  $MS^2$  spectrum of MC-LAzabu from PDB with *Microcystis* CAWBG11.

**Table A9.** Annotation of the  $MS^2$  spectrum of MC-LAzabu obtained from PDB with *Microcystis* CAWBG11. Fragments characteristic for MC-LAzabu are highlighted in bold script. Mdha, *N*-methyl dehydroalanine; Masp,  $\beta$ -methyl aspartic acid; Adda, 3*S*-amino-9*S*-methoxy-2*S*,6*S*,8*S*-trimethyl-10-phenyldeca-4*E*,6*E*-dienoic acid.

$m/z$	Annotation	Ion	Difference [ppm]
965.5085	$M + H^+$	-	- 0.6
947.4972	$(M - H_2O) + H^+$	-	- 1.4
831.4357	$(M - C_9H_{10}O) + H^+$	-	- 0.3
693.3818	Adda-Glu-Mdha-Ala-Leu - $NH_3 + H^+$	$y^5/b^5$	- 5.7
540.2899	Mdha-Ala-Leu-Masp-Azabu + $H^+$	$c^5$	+ 1.8
509.2631	Adda-Glu-Mdha + $H^+$	$z^3$	- 3.0
457.2500	Ala-Leu-Masp-Azabu + $H^+$	$c^4$	- 3.8
386.2146	Leu-Masp-Azabu + $H^+$	$c^3$	+ 0.0
375.1901	$(Adda - C_9H_{10}O)-Glu-Mdha + H^+$	$z^5$	- 3.6
273.1319	Masp-Azabu + $H^+$	$c^2$	+ 4.7
<b>268.1658</b>	<b>Mdha-Ala-Leu + <math>H^+</math></b>	<b><math>y^3/b^3</math></b>	+ 0.8
213.0878	Glu-Mdha + $H$	$y^2/b^2$	+ 3.6

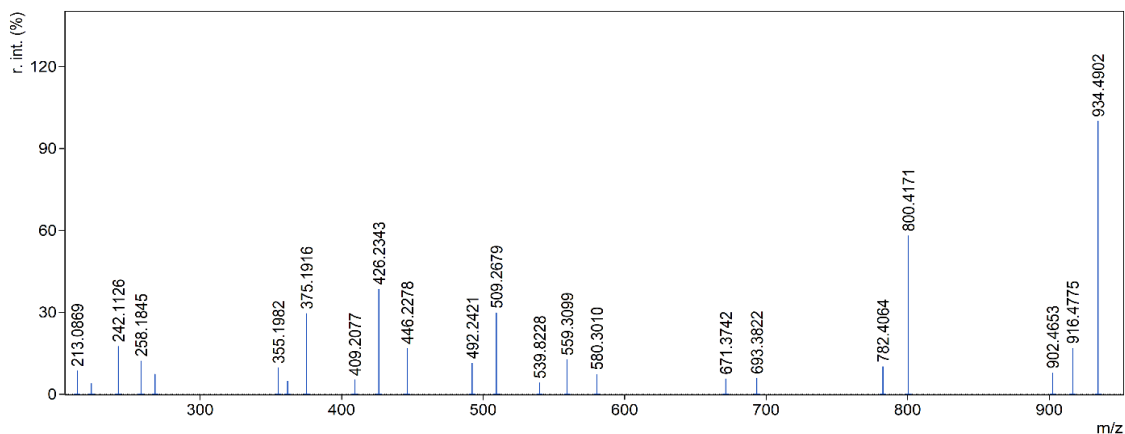


**Figure A93.** MS<sup>2</sup> spectrum of MC-LPrgly from PDB with *Microcystis* CAWBG11.

**Table A10.** Annotation of the MS<sup>2</sup> spectrum of MC-LPrgly obtained from PDB with *Microcystis* CAWBG1. Fragments characteristic for MC-LPrgly are highlighted in bold script. Mdha, *N*-methyl dehydroalanine; Masp,  $\beta$ -methyl aspartic acid; Adda, 3*S*-amino-9*S*-methoxy-2*S*,6,8*S*-trimethyl-10-phenyldeca-4*E*,6*E*-dienoic acid.

<i>m/z</i>	Annotation	Ion	Difference [ppm]
934.4902	M + H <sup>+</sup>	-	- 2.0
916.4775	(M - H <sub>2</sub> O) + H <sup>+</sup>	-	- 4.4
902.4653	(M - H <sub>3</sub> COH) + H <sup>+</sup>	-	- 0.6
800.4171	(M - C <sub>9</sub> H <sub>10</sub> O) + H <sup>+</sup>	-	- 2.3
782.4064	(M - C <sub>9</sub> H <sub>10</sub> O - H <sub>2</sub> O) + H <sup>+</sup>	-	- 2.5
<b>693.3822</b>	<b>Adda-Glu-Mdha-Ala-Leu + H<sup>+</sup></b>	<b>z<sup>5</sup></b>	<b>- 5.2</b>
671.3742	Mdha-Ala-Leu-Masp-Prgly-(Adda - C <sub>9</sub> H <sub>10</sub> O) + H <sup>+</sup> Prgly-(Adda - C <sub>9</sub> H <sub>10</sub> O)-Glu-Mdha-Ala-Leu + H <sup>+</sup>	y <sup>6</sup> /b <sup>6</sup>	- 3.1
580.3010	Adda-Glu-Mdha-Ala + H <sup>+</sup>	z <sup>4</sup>	- 1.2
<b>559.3099</b>	<b>Adda-Glu-Mdha-Ala-Leu + H<sup>+</sup></b>	<b>z<sup>5</sup></b>	<b>- 4.8</b>
446.2278	(Adda - C <sub>9</sub> H <sub>10</sub> O)-Glu-Mdha-Ala + H <sup>+</sup>	z <sup>4</sup>	- 1.6
426.2343	Ala-Leu-Masp-Prgly + H <sup>+</sup>	c <sup>4</sup>	- 1.0
409.2077	Ala-Leu-Masp-Prgly + H <sup>+</sup>	y <sup>4</sup> /b <sup>4</sup>	- 1.2
375.1916	(Adda - C <sub>9</sub> H <sub>10</sub> O)-Glu-Mdha + H <sup>+</sup>	z <sup>3</sup>	0.4
355.1982	Leu-Masp-Prgly + H <sup>+</sup>	c <sup>3</sup>	1.8
<b>268.1654</b>	<b>Mdha-Ala-Leu + H<sup>+</sup></b>	<b>y<sup>3</sup>/b<sup>3</sup></b>	<b>- 0.7</b>
242.1126	Masp-Prgly + H <sup>+</sup>	c <sup>2</sup>	- 3.7
231.0869	Glu-Mdha + H <sup>+</sup>	y <sup>2</sup> /b <sup>2</sup>	- 0.5



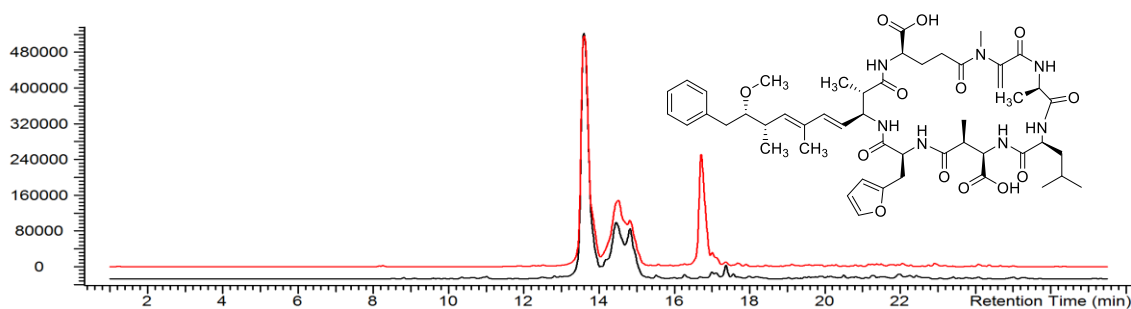


**Figure A94.** EIC ( $m/z$  976.4, pos. mode) overlay of a *Microcystis* CBT 275 control culture (black, lower trace) and a culture grown with 30  $\mu$ M Furala (red, upper trace).

	Formula	Ion	Measured $m/z$	Calculated $m/z$	Difference (Da)
MC-LFurala	$C_{50}H_{69}N_7O_{13}$	$[M+H]^+$	976.4	976.5	- 0.1

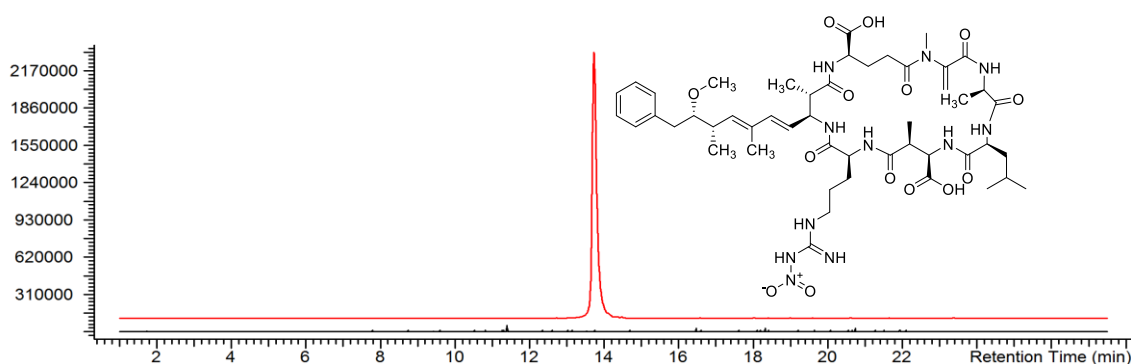


**Figure A95.** EIC ( $m/z$  1040.5, pos. mode) overlay of an *M. aeruginosa* CBT 480 control culture (black, lower trace) and a culture grown with 30  $\mu$ M Narg (red, upper trace).

	Formula	Ion	Measured $m/z$	Calculated $m/z$	Difference (Da)
MC-LNarg	$C_{49}H_{73}N_{11}O_{14}$	$[M+H]^+$	1040.5	1040.5	0.0

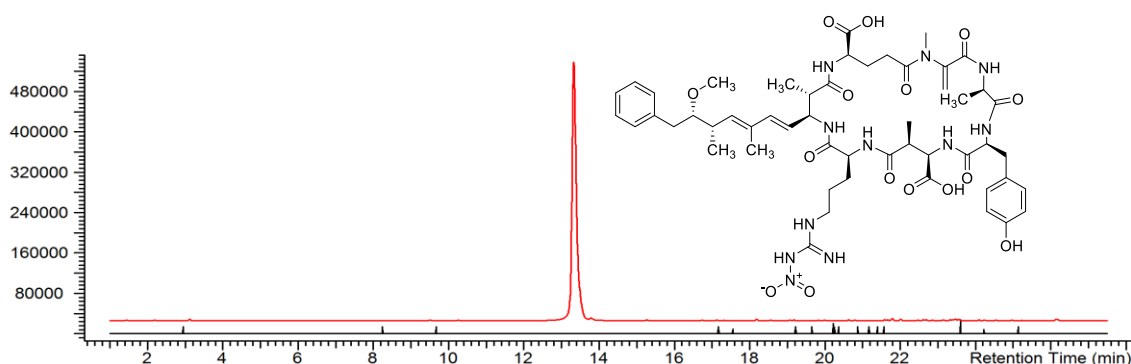


**Figure A96.** EIC ( $m/z$  1090.5, pos. mode) overlay of a *Microcystis aeruginosa* CBT 480 control culture (black, lower trace) and a culture grown with 30  $\mu$ M Narg (red, upper trace).

	Formula	Ion	Measured $m/z$	Calculated $m/z$	Difference (Da)
MC-YNarg	$C_{52}H_{71}N_{11}O_{15}$	$[M+H]^+$	1090.5	1090.5	0.0

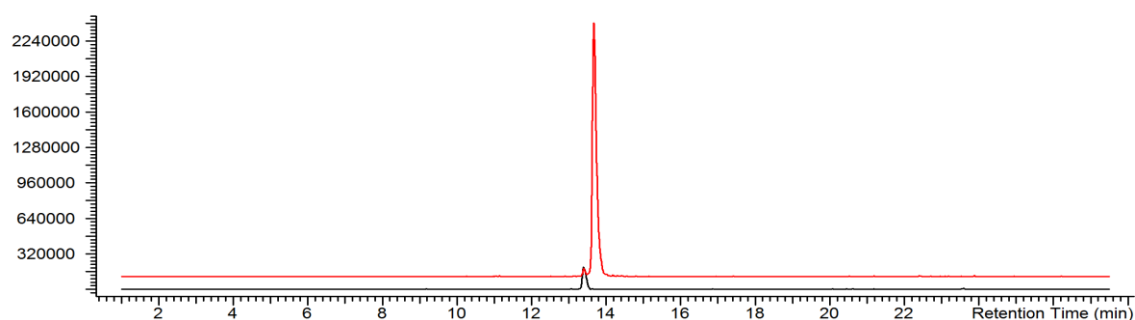


**Figure A97.** EIC ( $m/z$  1040.5, pos. mode) overlay of a *Microcystis* CBT 1 control culture (black, lower trace) and a culture grown with 30  $\mu$ M Narg (red, upper trace).

	Formula	Ion	Measured $m/z$	Calculated $m/z$	Difference (Da)
MC-LNarg	$C_{49}H_{73}N_{11}O_{14}$	$[M+H]^+$	1040.5	1040.5	0.0

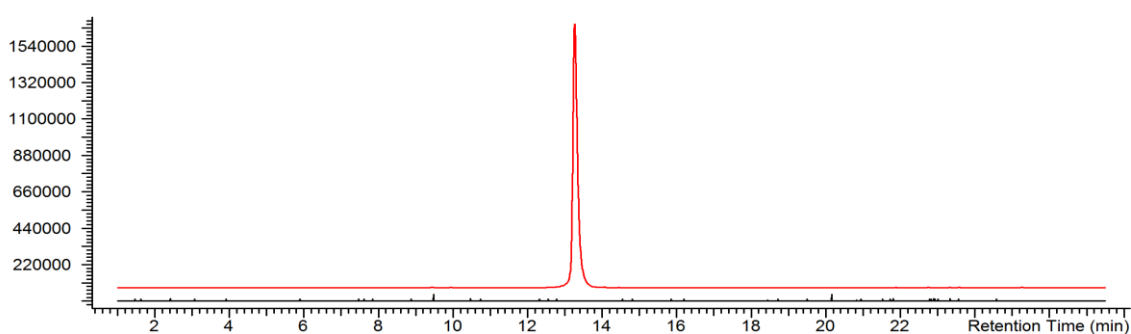


**Figure A98.** EIC ( $m/z$  1090.5, pos. mode) overlay of a *Microcystis* CBT 1 control culture (black, lower trace) and a culture grown with 30  $\mu$ M Narg (red, upper trace).

	Formula	Ion	Measured $m/z$	Calculated $m/z$	Difference (Da)
MC-YNarg	$C_{52}H_{71}N_{11}O_{15}$	$[M+H]^+$	1090.5	1090.5	0.0

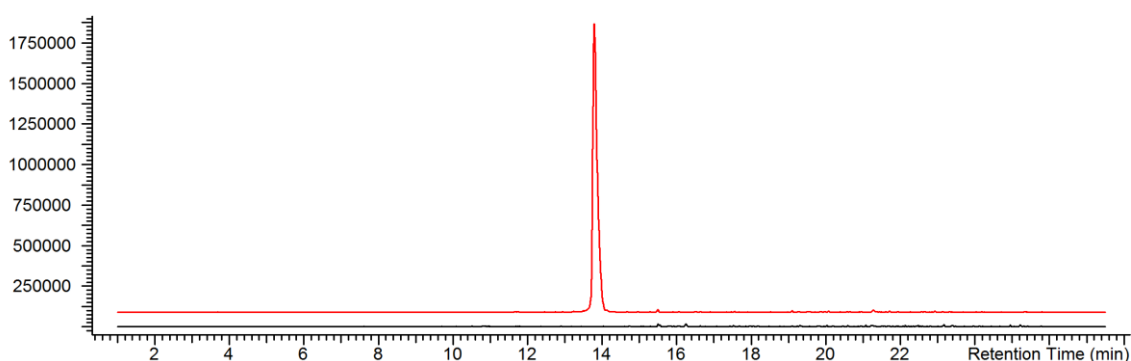


**Figure A99.** EIC ( $m/z$  1040.5, pos. mode) overlay of a *Microcystis* CBT 275 control culture (black, lower trace) and a culture grown with 30  $\mu$ M Narg (red, upper trace).

	Formula	Ion	Measured $m/z$	Calculated $m/z$	Difference (Da)
MC-LNarg	$C_{49}H_{73}N_{11}O_{14}$	$[M+H]^+$	1040.4	1040.5	-0.1

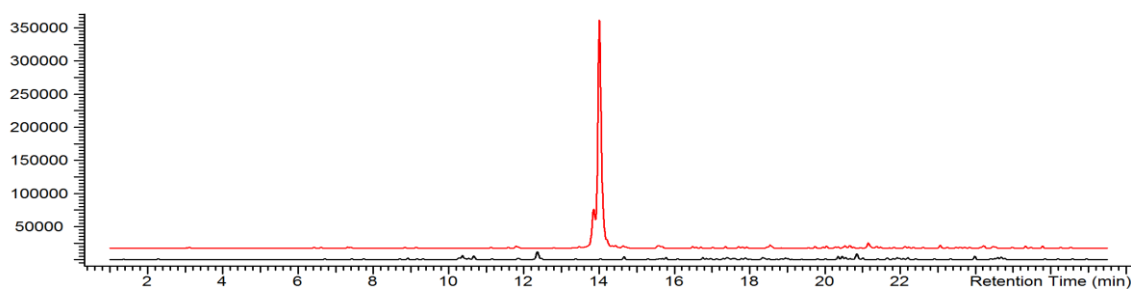


**Figure A100.** EIC ( $m/z$  1040.5, pos. mode) overlay of a *Microcystis* CBT 959 control culture (black, lower trace) and a culture grown with 30  $\mu$ M Narg (red, upper trace).

	Formula	Ion	Measured $m/z$	Calculated $m/z$	Difference (Da)
MC-LNarg	$C_{49}H_{73}N_{11}O_{14}$	$[M+H]^+$	1040.5	1040.5	0.0

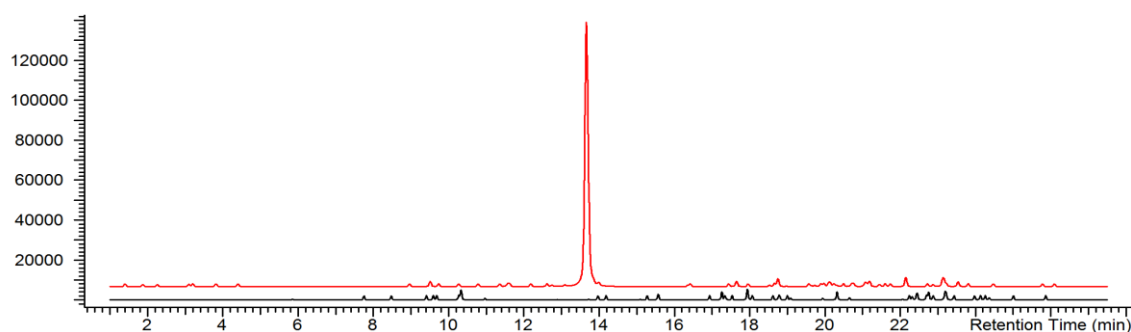


**Figure A101.** EIC ( $m/z$  1090.5, pos. mode) overlay of a *Microcystis* CBT 959 control culture (black, lower trace) and a culture grown with 30  $\mu$ M Narg (red, upper trace).

	Formula	Ion	Measured $m/z$	Calculated $m/z$	Difference (Da)
MC-YNarg	$C_{52}H_{71}N_{11}O_{15}$	$[M+H]^+$	1090.4	1090.5	-0.1

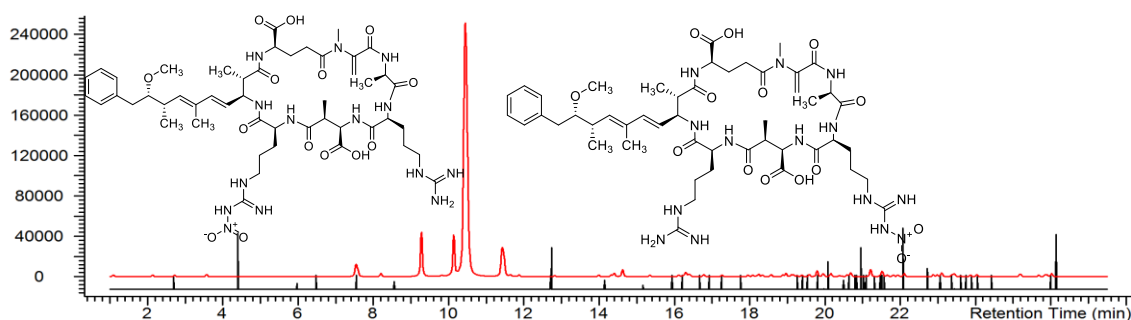


**Figure A102.** EIC ( $m/z$  1083.5, pos. mode) overlay of a *Microcystis* CBT 633 control culture (black, lower trace) and a culture grown with 30  $\mu$ M Narg (red, upper trace). The occurrence of two peaks indicates the co-formation of both isomers.

	Formula	Ion	Measured $m/z$	Calculated $m/z$	Difference (Da)
MC-RNarg	$C_{49}H_{74}N_{14}O_{14}$	$[M+H]^+$	1083.5	1083.5	0.0
MC-NargR			1083.5		0.0

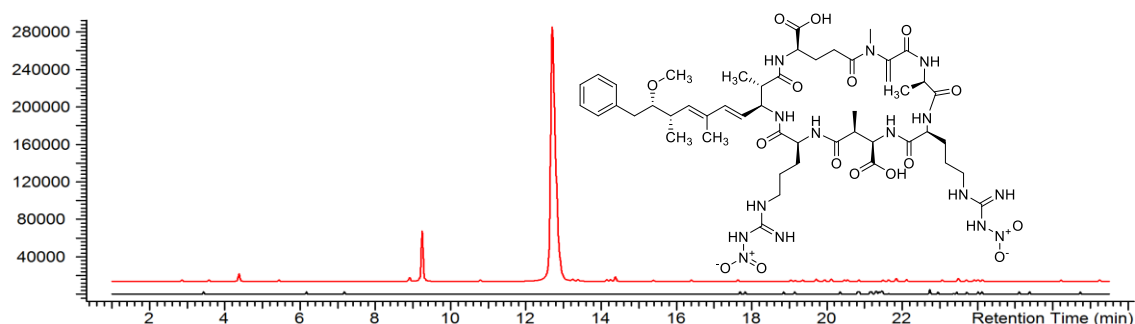


**Figure A103.** EIC ( $m/z$  1128.4, pos. mode) overlay of a *Microcystis* CBT 633 control culture (black, lower trace) and a culture grown with 30  $\mu$ M Narg (red, upper trace).

	Formula	Ion	Measured $m/z$	Calculated $m/z$	Difference (Da)
MC-NargNarg	$C_{49}H_{73}N_{15}O_{16}$	$[M+H]^+$	1128.4	1128.5	- 0.1

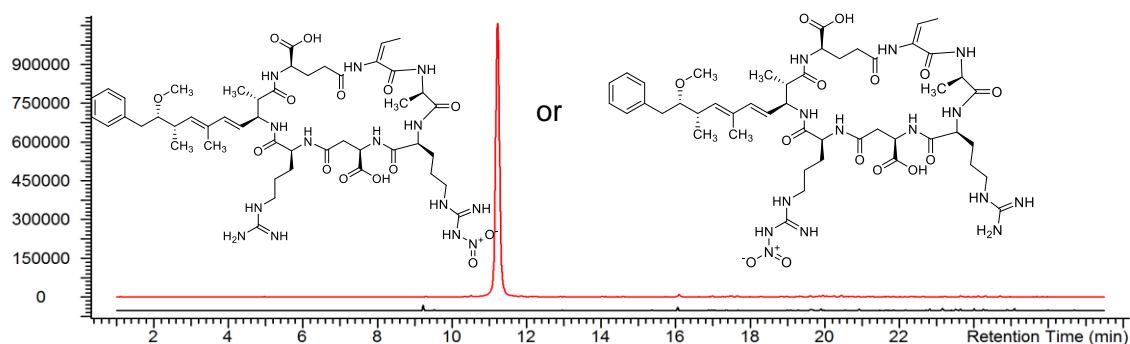


**Figure A104.** EIC ( $m/z$  1069.5, pos. mode) overlay of a *Planktothrix rubescens* CBT 329 control culture (black, lower trace) and a culture grown with 30  $\mu$ M Narg (red, upper trace). Since PDB of *Planktothrix rubescens* CBT329 was proof of concept only, the structure of the isomer was not determined.

	Formula	Ion	Measured $m/z$	Calculated $m/z$	Difference (Da)
[D-Asp <sup>3</sup> ,E-Dhb <sup>7</sup> ]MC-NargR or -RNarg	$C_{48}H_{72}N_{14}O_{14}$	$[M+H]^+$	1069.5	1069.5	0.0

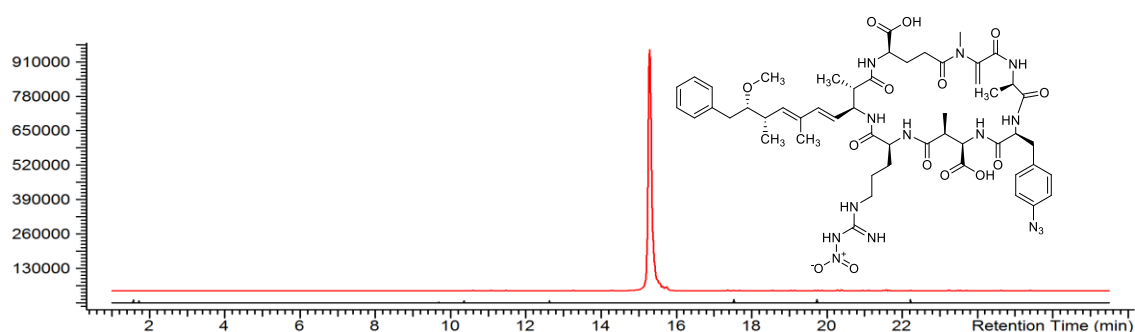


**Figure A105.** EIC ( $m/z$  1115.4, pos. mode) overlay of a *M. aeruginosa* CBT 480 control culture (black, lower trace) and a culture grown with 30  $\mu$ M Azphe and 30  $\mu$ M Narg (red, upper trace).

	Formula	Ion	Measured $m/z$	Calculated $m/z$	Difference (Da)
MC-AzpheNarg	$C_{52}H_{70}N_{14}O_{14}$	$[M+H]^+$	1115.4	1115.5	- 0.1

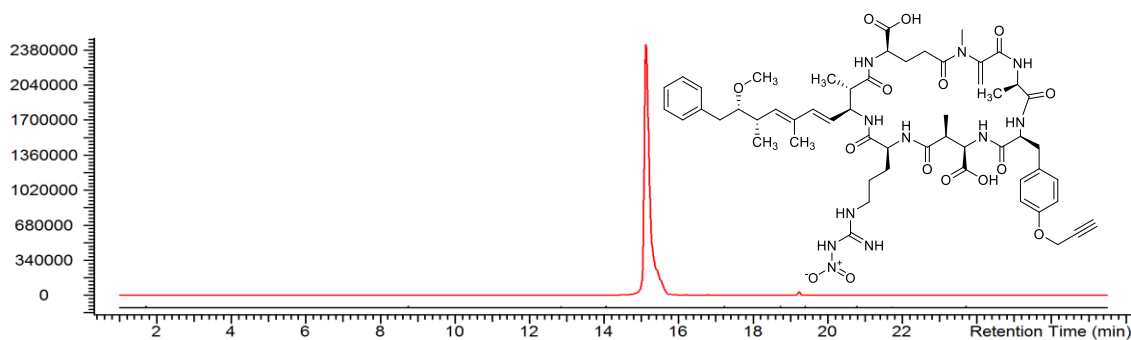


**Figure A106.** EIC ( $m/z$  1128.4, pos. mode) overlay of an *M. aeruginosa* CBT 480 control culture (black, lower trace) and a culture grown with 30  $\mu$ M Prtyr and 30  $\mu$ M Narg (red, upper trace).

	Formula	Ion	Measured $m/z$	Calculated $m/z$	Difference (Da)
MC-PrtyrNarg	$C_{52}H_{70}N_{14}O_{14}$	$[M+H]^+$	1128.4	1128.5	- 0.1

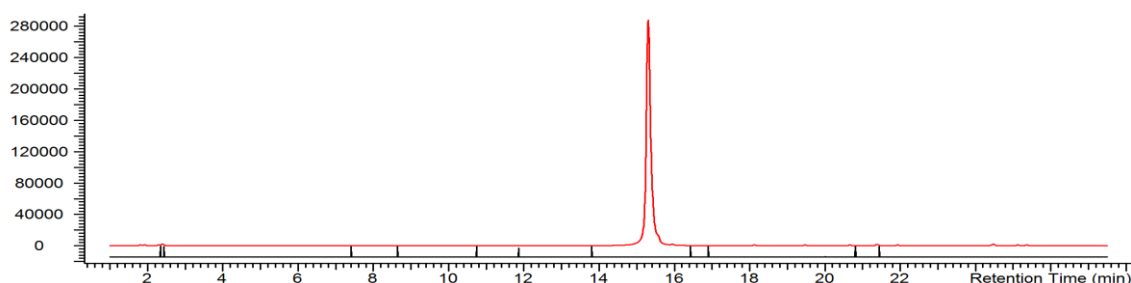


**Figure A107.** EIC ( $m/z$  1115.4, pos. mode) overlay of a *Microcystis* CBT 1 control culture (black, lower trace) and a culture grown with 30  $\mu$ M Azphe and 30  $\mu$ M Narg (red, upper trace).

	Formula	Ion	Measured $m/z$	Calculated $m/z$	Difference (Da)
MC-AzpheNarg	$C_{52}H_{70}N_{14}O_{14}$	$[M+H]^+$	1115.4	1115.5	- 0.1

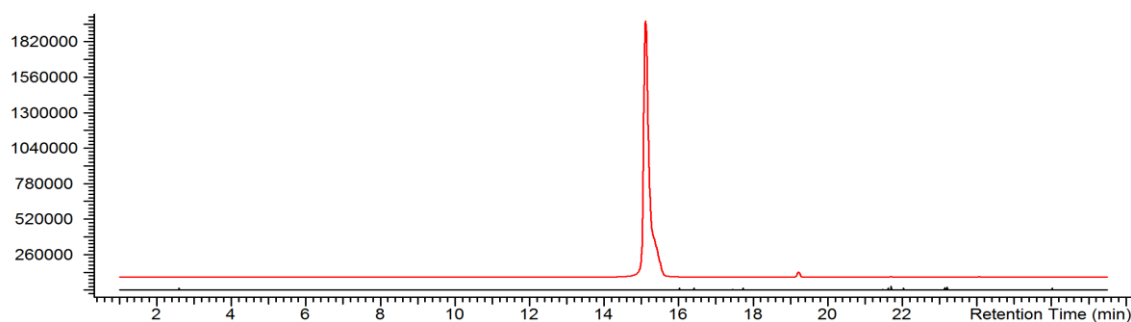


**Figure A108.** EIC ( $m/z$  1128.4, pos. mode) overlay of a *Microcystis* CBT 1 control culture (black, lower trace) and a culture grown with 30  $\mu$ M Prtyr and 30  $\mu$ M Narg (red, upper trace).

	Formula	Ion	Measured $m/z$	Calculated $m/z$	Difference (Da)
MC-PrtyrNarg	$C_{52}H_{70}N_{14}O_{14}$	$[M+H]^+$	1128.4	1128.5	- 0.1

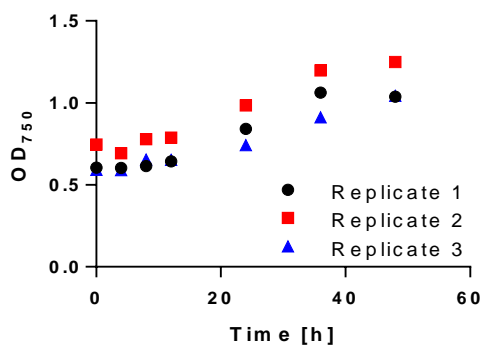


**Figure A109.** Growth of the three *M. aeruginosa* CBT 480 replicates (black circles, replicate 1; red squares, replicate 2; blue triangles, replicate 3) monitored as OD<sub>750</sub> supplemented with 50 µM Prtyr over 48 h.

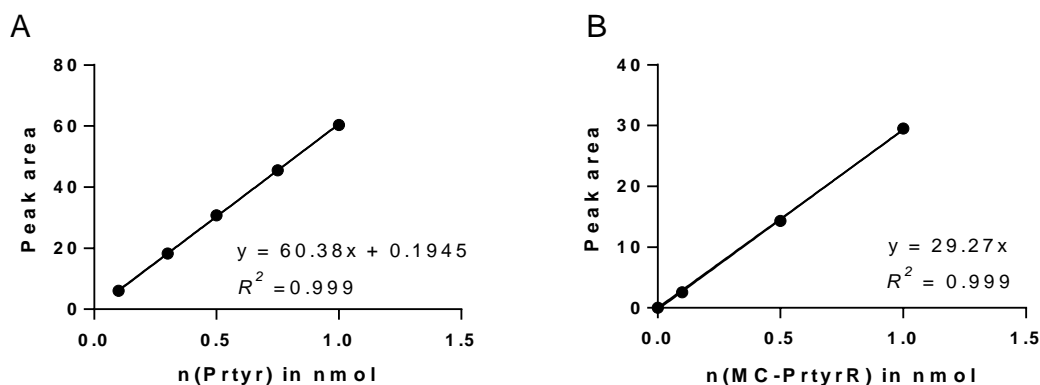


**Figure A110.** Calibration curves for the quantification of Prtyr and MC-PrtyrR. (A) Calibration curve for Prtyr quantification from 0.1 to 1 nmol Prtyr on-column. The equation obtained from linear regression and the goodness of fit ( $R^2$ ) are depicted in the graph. (B) Calibration curve for Prtyr quantification from 0.1 to 1 nmol MC-PrtyrR on-column. The equation obtained from linear regression and the goodness of fit ( $R^2$ ) are depicted in the graph.

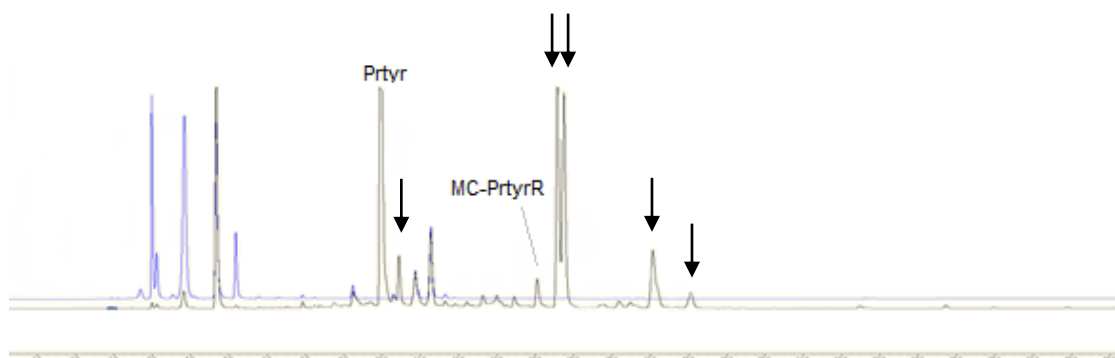


**Figure A111.** HPLC-Fluorescence chromatogram ( $\lambda_{\text{ex}}$ : 404 nm;  $\lambda_{\text{em}}$ : 480 nm) overlay of an *M. aeruginosa* CBT 480 supplemented with Prtyr extract (black trace) and *M. aeruginosa* CBT 480 control extract after conjugation with 3-azido-6-bromo-7-hydroxycoumarin (**4**). Black arrows indicate fluorescent peaks which cannot be linked to background fluorescence or known products.

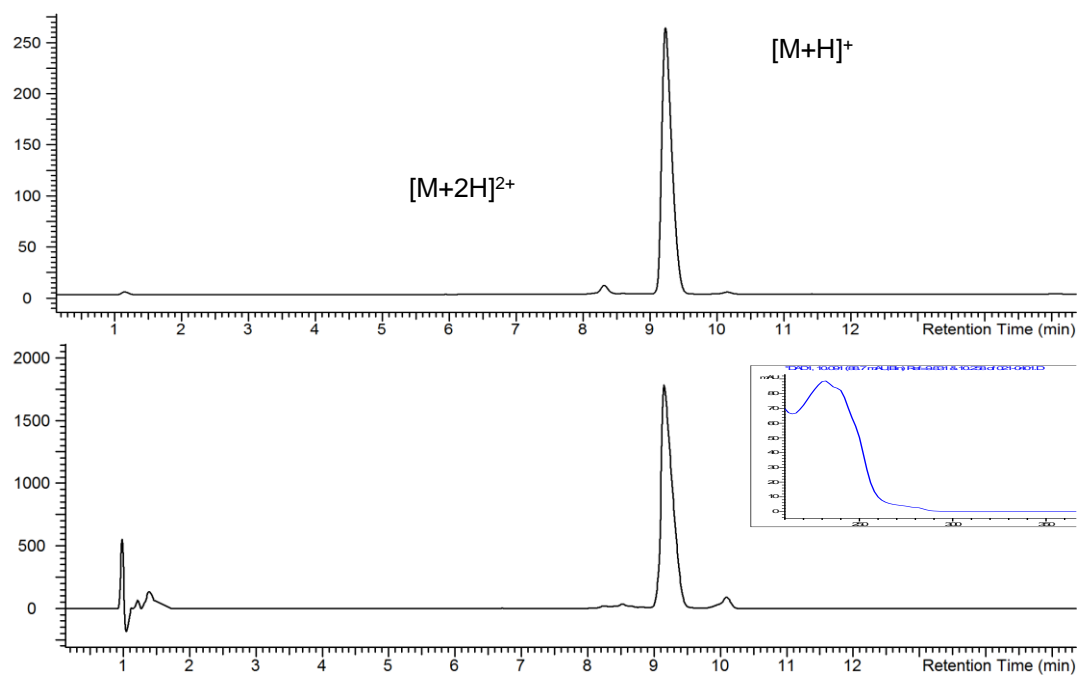


**Figure A112.** HPLC-ELSD chromatogram (top) and HPLC UV chromatogram (230 nm, bottom) of MC-PrtyrR (**3**) isolated from *M. aeruginosa* CBT 480. The compound at  $t_R$  10.1 min shows a microcystin-like UV spectrum (insert) and an  $[M+H]^+$  ion at  $m/z$  1097.5, indicating it to be  $[\text{Glu}(\text{OMe})^6]\text{MC-PrtyrY}$  (artifact from the isolation with MeOH/TFA).

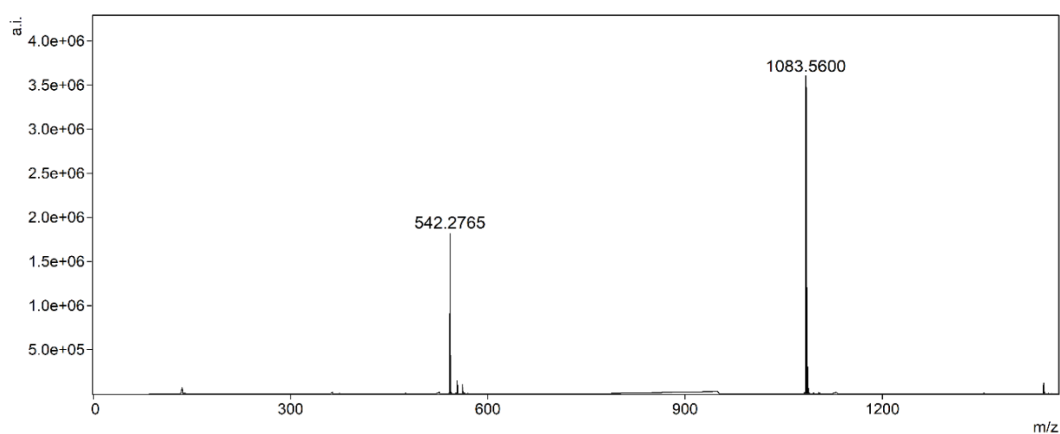
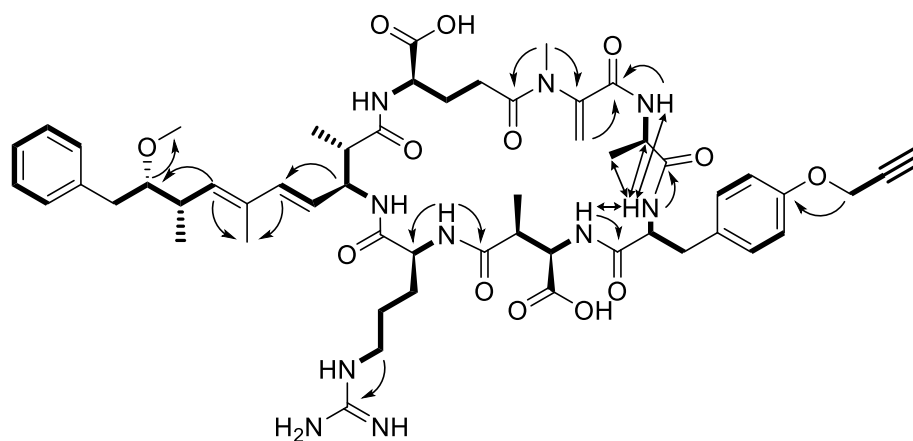


**Figure A 113.** HRMS spectrum of MC-PrtyrR (**3**) isolated from *M. aeruginosa* CBT 480.

**Table A11.**  $^1\text{H}$  and  $^{13}\text{C}$  NMR (600/150 MHz, DMSO- $d_6$ ) spectroscopic assignments for **3**.

unit	position	$\delta_{\text{C}}$	$\delta_{\text{H}}$ (J in Hz)	unit	position	$\delta_{\text{C}}$	$\delta_{\text{H}}$ (J in Hz)	
Ala	1	172.1		Adda	1	172.8		
	2	47.0	4.47, m		2	43.4	2.72, m	
	3	16.9	1.08, d (7.3)		3	54.4	4.35, m	
	NH		7.27, m		4	126.2	5.33, dd (15.4, 7.8)	
Prtyr	1	170.2			5	135.5	6.11, d (15.4)	
	2	58.0	4.03, m		6	132.0		
	3a	35.5	2.99, m		7	135.3	5.46, d (9.7)	
	3b		2.90, m		8	35.4	2.56, m	
	4	131.0			9	85.8	3.25, m	
	5/9	130.0	7.25, m		10a	37.0	2.73, m	
	6/8	114.5	6.84, d (8.6)		10b		2.69, m	
	7	155.8			11	16.0	0.94, d (6.8)	
	NH		7.79, d (7.2)		12	12.5	1.56, s	
	p-1	55.30	4.74, d (2.4)		13	15.9	0.98, d (6.8)	
p-2	79.4		14		57.4	3.19, s		
p-3	78.1	3.53, t (2.4)	15	139.2				
Masp	1	170.1		16/20	129.2	7.19, m		
	2	55.3	4.21, m	17/19	128.1	7.27, m		
	3a	39.4	3.13, m	18	125.9	7.18, m		
	4	15.0	0.92, d (7.3)	NH		7.60, br. s		
	NH		8.11, d (9.2)	Glu	1	174.5		
Arg	1	173.9			2	52.9	4.39, m	
	2	51.2	4.2, m		3a	25.9	1.97, m	
	3	28.0	1.98, m		3b		1.81, m	
	4a	25.5	1.38, m		4a	31.3	2.32, m	
	4b		1.31, m		4b		2.28, m	
	5	40.3	3.01, m		5	175.2		
	6	156.6			NH		9.13, br. s	
	N $\square$ H		8.92, d (9.2)		Mdha	N-Me	37.5	3.15, s
	N $\square$ H		7.44, m		1	162.4		
				2	144.8			
			3a	114.1	5.85, s			
			3b		5.43, s			





TOCSY spin systems in bold, key HMBC correlations indicated by curved arrows, ROESY correlations proving the incorporation of Prtyr in position 2 indicated by double-headed straight arrows.

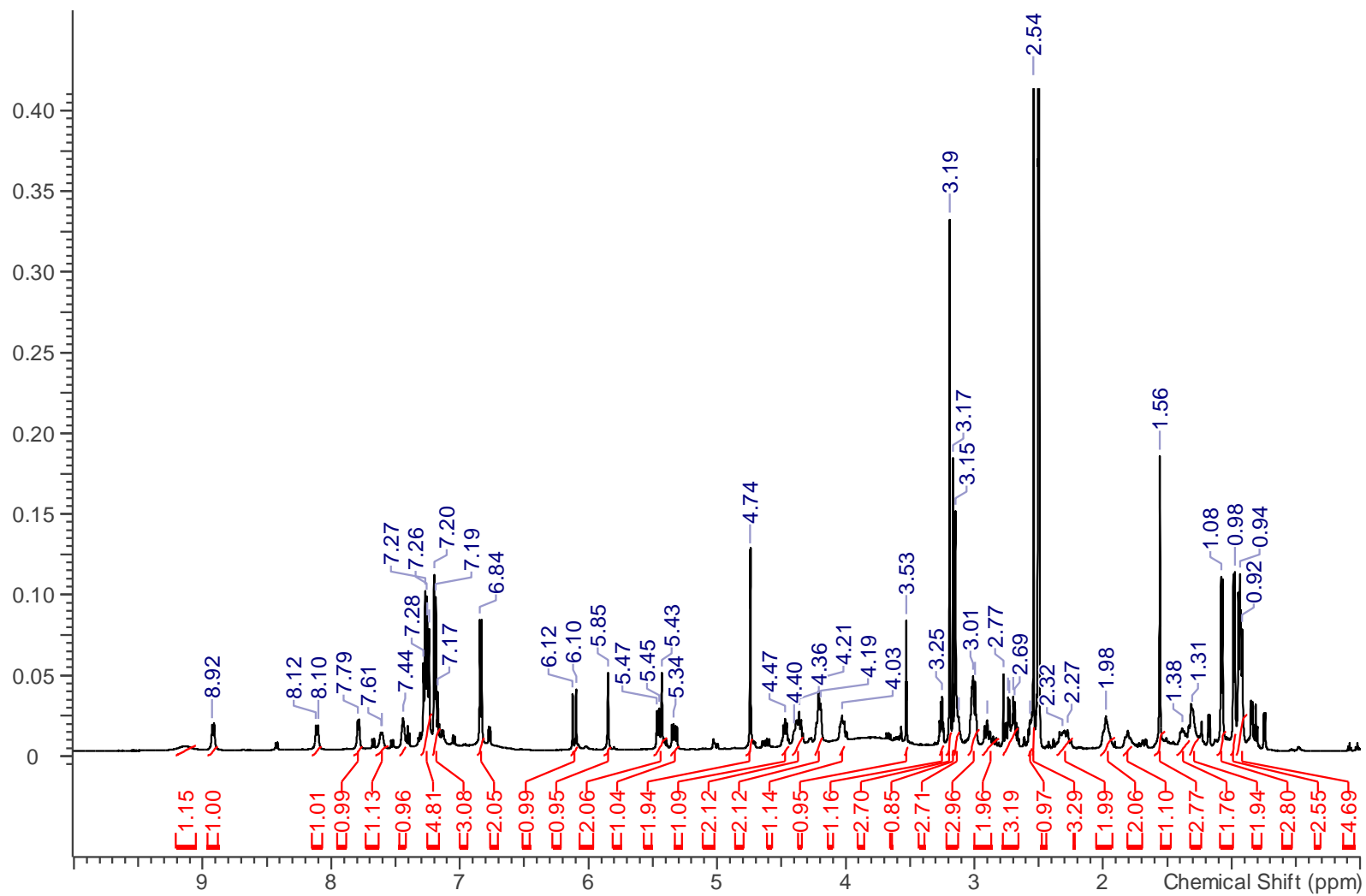


**Figure A114.**  $^1\text{H}$  NMR spectrum (600 MHz) of **3** in  $\text{DMSO-d}_6$  (overview from 0 to 10 ppm).

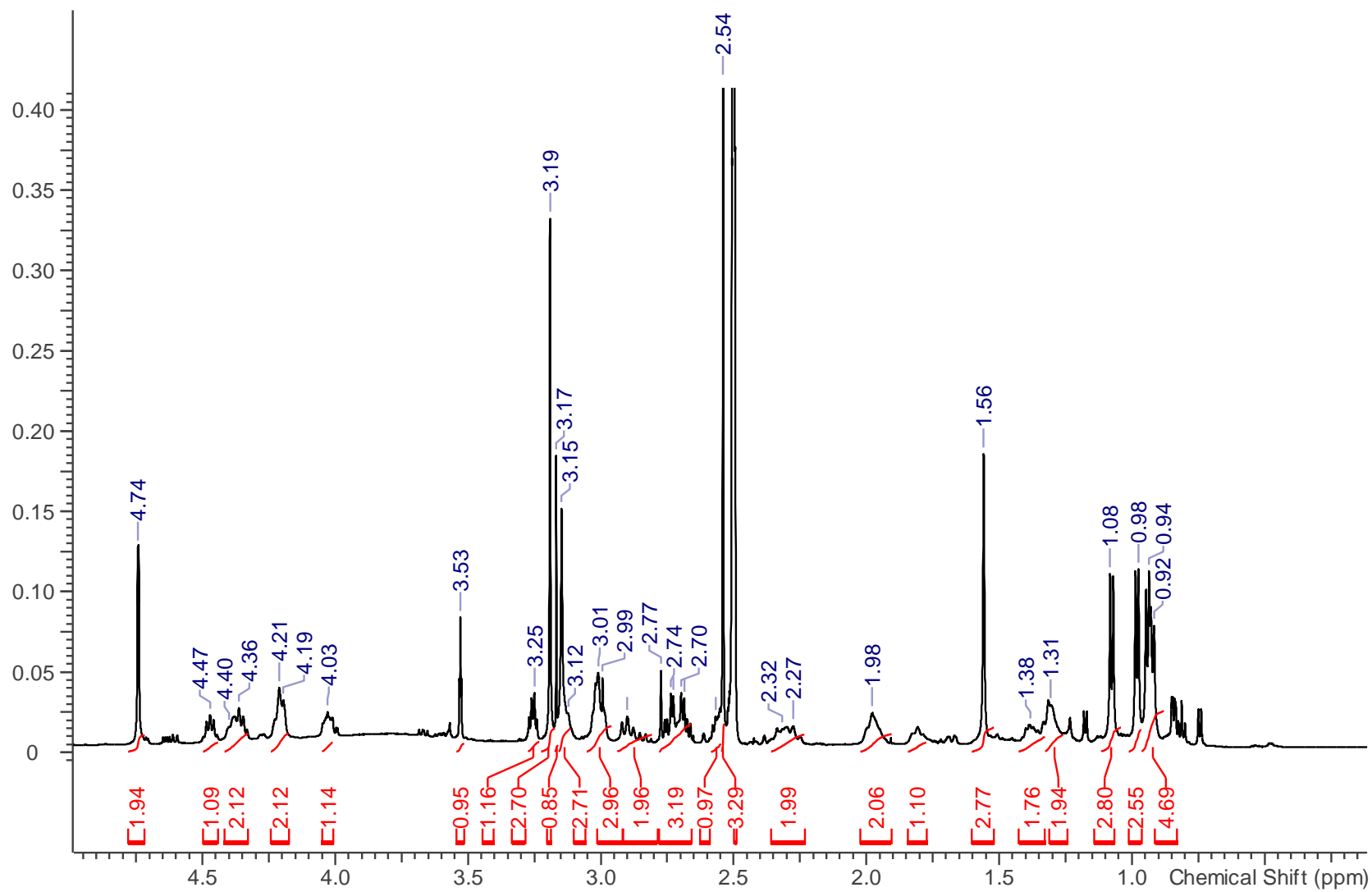
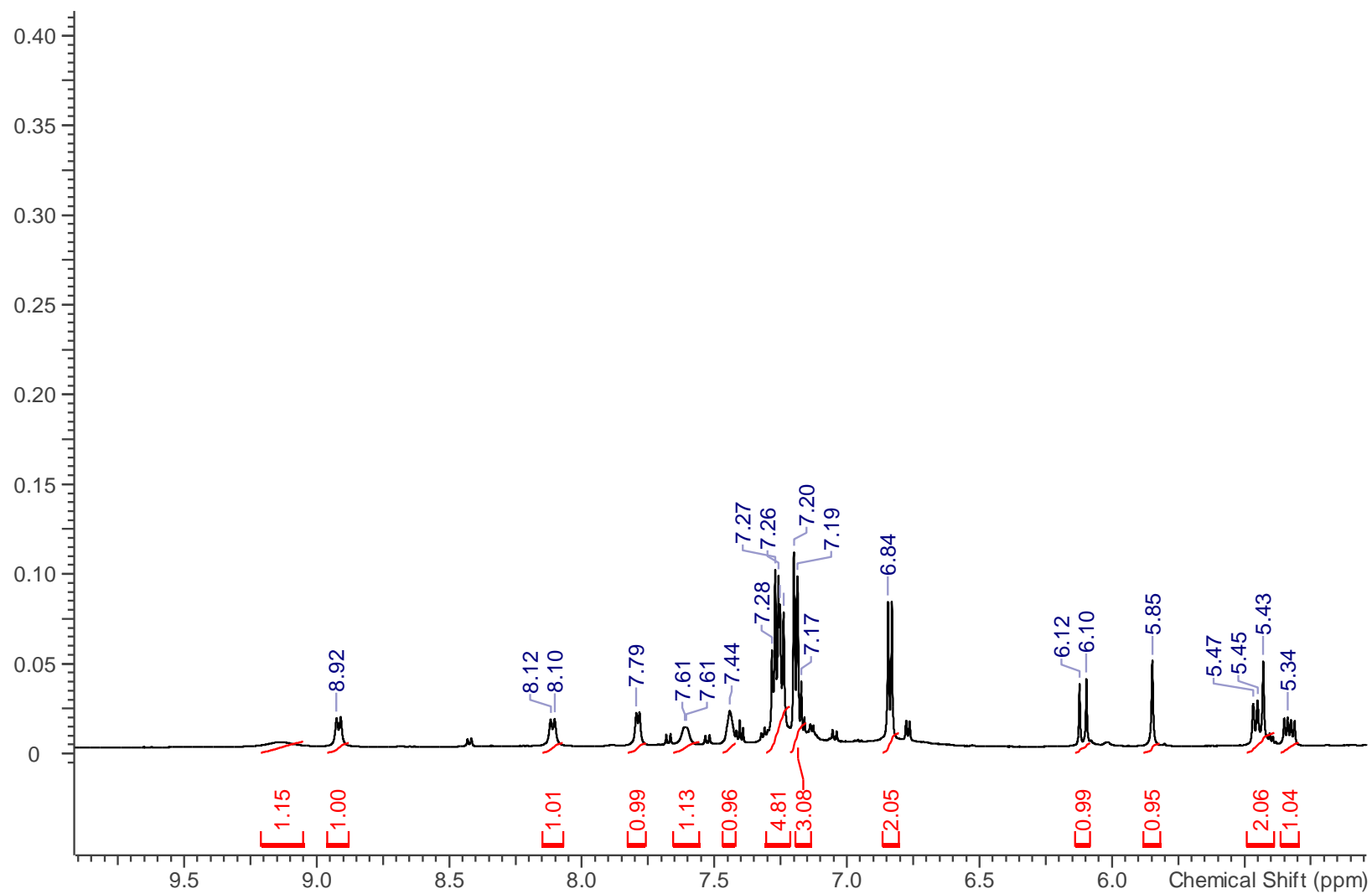


Figure A115. <sup>1</sup>H NMR spectrum (600 MHz) of 3 in DMSO-d<sub>6</sub> (0 to 5 ppm).



**Figure A116.** <sup>1</sup>H NMR spectrum (600 MHz) of **3** in DMSO-d<sub>6</sub> (overview from 5 to 10 ppm)

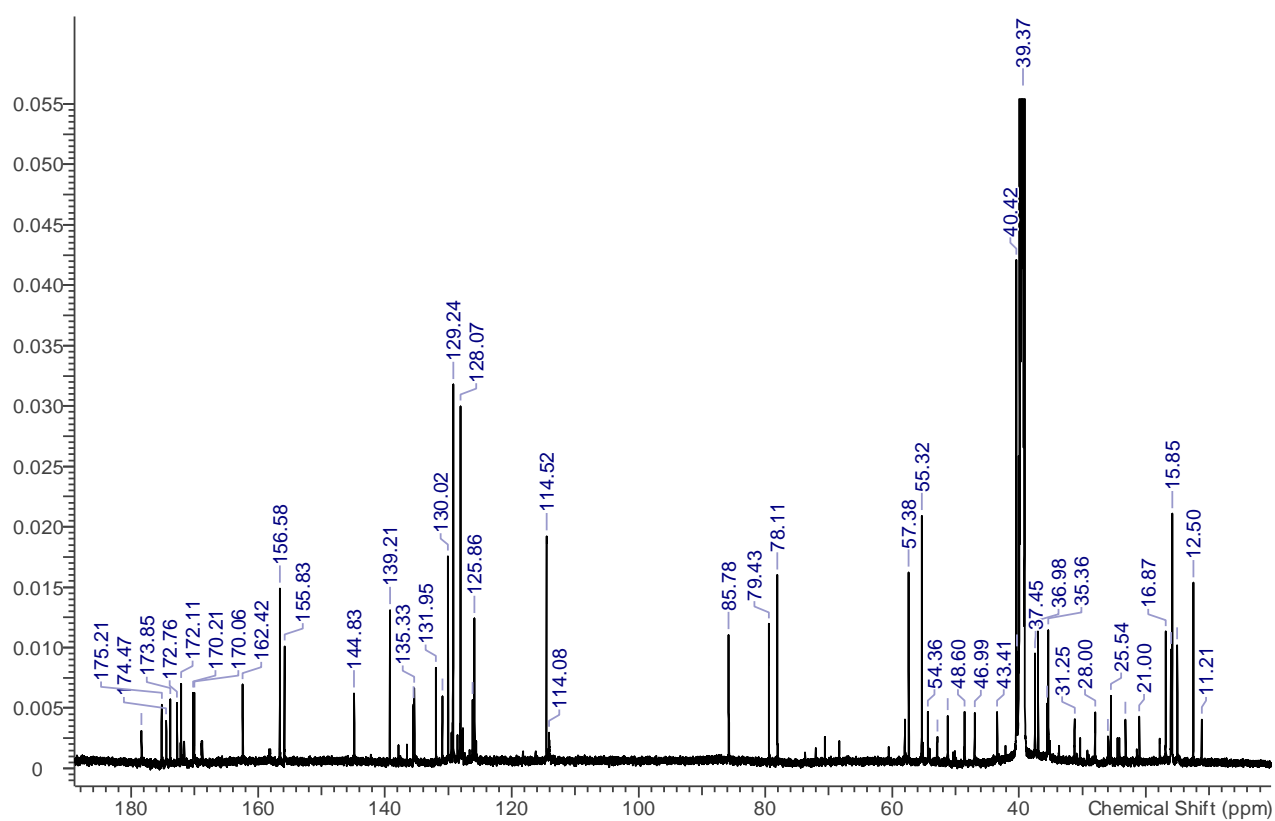


Figure A117.  $^{13}\text{C}$  NMR spectrum (150 MHz) of **3** in  $\text{DMSO-d}_6$ .

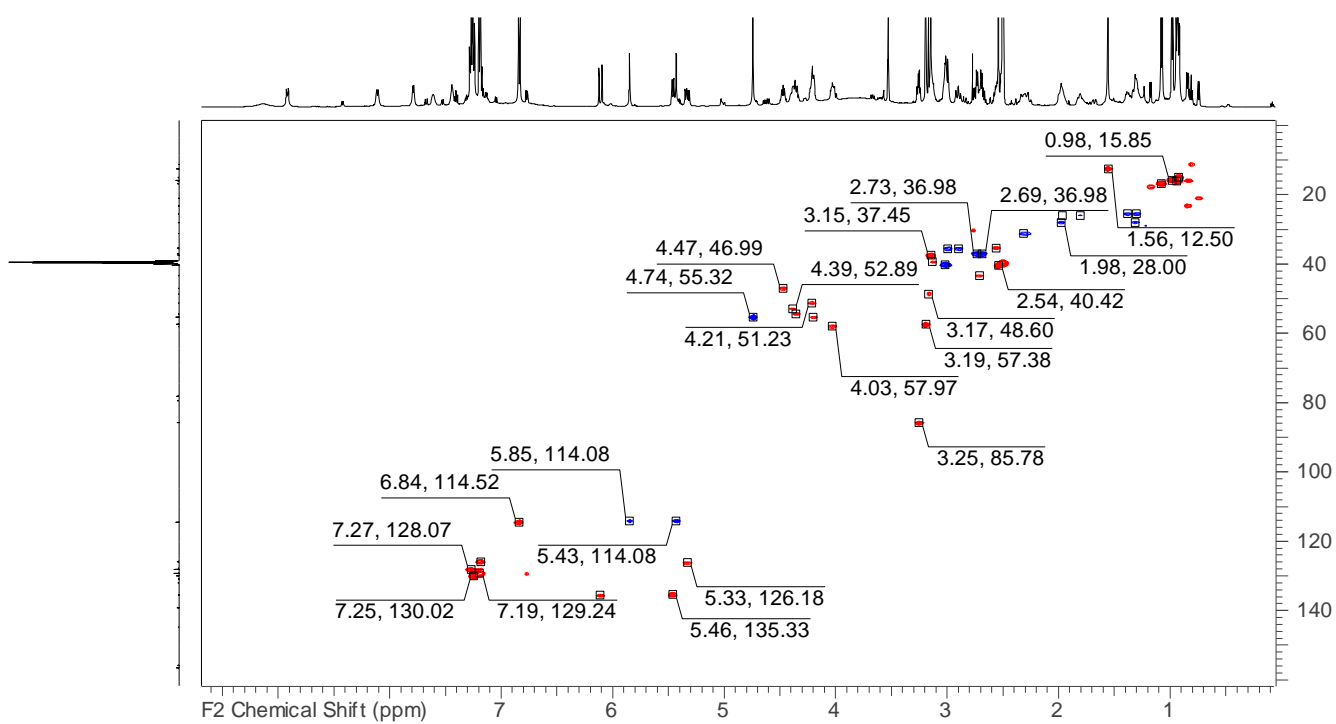


Figure A118. HSQC-DEPT NMR spectrum of **3** in  $\text{DMSO-d}_6$ .

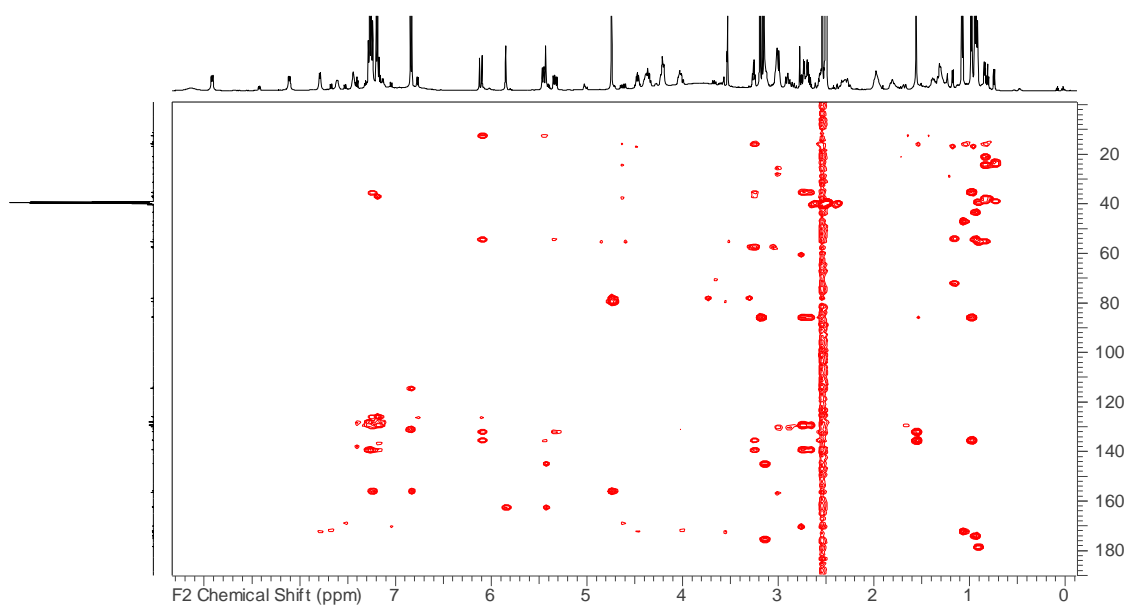


Figure A119. HMBC NMR spectrum of **3** in DMSO- $d_6$ .

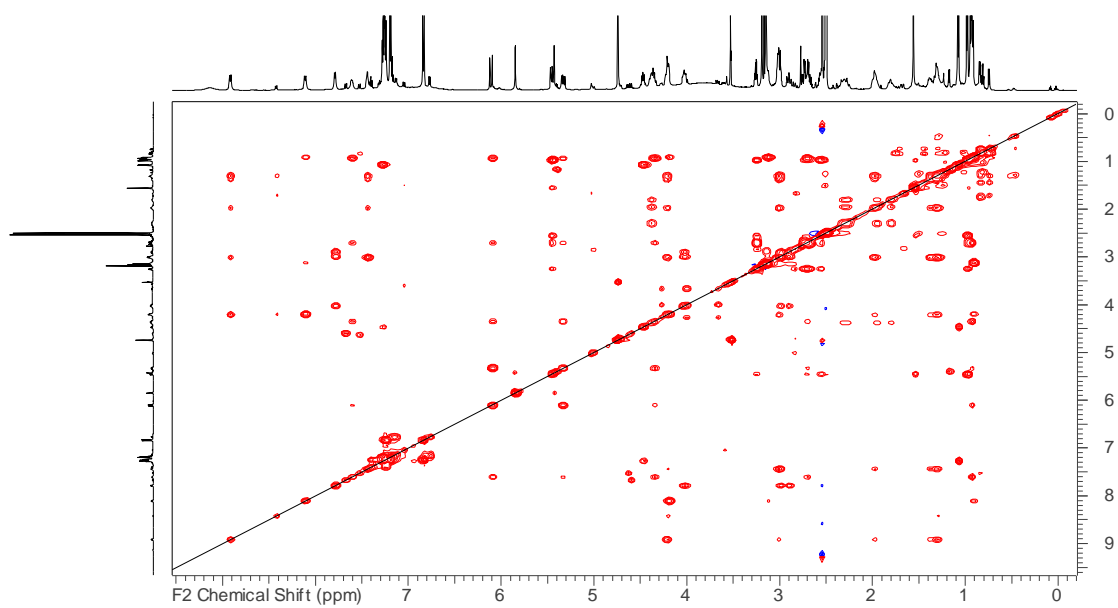


Figure A120. TOCSY NMR spectrum of **3** in DMSO- $d_6$ .

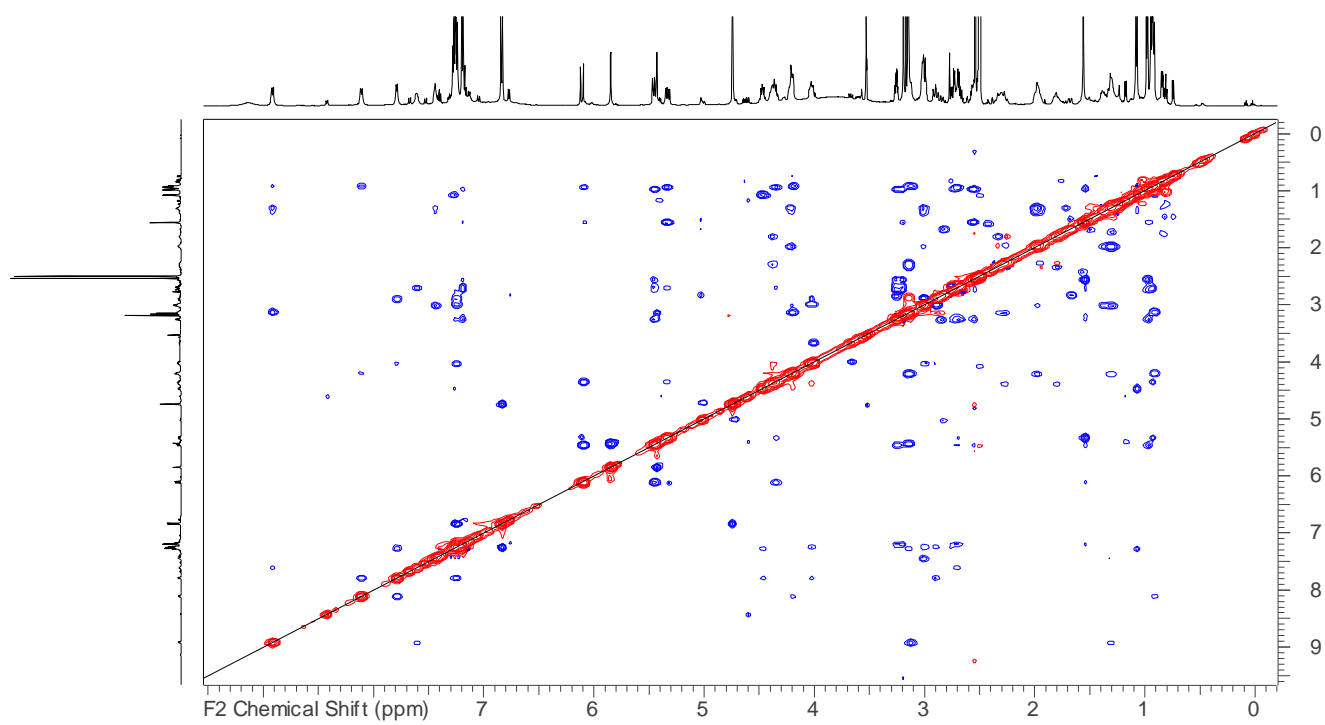


Figure A121. ROESY NMR spectrum of **3** in DMSO-d<sub>6</sub>.

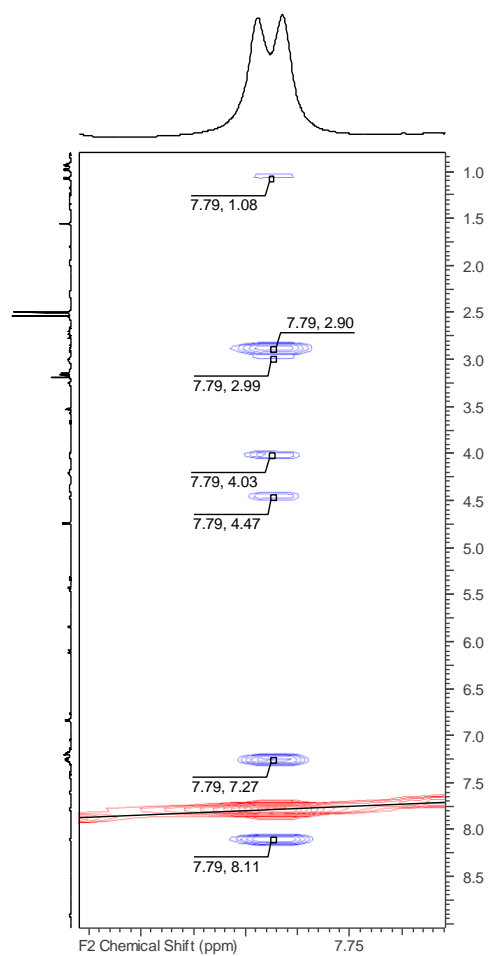
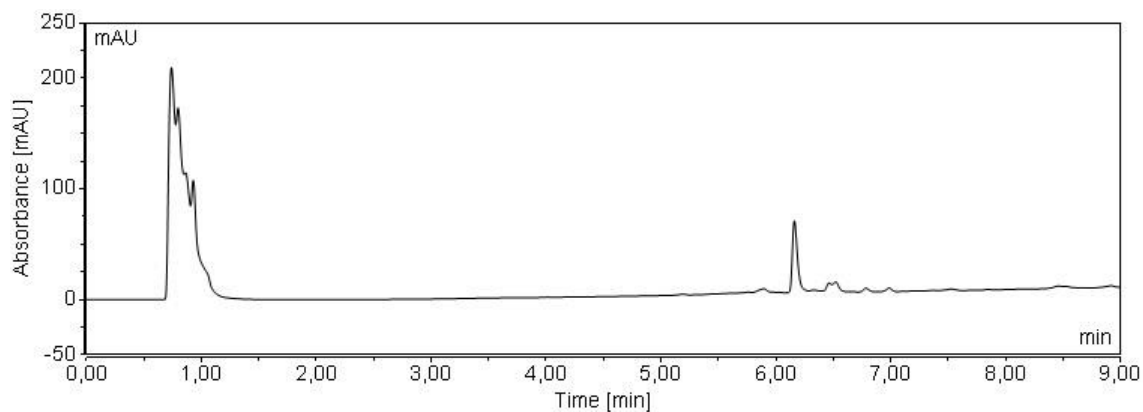
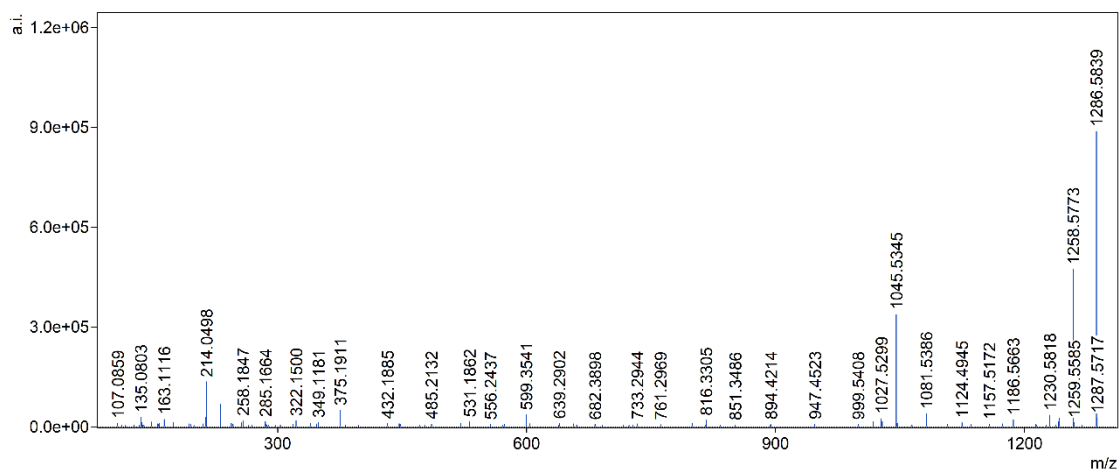


Figure A122. ROESY correlations of the Prtyr NH proton (7.79 ppm).



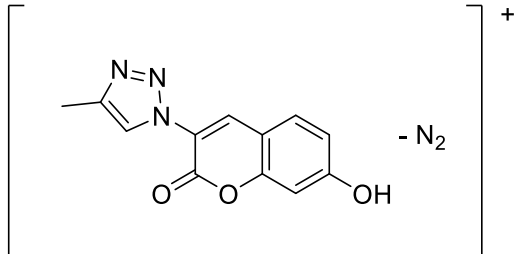
**Figure A123.** HPLC-UV chromatogram (254 nm) of MC-(O-((7-hydroxy-2H-chromen-3-yl)-1H-1,2,3-triazol-4-yl)methyl)YR (**5**). Injection peak due to the sample solvent (DMSO).



**Figure A124.** MS<sup>2</sup> spectrum of MC-(O-((7-hydroxy-2H-chromen-3-yl)-1H-1,2,3-triazol-4-yl)methyl)YR (**5**).



**Table A12.** Annotation of the MS<sup>2</sup> spectrum of MC-(O-((7-hydroxy-2H-chromen-3-yl)-1H-1,2,3-triazol-4-yl)methyl)YR (**5**). Mdha, *N*-methyl dehydroalanine; Adda, 3S-amino-9S-methoxy-2S,6,8S-trimethyl-10-phenyldeca-4E,6E-dienoic acid.

Fragment	Formula	Structure	Measured <i>m/z</i>	Calculated <i>m/z</i>	Difference (Da)
M + H <sup>+</sup>	C <sub>64</sub> H <sub>80</sub> N <sub>13</sub> O <sub>16</sub>	-	1286.5839	1286.5841	0.0002
M - N <sub>2</sub> + H <sup>+</sup>	C <sub>64</sub> H <sub>80</sub> N <sub>11</sub> O <sub>16</sub>	-	1258.5773	1258.5779	- 0.0006
M - C <sub>12</sub> H <sub>6</sub> N <sub>3</sub> O <sub>3</sub> + H <sup>+</sup>	C <sub>52</sub> H <sub>74</sub> N <sub>10</sub> O <sub>13</sub>	MC-YR + H <sup>+</sup>	1045.5345	1045.5353	-0.0008
M - C <sub>12</sub> H <sub>8</sub> N <sub>3</sub> O <sub>4</sub> + H <sup>+</sup>	C <sub>52</sub> H <sub>72</sub> N <sub>10</sub> O <sub>12</sub>	MC-YR - H <sub>2</sub> O + H <sup>+</sup>	1027.5299	1027.5247	+ 0.0052
b <sup>3</sup> /y <sup>3</sup>	C <sub>31</sub> H <sub>46</sub> N <sub>6</sub> O <sub>6</sub>	Masp-Arg-Adda + H <sup>+</sup> Arg-Adda-Glu + H <sup>+</sup>	599.3541	599.3552	- 0.0009
b <sup>3</sup> /y <sup>3</sup>	C <sub>20</sub> H <sub>27</sub> N <sub>2</sub> O <sub>5</sub>	(Adda -C <sub>9</sub> H <sub>11</sub> O -NH <sub>2</sub> )-Glu-Mdha	375.1911	375.1914	-0.0003
M - C <sub>52</sub> H <sub>72</sub> N <sub>12</sub> O <sub>13</sub>	C <sub>12</sub> H <sub>8</sub> NO <sub>3</sub>		214.0498	214.0504	- 0.0006

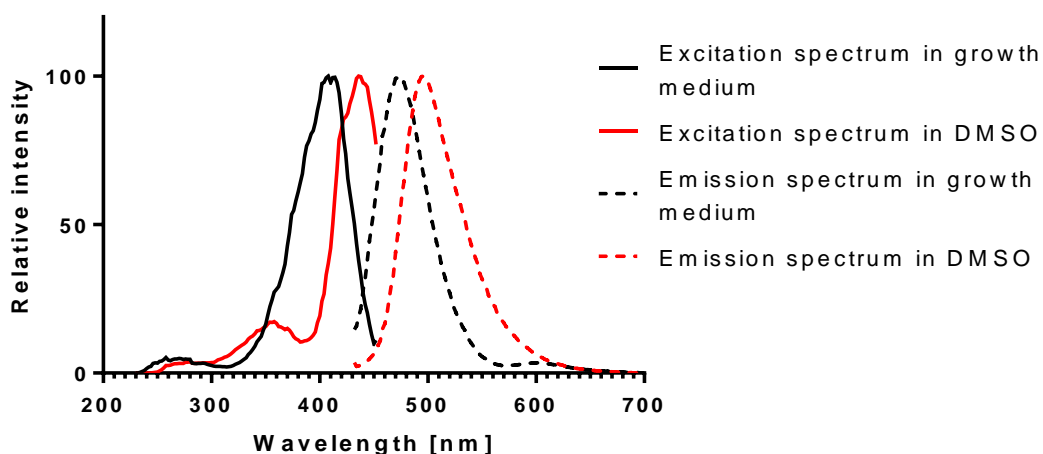


**Figure A125.** Excitation (solid lines) and emission (dashed lines) spectra of MC-(O-((7-hydroxy-2H-chromen-3-yl)-1H-1,2,3-triazol-4-yl)methyl)YR (**5**) in growth medium (black lines) and DMSO (red lines).

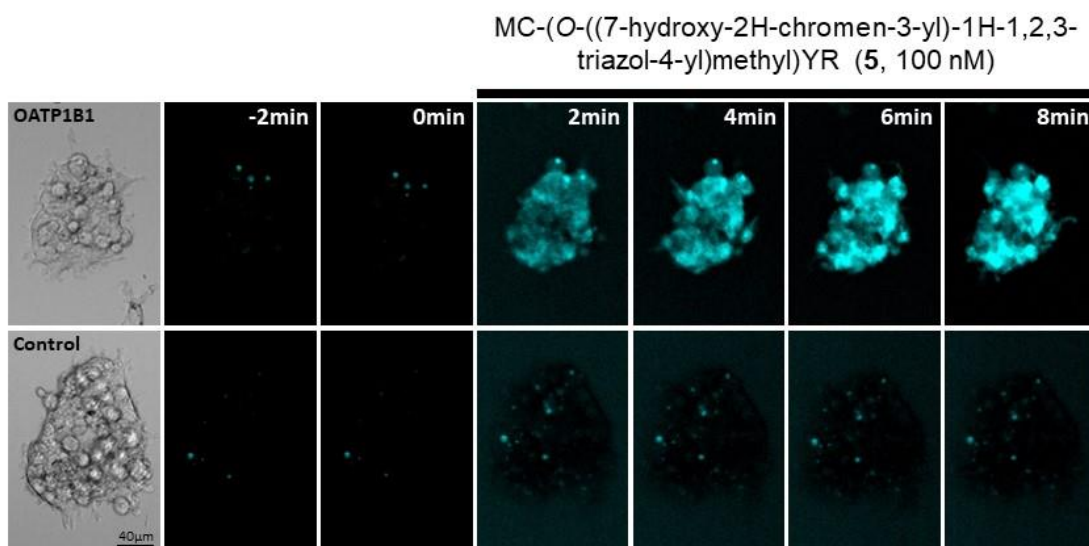


**Figure A126.** Fluorescence time-lapse microscopy of OATP1B1<sup>+</sup> HEK293 cells (upper row) and the corresponding control cells (lower row) before and after exposure to 100 nM MC-(O-((7-hydroxy-2H-chromen-3-yl)-1H-1,2,3-triazol-4-yl)methyl)YR (**5**). The first picture of each row depicts the brightfield image of the selected cell colony. After 8 min, the increase in fluorescence intensity was not visually discernible anymore.

## A.6. Copyright Licenses

**Document A1.** Copyright license for the reproduction of Figure 4.

RightsLink Printable License

<https://s100.copyright.com/CustomerAdmin/PLF.jsp?ref=468f35a7-91...>

### AMERICAN ASSOCIATION FOR CANCER RESEARCH LICENSE TERMS AND CONDITIONS

May 27, 2020

---

This Agreement between University of Tübingen ("You") and American Association for Cancer Research ("American Association for Cancer Research") consists of your license details and the terms and conditions provided by American Association for Cancer Research and Copyright Clearance Center.

License Number	4814260133859
License date	Apr 22, 2020
Licensed Content Publisher	American Association for Cancer Research
Licensed Content Publication	Cancer Research
Licensed Content Title	Recent Advances of Cell-Cycle Inhibitor Therapies for Pediatric Cancer
Licensed Content Author	Christopher C. Mills,EA. Kolb,Valerie B. Sampson
Licensed Content Date	Dec 1, 2017
Licensed Content Volume	77
Licensed Content Issue	23
Type of Use	Thesis/Dissertation
Requestor type	academic/educational
Format	print and electronic
Portion	figures/tables/illustrations

Number of figures/tables /illustrations	1
Will you be translating?	no
Circulation	5
Territory of distribution	Worldwide
Title	Microcystins as lead structures for anticancer therapy
Institution name	University of Tübingen
Expected presentation date	Jul 2020
Order reference number	Thesis_Figure 4
Portions	Figure 1
Requestor Location	University of Tübingen Auf der Morgenstelle 28 Tübingen, 72076 Germany Attn: University of Tübingen
Total	0.00 EUR

**Terms and Conditions****American Association for Cancer Research (AACR) Terms and Conditions****INTRODUCTION**

The Publisher for this copyright material is the American Association for Cancer Research (AACR). By clicking "accept" in connection with completing this licensing transaction, you agree to the following terms and conditions applying to this transaction. You also agree to the Billing and Payment terms and conditions established by Copyright Clearance Center (CCC) at the time you opened your Rightslink account.

**LIMITED LICENSE**

The AACR grants exclusively to you, the User, for onetime, non-exclusive use of this

material for the purpose stated in your request and used only with a maximum distribution equal to the number you identified in the permission process. Any form of republication must be completed within one year although copies made before then may be distributed thereafter and any electronic posting is limited to a period of one year. Reproduction of this material is confined to the purpose and/or media for which permission is granted. Altering or modifying this material is not permitted. However, figures and illustrations may be minimally altered or modified to serve the new work.

#### **GEOGRAPHIC SCOPE**

Licenses may be exercised as noted in the permission process

#### **RESERVATION OF RIGHTS**

The AACR reserves all rights not specifically granted in the combination of 1) the license details provided by you and accepted in the course of this licensing transaction, 2) these terms and conditions , and 3) CCC's Billing and Payment terms and conditions.

#### **DISCLAIMER**

You may obtain permission via Rightslink to use material owned by AACR. When you are requesting permission to reuse a portion for an AACR publication, it is your responsibility to examine each portion of content as published to determine whether a credit to, or copyright notice of a third party owner is published next to the item. You must obtain permission from the third party to use any material which has been reprinted with permission from the said third party. If you have not obtained permission from the third party, AACR disclaims any responsibility for the use you make of items owned by them.

#### **LICENSE CONTINGENT ON PAYMENT**

While you may exercise the rights licensed immediately upon issuance of the license at the end of the licensing process for the transaction, provided that you have disclosed complete and accurate details of your proposed use, no license is finally effective unless and until full payment is received from you, either by the publisher or by the CCC, as provided in CCC's Billing and Payment terms and conditions. If full payment is not received on a timely basis, then any license preliminarily granted shall be deemed automatically revoked and shall be void as if never granted. Further, in the event that you breach any of these terms and conditions, or any of the CCC's Billing and Payment terms and conditions, the license is automatically revoked and shall be void as if never granted. Use of materials as described in a revoked license, as well as any use of the materials beyond the scope of an unrevoked license, may constitute copyright infringement and the publisher reserves the right to take any and all action to protect its copyright in the materials.

#### **COPYRIGHT NOTICE**

You must include the following credit line in connection with your reproduction of the licensed material: "Reprinted (or adapted) from Publication Title, Copyright Year, Volume/Issue, Page Range, Author, Title of Article, with permission from AACR".

#### **TRANSLATION**

This permission is granted for non-exclusive world English rights only.

#### **WARRANTIES**

Publisher makes no representations or warranties with respect to the licensed material.

#### **INDEMNIFICATION**

You hereby indemnify and agree to hold harmless the publisher and CCC, and their respective officers, directors, employees and agents, from and against any and all claims arising out of your use of the licensed material other than as specifically authorized pursuant to this license.

**REVOCATION**

The AACR reserves the right to revoke a license for any reason, including but not limited to advertising and promotional uses of AACR content, third party usage and incorrect figure source attribution.

**NO TRANSFER OF LICENSE**

This license is personal to you and may not be sublicensed, assigned, or transferred by you to any other person without publisher's written permission.

**NO AMENDMENT EXCEPT IN WRITING**

This license may not be amended except in a writing signed by both parties (or, in the case of publisher, by CCC on publisher's behalf).

**OBJECTION TO CONTRARY TERMS**

Publishers hereby objects to any terms contained in any purchase order, acknowledgement, check endorsement or other writing prepared by you, which terms are inconsistent with these terms and conditions or CCC's Billing and Payment terms and conditions. These terms and conditions together with CCC's Billing and Payment terms and conditions (which are incorporated herein) comprise the entire agreement between you and publisher (and CCC) concerning this licensing transaction. In the event of any conflict between your obligations established by these terms and conditions, and those established by CCC's Billing and Payment terms and conditions, these terms and conditions shall control.

**THESIS/DISSERTATION TERMS**

If your request is to reuse an article authored by you and published by the AACR in your dissertation/thesis, your thesis may be submitted to your institution in either in print or electronic form. Should your thesis be published commercially, please reapply.

**ELECTRONIC RESERVE**

If this license is made in connection with a course, and the Licensed Material or any portion thereof is to be posted to a website, the website is to be password protected and made available only to the students registered for the relevant course. The permission is granted for the duration of the course. All content posted to the website must maintain the copyright information notice.

**JURISDICTION**

This license transaction shall be governed by and construed in accordance with the laws of Pennsylvania. You hereby agree to submit to the jurisdiction of the federal and state courts located in Pennsylvania for purposes of resolving any disputes that may arise in connection with this licensing transaction.

Other Terms and Conditions:

v1.0

Questions? [customercare@copyright.com](mailto:customercare@copyright.com) or +1-855-239-3415 (toll free in the US) or +1-978-646-2777.



**Document A2.** Copyright license for the reproduction of Figure A2.

RightsLink Printable License

<https://s100.copyright.com/CustomerAdmin/PLF.jsp?ref=3b9d38b3-c7...>ELSEVIER LICENSE  
TERMS AND CONDITIONS

May 24, 2020

---

---

This Agreement between University of Tübingen ("You") and Elsevier ("Elsevier") consists of your license details and the terms and conditions provided by Elsevier and Copyright Clearance Center.

License Number	4835480285948
License date	May 24, 2020
Licensed Content Publisher	Elsevier
Licensed Content Publication	Chemistry & Biology
Licensed Content Title	Structural organization of microcystin biosynthesis in <i>Microcystis aeruginosa</i> PCC7806: an integrated peptide–polyketide synthetase system
Licensed Content Author	Daniel Tillett, Elke Dittmann, Marcel Erhard, Hans von Döhren, Thomas Börner, Brett A Neilan
Licensed Content Date	Oct 1, 2000
Licensed Content Volume	7
Licensed Content Issue	10
Licensed Content Pages	12
Start Page	753
End Page	764

Type of Use	reuse in a thesis/dissertation
Portion	figures/tables/illustrations
Number of figures/tables /illustrations	1
Format	both print and electronic
Are you the author of this Elsevier article?	No
Will you be translating?	No
Title	Microcystins as lead structures for anticancer therapy
Institution name	University of Tübingen
Expected presentation date	Jul 2020
Order reference number	JM_Figure A2
Portions	Figure 2
Requestor Location	University of Tübingen Auf der Morgenstelle 28 Tübingen, 72076 Germany Attn: University of Tübingen
Publisher Tax ID	GB 494 6272 12
Total	0.00 EUR
Terms and Conditions	

**INTRODUCTION**



1. The publisher for this copyrighted material is Elsevier. By clicking "accept" in connection with completing this licensing transaction, you agree that the following terms and conditions apply to this transaction (along with the Billing and Payment terms and conditions established by Copyright Clearance Center, Inc. ("CCC"), at the time that you opened your Rightslink account and that are available at any time at <http://myaccount.copyright.com>).

#### GENERAL TERMS

2. Elsevier hereby grants you permission to reproduce the aforementioned material subject to the terms and conditions indicated.

3. Acknowledgement: If any part of the material to be used (for example, figures) has appeared in our publication with credit or acknowledgement to another source, permission must also be sought from that source. If such permission is not obtained then that material may not be included in your publication/copies. Suitable acknowledgement to the source must be made, either as a footnote or in a reference list at the end of your publication, as follows:

"Reprinted from Publication title, Vol /edition number, Author(s), Title of article / title of chapter, Pages No., Copyright (Year), with permission from Elsevier [OR APPLICABLE SOCIETY COPYRIGHT OWNER]." Also Lancet special credit - "Reprinted from The Lancet, Vol. number, Author(s), Title of article, Pages No., Copyright (Year), with permission from Elsevier."

4. Reproduction of this material is confined to the purpose and/or media for which permission is hereby given.

5. Altering/Modifying Material: Not Permitted. However figures and illustrations may be altered/adapted minimally to serve your work. Any other abbreviations, additions, deletions and/or any other alterations shall be made only with prior written authorization of Elsevier Ltd. (Please contact Elsevier at [permissions@elsevier.com](mailto:permissions@elsevier.com)). No modifications can be made to any Lancet figures/tables and they must be reproduced in full.

6. If the permission fee for the requested use of our material is waived in this instance, please be advised that your future requests for Elsevier materials may attract a fee.

7. Reservation of Rights: Publisher reserves all rights not specifically granted in the combination of (i) the license details provided by you and accepted in the course of this licensing transaction, (ii) these terms and conditions and (iii) CCC's Billing and Payment terms and conditions.

8. License Contingent Upon Payment: While you may exercise the rights licensed immediately upon issuance of the license at the end of the licensing process for the transaction, provided that you have disclosed complete and accurate details of your proposed use, no license is finally effective unless and until full payment is received from you (either by publisher or by CCC) as provided in CCC's Billing and Payment terms and conditions. If full payment is not received on a timely basis, then any license preliminarily granted shall be deemed automatically revoked and shall be void as if never granted. Further, in the event that you breach any of these terms and conditions or any of CCC's Billing and Payment terms and conditions, the license is automatically revoked and shall be void as if never granted. Use of materials as described in a revoked license, as well as any use of the materials beyond the scope of an unrevoked license, may constitute copyright infringement and publisher reserves the right to take any and all action to protect its copyright in the materials.

9. Warranties: Publisher makes no representations or warranties with respect to the licensed material.

10. Indemnity: You hereby indemnify and agree to hold harmless publisher and CCC, and their respective officers, directors, employees and agents, from and against any and all claims arising out of your use of the licensed material other than as specifically authorized pursuant to this license.

11. No Transfer of License: This license is personal to you and may not be sublicensed, assigned, or transferred by you to any other person without publisher's written permission.

12. No Amendment Except in Writing: This license may not be amended except in a writing signed by both parties (or, in the case of publisher, by CCC on publisher's behalf).

13. Objection to Contrary Terms: Publisher hereby objects to any terms contained in any purchase order, acknowledgment, check endorsement or other writing prepared by you, which terms are inconsistent with these terms and conditions or CCC's Billing and Payment terms and conditions. These terms and conditions, together with CCC's Billing and Payment terms and conditions (which are incorporated herein), comprise the entire agreement between you and publisher (and CCC) concerning this licensing transaction. In the event of any conflict between your obligations established by these terms and conditions and those established by CCC's Billing and Payment terms and conditions, these terms and conditions shall control.

14. Revocation: Elsevier or Copyright Clearance Center may deny the permissions described in this License at their sole discretion, for any reason or no reason, with a full refund payable to you. Notice of such denial will be made using the contact information provided by you. Failure to receive such notice will not alter or invalidate the denial. In no event will Elsevier or Copyright Clearance Center be responsible or liable for any costs, expenses or damage incurred by you as a result of a denial of your permission request, other than a refund of the amount(s) paid by you to Elsevier and/or Copyright Clearance Center for denied permissions.

#### LIMITED LICENSE

The following terms and conditions apply only to specific license types:

15. **Translation:** This permission is granted for non-exclusive world **English** rights only unless your license was granted for translation rights. If you licensed translation rights you may only translate this content into the languages you requested. A professional translator must perform all translations and reproduce the content word for word preserving the integrity of the article.

16. **Posting licensed content on any Website:** The following terms and conditions apply as follows: Licensing material from an Elsevier journal: All content posted to the web site must maintain the copyright information line on the bottom of each image; A hyper-text must be included to the Homepage of the journal from which you are licensing at <http://www.sciencedirect.com/science/journal/xxxxx> or the Elsevier homepage for books at <http://www.elsevier.com>; Central Storage: This license does not include permission for a scanned version of the material to be stored in a central repository such as that provided by Heron/XanEdu.

Licensing material from an Elsevier book: A hyper-text link must be included to the Elsevier homepage at <http://www.elsevier.com>. All content posted to the web site must maintain the copyright information line on the bottom of each image.

**Posting licensed content on Electronic reserve:** In addition to the above the following clauses are applicable: The web site must be password-protected and made available only to bona fide students registered on a relevant course. This permission is granted for 1 year only. You may obtain a new license for future website posting.

17. **For journal authors:** the following clauses are applicable in addition to the above:

**Preprints:**

A preprint is an author's own write-up of research results and analysis, it has not been peer-reviewed, nor has it had any other value added to it by a publisher (such as formatting, copyright, technical enhancement etc.).

Authors can share their preprints anywhere at any time. Preprints should not be added to or enhanced in any way in order to appear more like, or to substitute for, the final versions of articles however authors can update their preprints on arXiv or RePEc with their Accepted Author Manuscript (see below).

If accepted for publication, we encourage authors to link from the preprint to their formal publication via its DOI. Millions of researchers have access to the formal publications on ScienceDirect, and so links will help users to find, access, cite and use the best available version. Please note that Cell Press, The Lancet and some society-owned have different preprint policies. Information on these policies is available on the journal homepage.

**Accepted Author Manuscripts:** An accepted author manuscript is the manuscript of an article that has been accepted for publication and which typically includes author-incorporated changes suggested during submission, peer review and editor-author communications.

Authors can share their accepted author manuscript:

- immediately
  - via their non-commercial person homepage or blog
  - by updating a preprint in arXiv or RePEc with the accepted manuscript
  - via their research institute or institutional repository for internal institutional uses or as part of an invitation-only research collaboration work-group
  - directly by providing copies to their students or to research collaborators for their personal use
  - for private scholarly sharing as part of an invitation-only work group on commercial sites with which Elsevier has an agreement
- After the embargo period
  - via non-commercial hosting platforms such as their institutional repository
  - via commercial sites with which Elsevier has an agreement

In all cases accepted manuscripts should:

- link to the formal publication via its DOI
- bear a CC-BY-NC-ND license - this is easy to do
- if aggregated with other manuscripts, for example in a repository or other site, be shared in alignment with our hosting policy not be added to or enhanced in any way to appear more like, or to substitute for, the published journal article.

**Published journal article (JPA):** A published journal article (PIA) is the definitive final record of published research that appears or will appear in the journal and embodies all

value-adding publishing activities including peer review co-ordination, copy-editing, formatting, (if relevant) pagination and online enrichment.

Policies for sharing publishing journal articles differ for subscription and gold open access articles:

**Subscription Articles:** If you are an author, please share a link to your article rather than the full-text. Millions of researchers have access to the formal publications on ScienceDirect, and so links will help your users to find, access, cite, and use the best available version.

Theses and dissertations which contain embedded PJAs as part of the formal submission can be posted publicly by the awarding institution with DOI links back to the formal publications on ScienceDirect.

If you are affiliated with a library that subscribes to ScienceDirect you have additional private sharing rights for others' research accessed under that agreement. This includes use for classroom teaching and internal training at the institution (including use in course packs and courseware programs), and inclusion of the article for grant funding purposes.

**Gold Open Access Articles:** May be shared according to the author-selected end-user license and should contain a [CrossMark logo](#), the end user license, and a DOI link to the formal publication on ScienceDirect.

Please refer to Elsevier's [posting policy](#) for further information.

18. **For book authors** the following clauses are applicable in addition to the above: Authors are permitted to place a brief summary of their work online only. You are not allowed to download and post the published electronic version of your chapter, nor may you scan the printed edition to create an electronic version. **Posting to a repository:** Authors are permitted to post a summary of their chapter only in their institution's repository.

19. **Thesis/Dissertation:** If your license is for use in a thesis/dissertation your thesis may be submitted to your institution in either print or electronic form. Should your thesis be published commercially, please reapply for permission. These requirements include permission for the Library and Archives of Canada to supply single copies, on demand, of the complete thesis and include permission for Proquest/UMI to supply single copies, on demand, of the complete thesis. Should your thesis be published commercially, please reapply for permission. Theses and dissertations which contain embedded PJAs as part of the formal submission can be posted publicly by the awarding institution with DOI links back to the formal publications on ScienceDirect.

### **Elsevier Open Access Terms and Conditions**

You can publish open access with Elsevier in hundreds of open access journals or in nearly 2000 established subscription journals that support open access publishing. Permitted third party re-use of these open access articles is defined by the author's choice of Creative Commons user license. See our [open access license policy](#) for more information.

### **Terms & Conditions applicable to all Open Access articles published with Elsevier:**

Any reuse of the article must not represent the author as endorsing the adaptation of the article nor should the article be modified in such a way as to damage the author's honour or reputation. If any changes have been made, such changes must be clearly indicated.

The author(s) must be appropriately credited and we ask that you include the end user license and a DOI link to the formal publication on ScienceDirect.

If any part of the material to be used (for example, figures) has appeared in our publication with credit or acknowledgement to another source it is the responsibility of the user to ensure their reuse complies with the terms and conditions determined by the rights holder.

**Additional Terms & Conditions applicable to each Creative Commons user license:**

**CC BY:** The CC-BY license allows users to copy, to create extracts, abstracts and new works from the Article, to alter and revise the Article and to make commercial use of the Article (including reuse and/or resale of the Article by commercial entities), provided the user gives appropriate credit (with a link to the formal publication through the relevant DOI), provides a link to the license, indicates if changes were made and the licensor is not represented as endorsing the use made of the work. The full details of the license are available at <http://creativecommons.org/licenses/by/4.0>.

**CC BY NC SA:** The CC BY-NC-SA license allows users to copy, to create extracts, abstracts and new works from the Article, to alter and revise the Article, provided this is not done for commercial purposes, and that the user gives appropriate credit (with a link to the formal publication through the relevant DOI), provides a link to the license, indicates if changes were made and the licensor is not represented as endorsing the use made of the work. Further, any new works must be made available on the same conditions. The full details of the license are available at <http://creativecommons.org/licenses/by-nc-sa/4.0>.

**CC BY NC ND:** The CC BY-NC-ND license allows users to copy and distribute the Article, provided this is not done for commercial purposes and further does not permit distribution of the Article if it is changed or edited in any way, and provided the user gives appropriate credit (with a link to the formal publication through the relevant DOI), provides a link to the license, and that the licensor is not represented as endorsing the use made of the work. The full details of the license are available at <http://creativecommons.org/licenses/by-nc-nd/4.0>. Any commercial reuse of Open Access articles published with a CC BY NC SA or CC BY NC ND license requires permission from Elsevier and will be subject to a fee.

Commercial reuse includes:

- Associating advertising with the full text of the Article
- Charging fees for document delivery or access
- Article aggregation
- Systematic distribution via e-mail lists or share buttons

Posting or linking by commercial companies for use by customers of those companies.

**20. Other Conditions:**

v1.9

**Questions?** [customercare@copyright.com](mailto:customercare@copyright.com) or +1-855-239-3415 (toll free in the US) or +1-978-646-2777.

## Appendix

---

RightsLink Printable License

<https://s100.copyright.com/CustomerAdmin/PLF.jsp?ref=3b9d38b3-c7...>

